A Palaeomagnetic Study of 3.5 to 3.2 Billion Year Old Rocks from the Barberton Greenstone Belt, South Africa

Thesis submitted in accordance with the requirements of the University of Liverpool for the Doctor in Philosophy by

Laura Roberts Artal

September 2014

A Palaeomagnetic study of 3.5 to 3.2 Billion Year Old Rocks from the Barberton Greenstone Belt, South Africa

Laura Roberts Artal

A palaeomagnetic study of some of the best preserved Palaeoarchaean (3.2 -3.6 Ga) rock successions in the world – the Barberton Greenstone Belt, South Africa – has been carried out in order to shed light on Early Earth processes. The aim is to improve the understanding of the long term evolution of the Earth and the surface conditions under which the first forms of life originated through using palaeomagnetic records. The study follows on from work by Layer et al., (1998), Yoshihara & Hamano (2004), Usui et al., (2009), Tarduno et al., (2010) and Biggin et al., (2011) that indicate that rocks from the Barberton Greenstone Belt have the potential to record a near-primary direction of remanence and a reversing geomagnetic field at ca. 3.5 Ga. The rocks of the Barberton Greenstone Belt are excellently preserved and have only been subjected to low grade metamorphism (greenschist facies), making them good candidates for palaeomagnetic studies. Here, new data obtained from three Onverwacht Group Formations and from the Nelshoogte Pluton are presented. The reliability of the new palaeomagnetic data is affected by the complex history and the age of the rocks but no more so than any other published study of rocks of this age. The Noisy Complex and the Nelshoogte Pluton are affected by lightning induced isothermal remanent magnetisations (IRMs) which result in poor quality results. Nevertheless, two new poles, produced by combining the new findings with previously published data, are calculated for the Komati and Hooggenoeg Formations. The new Komati pole shows improved clustering when compared to previous studies. Whilst the data of the Hooggenoeg Formation are encouraging, the results are ambiguous and open to interpretation. When combined with the results of Biggin et al., (2011) they exhibit considerably improved clustering when the directions are corrected for the tectonic deformation resulting in the formation of the Onverwacht Fold, dated at 3.23 Ga. The new results presented here support the findings of previous palaeomagnetic studies of the Barberton Greenstone Belt and support the existence of a stable geomagnetic field at ca. 3.5 Ga. The results presented here support the findings of Biggin et al., (2011) of moderate latitudinal plate motion during this time and do not rule out the hypothesis that the Pilbara Craton (Western Australia) and the Kaapval Craton (South Africa) were conjoined in the Palaeoarchaean.

“It is very hard to be brave," said Piglet, sniffing slightly, "when you're only a Very Small Animal."

Rabbit, who had begun to write very busily, looked up and said: "It is because you are a very small animal that you will be Useful in the adventure before us.”

Benjamin Hoff, *The Te Of Piglet*

Acknowledgements

I would like to thank my supervisory team for their continued help and support throughout this PhD. This thesis would not have been possible without the guidance of Andy Biggin who has taught me the majority of what I know about paleomagnetism. I would like to thank my secondary supervisors Mimi Hill and Betty Mariani. I am very grateful to Cor Langereis for not only many fruitful discussions, but for his endless hospitality during my various stints at Utrecht. Thanks also go to Maarten de Wit for helping us find the best sampling localities, for sharing his extensive knowledge of the Barberton and for teaching me how to drive a 4x4!

During this project, I spent a long time in the lab, both at Liverpool and at Utrecth. I met a lot of people along the way who contributed to my work. I'd like to thank everyone at the Fort Hoofddijk for making me feel welcome. I would like to especially thank the late Tom Mullender for teaching me how to get the most out of the equipment and for always looking out for me during my visits. I'd like to thank everyone at the Liverpool Geomag Lab for making it such a fun place to work over the past four years. Special thanks to Neil Suttie for putting up with the two chatter boxes in the office but, primarily for always having time to help me (which was often!). Elliot Hurst, for the endless favours and continued technical support. This experience would not have been the same without my officemates: Emma Hodgson and Megan Thomas; thank you for all the cups of tea, cake, support and good times. To the rest of the Liverpool PhD crowd, but especially Leanne Cowie, it's been a blast!

I have had a lot of help and support, not only through my time as a PhD student, from my friends: to the Barcelona girls for being there despite the distance; to the gang for always providing laughs and light relief but to the Woodcroft girls especially for our Tuesday night dates and always being at the end of the phone. There are a few more friends who don't quite fit into a group, you know who you are, big thanks!

Lastly, to all my family for all the encouragement and support ever since I was little. A very special thank you to James for always believing in me, even when I don't, I simply couldn't have done it without you. A little shout out to dad for dedicating countless hours to dutifully proofing this thesis. To mami and pap, thank you for the opportunities, for encouraging me to pursue geology and for teaching me that the sky is the limit. I wouldn't be where I am without your support.

Contents

1. Introduction

1.1. Overview

Our understanding of the Archean aged (4.0Ga to 2.5Ga) Earth is limited. Questions regarding early Earth evolution, structure, geodynamics, geochemistry and associated thermal and tectonic process, (if indeed tectonic process operated at that time) still remain largely unresolved.

The Archean rock record is limited when compared to the abundance of preservation of Proterozoic and Phanaerozoic aged rocks (2.5 Ga to present). It follows, that given the age of Archean terrains a considerable amount of Archean crustal material would be recycled over time (Tolstikhin and Kramers, 2008). Nevertheless, Archean aged rocks are found on all continents on Earth, preserved in crustal provinces (cratons) that range in size from <0.1 to 2.6 x 10^6 km^2 (Condie, 1981), across 260 Greenstone Belts (de Wit and Ashwal, 1995).

There is no strict definition for the term Greenstone Belt (de Wit and Ashwal, 1995); nonetheless they have come to be understood as super crustal sequences, dominated by ultramafic volcanics and often surrounded by intrusive units of tonalitic, trondhjemite and granodioritic composition (Condie, 1981; de Wit, 2004; Dilek and Furnes, 2014); together with which they are known as granitoid-greenstone-terrains . They tend to be metamorphosed to low grades (usually greenschist facies, hence their distinctive colouring and resulting name) and they can be extensively deformed and tectonised (de Wit and Ashwal, 1995). By no means are they strictly composed of volcanic materials, as many preserve sedimentary units (in some cases, up to 90% of an Archean Greenstone Belt can be made up of sedimentary successions, de Wit and Ashwal, 1995), but the tectonic setting of these sediments, as with the volcanic units, remains largely unclear. Perhaps one of the most distinguishing features of greenstone belts is the presence of extrusive ultramafic rocks known as komatiites, discovered by Viljoen and Viljoen in 1969, in the Barberton Greenstone Belt (BGB) of South Africa. Komatiites have attracted the attention of many researchers over time as they have no modern day equivalents and disappear from the rock

record after the ca 2.5Ga, at the end of the Archean with all but a few exceptions (Phanerozic aged komatiites are reported from the Gorgona Islanda, Colombia, Arndt et al., 2008).

The extensive study of greenstone belts can shed light on the processes that operated during the very early stages of the Earth's life. The lack of modern day komatiites, for instance, implies a change in the mantle conditions after the Archean (Arndt et al., 2008; Robin-Popieul et al., 2012). As greenstone belts represent remnants of the Earth's earliest crust they can contribute significantly to our understanding of how the crust came to be (Condie, 1981). However, whether plate tectonics operated during this time is subject to intense debate. Was the Archean crust too weak and mobile to behave as unbending plates? As a result were continuous subduction processes active? Or alternatively were geodynamics dominated by crustal growth and differentiation resulting from isolated events such as proposed mantle super-plumes, (Dilek and Furnes, 2014)?

The tectonic settings in which greenstone belts formed are poorly understood and highly debated, so by attempting to reconstruct the palaeoenvironments in which the volcanic and sedimentary successions formed it is possible to make contributions towards resolving these unknowns. In addition, greenstone belts might hold the key to the evolution of the first forms of life on the planet (Furnes et al., 2004; Furnes, 2001; Grosch and McLoughlin, 2014). Understanding the conditions under which these came to be has not only implications for the Earth, but can potentially provide insight into extraterrestrial forms of life.

Palaeomagnetism has a crucial role to play when it comes to better understanding the early Earth. A significant number of studies of rocks of Archean age, which yield very promising palaeomagnetic results, have been carried out (Biggin et al., 2011; Hale, 1987a; Hale and Dunlop, 1984; Layer et al., 1996; Layer et al., 1998; McElhinny and Senanayake, 1980; Strik et al., 2003; Strik et al., 2007; Suganuma et al., 2006; Tarduno et al., 2007; Usui et al., 2009; Yoshihara and Hamano, 2004). The results of these works point towards the existence of a global stable geomagnetic field at ca. 3.5Ga which in turn has implications for the behaviour of the early Earth's core, contributing in particular to our understanding of inner core nucleation and timing of onset of the geodynamo. The structure and nature of the field at this time is also of relevance, with some studies suggesting a potentially reversing field at ca. 3.2Ga (Layer et al., 1998; Tarduno et al., 2007), which combined with pa-

laeosecular variation data(Smirnov and Tarduno, 2004b) may imply the existence of a dipolar field.

Whether plate tectonics where active during this early stage of the Earth's history and in what way they might have operated remains a key questions to be answered. Palaeomagnetism can contribute to shedding light on the style of plate motions during the Archean. Presently, plate tectonics driven by mantle convection means that the Earth effectively loses heat; however, given that the early Earth's mantle and crust are thought to have been at higher temperatures than at present, plate tectonics as we understand them today might not have been active during the Archean (Hamilton, 1998). In particular, a hotter mantle would have meant the dominant role that plate subduction plays in present day tectonic regimes might not have been as effective. In fact, subduction might not have been viable at all given that Archaean plates might have been more buoyant that at present and the density gradient between the crust and mantle, which allows for subduction to occur, might not have existed (Nisbet & Fowler, 1983). Davies (2006 and 2008) proposed crustal settling in the Archaean as a means by which this buoyancy problem might be overcome but it seems an unlikely solution given that the mantle is thought to have been more fertile (Condie 2005) and convecting vigorously (Brandenburg & van Keken, 200&). As a result, 'flat subduction' where the subducting plate moves subhorizontally below the overriding plate has emerged as one model for Archaean geodynamics (Abbot et al., 1994). This model is supported by geochemical observations (mainly related to the presence of tonalite-trondhjemite-granodiorite, TTG, terrains in greenstone belts) and geodynamically, as discussed above. However, van Hunen & Moyen (2012) argue against this model, mainly due to the fact that if Archaean plates were largely buoyant, there would be no significant force to drive subduction (please refer to van Hunen & Moyen, 2012 for a more in depth discussion).

Instead, subduction might have been more episodic than it is today, be it on long-term scales (a few hundred million years) or on shorter time scales of a few million years (van Hunen & Moyen, 2012). With Archean slabs thought to have been weaker than at present, short lived subduction would have been driven by slabs frequently braking-off (van Hunen & van den Berg, 2008) with the subsequent slab pull reducing further plate convergence (van Hunen & Moyen, 2012). On longer time scales, a weak mantle could have meant the buld up of stress was insufficient to sustain continuous subduction (van Hunen & Mayon, 2012).

The current understanding of the geodynamic settings in which Archaean komatiites were erupted, particularly those erupted into oceanic settings, further support a style of plate tectonics which is not too dissimilar to at present, but which would be largely affected by higher mantle temperatures (Arndt, 2008). These elevated temperatures are thought to have generated mantle plumes which where more abundant and larger than those seen at present and which provide the mechanism by which komatiites were erupted (Arndt, 2008).

An all together alternative model, the stagnant lid convection regime, suggests that pressure-release melting of diapirs would result in a thick compositional boundary layer which would inhibit plate tectonics (Strik, 2004; Vlaar et al., 1994) but allowing heat loss via vertical tectonics instead. This is not dissimilar to the model proposed for plate tectonics on Venus. Recent work suggests rapid latitudinal motion of the lithosphere during the Archean (Biggin et al., 2011; Suganuma et al., 2006).

Palaeomagnetism has a large role to play in deciphering which of the plate tectonic models , discussed above, are more likely to have dominated during the Earth's early history. Palaeomagnetic directions and poles measure over time are used to estimate lateral plate motions associated with modern day style plate motions involving subduction. If similar plate motions can be identified in Archaean aged rocks then they support lateral plate motions at this time. However, if palaeomagnetic results for the Archaean appear stationary, they might point towards a stagnant lid model as proposed by Vlaar et al., (1994). If indeed lateral plate motions existed during the Archean, palaeomagnetism might play a role in distinguishing between the currently proposed models. For example, van Hunen & Moyen (2012) argue that intermittent plate tectonics is supported by varying apparent polar wander angular velocities reported by Strik et al., (2003), O'Neil et al., (2007) and Piper (2010).

The present day magnetosphere plays an important role in shielding the Earth from the electromagnetic radiation and ejected plasma resulting from solar flares and coronal mass ejections (CMEs) at the Sun. To what extent could an Archaean magnetic field shield the Earth's atmosphere from radiation from the Sun? The preservation of the atmosphere at this early stage in the planet's life might have proved crucial to the appearance of the first life forms; its existence would limit the evaporation of water as a result of erosion of the atmosphere from solar wind. Studies of the intensity of the field suggest intensities compa-

rable to those recorded during the Phanaerozic (Tarduno et al., 2007; Tarduno et al., 2010) meaning an Archaean geodynamo was capable of preventing atmospheric erosion.

Despite the promising and encouraging results from previous palaeomagnetic studies, they are not without their problems. Robust palaeomagnetic results rely on the preservation of the original natural remanent magnetisation (NRM) of the rocks studied. Archaean aged rocks (prior to 2.5 Ga) are prone to remagnetisations caused by metamorphism (through the formation of new magnetic minerals and/or wide spread thermal events), hydrothermal alteration, lightning strikes and sample handling during acquisition of and experimentation on samples. Even when original NRMs are isolated from the samples, knowing the precise age of the formation/unit sampled is paramount in order to constrain the age of the acquisition of the magnetisation within the rocks. Often, these combined criteria are not met by palaeomagnetic studies of Archaean rocks.

1.2. Aim and Motivation

In this work, new paleomagnetic results from the Barberton Greenstone Belt, South Africa are presented. A large dataset, spanning four individual formations across the BGB, was studied with the primary aim of reliably constraining the age of the magnetisation recorded by the rocks of the BGB in light of the uncertainties resulting from unsure age determination of NRM components and/or remagnetisations in previous studies. The results have implications for tectonic processes operating during the Archaean.

1.3. Thesis Structure

This thesis can be split into three main sections: a) Geological and palaeomagnetic background; b) palaeomagnetic study of four formations within the BGB, the Komati Formation, The Hooggenoeg Formation, the Noisy Complex and the Nelshoogte Pluton; c) Discussion and overarching conclusions, combining the findings of all four palaeomagnetic studies.

Geological and palaeomagnetic background

The first chapter in this thesis gives an overall background to the geology of the BGB as well as a summary of the present literature and its implications for the work presented in this thesis. However, it should be noted that these are brief summaries; detailed geological and palaeomagnetic backgrounds are provided on a chapter by chapter basis.

Palaeomagnetic studies

Results chapters cover the directional results obtained from four formations, of differing age, within the BGB. These chapters include detailed summaries of geological and palaeomagnetic backgrounds, as well as methodology and sampling rationale. All directional results are supported by rock magnetic characterisation and microscopy results. Results are placed in the context of previous paleomagnetic studies for the individual formations. In the case of the Noisy Complex and Nelshoogte Pluton chapters, analysis of the research and suggestions to improve the outcome of the findings are made.

Concluding remarks

The wider implications of the results presented in the palaeomagnetic studies are investigated here. Further analysis of the research is discussed as well as suggestions for further avenues of investigation.

2 Geology and Paleomagnetism of the Barberton Greenstone Belt

2.1. Geology of the Study Area

2.1.1. Stratigraphy

The BGB forms part of an ancient Archaean aged Craton, the Kaapval Craton, a small kernel of continental fragment thought to have formed prior to 2.5Ga (de Wit et al., 1992). In the BGB, rocks of mid-Archean age (4.0-3.0Ga), are preserved covering an area of about 1.2 x10^6 km^2 in north eastern South Africa (de Wit et al., 1992). During the first 0.6Ga of its life, the Craton underwent a period of crustal growth where the continental mass separated from the lithosphere below (de Wit et al., 1992). After this period, continental growth continued through crustal accretion and subduction-related processes (although

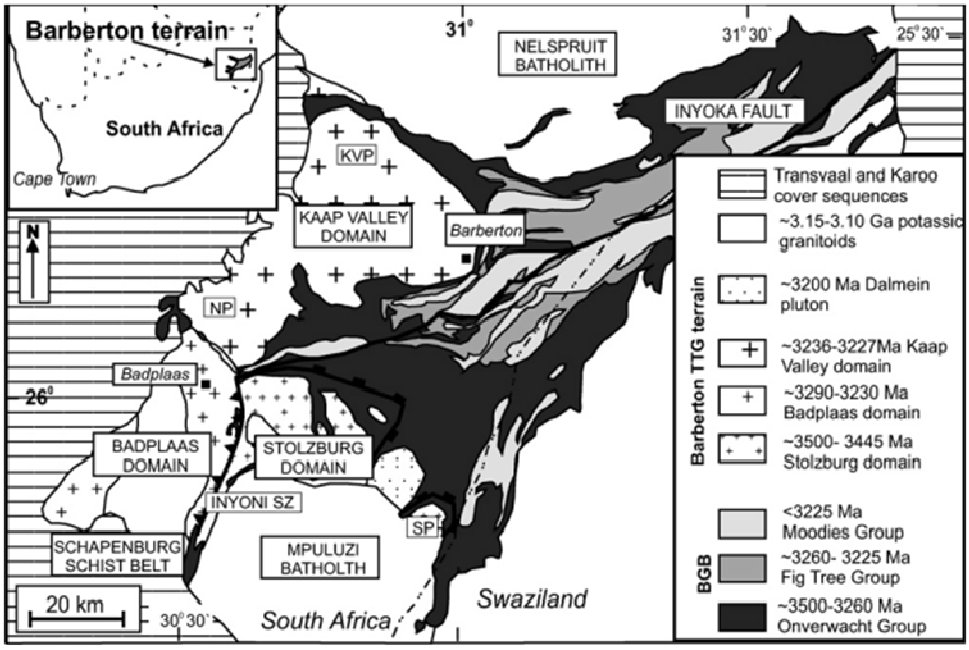

Figure 2.1. Simplified geological map of the BGB taken from Kirsters et al., (2010). NP, Nelshoogte Pluton; KVP, Kaap Valley Pluton; SP, Steynsdorp Pluton.

this is not a view wholly supported in the literature), from approximately 3.1-2.6Ga (de Wit et al., 1992).

The northern limit of the craton is defined by the also Archaean aged, Zimbabwe Craton, whilst to the west and south it has a contact with Proterozoic aged mobile belts. Jurassic volcanic deposits which have been folded mark the boundary of the craton to the west (de Wit et al., 1992). The vertical extent of the craton has been established using S-wave

velocities which indicate a deep and cold lithospheric root extending up to 350 km depth (de Wit et al., 1992). A simplified geological map of the craton is presented in Figure 2.1.

At its core the Kaapval Craton can be subdivided into three main domains, (the larger extent of the Kaapval can also be divided into further subdomains, but these are not relevant to the work presented in this thesis): the Ancient Gneiss Terrain, the southern Barberton Terrain and the northern Barberton Terrain (de Wit et al., 1992). The BGB is formed by the last two terrains, with rocks ranging in age from 3.54 and 3.08Ga (Armstrong et al., 1990; de Ronde and de Wit, 1994; de Wit, 1991; de Wit et al., 1992). Up to 3.65Ga old tonalitic rocks form the bulk of the Ancient Gneiss terrain to the south (Kröner et al., 1996). The boundary between the terrains is tectonic, with the Inyoka Fault acting as a boundary between the northern and southern terrains (Hofmann, 2005).

The BGB is a located in the eastern margin of the Kaapval Craton and constitutes a NE-SW trending tectono-metamorphic belt. The main stratigraphic sequences in the BGB were originally described in the work of Viljoen and Viljoen, (1969d) and are still used at present. The lowermost part sequences of the BGB are dominated by volcanic materials and known as the Onverwacht Suite. These are overlain by the predominantly fine grained sediments of the Fig Tree Group and capped by the Moodies Group, a dominantly coarse clastic sequence (de Wit et al., 2011). An alternative subdivision has been proposed by Lowe and Byerly (2007), where the supercrustal sequences and surrounding Tonalitic-Trondhjemitic Granitoid (TTG) terrains are divided into tectonostratigraphic suites. However, the subdivision has not been widely accepted in the literature given that it requires detailed understanding of the geochronology and thermal history of the BGB, which is not currently the case (de Wit et al., 2011).

The BGB is divided into three main lithostratigraphic groups: The Onverwacht Group, the Fig Tree Group and the Moodies Group. Of particular palaeomagnetic interest is the lowermost Onverwacht Group, given the abundance of volcanic materials which are likely to preserve a more stable and reliable remanence than the overlying predominantly sedimentary Fig Tree and Moodies Groups. This is not to say that these too can be of palaeomagnetic interest, however, the work presented in this thesis concentrates on results from Onverwacht Group. Some authors argue for a continuous stratigraphy across the rocks of the BGB (Lowe and Byerly, 1999b, 2007), whilst more recently, de Wit et al., (2011) argue for the Formations in the BGB to be split into ‘complexes’ bound by shear

zones and which represent potentially distinguishable tectonostratigraphic domains (Kisters et al., 2003). The lowest stratigraphic units of the Onverwacht Group are the Sandspruit and Theespruit Formations, dominated by komatiites to basalts and basalts to dacites, respectively. The Formations are found mostly in the southern part of the BGB within the Onverwacht Fold (OF) and the Steynsdorp Anticline (Lowe and Byerly, 1999b). The Sandspruit Formation is generally isolated from the main body of the BGB and appears as individual xenoliths of highly metamorphosed peridotites and basaltic komatiites (Lowe and Byerly, 1999b). The volcanics of the Theespruit Formation are interlayered with fine to coarse grained sedimentary units, with the entire sequence having been deformed and intruded by dykes and sills of felsic composition (de Wit et al., 2011). The volcanics are dominated by metamorphosed basalts, basaltic komatiites, as well as highly altered felsic volcanics and some pyroclastic units (Lowe and Byerly, 1999b). The exact age and structural relationship between the two Formations remains unclear, as is their relationships to the rest of the Onverwacht Group Formations. However, geochronology studies have suggested a depositional age for the Theespruit Formation of ca. 3530Ma (Kröner et al., 1996; Van Kranendonk et al., 2009a). The Formations have been extensively intruded by the surrounding 3460–3440 and 3210–3240 Ma tonalite to trondhjemite plutons (de Wit et al., 2011; Furnes et al., 2013; Lowe and Byerly, 1999b), which has caused the extensive metamorphism and deformation observed in the rocks (de Wit et al., 2011; Furnes et al., 2013). Peak metamorphic grade recorded in the Theespruit Formation along the edges of the Theespruit and Stolzburg plutons, reaches amphibolite facies indicating burial pressures and temperatures in the ranges from 6 to 8 kbar and 500°-700°C (Diener et al., 2005; Dziggel et al., 2002; Kisters et al., 2003; Lana et al., 2010a). These intense metamorphic conditions preclude the palaeomagnetic study of the lower Formations of the Onverwacht Group.

The Komati Fault/Shear/Schist Zone (KSZ), a 500m thick zone of tonalite dykes and sills as well as highly deformed talc-carbonates and serpentinised schists, marks the contact between the Theespruit Formation and the overlying Komati Formation (de Wit et al., 2011; Furnes et al., 2013; Lowe and Byerly, 1999b). For a detailed account of the stratigraphy and volcanology of the Komati Formation the reader is pointed towards Chapter 4 of this thesis. The minimum age for the Komati Formation is defined by the age of a cross-cutting felsic dyke sampled by Kamo and Davis, (1994) at 3467Ma. The Formation is dominated by layered massive serpentinised komatiites and komatiitic basalts, as well as spinifiex textured komatiites; towards the top of the sequence metabasalts with pyroxene spinifiex

textures and pillowed units become more prevalent (Dann, 2000; de Wit et al., 2011; Furnes et al., 2013). Mafic and ultramafic dykes, of unknown ages, commonly cross cut the volcanic units of the Komati Formation. The exact depositional environment for the ultramafic rocks of the Formation is undecided, with different authors supporting a range of tectonic settings: oceanic plateau (Arndt et al., 2008; Cloete, 1999), oceanic spreading centres (de Wit, 1987) or arc/back arc environments (Grove and Parman, 2004). Recent research (Grosch et al., 2009a; Grosch et al., 2009b) on chlorite composition within the komatiites suggests that previous metamorphic conditions reported at 200–510 °C and 2–5 kbar(Cloete, 1999), may overestimate the peak burial and heating temperatures.

Traditionally, the contact of the Komati Formation with the overlying Hooggenoeg Formation has been defined by the presence of a up to 10m thick metasomatised chert layer, the Middle Marker (MM), often used as a marker bed given its traceability across the OF. Despite authors acknowledging the presence of localised shearing and intrusive rocks along the contact of the two Formations, the stratigraphy has long been interpreted as being continuous (Lowe and Byerly, 1999b). However, recent work by Dann., (2000) de Wit et al., (2011) and Furnes et al., (2011) suggests the top of the Komati Formation is sheared throughout its outcrop in the southern BGB and therefore defined by a layer of silicified pillow lavas and breccias known as the Mbjega Shear Zone (de Wit et al., 2011). The formation of the Mbjega Shear Zone is thought to have occurred during either subseafloor weathering (Lowe and Byerly, 1986) or ocean floor metamorphism (de Wit et al., 2011; de Wit, 1987), therefore constraining the maximum age for the metamorphism observed in the Komati Formation and indicating it occurred soon after deposition of the Formation (de Wit et al., 2011). This is crucial to understanding to what extent thermal events might have affected the magnetisations preserved within the rocks of the Komati Formation.

The Hooggenoeg Formation is dominated by tholeiitic basalts, basaltic komatiites and ultramafic sills (de Wit et al., 2011; Lowe and Byerly, 1999b) up to 3 km in thickness. Detrial zircons measured from the MM give a maximum age for the Hooggenoeg Formation at 3472 ± 5 Ma (Armstrong et al., 1990). The stratigraphy of the Hooggenoeg Formation has been divided into a series of volcanic units/sequences capped by chert horizons (Furnes et al., 2011; Lowe and Byerly, 1999b) and is described in detail in chapter 5 of this thesis. Overall, the lowermost Hooggenoeg is characterised by massive tholeiitic and komatiitic basalts. Upwards, the Formation becomes dominated by basaltic pillow lavas with pyrox-

ene spinifiex textures (de Wit et al., 2011). The exact ages of the felsic intrusives which cross-cut the Hooggenoeg remain unclear but are argued to be related to the emplacement of the Solzburg TTG complex at ca. 3460-3437Ma, (Armstrong et al., 1990; de Wit, 1987; Grosch et al., 2011; Kamo and Davis, 1994). The Hoggenoeg Formation has been affected by a metamorphic event (peak temperatures do not exceed 400°C (Cloete, 1991; López-Martínez et al., 1992) soon after the extrusion of the ultramafic basalts (Brandl and de Wit, 1997). Fliegel et al., (2010) dated a metamorphic overprint, using secondary titanite minerals, at 3344Ga ± 60Ma and U/Pb dating. This age is in agreement with that of gabbroitic dykes which intrude the Komati and Hooggenoeg Formation at 3351±0.006 Ga (Fliegel et al., 2010; Kamo and Davis, 1994). Despite the exact causes of the metamorphism in the Hooggenoeg Formation being unclear, the age determinations support the interpretation that metamorphism of the rocks occurred after their extrusion. Furnes et al., (2011) interpret that the lavas of the Hooggenoeg Formation were erupted at volcanic centres underwater given the presence of pillow lavas and limited vesicularity. The presence of chert layers within the Hooggenoeg Formation may indicate significant hiatuses in the eruption of the lavas (Furnes et al., 2011). The geological evidence (see chapter 3) is supportive of the Hooggenoeg Formation arising in a tectonic setting akin to thin oceanic crust, not dissimilar to where ophiolites form above a subduction zones at present, (Furnes et al., 2013).

Defining the uppermost stratigraphy of the Hooggenoeg Formation is contentious. Originally described by Viljoen and Viljoen (1969b), the overlaying unit of the Hooggenoeg Formation is dominated by a broad zone of felsic volcanics which are capped by a thick chert horizon. The cherts are interbedded with felsic pyroclastic deposits, greywackes and iron rich shales, as well as layered tuffs and thick agglomerates. The sedimentary structures observed in the tuffs are thought to indicate deposition of ash fall deposits into shallow waters. In the subdivision of the Hooggenoeg Formation proposed by Lowe and Byerly (1999), the sedimentary packages were named the Buck Reef Chert (BRC) after the work of Hall, (1918) and ascribed to the overlying Kromberg Formation. Later work by de Vries et al., (2006a) highlighted that the contact between the BRC and the Hooggenoeg Formation is gradational and therefore does not warrant separation of the BRC from the Hooggenoeg. The BRC is incorporated into the stratigraphy of the Hoggenoeg Formation and renamed the Buck Ridge volcano-sedimentary complex (BR-vsc),(de Vries et al., 2006a). In the southern limb of the OF, de Wit et al., (2011) observed that the contact between the Hooggenoeg and BR-vsc is in fact unconformable and the geochemical signature of the

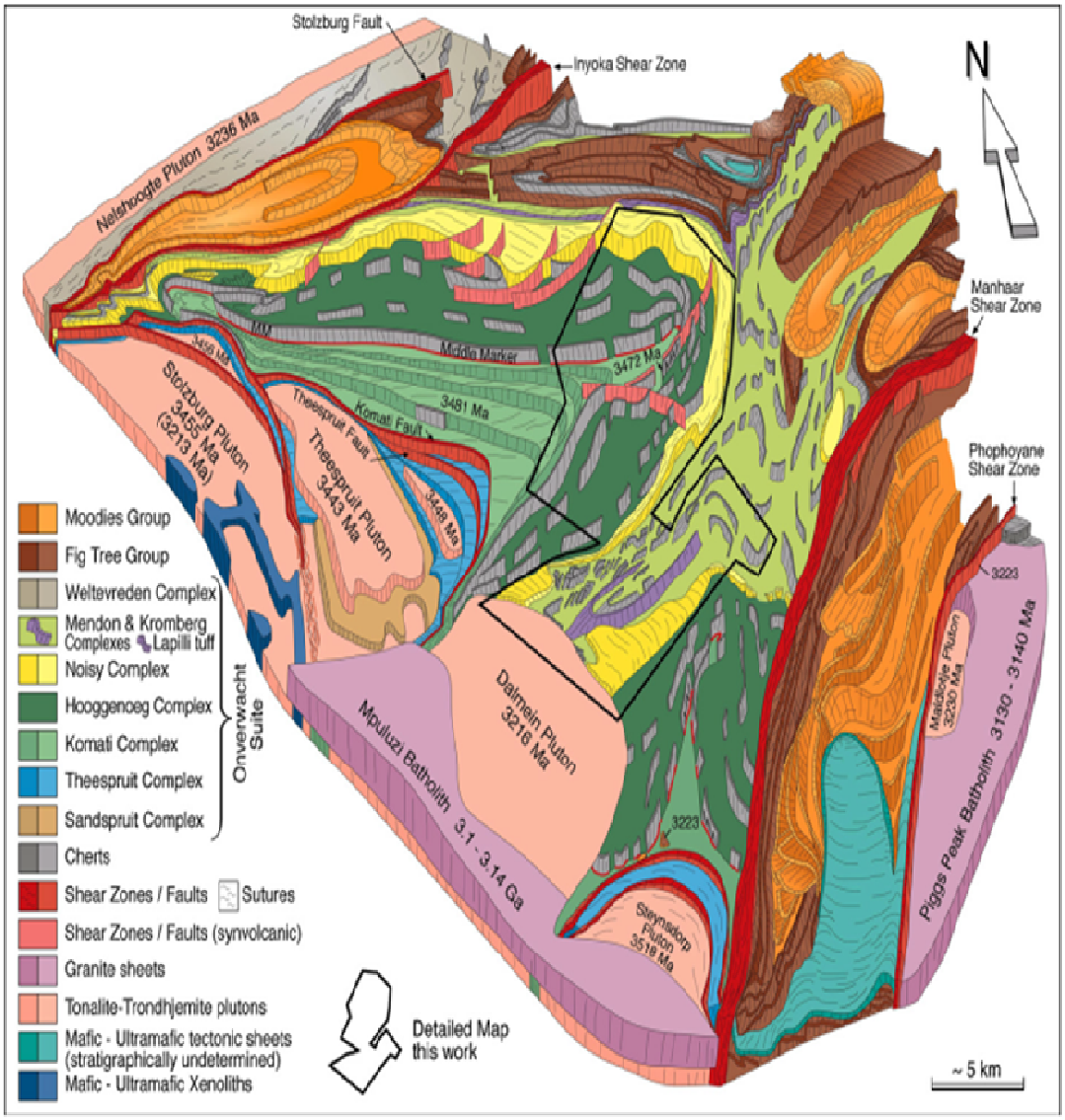

Figure 2.2. Simplified 3-D map illustrating the general geologic relationships of the southern Barberton Mountain Land, the area studied in this thesis. The Onverwacht Suite is subvertical and youngs northwards – into the belt. Please see Figure H, for further detail on the TTG terrain that surrounds the BGB. The figure is taken from de Wit et al., (2011). The solid black line in the centre of the figure is not relevant to the work presented in this thesis; the reader is referred to de Wit et al., (2011) and Furnes et al., (2011) where the authors carried out a detailed study of the lower Onverwacht Group in the area outlined in black, which is accompanied by a very detailed geological map.

volcanics of the two units distinct. Given this, de Wit et al., (2011) propose the creation of a new geological unit within the Onverwacht Group: The Noisy Complex. The new stratigraphy, to include the newly named complex is adopted across the work presented in this thesis. The oldest zircon age obtained for the Noisy Complex gives an age of 3457 ±0.7 (H. Jelsma, unpublished, in de Wit et al., 2011), whilst concordant U/Pb zircon dating of a tuff layer by Biggin et al., (2011), dates the complex at 3455.2±7.5Ma. Peak metamorphism

temperatures for the Noisy Complex are thought not to exceed 200-300°C as confirmed by fluid inclusion studies by de Vries and Touret, (2007) and paleomagnetism (Biggin et al., 2011; Tarduno et al., 2010; Usui et al., 2009). Proposed depositional environments for the rocks of the Noisy Complex range from reworking of coarse-fine grained felsic volcanics and airfall tuffs in a shallow marine environment by turbidite flows (Grosch et al., 2011; Lowe and Knauth, 1977) to volcanoclastics and tuffs extruded as a result of tectonic uplift along an active thrust in an intra-oceanic setting prior to 3455Ma (de Wit et al., 2011; de Wit, 1987; Grosch et al., 2011). Six detrial zircon ages, investigated by laser ablation (LA)- ICP-MS to constrain U-Pb and $^{207}Pb/^{206}Pb$, for the Noisy Complex established by Grosch et al., (2011) indicate a maximum depositional age of the unit of ca. 3432Ma. The depositional setting from the eruption of the Hooggenoeg lavas to the deposition of the Noisy Complex changed dramatically, from deep marine to shallow marine and allowing for the formation of a deep erosional unconformity, over a relatively short period of time, ca. 35 Ga (Furnes et al., 2011; Grosch et al., 2011). An arc-continent convergent margin would allow for the rapid transition in depositional environment, as is seen in, for example, the Phanerozoic ophiolites of Oman, (Grosch et al., 2011).

The Noisy Complex is overlain by the Kromberg Formation who's upper and lower contacts are tectonic in nature (de Wit et al., 2011). The Formation is predominately mafic and ultramafic volcanics, which are principally massive at the base of the unit and become pillowed stratigraphically upwards, as well as mafic and ultramafic intrusives (de Wit et al., 2011; Lowe and Byerly, 1999b). These are interbedded with chert layers, some of which preserve accretionary lapilli (Heinrichs, 1984a). The age of the Formation is poorly constrained due to it being bound by tectonic contacts. The paleomagnetism of the Kromberg Formation was not studied as part of the work presented in this thesis. For more detail on the geology of the Formation the reader is directed towards de Wit et al., (2011), Furnes et al., (2011), for detailed descriptions of the stratigraphy. Lowe and Byerly, (1999), also for detailed stratigraphy, but also for discussion on the inclusion of the BRC within the Kromberg. Furnes et al., (2013) present a detailed overall summary of the newly created tectonic complexes established in the work of de Wit et al., (2011) and Furnes et al., (2011). For details of the palaeomagnetic background of the Kromberg Formation the reader is directed to Biggin et al., (2011) and references therein.

Historically, the contact between the overlying Mendon Formation and the Kromberg Formation has been interpreted to indicated a change in the nature of cyclic volcanism from

predominantly basaltic volcanism in the Kromberg to komatiitic volcanism and local sedimentation in the Mendon Formation (Lowe and Byerly, 1999b). However, de Wit et al., (2011) argue that the top of the Formation is defined by a shear zone. Dating of zircons is unreliable as the cherts are thought to have been enriched in uranium (Rouchon and Orberger, 2008), but they give an age of 3310±2 and 3298±3 (Byerly et al., 1996) for the Formation. The sedimentary cherts are thought to have arisen from pyroclastic material deposited in shallow waters been transported to deeper waters via turbidites (Heinrichs, 1984a). Detailed mapping and logging (de Wit et al., 2011; Grosch et al., 2009a) may suggest that a thick chert and some komatiites are tectonically separated from the Mendon Formation and can no longer be included in its stratigraphy. Therefore, de Wit et al., (2011) argue this warrants the creation of a new tectonostratigraphic unit overlying the Mendon Formation to be known as the Ncakini Complex. For further reading on the Mendon Formation please see de Wit et al., (2011), Furnes et al., (2013), Furnes et al., (2011), Grosch et al., (2009a) and Lowe and Byrely, (1999), amongst others. The Mendon Formation marks the top of the Onverwacht Group and a transition into the more sedimentary rich units of the Fig Tree and Moodies Groups.

Neither the Fig Tree nor the Moodies Group have been studied in this thesis. Therefore, what follows is a very brief overview of the general stratigraphy to provide the reader with some basic background knowledge. The Fig Tree Group, dated at 3260–3226 Ma, is formed of siliciclastic and felsic volcanic rocks (Hofmann, 2005). The unit is capped by a thick layer of sandstones, mudstones and shales derived from turbidites (Lowe and Byerly, 1999b). North of the Inyoka Fault the Group can be subdivided into five stratigraphic units, whilst to the south, only two units are observed (Hofmann, 2005). Significant hydrothermal alteration has affected the rocks of the Fig Tree, with geochemical analyisis of barite and jaspilites horizons indicating a clear seawater signature (Hofmann, 2005). For detailed description of the stratigraphy of the Fig Tree group the reader is directed towards Hofmann, (2005), Lowe and Byerly (1999), Lowe and Nocita, (1999) and references therein.

The Moodies Group constitutes the uppermost unit within the overarching Swaziland Group. It is relatively well exposed in structurally isolated blocks (Lowe and Byerly, 1999b). The minimum age of the Moodies Group is obtained by LA-ICP-MS zircon U/Pb age at 3219 ± 9 Ma (Heubeck et al., 2013). The unit is dominated by quartzose sandstones which rangfrom fine grained to coarse grained and are thought to be deposited in shallow

-marine environments, such as deltas, rivers and the tidal zone (Heubeck et al., 2013). Conglomerates of pebble to cobble size are also common (Lowe and Byerly, 1999b). Volcanic material in the Group is rare, but a laterally continuous basaltic lava acts as a distinctive marker bed (Heubeck et al., 2013) which allows correlation of the Group across the BGB. Siltstones, shales and jaspilites are interbedded with the sandstones and indicate a mild deepening of the depositional environment (Heubeck et al., 2013; Lowe and Byerly, 1999b). In addition, reworked dacitic volcanoclastic material is interspersed within the Group. The lower Moodies group is dominated by a deepening-upward sequence where alluvial facies transgress into shelf facies whilst shallow water facies predominate in the upper section of the Group (Heubeck et al., 2013). The change in depositional style and setting has been attributed to the lowermost units being deposited in extensional tectonic setting whilst the uppermost Moodies represents syndepositional faulting as a result of basin uplift and shortening, ensuing the Group to be divided into a number of separate depositional basins, at ca. 3221Ma (Heubeck et al., 2013; Heubeck and Lowe, 1994). Folding of the Group at ca. 3215-3210Ma was followed by the intrusion felsic dykes (Heubeck et al., 2013). For further reading please see, amongst others: Bontognali et al., (2013); Byerly et al., (1996); Eriksson, (1977); Eriksson et al., (2006) Heubeck et al., (2013); Heubeck and Lowe, (1994) and, Lowe and Byerly, (1999).

The BGB, as are the majority of Archaean aged greenstone belts, is surrounded by tonalitic-trondjhemitic-granodioritc bodies (collectively known as the TTG Series). Notably, TTG series are absent from the post-Archean rock record. The plutons, of tonalitic to trondhjemitic composition were emplaced over a period of ca. 500Ma, from 3662 to 3105Ma (Kamo and Davis, 1994; Schoene et al., 2008c). The oldest of the plutons (e.g. Stenysdorp Pluton, Theespruit Pluton, Stolzburg Pluton, amongst others) are 3509-3227Ma in age (Kamo and Davis, 1994) and particularly rich in sodium. They intruded the BGB mostly along its southern limit, in contact with the Mpuluzi Batholith. The second stage of TTG pluton emplacement (at ca. 3227Ma, Armstrong et al., 1990) saw the formation of the large potassium dominated Kaap Valley and Nelshoogte Plutons, along the western margin of the BGB and the smaller Dalmein Pluton to the south. At the same time, large scale monzogranite-granodiorite batholiths, including the Pigg's Peak, Mpuluzi and Nelspruit batholiths, were extensively emplaced all around the BGB (Matsumura, 2014). The formation of the TTG terraine culminated with the emplacement of syenite-grantie complexes such as the Boesmanskop and Keens Zyn Doorns syenites, at ca. 3107

Ma (Kamo and Davis, 1994). See Figure 2.3, overleaf, for a 3-D map illustrating the main geological relationships between the units of the Onverwacht Group.

2.1.2. Deformation History

Over time, thermal and structural events may have lead to the overprinting of palaeomagnetic signals within the rocks of the BGB, for this reason, understanding the deformation regime across the BGB is crucial to this study. Given the age and complex geology within the BGB the exact correlation of deformation events remains controversial (Kisters et al., 2003). Nevertheless, four deformation phases (D1-D4) have been documented in the BGB (de Ronde and de Wit, 1994) which have resulted in significant faulting and folding and lead to a predominant subvertical orientation of the bedding (de Vries et al., 2006). The

Phase	Nature	Timing	Description	References
D0	Extension	>3458 ± 8 Ma	Mafic-ultramafic igenous activity; Normal Faulting and decollment; Metamorphism: greenschist to amphibolite facies through hydrothermal alteration and silicificatio leading to chert formation; Activity takes place on the ocean floor	de Wit (1986), de Ronde and de Wit (1994)
D1	Compression	3445-3416 Ma	Thrusiting and recumbent nappe formation; Intrusion of TTG plutons in southern part of BGB & intrusion of hyperbysall sills; Dynamothermnal metamorphism to greenschist and amphibolite facies	de Ronde and de Wit (1994)
D2	Compression	3229-3227 Ma	SE-NW orineted thrusting, tight isoclinal folding; Emplacement of TTG plutons to the NW and S of BGB; further greenschist-amphibolite facies metamorphims	de Ronde and de Wit (1994)
D3	Compression	3226-3084 Ma	Sedminatry activity predominates; NW thrusting and folding; minor intrusion oif tonalites	de Ronde and de Wit (1994)
D4	Extension	<3084 Ma	Sedimantation predominates; strike-slip faulting is accompanied by folding	de Ronde and de Wit (1994)

Table 2.1. Summary of the tectonic history of the BGB, modified after de Ronde and de Wit, (1994) and de Vries et al., (2006).

deformation records the onset of the accretion of the Kaapval Craton (de Wit et al., 1992). Table 2.1. summarises the main deformation stages in the BGB, and which are also described in detail below.

An early stage of mafic to ultramafic activity is often recognised in the literature as D0, (de Ronde and de Wit, 1994). During this time the volcanic successions and sedimentary Groups of the BGB were formed, likely on the ocean floor where ocean floor hydrothermal alteration and metamorphism was common (de Ronde and de Wit, 1994). The accretion of the BGB is thought to have taken place during the D1 and D2 stages (3445Ma and 3230 Ma by U-Pb zircon dating respectively, de Ronde and de Wit, 1994). The D1 event is characterised by a period of compression and sub-horizontal thrusting (de Vries et al., 2006a; Kisters et al., 2003) , which lead to overall shortening and folding of the BGB packages. The oldest of the TTG bodies (e.g. the Stolzburg Pluton) were emplaced synchro-

nously to the D1 deformation events (de Ronde and de Wit, 1994; Kisters et al., 2003). An intra oceanic subduction environment is proposed for this time (de Ronde and de Wit, 1994), but requires emplacement in an intra-oceanic setting, with the Onverwacht Group being akin to a modern day ophiolite (de Wit, 2004; de Wit, 1987), an interpretation which is not always accepted within the literature (Anhaeusser, 2010; Lana et al., 2010b; Van Kranendonk et al., 2009a).

D2, at ca. 3229-3227Ma (de Ronde and de Wit, 1994), gave rise to SE to NW thrusting and tight isoclinal folds as a result of overall compression (de Vries et al., 2006a). The intrusion of the 3227Ma aged Kaap Valley and Nelshoogte plutons is associated with the D2 deformation event (Kisters et al., 2003; Matsumura, 2014). De Ronde and de Wit, (1994) interpret that the D2 event marks the convergence of an arc and trench block in an arc-arc style setting.

A third and final, compressional event, D3, took place between 3226–3084 Ma by U-Pb and Pb-Pb zircon dating (de Ronde and de Wit, 1994; Kamo and Davis, 1994). This represents the most intense period of deformation recorded in the BGB and amalgamation of the arc and trench blocks of D1 and D2 (de Ronde and de Wit, 1994). It is another compressional event resultant from a NE-SW collision, along the Saddleback-Inyoka Fault, which amalgamated BGB terrains to the north and south (Kisters et al., 2003). As a result, the Saddleback-Inyoka Fault is interpreted to be a suture zone which binds the distinct terrains of the BGB (de Ronde and de Wit, 1994; De Ronde and Kamo, 2000a). The signature of this event dominates the present day structure of the BGB, with many of the folds and thrust zones in the belt oriented along a NE-SW axis (Kisters et al., 2003). The OF, which is within the area studied as part of this work, formed at this time. Prior to folding the strata in the OF had variable dips, therefore, despite being an anticline overall, in places it can present as a synform (De Wit et al., 1983; de Wit et al., 2011). It is likely the D3 folding is a continuation of the D2 deformation as folds from both events tend to be coaxial (de Ronde and de Wit, 1994). In addition, a marked change in sedimentary style resulted with Fig Tree Group sediments being replaced by the coarse grained sediments of the Moodies Group, deposited in an emerging to subaerial environment (de Ronde and de Wit, 1994; De Ronde and Kamo, 2000a; Kisters et al., 2003; Lowe, 1999a; Lowe et al., 1985), means that deposition of the Moodies Group is a direct result of the collision tectonism occurring during the D3 event.

The final deformation event, D4, marks a change to an extensional regime following the amalgamation of the BGB. This event occurred between 3227±1Ma (de Ronde et al., 1991) and 3084 Ma (Armstrong et al., 1990; de Wit et al., 1992). The event refolds the structures formed during the D2 and D3 events and is associated with strike-slip faulting of D3 shear zones.

A number of thermal events have affected the rocks of the BGB. Heating events are identified at ca. 3430Ma, 3.3Ga, 3.2, 3.0, 2.7 and 2.1Ga (de Ronde et al., 1991; Kamo and Davis, 1994; López-Martínez et al., 1992; Toulkeridis et al., 1994; Weis and Wasserburg, 1987) . Metamorphic grade in the BGB does not exceed greenschist to amphibolite facies (de Wit, 1987) and the rocks of the Onverwacht Group in particular have not been subjected to temperatures above 400°C (Biggin et al., 2011; Furnes et al., 2011). It is thought that peak metamorphic conditions were reached very soon after the formation and burial of the rocks on the seafloor (Knauth and Lowe, 2003b; López-Martínez et al., 1992; Schoene et al., 2008a). The conditions affecting individual formations and complexes are given alongside their stratigraphy in this chapter.

From ca. 3.95 to 3.85 Ga, the Moon was heavily bombarded by asteroids, during the Lunar Heavy Bombardment (LHB), which lead to the formation of the lunar Mare (Glikson, 2014). In recent work, it has been proposed that the Archean Earth was also heavily bombarded by asteroids, given the presence of spherule beds within the cherts of the BGB (Lowe and Byerly, 2010; Lowe et al., 2003; Sleep and Lowe, 2014). Of particular interest is spherule layer S2, located at the contact of the Onverwacht Group and the Fig Tree Group, dated at ca. 3.26Ga(Lowe et al., 2003). The bed is dominated by sand-sized spherules which result from the condensation of a rock vapour cloud after a large asteroid impact (Lowe et al., 2003; Sleep and Lowe, 2014). The layer is enriched in iridium and chromium isotopes, a signature typical of asteroid impacts. The rocks of the BGB were damaged by seismic waves and tsunamis resulting from the asteroid impact (Lowe, 2013). Sleep and Lowe,(2014) argue the presence of vertical chert dykes and veins, which are particularly well developed in the outcrop of the Mendon Formation in an area known as Barite Valley, are the surface expression of the asteroid impact and form as a result of downward flow of surface sediments into fracture formed at the seafloor (Sleep and Lowe, 2014). The dykes can extend up to 100m into the underlying stratigraphy (Sleep and Lowe, 2014). The spherule layer is heavily reworked and eroded implying the presence of a large scale tsunami resulting from the asteroid impact (Sleep and Lowe, 2014); alterna-

tively it is possible that seafloor failure caused density currents to rework the spherule layer or that a water column laden with spherules also resulted in density currents (Sleep and Lowe, 2014). The bolide diameter is estimated at 45 km (Johnson and Melosh, 2012) and the crater diameter is calculated at 478 km (Sleep and Lowe, 2014).The lateral extent of the damage caused by the impacting asteroid cannot be reliably established but the authors argue it is likely to have been several crater diameters (Sleep and Lowe, 2014). *P* waves and Rayleigh wave calculations indicate that the impact generated waves which exceeded the amplitudes expected from normal earthquakes. The rock weakening caused by the strong seismic waves lead to the Onverwacht Group rocks to move downslope, away from the edge of a submarine plateau, driven by gravity (Sleep and Lowe, 2014). The implications of an impact of such a large scale on the paleomagnetism of the rocks of the Onverwacht Group cannot be overlooked. Whilst the mechanism by which shock magnetism may impart an overprint in to the surrounding rocks is unclear, an impact of the size described in the work of Lowe et al., (2003), Lowe, (2013) and Sleep and Lowe, (2014) would very likely cause some remagnetisation of the rocks of the BGB. However, the positive conglomerate test (Biggin et al., 2011) obtained from the rocks of the Noisy Complex may rule out a full remagnetisation, if the age of the impact can be determined with certainty and is younger than the Noisy Complex.

2.2 The Early Earth

2.2.1. Archean Palaeomagnetism and Tectonic Reconstructions

The BGB is a good candidate for paleomagnetic study given that it is well preserved, has experienced, mostly low grades of metamorphism (no higher than 400° (Tice et al., 2004)) and is largely unaffected by pervasive structural deformation (de Wit et al., 2011). This means that many original textures and minerals are preserved; a prerequisite for obtaining reliable palaeomagnetic results. Understanding the ancient magnetic field is also limited by these very factors, meaning characterisation of the geodynamo in the Precambrian through palaeomagnetic studies is hampered by the age and thermochemical history of the rock sequences which can shed light on its early structure. Nevertheless, improvement of experimental techniques and theoretical modelling of the field mean that progress is being made in the field.

Geomagnetic field intensity measurements at the surface of the planet can shed light on the dynamo. Long-term changes in the strength of the field are likely associated with changes in core mantle boundary conditions and/or at the contact between the inner and outer core (Macouin et al., 2004). Tarduno et al., (2007) present virtual dipole moment (VDM) strengths that are comparable to the present day field strength which decrease by up to half when cooling rate effects are considered (Aubert et al., 2009). Whether the VDM has seen a steady increase through time (Macouin et al., 2004) or a sharp increase at between 2.1-2.7Ga as a result of the nucleation of inner core and onset of convection (Hale, 1987b) remains unresolved (Aubert et al., 2009).

The structure of the geomagnetic field at this early stage in the Earth's history is also of relevance. A clear indication of a dipolar field would be given by the presence of reversals in the rock record and there is tentative evidence for this prior to ca. 3.0Ga from studies of the Kaap Valley Pluton (Layer et al., 1996; Tarduno et al., 2007), the Nelshoogte Pluton (Layer et al., 1998) and directions from the Noisy Complex and Duffer Formation (Pilbara Craton, Western Australia) from the work of Biggin et al., (2011). However, the strength of these results is limited by data quality and in some cases a questionable primary NRM.To date, the oldest recorded reversal of the field is obtained from the Nullagine Synclinorium (and Meentheena Centrocline) of the East Pilbara Basin (Strik et al., 2003). The dipolarity of the field has also been considered in terms of latitude dependence in palaeosecular variation (PSV) (Smirnov and Tarduno, 2004a) but Aubert et al., (2009) highlight the limitations of this method given the absence of antipodal directions in the dataset presented (see also Dunlop and Yu, 2004) and the difficulty of separating dipolarity effects from secular variation. Also using the PSV, Biggin et al., (2008) established the dynamo was more stable 2.4-2.8Ga ago than it is currently; possibly owing to the ongoing growth of the inner core. Studies of the direction of the geomagnetic field, using the fundamentals of the GAD theory, allow for palaeomagnetic poles to be used to determine palaeogeographic reconstructions.

The existence of supercontinents during the history of the Earth is not uncommon (e.g. Pangaea ~300Ma), but establishing the presence of one during the Archean is complex. The existence of a super continent during the Archean has been proposed on the basis of correlation of volcanic and sedimentary stratigraphic units (Cheney, 1996), as well as palaeomagnetic (Strik et al., 2003; Zegers et al., 1998) , structural (Zegers et al., 1998) and environmental (de Kock et al., 2009) similarities. Cheney, (1996) argues three sequences of

the Transvaal succession (2.7-2.1Ga) in the northeastern part of the Kaapvaal Craton can be correlated via sequence stratigraphy, lithostratigraphy, and lithofacies to three similar units in Pilbara Province of Western Australia. The similarities are observed between the Ventersdorp Supergroup in Kaapvaal and the upper part of the Fortesque Group in Pilbara. The second correlatable sequence is dominated by sediments and banded-iron formations of the Griqualand West successions in the Kaapvaal and the Hamersley Group in the Pilbara. The Pretoria and Postmasburg Groups in the Kaapvaal and the lower part of the Wyloo Group in the Pilbara are also argued to be stratigraphically similar. The evidence presented by Cheney, (1996) supports that at some time between ca 27 and 2.1Ga, the Kaapval and Pilabara Cratons were once part of a larger supercontinent, known as Vaalbara. The work of Zegers et al., (1998) contributed geochronological, structural and palaeomagnetic evidence to further support the findings of Cheney, (1996), in addition to pushing back the age of the existence of Vaalbara to 3.1Ga. By taking the palaeomagnetic poles of the 2860 ±20Myr Millindina Complex (PC, from the Pilabara Craton of Schmidt and Embelton, (1985)) and those of the Kaapval Usushwana Complex (KC, 2871 ±30Ma of Layer et al., (1988)) and plotting them on the present day North pole, Zegers at al., (1998) are able to show the Pilbara and Kaapval Cratons are brought closely together and this supports the Vaalbara theory. Given the lack of longitudinal constraints, Zegers et al. (1996) explore a number of configurations for the Vaalbara supercontinent arguing the best fit is where the Pilbara towards the east of Kaapvaal, with the lineaments in the cratons shown to be sub-parallel, as they can be correlated geologically and through kinematic models.

Through studying the structural relationships between the two Cratons Zegers et al., (1998) conclude that the timing and tectonic evolution of the PC and KC show striking similarities. The exact timing of break-up of the proposed supercontinent is uncertain however Zegers et al., (1998) highlight the lack of evidence (amongst others, see Zegers et al., 19996, for an in depth discussion) of the Vredevort impact event at 2.023 Ga (Kamo et al., 1996) in the Pilbara Craton (when there is extensive evidence in the Kaapval Craton) indicates that the supercontinent must have rifted apart by this time. This implies a period of cratonic stability for Vaalbara of ca. 400Myr which is comparable to the stability of younger supercontinents such as Gondwana (600-180Ma) (Zegers et al., 1998). New palaeomagnetic poles obtained from the Pilbara Craton by Strik et al., (2003) meant further validation of the Vaalbara theory, despite the limitations of any potential reconstructions as a result of the lack of longitudinal constrains. To address this issue de Kock et al., (2009)

sampled the Allanbridge Formation of the Kaapval Craton and undertook a great-circle arc analysis of the results, comparing the new Kaapval poles to poles of similar age in the Pilbara Craton. This method highlighted there was evidence of common motion between the two continents making the theory of a Vaalbara supercontinent more robust by constraining the relative longitudinal separation between the Kaapval and Pilbara Cratons (de Kock et al., 2009). The authors rule out a reconstruction in the opposite hemisphere, given polarity ambiguity, as it would contradict the geological evidence which favours the existence of the supercontinent. In the new reconstruction of de Kock et al., (2009) the Pilbara Craton would be immediately to the north west of the current location of the Kaapval Craton. De Kock et al., (2009) favour this reconstruction over that of Zegers et al., (1998), as not only does it address the issues associated with constraining the longitude of the reconstruction, but also as paths between the poles compared are continuous as opposed to parallel whilst still ensuring good geological correlation. The scarcity of Palaeoarchaean poles limited the work of de Kock et al. (2009) in so far as they restrict the possibility of comparing great-circle distances between successive poles. However, comparison of the few available poles suggests that Vaalbara would have not existed later than 1.8Ga, which is in agreement with the findings of Zegers et al., (1996). Please see de Kock et al., (2009) for a more detailed discussion. Biggin et al., (2011) test the possibility that Vaalbara might have existed deeper into the Archean at ca. 3.45-3.48Ga by comparing palaeomagnetic results from Onverwacht Group (Biggin et al., 2011) to poles of the similar age in the Pilbara; the Duffer Formation pole DUF; 3470±6 Ma; (McElhinny and Senanayake, 1980; McNaughton et al., 1993), associated with a positive fold test and the Marble Bar Chert (MBC; 3456–3476 Ma; (McElhinny and Senanayake, 1980; McNaughton et al., 1993; Suganuma et al., 2006)). The results indicate a quasi-continuos apparent polar wander path between the Kaapval and Pilbara Cratons (Biggin et al., 2011). Whilst the results are encouraging, uncertainties associated with the reliability of the directions isolated from the samples (Usui et al., 2009) and the fact that the best grouping of the directions is observed when the polarity of the Pilbara poles is reversed means that the outcome of the test is inconclusive. Therefore, more data is required to validate the existence of the Vaalbara supercontinent into the late Archean and to establish whether the Zegers et al., (1998) or the de Kock et al., (2009) fit is more robust.

3. Magnetism and Methodology

A brief introduction to key principles of geomagnetism and paleomagnetism are given here. The aim is to provide the reader with some background of some of the terminology used throughout this section. For comprehensive explanations and discussion of geomagnetic theory please refer to:

- Butler. R.F, 1992, Paleomagentism: Magnetic Domains to Geological Terranes.
- Dunlop, D.J., and Özdemir, Ö., 2001, Rock Magnetism: Fundamentals and frontiers.
- Gubbins, D. and Herrero-Bervera, E., 2007, Encyclopaedia of Geomagnetism and Paleomagnetism.
- Tauxe, L., 2010, Essentials of Paleomagnetism.

The methodologies described here apply to the experiments that were performed on the samples as part of this work with the aim to characterise their rock magnetic carriers and the natural remenant magnetisation. A brief outline of the details of each methodology is given here.

3.1. Some Basic Principles

3.1.1. The Geomagnetic Field

The Earth's present day magnetic field is generated through the rotation and convection of an electrically conducting fluid in the outer core through some form of dynamo action (Merrill et al., 1998). The present day geomagnetic field at the Earth's surface is dominantly a geocentric axial dipole (GAD) with some contribution from equatorial dipole and non dipole sources. Both the dipole and non dipole field vary over time (Merrill et al., 1998). At the Earth's surface, the magnetic field can be defined by its intensity (H), declination (*D*) and Inclination (*I*), as shown in Figure 3.1. The vertical (H_V), horizontal (H_H), geographic north (H_N) and east (H_E) component of the field are given by the formulas below:

$$H_v = H \sin I$$

$$H_H = H \cos I$$

$$H_N = H \cos I \cos D$$

$$H_E = H \cos I \sin D$$

The direction of the geomagnetic field is fully described when the declination (*D*) and inclination (*I*) are known, as shown in Fig. 3.1. In addition, if all the field components are known, its total intensity can be calculated:

$$H = \sqrt{H_N^2 + H_E^2 + H_v^2}$$

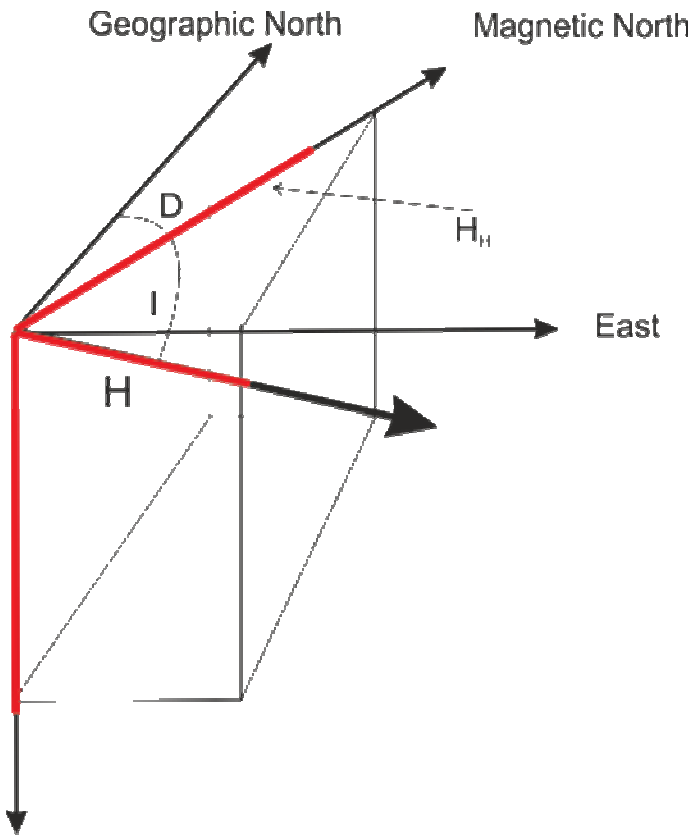

Figure 3.1. Components of the geomagnetic field. The total of the geomagnetic field vector (H) can be resolved into a vertical component Hv = sin I and a horizontal component where Hh= H cos I. Inclination, *I*, is measured positive down between the horizontal and H and ranges between -90 to +90°. The declination, *D*, is the azimuth measured clockwise from geographic north and the horizontal component of H, the angle can range between 0-360°. This figure is modified from Butler, (1992).

In the northern hemisphere, the magnetic inclination is mostly downward, whilst in the southern hemisphere it is mostly upward (Merrill et al., 1998).

The deep structure of the early Earth may have been significantly different to the present day and so it cannot be assumed that the ancient magnetic field would be the same as at present. Conditions within the fluid outer core, such as heat flow across the core mantle boundary (CMB) and the size of the inner core may have been considerably different, which would considerably change how the field was defined (Merrill et al., 1998).

With time, the magnitude and direction of the Earth's magnetic field change, this is defined as geomagnetic secular variation. Since measurements

3.1.2. Ferromagnetism, Paramagnetism, Diamagnetism

Atoms have atomic magnetic moments resulting from the movement of electrons in their orbitals as well as the spin of the electrons. If adjacent magnetic moments are parallel to one another, interact strongly then the material will behave ferromagnetically. Ferromagnetic substances are characterised by their saturation magnetisation j_s, the point beyond which increasing the applied field will not result in the minerals acquiring an increased magnetisation. Saturation magnetisation decreases with temperature and drops to zero once the Curie temperature (T_c) of the mineral carrying the magnetisation is reached. Once T_c is reached the material will behave paramagnetically or diamagnetically. Another characteristic of ferromagnetic minerals is their capacity to retain a permanent magnetisation in the absence of an applied field, known as hysteresis. A uniformally magnetised ferromagnetic grain which is elongated (non-spherical) mean surface magnetic charge are unevenly distributed at the grain boundary (if magnetised along its length, the grain will have a much lower magnetostatic energy than if magnetised along its width), leading to shape anisotropy. If magnetised along the long axis, only a small area of the grain will be covered by magnetic charges. The difference between magnetisation along the long axis of a grain versus magnetisation perpendicular to the long axis results in an energy barrier which impedes the rotation of j_s through the perpendicular direction (Butler., 1992; Tauxe, 2010). A mineral's microscopic coercive force (*hc*) is the magnetic field required to force j_s over the energy barrier. Similarly, in a bulk sample the total magnetisation is known as bulk magnetisation (J), and can be removed by the bulk coervcive force (H_c). Magnetite and hematite are ferromagnetic minerals. If magnetic moments are aligned with one another within a layer in a substance, but magnetisation in individual layers is

antiparallel the overall effect is for the moments to cancel each other out and the sample to carry a net magnetisation of zero; this known as antiferromagnetic. Substances which are ferrimagnetic have layers of antiparallel magnetic moments which are unequal. The net effect being that magnetisation is in the direction of the larger moment(, Butler.R.F, 1992). Ferromagnetic grains with short relaxation times are referred to as superparamagnetic (SP) and are unreliable recorders of the magnetic field as a result, (for a detailed discussion on relaxation times, please see below).

Paramagnetic substances have atomic magnetic moments which can be aligned, but do not interact with one another. In the absence of an applied magnetic field the moments will be randomly orientated and the sample will have no net magnetisation. Under the influence of an applied magnetic field the atoms will acquire a magnetisation which is parallel to that field, however, when the substance is no longer under the influence of an applied magnetic field, the magnetisation will drop to zero. If a material acquires a magnetisation linearly to an applied magnetic field but in the opposite direction to, then it is behaving diamagnetically. In this situation arises when a substance does not contain atomic magnetic moments due to electron spin. All substances are diamagnetic but the paramagnetic or ferromagentinc signal swamps the effects of diamagnetism. Diamagentic substances are characterised by a negative magnetic susceptibility (Butler.R.F, 1992).

3.1.3. Domains

A domain is a region of a particle that is uniformly magnetised. The size of a single domain grain is so small that the energy required to build domain walls is larger than the decrease in magnetostatic energy achieved by doing so. Larger grains contain multiple domains and are known as multidomain grains (MD). Individual domains are separated by domain walls. The magnetic properties of SD and MD grains are hugely different. However, the majority of palaeomagnetic theory is based on the behaviour of SD grains. Between the large sizes of SD grains and small MD grains a third category of grain exists: pseudo-single domain (PSD). The grain sizes for PSD magnetite range from 1-10µm (Butler.R.F, 1992). They are important carriers of magnetisation in the rock record.

3.1.4. Types of Magnetism Acquired by Rocks

As a rock is formed, it acquires a magnetisation which is, in general, parallel to the Earth's magnetic field at that time and place. In the case of the igneous units studied in this thesis, this occurs as the magnetic moments within the rocks align themselves with the ambi-

ent geomagnetic field as the lavas/intrusives cool after extrusion/emplacement. A mechanism by which magnetic minerials will equilibrate in an applied field, results from forcing the magnetic moments to rotate through the anisotropy energy barriers (see section 3.1.2) as a result of thermal activiation (Butler., 1992; Tauxe, 2010). The simplest effect of thermal activation is the natural decay of remanent magnetisation over time and the acquisition of a new "viscous" magnetisation aligned with the ambient field. At a given temperature some of the grains will have enough energy to overcome the anisotropy energy and j_s will be rotated to the 'easy' axis.In this situation, the temperature required to achieve this on laboratory timescales is known as the (un)blocking temperature. Given enough time, in a zero-field environment, all the moments will become randomised and magnetisation in the sample will decay to zero. The time for a remanent magnetisation to decay to 1/e of its original magnitude is referred to as the relaxation time, (Butler.R.F, 1992; Tauxe, 2010).

Prior to any laboratory treatment the measured intensity and direction of the field in a sample is known as the NRM. The NRM is often constituted of more than one component. The primary NRM is that acquired by a rock as it is first formed.

As well as the primary NRM, the NRM of a rock may also include secondary NRM components which overprint and obscure the primary NRM signature. The causes of acquisition of secondary NRMs are varied and can included chemical changes in the rock, such as hydrothermal alteration or burial metamorphism, which might also affect the ferromagnetic minerals; proximity to areas affected by lightning strikes; reheating of the rocks whether it be through burial or proximity to the emplacement of intrusive units (e.g. dykes, sills and/or plutons/batholiths) and/or subsequent emplacement of further volcanic units; and long-term exposure the magnetic field.

Primary NRMs can be acquired in three main ways:

a) as a thermoremanent magnetization (TRM), which is acquired during cooling of the rocks below their Curie Temperature. This is the form of primary NRM acquired by the majority of igneous rocks.

b) chemical remanent magnetization (CRM), formed by growth of ferromagnetic grains below the Curie Temperature (T_c, in the case of a ferromagnetic minerals, the temperature at which the mineral loses the ability to retain magnetisation), as result of, for exam-

ple, metamorphic or hydrothermal alteration. In addition, if ferromagnetic minerals are exposed to elevated temperatures, they may acquire a thermochemical remanent magentisation (TCRM) as result of chemical alteration. For example, titanomagnetite exposed to elevated temperatures can continue to exsolve in a solid solution series below its Curie Temperature as a consequence of oxidation. A CRM can be acquired one of two ways: it may result from the alteration of minerals already existing in the rock; alternatively it may be acquired when a ferromagnetic mineral is precipitated out of a solution. In both cases, this occurs at temperatures below the mineral's blocking temperature. This is particularly relevant to the rocks of the Onverwacht Group given that they are extensively serpentinised. Therefore, the source of any magnetisation the BGB rocks may record should be considered in light of a potential CRM or TCRM.

c) a detrital remanent magnetization (DRM), resulting from the alignment of detrital ferromagnetic minerals with the ambient field as they form sediments. In an ideal scenario, the TRM is acquired by a rock which is dominated by single domain grains (SD), but this is seldom the case. In reality, truly SD grains are relatively rare within most igneous rocks, which tend to be dominated by PSD and MD grain sizes (Butler., 1992; Tauxe, 2010). Grains larger than 10µm tend to acquire the TRM inefficiently and are prone to acquiring secondary magnetisations. This means that SD and PSD grains are likely to reliably record a primary NRM whilst MD sized grains are more liable to later overprints as a result of subsequent heating and/or burial events. It is known extrusive volcanic rocks which cooled quickly have relatively small grain size distributions in the SD and PSD range, whilst intrusive rocks tend to have a larger percentage of MD sized grains (Butler.R.F, 1992). However, given the age of the samples studied in this work, despite them being predominantly extrusive with the exception of the Neelshoogte Pluton samples, it would be imprudent to assume that a solely primary magnetisation will be recorded, even if the magnetic carriers fall within the SD-PSD grain size range.

Other types of magnetisation that should be considered when interpreting the results of this study include: viscous remanent magnetisation (VRM) which results from exposure to a weak magnetic field over a period of time (applicable to the rocks of the BGB given their age) and a thermoviscous remanent magnetisation (TVRM) also of relevance to the BGB samples as it is acquired during prolongued heating events subsequent to the emplacement of the rocks. Isothermal remanent magnetisation (IRM) may also be of importance when understanding the potential magnetic signal in the studied samples. An IRM is im-

parted during exposure to a strong magnetic field over short periods of time. A natural IRM is acquired as secondary component as a result of lightning strikes (the magnetic field within 1 m of a lightning bolt can be between 10 to 100 mT, Butler, 1992). Given the mountainous nature of the BGB, in an otherwise mostly flat landscape, thunder storms are common. Care was taken when selecting sampling sites to avoid those which were overly exposed or at the top of ridges. In addition, where lightning strikes were of concern, samples from a site were collected over a larger area to minimise the effect of any potential imparted IRM. Nevertheless, when considering the results of the BGB the effect of a lightning induced IRM must be assessed. IRMs can also be imparted during laboratory by placing samples in a strong magnetic field.

3.1.5. Demagnetisation Techniques

Information about the direction of the ancient magnetic field preserved in the rocks of the BGB is obtained by performing stepwise demagnetisation experiments. As discussed previously, given the geological history of the rocks it is likely they preserve multiple components of magnetisation. In order to isolate the characteristic NRM it is necessary to selectively remove the secondary NRM overprints within the sample by performing partial demagnetisation experiments.

Thermal demagnetisation (TH) techniques require a sample to be heated, in a step-wise manner, to a temperature below the Curie temperature of the minerals within the sample (which is usually established prior to the TH experiment with the aid of rock magnetic characterisation see section 3.2) and then cooling the sample back down to room temperature in the absence of an applied magnetic field. This results in the moments within grains which have an unblocking temperature below the heating temperature to become randomised and removes a partial thermoremenant magnetisation (Butler.R.F, 1992), thus exploiting the relationship between relaxation time and temperature (Tauxe, 2010). Grains carrying VRM components will be those with short relaxation times and therefore low unblocking temperatures. This VRM can therefore be selectively removed by heating the sample above their unblocking temperature. The grains which hold a more stable magnetisation (because they have longer relaxation times and therefore a higher blocking temperature) will require heating to higher temperature in order to remove the magnetisation. Schematically, this principle is explained by the figure below, taken from Butler, (1992).

Exposing a sample to an alternating magnetic field (AF), with a sinusoid waveform (oscillatory), will also result in removal of the magnetisation held by the sample. During the experiment, the sample is usually held within a holder which is free to tumble within the axis of the coil generating the field. The net effect is that all axes of the sample will be fully demagnetised during the experiment. A magnetic field is applied to the sample and with every half cycle of the sinusoid waveform the applied field is decreased by a small amount (usually 1 mT). During the ascending part of the sinusoid waveform grains with a coercivity equal to (or lower) than the applied field will be forced to point in the direction of the field and essentially become 'stuck' in that orientation. The field then passes through zero and onto a maximum in the opposite direction where the magnitude of the field is decreased by say, 1 mT, pulling all grains with coercivites less than or equal to the new applied field to point in the opposite direction. In the next upward cycle of the waveform, this is repeated, again decreasing the applied field after each half cycle. This results in the magnetic moments of grains with very similar coercivites being forced to point away from one another and therefore cancelling each other out. Only the grains with coercivities higher than the applied field will retain an NRM (Butler.R.F, 1992; Tauxe, 2010). This means AF demagnetisation is particularly suited to removal of secondary NRMs carried by MD grains, as these tend to have low coercivities when compared to SD or PSD grains. As will be discussed later, AF was chosen (often in conjunction with thermal demagnetisations) for the samples of the BGB. Often, it resulted in clearer Zijderveld plots than purely thermal experiments, likely owing to the predominance of MD grains in the samples of the BGB.

3.2. Methodology

This section briefly covers the techniques and methodologies used throughout this thesis. Details of individual number of experiments performed, relevant to each formation studied, are given in the results chapters.

3.2.1. Sampling

The bulk of samples from the BGB were collected during a field campaign in South Africa which took place in May/June 2011. This work was carried out by the author and Andrew Biggin primarily. During the early stages of the field work, guidance and assistance were provided by Marteen de Wit, without whose insight and extensive knowledge of the BGB the field work would not have been as successful. The sampling rationale for individual

Figure 3.2 (a) Surface sample cores being drilled by the author; (b) An example of a sampling site, this particular site is from the Hooggenoeg Formation; (c) Sun compass was used for orientation of samples, as well as a standard magnetic compass. In the photograph directions from the two are being compared; (d) The author drilling drill core samples from the BARB cores; (e) An example site from the BARB drill cores. Site seen here belongs to the Komati Formation.; (f) Rough sketch indicating subdivision of core sample into specimens and also showing how sample names were allocated.

sites is given in the results chapters. Areas to be targeted for sampling were determined prior to the field work; individual sampling sites were selected once in the field depending on factors such as accessibility, proximity to water, potential for the samples to have been lightning struck, amongst others. In particular, opportunities to carry out field stability tests which would assist in constraining the age of any primary NRM recorded in the rocks were sought out.

This thesis has benefited from a collaboration with the ICDP (International Continental Scientific Drilling Program) sponsored Barberton Greenstone Belt Drilling Project (BARB), see the BARB project website (http://www.peeringintobarberton.com/index.html) and Coetzee, (2014) for further details. The aims of the drilling project were to gain a better understanding of the process at the Earth's surface during the Archean. Complete sections of stratigraphy are not preserved in the outrcrops of the BGB. Drilling of the BGB will allow the study of stratigraphically continuous sections where contacts between lava flows and unweathered volcanoclastics and sediments are exposed. In terms of palaeomagnetic study the samples from the drill cores are valuable due to them being unweathered and protected from lighting induced remagnetisations. As the core was logged prior to palaeomagnetic sampling it allowed for targeted selection of sites on the basis of their potential for palaeomagnetic stability field test. For further details on the drilling programme and cores sampled please turn to Chapter 4. A further sampling trip was carried out by the author in July 2012 to collect samples from the BARB cores.

Samples collected during the field work carried out in 2011 will be referred to as surface samples; whilst samples obtained from the BARB cores will be generally known as the drill core samples, to easily distinguish the two groups.

Samples were drilled using a portable, petrol driven STIHL BT 45 drill modified to ensure a constant water supply, to avoid heating of the samples and possible remagnetisation. Locations were recorded using a Global Positioning System (GPS). Samples were oriented using a magnetic and sun compass. Y-east of true North (YETN) and the dip of the core were recorded. An orientation mark was made along the azimuth (representing the Z axis) of each individual sample with a brass marker before removing them from the country rock with a non-magnetic tool.

During collection of surface samples, each sampling site was sketched, with individual sampling positions marked on the sketch. In addition, photographs were taken and the exact

position of the site was determined using a Global Positioning System (GPS). Photographs in Fig. 3.2 (a to c) show the author during the surface sampling campaign in the BGB. In the case of the BARB samples, the exact depth, along the core, of the sampling site, as well as the exact depth of each individual sample was recorded. Sketches of the sampling sites were made and these were further documented using photographs. Details of the drilling and orientation of both the surface and drill core samples, (which are accompanied by sketches) are given within individual results chapters. Figure 3.2 (d) shows the set-up for the drilling of the ICDP cores.

Sampling sites were named after the formation from which they were taken and to differentiate them from samples collected in previous studies (e.g., Biggin et al., 2011) the initial of the author was included. Sites from the Komati Formation, for example, were named LKM. Samples were named using a standard palaeomagnetic scheme (see Butler., 1992 for further details). Individual core samples were subdivided into ~2.5 cm long specimens. The top and bottom ~10mm of each core were also removed. Figure 3.2 (e and f) illustrate an example of how both the surface and mini-core samples were named. The bottom section was utilised for rock magnetic characterisation experiments. Individual 2.5cm specimens were utilised in demagnetisation experiments. In the majority of the cases the drill core samples were not sufficiently long to be subdivided into specimens. A small thickness of the sample was removed from the base of the specimen to carry out rock magnetic characterisation. The individual 2.5cm specimens were utilised in demagnetisation experiments.

3.2.2. Rock Magnetic Characterisation

A suite of rock magnetic investigations have been used to determine the properties of the magnetic particles in the samples of the BGB samples. Here a brief overview of the overall methodology is given. To supplement the findings of the rock magnetic work, microscopy investigations were also carried out.

3.2.2.1. Rock Magnetic Work

Hysteresis, back field coercivity, isothermal remanent magnetisation and thermomagnetic experiments were carried out on a Magnetic Measurements Variable Field Translational Balance (VFTB). A combination of crushed and mini core samples, ranging in weight from 120-250mg, was used. Whole samples were more commonly used during early experiments as they are less susceptible to oxidation and alteration than crushed samples. How-

ever, due to the breaking of a number of expensive mini-drill bits the majority of the samples used were crushed. The benefit of using crushed samples is that the thermal lag between the centre of the sample compared to the exterior is reduced whilst at the same time reducing the effects of inhomogeneities within samples. Samples were secured within the sample holder by means of quartz wool which has the added advantage of limiting vibration of the sample.

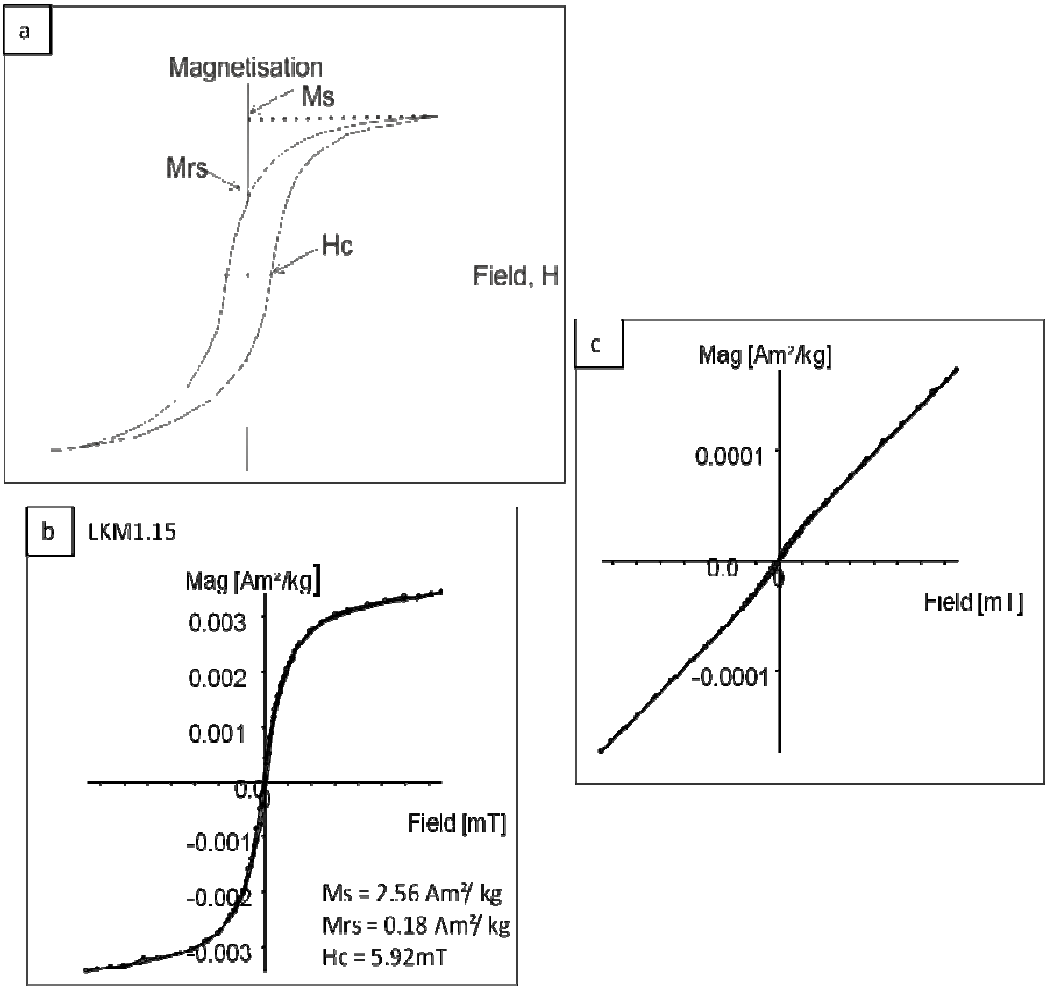

Figure 3.3. Example Hysteresis Plots. (a) Modified from Butler, 1992, shows a sample dominated by SD grains. Rock magnetic parameters which can be obtained from the hysteresis loop are also shown. (b) A Komati Formation sample which is dominated by MD behaving grains. (c) A Komati Formation sample which has a strong paramagnetic contribution and has to be corrected prior to rock magnetic parameters being calculated.

Hysteresis loops, as shown in Fig. 3.3, were produced by measuring the magnetisation of a sample while the applied field is incrementally cycled between high values (~1000mT) in the plus-minus direction. Analysis of hysteresis loop data, using the RockMag Analyzer Programme (Leonhardt, 2006), gives information on three parameters: Mrs, Ms, and Hc. Together with Hcr, the ratios of these can then be used to produce a Day Plot (Day et al., 1977) which allows characterisation of the domain states within a sample. In a hysteresis

loop magnetisation of the samples is plotted vs. an applied field. In an applied field a ferromagnetic solid will acquire a magnetisation resulting from the interaction of adjacent magnetic moments. If the a sufficiently strong magnetic field is applied during the experiment the sample will reach it's saturation magnetisation, M_s. Once the applied field is removed, the magnetisation that is retained by the sample is given by Mrs, the saturation remanence. Coercivity, Hc, measures how easily a sample can acquire a magnetisation applied in a new direction. Grains with large coercive forces, SD grains, result in wide hysteresis loops (an example of which is shown in Fig. 3.3. (a), whilst MD grains, which have lower coercive forces yield thin hysteresis loops, as can be seen in Fig. 3.3 (b). If the sample is dominated by the paramagnetic or diamagnetic contribution, then the hysteresis plot is close to linear and the magnetisation is reduced to zero when the applied field is removed. This behaviour is illustrated in Fig 3.3 (c). Paramagnetism and diamagnetism produce non-zero high field susceptibility values χhf, which can be removed (by extending χhf back to a Field = 0). In some cases, the paramagnetic contribution dominates the sample and it is unlikely the ferromagnetic contribution can be isolated , meaning it is not possible obtain hysteresis parameters.

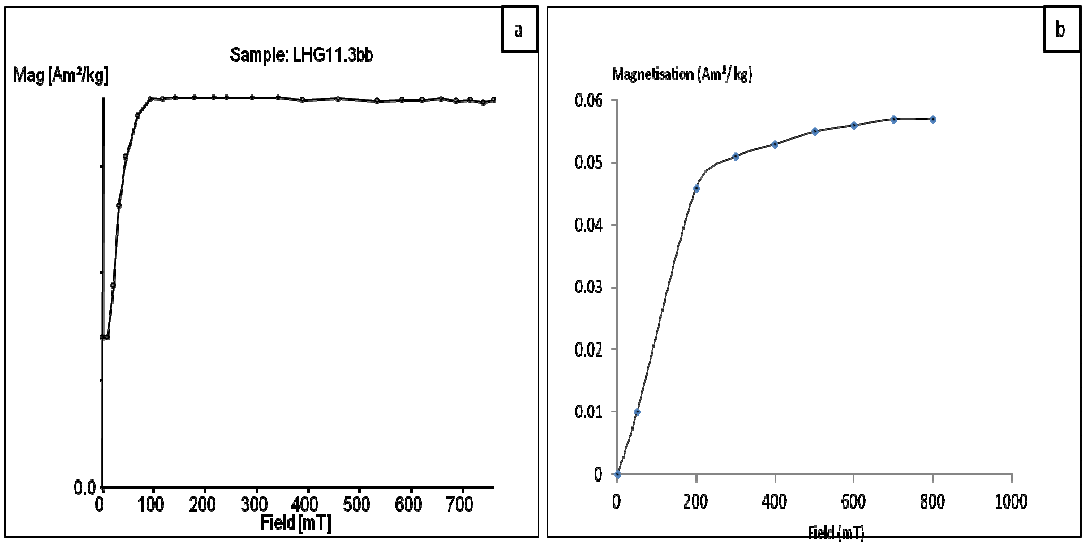

Figure 3.4. Example Isothermal remanent magnetisation curves (a) shows a material which fully saturates in an applied field, e.g. Magnetite saturates between 100-300mT. (b) an example of a material which does not fully saturate in an applied field, e.g. Haematite.

From Isothermal remanent magnetisation curves, IRM, the coercivity of remanence, Hcr, was obtained. During the experiment a stepwise field wa applied to the sample and out of field measurements taken. Hcr is a measure of the field required to remove the remanence once the sample has become fully saturated and can be used to establish the coercivity of particular minerals., e.g. Magnetite (see Fig 3.4a), saturates between 100-300mT whilst Haematite may not saturate during the experiment, as shown in Figure 3.4b . Once

all rock magnetic parameters were obtained, they were plotted on the Day plot to obtain information about the grain size of the magnetic particles. The ratio of the saturation of remanance and magnetisation remenance (Mrs/Ms) is plotted vs. the ratio of coercivity of remanence and coercivity (Hcr/Hc). The lower the Mrs/Ms ratio, and the greater the Hcr/Hc ratio, the greater the grain size.

Using the VFTB, which is shown in Fig. 3.5a, strong field thermomagnetic experiments were carried out to establish the Curie Temperature (T_c). The sample were heated incrementally up to 700°C and the magnetisation recorded while a field in excess of 300mT was applied. The sample was then cooled back down to room temperature remaining infield. Curie Temperatures are manifested as sharp changes in the slope of the produced thermomagnetic curve. A single T_c is obtained when the magnetic carriers within the sample are homogeneous. An example of this behaviour is given in Fig 3.5b. Multiple T_c result from samples which contain more than one ferromagnetic mineral assemblage. Pure magnetite has a T_c of 580°C. Impurities within the magnetite structure, such as inclusion of titanium (titanomagnetite) or the deficiency of iron (producing maghaemite) can significantly change the observed T_c. Thermochemical alteration during the thermomagnetic experiments results in the irreversible thermomagnetic plots (Fig 3.5c). In this study, alteration during the experiment has not been considered significant when the difference between the magnetisation measured on the heating and the cooling curve has been less than 10% (at the point where the curves are furthest apart). If a higher final magnetisation is observed, this implies a previously non-magnetic phase has become magnetic upon heating and results in the heating curve overlying the cooling curve. A lower final magnetisation results in cooling curve falling below the heating curve. Alteration (including oxidation) of magnetic minerals during the heating phase of the experiment implies an irreversible change in their magnetic properties. Heating of the sample may also lead to the formation of new magnetic phases. Alteration is often expressed by the presence of inversion humps, e.g., an inversion hump along the heating curve at ca. 350°C might indicate the presence of maghaemite(Davies, 2009). For an example see Fig. 3.5c. If a sample is dominated by minerals with high magnetic saturation these will dictate the signal of the thermomagnetic experiments. If magnetic minerals with low magnetic saturation are present within the sample, they may not be observed in the results, even if they carry most of the remanence. Stepwise heating experiments (also conducted on the VFTB, where a sample is heated, step-wise, at e.g. 50°C intervals, rather than in a single heating phase to 700°C) can help discern at what temperature alteration occurs. The use of IRM curves can

also assist in differentiating these behaviours. Curie Temperatures were estimated by means of the Rock Mag Analyzer software (Leonhardt, 2006) using the Moskowitz extrapolation method (1981) and second derivative approach (Leonhardt, 2006). Generally the second derivative approach was favoured as T_c were more accurately determined, especially in noisy samples.

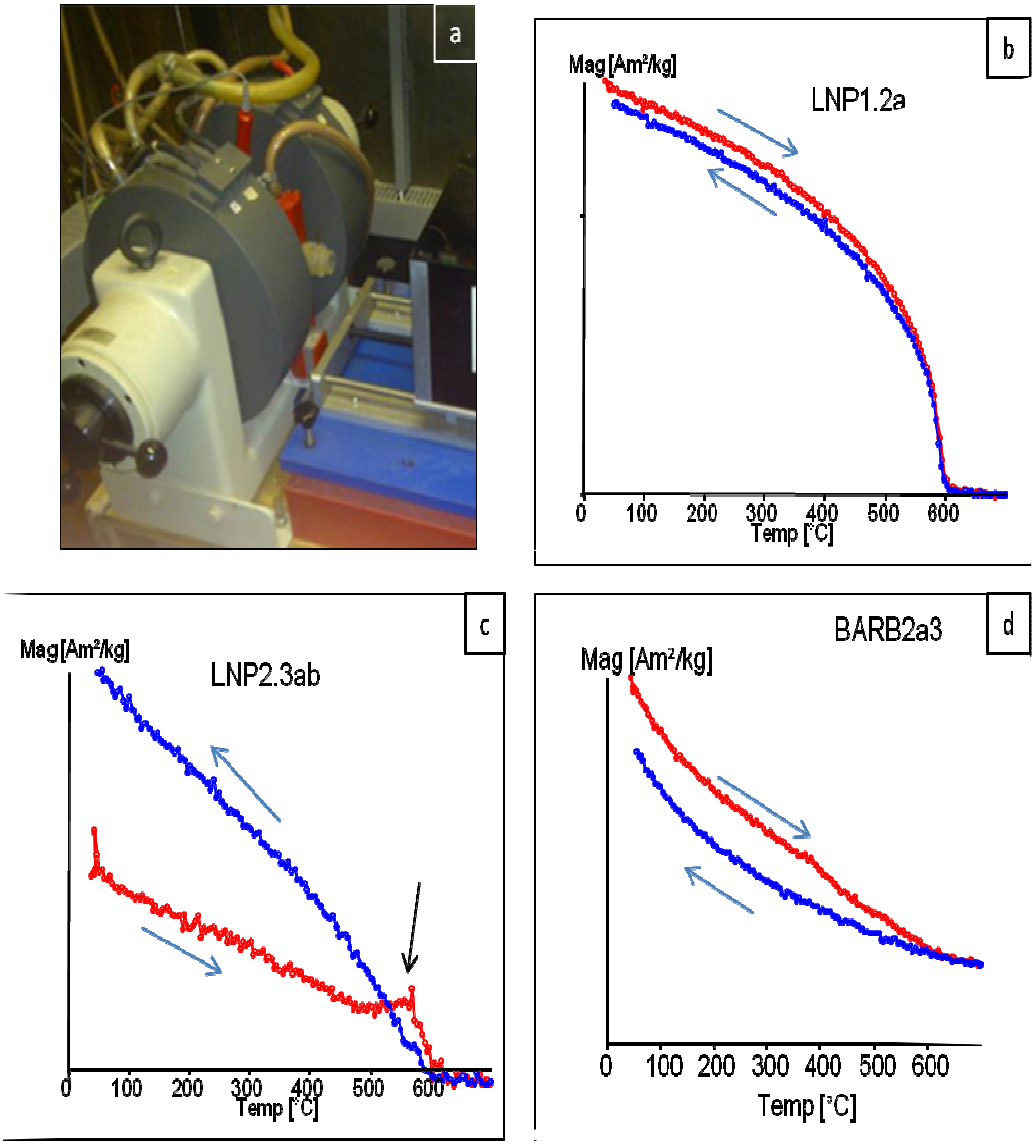

Figure 3.5. Examples of thermomagnetic experiments. (a) The MMVFTB equipment at Liverpool University. (b) An example of a fully reversible thermomagnetic curve. Curie Temperature is clearly represented which a clear change in slope at ca. 600°C (see the results chapters for explanations as to why elevated Tc were observed). (c) Non reversible thermomagnetic plot showing lower final magnetisation, note also the inversion hump highlighted by the black arrow; (d) higher final magnetisation, curves are reversible.

3.2.2.2. *Susceptibility Measurements*

To establish how prone to acquiring a magnetisation the rocks of the BGB are, room temperature susceptibility measurements (χ) were carried out on a Bartington Susceptibility meter. Samples were weighed and their susceptibility was measured at both low (465Hz) and high (4.7 KHz) frequencies. During the later stages of this research project an Agico Kappa Bridge Susceptibility meter (MFK1) was acquired by the Geomagnetism Laboratory at Liverpool allowing both room temperature and temperature dependant susceptibility measurements to be carried out. Using the Kappa Bridge magnetic bulk susceptibility as function of low temperatures (-196°C to 0°C) and of high temperatures (20°C to 700°C) was measured. Here samples of a weight of approximately ~330mg were crushed to a fine powder and inserted into a tube sample holder. The thermocouple is also inserted into the sample holder, ensuring there is sufficient sample to wrap around the base of the thermocouple. The high temperature experiment was carried out in argon, in order to reduce the potential for oxidation of magnetic minerals, thus minimising the effects of thermochemical alteration. The sample is then water cooled back down to room temperature. During the cooling experiment, the sample is cooled down to -196°C by adding liquid nitrogen and then continuously heated by the furnace in the Kappa Bridge up to 0° C.

Figure 3.6. The Agico Kappa Bridge at the Geomagnetism Laboratory , University of Liverpool.

Measuring bulk susceptibility as a function of temperature allows further characterisation of the magnetic carriers and was conducted in order to compliment the results obtained from the thermomagnetic experiments on the VFTB. From the low temperature experiment, the Verwey Transition (T_v) can be obtained (Verwey, 1939), which can indicate the presence of magnetite in a sample. At below 120K the lattice structure of magnetite is disrupted and changes from being cubic to slightly monoclinic as a result of reordering of Fe^{2+} and Fe^{3+} ions (Dunlop and Özdemir, 1997). The reordering in lattice structure leads to an abrupt change at T_v when measured on the Kappa Bridge (an example of which is

shown in Fig. 3.6), given that susceptibly measurements are dependent on crystalline anisotropy. However, the sharp peak is only observed is a sample contains pure magnetite, which is rare in nature. A broad peak, or a peak at lower T_v is not uncommon and indicates the remanance carrier contains impurities of titanium or may have been oxidised during the experiment. High temperature experiments are comparable to the VFTB thermomagnetic curves experiments but as the experiment is measured in much weaker fields than those applied during the VFTB experiments, it is less likely that paramagnetic contributions will swamp the ferromagnetic signal. From the high temperature experiment it is possible to observe T_c as a sharp drop in susceptibility (generally preceded by a peak).

Measuring frequency dependant susceptibility (χ_{fd}) can be used to establish grain size determination of the presence of superparamagnetic (SP) grains within a sample. Very narrow hysteresis loops can indicate the presence of SP grain sized particles (Dunlop and Özdemir, 1997; Tauxe, 1996). Very fine grained ferromagnetic particles show strong frequency dependence. Changing the frequency to which the sample is exposed to is equivalent to changing the amount of time available to the magnetic grains within the sample to react to a change in the applied field strength. Magnetic susceptibility as a function of frequency, from 976Hz to 3904Hz and onto 15616Hz, was measured at room temperature from individual, whole, specimens. The superparamagnetic constituent in a sample is given by:

$$Superparamagnetic\ constituent = \frac{(\chi_{lf} - \chi_{hf})}{\chi_{lf}}$$

Where χ_{lf} is the measured low frequency susceptibly and χ_{hf} is high frequency susceptibility.

3.2.2.3. Microscopy

Rock magnetic characterisation experiments were supplemented with microscopy studies to: a) better constrain the magnetic carriers, b) better understand the metamorphic alteration in the rocks of the BGB and its effect on the potential magnetic carriers. A selection of samples from each of the four BGB formations were studied using transmitted light microscopy and on a Philips XL30 tungsten filament Scanning Electron Microscope (SEM) fitted with for Electron Back Scatter Diffraction (EBSD) and Energy Dispersive Spectroscopy (EDS/EDX) technology. Thin sections were prepared by Paul Hands, at Birmingham

University. Details of which samples were studied and the selection rational are given in the individual Formation results chapters. Samples were studied using transmitted light microscopy prior to any SEM investigations, as thin sections require a carbon coat during SEM analysis to minimise charging effects (Prior et al., 1996), which obscures mineralogy observations in transmitted light.

Transmitted light microscopy was carried out on Meiji Technology Microscopes fitted with a Nikon camera, to establish the extent to which the samples had been altered during serpentinization and reheating. Identification of iron oxides was crucial and understanding their relationship to the surrounding mineralogy important to ascertain whether they are associated with the primary mineralogy of the sample. Given the complex history of the rocks of the BGB, the mineralogy of the samples is often very complex and it was difficult to establish a clear cooling history. Nonetheless amongst others, observation of freshness of minerals, as well as alteration of crystal rims and cores and textural relationships (e.g. phenocrysts in a fine grained matrix indicates a two stage cooling history; embayment of minerals indicates addition of mew magmatic material during emplacement of the rocks) were studied in order to better understand the mineralogy. All thin sections were studied under plain polarised light (PPL), cross polars (XPL) and reflected light (which is ideal for the study of opaque minerals, such as iron oxides).

Detailed discussion of SEM and BSE image acquisition is given in Prior et al., (1999 and 2002) and references therein. In BSE imaging the variation seen in the intensity of grey-scale colours indicate rough differences in mineral chemistry. Heavy elements (high atomic numbers) such as iron (Fe) appear brighter than atoms which are lighter, such as silicon (Si). This results from a shallower interaction of the electron beam with the targeted mineral. Therefore, this means iron oxides tend to be easily identifiable during the SEM investigations. EDX spectra can then be used to identify the main elements within the targeted mineral and so ascertain its exact mineral composition. In addition element maps can be created. The beam scans a given area of the thin section highlighting the presence of preselected atoms. This is useful to quickly identify areas in which there are large concentrations of Fe, which may indicate the presence of iron oxides (keeping in mind that minerals such as pyroxene, commonly found in volcanic rocks, can also be Fe rich).

3.2.3. Demagnetisation Work

Demagnetisation work was carried out at the Geomagnetism Laboratory at Liverpool University and at the Fort Hoofddijk, Paleomagnetism Laboratory at Utrecht University (The Netherlands). Small scale pilot studies were carried out at Liverpool, whilst the bulk of the samples were demagnetised at Utrecht University over a series of four visits.

At Geomagnetism Laboratory at Liverpool the batches of no more than 20 samples were demagnetised using a Magnetic Measurements thermal demagnetiser and a Magnetic Measurements supercooled thermal demagnetiser. The set-up of the equipment is seen in Fig. 3.7a. Subsequently measured on an Agico JR6 or JR6-A magnetometer (instrument sensitivity 2 $\times 10^{-6}$ A/m), shown in Fig 3.7b. Results are displayed using the REMA6W – Windows software. All equipment at Liverpool is hosted in Helmholtz cages. At Utrecht, batches of up to 40 samples were demagnetised using an ASC thermal demagnetiser and measured on a 2G Enterprises DC-SQUID magnetometer, as seen in Fig 3.7d, (noise level 3 $\times 10^{-12}$ Am^2 ,although the sample holder, whose magnetisation we attempted to correct , potentially increases the noise level by up to an order of magnitude. Thermal demagnetisation was performed stepwise (using increments of 10°C-100°C) up to 580°C.

In addition, to thermal (TH)demagnetisations, a series of alternating field (AF) demagnetisations were also carried out. The majority of these were performed at the Utrecht Laboratory using an AF demagnetiser (maximum 18 standard-sized samples, 25mm, or 36 mini cores, 12mm, demagnetised at one time with a peak alternating filed of 300mT). The photograph in Fig. 3.7e, shows the experimental set-up and Fig. 3.7h shows the sample holder. In addition the in-house built unique “robot”: a 2G magnetometer with an inline AF demagnetiser attached to an automatic sample handler which measures batches of up to 96 samples in three orientations was used for the majority of the AF demagnetisations (see Fig. 3.7f and Fig. 3.7g). In the work of Biggin et al., (2011) found that combining TH and AF demagnetisations gave relatively clean Zijderveld plots from samples of the Onverwacht Group. As a result, this methodology was also chosen for a selection of samples in this study. Samples were stepwise TH demagnetised up to 440°C (using increments of 40° C-100°C) and then AF demagnetisation (with increments of 5-10mT up to 110mT) was used to remove the remaining NRM. The additional advantage of this technique is that secondary magnetisation is fully removed by the thermal steps, whilst the robot allows for rapid and precise characterisation of the ChRM.

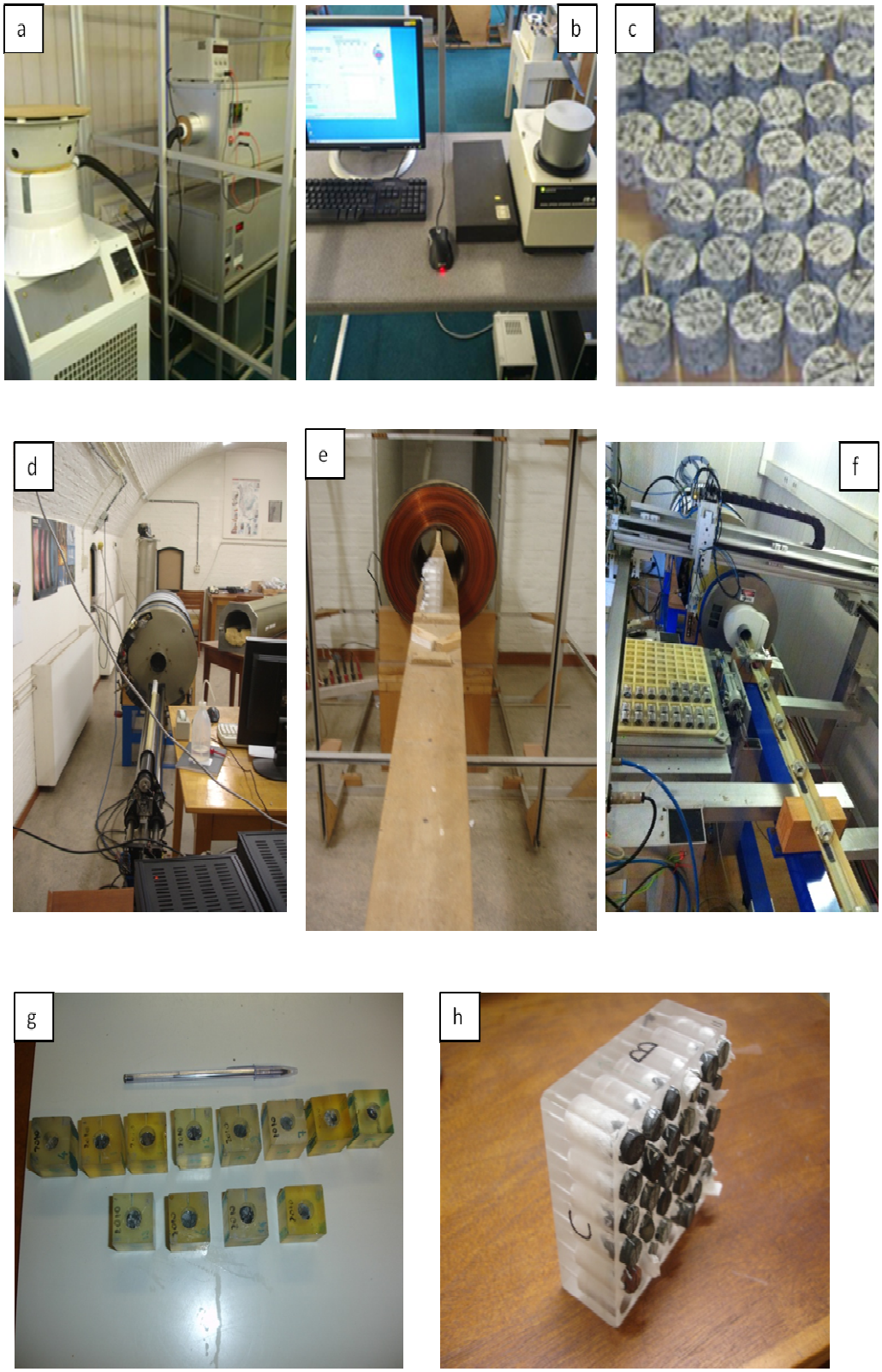

Figure 3.7. Photographs taken during the demagnetisation experiments. (a) MM Super supercooled thermal demagnetiser (top), 80 sample thermal demagnetiser (bottom) inside a Helmholtz cage, at the Geomagnetism Laboratory, Liverpool; (b) JR6-A at Liverpool; (c) standard cores specimens used for demagnetisations, from the Nelshoogte Pluton; (d) Enterprises DC-SQUID magnetometer, at the Paleomagnetism Laboratory, Utrecht; (e) ASC alternating field demagnetiser at Utrecht, sample holder containing 30 samples is in place; (f) The "robot": a 2G magnetometer with an inline AF demagnetiser attached to an automatic sample handler, at Utrecht; (g & h) Drill cores (mini cores) from the BARB Cores prepared for AF demagnetisation in The Robot and the ASC at Utrecht.

NRM directions were analysed with Zijderveld diagrams (Zijderveld, 1967). The analysis of the palaeomagnetic directions was conducted using principal component analysis and standard statistical analysis (Fisher, 1953; Kirschvink, 1980). Directions with a maximum angular deviation (MAD) lower than 15° were used in most cores, except for a few very weak samples.

3.3. Field Test of Palaeomagnetic Stability

As was introduce in the aims and motivations of this thesis (see 1.2), one of the main goals of the work presented here is to reliably constrain the ages of the magnetisations recorded by the rocks of the Onverwacht Group. This is especially significant as previous studies have, to a greater or lesser extent, had difficulty in achieving this.

Whilst laboratory demagnetisation techniques will allow for the isolation of palaeomagnetic directions, they are limited in their ability to shed light on the relative age of the magnetisation identified. Establishing the timing of acquisition of a ChRM is possible through the application of field test of palaeomagnetic stability, which relay on a careful sampling strategy, and geometric field relationships (Tauxe, 2010) to help determine the age of the magnetisation isolated.

There are a number of field test of palaeomagnetic stability which can be performed (fold tests, conglomerate tests, baked contact test, synfolding test and reversal test), but given the nature of the Formations studied here, only the fold test and baked contact test are relevant to this study; these are discussed in more detail below. For more information on the remaining test, the reader is directed to the texts recommended at the start of this chapter.

3.3.1. Baked Contact Test

As an igneous body intrudes into country rock, the contact zone within the host rock is heated above its Curie temperature, thus imparting a TRM (thermoremanent magnetisation) to the country rock immediately adjacent to the intrusion. The baked contact should now have the same remanence direction as the intrusive rock, which is likely to be in an entirely different direction to that of the country rock, especially if the units are significantly different in age. The temperature reached within the host rock decreases away from the intrusive rock and

so the remagnetisation is not complete. This means that the direction of magnetisation will gradually change for that of the intrusion to that of the country rock the further away from the intrusion. Uniform ChRM directions between the intrusive rocks, baked zone and unbaked host rocks can help establish the relative age of the magnetisations (provided the age of the intrusive unit is known).

The abundance of dykes within the Komati Formation in particular mean that sampling of the unit was designed to allow for the performance of a number of baked contact tests. Both the Hooggenoeg Formation and Noisy Complex are intruded by dykes, but none where sampled as part of this work.

3.3.2. Fold Test

The fold test, which can also be known as the bedding tilt test or tilt test, allows for the age of a set of directions to be determined relative to the age of a fold. This is achieved by deliberate sampling of units within the same formation but on the opposing sides of a fold (and thus with different strike and dip attitudes). If an isolated ChRM is acquired prior to folding, the ChRM directions observed from opposing limbs of the fold will be dispersed when plotted in stratigraphic coordinates. If however, the directions appear more tightly grouped when they have been corrected for the tilt of the fold (so as to restore the directions back to horizontal), then the magnetisation is likely to pre-date the folding event. Given that the Onverwacht Fold (OF) affects the Onverwacht units studied here, it presents the prefect opportunity to use this method to more robustly ascertain the relative age of the magnetisation isolated from the rocks studied in this thesis.

Note that, in order to perform the tilt corrections as part of this work, given that the OF is not only tilted but also plunges steeply (on average 92°), it necessary to take this into account when restoring the data sets back to horizontal. Site mean directions and their respective poles, (in geographic coordinates), were first treated to remove the 92° plunge, (as were the associated bedding data), before correcting for the tilting of the fold. Structural orientation of all sampling sites is given within the individual results chapters (4 to 7), within this thesis.

4 Palaeomagnetism of the Komati Formation

4.1. Introduction

As discussed elsewhere in this thesis (see Chapter 2), the oldest formations of the Onverwacht group are too severely affected by deformation processes and metamorphism to be of palaeomagnetic value. As a result, the Komati Formation is the oldest formation in the Onverwacht Group suitable for palaeomagnetic study.

Palaeomagnetic work has been carried out on the rocks of the Komati Formation by Hale & Dunlop, (1984), and Yoshihara and Hamano (2004), and also on the similarly aged 3452Ma ± 16 (Pidgeon, 1978) Duffer Formation of the Pilbara Craton, Western Australia by (McElhinny and Senanayake, 1980).The findings of these works point towards there being a stable geomagnetic field present at *ca* 3.5Ga. However, despite the encouraging results of these previous works, it is vital to address the fact that the rocks of the Komati Formation may not reliably record a primary NRM, as suggested by the work of Usui et al., (2009). If the formation of the magnetite in the Komati Formation volcanic is, in fact, associated to the 3.23Ga (see chapter 2), thermal and tectonic events that affected the BGB, as opposed to being formed during the eruption and emplacement of the rocks, it is possible the komatiites do not retain a 3.5Ga remenance. Palaeomagnetic field tests can be performed to assess the reliability of near-primary components, as shown by the positive conglomerate test of Usui et al., (2009), and further strengthened by the results of Biggin et al., (2011).

The komatiites of the Komati Formation are of broader geological interest as they can shed light on early Earth geodynamic models (Pollack, 1996; Dann, 2000). The evolution of the mantle during the Achaean is poorly constrained (Grove and Parman, 2004); however, it is generally accepted that melting of the mantle was widespread during the Archaean, resulting in thicker oceanic crust and significantly hotter magmas than those erupted presently (Arndt, 2003; Nisbet, 1982; Nisbet et al., 1993). Due to their unique chemical signature (MgO contents above 18%) the study of komatiites can give information about the mantle, as they provide evidence for the temperature and depth at which parental melt was generated (Grove and Parman, 2004). The mechanisms for the formation of Archean crust and how plate tectonics operated are hotly debated (Abbott et al., 2013; Bédard, 2006; de Wit et al., 2011; Furnes et al., 2013). A number of mechanisms for the tectonic setting in which komatiites can be produced have been proposed: 1) A mantle

plume setting(Arndt et al., 1998; Puchtel et al., 2013); 2) Mid-Ocean Ridge setting (de Wit, 1998; Parman et al., 2004) 3) Subduction setting (Furnes et al., 2013; Furnes et al., 2011; Parman et al., 2001; Parman et al., 2004). Which setting is plausible is highly dependent on the most controversial issues surrounding komatiites: are they generated by a hydrous mantle source at temperature moderately higher than at present (Grove, 1994; Parman et al., 1997; Parman et al., 2001) or are komatiites mostly formed in an anhydrous mantle, significantly hotter than at present (Arndt et al., 1998; Berry et al., 2008; Puchtel et al., 2013)? The lack of Komatiites in the more recent geological record, but particularly their abrupt decline into the Phanerozoic, has been linked to changes in the conditions of the mantle. An obvious interpretation is that the chemical change in the volcanic rocks being erupted at the surface reflects cooling of the mantle (Grove and Parman, 2004).

Whilst palaeomagnetism cannot directly contribute to the issues in this debate, there is potential for addressing the issues associated with scarcity and viability of palaeomagnetic data for the Archaean Aeon. Robust paleomagnetic results have implications for tectonic processes (Biggin et al., 2011). Confirmation of the presence of a viable and reversing field during the Palaeoarchean would place a strong constraint on processes occurring in the outer core during this time with implications for planetary evolution. Rates of apparent polar wander could also be constrained by the directional findings, shedding some light on mantle convection processes at the time and perhaps adding to the debate and big questions surrounding komatiite emplacement.

In order to constrain the reliability of previous paleomagnetic results by performing improved field stability tests, it was necessary to acquire a new data set for the Komati Formation. New sampling sites are shown along sites of previous studies in Figure 4.1. In addition, this would address the issues associated with scarcity of data for the Archean Eon. Surface samples were collected from six sites, west of the type section described by Viljoen and Viljoen, 1969. In addition, this work has benefited from access to oriented samples from the International Continental Drilling Programme (ICDP) Barberton Greenstone Belt Scientific Drilling Project, removing issues associated with lighting strikes and weathering of surface samples.

New paleomagnetic data for the Komati Formation, presented in this chapter, were noisy at both the specimen and site level, particularly for samples from the deep cores because of less precise orientation, associated with both the drilling and the sub-sampling of the

core, and drilling induced overprints. Despite this, two ancient components have been identified. One of these is dual polarity and may be associated with widespread intrusive activity at 3.2 Gyr. The other appears to be older and has a direction in agreement with previous results from the Komati Formation. When the improved pole is taken in conjunction with palaeomagnetic results from across the Onverwacht Group (Biggin et al., 2011), the validity of a near-primary age is supported.

This chapter begins with a summary of the geology of the Komati Formation and is followed by palaeomagnetic results previously published by Hale and Dunlop (1984), Hale (1987) and finally, Yoshihara and Hamano (2004). The bulk of the chapter describes the experimental methodology and results obtained from the current study. Description of directional results obtained from thermal demagnetisations is covered. This is followed by the description of magnetic carriers as established by rock magnetic characterisation and light and scanning electron microscopy. The findings are compared to the previous studies and discussed. Finally, conclusions are drawn.

4.2. Geology of the Komati Formation

The Komati Formation is the third youngest in the Onverwacht, see Chapter 2. The age range for the rocks of the Komatii Formation spans 3482-3472 Ma (Armstrong et al., 1990; Kamo and Davis, 1994; López-Martínez et al., 1992). The studies of Armstrong et al., (1990) and Kamo and Davis,(1994) give ages, established from zircons by conventional U-Pb isotope dilution and Sensitive High-Resolution Ion Microprobe (U-Pb), from a meta-gabbro and quartz-feldspar porphyry dyke which cross-cuts the Komati Formation, respectively. This is the dyke sampled as part of this work, site LKM2 (see Figure 4.4).It follows that the dyke would have been intruded into the lava flows of the Komati formation after their emplacement and, therefore, the age range given is a minimum age for the emplacement of the Komati Formation. A volcaniclastic bed at the base of the Formation has also been U-Pb zircon dated and gives the best lower bound constraint for the age of the Komati Formation at 3481 ± 2 Ma (Furnes et al., 2013). The underlying Theespruit Formation is dated at 3544 ± 3 – 3547 ± 3, (Kröner et al., 1996, using the vapour digestion technique). The Formation is composed of a succession of komatiite, komatiitic basalts and basaltic units thought to have been erupted rapidly due to the absence of sedimentary layers or erosional surfaces (Dann, 2000; Robin-Popieul et al., 2012; Viljoen and Viljoen, 1969c), in a submarine environment at approximately 2000m depth (Furnes et al., 2011). The komatiites which are black, containing predominantly olivine, have been almost en-

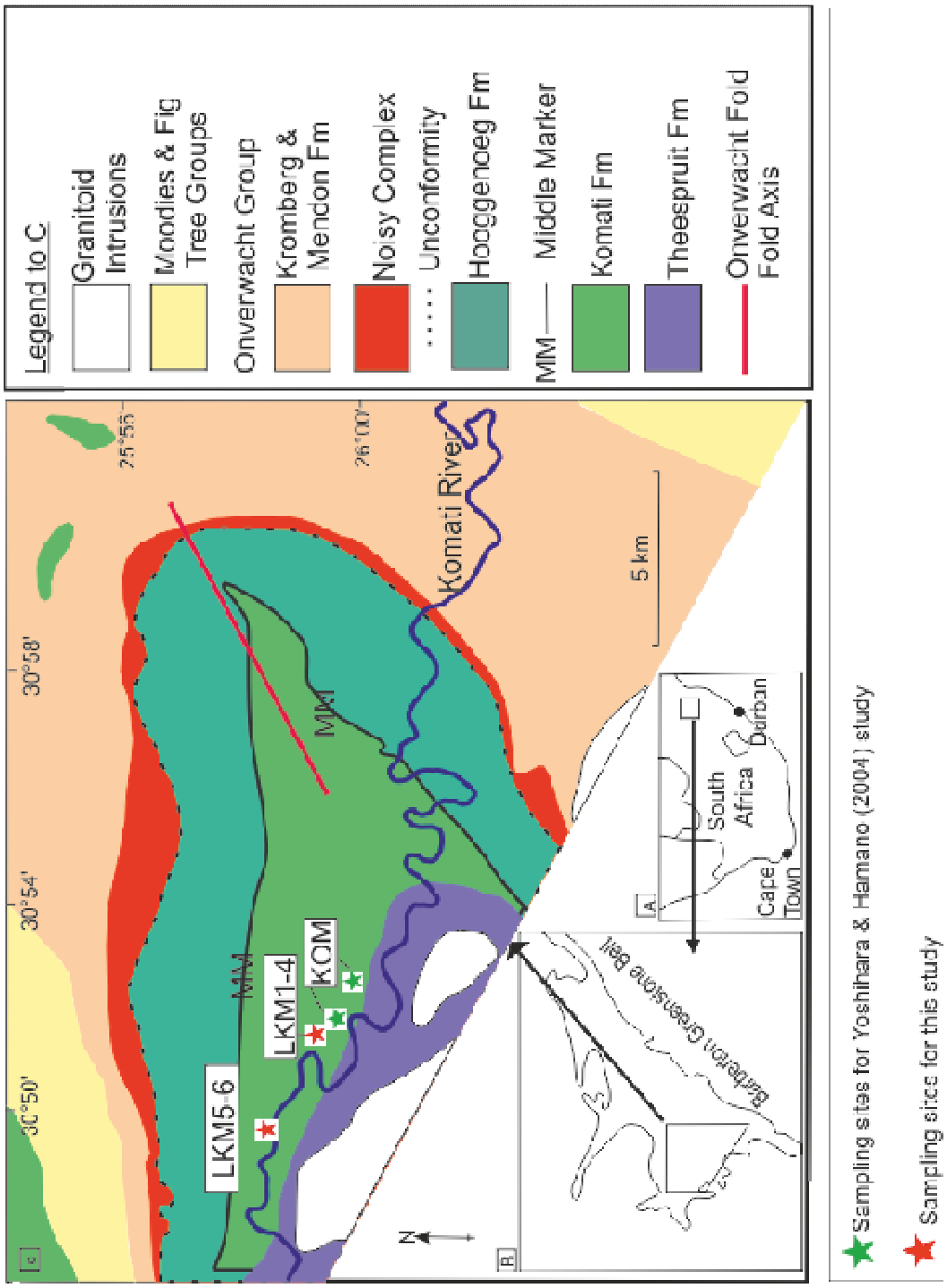

Figure 4.1. Location maps and simplified geological maps of the Barberton Greenstone Belt. Sampling sites from previous studies are shown. Green starts indicate the sites of Yoshihara and Hamano (2004); Surface sampling sites for this study are shown in red. Note that the Sandspruit Formation is not shown in this map, yet it is the oldest formation in the Onverwacht Group. Figure modified from De Wit et al. 2011.

tirely serpentinised (Dann, 2000), with MgO contents of 23-36 wt.% ((Viljoen et al., 1983). The komatiitic basalts are amphibole rich rocks which appear green in outcrop (Dann, 2000) and are characterised by a lower MgO content (11-24 wt.%,(Viljoen et al., 1983)). The lowest MgO content is in the basalts (4-9 wt.%(Viljoen and Viljoen, 1969b)), which contain mainly greenschist assemblages and are typically finer grained (Dann, 2000). The komatiitic basalts tend to contain varioles; vesicles are generally rare (Furnes et al., 2013). However, Dann (2001) observed up to 20-25% vesicles in the upper parts of some of the massive komatiites.

Komatiites are ultramafic rocks, present in almost all Archean terrains and defined by their elevated MgO content (above 18% MgO, (Nisbet, 1982). However, Kerr and Arndt (2001), argue that in addition to the high-Mg content, komatiites should also contain spinifiex textures to be defined as such. Research suggests they result from elevated mantle melting at depths in excess of 350Km (Arndt, 2003; Campbell et al., 1989; Nisbet et al., 1993) and result in lavas that are erupted at temperatures in the range of 1450°C (Parman et al., 1997) to 1600°C (Puchtel et al., 2013). Huppert & Sparks (1985), identified that komatiites flow turbulently and are therefore capable of thermally eroding (and potentially incorporating (Parman et al., 2001) their substrate). Komatiite flows are typically compositionally zoned, as can be seen in Figure 4.2, with an upper chill zone which often contains

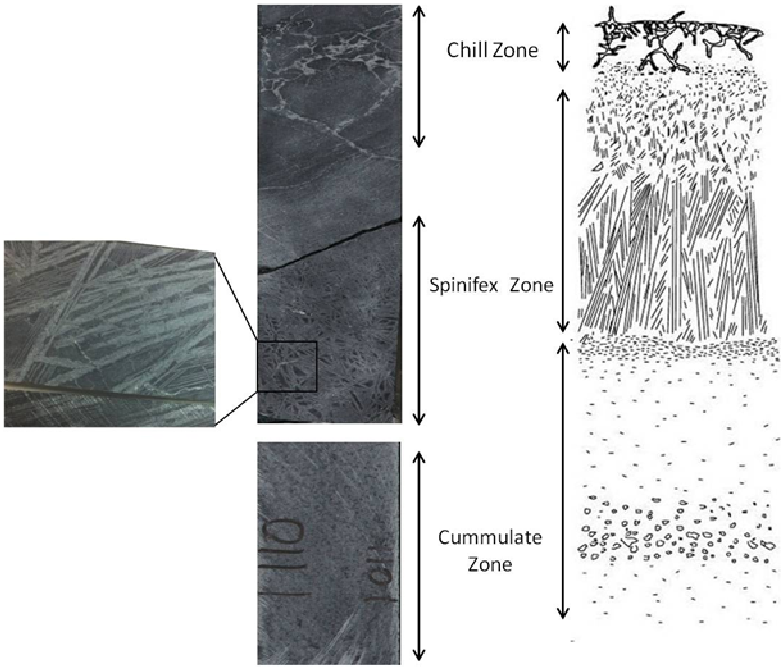

Figure 4.2 Sketch and photographs of a typical komatiite flow showing compositional zoning and characteristic zones. Figure modified from (Pyke et al., 1973). Photographs are from the BARB1 core, courtesy of Grace Cotezee and Allan Wilson. Numbers marked on the photographed core are not relevant to the work presented here.

fractures. The spinifiex zone forms the middle section of a flow and is characterised by random or aligned olivine or pyroxene laths, which can be up to 5cm in length, but tend to fine upwards. The lowermost section is dominated by mostly euhedral olivine (or pyroxene) cumulates (Pyke et al., 1973).

Komatiites are further subdivided into two major geochemical types based on their major and trace element contents. The Komatiites of the BGB are characterised by relatively low Al contents (Viljoen and Viljoen, 1969a), having low ratios of Al_2o_3/TiO_2. A feature not shared with any other Archean komatiites is their elevated CaO/Al_2O_3 ratios. Komatiites with this geochemical signature are known as Barberton-type komatiites or Al-depleted komatiites. Munro-type komatiites or Al-undepleted komatiites have higher Al_2o_3/TiO_2 ratios but lower concentrations of trace elements. All the komatiites identified across the globe have been metamorphosed (Arndt, 2003) and so understanding their original geochemical signature and what implications that has for the Archean mantle is difficult to ascertain. To what extent the original geochemical signature of komatiites can be altered by metamorphism is not fully understood. Some authors argue that the effects of metamorphism are minimal (Beswick, 1982) whilst others argue metamorphism causes modification of komatiitic rocks (Parman et al., 1997). Parman et al., (1997) argue that the compositional variation between komatiites is caused by metamorphism leading to the depletion of Na, Ca and K from the original geochemistry resulting in elevated MgO concentrations. They do not believe the compositional variation observed in komatiites results from olivine fractionation prior to the emplacement of the flows.

The Komati Formation is divided into two members: the Lower Komati and the Upper Komati (Dann, 2000). The Lower Komati is about 1.8Km thick with the lower boundary with the Theespruit Formation defined by the Komati Shear Zone. The unit is comprised of 50% komatiites and 50% komatiitic basalts (Robin-Popieul et al., 2012) which are predominantly massive, laterally continuous and of constant thickness (Dann, 2000). The unit is characterised by the presence of olivine-spinifex komatiities, which are absent in the overlying Upper Komati (Dann, 2000). There are a total of eight olivine komatiite layers in the unit, which can be further divided into: massive layers (the most common), spinifiex textured layers which occur in five distinct horizons and are relatively thin, and finally layers of vesicular komatiites (Dann, 2000). Due to the laterally extensive and massive nature of the layers, the Lower Komati rocks are interpreted to have been erupted into an environment with little topography such as a flat lavaplain(Dann, 2000). The presence of pillow

basalts, chilled margins at the top of flow units and reduced vesicularity (due to high emplacement pressures) indicate eruption of the Komati Formation into a submarine setting (Dann, 2000).

The Upper Komati is predominantly formed of pillowed flows (84±4%, (Dann, 2000) and pillow breccias, with minor proportions of sheet flows. The layers are characterised by pyroxene-spinifex texture and have a total thickness of 1.27Km (Robin-Popieul et al., 2012). The pillowed flows often thin down section and appear tilted with relation to underlying units, consistent with these being erupted in an environment where there was some local topography, potentially associated to the presence of faults in the region (Dann, 2000). The upper boundary of the Komati Formation is delimited by the Middle Marker Chert (3472 ± 5 Ma, detrial zircons, Armstrong et al., 1990), which is overlain by the Hooggenoeg Formation (de Wit et al., 2011).

Felsic, mafic and ultramafic sills and dykes intrude the Komati Formation (see Fig 4.3). It is important to appreciate that the exact age relationship between the intrusive units and the komatiites of the Komati Formation is still unclear (Dann, 2000. De Wit et al., 2011). The felsic intrusions (tonalite and gabbro compositions) can be dived into two sets that intrude the Komati Formation at different orientations and times (Dann, 2000). As outlined in Chapters 2 & 7 of this thesis, the rocks of the BGB are bordered on all sides by a granitoid-gneiss terrain characterised by tonalitic and trondhjemitic plutons (see also Chapter 7 for more detail). The plutonic rocks range in age from 3.51Ga to 3.11 Ga (Kamo and Davis, 1994). It is argued that the intrusion of felsic dykes into the rocks of the Onverwacht Group was associated with the emplacement of the plutonic rocks surrounding the Greenstone Belt (see de Wit et al., 2011 and Dann, 2000). The basis for the argument is the similarity in ages (of dykes that have been dated) and the composition of the dykes to that of the plutons. The age of the Tonalitic/ Trondhjemitic dyke sampled at the surface (site LKM2) is well constrained. The site was originally sampled in the work of Kamo & Davis, 1994. The age of the intrusion of the dyke is bracketed between 3476 ±2Ma and 3458 ±10Ma (dated by $^{207}Pb/^{207}Pb$ of concordant zircons). It is likely comagmatic to the emplacement of the Stolzburg, Doornhoek and Theespruit Plutons (de Wit, 1987; Kamo and Davis, 1994) of largely trondhjemitic composition and dated between 3460-3445Ma (Kamo and Davis, 1994). In addition, due to the dyke branching towards the East, intrusion is thought to have been from the West (Dann, 2000), consistent with it originating from the above mentioned Plutons. Sills of tonalitic composition are concentrated in the East of

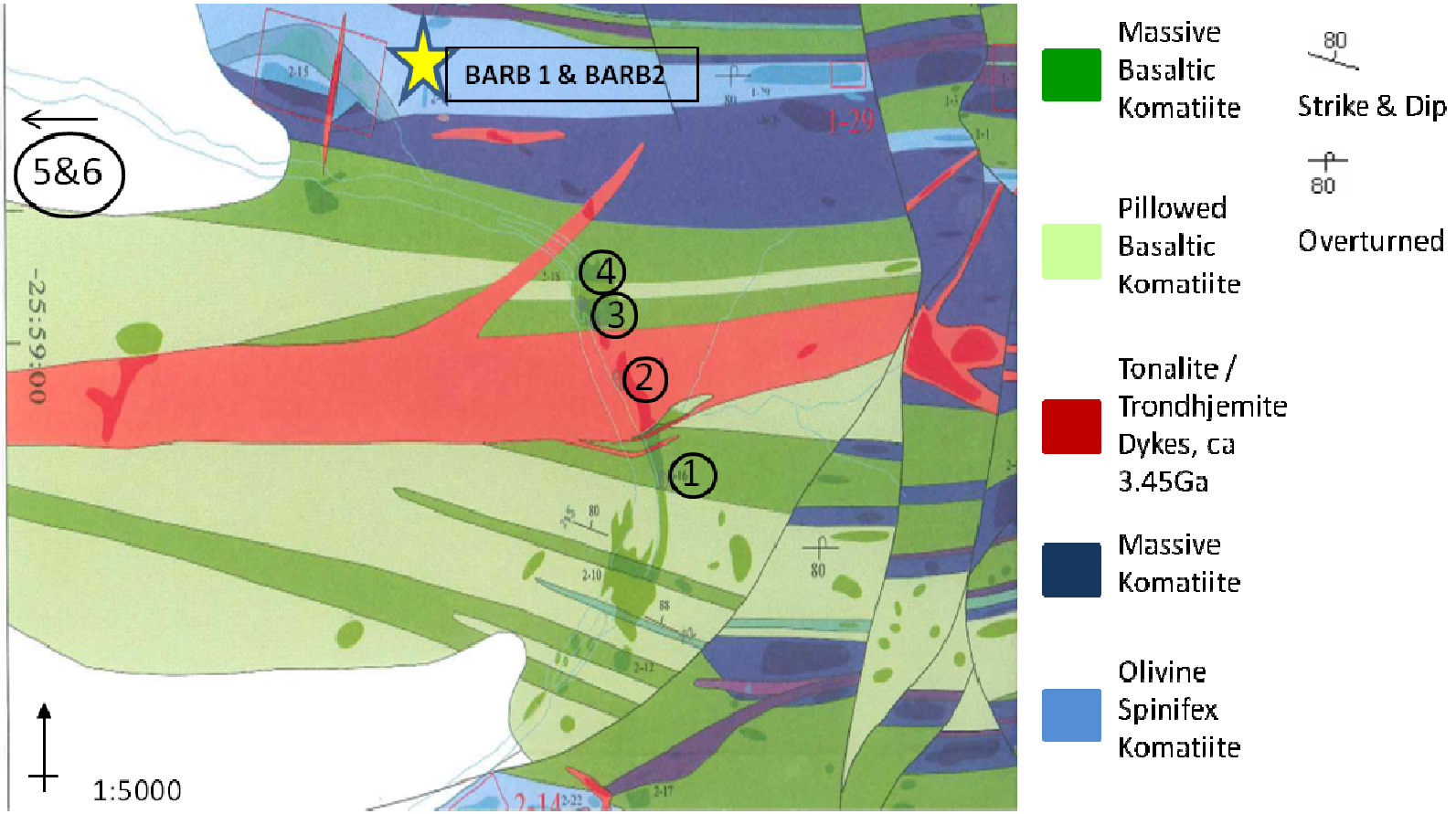

Figure 4.3 Detailed geological map showing four of the surface sampling sites and the drill core localities of BARB1 and BARB2 (yellow star). Note that surface sampling site, LKM2, samples a tonalite/trondhjemite dyke dated at ca. 3.45Ga (Kamo & Davies, 1994). Figure modified from Dann, 2000. Niote that the red box in top of the figure (close to the yellow star) is not relevant to the work presented here.

the Komati Formation, beyond the Spinifex Stream Fault. Dann, (2000) observed that these sills are texturally similar to the hypabyssal pluton, of tonalitic composition, that intrudes the upper Hooggenoeg Formation and which has been dated at ca. 3.445Ga. The sills are thought to be coeval with the emplacement of the Theespruit (3443 ± 4 Kamo and Davis, 1994 and consistent with Armstrong et al., 1990 and Krüner et al., 1991) and Doornhoek Plutons (3448 ± 4 Ma, Kamo and Davis,1990), as well as the dacitic rocks of the BR-vsc (see section 1.1 of chapter 5) (Dann, 2000). Thin vertical dykes and thicker sills of komatiitic basalt composition intrude the Lower Komati Formation. The dykes are concentrated along normal faults associated with deformation during the D2 stage. Dann, (2000) argues that due to composition similarities with the Upper Komati and Hooggenoeg Formation, these dykes are hypabyssal equivalents of the flows in the overlying statigraphy. Serpentinised dykes and sills of wehrlite (mafic) composition, age unknown, also intrude the rocks of the Komati Formation. Dann, (2000) observed that the wehrlite dykes intrude both the MM and cross-cut the tonalitic dykes, therefore postdating their emplacement. However, the age relationship between tonalite and wehrlite dykes is unclear and there is no evidence to suggest that at least some wehrlite dykes could predate the tonalitic intrusives (Dann, 2000). The wehrlite sills are seen to cross-cut the felsic intrusives, the diabase dykes (see below), as well as the komatiites and basalts of the Komatii Formation and so are potentially younger (Dann, 2000). Two ages of diabase (mafic) dykes intrude the Komati Formation. The early diabase dykes are of unknown age but are geochemically correlated to the mafic rocks of Onverwacht Group, in particular the basalts of the Kromberg Formation and so may be of similar age (Dann, 2000; de Ronde and de Wit, 1994). The late diabase dykes cross-cut major structures within the Komati Formation are thought to be associated to the dyke swarm that intrudes a large area of the Kaapval Craton, which is potentially related to the ca. 2.9Ga Ishwashana Complex of Swaziland (Dann, 2000).

The ages of the dykes in the BARB cores are unknown. Compositionally, the dykes sampled are most akin to the felsic intrusives described above. Therefore, one possibility is that they could be similar in age to the tonalitic/ trondhjemitic dyke of site LKM2 (3476 ±2Ma and 3458 ±10Ma , Kamo and Davis, 1990). Compositionally, the dykes in the BARB cores are also similar to the tonalitic plutons to the West of the BGB (Kaap Valley, Nelshoogte and Dalmein Plutons, 3230-3210Ma, (Kamo and Davis, 1994)). These plutons are thought to be geochemically related to the intrusives identified in the Fig Tree Group (Kamo and Davis, 1994). It seems that an age ca 3.4 for the dykes in the BARB cores is

more likely, due to there being a precedent for dykes of this age and composition in the rocks of the Komati Formation. However, until ages for the dykes are published, discussion of the ages of the BARB core dykes remains speculative.

The rocks of the Komati Formation have a sub-vertical dip and young towards the North. The rocks are arranged into regional scale folds (see Figure 4.1), that trend NE to SW and which plunge steeply to the NE or SW (de Wit et al., 2011). Prior to folding, the rocks of the Onverwacht Group were tilted and/or overturned and tectonically stacked (de Wit et al., 2011) by two major tectonic events (D_1 and D_2, details of which can be found in de Ronde and de Wit, 1994). The age of the folding is not well constrained and can only be determined by cross-cutting relationships established in the field. The rocks of the Komati Formation are folded in the Onverwacht Fold, which affects the Buck Ridge Sedimentary-Volcanic Complex (BRSVC as defined in de Wit et al, 2011), the youngest complex in the Onverwacht Fold, with a lower age of 3.4Ga (de Wit et al., 2011). Therefore, the Onverwacht Fold must be at most 3.4Ga. In addition, the NE-SW trending folds are thought to be caused by D_3 deformation (see de Ronde and de Wit, 1994) which is pervasive across the BGB. The deformation is thought to be synchronous with the deposition of the Moodies Group, thought to be younger than 3227 Ma (de Ronde and de Wit, 1994). Furthermore, the 3216 Ma Dalmain pluton (Kamo and Davis, 1994) cuts the limbs of the Kromberg Fold (de Wit et al., 2011), suggesting the D_3 deformation which caused the folding predates the emplacement of the pluton. Therefore, the Onverwacht Fold is thought to be in the region of 3.2Ga old (Kamo and Davis, 1994; Krüner et al., 1991).

The maximum metamorphic conditions recorded in the upper part of the Komati Complex, are 490–530 °C (Cloete, 1999), as determined by fluid inclusion geobarometry. This indicates greenschist grade metamorphism. These results indicate a maximum burial depth of 3.9kbar suggesting the rocks have only been subjected to burial metamorphism, as this is a depth similar to the total thickness of the overlying Barberton Supergroup (Van Kranendonk et al., 2009). The lowermost part of the Formation, in contact with the Theespruit Pluton, has also been affected by dynamic metamorphism (that associated with areas of moderate to high strain, e.g. fault structures – the contact between the two is tectonic and marked by the Komati Fault) as suggested by the 280°C retrograde temperatures recorded in this area (Van Kranendonk et al., 2009b). Here metamorphic grade is greenschist to amphibolites facies (Dann, 2000). The metamorphism of the Komati formation is inferred to be synchronous with the formation and burial of the komatiites on

the sea-floor (Schoene et al., 2008a), from $^{40}Ar/^{39}Ar$ studies on amphibole from serpentinised komatiites (de Ronde and de Wit, 1994; de Wit et al., 1982) and whole-rock K-Ar thermochronology (de Wit et al., 1982) and interpreted to have occurred sometime between 3460-3420Ma (de Ronde and de Wit, 1994; Kamo and Davis, 1994; López-Martínez et al., 1992).

4.3. Palaeomagnetic Background

Yoshihara & Hamano (2004) report palaeodirectional data from surface samples from the Komati Formation of the Barberton Greenstone Belt that are consistent with results previously published by Hale & Dunlop (1984). These results constitute the world's oldest unrefuted palaeomagnetic pole (See Figure 4.4.). This pole has been crucial in arguments for the existence of a viable geomagnetic field early in the Earth's history but does not yet have the support of rigorous field tests in constraining its age and viability.

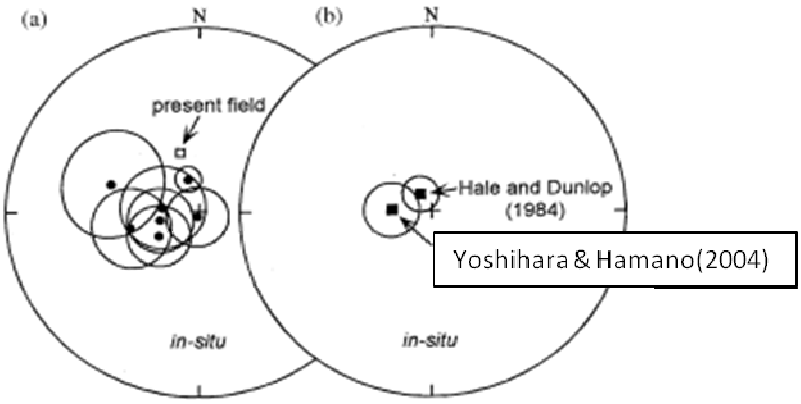

Figure 4.4. Taken from Yoshihara & Hamano (2004). (a) In situ directions. (b) In situ mean direction compared to results by Hale & Dunlop (1984). Solid symbols are plotted on the lower hemisphere. Open symbols are plotted on the upper hemisphere.

The main carriers of the Characteristic Remanent Magnetisation (ChRM) in Yoshihara & Hamano's study are identified as Ti-free magnetites presumed to behave as single domain grains which are stable upon heating to temperatures above 600°C. As part of this work Thellier-Thellier palaeointensity experiments were also performed and yielded low mean virtual dipole moment (VDM) estimates of (1.8± 1.3) x 10^{22} Am^2.

Yoshihara and Hamano (2004) sampled komatiites of peridotitic and basaltic composition. Thermal demagnetisation results showed that the peridotitic samples were strongly magnetised, with NRM intensities typically in the range of 1 to 20 A/m, whilst the basaltic komatiites were very weakly magnetised, with NRM intensities in the range of 10^{-5} to 10^{-4} A/m. The authors plotted Q_n ratios vs. NRM intensities (A/m) and samples clustered clearly into two groups (see Figure 4.5). Overall, peridotitic samples were found to be more stable, with unblocking spectra for high temperature components concentrated between 570-590°C, with over half the initial NRM intensity still remaining until after 570°C. The weaker basaltic samples gave less successful demagnetisation curves which were often found to be noisy, with high temperature components isolated above 400-500°C. For basaltic samples were it was possible to isolate characteristic components, directions were in agreement with those of the peridotitic samples

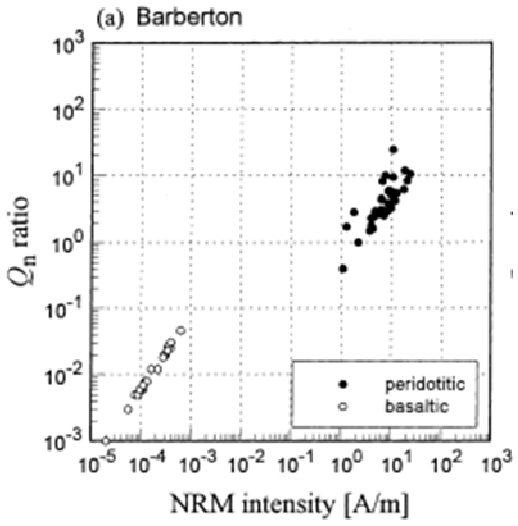

Figure 4.5. Plot of Qn ratios vs. NRM intensities for komatiite samples for the BGB, from Yoshihara & Hamano, 2004.

To better understand the magnetic carriers the authors conducted microscopic observations (SEM and energy dispersive X-ray analysis, EDX) of the peridotitic komatiites and found mainly serpentinised olivines, with MgO rich cores still preserved. Small grains and veinlets of magnetite (1-100 μm) were identified in the outer rims of the serpentinised olivines. The range of sizes of the magnetite grains observed in thin section means the magnetic carriers in the peridotitic komatiites are assumed to be a mixture of SD and MD grains.

The microscopic observations lead the authors to interpret the ChRM recorded in the Komati Formation to be of a secondary origin, associated to the serpentinisation process, which is caused by hydrothermal alteration of olivines and pyroxenes. Due to the olivine cores being preserved, it is thought exposure to a hydrous environment must have been short lived. The komatiitic rocks of the BGB are thought to have been extruded in a ridge or rift environment (Yoshihara and Hamano, 2004) and therefore serpentinisation would have occurred soon after extrusion. The authors argue that the magnetisation is therefore not a ChRM but rather a Chemical remenant magnetisation (CRM) acquired almost simultaneously to the formation of the komatiites. As the serpentinisation process occurs at relatively low temperatures, it is not a thermal remenant magnetisation (TRM) or thermochemical remenant magnetisation(TCRM).

However, Yoshihara & Hamano highlight that determining the timing of the acquisition of the ChRM isolated from the Komati Formation is still problematic. Hale & Dunlop (1984) and Hale (1987) argue that the recorded magnetisation is a thermal overprint (TRM) associated with the metamorphism caused by emplacement of the Theespruit Pluton (shown in Fig 2.2), which occurred after the serpentinisation process. Alternatively, Yoshihara & Hamano (2004) propose that the magnetisation could be a thermoviscous remenant magnetisation (TVRM) acquired over a period of time resulting from metamorphic events over the history of the BGB. The interpretation favoured by the authors is that the secondary grain growth CRM associated to the serpentinisation survived as a ChRM.

As part of the present study further surface samples from the Komati Formation were collected in the summer of 2011. The sampling sites are located to the West of those of Yoshihara & Hamano(2004) and Hale & Dunlop(1984), the rationale being to expand the geographical distribution of the data set and to attempt to carry out a fold test to investigate the reliability of any potential primary directions recorded by the samples. Sampling locations for this study and the previous works are shown in Fig .4.1.

Tectonically, the Komati Formation is affected by the formation of the Onverwacht Anticline at 3.2Ga. In the work of Yoshihara and Hamano (2004), site mean directions published are not corrected for the plunge of the fold. Re-sampling of the Komati Formation will allow for combination of our results with those already published and full interpretation of the site mean directions and pole positions by correcting both data sets for the formation of the Onverwacht Anticline.

Addition of the Komati Formation samples from ICDP Barberton Greenstone Belt drilling project to the existing surface samples was advantageous as it allows increased sample quantity which in turn should improve the statistical robustness of any potential directions. Surface samples can be affected by weathering processes and also lightning strikes (although surface sampling sites were chosen with care to minimise the risk of them being lightning struck). Drill core samples are expected to be unaltered by weathering processes and will not be affected by lightning strikes.

4.4. Methodology

4.4.1. Sampling

In May 2011, 101 core specimens sampled at six sites (LKM1-6) of the Komati Formation were collected as part as of a larger sampling trip of the Onverwacht Group.

Sites LKM1 and LKM3-LKM6 are of basaltic komatiite composition which are generally massive but contain some localised pillowed sections. The sites are a few hundred metres west of the classic komatiite outcrop described by the Viljoen brothers in 1969. Site LKM2 is a non uniform intrusive dyke of felsic composition, dated at 3.45Ga and ranging in thickness between 1-5m, as shown in Figure 4.9 (Kamo & Davis, 1994 and Dann, 2000; see also geological introduction for this chapter for more information). Sampling sites for this section of the Komatii Formation were chosen on the basis of performing a baked contact test around the felsic dyke. Yoshihara and Hamano's (2004) sites are located towards the East, well away from the expected influence of the dyke and, therefore, are not expected

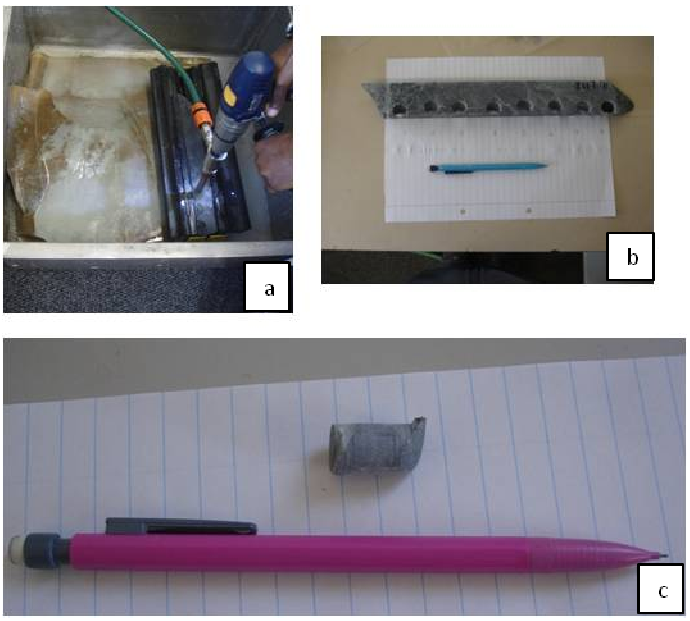

Figure 4.6. Drilling of the BARB mini-cores from the ICDP cores (a) Drilling set-up using a custom drill bit on an electrically powered hand drill. (b) Section of core showing a sampled drill site. (c) Example of a drilled mini-core. Approx size 12mm.

to be overprinted by the dyke emplacement. The same is true for sites LKM5 and 6, as they are 2km away from the dyke in a westerly direction**.** Sites LKM1 and LKM3 are in the immediate vicinity of the dyke, allowing for a baked contact test to be attempted. For an illustration of the sampling site relationships please refer to Fig. 4.10.

The OF provides a good opportunity to collect Komati Formation samples from each limb of the fold and therefore to perform a fold test to contribute to the efforts to ascertain the timing of acquisition of potentially primary ChRM. However, as part of this work, only samples from the northern limb of the fold were collected due to time constraints during the field work. In addition, the outcrops of the Komati Formation on the southern limb of the fold are closer to the Theespruit Pluton, so care when sampling in this area is required in order to avoid the amphibolite facies metamorphism which could have overprinted the original ChRM signature.

Early access to the ICDP drilled cores was granted in July 2012 for palaeomagnetic sampling. In total, 274 mini-core (diameter 12mm and length of ~ 20-25mm) samples were collected from a total of 26 sites across cores BARB1 to BARB4: 104 samples from BARB1, 45 samples from BARB2, 54 samples from BARB3 and 71 samples from BARB4 were collected. No samples were collected from BARB5. The drill cores of BARB1 and BARB2 sample the Komatii Formation. There is an overlap in the stratigraphy of 120m, at the base of BARB1 and the top of BARB2. The site selection for BARB 1 and BARB 2 was based on findings of Yoshihara & Hamano (2004), which indicated that peridotitic komatiites yielded stronger samples, which gave less noisy demagnetisation spectra and more stable directions than basaltic komatiites. The presence of a number of intrusive units meant that sites were also selected with the aim of performing baked contact tests. Site BARB1A sampled a hyloclastite unit and the aim was to perform a conglomerate test by sampling the clasts and matrix of the unit. Site BARB1D samples a dacitic intrusion; samples from sites BARB1B and C were selected to carry out a baked contact test on this section. Unfortunately, it was not possible to sample below site BARB1D due to the core being too friable in this area. Site BARB1F is an intrusive gabbro and sites BARB1E and BARB1G were selected to allow the performance of a baked contact test. The same is true for sites BARBI to BARBK. Sites BARB1H and BARB1L were selected as they were located away from any intrusive rocks and sampled units that fitted with Yoshihara & Hamano's description of the peridotitic komatiites that gave stable directions. Four sites have been sampled in BARB2. Sites here were selected because they too agree with the description of peridotitic

komatiites given by Yoshiahra & Hamano (2004). There was potential to carry out sampling across some baked contacts, but that was not possible due to the friability of the core and the need to preserve textures for other types of analysis. The age of the intrusive dykes found in BARB1 and BARB2 is unknown but is likely to be associated to the emplacement of the 3.2 and 3.45Ga tonalitic-trondhjemitic plutons (see section 1.1).

Lithologies were attributed to sites on the basis of the information acquired in the BARB drilling project logs. Whilst some obvious inconsistencies were found in the logs where komatiites had been recorded as gabbrotic dyke instrusions, the overall information recorded in the logs was assumed to be reliable. However, no geochemical or thin section work was carried out on the BARB samples collected as part of this study and, therefore, it is possible lithologies may have been misinterpreted.

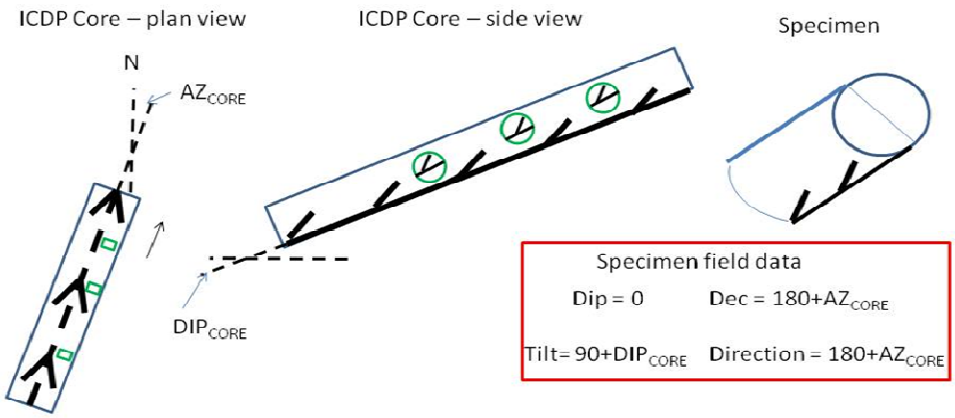

Figure 4.7. Sketch diagram illustrating the extra orientation required to establish the true orientation of the mini-cores. As the drill core was cut in half, along the orientation mark, the orientation and calculations shown here are true for mini-cores sampled from the right hand side of the core.

Drill cores were oriented at the drilling sites using a core orientation tool and the 'Eazymarker' system, which marks the core pieces with a gravity line at the bottom of the core. The orientation mark was traced with a red line. Half cores were placed in a convex boat used for core cutting, to be held securely in place; mini-core samples (were drilled out of the flat top of the core using a custom made drill bit on an electrically powered hand-drill, which was water cooled to avoid heating of the samples and possible remagnetisations (Figure 4.6.a). The mini-cores were drilled with respect to the orientation mark at the base of the core. As mini-cores were not drilled perpendicular to the orientation mark, it was necessary to carry out extra orientation corrections to establish the true orientation of the mini-cores, as is shown in 4.7.

4.4.2. Experimental Methodology

Rock magnetic characterisation experiments (as described in detail in Chapter 3, Section 3.2.2.1) have been carried out on 27 ICDP mini-core samples from BARB1 and BARB2 (at least one sample from each site has been measured), whilst at least one sample from each outcrop site, LKM1 to LKM6 have also been investigated. In cases where samples were proximal to an intrusion, more than one sample may have been investigated to establish if distance from the intrusive body has any effect on the rock magnetic properties.

Temperature dependant susceptibility measurements on eight mini-core sample from sites A-G of BARB1 have been carried out. In addition, cycled high temperature susceptibility measurements have been performed on samples F1 and F6 of core BARB1. A total of 95 measurements (which include measurement of sister samples) were made of bulk susceptibility from samples across LKM1 to LKM6.

4.5. Results

4.5.1. Directional Results

Three to ten samples, from each surface sampling site, were thermally demagnetised. A further 60 samples were also demagnetised using alternating field techniques. See Chapter 3, Section 3.3.1. for full experimental methodology. As a consequence of a mistake in the experimental procedure, it was not possible to use the results from the AF experiments for further analysis. In total 85 samples from the ICDP Drill cores have been AF or TH demagnetised.

The analysis of the palaeomagnetic data was conducted using principal component analysis and standard statistical analysis (Fisher,1953: Kirschvink,1980). Samples generally produce multi-component Zijderveld Plots with one stable overprint removed during stepwise demagnetisation prior to a characteristic remenant magnetisation (ChRM) component being isolated. In some cases, (discussed in more detail below) it was not possible to isolate a stable overprint and/or ChRM components. Recorded overprint and ChRM components generally had a maximum angular deviation (MAD) of less than 15°. Low NRM intensities in many sites result in very scattered directions that do not produce a reliable site mean direction. Figures 4.8 to 4.11 summarise the directional results, whilst Table 4.1. provides details of site lithologies and components isolated.

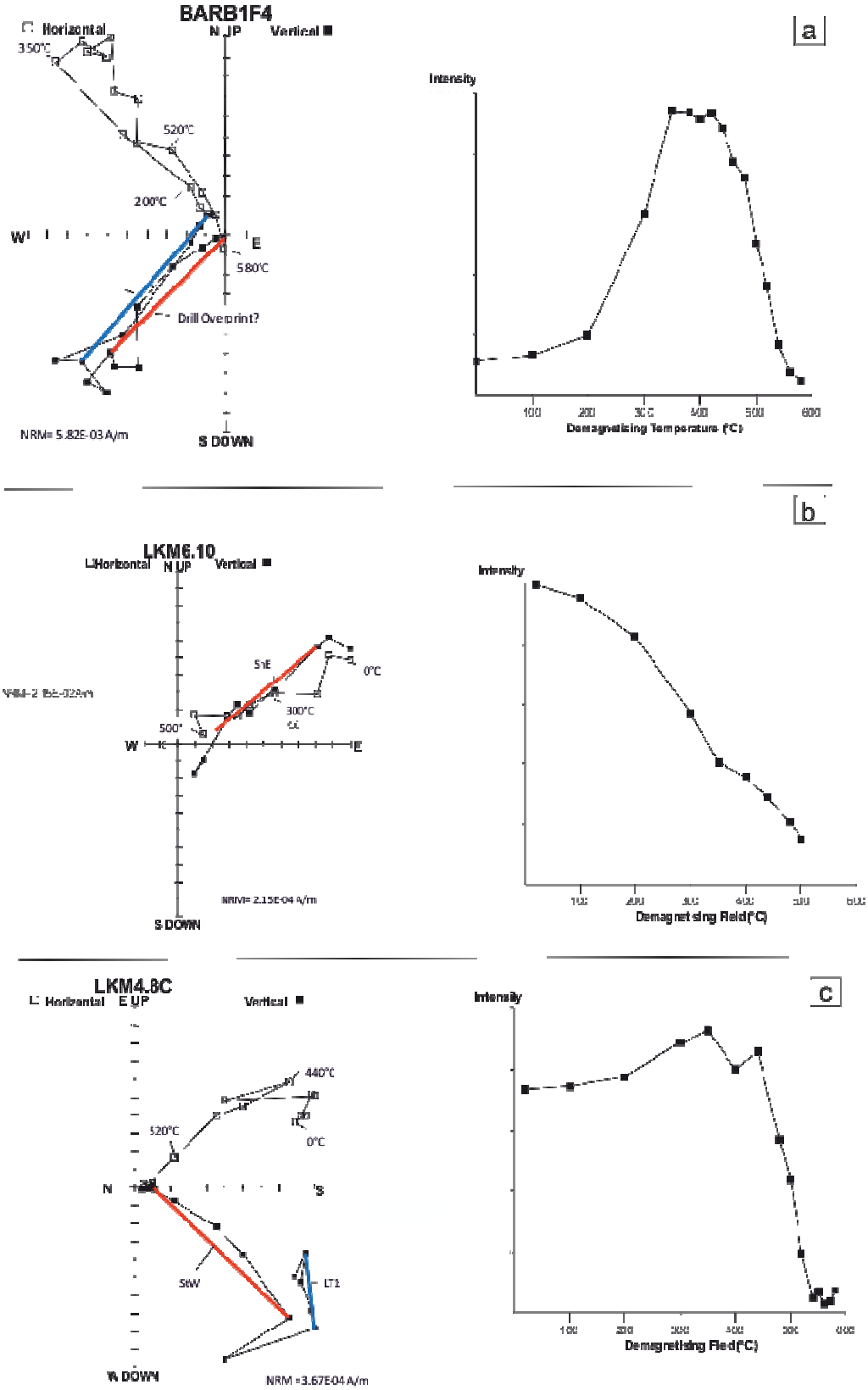

Figure 4.8. Results for thermal and alternating field demagnetisations of LKM surface samples and BARB cores;(a&e). Samples from sites across BARB1 and BARB2 are affected by a parallel and antiparallel drilling overprint (b&f). (c&g) Orthogonal plots for samples showing convergent component corresponding to a ShE component.(c&g) Samples LKM4.8c and LKM3.4a show a ShW. (d) A StW component is isolated above a shallow west component. (h) Samples from sites in the BARB1 core are characterised by a direction intermediate between the ShW and StW components. Temperature and/or AF demagnetisation field steps are indicated. All plots are in geographic coordinates.

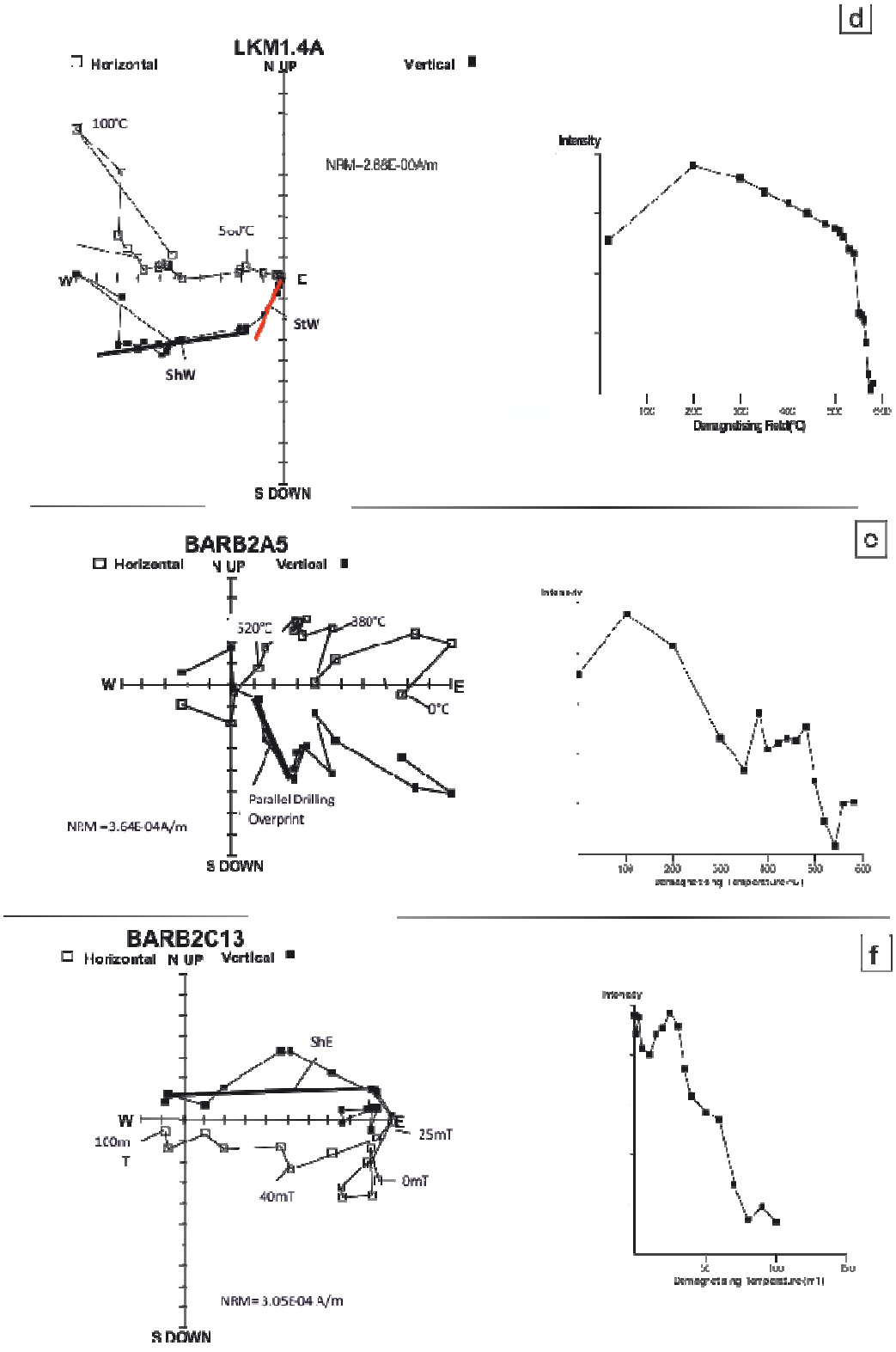

Figure 4.8. (cont.) Results for thermal and alternating field demagnetisations of LKM surface samples and BARB cores;(a&e). Samples from sites across BARB1 and BARB2 are affected by a parallel and antiparallel drilling overprint (b&f). (c&g) Orthogonal plots for samples showing convergent component corresponding to a ShE component.(c&g) Samples LKM4.8c and LKM3.4a show a ShW. (d) A StW component is isolated above a shallow west component. (h) Samples from sites in the BARB1 core are characterised by a direction intermediate between the ShW and StW components. Temperature and/or AF demagnetisation field steps are indicated. All plots are in geographic coordinates.

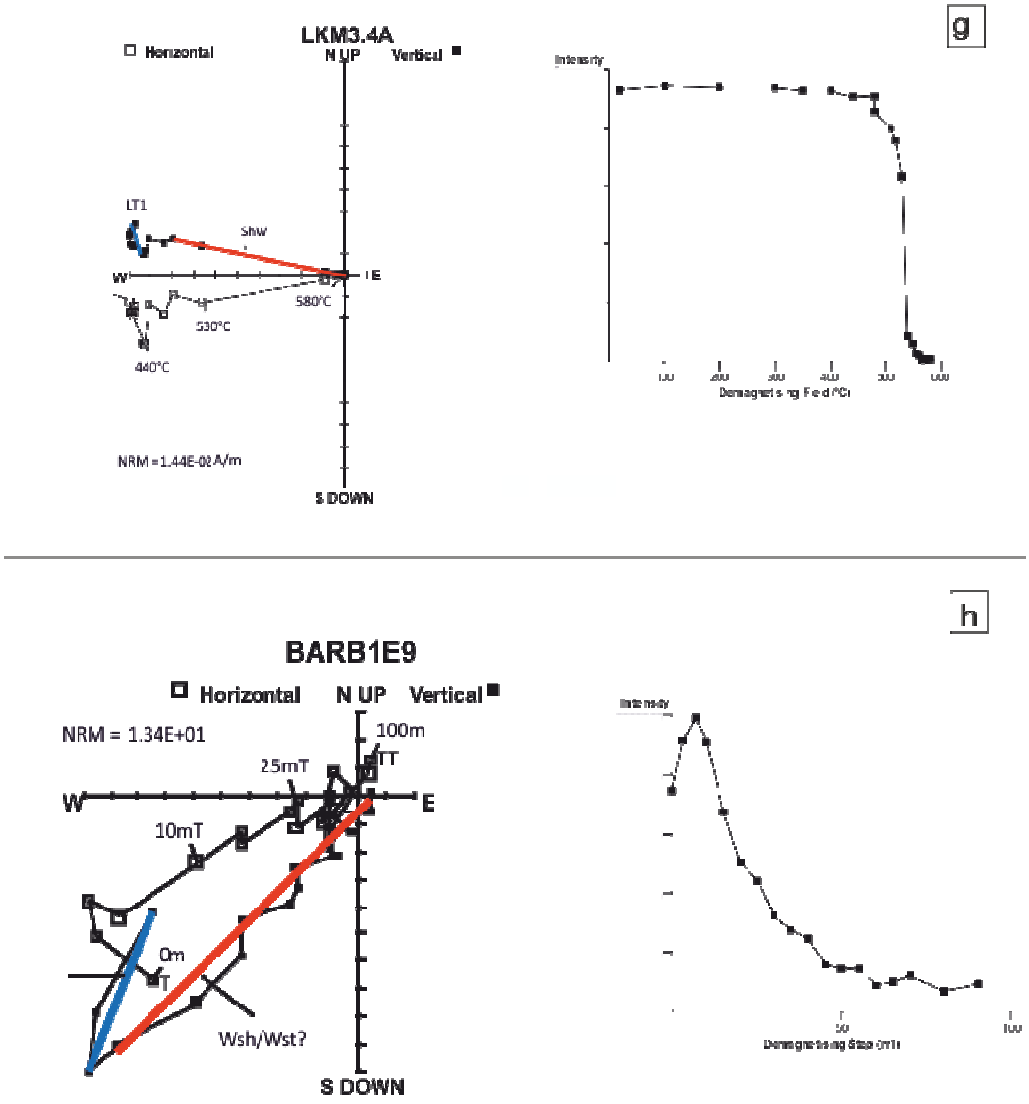

Figure 4.8. (cont.) Results for thermal and alternating field demagnetisations of LKM surface samples and BARB cores;(a&e). Samples from sites across BARB1 and BARB2 are affected by a parallel and antiparallel drilling overprint (b&f). (c&g) Orthogonal plots for samples showing convergent component corresponding to a ShE component.(c&g) Samples LKM4.8c and LKM3.4a show a ShW. (d) A StW component is isolated above a shallow west component. (h) Samples from sites in the BARB1 core are characterised by a direction intermediate between the ShW and StW compo-

Figure 4.9. Directional results of the Komati surface samples. Sketch of sampling localities is shown in addition to equal area projections showing predominant directions isolated in the sits. Low temperature components are shown in blue; high temperature components are shown in red.

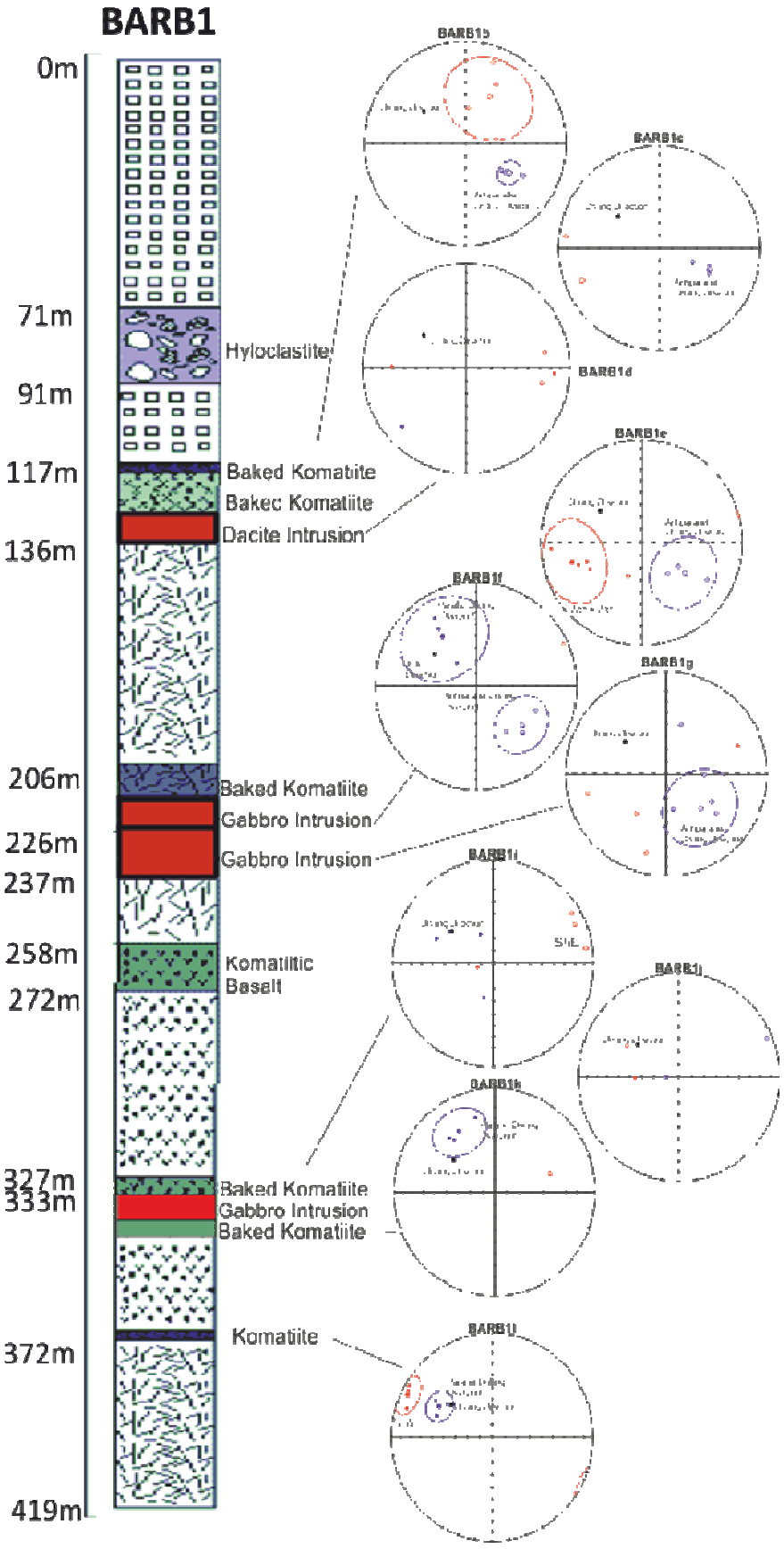

Figure 4.10. Directional results of the Komati BARB1 Core. Sketch log of sampled sites is shown in addition to equal area projections showing predominant directions isolated in the sites. Low temperature components are shown in blue; high temperature components are shown in red. Please refer to Fig. 4.12 for a legend to the symbols used in this figure.

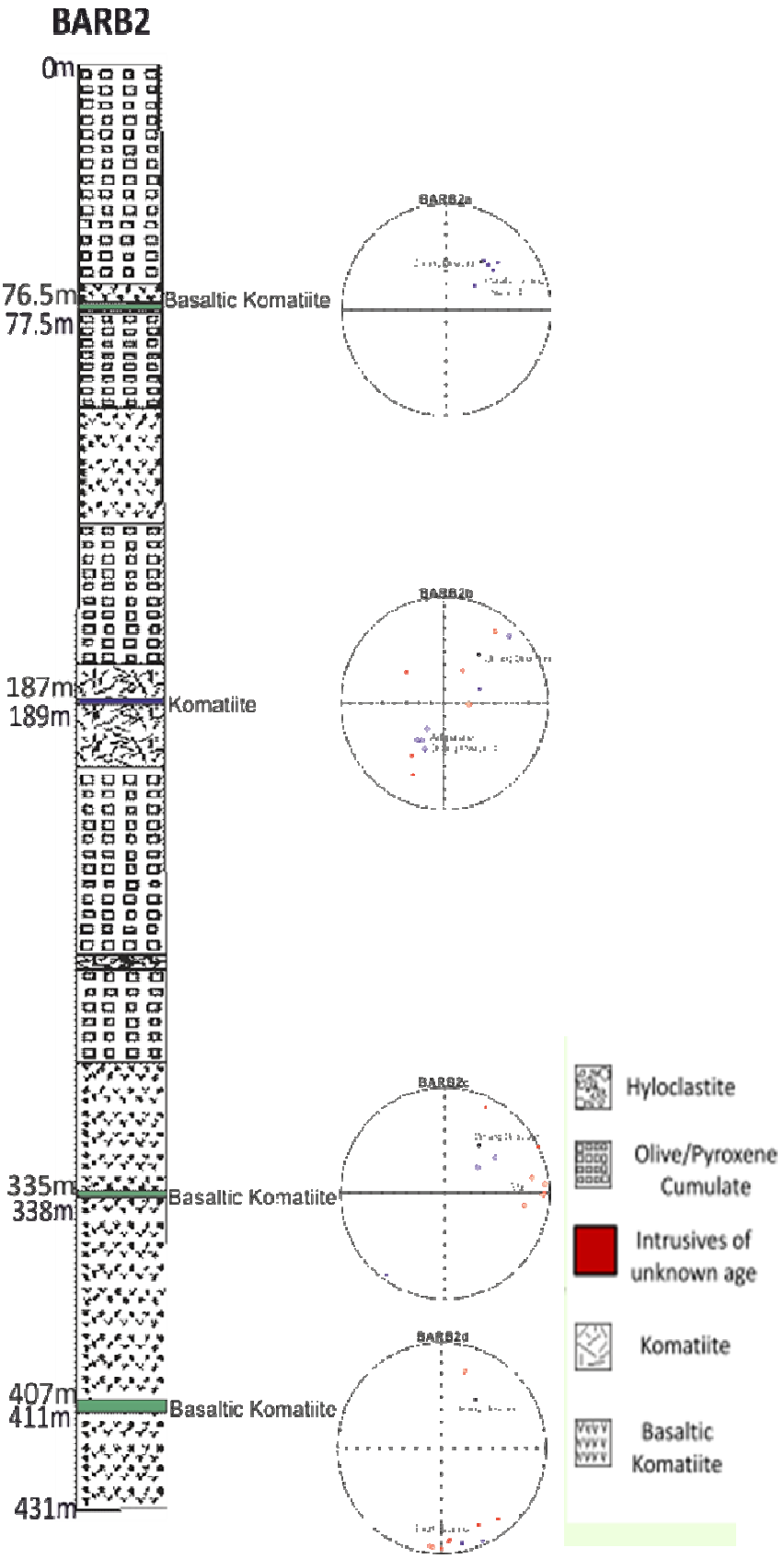

Figure 4.11. Directional results of the Komati BARB2 Core. Sketch log of sampled sites is shown in addition to equal area projections showing predominant directions isolated in the sites. Low temperature components are shown in blue; high temperature components are shown in red.

	Lithology	Site	Bedding Strike/Dip (°)	Lat (°)	Long (°)	Depth In Core (m)	Demag	N	NRM (A/m)	Component	T Range (°C/ mT)	Dm	Im	K	a95	n
Komati Formation	Baked Komatiite Flow	LKM1	288/84	-25.9855	30.84973	-	TH	7	1-5	LT1	100-350	342.2	-29.3	75.8	10.6	4
										ShW	500-560	271.1	14.3	51.5	9.4	6(7)
										StW	555-580	278.2	63.4	25.6	15.4	5
	Gabbrotic Dyke	LKM2	288/84	-25.9846	30.84925	-	TH, TH+AF	3	10^{-5}- 10^{-3}	Noisy ShW and StW direction as convergent						
	Baked Komatiite Flow	LKM3	288/84	-25.9842	30.84901 6	-	TH, TH+AF	7	10^{-3}- 10^{-1}	LT1	20-440	344.8	-54.3	15.5	17.6	6
										ShW	440-570	260.99356	-8.0285458	105.40118	5.4201774	8
	Komatiite Flow	LKM4	288/84	-25.9838	30.84871	-	TH, TH+AF	3	10^{-5}- 10^{-3}	Noisy StW direction as convergent component seen in only two samples						
	Basaltic Komatiite Flow	LKM5	288/84	-25.9747	30.82283	-	TH, TH+AF	7	10^{-4}- 10^{-3}	LT1	20-400	9.0498846	-32.960006	68.88712	14.968172	3
										StW	440-560	271.14159	66.530751	22.425666	16.511595	5
	Basaltic Komatiite Flow	LKM6	288/84	-25.9746	30.822783	-	TH	7	10^{-5}- 10^{-4}	Noisy - components very scattared to the N and E, mostly shallow						
	Hyloclastite	BARB1A	288/84	-25.9807	30.843689	72.42-72.70	TH, AF		10^{-3}-10^{-4}	Noisy components very scattered.						

Table 4.1. Overprint and high temperature directions measured in this study. Strike and dip refer to bedding planes measured in the field and validated against measurements from regional scale geological maps. Dec and Inc refer to the direction of the components in geographic coordinates before applying the plunging fold correction. N refers to the number of samples measured whilst n is the number of specimens used to calculate the site mean.

	Lithology	Site	Bedding Strike/Dip (°)	Lat (°)	Long (°)	Depth In Core (m)	Demag	N	NRM (A/m)	Component	T Range (°C/ mT)	Dm	Im	K	a95	n
Komati Formation	Baked Komatiite Flow	BARB1B	288/84	-25.9807	30.843689	117.71-118.03	TH, AF	6	3	AntiParallel DRILL	0-15	123.63795	-46.486481	92.526862	9.6021464	4
										NE-UP	15-100	27.964862	-47.045887	7.8215846	35.097796	4
	Baked Komatiite Flow	BARB1C	288/84	-25.9807	30.843689	118.75-119.16	TH, AF	5	10^{-2}	AntiParallel DRILL	0-560	113.1	-49.0	95.9	9.4300846	4
										ShW - StW ABOVE?	isolated above 40mT	-	-	-	-	2
	Dacite Intrusion	BARB1D	288/84	-25.9807	30.843689	119.91-120.16	TH, AF	4	10^{-1}	Noisy components very scattered, Shallow, E and W.						
	Baked Komatiite Flow	BARB1E	288/84	-25.9807	30.843689	208.71-215.82	TH, AF	5	10^{-4}	AntiParallel DRILL	0-350	125.2	-46.4	20.5	27.97835	3
										ShW	10 thru 60	254.4	29.4	18.2	29.7824	3
										StW	40-580	only seen in 2 samples				
	Gabbrotic Dyke	BARB1F	288/84	-25.9807	30.843689	218.88-219.43	TH, AF	3	10^{-2}-10^{-1}	AntiParallel DRILL	0-350	129.9	-40.2	31.9	22.214832	3
										DRILL OVERP?	10-580	325.52774	41.214589	13.561677	34.865923	3
	Gabbrotic Dyke	BARB1G	288/84	-25.9807	30.843689	222.55-222.87	TH, AF, TH+AF	7	1	AntiParallel DRILL	0-520	135.2	-49.6	17.1	30.747443	3
										Noisy components very scattered, Shallow, E and W.						
	Basaltic Komatiite Flow	BARB1H	288/84	-25.9807	30.843689	269.79-270.30	TH, AF	6	10^{-3}-10^{-1}	Noisy components very scattered.						

Table 4.1. (cont.) Overprint and high temperature directions measured in this study. Strike and dip refer to bedding planes measured in the field and validated against measurements from regional scale geological maps. Dec and Inc refer to the direction of the components in geographic coordinates before applying the plunging fold correction. N refers to the number of samples measured whilst n is the number of specimens used to calculate the site mean.

	Lithology	Site	Bedding Strike/Dip (°)	Lat (°)	Long (°)	Depth In Core (m)	Demag	N	NRM (A/m)	Component	T Range (°C/ mT)	Dm	Im	K	a95	n
Komati Formation	Baked Komatiite Flow	BARB1I	288/84	-25.9807	30.843689	329.76-329.97	TH, AF, TH+AF	5	10^{-3}	ShE	Noisy components very scattered, Shallow, E and W. 15-540	68.001165	-9.802268	47.119411	18.16372	3
	Gabbrotic Dyke	BARB1J	288/84	-25.9807	30.843689	330.77-331.68	TH, AF	6	10^{-3}		Noisy components very scattered. Mainly W and Steep					
	Baked Komatiite Flow	BARB1K	288/84	-25.9807	30.843689	332.38-332.61	TH, AF	3	10^{-3}	DRILL OVERP	1 thru 50	328.7	32.2	37.7	20.366219	3
	Komatiite Flow	BARBB1L	288/84	-25.9807	30.843689	371.63-373.67	TH, AF, TH+AF	6	10^{-4}	DRILL OVERP	5 thru 35	299.3	39.8	114.0	11.5974	3
										ShW	20mT/580	295.7	7.4	105.0	12.0921	3
	Basaltic Komatiite Flow	BARB2A	288/84	-25.9807	30.843689	76.11-76.51	TH, AF, TH+AF	6	10^{-3}-10^{-4}	DRILL OVERP	1mT-540	45.9	43.7	55.9	10.320416	5
	Komatiite Flow	BARB2B	288/84	-25.9807	30.843689	187.24-189.62	TH, AF	6	10^{-1}-1		Noisy, Overprint Rev Drill & Drill. NW, SW DOWN & UP.					
	Basaltic Komatiite Flow	BARB2C	288/84	-25.9807	30.843689	335.07-338.47	TH, AF	9	10^{-3}-10^{-4}	ShE	3 thru 90	74.7	-7.0	8.3	24.729215	6
	Basaltic Komatiite Flow	BARB2D	288/84	-25.9807	30.843689	390.84-400.25	TH, AF, TH+AF	7	10^{-1}-1	S-SHALLOW	0mT - 570	173.5	6.1	24.3	12.505845	7

Table 4.1. (cont.) Overprint and high temperature directions measured in this study. Strike and dip refer to bedding planes measured in the field and validated against measurements from regional scale geological maps. Dec and Inc refer to the direction of the components in geographic coordinates before applying the plunging fold correction. N refers to the number of samples measured whilst n is the number of specimens used to calculate the site mean.

4.5.1.1 Description of Overprint Components

4.5.1.1.1 LKM Surface samples

The komatiitic samples from the LKM sites, (see Figures 4.3 & 4.19), are characterised by two components, a low temperature overprint component and a high temperature component. Data collected from the trondhjemitic dyke (LKM2) and komatiitic basalt, LKM4, were scattered and it was not possible to isolate site means from the results. Scattered results are thought to be acquired during sample acquisition, due to inaccuracies in orientation, and handling during laboratory experiments. NRM intensities for the LKM sites ranged from 10^{-4} to 3.8 A/m. There is no obvious correlation between lithologies and measured NRM intensities, unlike that shown in the results of Yoshihara and Hamano (2004). Lithologies were attributed to sites during sampling on textural observations in the field. However, detailed geochemical analysis is required to accurately classify the rocks sampled, as suggested in Dann (2000). Detailed geochemical analysis is beyond the scope of this study and it is therefore possible that some sites classified as basaltic komatiites could in fact be komatiites and vice versa. This could explain the elevated NRM intensity of LKM1 when compared to the other LKM sites.

An in-situ, moderately steep and north component, LT1, observed in four sites (mean direction, declination/inclination (D/I)=351.43°/–42.29°, $\hat{k}$= 15.03, α95=10.19°), was generally removed by thermal demagnetisation in temperatures ranges from 20-440°C, although persisted to 480°C in samples from site LKM3 and to 540°C in samples from LKM1. The LT1 direction produces a pole (in geographic coordinates) that plots between the present-day field (PDF) and geocentric axial dipole (GAD) poles and therefore very likely records a recent field direction acquired as a viscous remenant magnetisation (VRM).

4.5.1.1.2 BARB Cores

The BARB core samples were particularly noisy and reflect the non-ideal rock magnetic characteristics (see section 3.2) and sample orientation problems. Six to eight samples, from each site, were demagnetised thermally or using an alternating field. NRM intensities for the BARB sites ranged from 10^{-4} to 6 A/m. As with the surface samples, no correlation is seen between lithology and NRM intensity recorded (Figure 4.12).

The drilling direction in BARB1 has an azimuth/dip (a/d)=307°/47° whilst in BARB2 the drilling direction is 036°/43°. Samples from both BARB1 and BARB2 are dominated by a pervasive overprint, which is observed in a parallel and antiparallel direction, in the drill-

ing direction and is, therefore, interpreted as a drilling induced overprint. Overprint components were generally removed by thermal demagnetisation to 400°C, although in site BARB1c they persisted up to 440°C. In most alternating field demagnetisation cases overprint components were removed by 15mT, although they persisted to 50mT in site BARB2d. In some cases, the samples do not preserve a primary direction as the demagnetisation spectra are fully dominated by the drilling overprint. This behaviour is clearly seen in BARB2a (Figure 4.12).

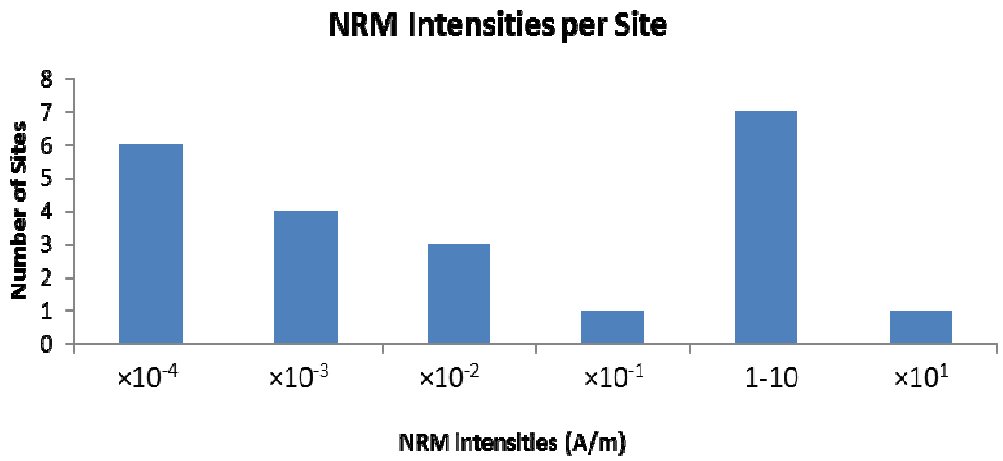

Figure 4.12. Histogram of NRM intensities measured per site across the Komati Formation. The range of intensities is evenly distributed across lithologies. Unbaked, baked and intrusives are represented in each NRM intensity range. Therefore, there is no obvious correlation between lithologies and intensity recorded.

4.5.2.1 Description of Characteristic Components

It was possible to isolate three characteristic components from the intrusives, baked and unbaked rocks from both the surface and core samples. Grouping of mean directions is calculated at sample level, rather than at site level due to the poor quality of individual site means. Table 4.1 shows details of the directional data.

4.5.2.1.1 Unbaked Units

A Steep West (StW) convergent high temperature mean direction, declination/inclination (D/I)=267°/64°,k=26, α95=7.1°, N=15) is observed in unbaked units of both komatiite (BARB1l and LKM4) and komatiitic basalt (LKM5) composition, as is shown in Fig. 4.10 and 4.11. The StW sample mean direction is also shown on a stereographic projection in Fig. 4.9. The direction is not clearly resolved in the BARB drill core sites. StW is isolated at temperatures between 440°C-580°C/70mT,(Fig.4.9). In some, but not all cases, the ShW direc-

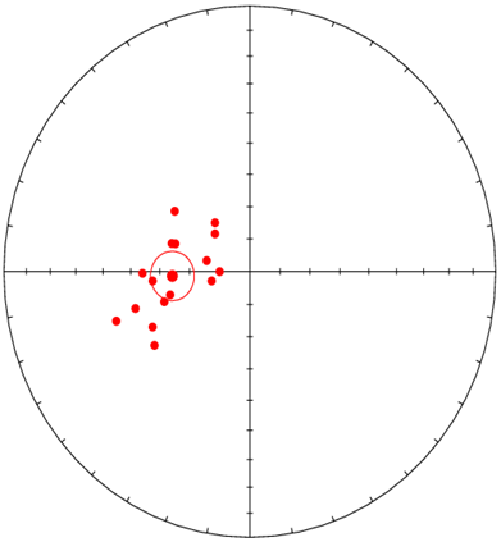

Figure 4.13. Stereographic projection of StW sample mean direction.

tion (see detailed description of this direction in section 4.5.2.1.2) is clearly seen to overprint the StW directions, (Fig. 4.8d). The StW direction is never observed in the intrusives, as can be seen in Figs.4.9 to 4.11.

The StW direction is consistent with results from previous studies, including Yoshihara & Hamano, (2004) and (Hale and Dunlop, 1984). The StW direction is commonly isolated from strong samples with NRM intensities above 1A/m. This is consistent with the behaviour observed by Yoshihara & Hamano, (2004). Despite this similarity, the unblocking behaviour between the StW direction isolated as part of this study and that in Yoshihara & Hamano's 2004 study is quite different. Yoshihara & Hamano, (2004), observe high unblocking temperatures, concentrated above 570°C, with over half of the initial NRM remaining until this temperature step. As described above, this is not the case for the StW in this study.

Sites LKM4 (komatiite), LKM6 (basaltic komatiite), BARB1a (hylocalstite) BARB1h (komatiitic basalt) and BARB1l (komatiite) also sample unbaked rocks. The directions isolated from samples in LKM4 are mostly scattered, but as is seen in Figure 4.9, (see the equal area projection for site LKM4), some samples do give a StW direction which is used in the calculation of the StW mean direction. Directions from LKM6, BARB1a, BARB1h were too scattered to yield meaningful results (see Figure 4.9 & 4.10).

Sites in drill core BARB2 sample only unbaked units of predominantly basaltic komatiite composition. As described in section 4.5.2.1.1 the rocks from site BARB2a (komatiitic basalt) are dominated by a pervasive parallel drilling overprint which overprints any primary signal. The same is true for komatiite rocks of BARB2b.

Site BARB1l records a Shallow West high temperature component (ShW) which is described in detail in section 4.5.2.1.2, below.

Site BARB2d (basaltic komatiite) does not preserve directions that are consistent with results from any of the other Komati Formation sampling sites (see figure 4.12). A single,

south east/south component is isolated in seven samples, with mean direction: declination/inclination (D/I)=173.5°/61°, k= 24.3, α95=12.5°). NRM intensities for the site are unusual when compared to the other sites. The site is located over 250m away from the nearest dyke, but only 30m away from the base of the core. Despite BABR2d being an amphibolites according to the BARB drill project cores, here it is interpreted as a basaltic komatiite given textural and petrological similarities with other sampled basaltic komatiites sampled as part of this study. Studied samples from BARB2d record a range of NRM intensities from 10^{-1} to 5 A/m.

4.5.2.1.2 Intrusive Units

As can be seen in Figures 4.9 & 4.10, the intrusive units of gabbrotic/dacitic composition, sampled as part of this work yield mostly inconclusive results. Whilst high temperature components have been isolated from the five intrusive units sampled, it was only possible to use directions from BARB1d, BARB1f and BARB1g to contribute towards calculating component means. Directions from site BARB1f are entirely overprinted by the drilling process with the exception of one sample which yields a ShE direction, described in detail below. The ShE direction is also isolated in some samples of site BARB1d. The results of site BARB1g are mostly scattered but one sample was used in the calculation of a ShW (also described in detail in section 4.5.2.1.3, below). The directions from sites LKM2 and BARB1j were too scattered to yield any meaningful results. The StW component is never observed in the intrusive units.

4.5.2.1.3 Baked Units

A total of seven baked units of both komatiitic and basaltic komatiite composition were sampled as part of this study.

A Shallow East high temperature component (ShE) was isolated in the baked rocks, as well as in the unbaked units and the intrusives (see text above), with unblocking temperature ranges between 200°C and 580°C/90mT by TH and AF demagnetisations. Characteristic Zijderveld Plots showing demagnetisation behaviour of the direction are shown in Fig.4.9b and f. Direction ShE was observed in six sites (mean direction, declination/inclination (D/I) =68.1°/–3.2°, k= 5, α95=15.4°, N=22). See Table 4.1. and Figs. 4.9 to 4.11.

Samples from a number of sites were seen to readily alter during TH demagnetisation. During TH demagnetisations, samples were reversed (along the Y-Zaxis), in the oven at

each demagnetisation step. If samples are prone to alteration and/or if residual field is significant, this results in the demagnetisation curves being characterised by a zigzag. This is clearly seen in of some of the Zijderveld plots (include Z-Plot of BARB1L6 to illustrate) from BARB1, as seen in Fig. 4.8a as well as h. Although directions for ShE component are scattered (k̂=5, see for example and may warrant the removal of potential outliers, when plotted against a curve for a standard Fisher distribution, the dataset fits the shape of the Fisher distribution accurately and so the removal of outliers is not justified (Figure 4.14).

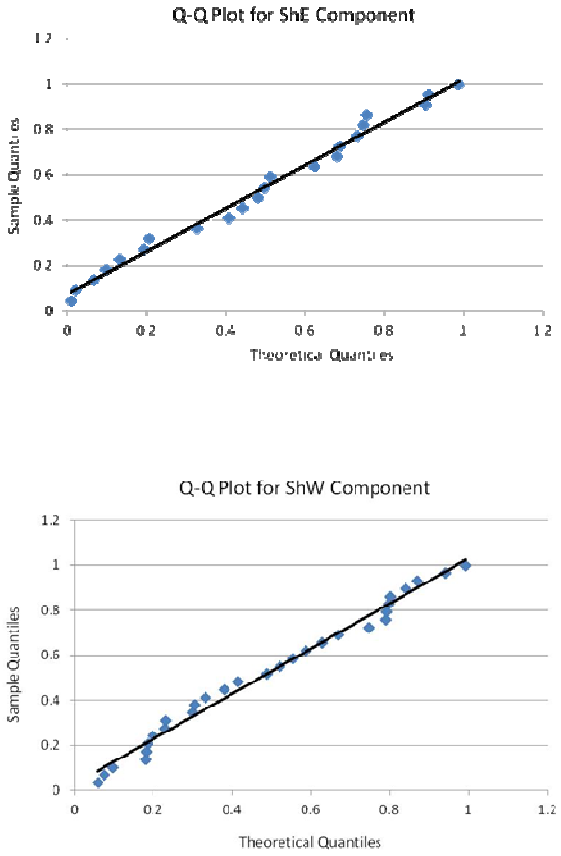

Figure 4.14. Quantile-Quantile Plots of quantile values for the ShE direction vs. a theoretical Fisher distribution (top); -Quantile values for the ShW direction vs. a theoretical Fisher distribution (bottom).

A Shallow West high temperature direction (ShW, mean direction, declination/inclination (D/I)=259.9°/7.2°, k̂= 13.3, α95=7.6°, N=29), was isolated in a total of seven sites: six baked and one unbaked unit. Unblocking ranges are between 20mT and 90mT/580°C by AF and TH demagnetisations. When plotted against a curve for a standard Fisher distribution, the dataset for the ShW components fits the shape of the Fisher distribution accurately and so the removal of outliers is not justified, as shown in Figure 4.14.

4.5.2.1.4 Field Tests

It is noteworthy that both the ShE and ShW components are associated with very weakly magnetised samples, with original NRM values ranging between 10^{-4} to 10^{-1} A/m. In addition, these directions are predominantly present in samples taken from the younger intrusions and associated baked komatiites.

A reversal test was carried out to establish if the ShE and ShW components are antipodal. The classification as described by (McFadden and McElhinny, 1990) was applied to the dataset and the dataset passes the reversal test with classification C. Although directions for ShW component are scattered ($\hat{k}$=13), quantile-quantile plots (Figure 4.14) show that both sets of data have a Fisherian distributed and so the standard reversal test can be applied without the need to remove outliers.

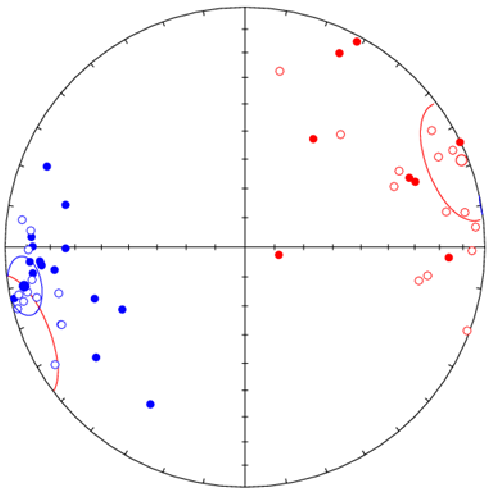

Figure 4.15. Stereographic projection of antiparallel directions of ShE (shown here in red) and ShW (shown here in blue).

The sampling strategy for both the surface and drill core sites was designed with the aim to constrain the ages and viability of potential near primary directions isolated from the samples, as described in 4.4..1. However, as seen in Figures 4.9 and 4.10 results from all sites that sampled intrusive and associated baked rocks yielded inconclusive results. In most cases this was a result of isolated ChRM directions being too scattered in either the intrusives or baked rocks, or because no ChRM directions were isolated. In total, four baked contact tests were attempted: one test was carried out on sites LKM1-LKM3 from the surface samples and three tests were attempted from sites BARB1b-BARB1d, BARB1e-BARB1g and BARB1i-BARB1k.

Sites LM1, LKM2 and LKM3 provide the most encouraging results of the four baked contact tests carried out. The directional results from LKM2, the dyke of trondhjemitic composition, are very scattered. The clustering of ChRM directions in site LKM3 is consistent with a ShW component. The ShW direction and the StW direction are isolated in LKM1 and some of the samples from this site clearly show the ShW overprinting the StW direction (see Figure 4.8d). Whilst this test remains inconclusive due to there being no clear ChRM direction isolated in the intrusive unit (although some samples do plot in the area which would be consistent with a ShW direction, as seen in Figure 4.9) both the baked units preserve the ShW direction. Given that the StW direction is seen at higher unblocking temperatures than the ShW direction in some samples of LKM1, it would not be unreasonable to assume that emplacement of the dyke caused overprinting of the StW direction by the ShW direction.

A comprehensive baked contact test, which sampled baked and unbaked units at an increasing distance from the intrusive unit, was attempted in sampling sites BARB1b-BARB1d (117.7-120.1m), as seen in Figure 4.10. However, it was not possible to sample the entirety of the proposed section of core below BARB1d due to it being too friable to drill for palaeomagnetic samples. Therefore, it was only possible to drill sites from the baked units above the dacitic intrusion at BARB1d, resulting in an inconclusive baked contact test. Site BARB1b, 2m away from the intrusion, gives ChRM directions which are scattered to the north east, inconsistent with any other directions isolated in the Komati Formation rocks. The lowermost samples in BARB1c are 50cm away from the intrusive unit and although there are insufficient directions to calculate a site mean, the results obtained are consistent with a ShW direction. Directions in the intrusive dacite are scattered but consistent with a ShE direction. As with sites LKM1-3 the results of this baked contact test are inconclusive, but point towards the ShE/ShW direction being associated with the emplacement of the intrusive units across the Komati Formation.

It is not possible to draw meaningful results from the baked contact test performed on sites BARB1e-BARB1g (208.7-222.8m, see Figure 4.9). In the BARB Drill Project logs site BARB1g is described as a komatiitic basalt unit containing pyroxene (and therefore targeted for sampling due to it likely being comparable to Yoshihara & Hamano's (2004) peridotitic samples). However, during sampling, I interpreted the overlying intrusive gabbro (BARB1f) to be thicker than was indicated in the BARB Drill project logs and to include site BARB1g, due to the petrology in hand specimen. At this depth the rocks are still medium

to coarse grained, light grey with milky white phenocrysts of plagioclase. This mineral assemblage is more consistent with a gabbro/trondhjemite composition than with a komatiite. Furthermore, it was not possible to sample below the depth of the dyke due to the orientation of the core not being reliable. Directions isolated from the baked komatiite in BABR1e indicate the presence of a ShW and/or StW component which are indistinguishable, possibly due to the ShW and StW components overlapping in the demagnetisation spectra. Whilst the results of this baked contact test are also inconclusive, the presence of the ShE component in the samples of the intrusive body reinforces the possibility that the ShE/ShW direction is associated with the emplacement of the intrusive units.

The sampling of sites BARB1i to BARB1k (329.7-332.6m) provided the final opportunity to perform a baked contact test from the rocks of core BARB1, see figure 4.9. Although site BARB1i (baked komatiite) is largely affected by the drilling overprint, it was possible to isolate the ShE component from three samples. Results from the intrusive gabbro (BARB1j) were found to be scattered and no meaningful direction was isolated from the unit. The samples from site BARB1k (baked komatiite) were entirely overprinted by the drilling of the core and no primary directions were isolated in this unit. This is perhaps the least conclusive of all the baked contact tests performed on the sites of the Komati Formation. Having said that, combined with the findings of the baked contact test discussed above, the isolation of the ShE component in the baked komatiites of site BARB1i is consistent with the shallow east/west direction being associated with the emplacement of the dykes.

4.6. Rock Magnetic Characterisation

The unblocking temperature spectra observed in the rocks of the Komati Formation suggest that the main magnetic carrier is magnetite (see Figure 4.8). Curie Temperatures (T_c)= 550°- 604°C established from thermomagnetic curves are indicative of the presence of magnetite and/or maghemite in the samples, Figure 4.16. VFTB thermomagnetic curves are highly reproducible, as shown in Fig. 4.16 sample LKM with the exception of LKM2 and LKM3, indicating that alteration on heating is minimal or non-existent. IRM acquisition curves exhibit saturation below 200-300mT (See Figure 4.17). In combination with hysteresis curve analysis, this suggests the presence of a low coercivity mineral, such as magnetite. In addition, analysis of hysteresis curves indicates samples are characterised by a combination of the ferromagnetic and paramagnetic fraction. Twelve of the 35 samples measured displayed dominantly paramagnetic behaviour as seen in Table 4.3. Hysteresis

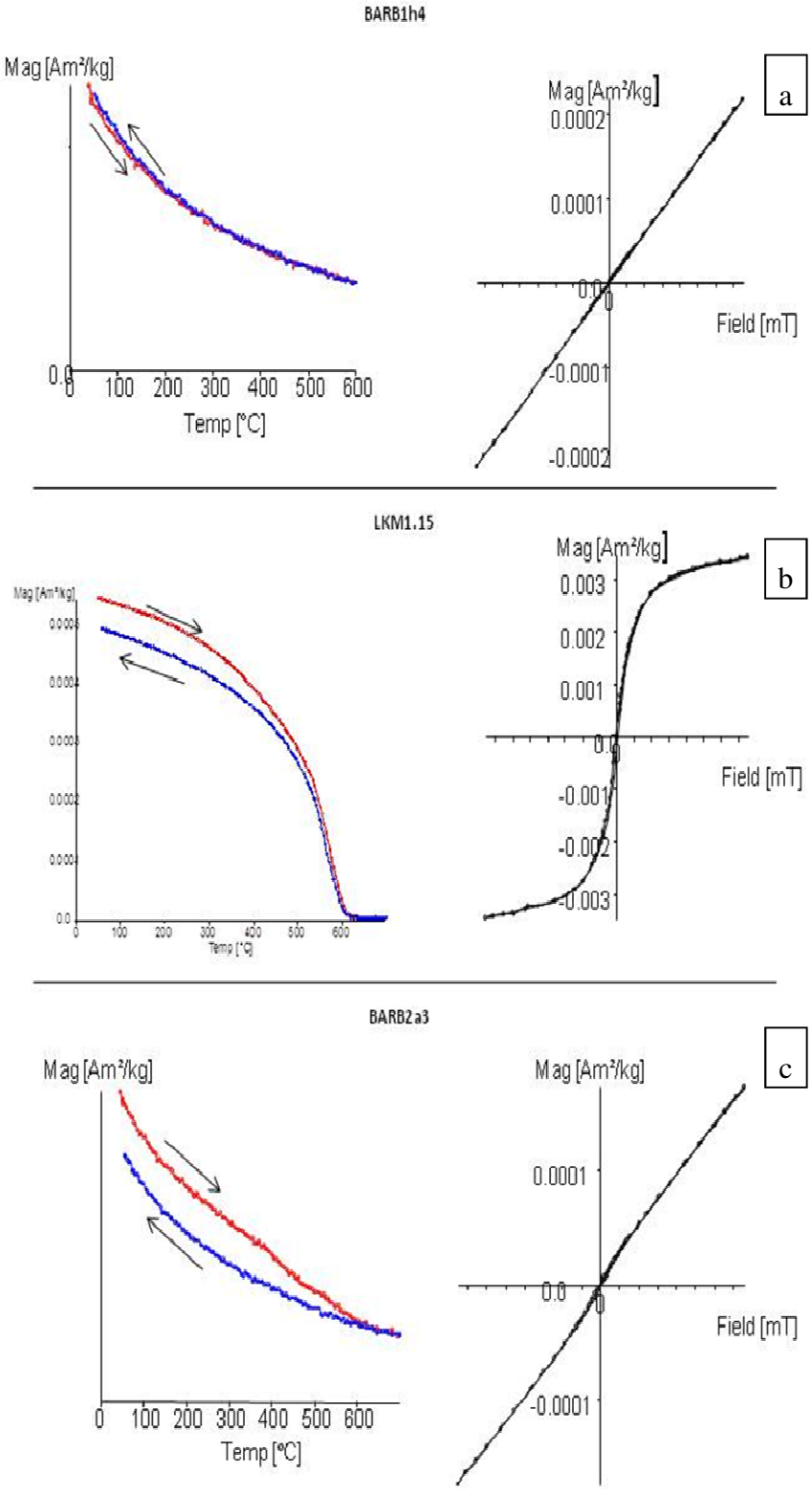

Figure 4.16. Thermomagnetic curves (left) and hysteresis loops (right) for samples BARB1h4 (a), LKM1.15 (b), BARB2a3 (c). Heating curves are shown in red and highlighted by the downward pointing arrow, whilst cooling curves are shown in blue and upward facing arrows, in the thermomagnetic curves. The chosen samples illustrate the common rock magnetic behaviour seen in samples of the Komati formation. (a) Samples are often dominated by the paramagnetic fraction, as is the case for BARB1h4. (b) Sample LKM1.15 shows little alteration upon heating and a very narrow hysteresis loop.

parameters and thermomagnetic curves measured for samples from the same site are reproducible and suggest uniform distribution of magnetic carriers throughout the individual units sampled (Fig. 4.16.a,b &c). Site LKM3 is the exception, sample LKM3.4bb is dominated by the paramagnetic fraction and the thermomagnetic curve shows no alteration; this is in agreement with magnetic susceptibility results obtained using the Kappa Bridge for the same sample. However, LKM3.9bb has a lesser paramagnetic contribution, a T_c 425°C and alters significantly on cooling.

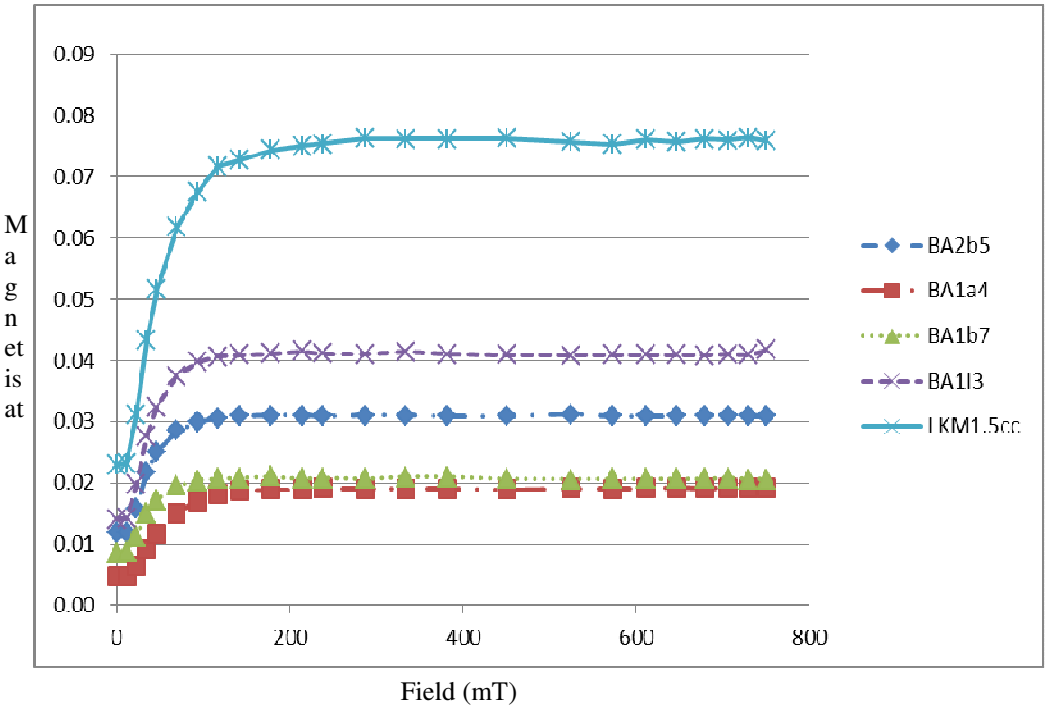

Figure 4.18. IRM acquisition curves for a selection of samples across the Komati Formation. Samples of the Komati Formation commonly saturate below 110mT.

Hysteresis parameters are plotted on a Day plot (M_{rs}/ M_s) and (H_{cr}/ H_c) (Day et al., 1977) and show all samples from this study plot in the MD (multi domain) and PSD (pseudosingle domain) sections of the plot (Figure 4.18). The narrowness of the hysteresis loops in some samples could suggest a contribution from the superparamagnetic fraction (Figure 4.16c), which can dominate the signal in some samples (Dunlop & Özdemir, 1997). Very fine grained particles show strong frequency dependence. Changing the frequency to which the sample is exposed is equivalent to changing the amount of time available to the magnetic grains within the sample to react to a change in the applied field strength. Therefore, measuring frequency dependent susceptibility (χ_{fd}) can be used to establish grain size. The magnetic susceptibility as a function of frequency was measured (at room tempera-

ture) for a sample from each Komati Formation site. A drop in magnetic susceptibility with increasing frequency would indicate the presence of superparamagnetic particles. As is shown in Figure 4.19 magnetic susceptibility does not change significantly when the frequency is increased (from 976Hz to 3904Hz and onto 15616Hz) for any of the measured samples. Therefore, despite the narrowness of the hysteresis loops, the presence of superparamagnetic particles can be ruled out for the samples of the Komati Formation.

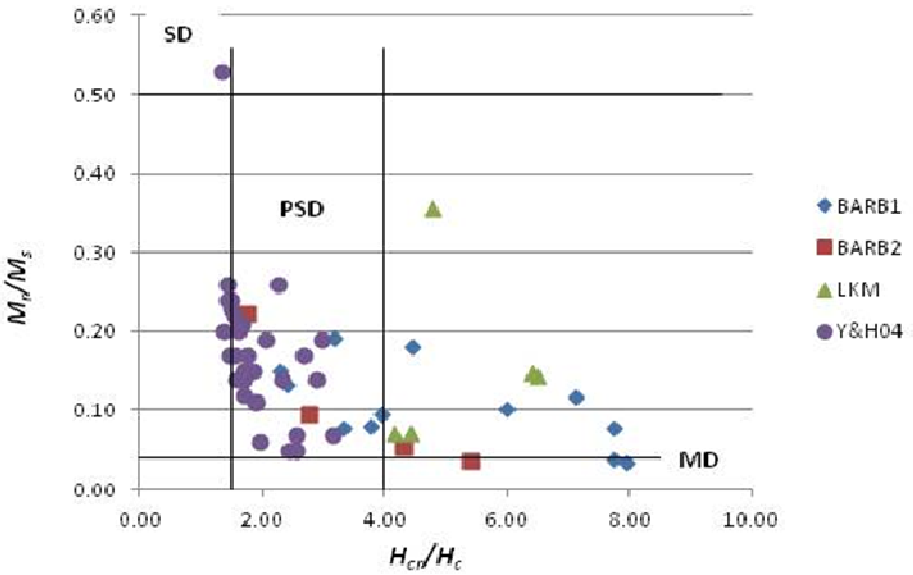

Figure 4.18. Day Plot, (Day et al., 1977) for samples of this study and also samples of the Komati Formation from Yoshihara & Hamano, 2004 (referred to as Y&H04, in plot). SD: Single Domain; PSD: Pseudosingle domain; MD: Multidomain.

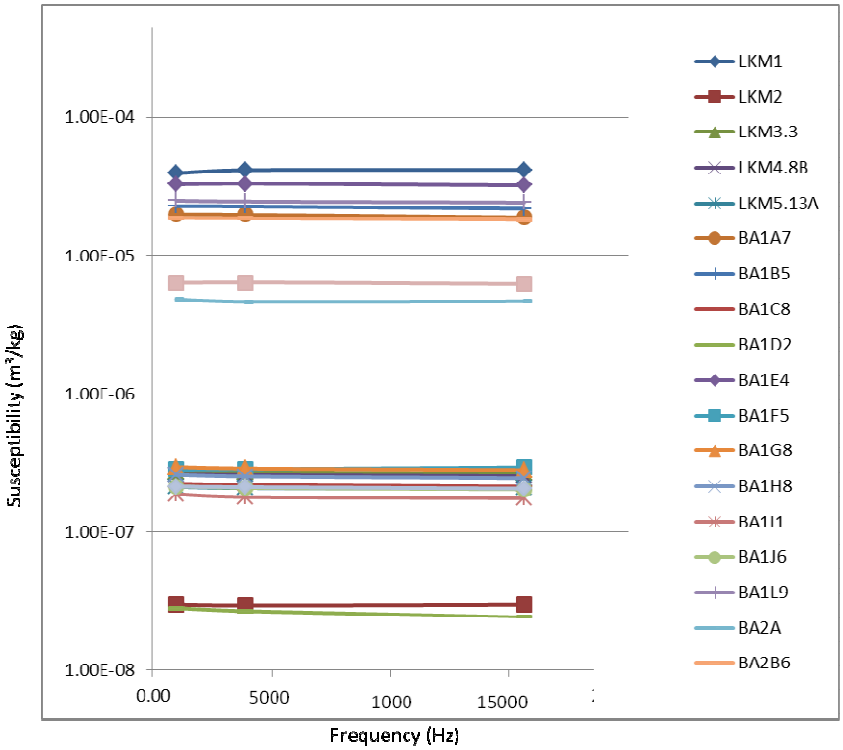

Figure 4.19. Magnetic susceptibility as a function of frequency. Variation of susceptibility with frequency is minimal and therefore suggests the samples do not contain superparamagnetic particles.

Magnetic susceptibility measured as a function of high and low temperature results from six surface samples and 16 BARB core samples support the findings of the experiments performed on the VFTB. In samples which are not dominated by the paramagnetic fraction, T_c is measured at 575°C- 585°C, indicating the presence of magnetite. Measured Verwey transitions at 140K also indicate the presence of magnetite. In cases where the signal is dominated by the paramagnetic contribution results can be noisy and T_c difficult to establish. Thermomagnetic curves are mostly reproducible in the sample set, with some exceptions (Figure 4.20), indicative of samples altering upon heating, as was observed in the thermal demagentisations.

The results presented mean establishing the mineral carrying the magnetisation in the samples of the Komati Formation is problematic. The T_c calculated in the VFTB experiments is indicative of maghemite, whilst the shape of the thermomagnetic curves is consistent with magnetite. The demagnetisation spectra observed in the samples (see Figure 4.8) are also consistent with magnetite. Both low and high temperature susceptibility experiments (curve shape and calculated T_c) are also consistent with magnetite. Maghemite is not an unlikely carrier, as it is a low temperature alteration product of magnetite (either

when exposed to hydrothermal alteration at the sea bed, likely for the Komati samples, or due to surface weathering). The discrepancy between T_c calculated from VFTB experiments and Kappa Bridge experiments was investigated further by measuring thermomagnetic curves and high temperature dependant susceptibility from the same sample from four sites. Of the four experiments conducted, T_c calculated from VFTB results ranges between 593°C-604°C (as expected from previous VFTB results). Inflection points measured from high temperature susceptibility results ranges between 574°C-577°C. See Figure 4.21 for a comparison of the results. Despite the T_c from the VFTB indicating the presence of maghemite, all other evidence is consistent with magnetite being the magnetic carrier. Comparing the high and low temperature magnetic susceptibility results to those of the VFTB indicates that the VFTB maybe overestimating the T_c for Komati Formation.

Rock magnetic characterisation of samples from BARB2d (which gives an anomalous direction, see section 4.5.1) shows the sample to be mostly ferromagnetic with a paramagnetic contribution, with coercivities lower than those observed in other BARB2 samples, but comparable with results from both BARB1 and LKM samples. The magnetic carrier is interpreted to be thermally stable, multidomain (see Day Plot, Fig. 4.18), maghemite.

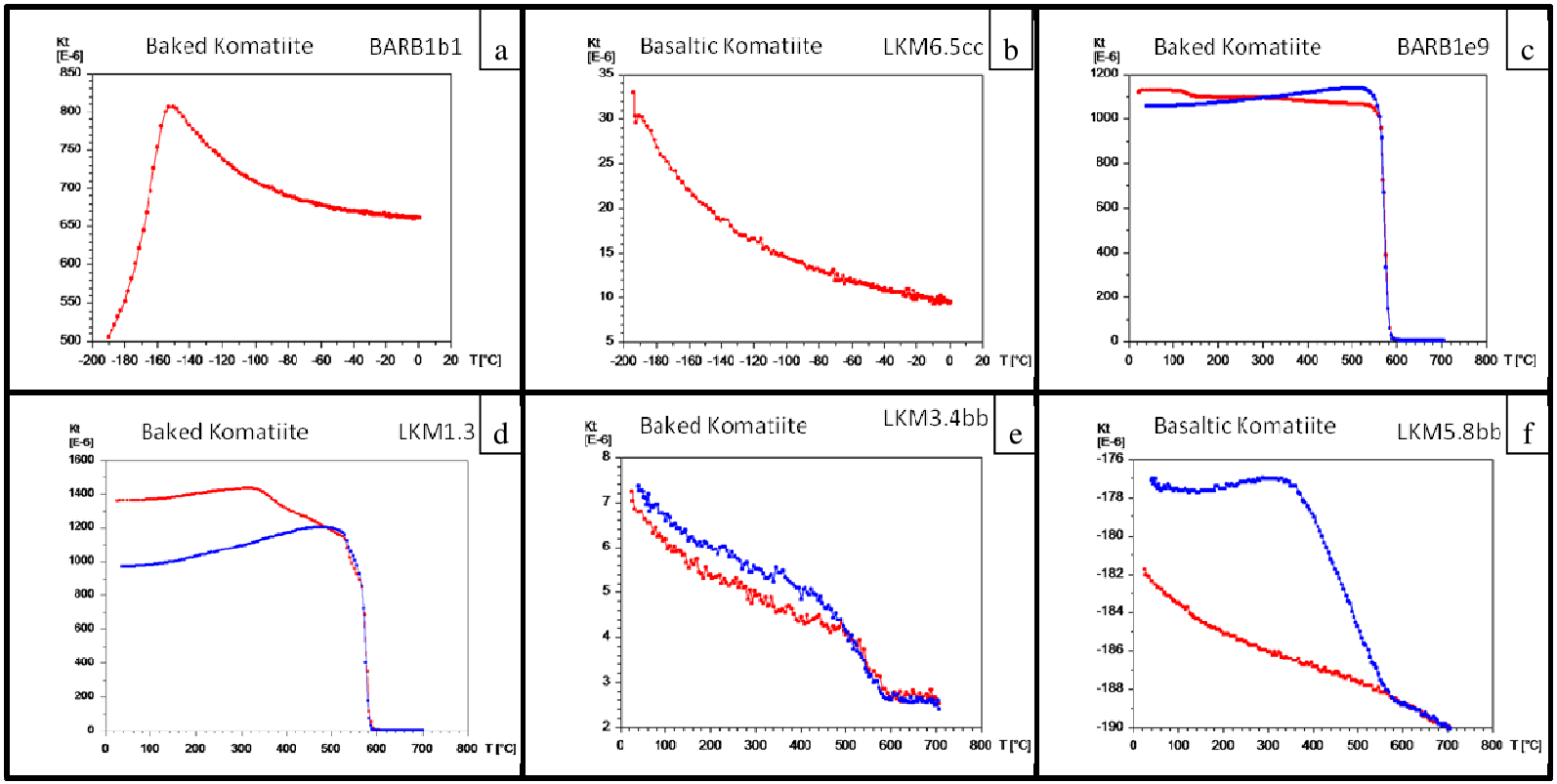

Figure 4.20 Magnetic susceptibility measured as a function of temperature, Kappa Bridge; (a) Verwey transition of magnetite as sample warms up from liquid nitrogen temperature (-196°C); (b) Sample is dominated by the paramagnetic fraction and so no Verwey transition is identified; (c&d) Surface and drill core samples showing magnetite as the magnetic carrier. Sample LKM1.3 shows alteration upon heating and a minor phase at Tc ~375°C; (e) LKM3.4bb is dominated by the paramagnetic fraction in VFTB results, but a Tc of 580°C is identified using the Kappa Bridge; (f) Sample alters significantly upon heating.

Site	Sample	Ms (Am^2/kg)	Mr (Am^2/kg)	Hc (mT)	Hcr (mT)	Mr/Ms	Hcr/Hc	Tc (°C)
BARB1	Ba1a1	1.95	0.07	3.44	27.34	0.03	7.95	596
	Ba1a4	5.35E-03	1.03E-03	8.64	27.34	0.19	3.17	
	Ba1a7	2.14	0.08	3.41	26.41	0.04	7.75	588
	Ba1b7	1.10	0.08	3.41	26.41	0.08	7.75	588
	Ba1c5	0.03	0.08	7.10	23.53	0.13	2.40	
	Ba1d5	1.22E-03	1.42E-04	8.11	57.62	0.12	7.11	548
	Ba1e9	0.97	0.10	7.41	44.33	0.10	5.99	588
	Ba1e9a	0.85	0.08	7.40	29.16	0.10	3.96	592
	Ba1e10	0.18	0.02	8.70	-	0.09	-	593
	Ba1f6	8.99E-03	1.62E-03	12.76	56.80	0.18	4.45	
	Ba1g9	6.08E-03	9.15E-04	25.13	57.62	0.15	2.29	
	Ba1h4				Paramagentic			
	Ba1h9				Paramagentic			
	Ba1i4				Paramagentic			
	Ba1i6				Paramagentic			
	Ba1j9				Paramagentic			
	Ba1k6				Paramagentic			
	Ba1l3	2.35	0.19	5.84	19.43	0.08	3.33	598
	Ba1l4	2.70	0.22	6.00	-	0.08	-	603
	Ba1l8	2.26	0.18	5.55	20.94	0.08	3.77	594

Table 4.2 Hysterisis parameters for the Komati Formation. M_s, saturation magentisation; M_r, saturation remenance; H_c, coercivity, H_{cr}, coercivity of remenance; T_c, Curie Temperature.

Site	Sample	Ms (Am^2/kg)	Mr (Am^2/kg)	Hc (mT)	Hcr (mT)	Mr/Ms	Hcr/Hc	Tc (°C)
BARB2	Ba2a3	0.01	2.30E-03	11.86	20.94	0.22	1.77	paramagentic
	Ba2b5	1.77	0.17	6.59	18.29	0.10	2.78	593
	Ba2b6	1.73	0.14	5.80	-	0.08	-	604
	Ba2c3				Paramagentic			
	Ba2d1	0.80	0.04	4.33	18.58	0.05	4.29	595
	Ba2d6	0.35	0.01	3.79	20.41	0.04	5.39	594
LMK1	LKM1.3cc	3.77	0.34	5.60	-	0.090318	-	603
	LKM1.5cc	3.7393E-06	2.6551E-07	6.04	25.07	0.07	4.15	588
	LKM1.15bb	2.56	0.18	5.92	26.20	0.07	4.43	600
LKM2	LKM2.5b	1.30E-03	4.61E-04	14.92	71.52	0.36	4.79	paramagentic
	LKM2.12bb				Paramagentic			
LKM3	LKM3.4bb	3.73E-03	5.34E-04	8.15	50.00	0.14	6.51	paramagentic
	LKM3.9bb	3.63E-03	2.89	8.28	53.07	0.15	6.41	419
LKM4	LKM4.4b				Paramagentic			
LKM5	LKM5.2cc				Paramagentic			
	LKM5.8bb				Paramagentic			
LM6	LKM6.3cc				Paramagentic			
	LKM6.5cc				Paramagentic			

Table 4.2 Continued

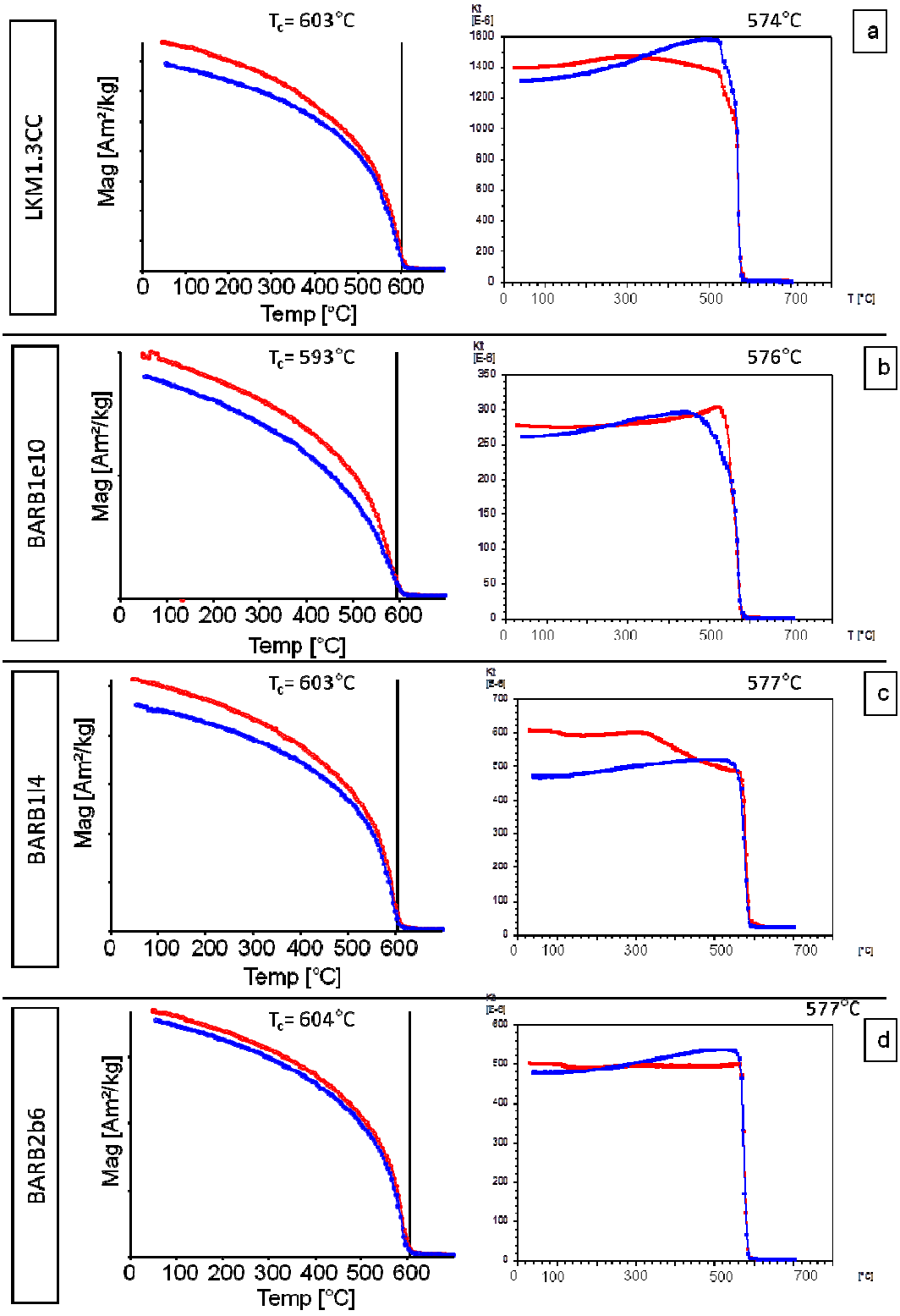

Figure 4.21. Comparing calculated T_c from VFTB acquired thermomagnetic curves and Kappa Bridge acquired temperature dependant susceptibility curves (both conducted at room temperature). Curves on the left correspond to VFTB acquired data, curves on the right correspond to Kappa Bridge acquired data.

4.7. Microscopy Observations

The rocks of the Komati Formation incorporate units that range in composition between komatiites, basaltic komatiites and basalts. These have been largely serpentinised (Dann, 2000) due to significant amounts of hydrothermal alteration. Samples from sites LKM1, LKM2 and LKM5 were examined using an optical microscope and Philips XL30 tungsten filament SEM to better understand the mineralogy and thermal history of the sample, whilst the scanning electron microscope (SEM) was also used to analyse the composition of the minerals. No thin sections of the BARB cores were available to be studied.

Sample LKM1.11 (baked komatiite, Fig. 4.22 e&f) was chosen due to its high NRM intensity values, in addition to rock magnetic results for the site being consistently dominated by the ferromagnetic fraction. Sample LKM2.6 (trondjehimitic intrusion, seen in Fig 4.22 g&h) was selected so as to compare the magnetic carriers within the komatiite host rocks with those found in the intrusive rocks, whilst sample LKM5.12cc (komatiitic basalt, shown in Fig 4.23 a-c) was selected due to it being representative of the sites where rock magnetic results were dominated by the paramagnetic fraction and characterised by low NRM intensities.

Previous results have shown that the common microscopic assemblage for the komatiites of the BGB is olivine (often altered to antigorite), clinopyroxene, chromite, tremolite, chlorite and magnetite (Parman et al., 1997; Viljoen and Viljoen, 1969a). Magnetite is formed as a result of the serpentinisation of olivine and is typically found along the edge of the olivine minerals, (Hale & Dunlop, 1984) as well as a metamorphic overgrowth on chromite (Parman et al., 1997; Viljoen and Viljoen, 1969a). The main cause for serpentinisation is hydrothermal alteration as a result of exposure of the rocks to a body of water and is consistent with the interpretation that the rocks of the Komati Formation were erupted in a submarine environment. Whilst metamorphism is heterogeneous and has altered the primary composition of the komatiites, primary igneous compositions and morphologies are retained (Parman et al., 1997). The mineralogy of the tonalitic dykes and sills which cross-cut the Komati Formation has not been studied in detail. Their primary composition is dominated by quartz and plagioclase; textures range from equigranular to porphyritic dependant on the thickness of the unit (Dann, 2000; Kamo and Davies, 1994).

Sample LKM5.12cc was found to be olivine rich but to have been almost entirely hydrothermally altered to serpentinite, giving the radial, spiralling textures see in Figure 4.22d.

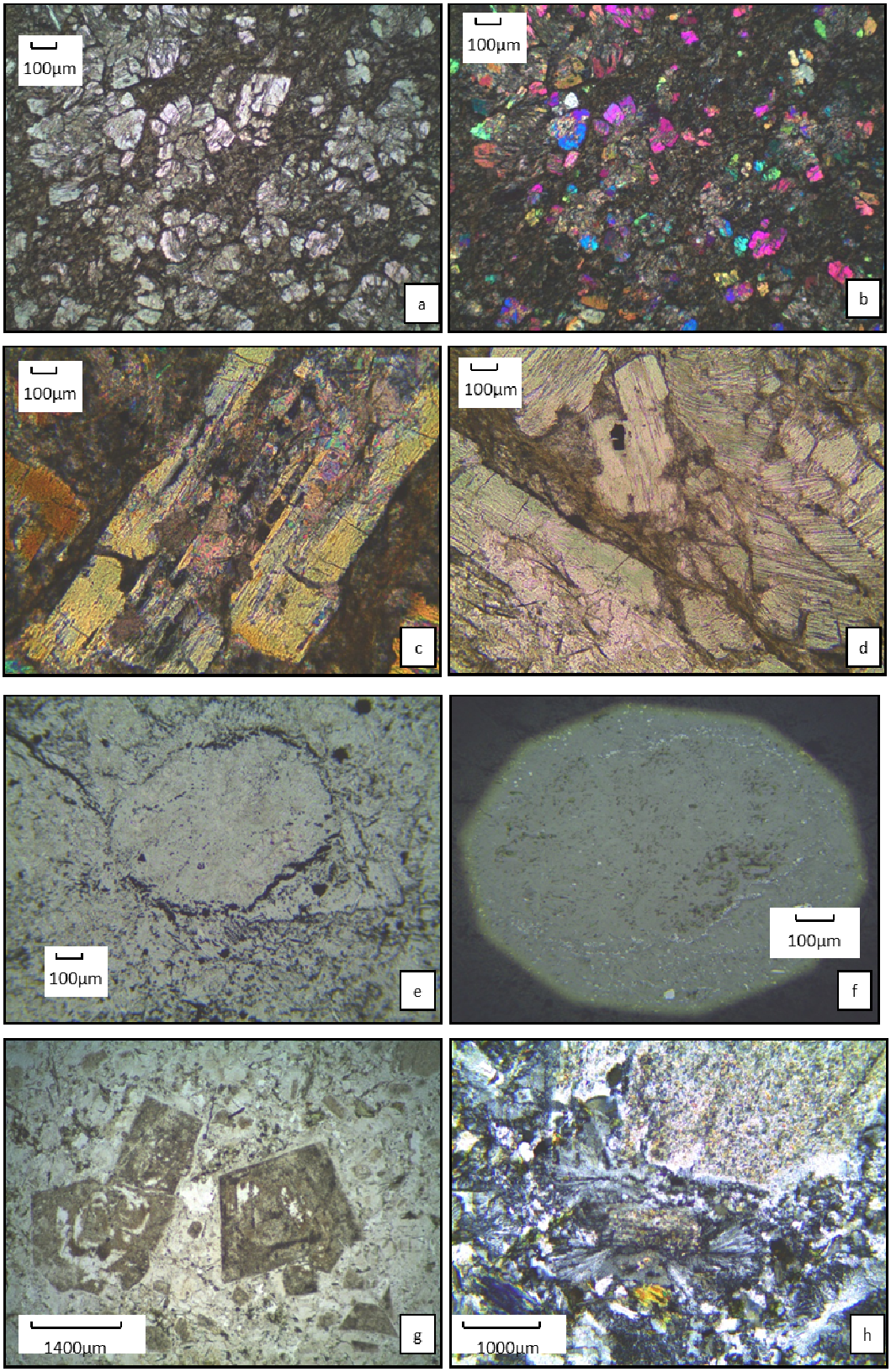

Figure 4.22 Optical Photomicrographs (a &b) show the primary mineralogy of the Komati Formation. Olive phenocrysts hydrothermally altered to serpentinite are surrounded by a groundmass of glass and plagioclase, sample LKM5.2cc. (c) Sericitization of plagioclase as seen in sample LKM5.12cc. (d) Radial spiralling structures typical of serpetinised olivines (chrysolite). (e & f) Reflected and transmitted light microscopy showing Fe-oxides forming along olivine mineral boundaries, as seen in LKM1.11. (g&h)Optical photomicrographs of sample LKM26 showing typical tonalitic mineral assemblage. Plagioclase phenocrysts are altered; groundmass consists, primarily, of quartz and chlorite.

However, the core of the olivine phenocrysts often remain intact, as shown by the high interference colours observed in cross polars and seen clearly in Figures 4.22a&b. This texture is indicative that the minerals were not in the presence of water for excessively long periods of time and consistent with the findings of Yoshihara and Hamano, (2004); (see also section 4.2 of this chapter for further details). Despite being logged as komatiitic basalt, the predominance of olivine suggests it is more likely a komatiite according to the classification of Dan, 2000, discussed in section 4.1 of this chapter. Relic olivine cores were observed, (Figure 4.22a&b). Typically, komatiites are characterised by limited amounts of plagioclase and this true for the thin section studied. Relic plagioclases (likely anorthite) were observed. Hydrothermal activity has caused the alteration of plagioclase to sericite (Figure 4.22c). A single grain of tremolite was also observed. Whilst reflected light microscopy revealed some opaque minerals, Figure 4.22e, when studied under transmitted light these had a yellowish tinge, more characteristic of iron sulphides, Fig. 4.22f.

Further work was carried out on the SEM to try and identify the opaque minerals and their relationship to the primary mineralogy. Energy dispersive X-ray spectra (EDX) were also acquired to try and identify the main minerals in the sample. Opaques tend to be bright when observed under the SEM and so minerals with these properties were targeted for X-ray analysis in order to identify likely FeO. However, no pure magnetite was identified. Opaque minerals were sparse and those identified had the mineral composition FeS and are, therefore, interpreted to be iron sulphides such as pyrite or pyrrhotite (See Fig. 4.23c). All the minerals expected to be identified in a komatiite were recognised: serpentine, chlorite, amphibole, tremolite/actinolite, sericite and clinopyroxene, seen in Figs 4.23a to c. However, no chromite was identified in sample LKM5.12cc. Due to the difficulties identifying Fe Oxides using electron imaging and EDX spectra alone (results of EDX spectra analysis are shown in Fig 4.23d), element x-ray mapping was carried out on three distinct areas of the sample to try and identify clusters of iron that may indicate the presence of Fe bearing opaque minerals. However, in all three maps produced, iron was found to be well scattered throughout the sample with no obvious clusters, indicating a lack of Fe bearing ore minerals (Figure 4.23g).

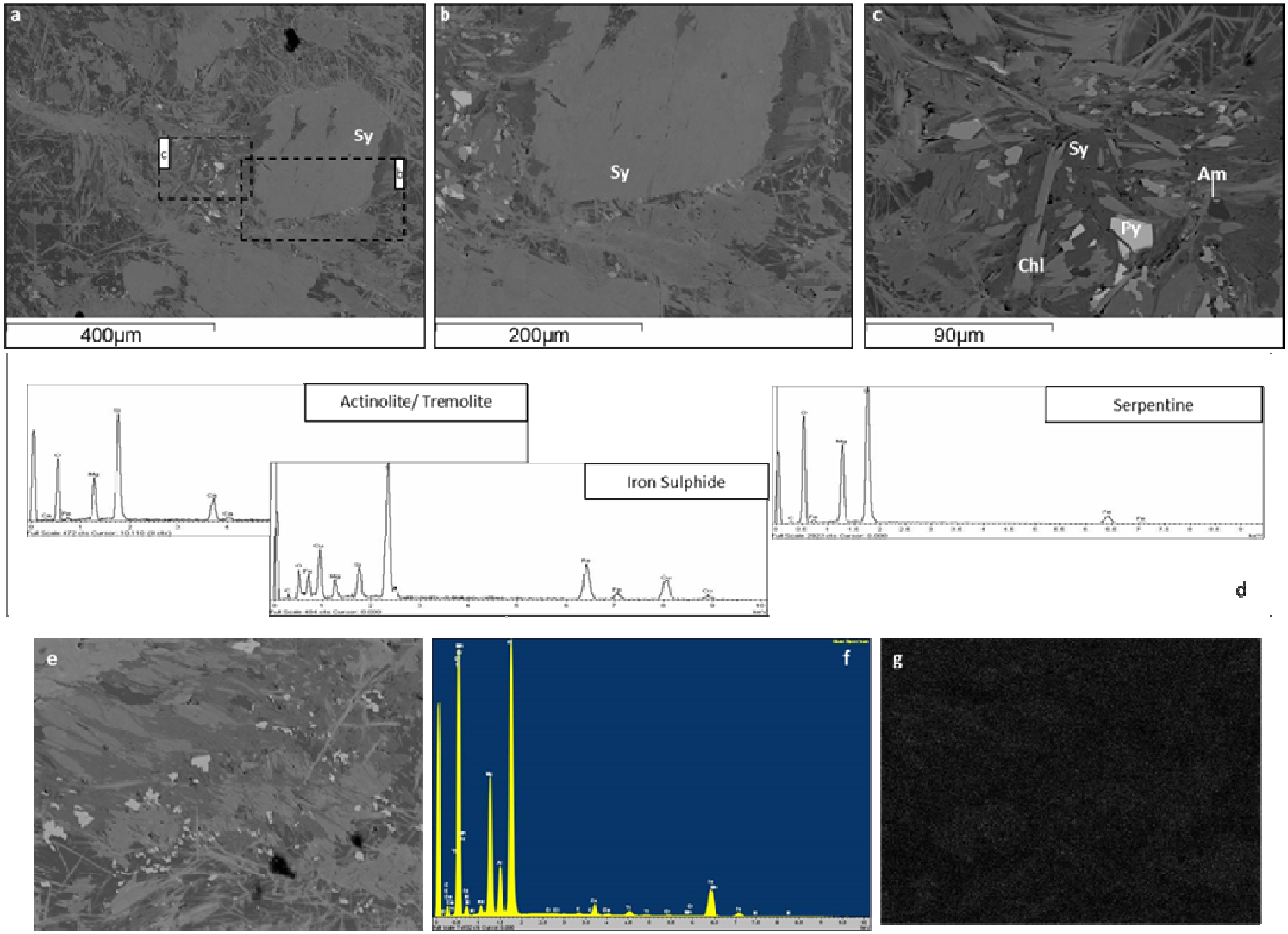

Figure4.23. Scanning Electron Micrographs of LKM5.12cc. (a) Area shows large serpentinised (Sy) olivines as well as chlorite (Chl), amphibole (Am), actinolite and iron sulphide. (b) Magnified area of edge of olivine mineral where magnetite is expected to be found. Pale grey and white minerals are clinopyroxene and actinolite. (c) Magnified area to left of large olivine seen in (a). Triangular, white mineal seen in centre of field of view (FOV) is identified as an Fe Sulphide, likely pyrite (Py). (d) EDX spectra showing main minerals identified in thin section. (e) Photomicrograph of an large area within LKM5.12cc, (f) sum EDX spectra of main element present in area (e); (g) Fe element X-ray map of area (e). Map indicates iron is well distributed across the imaged area, rather than concentrated, therefore indicating there are no Fe-Oxides in the thin section.

Sample LKM1.11 is almost entirely serpentinised indicating extensive alteration throughout. Under the optical microscope, the sample was found to be consistent with the description of a komatiite, as given by Dann 2000: the specimen was almost black due to an abundance of opaque minerals in the groundmass, as is evident in Figs 4.22e&f. Overall, the thin section was porphyritic with phenocrysts of olivine serpentinised to antigorite and chrysolite, as identified by the radial textures observed in some phenocrysts. Unlike sample LKM5.12cc, few of the olive cores remained intact, implying longer exposure to hydrothermal fluids, as expected given the extensive serpentinisation. Consistent with the findings of Hale & Dunlop, (1984), submicron blebs of magnetite were observed concentrated along the grain boundaries of the relic olivines, as seen in Figures 4.22e&f and 4.24a&c. These were identified using both transmitted and reflected light microscopy.

Analysis of the thin section in the SEM confirmed the findings of the optical microscopy work. Sample LKM1.11 was dominated in the main by minerals with a composition of Mg, O, Si and Fe, (as seen in the elemental spectra shown in Figure 4.24b), consistent with serpentine. In addition, a significant amount of chlorite (the product of the hydration of clinopyroxene, a common mineral in komatiites) was also identified. Iron oxides, likely magnetite, were identified along the majority of the relic olivine grain boundaries and in veinlets across the thin section. Mapping of abundances of elements across the thin section agreed with previous findings (see Figure 4.24d).

Sample LKM2.6 was characterised by a porphyritic texture dominated by twinned and zoned plagioclases. The groundmass consisted mainly of quartz, fine grained plagioclase and opaque minerals (see Fig.4.22g&h). Biotite is a common mineral in rocks of tonalitic composition; in a hydration reaction it can alter to chlorite which was extensive throughout the thin section, as shown in Figure 4.22a,b &d. The plagioclase phenocrysts also indicate the sample has been subjected to hydrothermal alteration, as many are sericitised, as can be seen in Fig 4.22h. The groundmass of the sample was too fine grained to image clearing using optical techniques; as a result, no opaque minerals were identified.

Additional work was carried out on the SEM to try and identify the opaque minerals. EDX spectra were also acquired to try and identify the main minerals in the sample. Bright and 'shinny' minerals, potentially FeO, were targeted for element analysis. Minerals with a high iron content were overall scarce within the sample, although a micron sized euhedral grain of titanomagnetite was clearly identified within the groundmass (see Figure 4.25a).

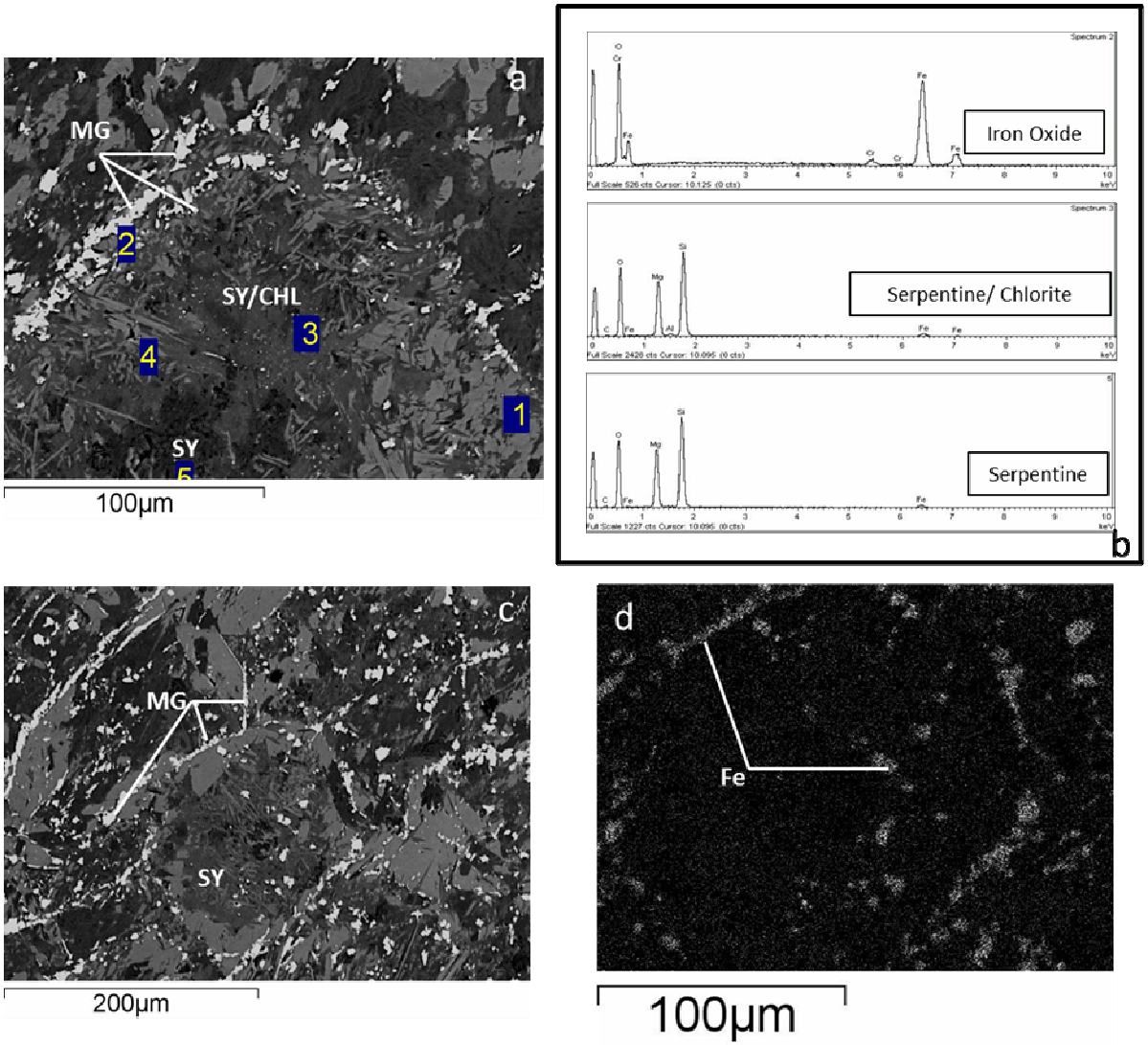

Figure 4.24. Scanning Electron Micrographs of LKM1.11. (a) Area shows large serpentinised olivines as well as chlorite (Sy/Chl). Iron oxides concentrate along the olivine grain boundary (Mg) (b) EDX spectra showing main minerals identified in thin section. (d) Fe element X-ray map of area (c). Note how Fe rich minerals are shown to cluster along the grains boundaries and within veinlets.

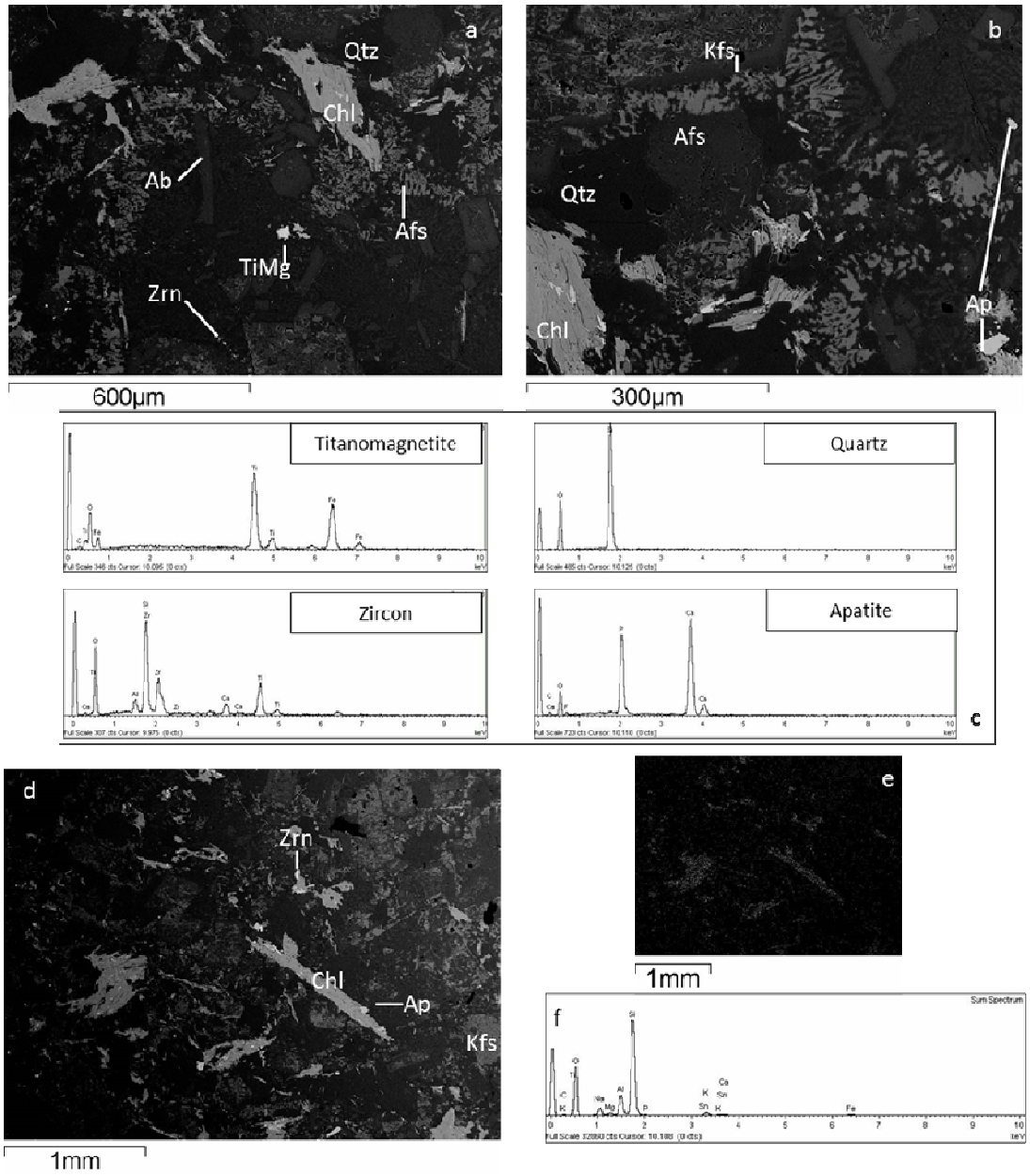

Figure 4.25. (a&b) Scanning Electron Micrographs of LKM2.6. The mineralogy observed is typical of a tonalitic rock: Biotite has been altered to chlorite (Chl), Quartz (Qtz), Albite (Ab), Zircons (Zrn), Alkali Feldspars (Afs) and K-felsdpar (Kfs). Note the large single titanomagnetite grain (TiMg). (c) EDX spectra showing main minerals identified in thin section. (e) Fe element X-ray map of area (d). Note how elevated Fe concentrations are identified within the iron rich chlorite minerals. (f) Sum EDX spectra showing major elements identified in the sampled area.

All the minerals expected to be identified in a rock of tonalitic composition were recognised: potassium and plagioclase feldspars, quartz, serpentine, chlorite, apatite and zircons, clearly identified in Figs 4.25a to d. Elemental mapping was carried out on three distinct areas of the sample to try and identify clusters of iron that may indicate the presence of Fe-bearing opaque minerals. However, in all three maps produced, iron was found to be well scattered throughout the sample with no obvious clusters, indicating a lack of Fe bearing ore minerals (See Figure 4.25e).

The findings of the microscopy work carried out on site LKM5 support the results of the rock magnetic characterisation experiments performed on the site. The samples of LKM5 were dominated strongly by the paramagnetic fraction. Given the apparent lack of iron oxide minerals, one might expect the ferromagnetic signal in the rock magnetic experiments to be weak. The microscopy work allowed identification of iron sulphides, such as pyrite, which could account for the strong paramagnetic contribution observed in the samples. Previous microscopy work carried out by Hale & Dunlop (1987) and Yoshihara and Hamano, (2004) indicates that magnetite grains in samples of the Komati Formation can be expected to micro to submicron scale (<1µm - 10µm) which is on the limits of the resolution of the optical and electron microscopes used to investigate the samples in the present study. Therefore, it is possible the sample may contain small proportions of very fine grained iron oxides which may not have been imaged.

The same is true of the sample studied from site LKM2. Iron oxides are accessory minerals in rocks of gabbrotic/tonalitic compositions. Therefore, it is not surprising that limited number of iron oxides were identified in the sample. This would account for the strong paramagnetic behaviour observed in the rock magnetic work. As is true for LKM5, it is also possible that iron oxides are more abundant in the sample, but are beyond the resolution of the instruments used.

In contrast, sample LKM1.11 was found be strongly ferromagnetic with high initial NRM intensities. The high abundance of micron to submicron sized iron oxide minerals along olivine grain boundaries would explain the rock magnetic properties of site LKM1. This provides a likely explanation for the variation in NRM intensities observed across the sites of the Komati Formation. Whilst no microscopy work was carried out on the sampled BARB core sites, it is possible samples from sites BARB1a, BARB1l and BARB2b, which also show high NRM intensity values, might be mineralogically similar to sample LKM1. This would also be consistent with samples which show high NRM intensities being komatiites under Dann's (2000) classification and peridotitic under the classification of Yoshihara and Hamano, (2004). The NRM intensities of site LKM1 are comparable to those of the peridotitic samples of Yoshihara and Hamano, (2004). The findings presented here indicate that petrological differences between the samples give rise to the variety of NRM intensities observed across the Komati Formation and are consistent with the findings of Yoshihara and Hamano, (2004).

The iron oxides identified in thin sections of sample LKM1.11 and LKM5.12cc were beyond the resolution of the SEM used. The EDX spectra acquired for the Fe Oxides cannot distinguish between minerals that have the same composition, i.e., magnetite and maghemite, but different lattice structures. If magnetite in the samples had been hydrothermally altered by low temperature oxidation to maghemite, one would expect to see cracking at the surface of the iron oxide grain (Tauxe, 2010). It was not possible to distinguish between the two potential carriers identified through rock magnetic characterisation using optical and electron backscatter imaging techniques.

4.8. Discussion

Two overprint directions of magnetisation were isolated from the rocks of the Komati Formation. The surface samples (LKM sites) are characterised by a low temperature direction (LT1) which is interpreted to be a present day field overprint. The drill core samples from the BARB cores are dominated by drilling-induced overprints (acquired during drilling of the original cores). The overprint is observed in a parallel and antiparallel to the drilling direction. The causes for the drilling overprint being observed in an antiparallel direction in some BARB core samples are not entirely clear.

Once viscous and drilling-induced overprints were removed, three directions of magnetisation were recognised in the samples of the Komati Formation. In order to establish the

timing of acquisition of the components identified in the samples, baked contact tests were attempted. Two of the directions of magnetisation (WSh and ESh) are seen in both baked and unbaked komatiites and in some intrusions. The shallow components were observed to be almost antipodal and therefore a reversal test on the dataset was applied. The components pass a reversal test.

A further magnetisation direction (WSt) is seen above WSh in some unbaked and baked komatiites but not at all in younger intrusives. Establishing the age of the component is crucial, as it has the potential to be the oldest palaeomagnetic pole. Comparison with previously published data sets will add to the robustness of and give a wider context in which to interpret the results presented here.

4.8.1. Sample handling Overprints (ICDP Drill Cores)

Three processes during the acquisition of the palaeomagnetic samples can induce an overprint: 1) Drilling of the cores induces an overprint usually directed in the vertical direction of the core (z); 2) cutting of the cores, with an overprint direction expected in the plane of the saw (x-y plane in specimen coordinates) and; 3) drilling of the mini-cores can also induce an overprint in the vertical direction of the mini-cores. Strong overprints induced by the processes above have the potential to obscure potential primary remanence held within the samples and so it is crucial to rule these out before interpretation of the directional dataset. During acquisition of the samples, every effort was made to reduce the likelihood of overprints by using water and other coolants.

There is no evidence in the Zijderveld plots that overprints have been induced in the BARB cores samples as a result of processes 2 or 3, see Figures 4.10 and 4.11. Samples affected by a drilling overprint would be expected to display a strongly unidirectional overprint component in the Zijderveld plots and directions clustered around that of the drilling orientation in an equal area projection. As is seen in Figures 4.10 & 4.11 , this is the case for the BARB cores studied. Therefore, samples have been affected by a drilling overprint. The overprint is observed in a parallel and antiparallel to the drilling direction. The causes for the drilling overprint being observed in an antiparallel direction in some BARB core samples are not entirely clear. I was not part of the drilling parties and fieldwork associated with acquisition of the drill core; therefore, the exact circumstances of core drilling are not clear. Possible causes for the unusual behaviour recorded in the samples could be: 1) the drilling casing and/or 2) misorientation of core sections. In order to prevent unsta-

ble upper formations from caving-in, it is common for the drill hole to be lined with metal casings. These are not directly water cooled during the drilling process (as water is supplied to the drill head via the drill string), but are often rotated in a reverse drilling direction in instances where they become stuck; this could induce a reversed drilling direction. In addition, greater depth is gained by addition of further sections of casing at the surface. Casing can be added in reversed orientations and so the magnetisation carried can be induced in an antiparallel direction to that in which the hole is being drilled. During drilling, drill core was recovered every 1.5m. Although great care was taken at the drilling sites to correctly link the base of the previously extracted section of core and the top of the newly extracted section of core, it is possible a few sections could have been misorientated. Whilst this would explain antiparallel drilling directions in sites BARB1c and BARB1e, it does not explain why we see parallel and antiparallel directions within a single core section - BARB1f, for instance. In addition, if sections of core had been misorientated, it was not obvious that this was the case during the sampling of the core. Therefore, this is considered an unlikely cause for the observed behaviour.

Another possibility that may account for the drilling overprint being observed in a parallel and antiparallel direction is that some of the studied samples are able to undergo self-reversals. Examples of self-reversals in natural rocks are rare and are thought to occur in maghematised submarine basalts, (Dunlop and Özdemir, 1997). pTRM acquisition experiments, as outlined by Doubrovine and Tarduno (2004), were carried out on three samples (BARB1e8, , BARB1f3 and BARB1l8) from the BARB cores to establish whether self-reversal might be observed in samples. The data set was not sufficient to reach conclusive results and so self-reversal as a mechanism for explaining the drilling overprint being observed in a parallel and antiparallel direction requires a considerable amount of work.

4.8.2. Comparison with Previously Published Palaeomagnetic Data

A number of palaeomagnetic studies have been performed on the rocks of the Barberton Greenstone Belt. Of those, there are three that are directly significant to the present study. Extensive reference has already been made to the work of Yoshihara & Hamano, (2004), which also sampled rocks of the Komati Formation. In addition, the work of Layer et al., (1994) on the Nelshoogte Pluton and the work of Tarduno et al. (2008) on the Kaapvalley Pluton are also relevant to the findings of this study.

Establishing the timing of the acquisition of the high temperature magnetisation is crucial to ascertain the viability and reliability of the poles calculated for the rocks of the Barberton Greenstone Belt. The complex geological history casts doubts over the feasibility of the findings. However, as discussed in the sections above, whilst field stability tests have not always been conclusive there is strong evidence the timing of the acquisition of the NRM is up to ca. 3.2-3.4a for the ShE and ShW components and at least ca.3.48Ga for the StW component. Comparison with previously published data can provide another means of validating the robustness of the findings of this study.

Layer et al., (1994), identified two antipodal shallow northeast (A-) and shallow northwest (A+) directions, (A-= (D/I)=104.0°/11.8°, $\hat{k}$= 7, α95=28°, n=6; A+=(D/I)=293.1°/7.0°, $\hat{k}$= 13, α95=13, n=11) in the 3179±18 Ma trondhjemitic Nelshoogte Pluton, (see also Chapter 7). In addition, this direction is also recorded in microgabbro dykes of similar age and the authors consider the directions were acquired simultaneously. Tarduno et al. (2007) studied the tonalitic Kaap Valley Pluton (3227±1Ma, Kamo and Davies, 1994). Whilst the focus of that study was measuring palaeointensities, the authors also identified two antipodal east (KVP+ = (D/I)=101°/56.1°, $\hat{k}$= 26.2, α95=13°, n=8) and shallow west directions (KVP- = (D/I) =273°/-24.1°, $\hat{k}$= 46, α95=7°, n=7). It is worthwhile comparing the directions for the ShE and ShW directions isolated in this study and those summarised above due to the possibility the intrusive units within the Komati Formation might be related to emplacement of these tonalitic plutons to the west of the BGB. Note, however, as discussed in detail in section 4.2 and 4.1.1 of this chapter, the torndhjemitic/tonalitic dyke (site LKM2) sampled as part of this study (3476 ±2Ma and 3458 ±10Ma, Kamo and Davis, 1994), is significantly older than the plutons studied in the works of Layer et al., (1994) and Tarduno et al. (2007).

The stereographic projection shown in Figure 4.26 compares the directions of this study with those of Layer et al. (1994). The ShW direction and the A+ direction are significantly different from one another, as neither their direction means nor their α95 confidence limits overlap; despite some of the sample directions being comparable. Direction means for ShE and A- direction do not overlap, but their α95 confidence limit envelopes do. Therefore it was necessary to perform a common true mean test for randomness to statistically compare the directions and establish if they are distinguishable from one another. The test gave a negative result, indicating the two directions do not share a common mean and are distinguishable from one another.

As shown in Figure 4.26 , the ShE and ShW directions in the Komati Formation are clearly distinguishable from the Tarduno et al. (2007) Kaap Valley Pluton KVP+ and KVP- directions. Whilst the directions fall close to one another, they share no common means.

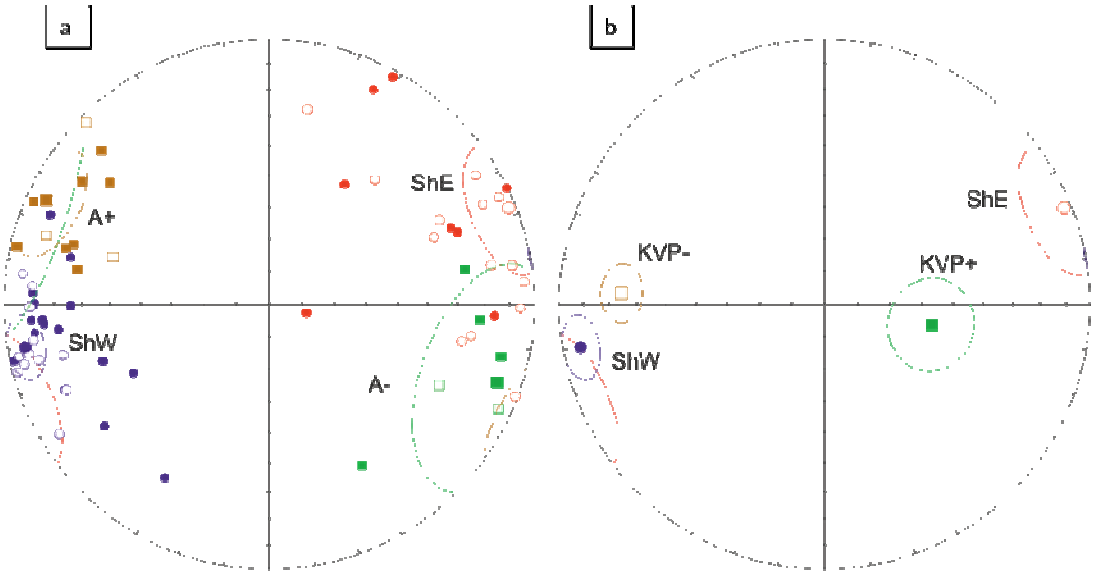

Figure 4.26. (a)Stereographic projection comparing directions from this study (ShE in red, ShW in purple) and directions from Layer et al. (1994) (A- in green, A+ in brown). (b) Stereographic projection comparing directions from this study (ShE in red, ShW in purple) and directions from Tarduno et al. (2007) (KPV+ in green, KPV- in brown).

The rocks of the Komati Formation are affected by the tectonic deformation (D_1 and D_2 stage, see section 4.1 of this chapter and Chapter 2 for further details) that resulted in the formation of the Onverwacht Fold, dated at 3.2Ga (Kamo and Davis, 1994; Krüner et al., 1991). Therefore, the ShE and ShW directions were tectonically corrected for the folding and plunging of the OF (see Table 4.3). A tectonically corrected virtual geomagnetic magnetic pole (VGP) was calculated for the combined ShE and ShW directions (λ= -29.2°/ϕ= 162.5°, A95=7.3, N=51, where N is number of samples).

The Kaap Valley and Nelshoogte Pluton have not been affected by the tectonic deformation that led to the formation of the OF in the BGB. As a result, in order to compare the VGPs of the ShE+ShW direction with those of the Kaapvalley Pluton and Nelshoogte, it was necessary to do so in geographic coordinates (the same is true for the mean directions compared above). As seen in Figure 4.27 the clustering of the directions does not improve in pole space and is indicative that the directions isolated in this study are not related to the directions present in the Nelshoogte or Kaap Valley Pluton.

Yoshihara and Hamano (2004), argue the steep direction recorded in their samples of the Komati Formation predates the creation of the OF fold; details of their evidence are given in section 4.1 of this chapter.

As is seen in Figure 4.27 and Table 4.3, when plotted in geographic coordinates, the StW mean direction calculated in this study is in agreement with the steep west direction isolated by Yoshihara and Hamano, (2009) and named here as the KOM direction, following Biggin et al., (2011). In addition, the StW direction is also in good agreement with the findings of Hale & Dunlop (1984), see also Figure 4.4.

In order to compare the results of the work presented here and those of Yoshihara & Hamano in stratigraphic coordinates it was necessary to recalculate the tilt-correction for the work of Yoshihara & Hamano, (2004), as the correction carried out by the authors failed to consider the plunge of the Onverwacht fold, (see Biggin et al. 2011). Tectonically corrected data for this study are consistent with full tilt-corrected values published by Biggin et al., 2011, see Table 4.3 and Figure 4.27. The clustering of the mean directions is slightly better in geographic coordinates than in stratigraphic coordinates (*K* decreases from 26 to 11.4 for the data presented in this study, see Table 4.3) .

Component	Lithology	NRM (A/m)	T Range (°C/mT)	Dm	Im	k	α95	N
ShE	Intrusives and Komatiites	$10^{-3}/10^{-4}$	200-580	68.1	-3.1	5	13.4	22
				138.8	*-29.6*	*12*	*11.2*	*22*
ShW	Intrusives and Komatiites	$10^{-3}/1$	20-90	259.9	7.2	13.3	7.6	29
				314.2	*24*	*21*	*6.6*	*29*
StW	Komatiites	$10^{-4}/1$	440-580	267	64	26	7.14	16
				24.9	*11.6*	*11.4*	*13.4*	*16*
KOM	Peridotiitic and Basaltic Komatiites	$10^{-4}/24$	300-590	272.3	72.6	26.3	12	7*
				27.9	*9.73*	*7.8*	*21.2*	*7**

Table 4.3. Mean directions used in this study. Directions in the upper line are given in geographic coordinates and directions in the *lower line* are given in stratigraphic coordinates. Directions given are all calculated as part of this study, with the exception of KOM (as per Biggin et al., 2011), which corresponds to the direction calculated in Yoshiara and Hamano's study of 2009. The direction was not tilt corrected by Yoshihara and Hamano (2009). The direction given in stratigraphic coordinates was calculated as part of the work presented in this thesis. N denotes number of samples used to calculate the sample mean. * denotes cases where site means were used instead of sample means (for reference, a total of 46 samples were used to calculate the KOM direction mean, Yoshihara and Hamano, 2009).

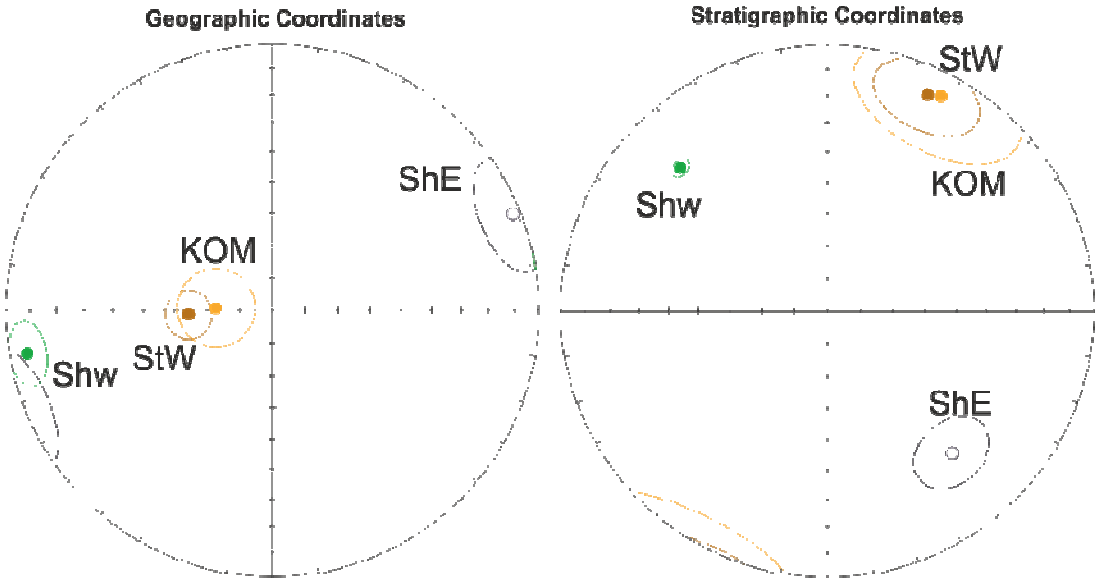

Figure 4.27. Equal area projection showing sample mean directions identified for this study (ShE, ShW and StW directions, see text for details). NRM components with filled (unfilled) points represent the lower (upper) hemisphere. The Yoshihara and Hamano (2011) steep west direction is also shown for comparison with the new data presented in this study (Y&H04 in brown). Tables 4.3 provide data shown in the plots.

Component	Lithology	λ	ϕ	A95	N
ShE +ShW	Intrusives and Basaltic Komatiite	-14.5°	296.8°	7.7	51
		-29.2°	*162.5°*	*7.3*	*51*
StW (This study & YH04)	Komatiite	-22.5°	-11.6°	7.82	14
		53.9°	*66.5°*	*12.7*	*14*

Table 4.4. VGPs calculated for directions isolated from the samples measured in this study. Poles given in italics are tectonically corrected. The pole for the StW direction has been calculated by combining the findings of this study and those of Yosihara and Hamano, (2004). The direction mean for the KOM pole published by Biggin et al. (2011) is calculated from site means. In order to maintain consistency, whilst the StW direction mean is determined from sample means, where possible, site means were used to calculate the new VGP.

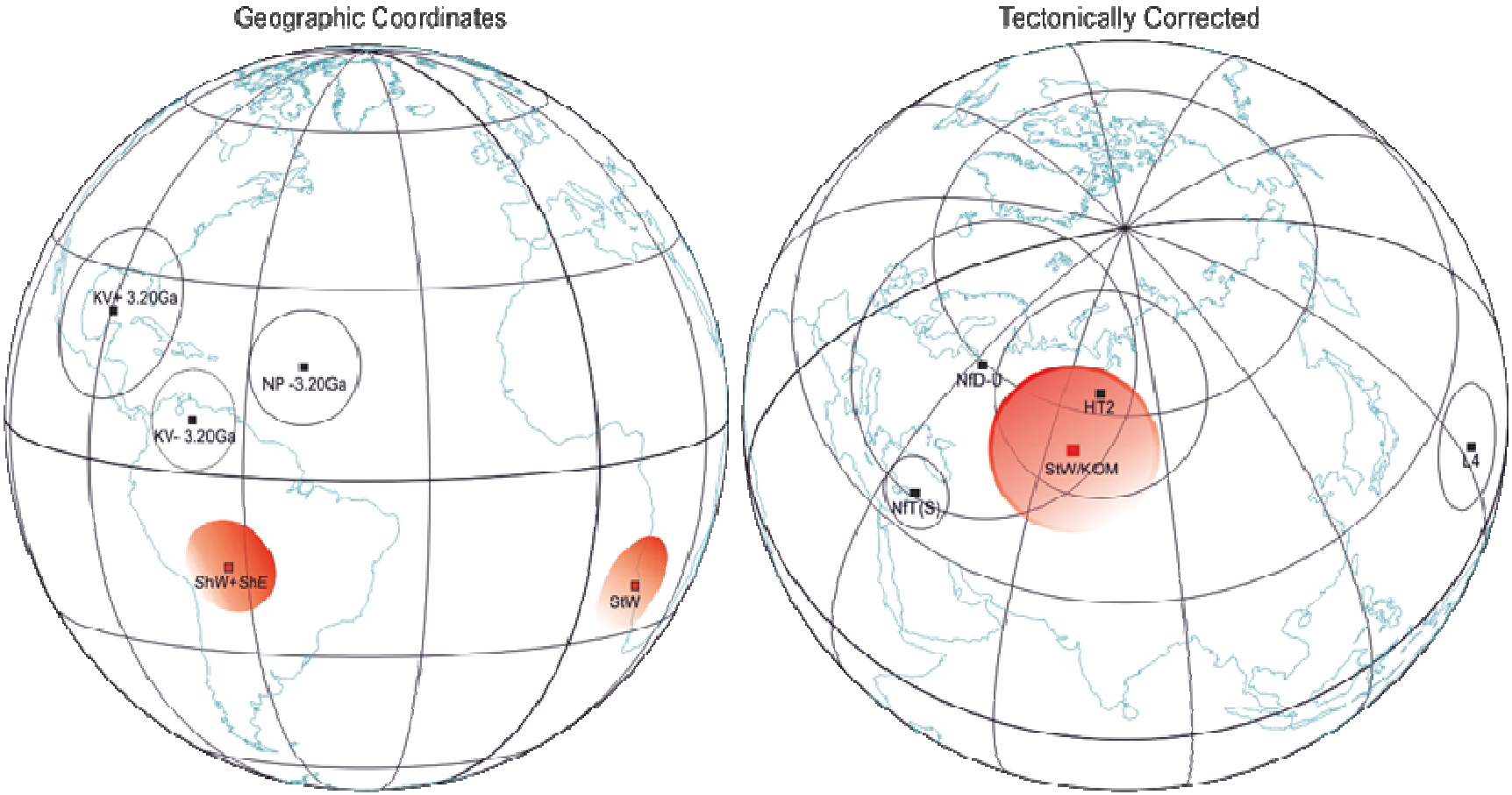

Figure 4.28. Poles produced for Komati Formation (this study) are shown in shaded red circles. (a) Poles are presented in geographic coordinates, unshaded circles are published poles of relevance to Komati Formation. KV+/- = Kaapval Pluton (Tarduno et al., 2007) and NP = Nelshoogte Pluton (Layer et al., 1994). (b) Poles are presented in stratigraphic coordinates NfD-U, HT2, L4 and NfT(S) = Onverwacht Group Poles, (Biggin et al., 2011).

It was not possible to perform a fold test combining the newly acquired data in this study and the results with those of Yoshihara and Hamano, due to all samples having been acquired from the northern limb of the OF.

When combined with the results of Yoshihara and Hamano, (2004), a new tectonically corrected VGP (λ= 53.9°/ϕ= 66.5°, A95=12.7, N=14), is calculated from a total of 67 samples and implies a palaeolatitude of 13.9°, see Figure 4.28.

4.8.3. Timing of Acquisition of Remanence

The age of the Tonalitic/ Trondhjemitic dyke sampled at the surface (site LKM2) is well constrained. The site was originally sampled in the work of Kamo & Davis, 1994. The age of the intrusion of the dyke is bracketed between 3476 ±2Ma and 3458 ±10Ma (dated by $^{207}Pb/^{207}Pb$ of concordant zircons). This age is also often used as the minimum age for the emplacement of the Komati Formation in the literature. The ages of the dykes in the BARB cores are unknown. However, their intrusion is likely associated with the emplacement of the plutons surrounding the Greenstone Belt, which are dated at ca. 3.45 and 3.2Ga (Kamo & Davis, 1994; Layer et al. 1998; Dann, 2000). The exact age relationship between the intrusive units and the komatiites of the Komati Formation is unclear (Dann, 2000). The emplacement of the dyke sampled in LKM2 is likely comagmatic to the emplacement of the Stolzburg, Doornhoek and Theespruit Plutons (de Wit, 1987; Kamo and Davis, 1994) of largely trondhjemitic composition and dated between 3460-3445Ma (Kamo and Davis, 1994). In addition, due to the dyke branching towards the East, intrusion is thought to have been from the West (Dann, 2000), consistent with it originating from the above mentioned Plutons.

The inability to constrain the ages of the intrusive units within the BARB cores means it is not possible to precisely time the acquisition of the ShW and ShE component isolated in these samples. The small number of obtained directions coupled with a high intrinsic scatter of the results of some sites adds to the difficulty of understanding the timing of acquisition of the ChRM, resulting in inconclusive baked contact tests. Nevertheless, the ShW and ShE directions are predominantly present in the younger intrusions and baked komatiities and absent from non-baked rocks, see Fig 4.9 & 4.10. The exception to this is site BARB1l, where a ShW and StW direction are indistinguishable, possibly due to the ShW and StW components overlapping in the demagnetisation spectra - a behaviour seen in a number of other samples in the dataset, as shown in Figure 4.8(d). Alternatively, the direc-

tion observed in BARB1l is indistinguishable from the drilling direction; it may be they are associated with a drilling overprint instead.

Unfortunately, there are no palaeomagnetic studies of the ca 3450Ma plutons to the south west of the BGB (Stolzburg, Doorhoek and Theespruit Pluton). So it was not possible to compare our results to the palaeomagnetism of these units. The field relationships established through the detailed study of the geology of the BGB by de Wit (1984, 1987, 2011), Kamo & Davies (1994), etc, in addition to the age of the LKM2 dyke, suggest that the maximum age for the ShW and ShE direction is that of the dyke emplacement, ca 3450Ma . This age is in agreement with the emplacement of the 3450Ma plutons, thought to be comagmatic with the emplacement of the dykes in the Komati Formation.

As the ages of the dykes sampled in the BARB cores are unknown and despite the correlation outlined above, Dann (2000)states that the exact relationship between the dykes and Komati Formation is poorly understood, it was important to compare our results with those of the younger 3.2Ga Plutons given the compositional similarities between the two. If indeed the ShE and ShW directions were acquired at ca.3450Ma then one would not expect to see a strong correlation between our results and those of Layer et al. (1994) and Tarduno et al., (2007), given the potential 200Ma difference between the two directions. The results presented in 4.5.2.1 support the argument that the ShW and ShE directions are older than the emplacement of the Kaap Valley and Nelshoogte Plutons.

The StW direction is seen at higher unblocking temperatures than the ShW and ShE components (Figure 4.8d). In addition, this direction is never observed in the younger intrusive rocks. The StW direction is consistent with previously published studies (Hale & Dunlop, 1984 and Yoshihara & Hamano, 2004), see detailed discussion in section 4.8.2. The evidence discussed in sections 4.5.1.1 and 4.2 suggests the StW direction predates the dyke emplacement and may record the field direction at the time of the emplacement of the Komatii Formation.

4.8.4. BARB2d

The shallow southeast/ south direction recorded in site BARB2d is not seen in any other site from the Komati Formation. A similar direction is reported by Stirk et al., (2007), from flood basalts of the 2.6Ga, Allanridge Formation of the Ventersdorp upergroup of the Kaapvaal Craton ((D/I)=188.7°/60.7°, $\hat{k}$= 82, α95=6.2°). However, the rocks of the Venters-

dorp Supergroup outcrop a considerable distance from the BGB; this, combined with the fact the observed southeast/south direction is not isolated in any of the Komati Formation sites, limits the viability of the direction being an overprint caused by the emplacement of the Allanridge flood basalts. As a result, it is not possible to say with certainty what gives rise to the unusual direction observed in BARB2d.

4.9. Conclusions

Following a paleomagnetic investigation of the rocks of the Komati Formation the new findings are placed in the context of previously published results for the Komati Formation, Onverwacht Group and rocks of the same age in the Kaapval Craton. Interpretation of the results has been hampered by the complex thermal and chemical history of the studied rocks leading to noisy results with scattered directions and inconclusive field stability tests. Once viscous and drilling-induced overprints were removed, three ChRM components were recognised. Two of these (ShE and ShW) are seen in both baked and unbaked komatiites and in some intrusions. A tentative age of ca. 3450Ma is proposed based on age and geological correlations between one of the sampled dykes and the Stolzburg, Doorhoek and Theespruit plutons. However, this age is far from certain and should be considered with caution until dating of the intrusive units in the Komati Formation is carried out and/or more conclusive field stability tests can be performed. In addition, these antipodal directions provide tentative evidence of a field reversal in the Komati Formation. However, these results must also be considered with caution given the noisy nature of the date set. A further component (WSt) is seen above WSh in some unbaked and baked komatiites but not at all in younger intrusives. This is indistinguishable from the characteristic component found by earlier studies performed on komatiites a few km away. The StW direction is thought to predate the dyke emplacement and may record the field direction at the time of the emplacement of the Komatii Formation, at ca. 3.5Ga. When combined with previously published data, the new results presented here increase the precision of the KOM/StW pole and therefore study provides further support for the validity of the world's oldest pole.

5 Palaeomagnetism of the Hooggenoeg Formation

1.1. Introduction

The rocks of the Hooggenoeg Formation immediately overlie those of the Komati Formation and, as occurs with the latter, they have not been severely affected by deformation processes and metamorphism and, therefore, remain of important palaeomagnetic value. The rocks of the Hooggenoeg Formation are the second oldest Onverwacht Group basalts studied as part of this work.

The broader implications of studying rocks of this age for understanding the evolution of the Earth during the Archaean has been discussed in Chapters 1 & 2 of this thesis. The results of previous palaeomagnetic studies have shown that robust data sets can contribute to our understanding not only of tectonic process (Biggin et al., 2011; de Kock et al., 2009; Smirnov et al., 2013; Strik et al., 2003; Zegers et al., 1998), but also strength of the Palaeoarchaean geodynamo (Tarduno et al., 2010; Yoshihara and Hamano, 2004), timing of inner core growth (Tarduno et al., 2007; Tarduno et al., 2010; Usui et al., 2009) and magnetopause standoff distances (Tarduno et al., 2010), amongst other parameters; hence adding to the overall understanding of the Palaeoarchaean Earth.

There is clear potential for the rocks of the Onverwacht Group to reveal important insight into how the Earth operated during Archaean times, as established by a number of studies (Biggin et al., 2011; Hale and Dunlop, 1984; Tarduno et al., 2007; Tarduno et al., 2010; Usui et al., 2009; Yoshihara and Hamano, 2004) . However, their age and the fact that the tectonic setting of their formation is still highly debated, means that establishing the time of the acquisition of remanences held by the rocks of the Onverwacht Group and their reliability is of fundamental importance. This can be achieved through performing further palaeomagnetic field tests, which rely on the geometric relationships of formations in the field to help ascertain the age of the magnetisation preserved in the sampled rocks. Successful palaeomagnetic field tests of the Onverwacht Group include a conglomerate test by Usui et al., (2009) followed by an encouraging result from Biggin et al., (2011) , both in the Noisy Complex. The rocks of the Hooggenoeg Formation present a perfect opportunity as there are several exposures over a thickness of up to 10 km across both the northern and southern limbs of the Onverwacht Fold (OF), as can be seen in Figure 5.1, making them ideal candidates for additional palaeomagnetic studies, particularly

given the successful, yet ambiguous (see a further discussion on this in section 5.3 of this chapter), results of previous work by Biggin et al., (2011).

The aim of this study was to acquire a new data set for the Hooggenoeg Formation, with particular focus on the units of the northern limb of the OF, as these have not been sampled as part of previous palaeomagnetic studies and provide a unique opportunity to constrain the reliability of previous results through performing improved field stability tests. Surface samples were collected from 14 sites; six sites were sampled in the central part of the northern OF, whilst a further eight site were sampled close to the Komati River approximately 3.6 km to the west of the sampling sites of Biggin et al., (2011), as shown in Fig. 5.1.

The new paleomagnetic data for the Hooggenoeg Formation show good agreement with the results previously obtained by Biggin et al., (2011). A low temperature component was identified and interpreted to be a present day overprint. A mid temperature component was also isolated from the samples and is likely associated with the emplacement of late Archean intrusive events. A new high temperature direction is observed in the samples of the northern limb of the fold. Whilst in geographic coordinates this direction is distinct from any others published previously, when the tectonic correction for the emplacement of the OF is applied, results cluster well with those of Biggin et al., (2011). This implies the two components are in fact the same. This constrains the age of the HT2 component to be at least as old as the folding of the OF, at ca. 3.2Ga, supporting the validity of a near-primary age for the magnetisation

In this chapter, the geology of the Hooggenoeg Formation is outlined, followed by a description of relevant previous paleomagnetic studies. Details of the experimental methodology follow including sampling techniques and rock magnetic characterisation. The bulk of the chapter is dedicated to the results of the characterisation of magnetic carriers within the samples and in particular the details of the directional components isolated from the studied units. The new results are then put in the context of previous palaeomagnetic studies. The chapter is finished with an overall summary and some concluding remarks.

5.2. Geological Background

The base of the Hooggenoeg Formation (shown in Figure 5.1), is defined by the Middle Marker (MM), a regionally extensive chert layer of silicified volcaniclastic and sedimentary material which can be up to 10 m thick and is interpreted to have been derived from metasomatic processes (de Wit et al., 2011; Lowe and Byerly, 1999b; Viljoen and Viljoen, 1969b). A detailed study by de Wit et al., (2011), suggests the contact between the MM and the Hooggenoeg Formation is along a shear zone, characterised by silicified pillow lavas and komatiitic breccias which are altered to flaser-banded quartz-carbonate-serpentine rocks, known as the Mbjega Shear Zone (de Wit et al., 2011). The oldest possible age for the Hooggenoeg Formation is obtained from detrital zircons from the MM, exposed along the southern limb of the Onverwacht Fold (OF), which give an age of ca. 3472 ± 5 Ma (Armstrong et al., 1990). The Formation is overlain by the newly named Noisy Complex (see Chapter 6, for details of the new nomenclature, but it is also known as the Buck Ridge volcano-sedimentary complex, BR-vsc). The nature of the contact with the Noisy Complex is highly debated in the literature due to it being structurally problematic: it consists of a section of felsic volcanics that are faulted, sheared and intruded, heavily, by ultramafic basalts and dacitic rocks. A highly brecciated chert (de Wit et al., 2011; de Wit et al., 1982; de Wit, 1987), indicates the contact with the Noisy Complex is along a shear zone (Geluk Shear Zone), along a thrust fault (Lowe and Byerly, 1999b). Alternatively de Vries, et al., (2006b) argue that the BR-vsc belongs within the stratigraphy of the Hooggenoeg Formation (see Chapter 6 for further details), arguing that the contact between the two units is transitional along a fault zone and characterised by numerous normal faults which act as conduits for the intrusion of the ultramafic and dacitic rocks.

Overall, the Formation comprises theoleiitic basalts intruded by basaltic to ultramafic sills; dykes are rare. The formation is well exposed, particularly on the southern side of the Onverwacht Fold (OF) and comprises the most continuous section of submarine volcanics in the Onverwacht Group (Furnes et al., 2013). In addition, the theoleiitic members are interlayered with basaltic komatiites and thin komatiites, as well as a number of cherts (de Wit et al., 2011; Lowe and Byerly, 1999b; Viljoen and Viljoen, 1969f). The Formation ranges in thickness between 2.5-3.0 Km (Dann, 2000; de Vries et al., 2006b; de Wit et al., 2011; de Wit, 1987; Furnes et al., 2011; Viljoen and Viljoen, 1969f). Pronounced thickness variations occur along the southern limb of the OF, with an overall increase across a distance of 3 Km along NE-SW strike (from 2Km in the NE to 5Km in the SE) due to significant intru-

sion of mafic and ultramafic rocks along strike (Furnes et al., 2013). Given the uncertain nature of the tectonic contact with the overlying Noisy Complex and the significant thickness variations, the original width and the specific age-range for the Hooggenoeg Formation is unknown (de Wit et al., 2011). For an in-depth geological map of the broader study area, the reader is directed to the work of de Wit et al., (2011).

Viljoen and Viljoen (1969f) first described the geology of the volcanic units of the Hooggenoeg Formation. The thorough mapping, petrological and geochemical work conducted by the authors remains the foundations for how the geology of the Hooggenoeg Formation is understood today. The regional scale alteration of the unit due to silification, serpentinisation, carbonation and ferruginisation (de Wit et al., 2011; de Wit et al., 1982; de Wit, 1987; Grosch et al., 2009a; Viljoen and Viljoen, 1969e, f) led Viljoen and Viljoen, (1969) to misinterpret the volcanism of the Hooggenog Formation as a series of repeating felsic cycles of volcanicity which are now known to result from silicification and alteration of mafic and ultramafic units (Byerly et al., 1983; de Wit et al., 1982; de Wit, 1987; Lowe and Byerly, 1999b; Lowe et al., 1985). Since the work of the Viljoen brothers in the 1960s, a significant and continuous effort to understand the geology and structural history of the Hooggenoeg Formation ensued. Here we will focus on the works of Lowe and Byerly, (1999), de Wit et al., (2011), Furnes et al., (2011) and Furnes et al., (2013) as they provide the most up to date description of the volcaninc units of the Hooggenoeg Formation. Other relevant works (and references therein), which may be of interest of to the reader, are referenced throughout this chapter.

Lowe and Byerly (1999), divided the Hooggenoeg Formation into six volcanic members (H1 to H6), traceable across not only the OF but also the Kromberg Anticline to the south east, although the type section is located in the northern limb of the OF. Furnes et al., (2011) studied the stratigraphy of the Hooggenoeg Formation in the southern limb of the OF and identified eight to nine continuous volcanic sequences, corresponding to eruptive phases (VS1–VS9), separated by chert layers, over a total of 15 logged vertical profiles. The sequences of Furnes et al., (2011) can be broadly correlated to those of Lowe and Byerly (1999), Figure 5.2. However, Furnes et al., (2011) identify more chert capping layers resulting in a more detailed understanding of the Formation. The lowermost sequence, H1, is assigned to the rocks of the MM. Original volcanoclastic material has been silicified and metasomatised to cherts which are carbonate rich (Lowe and Byerly, 1999b; Viljoen and Viljoen, 1969e, f). Unit H1 is conformably overlain by a thick, massive and pillowed

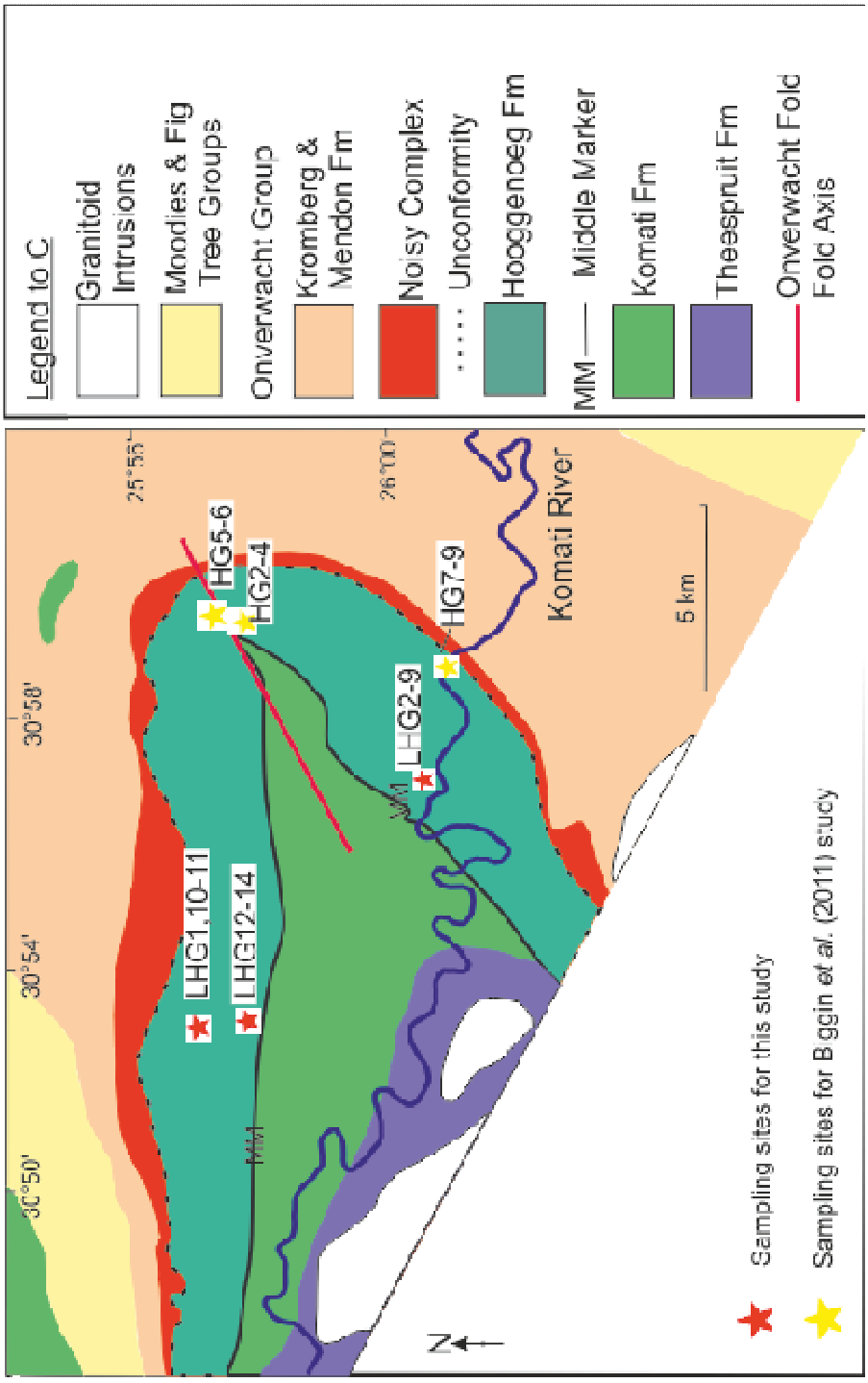

Figure 5.1. Geological map of the Onverwacht Group, based on the map of de Wit et al., (2010). The Hoogenoeg Formation is shown in the dark green colour. Sampling sites for this study are shown with red stars, whilst the sampling sites of Biggin et al., (2011) are represented by a yellow star. The axis of the Onverwacht Fold (OF) is represented by the red line. Samples LHG1 and LHG1 and LHG10-14 are take from the northern limb of the fold, whilst samples LHG2-9 and the sites of Biggin et al., (2011) are all collected in the southern limb of the fold.

tholeiitic sequence (H2) and capped by a black chert layer (H2c). The individual units range in thickness in the order of hundreds of meters and display complex lateral and vertical interlayering (Lowe and Byerly, 1999b). Interbedded cherts in the sequence are rare, but become more common towards the upper part of H2. In Furnes et al., (2011) VS1, the unit is thicker and comprises mainly massive non-pillowed basalt lavas. The sequence includes the MM, in addition to a further overlying chert horizon. Sequence H3 overlies H2 and is characterised by its abundance of variolitic pillows and spinifex-bearing basaltic komatiites (Lowe and Byerly, 1999b). Pillowed units are predominant at the base of the sequence, whilst spinifex basaltic komatiites are more common towards the upper part of H3. There are rare, 1m thick layers of chert present in the uppermost sections of the sequence (Lowe and Byerly, 1999b). Furnes et al., (2011) largely agree with the description given by Lowe and Byerly but also highlight the presence of two thin volcanic breccia horizons in the central part of the VS2 sequence. An up to 20m thick chert, which closely resembles the MM, marks the top of H3 and is defined by a lowermost layer of metosomatised ash and an uppermost layer of airfall dust, accretionary lapilli and ash (Lowe and Byerly, 1999b). In contrast to the findings of Lowe and Byerly, (1999), Furnes et al., (2011) identified a total of seven chert layers between H1 and H3 members but acknowledge they are obscured by a combination of poor exposure and predominance of intrusives which makes identification difficult. Sequence H4 is a 250m to 350m thick sequence of basaltic komatiites and basalts where pyroxene spinifex is common. The sequence includes rare, thin hyaloclastite breccias (also observed in the BARB cores of the Komati Formation, see Chapter 4). The lower part of the section is intruded by dykes and sills of largely komatiitic composition, whilst the uppermost divisions are generally predominantly pillowed and spinifex-free (Lowe and Byerly, 1999b). Furnes et al., (2011) VS3 sequence is comparable to H4, but does not include breccias and the authors highlight the presence of non-vesicular, but variolitic pillows with the komatiites. Sequence H4 is also capped by a chert layer, which in this instance is discontinuous and consists of mainly reworked volcanicalstic sediments and some airfall tuffs (Lowe and Byerly, 1999b). The sequence is overlain by a massive and pillowed theoleiitic basalt which marks the end of the mafic volcanism in the Hooggenoeg Formation (H5). The sequence is capped by a thin (1-2m) black chert (Lowe and Byerly, 1999b). All the cherts which cap individual sequences within the Formation are characteristically underlain by up to 10m of silicified basalts. Whilst Furnes et al., (2011) agree that VS4 is a thick, generally massive unit, it is poorly exposed in the southern limb of the OF. The capping chert of the VS4 is correlated by the

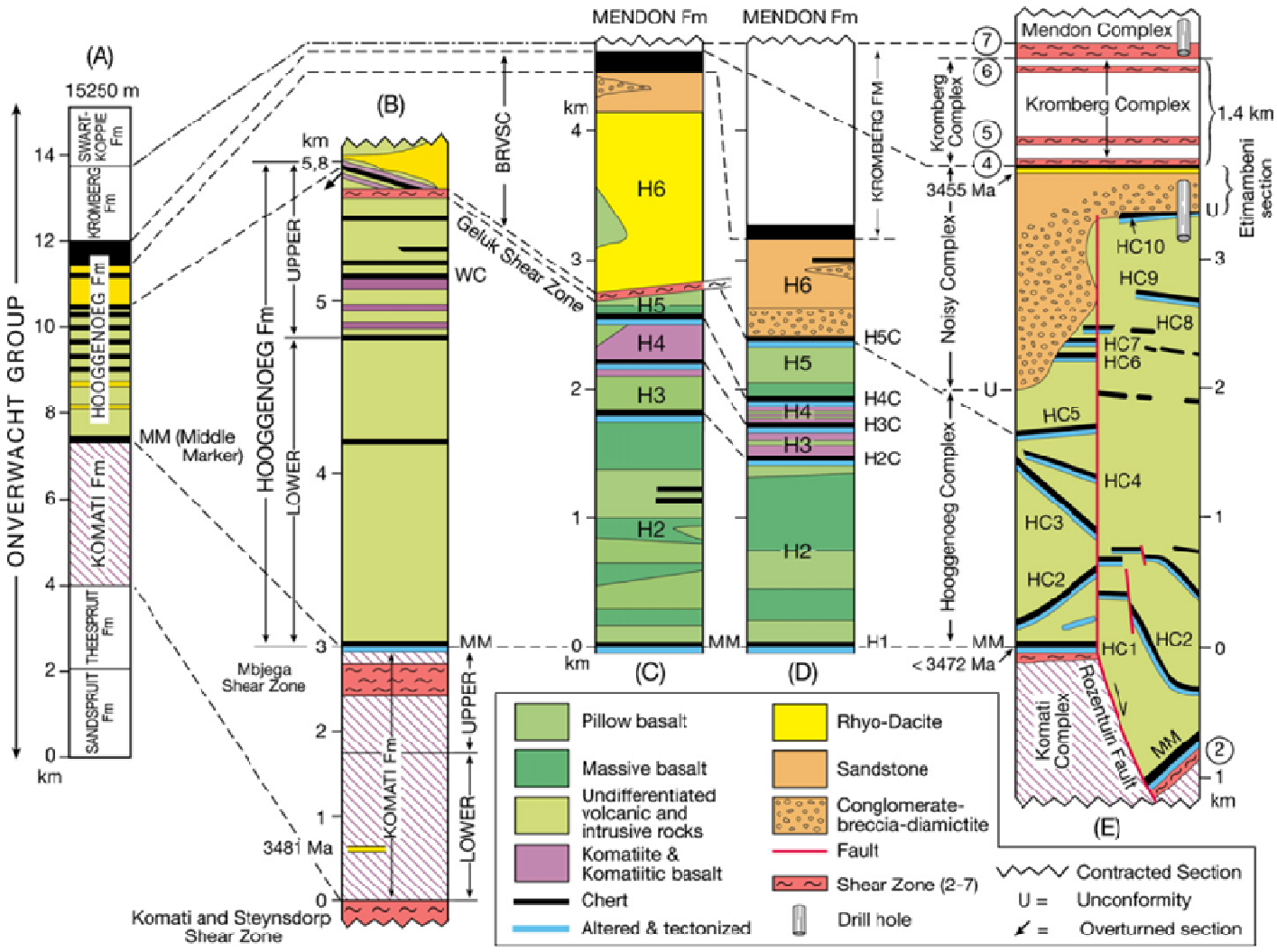

Figure 5.2. This figure is taken from the work of de Wit et al., (2011). Simplified stratigraphic sections are compiled from the work of A = Viljoen and Viljoen, 1969b, B = Dann and Grove, 2007 (BRVSC after de Vries et al., 2006), C+D = Lowe and Byerly, 1999, 2007, from the northern and southeastern limbs of the Onverwacht Fold, respectively; and E= the composite section derived from detailed logging and mapping by de Wit et al., (2011) and Furnet et al., (2011). Note that in sections C and D, H refers to volcanic sequences, established by Lowe and Byerly as described in the text in this chapter. Units labelled in the style H2C, in sections C, D and E correspond to chert horizons. As described in the text, HC5 can be use to correlate stratigraphic units across both limbs of the OF and between the work of Lowe and Byerly (1999, 2007) and the work of de Wit et al., (2011) and Furnes et al., (2011; 2013).

authors with the capping chert at the top of the H5. The uppermost member of the Hooggenoeg Formation, H6, marks the onset of both intrusive and extrusive felsic volcanism. It is a complex sequence of massive dacitic intrusive rocks associated with volcanic breccias, conglomerates, dacitic tuffs, overturned blocks and debris-flow deposits (Lowe and Byerly, 1999b). The complex morphology of the unit is affected largely by the presence of the Geluk shear zone which marks the top of the Hooggenoeg Formation (according to Lowe and Byrely, 1999). In their work of 2007, through detailed logging of an alternative section, Lowe and Byrely identified that the uppermost H6 sequence is not always preserved/present and instead H5 is immediately capped by the Noisy Complex, which they consider belongs to the Hooggenoeg Formation (see Figure 5.2). The section logged in detail by Furnes et al., (2011) is thicker and consists of a further five capping cherts and four more volcanic sequences, VS5-VS9. In addition, no transition to felsic volcanism is observed in the area studied by Furnes et al., (2011). The remaining volcanic sequences of Furnes et al., (2011) are at least 1400m thick and comprise mainly thick basaltic komatiite units. These vary between being massive and pillowed and are interlayered with thin and rare volcanic breccias. The sequences are heavily intruded by rocks of mafic and ultramafic composition. This area is affected by vertical faults, with the Rosentuin Fault extending throughout the entire thickness of the Formation and through which a gabbrotic/dirotitic dyke (dated at 2.9-3.0 Ga) has intruded the Hooggenoeg. The tectonic activity is thought to have been contemporaneous with volcanism but later reverse movement along the fault may have resulted in the relative uplift of the southern block (Furnes et al., 2011).

The rocks of the Hooggenoeg Formation have been affected by four major thermal events (discussed in more detail in Chapter 2), at 3.2Ga, 3.1Ga, 2.7Ga and 2.1 Ga (de Ronde et al., 1991; Kamo and Davis, 1994; Toulkeridis et al., 1994). It is thought that the rocks of the Hooggeneog Formation have not been reheated since the Palaeoproterozic, as evidenced from results of radioisotopic studies by de Ronde and de Wit., (1994) , de Wit et al.,(1992) and Weis and Wasserburg, (1987). The rocks of the area studied are folded within the Onverwacht Fold (OF), however, the exact age of the fold is unclear (de Wit et al., 2011). The youngest age given for the BR-vsc is ca.3.4Ga. To the southeast of the OF, both limbs of the Kromberg Fold, thought to have formed at a similar time to the OF, is cross-cut by the 3216Ma Dalmain pluton (Kamo and Davis, 1994) and, therefore, the folding event must predate the emplacement of the pluton, giving a minimum age for the deformation at ca. 3.2Ga. De Wit et al. (2011) assume that this is also the age for the formation of the

OF. This is supported by dating of folding and thrusting in the centre of the BGB at 3230-3228Ma (de Ronde and de Wit, 1994; De Ronde and Kamo, 2000; de Wit et al., 2011).

At a similar time, the volcanic sequences of the Upper Onverwacht Group were buried immediately after their formation on the sea floor (de Ronde and de Wit, 1994; de Wit et al., 1992; de Wit, 1987; Knauth and Lowe, 2003; Lowe, 1999a; Schoene et al., 2008), leading to their metamorphism. Peak metamorphic conditions did not exceed 400°C or low-grade amphibolites facies, although the majority of the units are metamorphosed to greenschist facies (Cloete, 1991; López-Martínez et al., 1992; Schoene et al., 2008b) . The minimum age for the metamorphism recorded by the rocks is estimated at ca. 3.23Ga, given by the U-Pb age determinations for the synkienmatic intrusion and sphene (Diener et al., 2005; Dziggel et al., 2005).

Furnes et al., (2011) interpret that the lavas of the Hooggenoeg Formation were erupted underwater given the presence of pillow lavas and limited vesicularity. It is using the limited abundance of vesicles in the Formation that they infer eruption depths of 2.4-4 Km below water (Furnes et al., 2011). Vesicularity varies laterally within volcanic sequences indicating that the Southern Hooggenoeg Formation was at times erupted into shallower waters than the north (this is particularly true in sequence VS2). Overall, abundance of vesicles decreases upwards through the sequences indicating that the uppermost basalts were erupted into deeper waters(Furnes et al., 2011).

Using the inference that size and durability of magma chambers can be determined by the extent of individual magma fluxes (Smith and Cann, 1993), Furnes et al., (2011) argue that the massive lavas were erupted at volcanic centres (which are generally characterised by larger volumes of erupted material), whilst the pillowed lavas originate from volcanoes with smaller magma chambers. The massive lavas in particular, are characterised by thickness variations across stratigraphy and Furnes et al., (2011) interpret these to represent sections through volcanic ridges and/or shield volcanoes.

The presence of up to 20m thick chert layers within the Hooggenoeg Formation (Furnes et al., 2011) may indicate significant hiatuses in the eruption of the lavas. The cherts, studied in detail by Lowe, (1999b) consist of 75% fine grained volcaniclastic/pyroclastic material, as well as biogenic sediments, sediments derived from the weathering of older rocks and direct chemical precipitates (Furnes et al., 2011). The geochemistry and textures pre-

served in the volcanicllastic material suggests phreatomagmatic plinian eruptions are the source of the material (Stiegler et al., 2008), indicative of eruption in relatively shallow waters opposing the deep water eruptive setting proposed for the thick basaltic units of the Hooggenoeg Formation . Furnes et al., (2011) reconcile this problem by arguing that as ash fall of modern Plinan fall out can disperse over an area of thousands of kilometres squared, (Self and Sparks, 1978), it is likely the source volcanoes would have been quite some distance away from the eruptive centres of the Hooggenoeg lavas. An alternative explanation is that the volcaniclastic material was introduced during periods of quiescence, as a result of transport of material to the deep waters via turbidity currents (Heinrichs, 1984; Stanistreet et al., 1981).

The tectonic setting in which the Onverwacht Group was formed is a highly debated topic and has been discussed in more detail in Chapter 2. Furnes et al., (2011) argue that given that the rocks of the Onverwacht Group do not form a continuous eruptive sequence (de Wit et al., 2011; Grosch et al., 2009a), the originally reported thickness of the Group (ca. 15km) by Viljoen and Viljoen, (1969b) amongst others, may not be truly representative. When combined with the deep water eruptive settings, faulting contemporaneous to the volcanic activity and komatiites being broadly comparable to boninites, the evidence is supportive of a tectonic setting akin to thin oceanic crust, not dissimilar to where ophiolites formed above a subduction zone(Furnes et al., 2013). As a result, the rocks of the Hooggenoeg Formation are interpreted to be formed in Palaeoarchean oceanic crust, in connection with subduction, with an associated island arc (at an unknown distance from the main eruptive centre), which supplied the volcaniclastic material which was later silicified into cherts (Furnes et al., 2013; Furnes et al., 2011).

5.3. Palaeomagnetic Background

A single, detailed palaeomagnetic study of the rocks of the Hooggenoeg Formation was carried out by Biggin et al., (2011). The work follows on, not only from previous palaeomagnetic studies of rocks of the Onverwacht Group(Hale and Dunlop, 1984; Usui et al., 2009; Yoshihara and Hamano, 2004), but also other studies of Archaean aged rocks (Layer et al., 1996; Suganuma et al., 2006; Tarduno et al., 2006), all of which have yielded encouraging results and point towards a stable, and potentially reversing, geomagnetic field in the Archaean. Aside from the work of Usui et al., (2009), the other studies fail to support their findings with robust palaeomagnetic field test that will help constrain the ages

of the primary directions isolated from the measured samples. Biggin et al., (2011) acknowledge the findings are encouraging and exciting but establishing the reliability of results is crucial to furthering our understanding of the Archaean geomagnetic field.

The work of Biggin et al., (2011) covered the Hooggenoeg Formation, the Noisy Complex and also Kromberg Formation. Here we will focus exclusively on their findings in relation to the Hoggenoeg Formation. The authors sampled a total of 8 sites in the southern limb of the OF, as shown in Figure 5.1. Sites HG2-6 were sampled close to the fold hinge, whilst sites HG7-9 were sampled further south, along the Komati river in close proximity to the contact with the Noisy Complex. All sites, with the exception of HG2, sampled volcanic flows of basaltic composition. HG2 sampled an intrusive dyke which is also basaltic in composition. Samples were demagnetised using thermal (TH) and alternating field (AF) stepwise demagnetisations. A combined TH (up to 430°-480°C) and AF demagnetisation technique was utilised on some samples given that AF measurements could be preformed quickly on an in-house built AF demagnetiser at Utrecht University (see Section 5.4 of this chapter for more detail on this technique), whilst still ensuring viscous components were fully removed.

	Component	Estimated age (Ma)	Dec (°C)	Inc (°C)	k	α95 (°)	N	Pal-lat (°)	λ (°C)	ϕ (°C)	A95 (°)	dp	dm
Biggin et al., (2011)	LT1	~0-250	350.7	-60.6	50.0	9.6	6	-41.6	72.6	234.9	12.0	11.1	14.6
			282.3	*61.5*	*56.9*	*9.0*		*42.7*	*-9.0*	*344.3*	*11.0*	*10.7*	*13.9*
	LT2	1800-2054	162.8	-66.0	18.8	14.3	7	-48.9	-13.6	199.5	22.2	19.3	23.5
			109.8	*64.2*	*11.9*	*18.3*		*45.9*	*0.1*	*14.8*	*27.4*	*15.2*	*19.0*
	MT	~2.7 Ga?	321.8	85.6	50.4	13.1	4	81.2	-19.0	25.3	25.6	25.7	26.0
			18.9	*4.0*	*17.6*	*22.5*		*2.0*	*56.6*	*67.0*	*21.5*	*11.3*	*22.5*
	HT1	<3230	169.8	58.1	121.9	6.1	6	38.8	-74.6	62.4	7.5	6.6	9.0
			44.1	*-22.9*	*16.8*	*16.8*		*-11.9*	*46.2*	*110.8*	*16.5*	*9.5*	*17.8*
	HT2	3472-3455	36.9	62.9	37.3	15.3	4	44.4	12.0	57.0	22.2	18.9	24.0
			16.5	*-9.2*	*14.6*	*24.9*		*-46.0*	*63.4*	*70.3*	*16.1*	*12.7*	*25.1*

Table 5.1. Mean Directions and poles calculated by Biggin et al., (2011). The lower direction, given in italics, for each component is given in stratigraphic coordinates. The upper direction is given in geographic coordinates. Pal-lat is the palaeolatitude associated with the mean direction (assuming a GAD) and λ and ϕ are the latitude and longitude of the associated (north poles). A95, dp and dm are 95% confidence parameters for the mean pole.

Rock magnetic observations and detailed thin section work revealed the magnetic signal in the rocks of the Hooggenoeg was recorded by pseudo-single domain (PSD) grains or a combination of single domain grains (SD) and multi-domain grains (MD) of Ti-poor titanomagnetite or magnetite (Biggin et al., 2011). Zijderveld Plots were found to be generally multi-component with at least one overprint component isolated prior to a stable characteristic remanent magnetisation (ChRM) being identified. The first of three over-

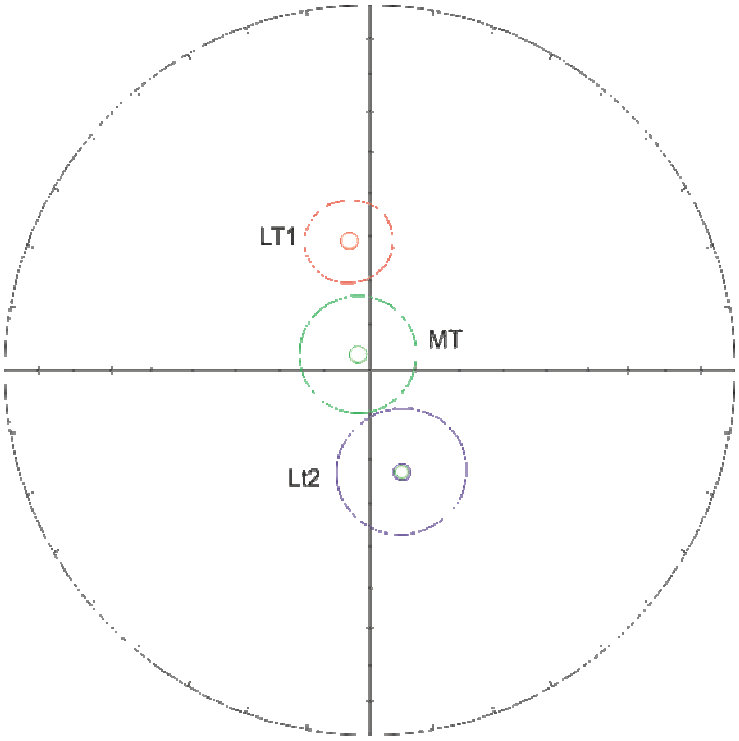

Figure 5.3. Equal area projection of Biggin et al., (2011) overprint components. Directions for the plotted components are taken from table A and based on the work of Biggin et al., (2011). Directions are plotted with the α95 confidence limit envelope. LT1 is shown in red, whilst LT2 is shown in blue. Component MT is shown in green.

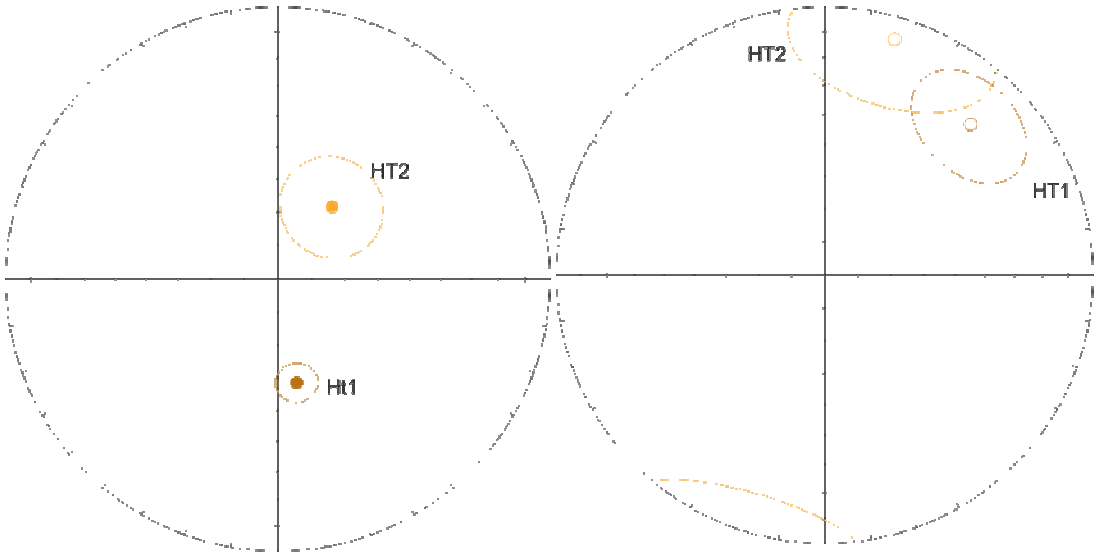

Figure 5.4. Equal area projections showing high temperature components as describe by Biggin et al., (2011). On the left, high temperature components, HT1 and HT2 are shown in geographic coordinates. Directions are plotted with the α95 confidence limit envelope. HT1 is shown in brown, whilst HT2 is shown in yellow. On the right, components are plotted in geographic coordinates. On the left, the components are shown in stratigraphic coordinates, having been tectonically corrected for the influence of the OF. Directions for the plotted components are taken from table A and based on the work of Biggin et al., (2011).

print directions isolated was LT1, (for all three overprint direction, see Figure 5.4), isolated between 250° and 460°C and thought to represent a present day overprint given that the pole for the direction plots between the present-day field (in South Africa) and the geocentric axial dipole (GAD), see Table 5.1 for further details of the direction. The component LT2 was isolated in the temperature ranges between 100°C and 440°C across seven sites, but only one of those was a Hooggenoeg Formation site. The LT2 direction was seen to overlap with poles produced from a wide spread thermal event associated with the emplacement of the 2054.4± 1.3 Ma Bushveld Complex (Letts et al., 2009), a large scale intrusive event some 200 km from the BGB (Biggin et al., 2011). The third overprint component, MT, was observed in a total of four studied sites and isolated in temperature ranges between 370°C and 430°C/ 35mT. It is a predominantly near vertical down component (Biggin et al., 2011) similar to that preserved in the 2714±8 Ma (Armstrong et al., 1990) rocks of the Westonara Basalt in Ventersdorp Supergroup (outcrops between 25°S/26°E and 30°S/24°E, some 680 km west of the town of Barberton at it's northernmost outcrop, Strik et al., 2007) and the Modipe Gabbro intrusion (outcrops along the South Africa and Botswana border at ca. 24°39' and 26°10', Evans and McElhinny, 1966). In two sites, L3 and L4, the component is isolated at higher temperatures (480°C), above the unblocking temperatures of LT2, meaning it could be related to interplate magmatism of the Waterberg and Soutpansberg Supergroups (located north of the Bushveld Complex) acquired prior to 1.8 Ga (Biggin et al., 2011). The authors offer the interpretation that the direction may have been acquired prior to the LT2 direction, during a ca.2.7Ga event (de Ronde et al., 1991) and was later overprinted by the thermal event that imparted the LT2 direction.

Biggin et al., (2011) isolated two ChRM directions from six of the eight sampled sites. Direction HT1 was removed above temperatures of 340°C in sites HG2 and HG3, close to the axis of the OF. Grouping of the direction is better in geographic coordinates than in stratigraphic coordinates, once a correction for the formation of the OF is applied. As such, Biggin et al., (2011) determined that the direction is younger than the 3.2Ga OF. Establishing the timing of the acquisition of the direction beyond that is complicated. The most straight forward option is that HT1 represents an overprint associated with a large thermal event at 3.1Ga(Toulkeridis et al., 1994) or the igneous events in the BGB between 2.9-3.0 Ga (de Wit et al., 2011; Schoene et al., 2008b). However, the antipode of the HT1 direction is consistent with the pole obtained for the Karoo by Strik et al., (2007); a Mesozoic to Cenozoic aged large igneous province north of the BGB. The LT2 and MT direc-

tions are considered to be older than ca. 180 Ma and therefore, would mean a chemical remagnetisation caused the HT1 overprint and allowed preservation of a more ancient field to be preserved at lower unblocking temperatures (Biggin et al., 2011).

At temperatures above 460°C, in sites HG5,6,7 and HG9, a moderately –steep down direction was isolated, HT2. A Monte Carlo common true mean test shows that despite the similarity between the HT2 direction and the MT overprint, the directions are statistically distinguishable (Biggin et al., 2011). The same is true when the HT2 pole, in geographic coordinates, is compared to the Bushveld Complex poles. Biggin et al., (2011) attempted a fold test to establish the timing of the acquisition of the HT2 component. The directions cluster more poorly in stratigraphic coordinates than they do in geographic coordinates (see Figure 5.4) but is inconclusive partly due to the limited data set, as the direction was only observed in four sites (Biggin et al., 2011). In addition, despite the sites having somewhat different bedding plane measurements (HG5-6 (Strike/Dip) = 348°/100° and HG8-9 (Strike/Dip) = 55°/90°), the sites sampled are on the same limb of the OF, one might expect more conclusive results if data had been available for the northern limb of the OF.

5.4. Methodology

5.4.1. Sampling

In May 2011, 152 core samples were sampled at 14 sites (LHG1-14) of the Hooggenoeg Formation, collected as part as of a larger sampling trip of the Onverwacht Group. All sites sampled in the Hooggenoeg Formation sample basaltic komatiites (for a detailed description of the komatiities of the Hooggenoeg Formation, see Section 5.2 of this chapter; in addition, for a detailed description of komatiites in general, see Chapter 4), however, it was beyond the scope of this work to characterise the geochemistry of the sampled units in detail. Sites LHG1 and LHG10-14 were sampled in the Northern limb of the OF fold, as seen in Figure 5.1. Site LHG1 is thought to be of basaltic komatiite composition and generally massive. The unit appears jointed and sometimes contains pillows which can be highly vesicular in places. The vesicles are a good indicator of younging direction in the unit. In order to avoid the more likely severe quenching and hydrothermal alteration associated with the pillow edges, samples were collected in the centre of the pillow lavas. Site LHG10 is located stratigraphically below LHG1. Just over 100m away from site LHG10, is site LHG11 a pillowed lava unit, see Figure 5.5 (e&d). The unit dips into a stream, in close proximity of which the unit appears more massive, as a result of the smoothing of the rocks

caused by water erosion. This unit is stratigraphically below LHG10. Sites LHG12-14 are more weathered in comparison to the other LHG sites, in particular their red colouring is striking when compared to the dark grey colouring of all other LHG sites, as is shown in Figure 5.5 (c&f). Sites LHG12 and LHG14 contain a mixture of massive and pillowed sections. The pillows are smaller, less well formed and less abundant than in other northern limb sites. The massive parts of the unit are heavily fractured. Site LHG13 is also weathered and generally massive, with no evidence of pillows or vesicularity. Vesicularity is a feature typical of the lower units within the Hooggenoeg Formation. The unit becomes more varilotic up stratigraphy owing to increasing water depths due to the evolution of the subsiding oceanic basin in which they were originally deposited (M.J. de Wit, pers. comm.).

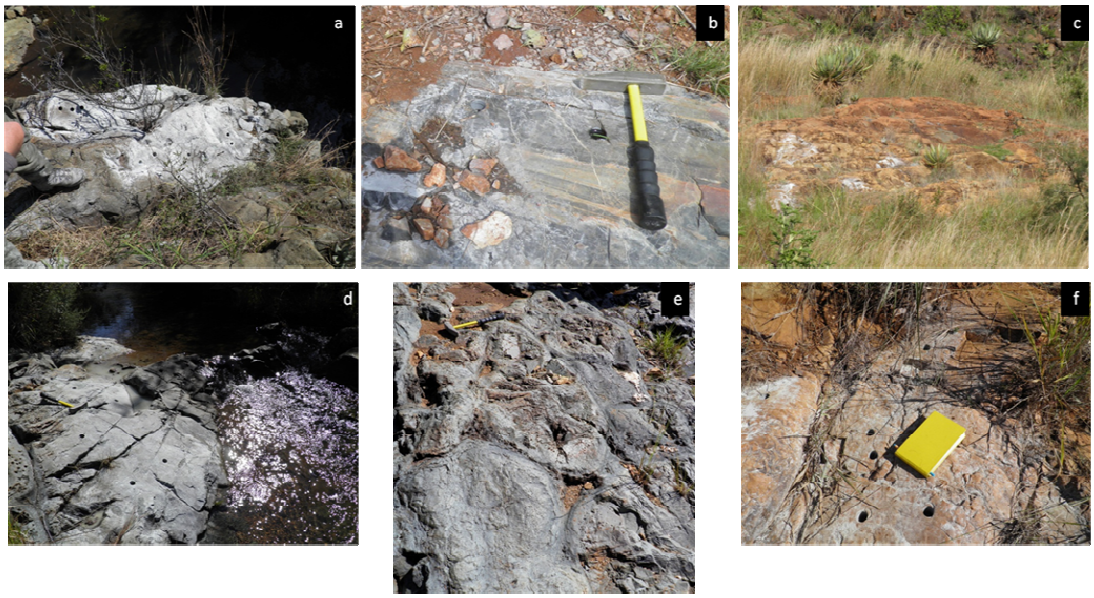

Figure 5.5. Photographs of some of the Hooggenoeg Sampling sites. (a) Site LHG8, note the dark colour of the volcanincs in the southern limb of the OF fold. (b) Site LHG9, a chert layer within the Hooggenoeg Formation. Note the colour banding within the chert, indicative of impurities within the silicified layers, see section 1.2 of this chapter for further details. (c) LHG13. Note the red weathering colour observed in the sites of the Northern limb of the OF. (d & e) LHG11. (e) shows the pillow lavas observed in the site, note how vesicularity is limited and restricted to the edges of the pillow. (f) Close up of sampling site LHG14, from the base upwards samples LHG12.2 to LHG12.6.

Sites LHG2-9 were sampled in the southern limb of the OF fold (see Figure 5.1), ~3 km away from sampling sites HG7-9 of Biggin et al., (2011). All southern limb sites are thought to be of basaltic komatiite composition. The exception is site LHG8 which could be komatiitic or peridotitic in composition, given the presence of well preserved spinifex texture. LHG9 is also an exception, it is the only site of the sites sampled in the Hooggenoeg Formation that is not basaltic in origin. The unit comprises a volcanoclastic unit which has been subsequently altered via silicification to a chert(Hofmann et al., 2013; Lowe, 1999b).

This means that the chert is largely (in the case of the Onverwacht Group cherts it is typically >75%, Lowe 1999) comprised of microcrystalline silica in the form of microquartz and/or chalcedony (Lowe, 1999b). The sampled chert (Figure 5.5 (b)), was banded and exhibited white (microquartz and/or chalcedony), red and dark grey colours, indicating it is an impure chert containing also iron oxides (leading to the reddish colour) as well as carbonaceous matter, ash, clay, dolomite and siderite, resulting in the dark grey colouring (Lowe, 1999b). In addition, the unit is crosscut by a series of cm scale quartz veins. Sites LHG2-7 are overall massive, with pillows only being observed in site LHG5. As with the northern limb sites, pillow edges were avoided when sampling to ensure the quality of the samples.

The OF provides a good opportunity to collect Hooggenoeg Formation samples from each limb of the fold and therefore to perform a fold test to contribute to the efforts of ascertaining the timing of acquisition of potentially primary ChRM. The southern limb sites were sampled with the aim to validate the findings of Biggin et al., (2011) as well as increase the available data set, in hope of producing yet more robust results. The northern limb of the OF fold was previously unsampled. The new sample set gives the opportunity to validate results over a large geographical area, but primarily allows for a fold test to be performed.

5.4.2. Experimental Methodology

A suite of rock magnetic investigations have been used to determine the properties of the magnetic particles in the samples of the Hooggenoeg Formation. These are described in detail in Chapter 3, Section 3.2.2.1) . Experiments have been carried out on 29 samples from across all sited. With the exception of sites LH10 and LHG11 (were only one sample was measured), at least two samples from each site have been investigated.

Three to eleven samples from each sampling site were either thermally (TH) demagnetised or a combined thermal and alternating field (AF) technique was applied. On average, a total of 14-25 specimens were measured from each site. Site LHG9 is the exception; where only five individually oriented samples were collected. See Chapter 3, Section 3.3.1. for full experimental methodology.

5.5. Results

5.5.1. Directional Results

Three to eleven samples from each sampling site were either thermally (TH) demagnetised or a combined thermal and alternating field (AF) technique was applied. On average, a total of 14-25 specimens were measured from each site. Site LHG9 is the exception; where only five individually oriented samples were collected. See Chapter 3, Section 3.3.1. for full experimental methodology.

NRM intensities for the samples range from 10^{-6} to 1 A/m. These intensities are comparable to NRM intensities measured in other Archaean aged volcanic rocks (Biggin, 2009; Strik et al., 2003; Strik et al., 2007). In addition, they are comparable to previously published NRM intensities for the rocks of the Hooggenoeg Formation (Biggin et al., 2011) and the NRM intensities measured for the komatiites of the Komati Formation in this study (Chapter 4).

The analysis of the palaeomagnetic data was conducted using principal component analysis and standard statistical analysis (Fisher,1953: Kirschvink,1980). Samples generally produce multi-component Zijderveld Plots with two stable overprint magnetic directions removed during step-wise demagnetisation prior to a characteristic remenant magnetisation (ChRM) component being isolated. In some cases, (discussed in more detail below) it was not possible to isolate a stable overprint and/or ChRM components. Recorded overprint and ChRM components generally had a maximum angular deviation (MAD) of less than 15°. Low NRM intensities in some sites result in scattered directions that do not produce a reliable site mean directions. Figures 5.8, 5.9, and 5.10 summarise the directional results, whilst Table 5.2 provides details of site lithologies and components isolated.

5.5.2. Description of Overprint Directions

5.5.2.1 Low Temperature Magnetisation (LT)

A low temperature direction of magnetisation (LT1) was identified in seven of the measured sites, see Figure 5.6 a,d and e & Figure 5.7 a, c, d and f. The direction is to some extent scattered but mostly directed towards the north and moderately steep (mean direction, declination/inclination (D/I)=336.2°/–42.1°, $\hat{k}$= 4.2, α95=33.6°), and was generally removed by thermal demagnetisation in temperatures ranges from 20-400°C, although persisted to 440°C in samples from site LHG3, LHG10 and LHG11. The LT1 direction pro-

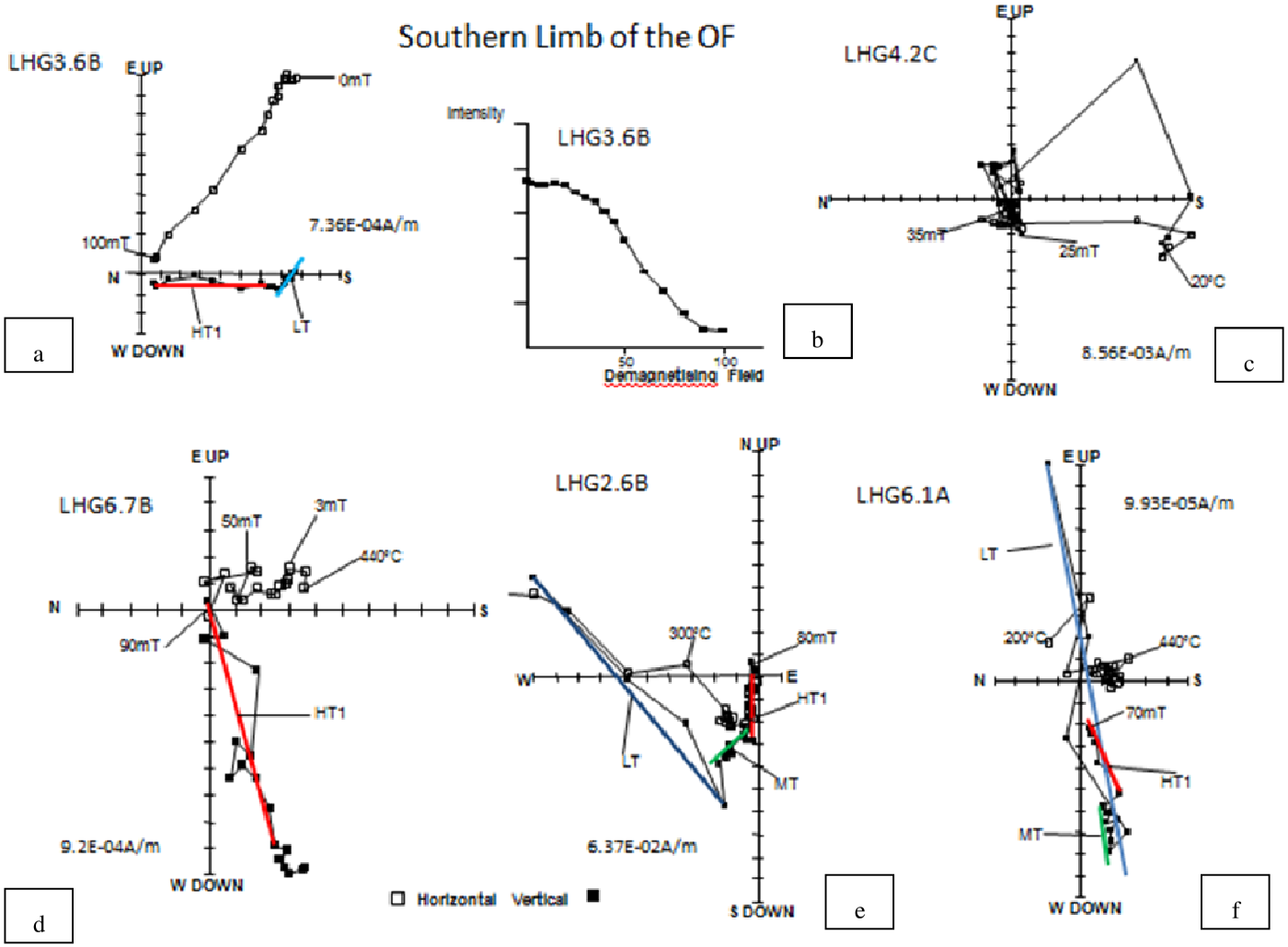

FIGURE 5.6—. Orthogonal vector plots for samples from the southern limb of the Onverwacht Fold (OF) and representative demagnetisation diagram . (d&e) The majority of samples show two components of magnetisation. Samples LHG2.6B and LHG6.1A show three components of magnetisation. (c) In sample LHG6.7B the low temperature component is not shown, making it easier to view the high temperature component. (b) LHG4.2C is a particularly noisy sample and highlights the difficulties associated with

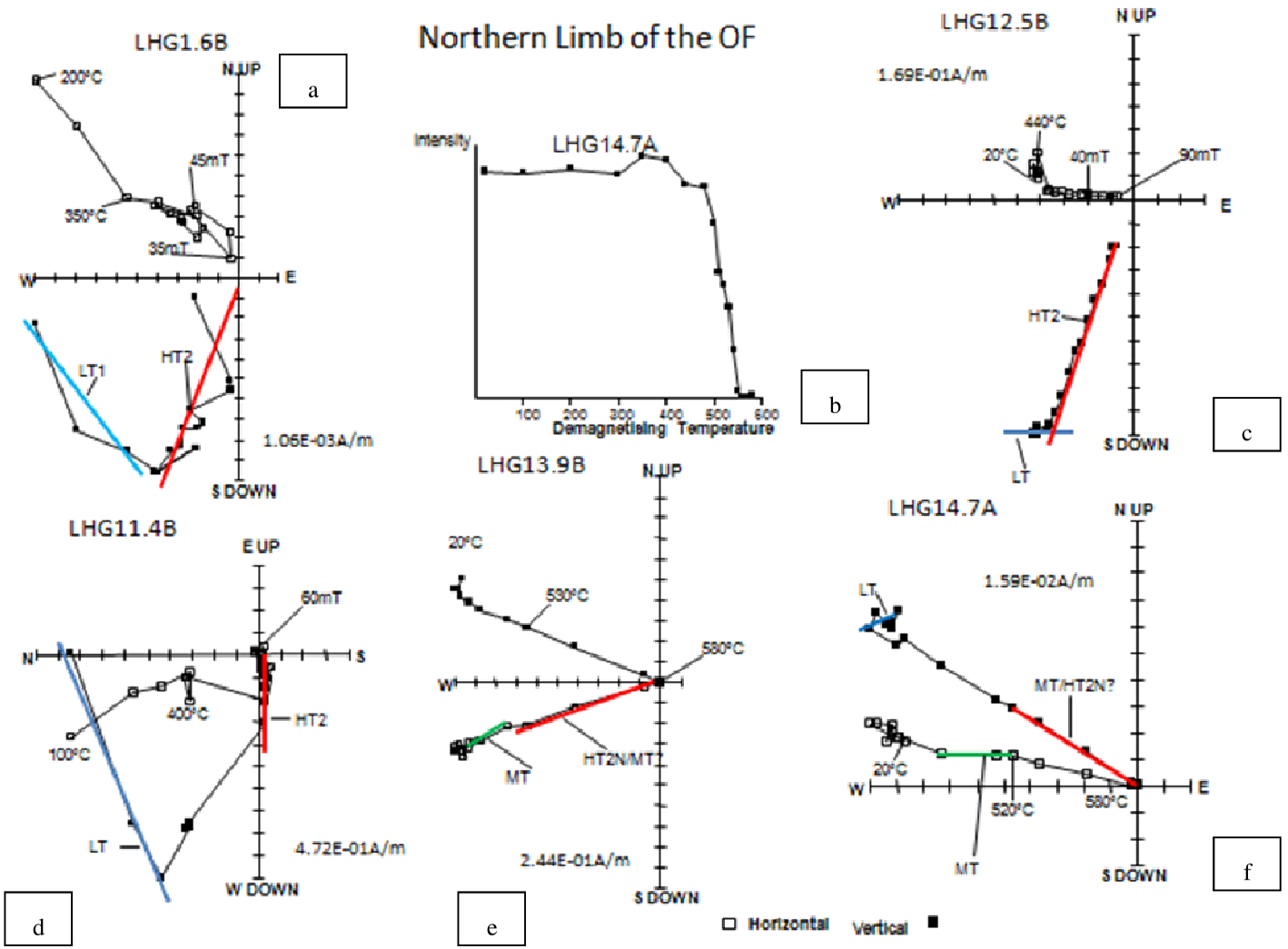

FIGURE 5.7—. Orthogonal vector plots for samples from the northern imb of the Onverwacht Fold (OF) and representative demagnetisation diagram. (a&d) The majority of samples show two components of magnetisation. A low temperature overprint is removed prior to a high temperature component. (e&f) Samples LHG13.9B and LHG14.7A are shown as examples were a 'dog leg' is seen between themed temperature and high temperature components.

duces a pole (in geographic coordinates) that plots between the present-day field (PDF) and geocentric axial dipole (GAD) poles and therefore very likely records a recent field direction acquired as a viscous remenant magnetisation (VRM).

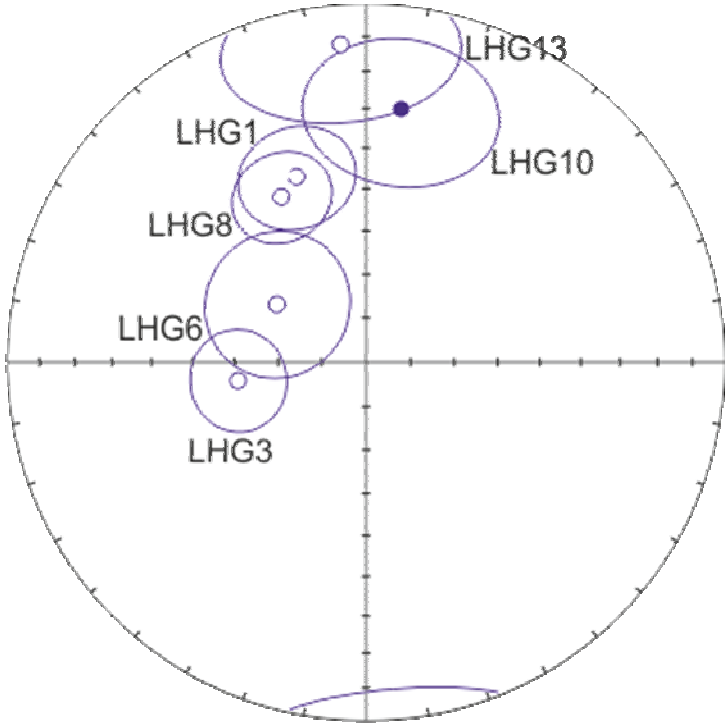

Figure 5.8. Equal area projection showing site mean directions for component LT1, in geographic coordinates. Filled (unfilled) points representing the lower (upper) hemisphere and ellipses indicating α 95 cones of confidence.

Low temperature directions of magnetisation were isolated, by thermal demagnetisation, from samples in the remaining seven sites (LHG2,4,5,7,9,12 and 14). Unblocking temperatures were consistent with those from the sites which yielded the LT1 component. Whilst directions from some samples in sites LHG2, LHG4 and LHG7 were comparable to the LT1 direction, the majority of the isolated directions in the sites were scattered; as a result, it was not possible to calculate a meaningful site mean direction for these sites.

5.5.2.2 Mid Temperature Magnetisation (MT)

A second intermediate stability direction of magnetisation was observed in the majority of the measured sites. The direction is usually isolated in the temperature ranges 400°C/0mT - 530°C/35mT, with the exception of sites LHG2,5 and LHG10 were it persisted up to 50mT in some samples. In most sites, the directions are too scattered to obtain a meaningful site mean. Moreover, sites LHG4,7, 9 and LHG12 produced three, or less, samples with a mid temperature direction and therefore it was also not possible to combine the isolated directions to produce a site mean.

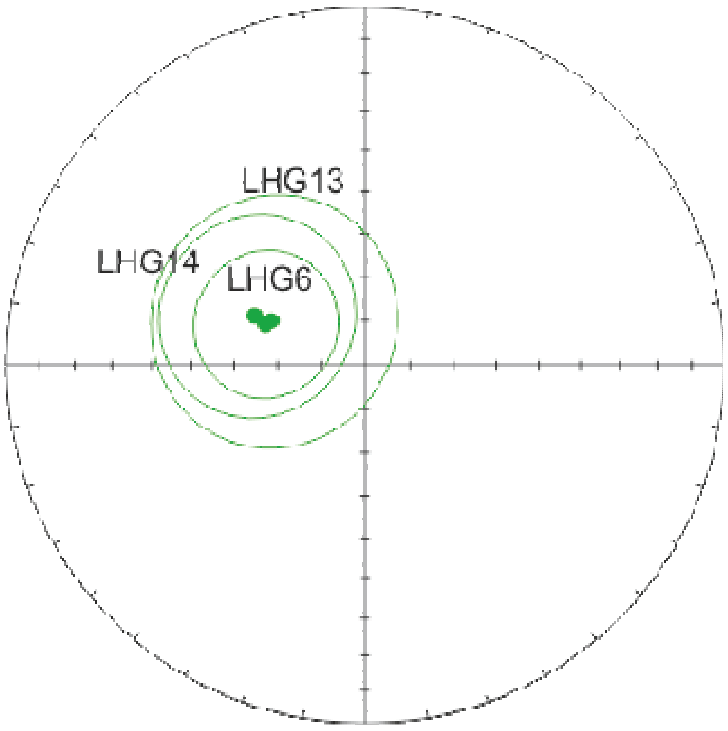

Figure 5.9. Equal area projection showing site mean directions for component MT, in geographic coordinates. Filled (unfilled) points representing the lower (upper) hemisphere and ellipses indicating α 95 cones of confidence.

In three sites, LHG6, LHG13 and LHG14, the second overprint direction, MT, was well clustered and was observed to be directed near vertical downwards and was removed by thermal and alternating field demagnetisation between 400°C and 45mT. The MT component has a mean direction of declination/inclination (D/I)=293.8°/64.67°, ƙ= 144, α95=3.2° n=3. The direction was also identified in a number of other sites, but individual samples gave results which were too scattered results to produce a reliable mean direction.

5.5.3. Description of High Temperature Magnetisation(HT1 and HT2N)

High Temperature convergent directions of magnetisation were isolated and gave consistent directions in eight sites from the Hooggenoeg Formation. The directions fell in two directional clusters. The first direction is HT1, as identified previously by Biggin et al (2011). It has a southerly, moderately steep direction (mean declination/mean inclination (D/I) = 165.9°/71.2°, ƙ= 36.5, α_{95}=15.4°, n=4). HT1 is isolated in samples from sites LHG2, LHG3, LHG4 and LHG6, all of which are located on the southern limb of the OF fold, as is shown in Figure 5.1. This direction was isolated above 480°C in all sites, except for LHG4 were it was identified at 400°C.

	Lithology	Site	Bedding Strike/Dip (°)	Lat (°)	Long (°)	Demag	N	NRM (A/m)	Component	T Range (°C/mT)	Dm	Im	k	a95	n
Hooggenoeg Formation	Komatiititc Basalt	LHG1	301/102	-25.9527	30.8809	TH, TH+AF	10	10^{-4}- 10^{-3}	LT1	20-400°C	339.3	-44	20.6	12.5	8
									MT	350°C/10-500°C/30	Scattered - shallow down to N				
									HT2	440°C/3-540°C/70	274.2	65	184.4	6.8	4
		LHG2	59/82	-26.0175	30.9536	TH, TH+AF	13	10^{-4}- 10^{-2}	LT	20-400°C	Scattered - up and NW				
									MT	400°C/0-50	Scattered - steep down to west				
									HT1	480°C/10-560°C/70	190.2	66.7	11.6	38	3
		LHG3	59/82	-26.0173	30.9547	TH, TH+AF	10	10^{-4}- 10^{-3}	LT1	20-440°C	261.6	-60.3	46.8	11.3	5
									MT	350°C/0-440°C/35	Scattered/smeared - steep down to west				
									HT1	480°C/25-560°C/90	179.9	64.4	16.4	15.3	7
		LHG4	59/82	-26.1794	30.9519	TH, TH+AF	10	10^{-3}- 10^{-2}	LT	20-400°C	Scattered to the NW both up and down				
									MT	0-35	west and shallow				
									HT1	400°C/0-530°C/70	174.1	73.2	72.5	9	5
		LHG5	59/82	-26.0196	30.9515	TH, TH+AF	11	10^{-4}- 10^{-2}	LT	0-400°C	Scattered - down to SW				
									MT	480°C-50	317.2	67.8	4.1	52.1	4
									HT	500°C/0 -560°C/90	No consistent HT identified				
		LHG6	59/82	-26.0200	30.951	TH, TH+AF	12	10^{-4}- 10^{-3}	LT	20-400°C	302.8	-65.7	12.1	16.6	8
									MT	0-35	292.1	65.3	17.2	16.6	6
									HT1	480°C/35-570/90	180.6	68.6	194.8	4.3	7
		LHG7	59/82	-26.0203	30.9524	TH, TH+AF	9	10^{-4}- 10^{-2}	LT	20-400°C	Scattered - steep up				
									HT	440°C/7-550°C/90	Scattered to the South				
		LHG8	59/82	-25.7818	30.8832	TH, TH+AF	11	10^{-4}-10^{-3}	LT	20-400°C	332.8	-47	19	10.8	11
									MT	0-35	No consistent MT identified				
									HT	480°C-90	68.1	82.6	15	12.2	11
	Chert	LHG9	59/82	-25.9491	30.8681	TH, TH+AF	6	10^{-4}-10^{-2}	LT	100-480°C	Shallow down to the West.				-
									HT	440°C/0-580°C/40	Scattered to the N, NE up and down.				-
	Komatiititc Basalt	LHG10	301/102	-25.9527	30.881	TH, TH+AF	12	10^{-4}-10^{-3}	LT1	20-440°C	7.9	29.5	10.6	19.4	7
									MT	350°C/0-530°C/50	Scattered, down N to W				
									HT	480°C/0-580°C/90	Scattered, to the SW to NW, up and down				
		LHG11	301/102	-25.9532	30.881	TH, TH+AF	12	10^{-3}-1	LT1	20-440°C	329.2	-53.6	6.9	24.7	7
									MT	300°C/3-500°C/35	Scattered, down to the E				
									HT2	480°C/0-580°C/90	313.4	78	20	21.1	4
		LHG12	301/102	-25.9667	30.8806	TH, TH+AF	12	10^{-1}-10^{-1}	LT1	20-400°C	Scattered to the NE to SE, steep down				
									MT	440-510°C	No consistent MT identified				
									HT2	480°C/0-580°C/90	283.6	67.4	38.6	9.8	7
		LHG13	301/102	-25.9677	30.8795	TH, TH+AF	11	10^{-2}-10^{-1}	LT1	20-400°C	355.3	-12.1	13.8	21.3	5
									MT	400-530°C	296.3	66.3	6.4	28.6	6
									HT2	520°C/0-580°C/90	307.5	70.7	71.2	7.2	7
		LHG14	301/102	-25.9678	30.8795	TH, TH+AF	9	10^{-1}- 10^{-1}	LT	20-400°C	Scattered, mostly up to the S				
									MT	440°C-540°C/45	291.3	72.5	90.3	22.8	3
									HT2	480°C/25-580°C/90	294	62.4	235.3	5	5

Table 5.2. Overprint and high temperature components measured in this study. Strike and dip refer to bedding planes measured in the field and validated against measurements from regional scale geological maps. Dec and Inc refer to the direction of the components in geographic coordinates before applying the plunging fold correction. N refers to the number of samples measured whilst n is the number of specimens used to calculate the site mean.

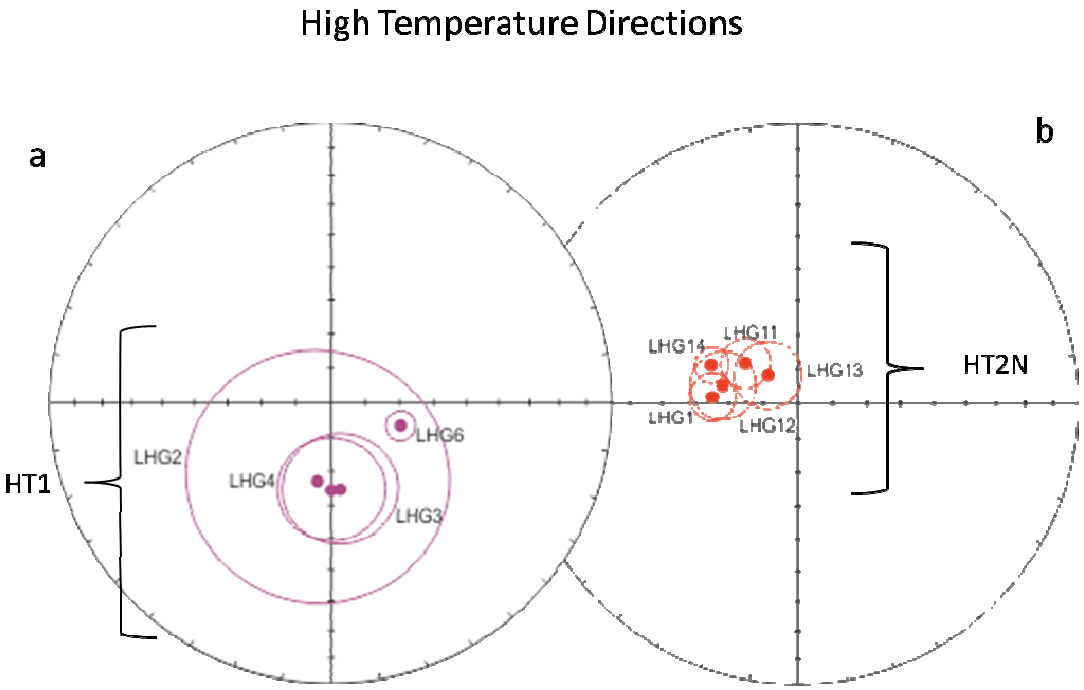

Figure 5.10. Equal area projections showing site mean directions for high temperature components. (a) Sites from the southern limb of the OF display the HT1 direction, whilst from the sites on the northern limb of the OF component HT2 isolated (b). Filled (unfilled) points representing the lower (upper) hemisphere and ellipses indicating α 95 cones of confidence.

The second cluster of ChRM directions, HT2N (to distinguish it from HT2 of Biggin et al., (2011), which from now on will be referred to as HT2S), are directed north east and moderately steep down (mean declination/mean inclination (D/I) = 289.0°/66.8°, $\hat{k}$= 154.4, α_{95}=7.4°, n=4). This direction was only identified in samples collected from sites in the northern limb of the fold: sites LHG1 and LHG12-14. This direction was isolated above 480°C in all sites, except for LHG14 were it was identified at 400°C. The direction is distinct from the previously identified HT1 component, (see Figure 5.10).

No site mean direction was calculated for LHG5. Although high temperature directions were obtained from 12 out of the 22 measured specimens the directions were overall very scattered. Interpretation of the Zijderveld plots was difficult given the particularly noisy nature of the plots. The poor quality of the results might be explained by the low NRM intensities measured from this site (9 x10^{-4} to 1 x10^{-2} A/m). Added to which, at high

AF steps (60-90mT) for samples demagnetised using the combined TH and AF approach, the high temperature component veered away from the origin, indicating the samples may have been affected by a gyroremanent magnetisation (GRM) acquired during the AF demagnetisation experiment. Crucially, specimens measured from the same sample often gave very different directional results and therefore their reliability has to be questioned. This is the case for eight of the measured specimens and therefore, these directions where not used to calculate a site mean. The remaining four directions (calculated from four individual specimens) are too scattered for a meaningful site direction to be calculated.

Results from site LHG7 were not included in the HT1 or HT2N direction means. Eight of the 18 specimens measured produced high temperature direction. The remaining ten samples were, in most cases, fully demagnetised by 400°C and characterised by a single component of magnetisation above which the Zijderveld Plot became too noisy for any further interpretation. The uni-vectorial nature of the Zijderveld Plots and rapid loss of NRM at low demagnetisation temperatures suggests, at least in some cases, that the site might have been affected by lightning strikes. Multi-component Zijderveld Plots are obtained for samples LHG7.3, LHG7.4, LHG7.10 and LHG7.12, (LHG7.11 was not measured). Directions measured from individual specimens from core samples LHG7.10 and LHG7.12 agreed well with one another. However, the directions obtained from these samples are scattered and cannot be used to calculate a site mean. The measured NRM intensities for the site are low (9.58×10^{-4} to 3.05×10^{-2} A/m) when compared to other lightning struck samples identified in this study (up to 89 A/m in the Noisy Complex and up to 40 A/m in the Nelshoogte Pluton, see Chapters 6 & 7 respectively). However, this does not preclude the possibility that site LHG7 might have been affected by lighting. The overall low NRM intensity suggest that none of samples collected from the site have been directly struck by lightning, however lightning strikes can affect the NRM of a surface outcrop by as much as 25 m² (Graham, 1961), therefore, it is not unlikely that these samples would have felt the effect of nearby lightning strikes. The multi-directional behaviour observed in samples LHG7.10 and LHG7.12 in particular, might be indicative of these samples being at a greater distance from the area of outcrop effected by lightning, given that their measured NRMs are also lower (9.58×10^{-4} and 1.2×10^{-3} A/m, respectively) than the NRM intensities measured for samples LHG7.1 to LHG7.9 which range 7.3×10^{-2} to 1.16×10^{-1} A/m.

Site LHG9 is the only site of those sampled in the Hooggenoeg Formation that is not basaltic in origin. Only five oriented cores and three hand samples were collected at this locality given that cherts are extremely hard and therefore particularly time consuming and difficult to drill. A high temperature direction of magnetisation was measured in three of the specimens demagnetised. Despite the original volcanic material having the potential to record a primary magnetisation (e.g. the HG1 tuff of the Noisy Complex, as sampled by Biggin et al., (2011)), the replacement of the primary mineralogy by silica means that, in general, cherts are not good magnetic recorders. Combined with the limited number of samples available it was unlikely that site LHG9 would yield a meaningful site mean direction regardless of the effort made to sample the dark grey and red bands over the white bands.

Some samples of site LHG11 present a direction that is similar to the HT2N mean direction. High temperature directions from this site are generally scattered but the calculated site mean is broadly comparable to the HT2N direction. The unblocking temperatures of the isolated directions are within the range described above for the HT2 components. However, six of the 14 measured specimens produced very noisy Zijderveld plots, from which it is not possible to distinguish a high temperature component. NRM intensities for this site range between 4.11 $x10^{-2}$ to 1.03 A/m, which are comparable with other Archean aged rocks and particularly the komatiites of the Komati Formation. Nevertheless, the NRM intensities of samples LHG11.2 and LHG11.12, in excess of 1 A/m, are higher than any other NRM intensity measured for the Hooggenoeg Formation. It would not be unreasonable to attribute the elevated NRM intensities to a lightning strike. The Zijderveld plots for these samples are noisy but do not have the characteristic univerctorial behaviour expected from lightning struck samples. Whilst the maximum angular deviation (MAD) for the directions is low (2-3°), given the overall scatter of the individual directions and unreliable nature of some of the Zijderveld Plots due to them being noisy, as well as the large range in measured NRM intensities, the mean direction for site LHG11 was not used to calculate the HT2 component direction.

5.6. Rock Magnetic Characterisation

Of the 29 samples for which rock magnetic experiments were performed only samples from site LHG4, LHG11, LHG12 and LHG13 show a ferromagnetic contribution. The ferromagnetic signal is completely swamped by the paramagnetic fraction in samples from sites LHG1-3 and LHG5-10, as is sample LHG12.6bb and site LHG14, as is shown in Figure 5.11. As a result it was not possible to obtain magnetic parameters (Saturation magnetisation: M_s M_r, Corecivity: H_c; H_{cr}) from these sites.

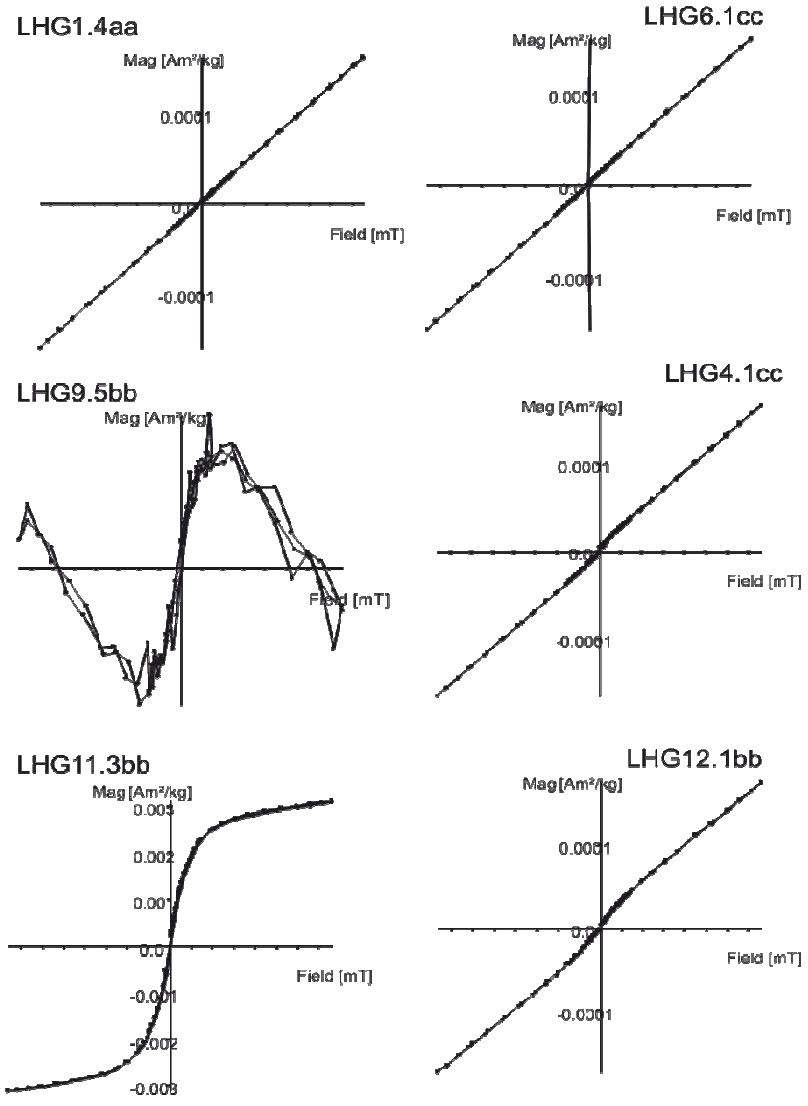

Figure 5.11 Representative hysteresis curves, acquired from the VFTB, for sites across the Hooggenoeg Formation. Samples LHG1.4aa and LHG6.1cc displayed dominantly paramagnetic behaviour. It was not possible to obtain rock magnetic data from these samples. Samples LHG12.1bb also shows a strong paramagnetic contribution, where the hysteresis loop had to be significantly corrected to remove that contribution in order to obtain rock magnetic parameters, but less so than LHG4.1cc. Sample LHG11.3bb is strongly dominated by the ferromagnetic fraction. LHG9.5b is taken from a chert horizon within the Hooggenoeg Formation, and displays predominantly diamagnetic behaviour; given its mineralogy the samples from this site where not expected to yield good rock magnetic parameters.

Of the three LHG4 samples measured, only results from one had a strong enough ferromagnetic contribution for magnetic parameters to be obtained. However the paramagnetic contribution was still significant and a considerable correction was applied to remove the contribution before results were obtained. The same is true for samples LHG12.1bb and samples from site LHG13. The measured sample from site LHG11 was strongly dominated by the ferromagnetic contribution and a very minor correction of the paramagnetic contribution was required to characterise the samples rock magnetic properties.

Thermomagnetic curves for samples from sites LHG1-3 and LHG5-10 (Figure 5.12) and also LHG4.1cc and LHG12.1bb (which gave good magnetic parameters) were too strongly dominated by the paramagnetic fraction for Curie Temperatures (T_c) to be established. However, the majority of the samples showed significant alteration with a new magnetic phase being formed during the heating step, (Figure 5.12). This behaviour is most pronounced in samples LHG2.3bb and 4.5dd. Sample LHG8.6cc shows significant alteration with the heating curve appearing over the cooling curve, indicating an originally magnetic phase is lost during the heating of the sample. An inflection point is seen at 599°C in the heating curve (Figure 5.12b), but is not reproducible in the cooling curve and is therefore thought to be an alteration temperature. The sample has a further pronounced change in slope at ca.200°C in the cooling curve, possibly indicating the formation of pyrrhotite during heating.

During thermomagnetic experiments, samples from sites LHG6 and 7, as well as samples LHG2.6cc, LHG10.1aa, LHG11.3bb and LHG12.1bb give perfectly reproducible heating and cooling curves, or otherwise the difference between the curves is below 10% (difference in original Am^2/Kg and final Am^2/Kg) and therefore the alteration is not considered to be significant. It is noteworthy that it was not possible to calculate a T_c for sample LHG2.6cc (see Figure 5.12e), however, an inflection point at 464°C was observed on heating and is interpreted as the sample undergoing alteration .

It was possible to calculate a T_c for sample LHG11.3bb given at 567°C, as well as for samples from site LHG13 where T_c ranged from 555°C -570°C. In addition, IRM acquisition curves exhibit saturation below 100mT suggesting the presence of a low coercivity mineral, such as magnetite. The slightly lower than expected T_c for magnetite might suggest the sample contains some impurities, indicating the presence of titanomagnetite; which is

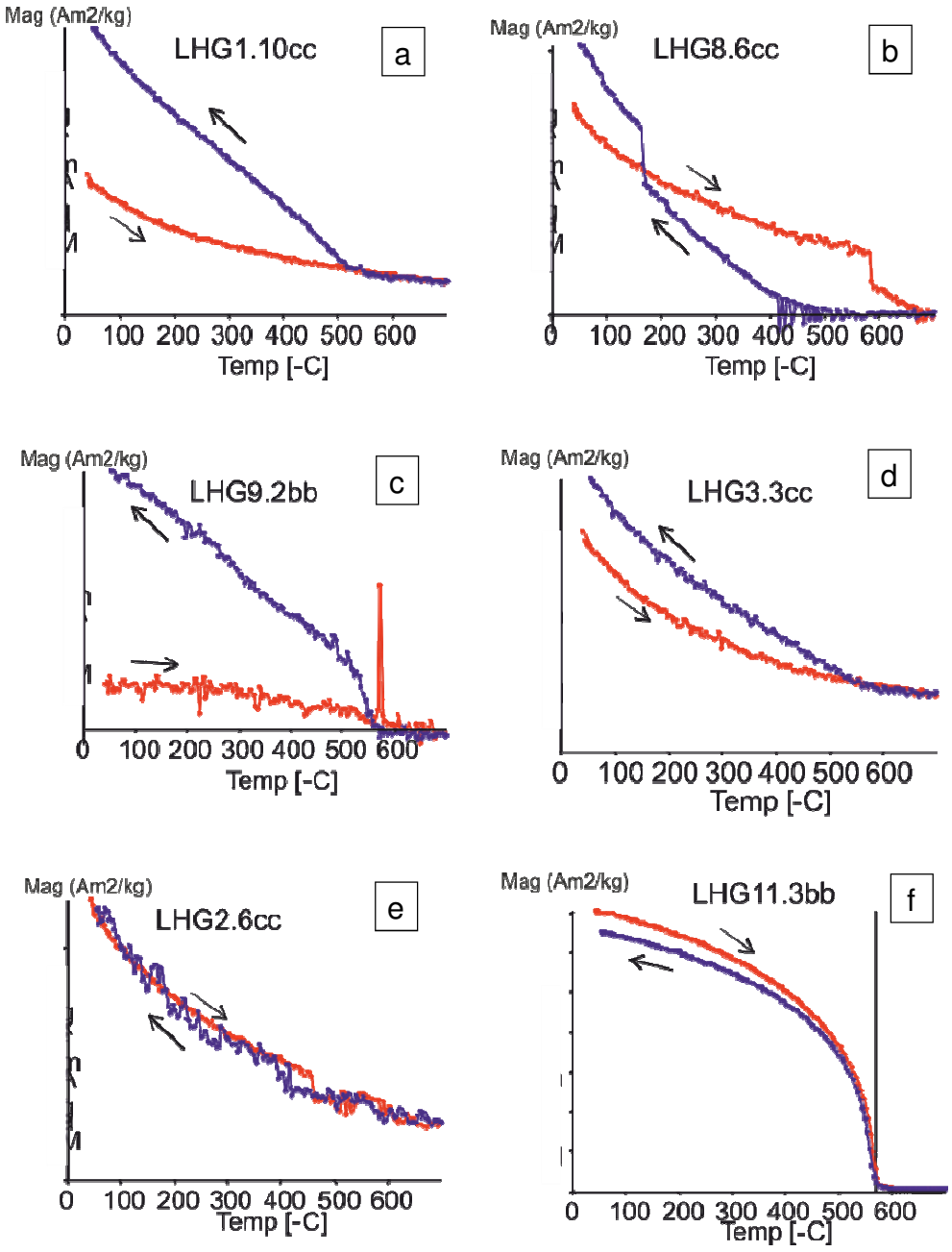

Figure 5.12. Representative thermomagnetic curves, acquired from the VFTB, for sites across the Hoogge-noeg Formation. Downwards arrows (red line) indicates the heating cycle, whilst upwards arrows (blue line) indicate the cooling cycle. Significant alteration on both the heating and cooling cycle is observed in samples LHG1.10cc (a), LHG8.6cc (b), LHG9.2bb (c) and LHG3.3cc (d). It was not possible to obtain Tc from samples LHG1.10cc (a) and LHG3.3cc (d) due to them being dominated by the paramagnetic fractions. Although samples LHG8.6cc and LHG9.2bb (b and c, respectively) both display a change in slope in during the heating cycle (and also the cooling cycle in LHG8.6cc), these are not considered Curie Temperatures are they are not reproducible and more likely indicate alteration occurring at that temperature. Samples LHG2.6cc (e) is strongly dominated by the paramagnetic fraction but heating and cooling curves are fully reproducible, therefore indicating no alteration on heating of the sample. Sample LHG11.3bb (f) is dominated by the ferromagnetic contribution, the curves are fully reproducible and a clear Tc is observed. The downwards arrow on the thermomagnetic curve represents a heating cycle, whilst the upward arrow indicates the cooling cycle.

Site	Sample	Ms (Am^2/kg)	Mr (Am^2/kg)	Hc (mT)	Hcr (mT)	Mr/Ms	Hcr/Hc	Tc (°C)
LHG1	LHG1.4aa				Paramagentic			
	LHG1.10cc				Paramagentic			
LHG2	LHG2.3bb				Paramagentic			
	LHG2.6CC				Paramagentic			
LHG3	LHG3.3cc				Paramagentic			
	LHG3.9bb				Paramagentic			
LHG4	LHG4.1cc	5.69E-03	2.12E-03	18.1	31.10	0.37	1.72	paramagentic
	LHG4.9dd				Paramagentic			
	LHG4.10dd				Paramagentic			
LHG6	LHG5.5cc				Paramagentic			
	LHG6.1cc				Paramagentic			
	LHG6.4bb				Paramagentic			
	LHG6.11cc				Paramagentic			
LHG7	LHG7.2cc				Paramagentic			
	LHG7.5bb				Paramagentic			
	LHG7.12bb				Paramagentic			
LHG8	LHG8.3cc				Paramagentic			
	LHG8.6cc				Paramagentic			
	LHG8.12cc				Paramagentic			
LHG9	LHG9.2bb				?			
	LHG9.5bb				?			
LHG10	LHG10.1aa				Paramagentic			
LHG11	LHG11.3BB	2.29	0.07	2.72	18.70	0.03	6.88	567
LHG12	LHG12.1bb	1.52E-02	1.26E-03	8.9	36.75	0.08	4.15	paramagentic
	LHG12.6bb				Paramagentic			
LHG13	LHG13.2bb	1.42E-02	1.89E-03	12.39	36.48	0.13	2.94	555
	LHG13.7bb	2.06E-08	1.97E-09	5.90	45.00	0.10	0.76	570
LHG14	LHG14.1a				Paramagentic			
	LHG14.3bb				Paramagentic			

Table 5.3. Hysterisis parameters for the Hooggenoeg Formation. M_s, saturation magentisation; M_r, saturation remenance; H_c, coercivity, H_{cr}, coercivity of remenance; T_c, Curie Temperature.

also consistent with the hysteresis curve analysis (Figures 5.11 and 5.12). Hysteresis parameters for LHG4.1cc, LHG11.3bb, LHG12.1bb and the LHG13 samples are plotted on a Day plot for magnetite showing (M_{rs}/ M_s)vs (H_{cr}/ H_c) and indicate samples from these sites plot are scattered across the plot. Given the significant paramagnetic contribution that had to be removed from the majority of the samples, hysteresis plots were noisy and therefore might explain some of the scatter observed. Sample LHG11.3bb falls in the region of the MD (multi domain) mixing line (Dunlop, 2002), of the plot (Figure 5.13) and is the most reliable result given that no correction was applied to the data in order to obtain the rock magnetic parameters.

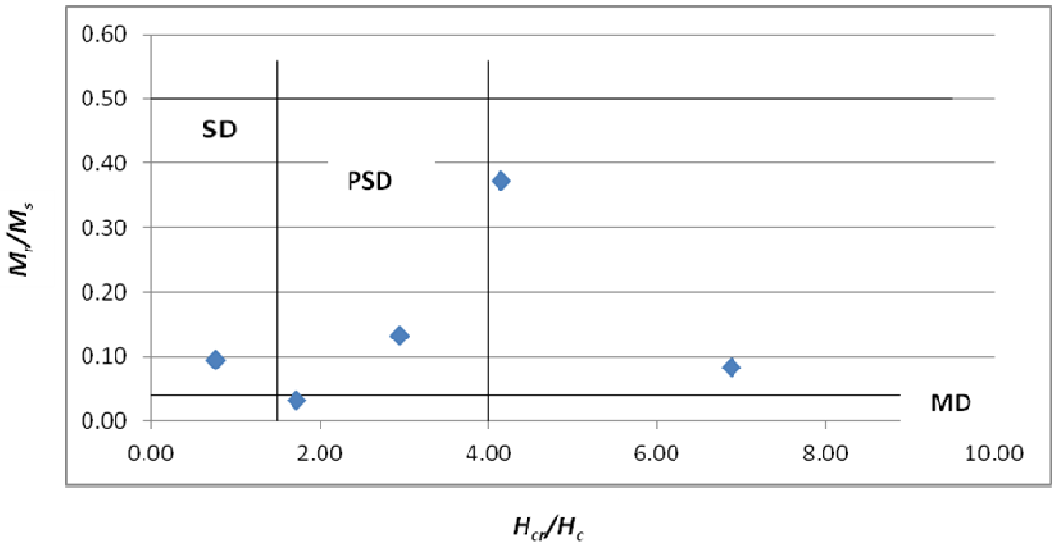

Figure 5.13. Day plot for LNP rock magnetic results. Theoretical Day plot after Day et al., (1977) and Dunlop (2002). SD: Single Domain; PSD: Pseudosingle domain; MD: Multidomain.

It should be noted that during rock magnetic characterisation of samples from the Komati Formation (see section 9 of Chapter 4) it was observed that there was a discrepancy between T_c calculated from the VFTB and those calculated using results measured on the Kappa Bridge. On further investigation it was discovered that the thermocouple in the VFTB oven was in the wrong position; as opposed to being flush against the sample and measuring the sample temperature it was found to be withdrawn from the sample and measuring a temperature gradient within the oven. The rock magnetic experiments for the Hooggenoeg Formation were performed almost two years prior to the issue being discovered, however, it is not known for how long the thermocouple was misaligned, therefore it is important to note that the T_c reported above may not be entirely reliable, (please see Chapter 4 for more details on this issue).

Nevertheless, the hight and low magnetic susceptibiltiy results from 12 samples (1 for each site) support the findings of the experiments performed on the VFTB. The majority of samples are dominated by the paramagentic fraction. No Verwey transitions were observed in the samples during the low temperature experiments. The curves have the characteristic shape for paramagnetic samples of 1/T. The thermomagnetic curves are reproducible in samples LHG6.4bb,LHG7.2ab, LHG8.12cc and LHG10.6bb, indicating no alteration of the sample occurs during heating. Samples from sites LHG1-5 alter significantly on heating, as the thermomagnetic curves are not reproducible, despite the experiments being carried out in argon to minimise oxidation (see Fig. 5.14d). No T_c equivalent was established from any of the above samples as the signal was too dominated by the paramagnetic contribution resulting in noisy results with no obvious T_c. As with the thermomagnetic curves obtained from the VFTB experiments, samples which alter significantly display changes in slope (always in the cooling curve during Kappa Bridge experiments). The temperature at which the change in slope is observed at between 539°C and 580°C and is indicative of the oxidation of magnetite or titanium poor magnetite during heating. Samples LHG11.1bb (shown in Fig 5.14c), LHG12.bb and LHG13.7bb are the exception. The results, comparable to the VFTB experiments, show a significant contribution of the ferromagnetic fraction, meaning clear Verwey transition (only in sample LHG11.1bb, as shown in Fig.5.14c)) and T_c are determined for the sample at 140K and between 558-575°C, respectively.

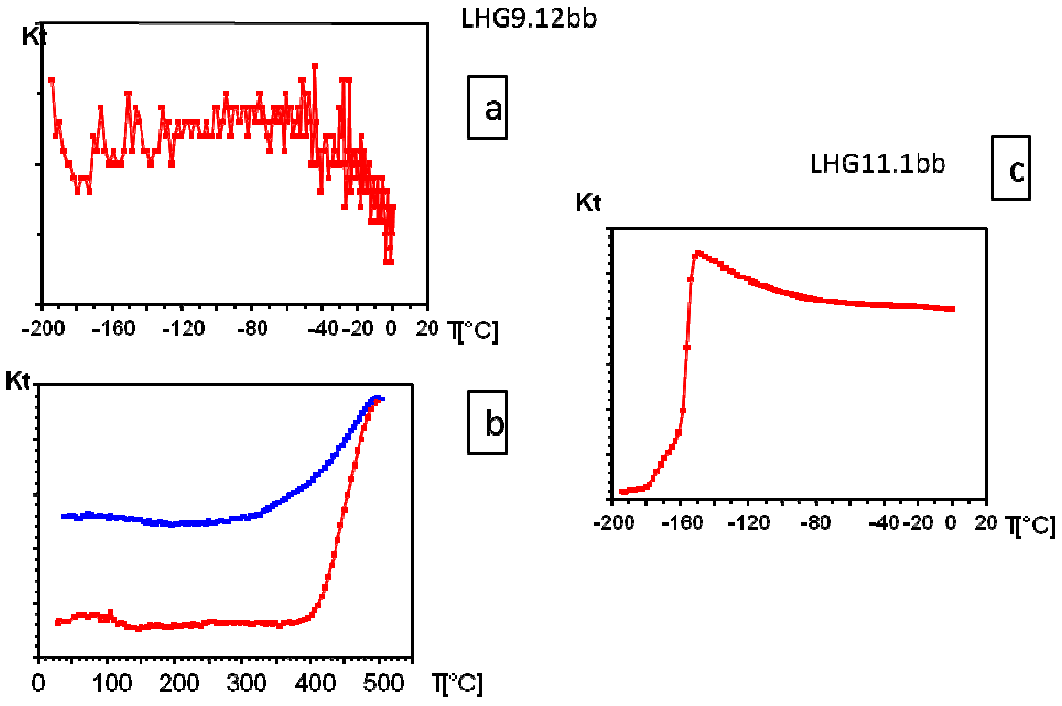

Figure 5.14 (Description on following page).

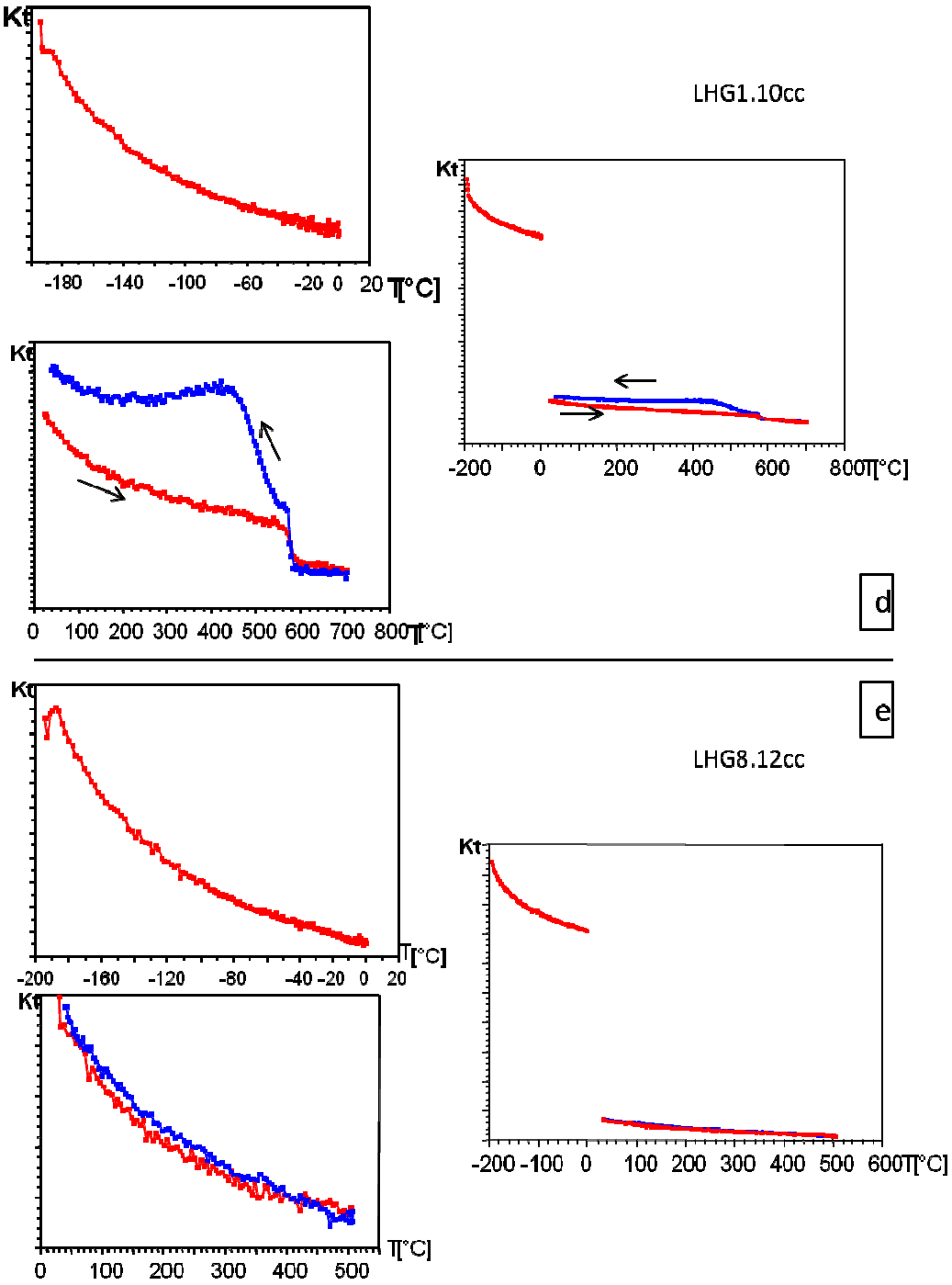

Figure 5.14 continued. Representative temperature dependant susceptibility measurements for samples across the Hooggenoeg Formation sites. Low (-200°C to room temperature) temperature dependant susceptibly and high (0°C to 700°C) temperature dependant susceptibility (carried out in argon), corrected for the sample holder, are show on the left (above and below respectively). Downward arrows on the high temperature dependant susceptibility indicates the heating cycle, whilst upwards arrows indicate the cooling cycle. Combined results for low and high temperature experiments are displayed on the right, however, it should be noted these are not corrected for the contribution the sample holder may have to the susceptibility. (d&e) Samples LHG1.10cc and LHG8.12cc are dominated by the paramagnetic contribution, meaning no Hopkinson's Peak is observed. LHG1.10cc alters significantly on heating, however a T_c can be obtained from the sample. (a &b) Sample LHG9.12bb alters significantly during the high temperature experiment as a new mineral phase forms during the experiment. (c) Sample LHG11.1bb is dominated by the ferromagnetic contribution, in agreement with the results of the VFTB experiments.

Note that the temperatures measured at the inflection point of the heating curves with the Kappa Bridge are in agreement (within experimental error) of those calculated after VFTB experiments. As discussed above, VFTB and Kappa Bridge results seem to be in broad agreement and it is possible that the VFTB experiments were not affected by the same issues as the other Formations studied as part of this work. However, it cannot be ruled out entirely and should be considered when interpreting the results presented here .

Samples from site LHG9 (see Fig.5.14a&b) are unusual in their behaviour, largely owing to their lithology. Unlike the rest of the samples of the Hooggenoeg Formation, they are primarily sedimentary in composition and their magnetic signature is distinct from the rest of the samples too. See the hysteresis loop in Figure 5.11 where once the sample has reached saturation magnetisation, the magnetisation drops markedly. Although the VFTB thermomagnetic curve is typical for a paramagnetic sample, the thermomagnetic curve for the Kappa Bridge experiment indicates the sample continued to gain significant magnetisation after reaching 400°C and altered significantly throughout the experiment.

The results presented above mean establishing the mineral carrying the magnetisation in the samples of the Hooggenoeg Formation is problematic. The samples from the majority of sites are dominated by the paramagnetic fraction and therefore it is not possible to obtain rock magnetic characteristics for the majority of the sites. It would not be appropriate to assume that the rock magnetic characteristics obtained from sites LHG11 and LHG13 are representative of the whole of the Hooggenoeg Formation. Despite the overall similarities in composition of the units sampled, it would be imprudent to expect homogeneity over such a large geographical area, particularly when during sampling it was observed that emplacement conditions and weathering of samples (amongst other properties) where notably different between sites.

5.7. Microscopy Observations

The rocks of the Hooggenoeg Formation incorporate units that range in composition between komatiites, basaltic komatiites and tholeiitic basalts (de Wit et al., 2011). Samples from sites LHG1, LHG4, LHG7, LHG10, LHG11 and LHG13 examined using an optical microscope and Philips XL30 tungsten filament SEM to better understand the mineralogy and

thermal history of the sample, whilst the scanning electron microscope (SEM) was also used to analyse the composition of the minerals.

It should be noted, samples for microscopy study were chosen prior to the bulk of the directional and rock magnetic characterisation of the samples was complete. Samples LHG4.1bb and LHG7.3aa were chosen due to being from the southern limb of the OF. Samples LHG1.6a, LHG10.2aa, LHG11.9bb and LHG13.8ab were chosen due to having been collected in the northern limb of the fold. Samples in the northern limb of the fold were collected in two distinct clusters (see Figure 5.1) so it was important the microscopic properties of each locality were studied. Preliminary interpretation of rock magnetic characterisation and demagnetisation results had indicated that samples from sites LHG12 to LHG14 yielded the best quality results, therefore, samples LHG13.8ab was chosen with the aim to identify mineralogical differences which might explain the better quality data.

Previous results have shown that the common microscopic assemblage for the komatiites of the BGB is olivine (often altered to antigorite), clinopyroxene, chromite, tremolite, chlorite and magnetite (Parman et al., 1997; Viljoen and Viljoen, 1969a). Magnetite is formed as a result of the serpentinisation of olivine and is typically found along the edge of the olivine minerals, (Hale & Dunlop, 1984) as well as a metamorphic overgrowth on chromite (Parman et al., 1997; Viljoen and Viljoen, 1969a), in the case of the komatiites of the Komati Formation. The main cause for serpentisinsation is hydrothermal alteration as a result of exposure of the rocks to a body of water and is consistent with the interpretation that the rocks of the Hooggenoeg Formation were erupted in a submarine environment. Whilst, metamorphism is heterogeneous and has altered the primary composition of the komatiites, primary igneous compositions and morphologies are retained (Parman et al., 1997). Particularly well preserved are the pyroxene crystals. Associated with these, small amounts of actinolite are usually present, owing to the alteration of the pyroxene during metamorphism(Viljoen and Viljoen, 1969f). Epidote is ubiquitous(Viljoen and Viljoen, 1969f) and is a product of hydrothermal alteration of pyroxenes and amphiboles and occurs in association with titanium-rich minerals such as titanite ($CaTiSiO_2$). Chlorite is also common, as are small amounts of quartz and carbonates(Viljoen and Viljoen, 1969f). The mineralogy of the komatiites of the Hooggenoeg Formation has been documented in detail by Biggin et al., (2011). They found that mineralogy of the studied samples was dominated by secondary amphibolites (usually tremolite/actinolite), chlorite and epidote. Opaque grains were observed in association with the secondary minerals (found to be sub

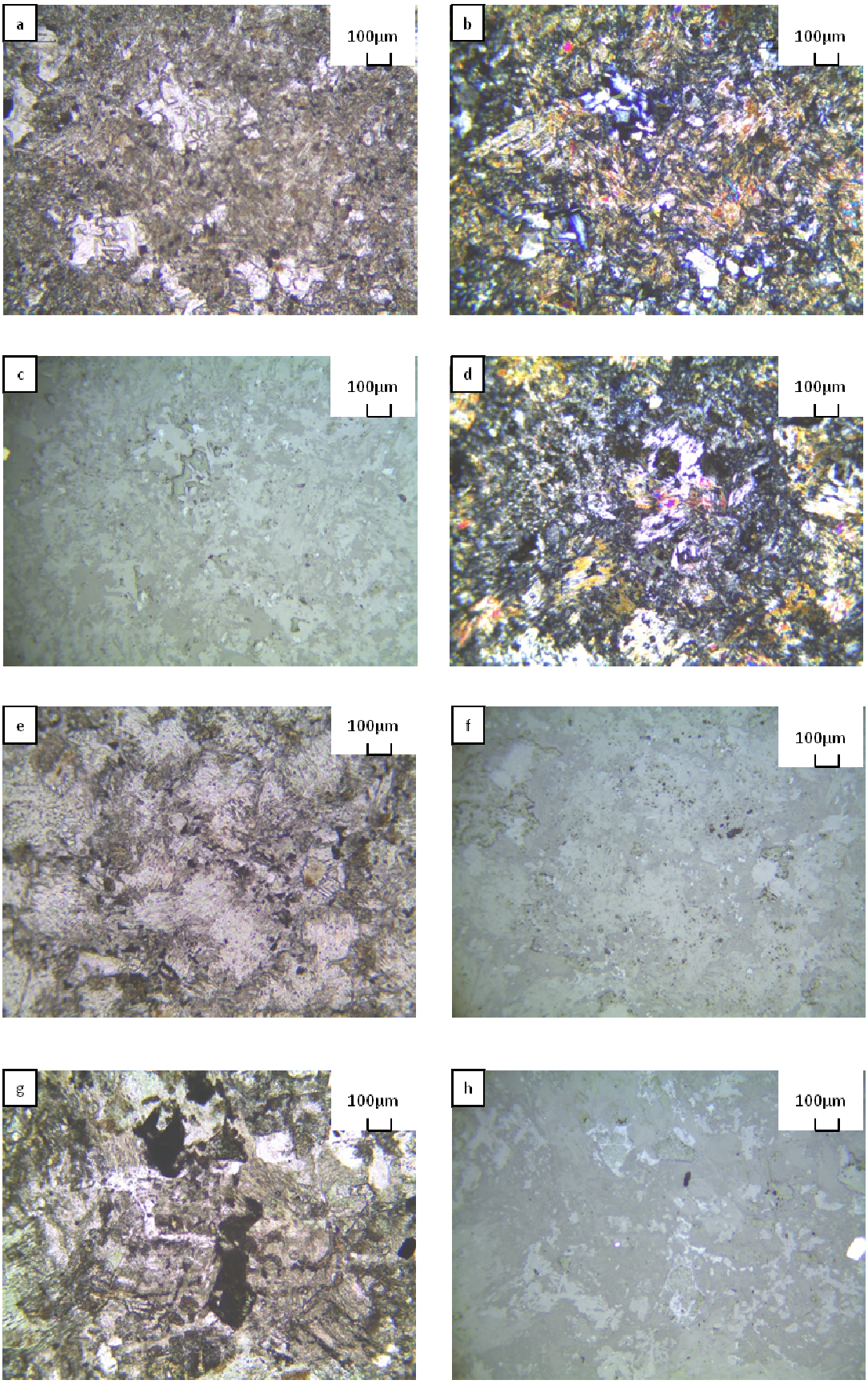

Figure 5.15 (Figure caption on following page).

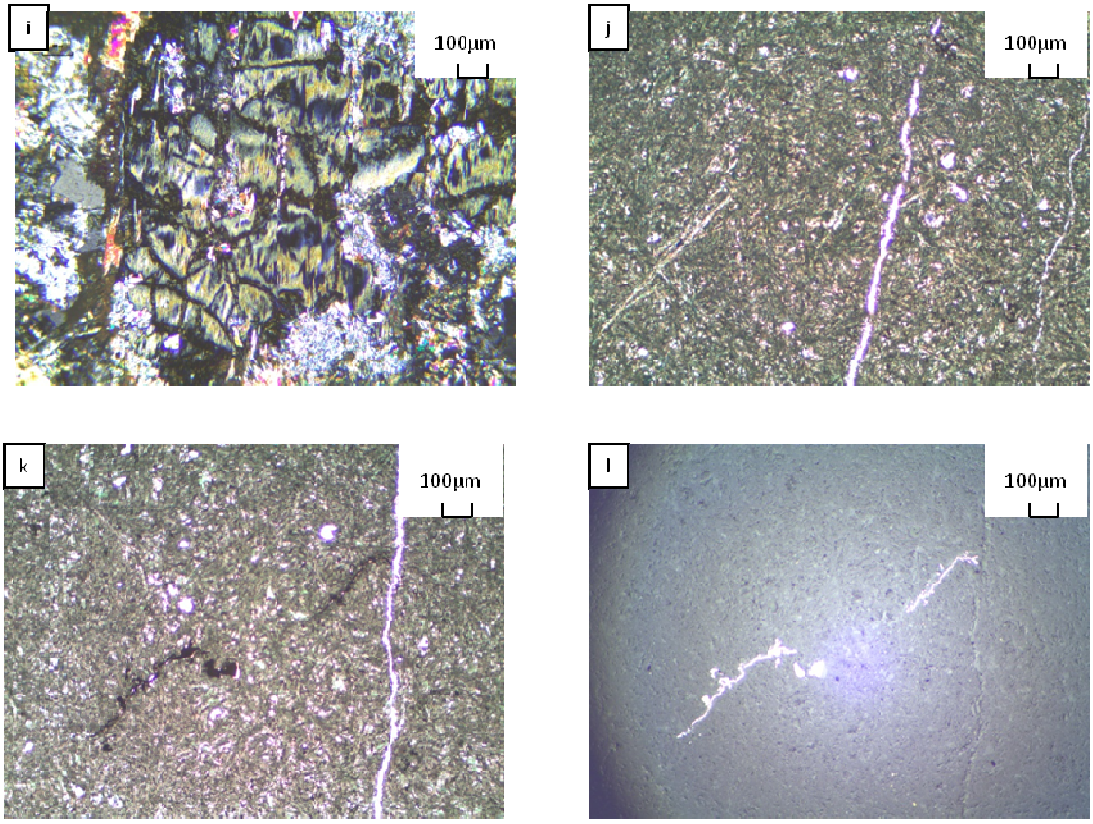

Figure 5.15. continued from overleaf. Representative photomicrographs of the samples studied under the optical microscope. (a,b,c) Representative photomicrographs of sample LHG4.11bb, plain polarised light (PPL), cross-polarised light (XPL) and reflected light, respectively. Note the alteration of the samples meaning intact original mineralogy phenocrysts are rare. The same is true for sample LHG7.3aa (d,e,f). Here opaque grains are seen in PPL (e) around the phenocryst rims and their presence is confirmed under reflected light (f). (g)Sample LHG10.2aa appears to have large opaque grains observed in plain polarised light, centre of field of view (FOV) and to the right of the FOV, however, in reflected light (h) only the euhedral grain to the right of the FOV is bright and therefore interpreted as an opaque mineral. (i) Heavily sericitised plagioclases are observed in sample LHG10.2aa. Photomicrographs for sample LHG11.9bb under transmitted light (j & k) and under refelected light (l). The sample is characterised by aphinitic texture; (k&l) Opque minerals were observed to concentrated within a vein, they are black in plain polarised light in (k) and bright under reflected light in (l).

-micron to tens of microns in size), which is indicative of the magnetisation not having arisen prior to the metamorphism of the samples. The observed mineralogy was interpreted to have arisen from hydrothermal alteration which resulted in the chloritised glassy matrix observed in some of the pillow lavas. However, the hydrothermal action was not severe enough to destroy the ichnofossils preserved in the earlier volcanic glass (Biggin et al., 2011).

Samples LHG4.1bb, LHG7.3aa, LHG10.2aa and LHG11.9bb were studied under the optical microscope. Samples were found to be pyroxene rich but significantly altered to secondary amphiboles. Olivines were observed in samples LHG4.1bb and LHG7.3aa but where scarce and significantly altered. All samples, inclusive of LHG11.9bb are characterised by a strong green colouring, both in hand specimen and thin section, but this is particularly striking in the case of LHG11.9bb. The colouring can be attributed to the presence of actinolite and chlorite which replace the primary minerals. Cores of the olivine and pyroxene phenocrysts do not often remain intact, but can be distinguished by the high interference colours observed in cross polars and seen clearly in Figure 5.15 (b and d). In addition, although komatiites are typically characterised by limited plagioclase, sericiteised relic plagioclases (likely anorthite) were observed in samples LHG4 to LHG10. It is likely hydrothermal activity has caused the alteration of plagioclase to sericite, shown in Figure 5.15 i, in addition to some serpentinization of the olivines. However, the limited preservation of the some of the phenocryst cores is indicative that the minerals might have been in the presence of water for moderately long periods of time. Whilst samples LHG7.3aa and LHG10.2aa are generally coarse grained with phenocrysts identifiable by the naked eye (porphyritic texture), LHG4.1bb, and particularly LHG11.9bb, are considerably finer grained and domainated by aphanitic texture, as seen in Figure 5.15 (j,k and l). As a result, identification of mineral phases was complicated. Reflected light microscopy revealed some opaque minerals (Figure 5.15 (f,g,h,k), particularly along the mineral edges of chlorite and pyroxene grains, as would be expected if they result from the alteration of the primary mineralogy by hydrothermal action. Opaque minerals in LHG10.2 were rare, but when observed, particularly large (micron scale). When studied under transmitted light these were ‘bright’, characteristic of iron oxides.

Further work was carried out on the SEM, on samples LHG1.6,LHG11.9bb, LHG13.8ab, to try and identify the opaque minerals and their relationship to the primary mineralogy. Energy dispersive X-ray spectra (EDX) were also acquired to try and identify the main min-

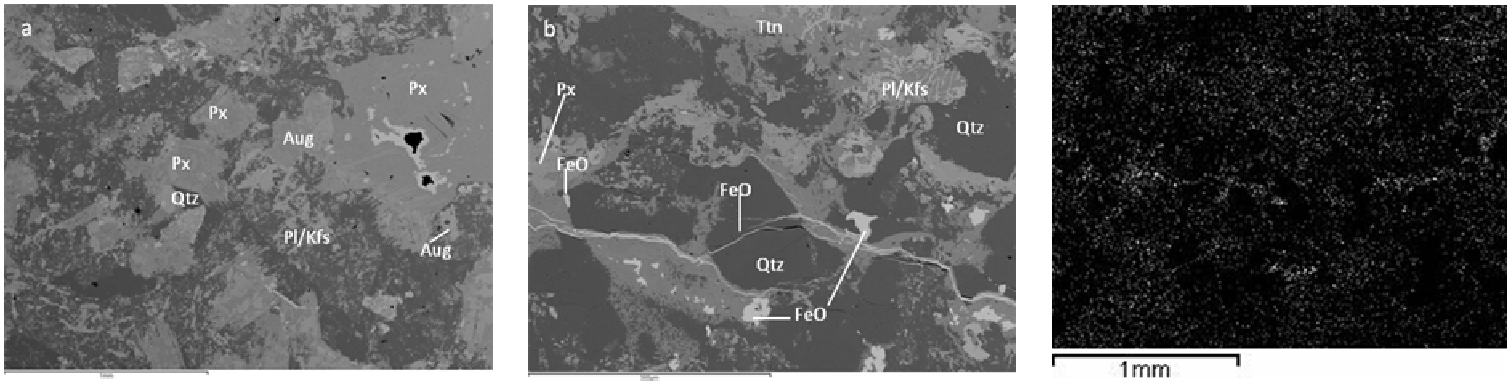

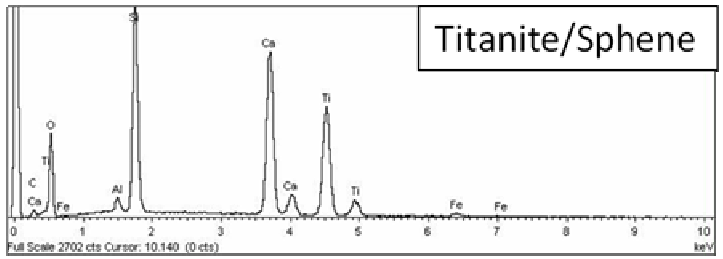

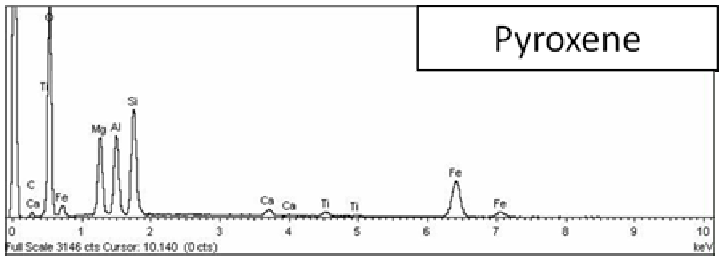

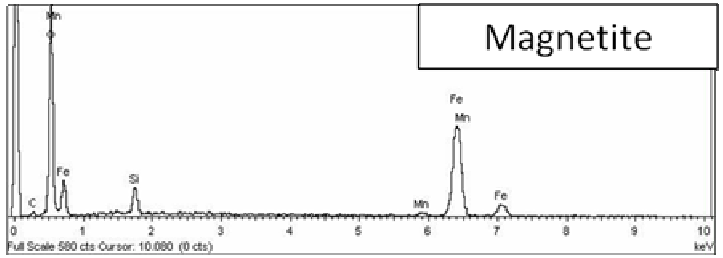

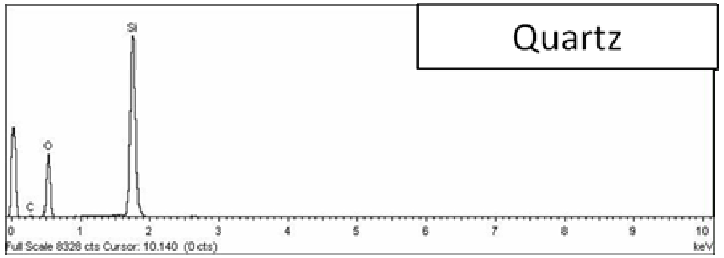

Figure 5.16. Scanning Electron Micrographs of LHG1.6. (a &b) Mineralogy of the sample includes Quarts (Qtz), Pyroxene (Px), Augite (Aug), Plagioclase feldspar (Pl) with potassium feldspar overgrowths (Kfs), Iron oxides (FeO) are identified within a vein and larger subhedral grains are also observed as inclusion within Qtz and the rims of the Pl. The element map for Fe shown above highlights the abundance of Fe deposited within the vein and some of the magnetite identified in (b). Representative EDX spectra for some of the minerals identified in the thin section are also shown.

erals in the sample. Opaques tend to be bright when observed under the SEM and so minerals with these properties were targeted for X-ray analysis in order to identify likely FeO.

Analysis of the thin section in the SEM confirmed the findings of the optical microscopy work, whilst aiding the identification of the primary mineralogy characterisation of opaque minerals observed using optical microscopy. Sample LHG1.6 was overall dominated by minerals with a composition of Ca, Fe, Si, Al and O, (as seen in the elemental spectra shown in Figure 5.16), consistent with augite. In addition, a significant amount of chlorite (the product of the hydration of pyroxene, a common mineral in komatiites) was also identified. Titanite (sphene) was also considerable. In addition, significant plagioclase feldspar with potassium feldspar overgrowths was observed. Rare quartz, sericite and a few zircons (initially mistaken for iron oxides, given their euhedral habit and brightness) were also observed in the thin section. Euhedral shaped, micron to submicron scale Iron oxides, likely magnetite, were identified along the majority of the relic pyroxene grain boundaries (shown in Figure 5.16(b)) and in a large vein across the thin section. However, the vein is seen to cross-cut the phenocsysts in the thin section and is therefore likely secondary and formed after the primary mineralogy developed. Mapping of abundances of elements across the thin section agreed with previous findings (see Figure 5.16 c).

Sample LHG11.9 was characterised by minerals with a composition of Ca, Fe, Si, Al and O, (as seen in the elemental spectra shown in Figure 5.17), consistent with augite. In addition, chlorite (the product of the hydration of pyroxene, a common mineral in komatiites) was also identified. Titanite (sphene) was also considerable. In addition, significant plagioclase feldspar was observed. EDX spectra characterised a mineral to have a composition of Ca, O, which is consistent with carbonate. Viljoen and Viljoen, (1969b) report carbonate in samples of the Hooggenoeg Formation. Silicate minerals (quartz was identified in this sample) are easily converted to carbonates by hydrothermal reactions with solutions containing CO_2 (one of the main gases produced during mafic volcanism). An alternative interpretation is that the EDX spectra was not allowed to run long enough, for the mineral composition to be fully resolved. A standard element map of abundances of elements across the thin section acquired for the studied samples contained on average 25 frames. These reveal the presence of sodium (Na) and aluminium (Al) in the vicinity of the Ca, O rich mineral. An elemental map was acquired over a period of over 30 minutes (in excess of 300 frames) which showed the mineral to be a highly zoned plagioclase. The core of the mineral was very Ca rich, whilst the rim contained more Na (as well as Ca, and O), typical

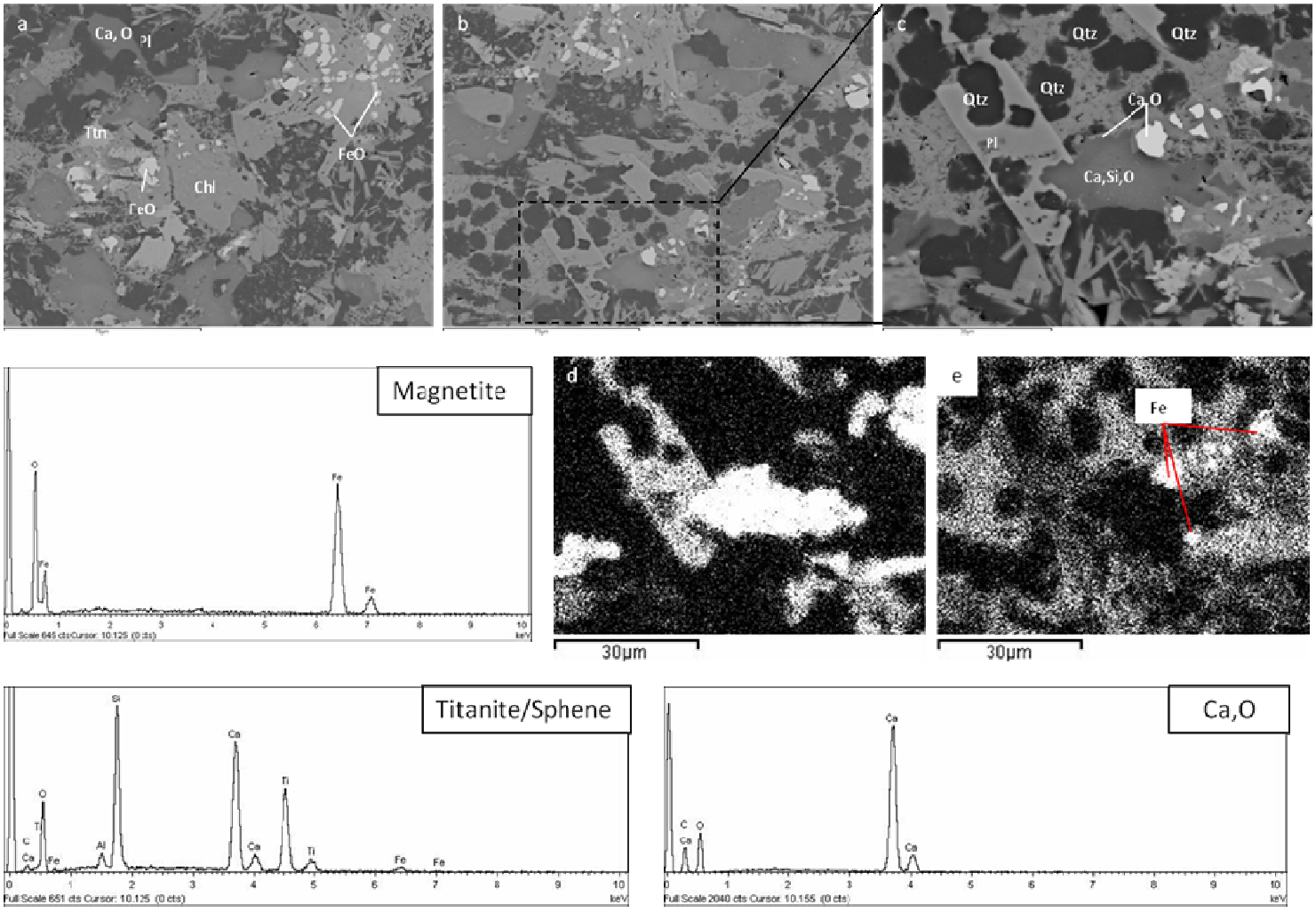

Figure 5.17. Scanning Electron Micrographs of LHG11.9bb. (a, b, c) Show mineralogy expected of a rock of basaltic komatiite composition which has been altered by the presence of hydrothermal fluids: quartz (Qtz), Plagioclase (Pl) which appears in a larger abundance than in other komatiitic basalts studied in this thesis (Komati Formation samples), Chlorite (Chl), Augite , and Titanite/Sphene (TTn). Iron- oxides including magnetite (Mag), were identified in the sample, as seen in a and in element maps for iron (e). (b & c) Highlight an area were substantial amount carbonate was measured, embayed with a plagioclase grain, (d) a detailed element map of Ca highlight the abundance of the chemical within the sample. of Magnified area of edge of olivine mineral where magnetite is expected to be found. (f) Fe element X-ray map of area. Selected EDX spectra showing minerals identified in thin section.

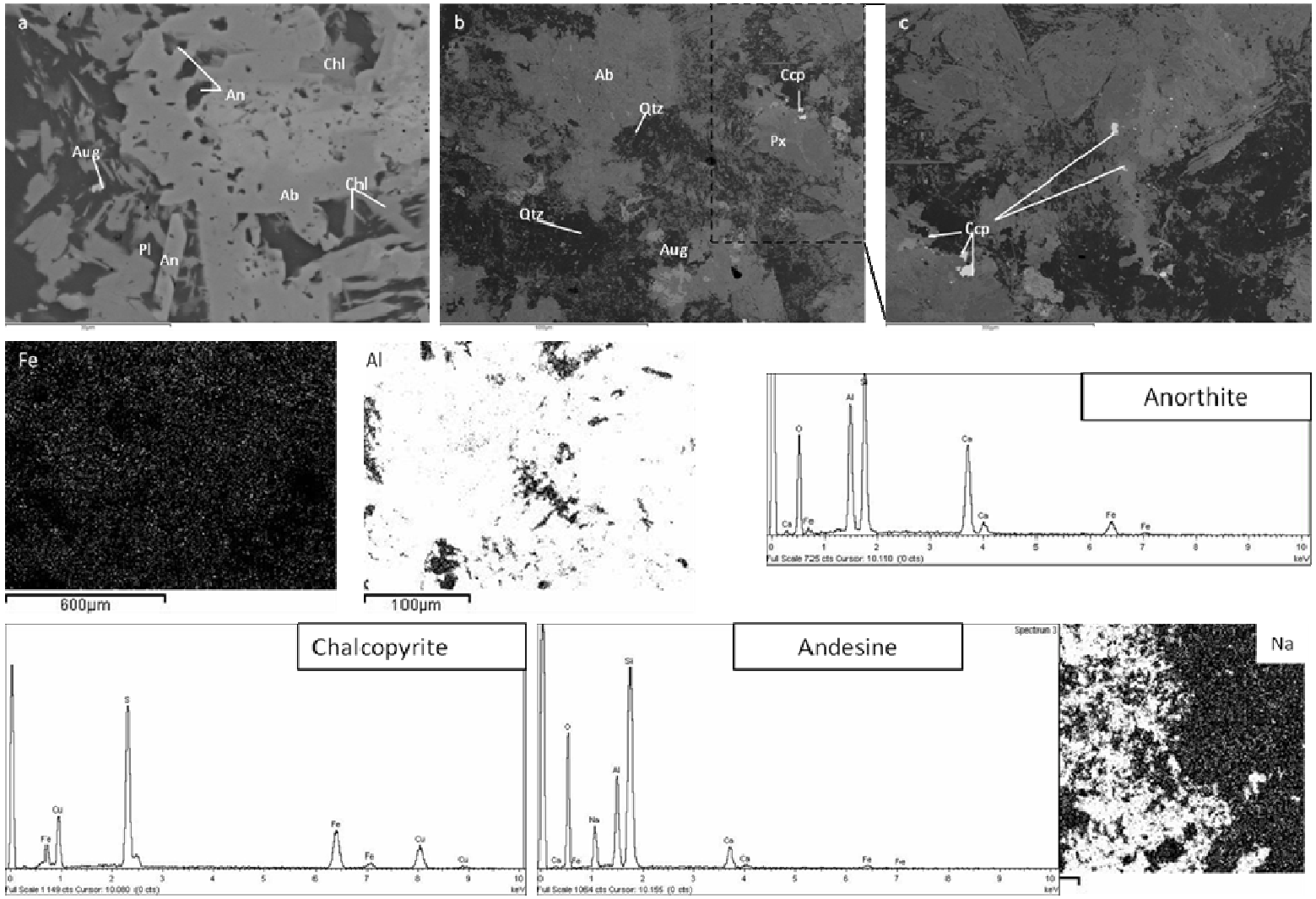

Figure 5.18. Scanning Electron Micrographs (a,b & c) of LHG13.8ad in addition to representative element maps (Fe, Al & Na) and selected EDX spectra for typical minerals found in the thin section. Minerals identified within LHG13.8bb include Albite (Ab), Plagioclase (Pl), Anorthite (An), Chlorite (Chl), Quartz (Qtz), Augite (Aug), Pyroxenes (Px) and chalcopyrite (Ccp). The element map for iron (Fe) shows that Fe is distributed evenly throughout the sample and no particularly bright clusters can be picked out, indicating a limited abundance of iron oxides. Element maps for Alumininum (Al) and Sodium (Na) highlight how dominated by plagioclase the sample is, this is unusual for basaltic komatiites which tend to be depleted in silicates.

of a zoned plagioclase. Micron to submicron scale, euhedral shaped, Iron oxides, identified as magnetite, were observed along edges of pyroxene phenocrysts.

EDX spectra analysis of sample LHG13.8ab (Figure 5.18) identified the main mineral phases in the sample to be plagioclase (albite and anorthite), as well as augite, often altered to chlorite. When compared to samples LHG1.6 and LHG11.9bb, it was noted that the mineralogy of sample LHG13.8ab was less diverse. Plagioclases were micron to millimetre in scale and observed to have a 'pitted' texture (Figure 5.18 (a)). Euhedral, bright, opaque minerals were identified within the silica rich minerals and also as inclusions within chlorites (which indicate they are of primary origin). EDX spectra analysis identified the opaque minerals to be chalcopyrite (Cu,Fe,S) which is typically antiferromagnetic (see Figure 5.18).

The findings of the microscopy work carried out on sites LHG1, LHG4, LHG7, LHG10 , LHG11 and LHG13 compliment the results of the rock magnetic characterisation experiments performed on the sites. The samples of LHG1,4,7,10 and 13 were dominated strongly by the paramagnetic fraction. Given the limited number of iron oxide minerals, one might expect the ferromagnetic signal in the rock magnetic experiments to be weak. The microscopy work allowed identification of copper iron sulphides, such as chalcopyrite, which could account for the strong paramagnetic contribution observed in the samples. Previous microscopy work carried out by Biggin et al., (2011) and the observations made as part of this work, indicates that magnetite grains in samples of the Hooggenoeg Formation can be expected to be micro to submicron scale (<1µm - 10µm) which is on the limits of the resolution of the optical and electron microscopes used to study the samples in the present study. Therefore, it is possible the sample may contain small proportions of very fine grained iron oxides which it may not have been imaged. In contrast, sample LHG11 was found be strongly ferromagnetic with high initial NRM intensities. The high abundance of micron to submicron sized iron oxide minerals along olivine grain boundaries would explain the rock magnetic properties of site LHG11. The mineralogy of the rocks of the Hooggenoeg Formation is discussed further in sections 5.8.13 in light of the palaeomagnetic results.

5.8. Discussion

Two overprint directions were isolated from the rocks of the Hooggenoeg Formation. The samples are characterised by a low temperature direction (LT1) which is interpreted to be

a present day field overprint. A further overprint direction was isolated above the LT1 direction, in middling temperature ranges, MT.

Once overprint directions were removed, two high temperature directions were recognised in the samples of the Hooggenoeg Formation. The HT1 direction is isolated from the southern limb of the OF whilst the HT2N direction is isolated from the northern limb of the OF. Comparison with previously published data sets will add to the robustness of and give a wider context in which to interpret the results presented here. To that effect, the results presented as part of this study will be compared to the findings of the work by Biggin et al., (2011).

Establishing the timing of acquisition of the directions identified in the samples is crucial. In order to do so, a fold test was attempted using the newly discovered HT2N direction in the northern limb of the OF, which has not been previously sampled. In addition, the age of the MT component and HT1 direction will also be discussed.

5.8.1.Comparison with Previously Published Palaeomagnetic Data

Establishing the timing of the acquisition of the direction is crucial to ascertain the viability and reliability of the poles calculated for the rocks of the Barberton Greenstone Belt. The complex geological history casts doubts over the soundness of the findings of this and previous studies. In conjunction with palaeomagnetic field stability tests comparison with previously published data can provide a means of validating the robustness of the findings of this study.

A number of palaeomagnetic studies have been performed on the rocks of the Barberton Greenstone Belt and will be discussed on a broad basis, as required. Of direct relevance to the results presented here is the study of the Hooggenoeg Formation by Biggin et al., (2011) and to which extensive reference has already been made throughout this chapter.

Biggin et al., (2011), identified a low temperature overprint direction, LT1, a generally north and steep direction (D/I)=350.7°/-60.6°, $\hat{k}$= 50, α95=9.6°, n=6. In addition they identify a second overprint direction, MT; a near vertical downwards direction with mean direction (D/I)=321.8°/85.6°, $\hat{k}$=50.4 50, α95=13.1°, n=4. Two ChRM components are also established in the study of Biggin et al., (2011), HT1 (D/I)=169.8°/58.1°, $\hat{k}$=121.9, α95=6.1°, n=6 and HT2 (D/I)=36.9°/62.9°, $\hat{k}$=37.8, α95=15.3°, n=4. For a more detailed overall de-

scription of the work carried out by Biggin et al., (2011), as well as of these directions please see the results section of this chapter.

5.8.1.1 Overprint Direction LT1

As discussed in the results section of this Chapter the LT1 overprint direction is identified in seven of the studied sites. As seen in the equal area projection in Figure 5.19(a), the site mean directions calculated for the LT1 direction are smeared over a range of declinations and inclinations. In the case of Biggin et al., (2011) the LT1 direction is better clustered, see Figure 5.19 (b). Nevertheless, the clustering of the LT1 direction calculated as part of this study is reasonable considering the age of the samples, as well as the low NRM intensity values and the somewhat poor quality of the resulting Zijderveld Plots. When compared to the data set of Biggin et al., (2011), we see that our LT1 direction agrees relatively well with the LT1 direction identified as part of the work by Biggin et al., (2011). In geographic coordinates The LT1 direction of Biggin et al., (2011) produces a pole that plots between the present-day field (PDF) and geocentric axial dipole (GAD) poles. Therefore it is very likely it records a recent field direction (Biggin et al., 2011). The same is true for the LT1 direction calculated as part of this work. The new data presented here is in agreement with the findings of Biggin et al. 2011 and so contributes to the argument that the LT1 component is a recent day overprint.

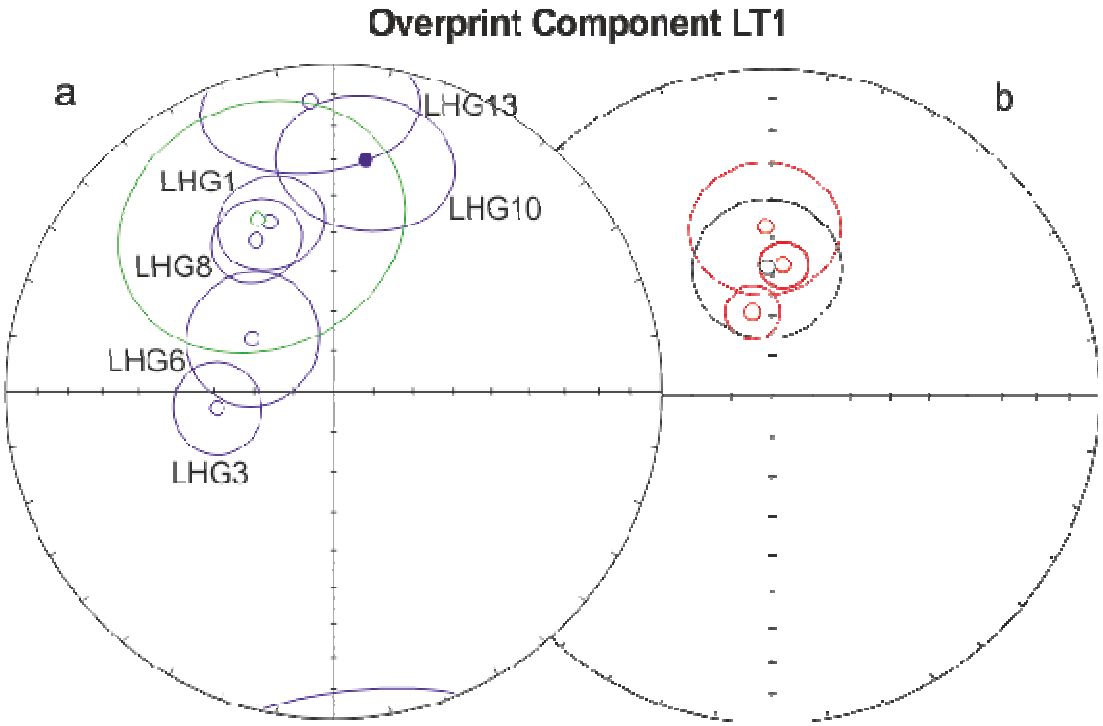

Figure 5.19. Equal area plots showing overprint component site mean directions. (a) Site mean directions from this study are shown in blue. The direction mean is shown in green. (b) Site mean directions calculated by Biggin et al., (2011) are shown in red. The direction mean is shown in black. In this figure, only directions obtained from Biggin et al., (2011), Hooggenoeg samples (HG) are shown. The direction mean has shown has been recalculated using only the three LT1 direction means obtained from HG samples. This is to ensure a fair comparison of the newly presented data set. However, the direction mean calculated by Biggin et al., (2011) which includes LT1 directions obtained from the Kromberg Formation and Noisy Complex is very close to that calculated here, see Table 5.1 and Figure 5.3, were the LT1 direction as calculated by Biggin et al., (2011) is shown. Filled points represent the lower hemisphere whilst unfilled points represent the upper hemisphere. Ellipses indicating α 95 cones of confidence.

5.8.1.2 Overprint Directions LT2 and MT

In the work of Biggin et al., (2011) the LT2 component is isolated in one Hooggenoeg Formation site, five Kromberg Formation (which directly overlies the Hooggenoeg Formation and dated at 335-3445 Ma) sites and one Noisy Complex site. Biggin et al., (2011) argue that the LT2 direction predates the acquisition of the MT direction (discussed in more detail below). The LT2 direction is not observed in the samples measured as part of this study. However, given that only Hooggenoeg Formation samples have been studied here and that LT2 was only observed in site HG3 of the Hooggenoeg in Biggin et al., (2011) it is not unreasonable to assume that the MT component in the sites studied here have fully overprinted the LT2 signal. This might imply that the LT2 overprint is not widespread across the entirety of the Onverwacht Group.

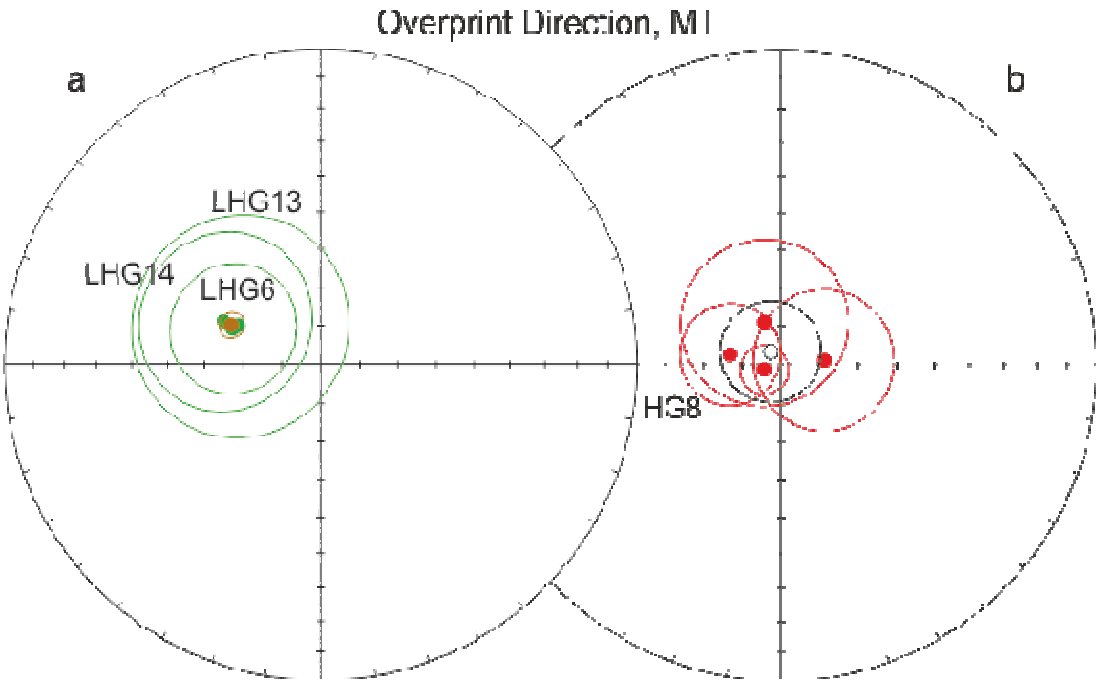

Figure 5.20. Equal area plots showing MT overprint direction site mean directions, in-situ (a) Site mean directions from this study are shown in green. The direction mean is shown in brown. (b) Site mean directions calculated by Biggin et al., (2011) are shown in red. The direction mean is shown in black. In this figure, all MT direction means obtained from Biggin et al., (2011), irrespective of Formation are show: Hooggenoeg samples (HG8), the remaining three directions are obtained from the Kromberg Formation. Filled points represent the lower hemisphere whilst unfilled points represent the upper hemisphere. Ellipses indicating α 95 cones of confidence.

Direction MT was observed in three sites LHG sites, whilst Biggin et al., (2011) observed the component in only one HG site (HG8) and in a further three Kromberg Formation sites. As is seen in Figure 5.20, the MT direction means from both studies do not overlap, nor do their α95 confidence limit envelopes. However, individual site mean direction α95 confidence limit envelopes do overlap, particularly the LHG and HG components. Therefore it was necessary to perform a common true mean test (McFadden and McElhinny, 1990) to statistically compare the directions and establish if they are distinguishable from one another. The test gave a negative result, indicating the two directions do not share a common mean and are distinguishable from one another (G=21.5° when the critical angle is Gc= 14.5°). However, as the Biggin et al., (2011) MT direction includes samples from the Kromberg Formation a common true mean test was carried out to establish if the MT directions observed in the Hooggenoeg Formation samples were statistically related. Site mean directions from HG8 and LHG14 seemed to cluster nearest to one another and pass a common true mean test with classification C (critical angle = 18.9°, G = 7.2). When the site mean direction from HG8 is compared to the site mean directions calculated for LHG6 and LHG13, the test for a common true mean is indeterminate. Therefore this indicates that the HG8 direction can be included into a new MT direction mean with the LHG samples. As the Kromberg site means are statistically distinguishable from those of the Hooggenoeg, it is proposed that the direction is split, creating an MT direction that in the Kromberg Formation (MTK) which is distinguishable from the MT direction in the Hooggenoeg (MTH). The new MTH has direction (D/I) = 291.9°/67.8°, $\hat{k}$= 157.8, α_{95}=7.3°, n=4). The MTK direction (recalculated using Biggin et al., (2011) data) gives (D/I) = 11.7°/86.2°, $\hat{k}$= 53.2, α_{95}=17.0°, n=3).

Crucially, the MT direction is seen in sites from the northern limb of the OF (LHG 13 and LHG14) as well as sites from the southern limb of the fold (HG8 and LHG6). Clustering of directions in geographic coordinates of the LHG sites is remarkable ($\hat{k}$= 144) and the addition of the HG8 means $\hat{k}$ is further improved to 158. This implies that the MT overprint post dates the formation of the OF fold, at ca. 3.2Ga. If this were not the case, one would expect to see directions which clustered away from one another in geographic coordinates (for sites on opposite limbs of the fold), with improved clustering only after a tectonic correction was applied.

5.8.1.3 High Temperature Direction, HT1

Four sites from the Hooggenoeg Formation measured in this study gave a site mean direction which clustered fairly steeply to the south and was generally isolated above 480°C. This is in agreement with the HT1 direction isolated by Biggin et al. (2011) in two Hooggenoeg Formation sites and a further five Kromberg Formation sites (which directly overlies the Hooggenoeg Formation and dated at 335-3445 Ma) . In the interest of comparing like for like, in the first instance, when plotting the HT1 directions on an equal area projection, only the results obtained from the Hooggenoeg Formation have been plotted. It is clear, from Figure 5.21 (a), that the site mean directions from the LHG and HG sites overlap (despite the LHG samples having a larger uncertainty) and that the directions from both studies should be combined to produce a new mean direction and pole. The new in-situ HT1 direction calculated from the Hooggenoeg Formation sites gives (D/I) = 168.7°/63.3°, $\hat{k}$= 343, α_{95}=3.6°, N=6, with a pole of latitude (λ) and longitude (ϕ) of (λ/ ϕ) = -69.0°/53.7, A95= 18.5, N=10. When this direction is compared to the direction mean calculated by also including the Kromberg site mean directions of Biggin et al., (2011) it becomes obvious there is no clear reason to disregard the Kromberg directions, as the HT1 direction mean is given by (D/I) = 168.7°/63.3°, $\hat{k}$= 91.9, α_{95}=5.06°, N=10, which is clearly comparable to the HT1 direction calculated only from the Hooggenoeg sites. From this, a new pole is calculated for the HT1 of (λ/ ϕ) = -69.0°/53.7°. The new pole is plotted in Figure 5.25 and can be compared to other poles of the Kaapaval Craton as well as the results of other Onverwacht Group Formations of Biggin et al., (2011).

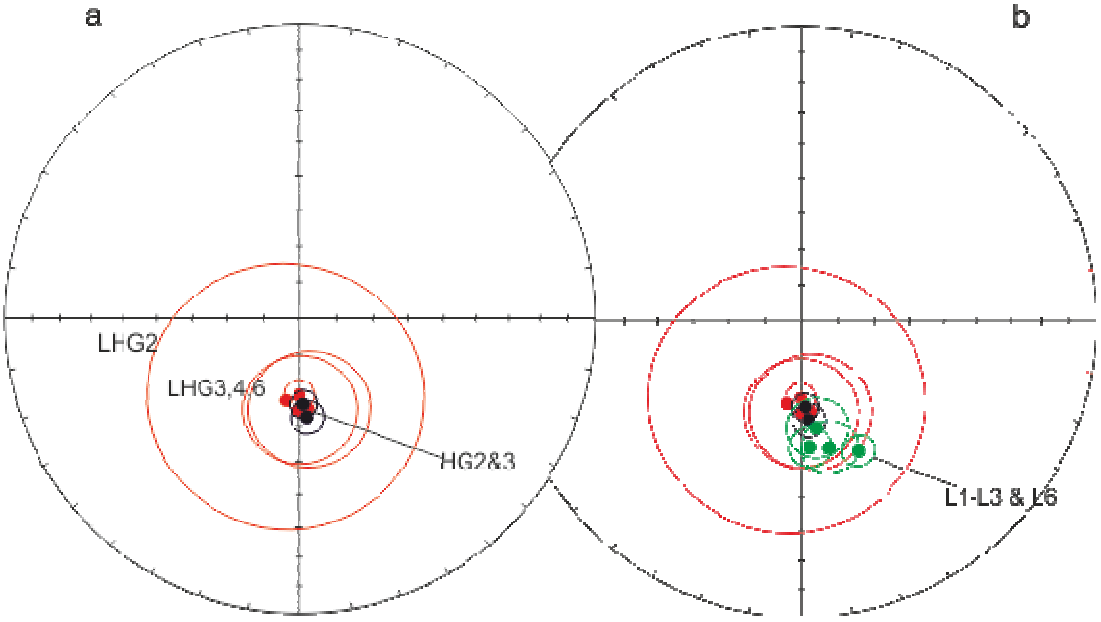

Figure 5.21. Equal area plots showing HT1 site mean directions in geographic coordinates. (a) Site mean directions from this study are shown in yellow. Site mean directions calculated by Biggin et al., (2011) are shown in black. (b) Site mean directions are shown again, in this equal area plot. In addition the Hoogge-noeg Formation site means, the Kromberg Formation means, as calculated by Biggin et al., (2011), are in-cluded (shown in pink). The HT1 direction show good clustering. Filled points represent the lower hemi-sphere. Ellipses indicating α 95 cones of confidence.

Interestingly, this direction is only observed in sites from the southern limb of the OF. In the case of Biggin et al., (2011) the most obvious explanation is that this is due to sampling bias, as no samples were collected in the northern limb of the fold as part of that study. Biggin et al., (2011) highlight that the HT1 pole is comparable to the younger 180Ma Karoo Large Igneous Province pole which caused wide spread overprinting throughout the Kaapval Craton (Strik et al., 2007). If this is the source of the direction, then it is younger than the LT2 and MT directions and would require a chemical remagnetisation which would record a more ancient magnetic field at lower blocking temperatures (Biggin et al., 2011). Alternatively, it is possible the similarity between the HT1 direction and the younger poles is coincidental, and that, while HT1 was acquired subsequent to the formation of the OF and is therefore older than LT2 and MT (Biggin et al., 2011). The thermal events at 3.1Ga (Toulkeridis et al., 1994) or the large igneous events at 2.9 and 3.0Ga (de Wit et al., 2011; Schoene et al., 2008b) are likely candidates for imparting the direction (Biggin et al., 2011). From the new, improved HT1 direction presented in this work (which agrees well with the direction of Biggin et al., (2011)), there is no further evidence that would favour either of these interpretations and therefore they both remain valid. However, in either situation the implication is that the event which caused the HT1 magnetisation was widespread and so unusual that its signature is not seen in the rocks of the northern limb of the OF. There are indications that the magnetic carriers in either limb of the fold could be somewhat different. The rock magnetic indications seem to suggest that, at least some of the sites (e.g. LHG11), in the northern limb of the OF are dominated by ferromagnetic minerals whilst the southern limb sites are dominated by the paramagnetic contribution. NRM intensities in the southern limb of the fold are lower (10^{-4} to 10^{-3} A/m) than in the northern limb of the fold (10^{-2} to 10^{-1} A/m). At the same time, the microscopy work did not indicate any obvious mineralogical differences between the two limbs of the fold and personal communication with M.J. de Wit on this subject clarified there are no significant lateral heterogeneities in the basalts across the OF. A shortcoming of the work presented here, however, is the fact that no southern limb samples were studied under the SEM and this would be recommended in any future work, as the optical investigations are limited in the resolution of the grain sizes that can be studied and it is

possible that differences regarding the magnetic carriers would only be observed at a micron or submicron scales. With the available data set it is not possible to fully clarify why the HT1 direction is only observed in the southern OF.

5.8.1.4 High Temperature direction, HT2N

A second high temperature direction was isolated from the LHG sites, from the northern limb of the OF (for clarity, this will be referred to as HT2N). In the results section of this chapter, the direction has been interpreted as an HT2 direction, after Biggin et al., (2011), who isolate an HT2 component in the southern limb of the fold (throughout this discussion referred to as HT2S). In geographic coordinates, the directions do not cluster well with any of the other high temperature directions identified in this study or by Biggin et al., (2011).

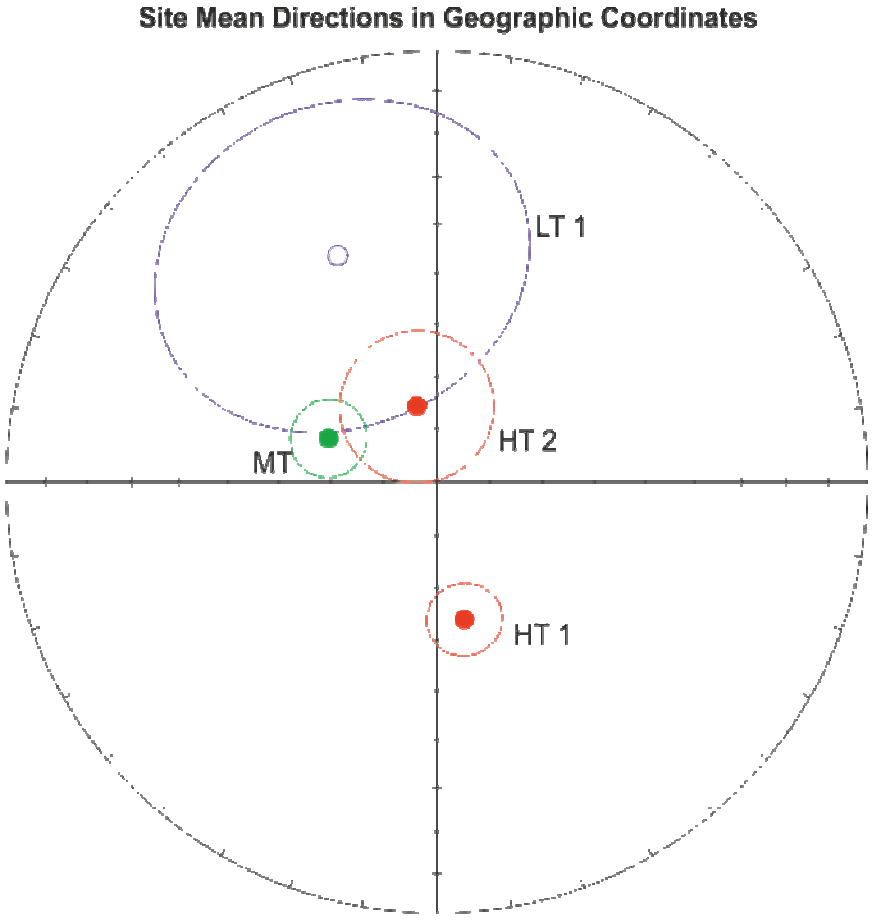

Figure 5.22. Summary equal area plot showing site mean directions, in geographic coordinates, calculated as part of this study. Overprint directions LT1 and MT are shown in blue and green respectively. High temperature directions are shown in red, HT1 and HT2. HT direction are combined with the results of the previous study of Biggin et al., (2011), please see discussion for details. Filled points represent the lower hemisphere whilst unfilled points represent the upper hemisphere. Ellipses indicating α 95 cones of confidence.

The similarity of the MT directions to the HT2 direction obtained from the LHG samples should be considered in light of the findings presented (see Figure 5.22). In addition, there is no evidence that the HT1 overprints the HT2N (or HT2S) directions, which combined with the similarity of the directions suggests the simplest interpretation is that the HT2 direction is a remagnetisation of MT age. This would imply that the MT direction is exclusively preserved in the northern limb of the fold, fully overprinting any older magnetisations (whether they be of HT1 or HT2 age). If this is the case, then it raises the question as to why the MT overprint did not cause remagnetisation of the HT1 and HT2S directions in the southern limb of the fold. Furthermore, this means the age of the HT2S direction cannot be further constrained using the results of this data set.

An alternative interpretation can be investigated if the HT2N direction is considered to be older than the MT direction. Whilst the evidence is far from conclusive, there are some indications that this may be a possibility and these are explored further. In site LHG6 the MT overprint is seen below the HT1 direction, suggesting that the MT1 direction must be younger and have been acquired prior to the HT1 direction. In sites LHG13 and LHG14 the MT direction is seen below the HT2 direction, but this in its self is not conclusive enough as the directions are indistinguishable. In some of the samples from these sites there is no evidence of two direction (see Figure 5.7 a,c and d), producing only a small LT component above which an MT/HT2N component is observed, straight to the origin. However, in other samples (Figure 5.7 e & f) there is a dog leg in the demagnetisation curves at ~400° c/35mT (these temperatures vary slightly from sample to sample) which has lead to the interpretation of two separate directions. The unblocking temperatures observed for the MT direction in sites LHG13 & 14 are consistent with those observed for the MT direction in site LHG6 and distinct from the higher unblocking temperature of the HT2 direction (>480°C). This behaviour is not exclusive to the samples presented in this work, Biggin et al., (2011) observe the HT2 direction above the MT direction in site HG8, albeit in this instance the directions are more easily distinguishable as the HT2 from the southern limb (which is steep to the north) is observed. The final point in favour of a younger age for the MT component is discussed in section 5.5.2.2 of this chapter; the MT direction is observed in both the northern and southern limbs of the OF, with directions clustering well in geographic coordinate and therefore implying an acquisition age which post-dates the formation of the OF. On the other hand, below a fold test is performed using the HT2N and HT2S directions which suggests the HT2 direction is potentially as old as the formation of the OF. However, if the interpretation that the MT direction in the northern limb of the

fold does indeed overprint any older magnetic signal the success of the fold test carried out from the northern limb and southern limb HT2 direction is purely coincidental.

The HT2S direction identified by Biggin et al., (2011) produces a pole (in geographic coordinates) distinct from any published Kaaapval Craton poles of Archean or Paleoproterozoic age (Biggin et al., 2011). If the acquisition of the HT2 magnetisation predates the formation of the OF, one would expect the HT2 site mean directions from each limb of the fold to be dispersed in geographic co-ordinates. When compared in stratigraphic coordinates the directions are seen to cluster much better after structural correction, $\hat{k}$ = 13.5 in geographic coordinates and increases to $\hat{k}$ = 29 in stratigraphic coordinates. On this basis, the HT2 direction identified as part of this work in the northern limb of the OF is considered comparable to the direction identified by Biggin et al., (2011).

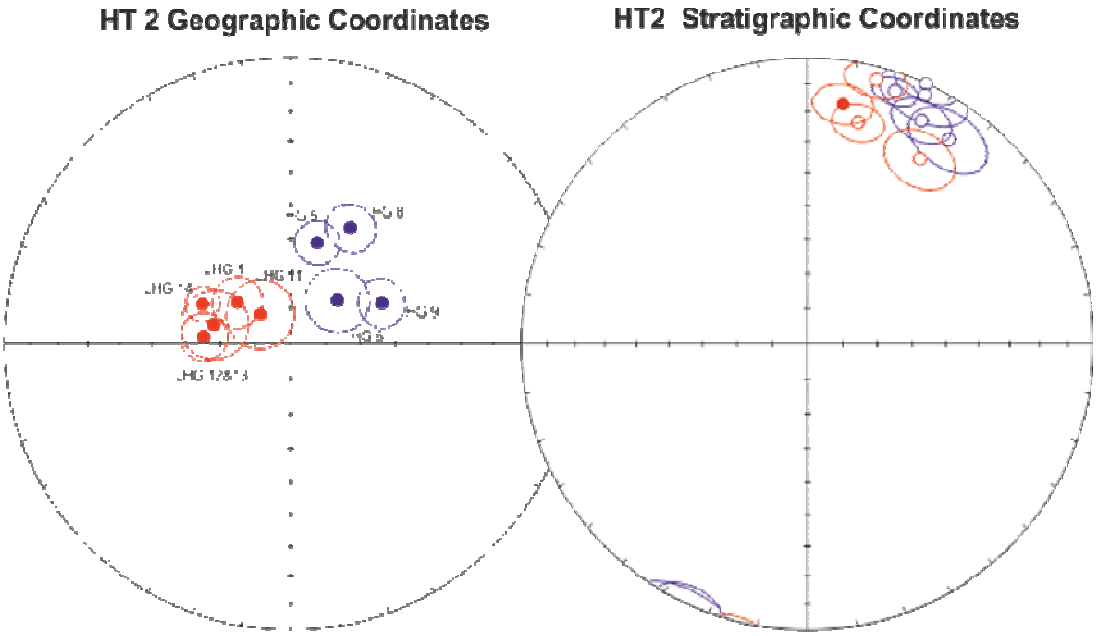

Figure 5.23. Equal area plots showing HT2 component site mean directions. (a) Site mean directions of HT2 component in geographic coordinates; samples from this study are shown in red. Site mean directions calculated by Biggin et al., (2011) are shown in blue. (b) Once the tectonic correction to account for the formation of the OF, HT2 directions from this study (red) and those of Biggin et al., (2011) show improved grouping. Filled points represent the lower hemisphere. Ellipses indicating α 95 cones of confidence.

The discussion above forms the basis of a fold test (bedding-tilt test, see Figure 5.23) which can determine the relative age of a ChRM magnetisation. If the ChRM is acquired prior to folding, the ChRM directions observed from opposing limbs of the fold will be dispersed when plotted in geographic coordinates. In stratigraphic coordinates, when a structural correction is applied to the directions, so as to restore them back to horizontal, the directions are seen to converge (Butler.R.F, 1992; Graham, 1949; McElhinny, 1964). As described above, when a structural correction is applied to the HT2 directions to ac-

count for the steeply plunging OF, clustering of the directions is improved significantly, from a ƙ value of 13 which increases to a ƙ value of 29. This therefore means that the ChRM must have been acquired syn-folding or prior to the folding event which resulted in the OF at ca. 3.2 Billion years, dated indirectly from field relationships, de Wit (2011). However, this field stability test cannot distinguish between magnetic acquisition prior to the folding event or as a result of the formation of the fold. A full unfolding of the structure may overcorrect directions, whereas the best grouping of the directions may be obtained only as the structure is partially unfolded (Butler.R.F, 1992; Tauxe and Watson, 1994). In addition, comparing grouping of directions alone cannot account for the complexities of the geomagnetic field, nor for the intricate structural relationships which may not be fully understood (Tauxe and Watson, 1994). Applying a bootstrap fold test (Tauxe and Watson, 1994) can overcome the short comings of the fold test as proposed by McElhinny, (1964) and applied above. The results of the test (shown in Figure 5.24) confirm the results of the simpler fold test and suggest the best grouping of the HT2 directions from the opposing limbs of the OF is achieved at pre- or early syn-folding stage. This means the age of the magnetisations recorded by the HT2 direction in the rocks of the Hooggenoeg Formation is constrained by the age of the OF at 3.2Ga. When combined with the results of Biggin et al., 2011, a new tectonically corrected VGP, λ= 59.9°/ϕ= 78.7°, A95=6.9, N=9), is calculated from a total of 9 sites and implies a palaeolatitude of -4.3° for the Hooggenoeg Formation , plotted structurally corrected in Figure 5.25.

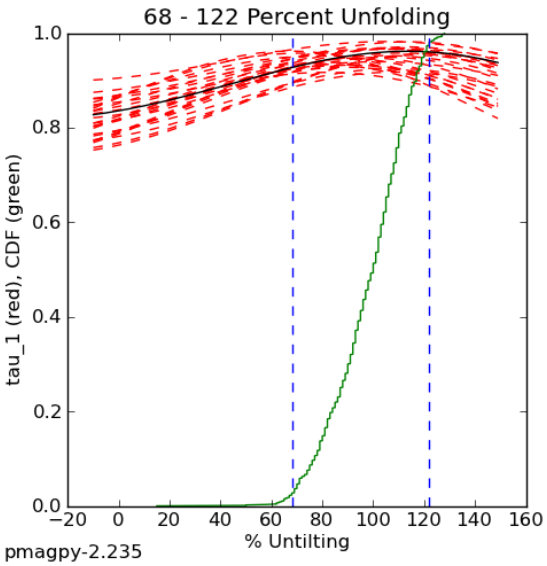

Figure 5.24 Results of a bootstrap fold test as per the method of Tauxe and Watson, 1994. The test was applied to individual site mean directions from the HT2 direction, to establish if the improved clustering observed after tectonic correction was indeed robust, thus establishing timing of the acquisition of the HT2 direction.

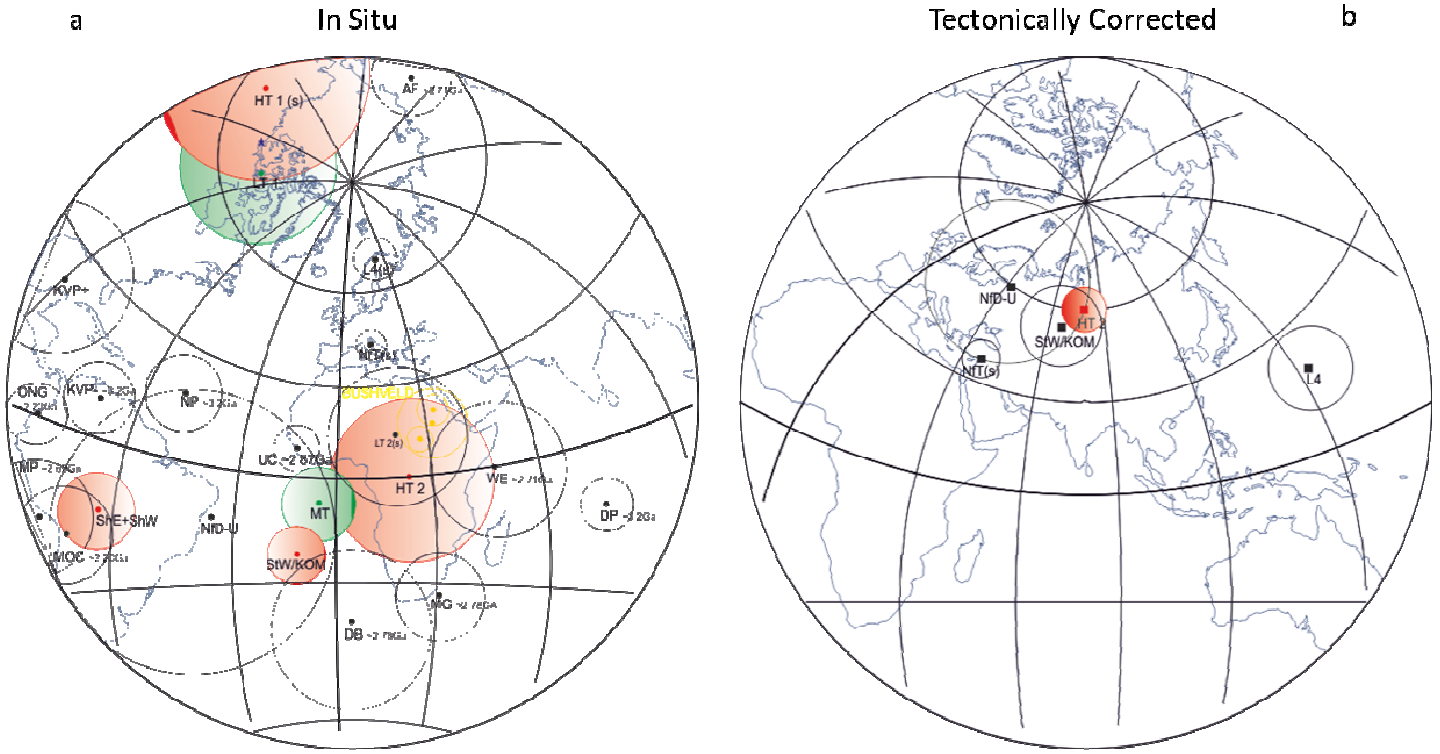

Figure 5.25. Average poles produced from this study of the Hoggeneong Formation (seeTable 5.3) are shown in geographic coordinates in (a) by the shaded: green = low and medium temperature overprint components; red = ChRM components. The new components calculated for the Komati Formation and presented in this thesis are also plotted in red (ShE+ShW and StW/KOM). (s) alongside a pole indicates the poles are south, otherwise all poles are north. The purple star indicates the pole obtained from the present-day field (PDF) direction for the BGB. For comparison poles older than 2Ga for the Kaapval Craton are shown by black unfilled circles. Bushveld poles (after Letts et al., 2009) are shown in yellow. L4+ = Kromberg Formation (Biggin et al., 2011); NfT and NfD-U = Noisy Complex (Biggin et al., 2011); LT2 = Hoggenoeg and Kromberg Formation (Biggin et al., 2011); AF = AllanBridge Fm (de Kock et al., 2006); DB = Deerdepoort Basalt (Wingate, 1998); ONG = Ongeluk lava (Evans et al., 1997); DP = Dalmein Pluton (Tarduno et al., 2007); KV+/- = Kaap Valley Pluton (Tarduno et al., 2007); MG = Modipe Gabbro (Evans and McHennily, 1966); MOC = Mamatwan Ore Complex (Evans et al., 2001); MP = Mbabane Pluton (Layer et al., 1988,1989) ; UC =Usushwana Complex (Layer et al., 1998)WE = Westonaria Basalt (Strik et al., 2007).

(b) Average Poles shown are tectonically corrected. New HT2 direction, thought to be older than 3.2 Ga (see text) compared to similarly aged Onverwacht Group poles calculated by Biggin et al., (2011): NfT, NfD-U and L4, as well as the StW/KOM pole calculated in Chapter 5 of this thesis.

5.9. Conclusions

A palaeomagnetic investigation of the rocks of the Hooggenoeg Formation has been carried out. The new findings presented in this chapter have been placed in the context of previously published results for the Hooggenoeg Formation, Onverwacht Group and rocks of the same age in the Kaapval Craton. Given the age of the rocks and their complex thermal and chemical history the results were found to be noisy, often resulting in scattered directional results and therefore overall not straightforward to interpret. A low temperature overprint direction (LT1) was interpreted as a present day field (PDF) overprint. A further mid temperature overprint which was observed in samples of both the southern and northern limbs of the Onverwacht Fold (dated at 3.2Ga, de Wit et al., (2011), indicating that the MT direction postdates the formation of the fold and is therefore younger than 3.2Ga. Thermal events across the BGB at ca. 2.7 (de Ronde et al., 1991) could be the source of the magnetisation and are consistent with a post-D2/D3 age. High temperature direction , HT1, is isolated exclusively in the rocks of the southern OF. A new component direction and pole is calculated for the HT1 direction as it agrees well with the direction previously isolated from the Hoggeneogg Formation by Biggin et al., (2011). The error envelope of the pole is now larger, so despite confirming the results of Biggin et al., (2011) the result is less precise. In addition, the results presented here cannot contribute to determining the age of the HT1 magnetisation as it was not possible to carry out any palaeomagnetic field test. The results from the northern limb of the fold remain somewhat unclear. A high temperature direction HT2N is isolated in samples of the northern limb of the fold but is not fully distinguishable from the MT direction. Tentative evidence to suggest that the directions are indeed of different ages is presented but it is certainly not conclusive. Nevertheless, the HT2N direction, combined with the HT2S direction identified by Biggin et al., (2011) in the southern limb of the OF can be used to carry out a fold test which indicates that the HT2 direction was acquired prior to or during the formation of the OF. If the HT2N and MT directions are shown to be distinguishable, this means the minimum age for the HT2 direction is 3.2Ga and indicates a stable geomagnetic field was present in the Archean. In addition the new pole calculated for the HT2 direction places the BGB at equatorial latitudes at the time of the acquisition of the HT2 magnetisation.

6 Palaeomagnetism of the Noisy Complex

6.1. Introduction

The named Noisy Complex (de Wit et al., 2011) is the youngest formation of the Onverwacht Group studied as part of the work presented in this thesis. The overlying Kromberg and Mendon Formations include thick basaltic packages but are dominated by volcanicalstic and sedimentary sequences, with a number of interbedded cherts. Furthermore, particularly in the case of the Mendon Formation, deformation has resulted in the units being divided across the BGB by a number of narrow structural blocks (Lowe and Byerly, 1999b), making correlation of individual packages across the length of the BGB difficult. The difficulties associated with the sampling of the uppermost units of the Onverwacht Group, combined with the lack of any significant palaeomagnetic studies which would allow the results to be put into palaeomagnetic context and the time constraints associated with a short field season meant a focus on the middle sections of the Onverwacht Group was determined. The promising palaeomagnetic results already published for the rocks of the Noisy Complex provided further reason to develop our understanding of the palaeomagnetic record of the middle units of the Onverwacht Group.

Previous palaeomagnetic work carried out on the rocks of the Noisy Complex can be found in studies by: Biggin et al., (2011); Tarduno et al., (2010) and Usui et al., (2009). As is true for the two other Onverwacht Formations studied in this thesis, despite the encouraging results that point towards a stable geomagnetic field being present at the time of the formation of the Noisy Complex, it is vital to establish the reliability of the age of the magnetisation recorded in the rocks of this formation. Palaeomagnetic field tests can be performed to assess the reliability of the near-primary components, as shown by the positive conglomerate test of Usui et al., (2009) and strengthened by the later work of Biggin et al., (2011). Due to the complex tectonic history of the rocks of the BGB, the interpretation of the results presented in the previous studies is complicated and they remain tentative attempts at dating the magnetisation locked in the rocks of the Noisy Complex.

In order to further constrain the reliability of the results presented in previous paleomagnetic studies, it was necessary to acquire a new data set for the Noisy Complex, so as to perform improved field stability tests. Collection of new samples would further add to the dataset available for the Noisy Complex, allowing for more robust interpretation of new results, particularly in light of the findings published by previous authors. As swwn in Fig-

ure 6.1, surface samples were collected from four sites, in the northern limb of the Onverwacht Fold, in a previously unsampled area to the west of the localities of Tarduno et al., (2010).

New paleomagnetic data for the Noisy Comple Complex, presented in this chapter, were noisy both at the specimen and site level and often affected by lightning strikes and the effects of weathering.

This chapter outlines the geological context of the samples collected for this study, as well as including a short summary of previous palaeomagnetic studies of the rocks of the Noisy Complex. The chapter focuses on the directional results obtained from the samples collected in addition to establishing the carriers of the magnetisation via rock magnetic characterisation and optical and scanning electron microscopy. The new results are put into the context of the already published work. The chapter concludes with some final observations and conclusions.

6.1.1.Geology of the Noisy Complex

6.1.1.1 Stratigraphic Context

In 1969, Vijoen and Viljoen mapped and described the upper formations of the Onverwacht Group, including the Hooggenoeg Formation, the Kromberg Formation and the Swatkoppie Formation [now interpreted to be structurally disturbed parts of other units within the Onverwacht Group, (Lowe and Byerly, 1999b)]. They observed that in the type area in the Western Limb of the Onverwacht Fold (OF), the main feature of the Hooggenoeg Formation was the apparent cyclicity of the volcanism recorded in the sequence. They distinguished that the base of the Hooggenoeg formation is characterised by ultramafic basalts which can be massive and pillowed, whilst towards the top of the sequence felsic volcanic materials interspersed with cherts become more predominant. The uppermost part of the formation is dominated by a broad zone of felsic volcanics which are capped by a thick chert horizon. Viljoen and Viljoen (1969) identified that this uppermost layer can be traced over the total strike distance (56 km) of the western limb of the Onverwacht Anticline. The felsic volcanics are described as being massive, structureless feldspar porphyries which fine upwards into dense light grey sericitic volcanics thought to be of pyroclastic origin. The unit is capped by 112m thick black and white cherts, with some banded iron formations too. Bedded felsic pyroclastic deposits, greywackes and iron rich shales are interbedded within the cherts. In the Eastern limb of the OF, the section is

characterised by layered tuffs with visible bedding and flame structures as well as thick agglomerates. Viljoen and Viljoen (1969) argue that the emplacement of the uppermost layer of the Hooggenoeg Formation was during a lull in explosive activity which emplaced the lower Hooggenoeg as near-surface intrusives and/or extrusives. The sedimentary structures observed in the tuffs are thought to indicate deposition of ash fall deposits into shallow waters.

Following the classic work of Viljoen and Viljoen in 1969, a number of authors continued to study the rocks of the upper Hooggenoeg Formation (de Ronde and de Wit, 1994; de Wit et al., 1982; de Wit, 1987; Lowe and Byerly, 1999a; Lowe et al., 1985). The interpretations of Viljoen and Viljoen, (1969) remained true for the most part. Better understanding of the alteration caused by hydrothermal process that affected the rocks of the BGB led to the reinterpretation of the cyclic volcanic activity and the understanding that the felsic units are in fact silicified mafic and ultramafic volcanic deposits (de Wit et al., 1982; de Wit, 1987). In addition, the work of Lowe and Byerly, (1999b) proposed a new stratigraphic classification of the rocks within the Onverwacht Group. In this new classification the Hooggenoeg Formation was subdivided into six stratigraphic units (H1-H6). Unit H6 comprised the thick sequence of felsic volcaniclastic and volcanic rocks. The silicified sedimentary rocks of the uppermost Hooggenoeg Formation were named the Buck Reef Chert (BRC) after the work of Hall, (1918). However, Lowe and Byerly (1999) argued that the BRC belong at the base of the overlying Kromberg Formation, rather than at the top of the Hooggenoeg Formation. In the new stratigraphic regime, the BRC became unit K1 of the Kromberg Formation. The authors further divided the BRC into four subdivisions -for details the reader is directed to Lowe and Byerly, (1999b) and Lowe and Worrel, (1999).

The reassignment of the BRC to the Kromberg Formation was controversial and many authors did not adopt this reclassification amongst them Brandl and de Wit, (1997). An extensive mapping project was undertaken by de Vries et al., (2006) to better understand the stratigraphic architecture of the BRC. The authors highlight that the contact between the BRC and underlying stratigraphy is gradational (as previously identified by Lowe and Worrel, (1999); Viljoen and Viljoen, (1969b)), and there is no regional unconformity (despite there being some local unconformities) at the base of the BRC which would warrant stratigraphic separation from the Hooggenoeg. Furthermore, de Vries et al., (2006) consider that the felsic volcanics and the BRC are closely related and therefore introduce the Buck Ridge volcano-sedimentary complex (BR-vsc) as a new stratigraphic unit. The

work of de Vries et al., (2006) focused on the north-western limb of the OF fold. Detailed logging and mapping in the south-eastern limb (Etimambeni Section) of the fold by de Wit et al., (2011) shows that the base of the BR-vsc has an unconformable contact with the Hooggenoeg Formation. The geochemical signature of the volcanics within the Hoogge-

Figure 6.1 Geological map showing sampling localities for this study (white star) and sampling site of previous works. CG1, CG2 and CGM correspond to sites sampled by Biggin et al., (2011); NfD-T corresponds to sites sampled by Tarduno et al., (2010); NfT-U correspond to localities sampled by Usui et al., (2009). Map modified from de Wit et al., (2011).

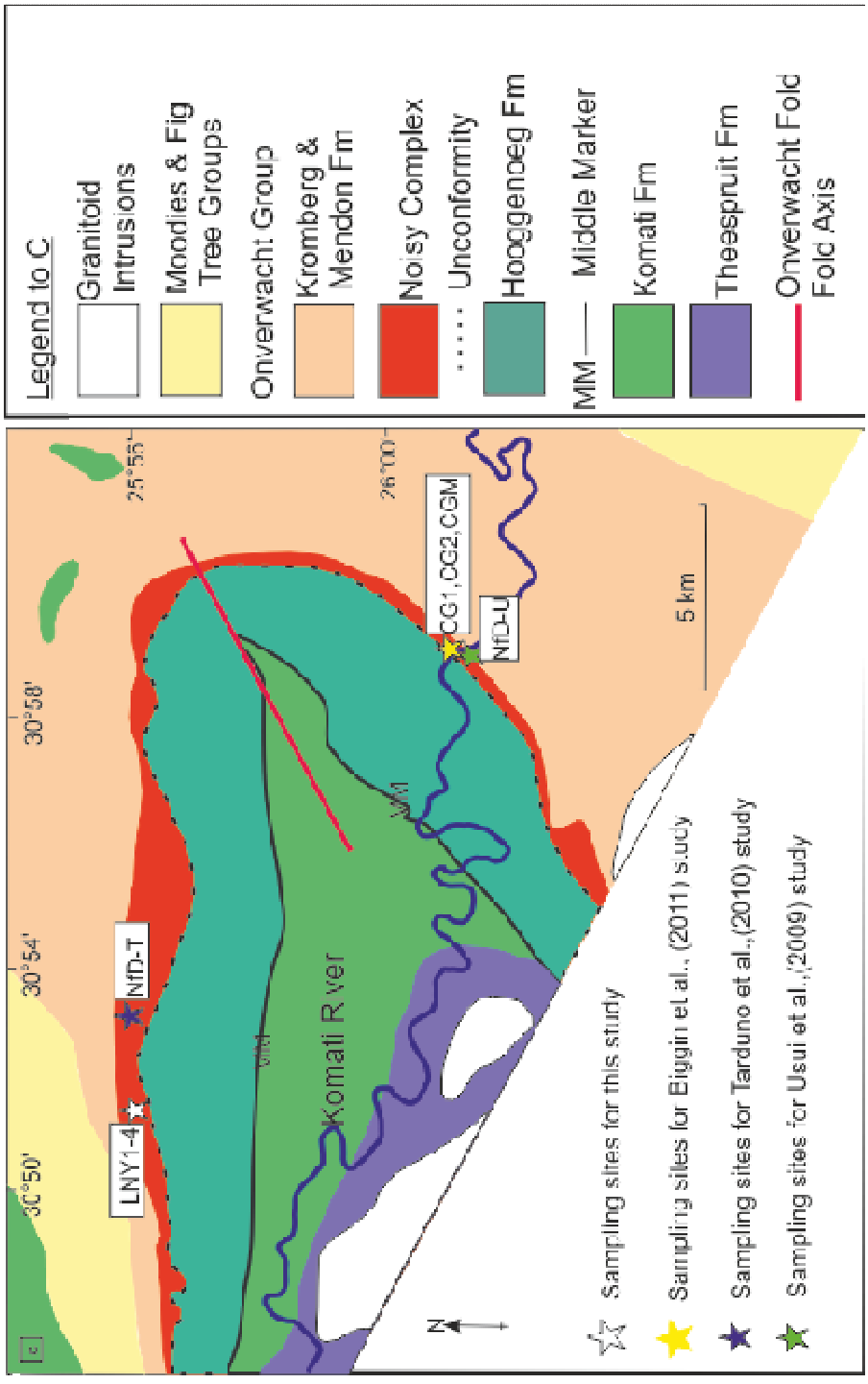

noegg Formation and the BR-vsc is also very different (Furnes et al., 2011). Therefore, de Wit et al., (2011) propose the creation of a new geological unit within the Onverwacht Group: The Noisy Complex. In the study area the Noisy Complex is presented as a predominantly clastic sedimentary sequence with no lavas, although there is a tuff in the uppermost part of the section studied. Concordant U/Pb zircon dating gives an age of 3455.2 ± 7.5 Ma (Biggin et al., 2011) for the tuff. This is consistent with previously published ages for the BR-vsc: 3451±5 Ma (De Vries, 2004), 3445 ± 6 Ma (de Wit et al. 1987, Kamo and Davis, 1994) and 3451±5 Ma (de Vries et al., 2006). De Wit et al., (2011) argue this is further evidence that the new Etimambeni Section should be merged with the BR-vsc to form the Noisy Complex. For further details on dating of the Noisy Complex, the reader is directed to de Wit et al., (2011) and references therein.

The newly created Noisy Complex nomenclature is not adopted by Grosch et al., (2011). The drilling of three boreholes in the mid-upper Onverwacht Group (Kromberg, Noisy and Hooggenoeg Formations) in 2008 by the Barberton Scientific Drilling Program (BSDP) allowed further detailed study of the Noisy Formation. The drill core was obtained along the south-eastern limb of the OF fold; for full details of the drilling operations the reader is directed towards Grosch et al., (2009a).The recovered core allowed Grosch et al., (2011) to carry out a detailed chronostratigraphic study of the Noisy Formation. Detrial zircon ages from the study argue for a maximum depositional age for the Noisy Formation at ca.3432Ma and also represent the maximum age of the unconformity identified both in the new drill core and by de Wit et al., (2011) in the Etimambeni Section. Further detrial zircon ages from the study suggest the source of the clasts (see section 1.1.2, this chapter for stratigraphy details) within the conglomerate units is diverse and includes the BR-vsc, the Hooggenoeg pillow lavas and cherts, the Stoltzburg and Theesrpuit Plutons, as well as rocks from the Ancient Gneiss Complex (AGC, see Chapter 2 for further detail). The authors argue, given the chronological and stratigraphic evidence, the Noisy Formation on the south-eastern limb of the OF cannot be correlated with the BR-vsc in the north-western limb of the OF, as proposed by de Wit et al., (2011). Grosch et al., (2011) agree that the unconformable contact, the difference in ages of the two units, as well as the contrasting lithologies mean that the Noisy Formation is distinct from unit H6 (which includes the BR-vsc) of the Hooggenoeg Formation. Despite the evidence presented by Grosch et al. (2011), the authors do not consider the lack of outcrop of the Noisy Formation on the north-western limb of the OF.

The newly created stratigraphic of the Onverwacht Group, which includes the Noisy Complex, is adopted within the work presented in this chapter and thesis, as is shown in the geological map in Figure 6.1.

6.1.1.2 Stratigraphy

The north-western limb of the OF the Noisy Complex, as studied by de Vries et al., (2004) is exposed as a laterally extensive, east-west striking and steeply dipping (in some places overturned) unit which youngs to the North. At this type locality, the unit is approximately 2 Km thick. It is cross-cut by NE-trending faults that affect the entire north-western limb of the OF.

De Vries et al. (2004) divide the BR-vsc section into two parts: the lower BR-vsc, which is poorly exposed but dominated by massive, occasionally pillowed, basalts with minor komatiites. These are interbedded with silicified sedimentary rocks which preserve cross bedding and grading. These features indicate deposition in a subaqueous environment. The upper part of the section becomes dominated by bimodal styles of volcanism: generally massive porphyritic felsic lava flows, which in places are columnar jointed and flow banded. These are interpreted to indicate a phase of shallow intrusive or extrusive volcanism. Towards the west, the section is generally finer grained and consists mainly of volcaniclastic deposits: tuffs with rare accretionary lapilli layers. In conjunction with the presence of conglomerates, these features indicate the erosion and transport of the volcanic material in a potentially shallow water environment. The presence of accretionary lapilli indicates the volcanism could be explosive at times. The section is capped with the previously know BRC, consisting of silicified volcaniclastic material, banded sedimentary cherts and iron-rich bands which suggest a slight deepening of the depositional environment. Well-banded silicified sedimentary rocks are indicative of a near-shore setting. The lower section of the BR-vsc shows thickness variations in the order of hundreds of metres. Stratigraphically upwards the thickness variations across the section diminish with the uppermost part of the section being largely unaffected.

The lower part of the BR-vsc is intruded by massive felsic intrusions which were likely emplaced along the NE-trending faults. The intrusions are quartz and feldspar rich. A sample from the core of one of the intrusions is dated by U-Pb SHRIMP at 3451 ± 5 Ma (de Vries et al., 2006). Felsic sills project from the northwestern sides of the massive felsic intrusions. In addition, quartz and plagioclase rich felsic porphyritic dykes with a fine grained

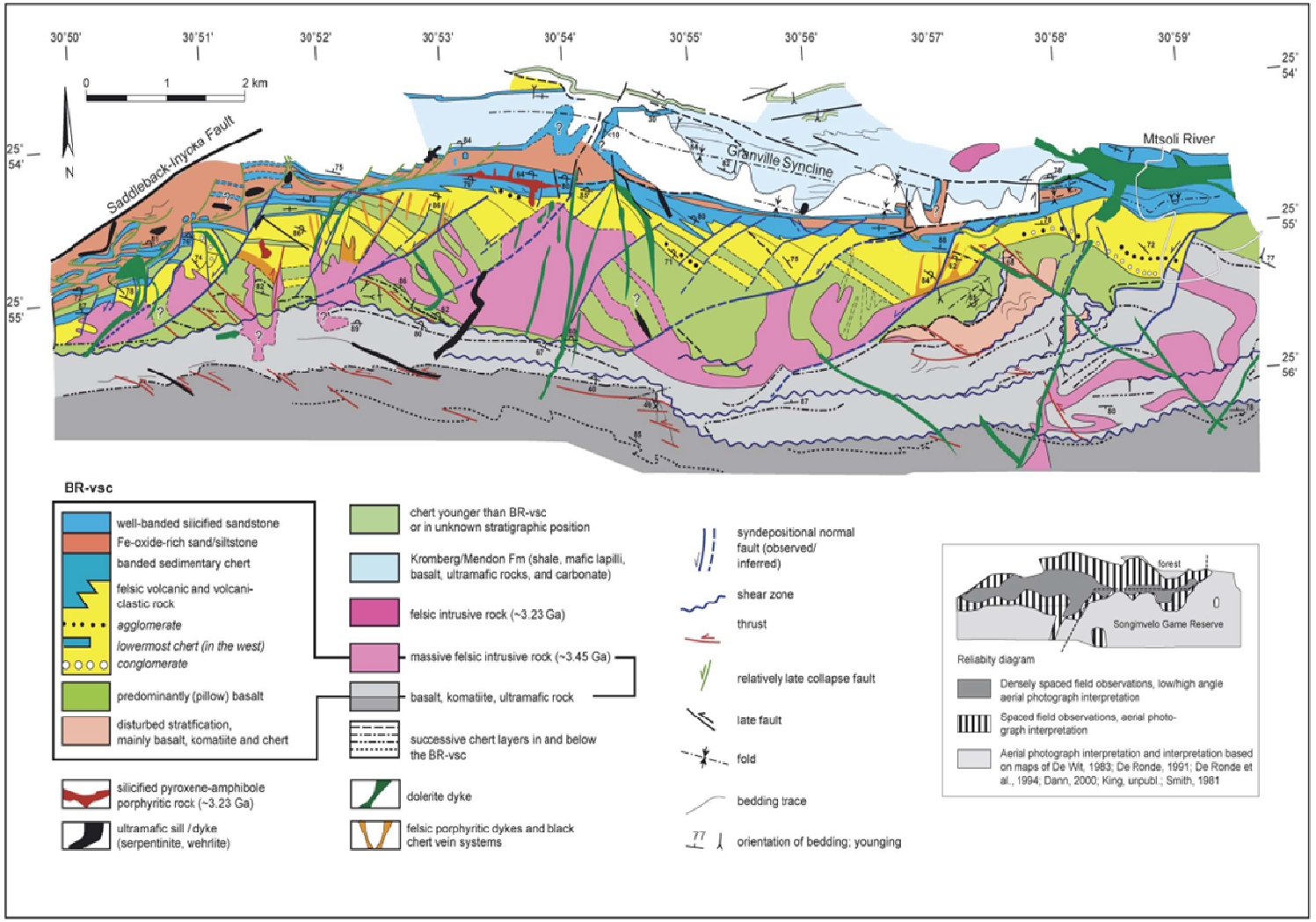

Figure 6.2. Geological map of the Noisy Complex, in the north-western limb of OF fold, taken from de Vries et al., (2004). As the orientation of the bedding in the area is near -vertical the map can also be interpreted as a cross-section through the BR-vsc section.

groundmass intrude the lower and upper parts of the BR-vsc. Metre wide black cherts occur in association with the porphyritic dykes. Mafic intrusions of mainly doleritic compositions intrude the western part of the section. These are dated by U-Pb SHRIMP at 3228 ± 3 Ma (de Vries et al., 2006). Coarse grained undated wehrlite dykes, as described by Dann, (2000), also traverse the BR-vsc section.

Thickness variations, which are more severe and display the largest stratigraphical offsets in the lower parts of the section, are attributed to listric normal faults which de Vries et al., (2004) interpret as syndepositional. In the westernmost part of the section (see Fig 6.2, from 30°51' to 30°53') a roll-over anticline associated to the deformation is observed. The concentration of clastic deposits on the down-thrown sides of the NE normal faults and the distribution of the felsic rocks indicate that deposition in the area was dominated by an extensional regime with accommodation space being created by the normal faults. The emplacement of the massive felsic intrusion is along the faults and takes up some of the accommodation space created during extension. The dating referred to above indicates that emplacement of the felsic rocks is contemporaneous to the extrusive volcanism in the upper part of the BR-vsc section.

The Etimambeni section (182m, see Figure 6.3), in the south-eastern section of the OF, crops out along the Komati River Gorge. As described by de Wit et al.,(2011) there are no lavas present in the section, which is dominated by well-bedded clastic sedimentary rocks. At this locality, the contact with the underlying Hooggenoeg Formation is unconformable, whilst the upward contact with the Kromberg Formation is defined by the presence of a shear zone (Etimambeni Shear Zone). The lowermost part of the section comprises a diamictite [a lithified, unsorted conglomeratic sand which can also include coarser particles, mainly in a mud matrix (Allaby and Allaby, 2008)], which is normal and inversely graded and includes cyclic layers of conglomerates, sandstones and cherts. The angular clasts in the conglomerate include banded cherts and fuchsite-rich clasts which the authors propose are derived from the underlying Hooggenoeg Formation. The clasts and the matrix have undergone extensive hydrothermal alteration leading to the formation of sericite, fuchsite, carbonates and magnetite (Biggin et al., 2011; de Vries and Touret, 2007; de Wit et al., 2011). The diamictite is interpreted as a debris-flow. The deposits in the middle part of the section are thought to be fluvial deposits, given the presence of well-sorted massively bedded (in places seen to in-fill channels) clast supported conglomerates. Overlying the fluvial deposits is anormally graded and bedded sandstone display-

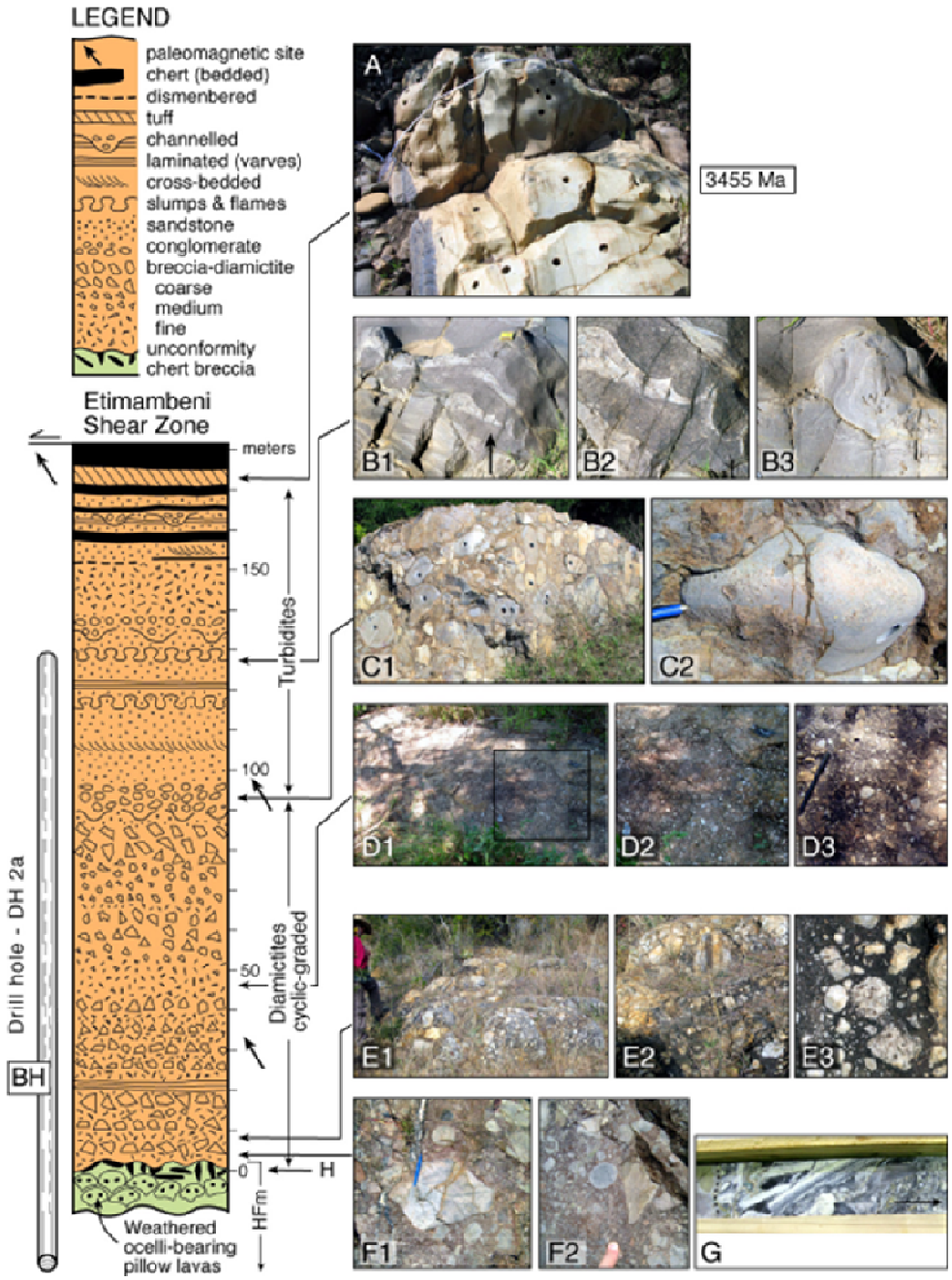

Figure 6.3. Figure taken from (de Wit et al., 2011). Detailed log of the Etimambini section, showing also the location of a drill hole (Grosch et al., 2009a). Photographs also in de Wit et al., (2011). A) Felsic tuff sampled by Biggin et al. (2011). B) Flame structures in upper parts of the section. C) Conglomerates with chert clasts. D) Diamictites characterstic of the lowermost part of the section. E & F) Coarse grained diamictite. G) Brecciated chert. For more detail on individual photographs and lithological descriptions the reader is directed towards de Wit et al., (2011).

ing a range of sedimentary structures, including flame structures. These are overlain by a thin 1-2m thick felsic tuff (sampled for palaeomagnetic studies by Biggin et al., 2011, see also section 1.2), dated at 3455 ± 7.5Ma by concordant U/Pb zircons (Biggin et al., 2011). The uppermost 20m of the section is dominated by laminated and bedded cherts.

Overall, the geology of the Noisy Formation, as described by Grosch et al., (2011), from the drill core (obtained as part of the BSDP) and field observations is in agreement with that of the Etimambini section described by de Wit et al., (2011). The uppermost section of the unit is interpreted to be deposited as turbidity current, given the convoluted bedding, flame structures and slumping observed in the tuffaceous and sandstone layers. As a result, Grosch et al., (2011), argue the airfall tuff, as interpreted by de Wit et al., (2011) and sampled for palaeomagnetic purposes by Biggin et al., (2011) - see section 6.2 of this chapter- is, in fact, not a primary airfall deposit, but rather a reworked sedimentary deposit which cannot be used as a chronostratigraphic marker; the implication being that the 3455.2 ± 7.5 Ma age of Biggin et al., (2011) should be attributed to the underlying clastic sediments. Whilst de Wit et al., (2011) argue the majority of the clasts in the lower diamicties are mainly dacitic in composition, observations from the drill cores indicate meta-igneous and metasedimentary clasts are also present. Grosch et al. (2011) interpret this to mean the provenance of the clasts is derived from the underlying Hooggenoeg Formation and BR-vsc. Furthermore, a wide range of detrial zircon ages, obtained from the lower units of the Noisy Formation indicates diverse detritus sources for the clasts of the diamictite. These could include zircons from the Steyndorp Block and the Phophonyane Shear Zone (PSZ) and the Ancient Gneiss Complex (AGC); for further detail on the overall structure of the Kaapval Craton the reader is directed to chapter 2. The implication of these findings is crucial to our understanding of the early Earth, as it is indicative that some of the proto-continental blocks that make up the Kaapval Craton might have, at the time of deposition of the Noisy Formation, been accreted and therefore provide evidence for tectonic processes being in operation at ca.3432Ma. In the geodynamic model proposed by Grosch et al., (2011), the unconformity at the base of the Noisy Formation indicates a period during which the depositional environment changed from a deep marine setting where pillow lavas were erupted [the Hooggenoeg Formation, (Furnes et al., 2011)] to a shallow marine setting. This rapid change in depositional environment is argued to be comparable to arc-continent convergent margins and ophiolite obduction processes (Grosch et al., 2011).

6.2. Palaeomagnetic Background

Three previous palaeomagnetic studies have been published for the rocks of the Noisy Complex: Biggin et al., (2011); Tarduno et al., (2010) and Usui et al., (2009).

The work of Usui et al., (2009) focused on the conglomerates in the Noisy complex. Samples, collected from the southern and the northern limb of the Onverwacht Fold (see Figure 6.1), from both the parent body and clasts were studied as part of the work. Microscopic analysis carried out on the clasts indicated that these were microcrystalline and formed almost entirely of plagioclase and quartz, with some phenocrysts of the same minerals. Accessory minerals include magnetite and apatite. Rock magnetic characterisation of the clasts suggests the magnetic carriers are dominated by MD grains of magnetite with a possible contribution from goethite or haematite. In addition, due to the constriction of the hysteresis loops at the waist, the authors suspect a contribution of SP grains. Typical demagnetisation results and equal area projections of the directions can be seen in Figure 6.4.Two directions of magnetisation are identified in the conglomerate clasts. A low temperature direction (LT) is removed by 500°C which can consist of multiple components. The LT direction (D = 388.4°, I = -60.3°, α95 = 6.5, k = 45.5) clusters close to the overprints observed in the Kaapval Craton that are caused by the emplacement of the Karoo Large Igneous Province ca. 180Ma (Strik et al., 2007). The LT direction is also close to the present day field at South Africa. A high temperature direction (HT) is removed at temperatures between 500-560°C, with directions being scattered. The authors of the study performed a Watson's test (Watson, 1956) to investigate the randomness of the HT direction, which found that the 14 samples tested were from a statistically random population (R=2.37). Therefore, the authors argue this is evidence for the clasts having acquired their magnetisation prior to their deposition in the conglomerate. Five sites were sampled in the dacite source rock (conglomerate). LT directions were isolated from three sites in the temperature range 75°-425°C. The LT direction is consistent with a present day field or Karoo age overprint. Samples from three sites are affected by lightning strikes. Consistent high temperature components with unblocking temperatures in the range of 550°-580°C, were isolated from three sites. Usui et al., (2009) interpret this direction to be a TRM acquired at ca. 3445Ma. However, the authors acknowledge the scatter in the data set and propose two alternative mechanisms by which the primary component could have been acquired:

a) Through remagnetisation of all conglomerate clasts, prior to their incorporation into the conglomerate, caused by Archaean lightning strikes. However, the authors acknowledge that it is not fully understood whether the Archaean atmosphere was able to generate lightning strikes.

b) Alternatively, there might not have been an internal geodynamo capable of generating a field during Archaean times (Labrosse et al., 2007) and the magnetisation could result from the influence of an external magnetic field generated by the interaction of solar wind and the atmosphere.

Whilst the results of the study cannot entirely disprove either of these options (paleointensity might clarify the issue, as lightning strikes would require samples to record very high field values, whilst an externally generated signal would yield very low field values and highly variable directions), the simplest explanation is that the magnetisation is a CRM acquired from the hydrothermal alteration.

The work of Usui et al., (2009) was followed by the work of Tarduno et al., (2010) which focused on the palaeointensity recorded by a dacitic intrusion of the Noisy Complex (samples were collected in the Northern limb of the Onverwacht Fold, see Figure 6.1). The aim of the study was to measure the palaeointensity as recorded by SD magnetite inclusions found in single silicate (plagioclase or quartz) crystals. The advantage of this technique is that it minimises the effects of non ideal behaviour: the effects of alteration caused by heating of the samples in traditional Thellier-Thellier experiments (Thllier & Thellier, 1959) ; it is also argued to shield magnetite from weathering/hydrothermal alteration and to minimise non-ideal behaviour of MD and PSD grains. The methodology was developed by Cottrell and Tarduno (1999) and has been used on a number of other studies, of which that of Tarduno et al., (2007) on the Kaapvalley Pluton is most relevant to the work presented in this thesis and which is discussed in further detail in Chapter 7. The results of the study would help clarify the source of the scattered HT component isolated in the work of Usui et al., (2009). Single domain to pseudo-single domain magnetite was isolated in single quartz crystals and Thellier-Coe paleointensity measurements (Coe, 1967) performed on unoriented samples. Two components of magnetisation were isolated from the samples. A low temperature component isolated at temperatures no higher than 450°C, in addition to a univectorial component isolated at higher temperatures. A total of 12 samples yielded results with an average paleointensity of 28.04± 4.3 μT; an intensity too high to have been generated in the absence of a geodynamo and

therefore precluding either of the exotic scenarios proposed by Usui et al. (2009). In addition, the authors were able to establish the paleoinclination for the BGB (-44.5° ± 11.1°) from two oriented samples (see Cottrell &Tarduno, (2000) and Tarduno et al., (2006) for details on the technique for obtaining oriented quartz crystals from thin-sections).

Biggin et al., (2011) sampled four Noisy Complex sites, in the southern limb of the fold, along the Komati River (CG1, CG2, CGM, NfT, see Figure 6.5). Three sites sampled the Noisy Complex conglomerates, whilst one site sampled a volcanic tuff. Biggin et al., (2011) isolate overprint components from all four sites which were unblocked at temperatures below 460°C with the exception of site CG2 where overprint directions persisted up to 550°C. ChRM components were isolated from three of the four sites, with the components being unblocked in the temperature range 400°C to 580°C/110mT. The ChRM directions from sites CG1 and CG2 were found to be scattered, but when combined with the data of Usui et al., (2009) gave a positive conglomerate test, meaning the conglomerate records a near-primary remenance of ca. 3.4Ga. The overprint and ChRM components isolated in site NfT often overlapped, therefore the ChRM was not always fully resolved. The authors acknowledge that hydrothermal alteration is the likely cause for the formation of the magnetic minerals which carry the remenance preserved in the samples, but argue that this is not problematic, as alteration likely took place soon after emplacement of the Complex. The new directions obtained in the study are compared to the previously published studies. Biggin et al., (2011) refer to directions isolated by Usui et al., (2009) as NfD-U and NfD-T for those presented by Tarduno et al., (2010). For ease of comparison this nomenclature will be adopted throughout this chapter. The previous studies had made no attempt to correct for the tectonic deformation leading to the formation of the Onverwacht Fold. Biggin et al., (2011) noted that the NfD-U and NfD-T directions do not cluster well in geographic or tectonic coordinates. In addition, NfD-T falls close to the LT1 direction identified by both Usui et al., (2009) and Biggin et al., (2011) and so could be a present day overprint. This has implications for the paleointensity results presented by Tarduno et al., (2010) and casts doubts over the timing of the acquisition of the magnetisation preserved in the single crystals. It also compromises the palaeolatitude calculated by Tarduno et al., (2010).

When plotted in stratigraphic coordinates, Biggin et al. (2011) find that NfD-U and NfT components cluster better than in geographic coordinates, indicating that the components predate the formation of the Onverwacht Fold at 3.2Ga. The findings are reinforced

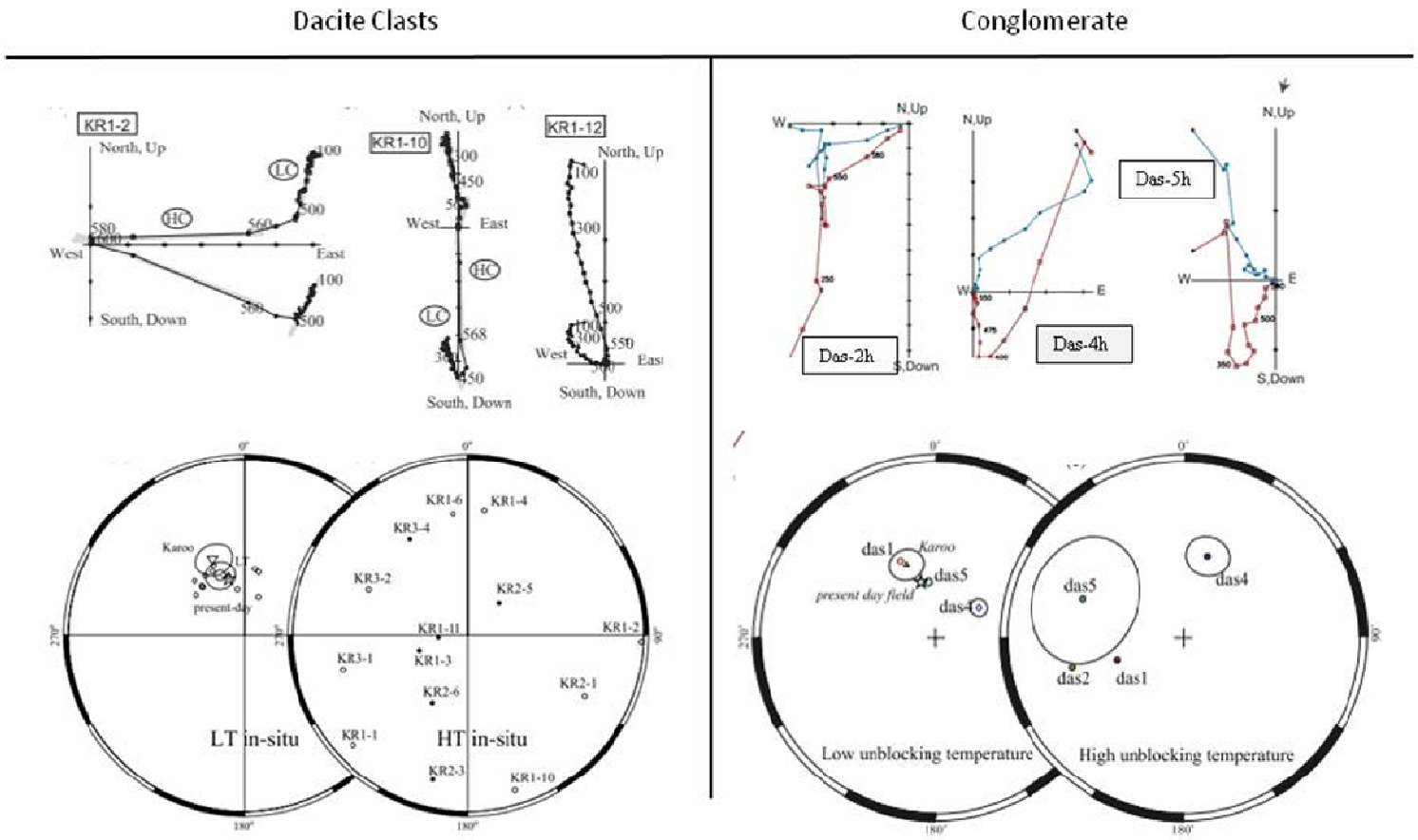

Figure 6.4. Orthogonal vector plots and equal area projections, showing demagnetisation and clustering of directions for dacite clasts and conglomerate samples, from Usui et al., (2009). All results are in geographic coordinates as the authors did not attempt a tectonic correction.

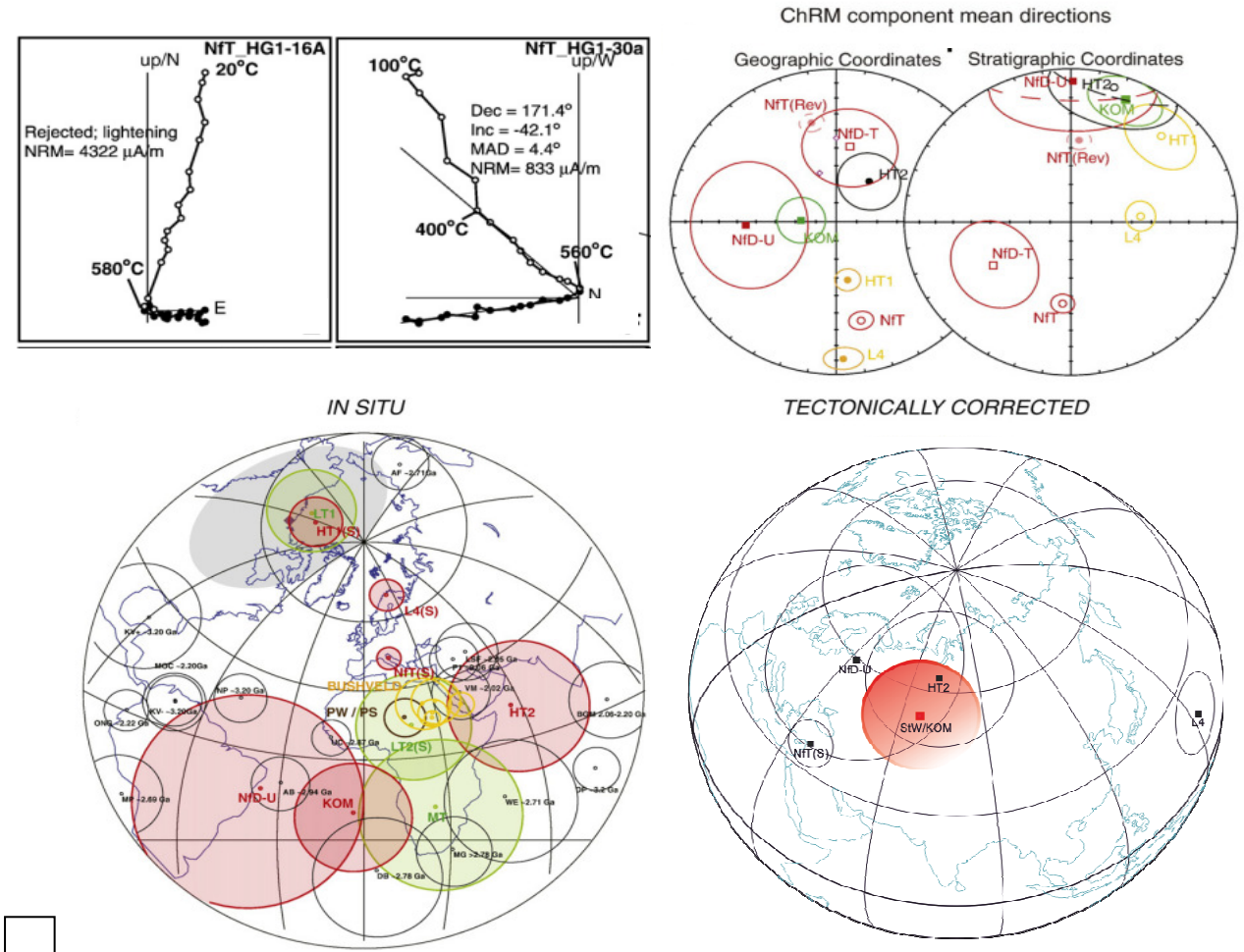

Figure 6.5. Directional results taken from Biggin et al., (2011) and results presented in this thesis. a) Representative demagnetisation orthogonal vector plots for samples of the Noisy Complex. b) ChRM components directions in geographic and stratigraphic coordinates. Filled points represent the lower hemisphere, open points represent the upper hemisphere. c) Average pole produced in Biggin et al. (2011) study shown as shaded circles, unshaded circles represent work previously published by other authors. The poles relevant to the work discussed in this chapter are: NfD-U, NfD-T and NfT(S, where S indicates the pole is South). NfD-U and NfT poles cluster better once the tectonic correction is applied, indicating the magnetisation predates the formation of the Onverwacht Fold.

when results are plotted in pole space where the directions are seen to overlap, as shown in Figure 6.4.

As part of this study, surface samples from the Noisy Complex were collected in the summer of 2011. The sampling sites are located in the Northern limb of the Onverwacht Fold, to the West of those of Tarduno et al., (2007) and Usui et al., (2009)- the rational behind the location of the sampling sites being to expand the geographical distribution of the data set and carry out a fold test utilising the results of Usui et al., (2009) and Biggin et al., (2011) from the Southern limb of the fold, with the aim of further investigating the reliability of the primary directions identified in the previous studies.

6.3. Methodology

6.3.1. Sampling

In May 2011, 46 core specimens were sampled at four sites (LNY1-4, as seen in Fig. 6.1) of the Noisy Complex, collected as part of a large sampling trip of the Onverwacht Group. Samples were drilled using a portable, petrol driven Stihl BT 45 drill modified to ensure a constant water supply, to avoid heating of the samples and possible remagnetisation. Locations were recorded using a Global Positioning System (GPS). Samples were oriented using a magnetic and sun compass. Y-east of true North (YETN) and the dip of the core were recorded. An orientation mark was made along the azimuth (representing the Z axis) of each individual sample with a brass marker before removing them from the country rock with a non-magnetic tool.

The locality is relatively inaccessible (via remote forest tracks) and there is no water supply readily available, meaning it is not the ideal candidate for palaeomagnetic study but precisely for these reasons offered an attractive alternative to localities of previous studies. However, the locality is positioned at the top of a ridge and lightning prone outcrops in the area are unavoidable.

Site LNY1 is located close to iron-rich banded cherts of the uppermost parts of the Noisy Complex (see Fig. 6.2, LNY1 is located at 25° 55.5’ S/ 30° 51.3’E). The Noisy Complex outcrops in the sampling area are faulted, complicating the identification of rocks belonging to the Noisy Complex versus those belonging to the overlying Kromberg Formation. The unit sampled as part of site LNY1 has a subvertical dip coincidental with the strike of a nearby banded, iron-rich chert. The volcanics of the Noisy Complex in this area are ex-

pected to be pale grey, quartz and feldspar rich reflecting their felsic composition. The rocks of site LNY1 are dark and fine grained indicative of a mafic composition. Therefore, site LNY1 is thought to sample a dyke/sill of unknown age: possibly a feeder dyke for the Mendon Formation (de Wit.2011, pers comm.).

The rocks of sites LNY2-4 are light grey in colour, very fine grained and contain phenocrysts of plagioclase and quartz. The Noisy Complex outcrop in this area is characterised by fractures which lead to formation of large blocks (50-100cm scale). During sampling, these fractures were avoided so as to reduce weathering effects on collected samples. In the vicinity of the drilling sites there are loose grey/brown, vesicular blocks of less crystalline material thought to be comparable to the tuffs described in the Etimambeni section (see section 6.1).

6.3.2. Experimental Methodology

A total of 31 discrete core samples, from four sites, were subjected to demagnetisation treatment. The discrete core samples were further subdivided to create specimens, of which a total of 41 were demagnetised using the combined thermal and AF treatment, whilst 33 were demagnetised using thermal techniques alone. For details of the demagnetisation techniques please see section 3.3.1 of this thesis.

Rock magnetic experiments (described in detail in Chapter 3, Section 3.2.2.1) have been carried out on 7 core samples from LNY1 to LNY4. With the exception of sites LNY1 (due to it not being part of the Noisy Complex) , at least two samples from each site have been investigated. Temperature dependant susceptibility measurements were carried out on four mini-core sample from sites LNY1 to LNY4. In addition a total of 28 bulk susceptibility measurements (which include measurement of sister samples) were made of bulk susceptibility from samples across LNY1 to LNY4.

6.4. Results

6.4.1. Directional Results

The analysis of the palaeomagnetic data was conducted using principal component analysis and standard statistical analysis (Fisher, 1953: Kirschvink,1980). On the whole, samples were characterised by a single component of magnetisation. Samples from sites LNY2 to LNY4 did produce some multi-component Zijderveld Plots with one stable overprint re-

moved during step-wise demagnetisation prior to a characteristic remanent magnetisation (ChRM) component being isolated. In most cases, (discussed in more detail below) the isolated directions were too scattered to produce a reliable site mean. In some cases it was not possible to isolate a stable overprint and/or ChRM components. Recorded overprint and ChRM components generally had a maximum angular deviation (MAD) of less than 15°. Low NRM intensities in many samples resulted in very scattered directions that did not produce a reliable site mean direction.

The mafic samples of LNY1 are dominated by a single component of magnetisation. The felsic samples from the LNY2-4 sites are often characterised by two components, a low temperature overprint component and a high temperature component. However, in all the sites, single components of magnetisation are observed. Data collected from the sill/ dyke (LNY1) and felsic rocks of LNY2-4, were scattered and it was not possible to isolate site means from the results. NRM intensities for the LNY sites ranged from 10^{-3} to 89 A/m.

In some cases the samples are weakly magnetised which adds significant noise to the data. In addition, in hand specimen the samples were noted to be considerably altered. Sample acquisition and handling could further contribute to the poor quality of the results.

6.4.1.1 LNY1

A total of ten samples were collected from site LNY1. Of those, six core samples, further subdivided into specimens, were subjected to demagnetisation treatment. All the measured samples are characterised by a single component of magnetisation which is isolated in the temperature range 0-90mT/ 20-580°C. The directions obtained from the LNY1 samples (Figure 6.6) are scattered and, therefore, it was not possible to calculate a meaningful site mean direction.

The measured intensities from the samples of the LNY1 site are in the range 22-89A/m. The elevated intensities recorded by the samples, when compared to intensities of other Archean aged rocks [4300µA/m-44µA/m for Noisy Fm samples in Biggin et al., (2011)] in combination with the single component behaviour observed in the samples indicates that the samples of this site have acquired an overprint associated with lightning strikes. The

samples were collected at the top of a ridge and care was taken to select localities which were more sheltered and less likely to have been affected by lightning. However, given the location of the sampling site it is a likely justification.

The exception to this is sister sample LNY1.3aa which produces a multi-component Zijderveld Plot, showing a low temperature overprint unblocked between 20-200°C with a high temperature component unblocked above 520°C. However, sister sample LNY1.3a shows a clear overprint acquired due to a lightning strike. The high temperature component direction for sample LNY1.3aa agrees well with the single component direction of LNY1.3a. This would indicate that given the low unblocking temperature of the overprint component, a less stable part of the blocking temperature spectra was contaminated.

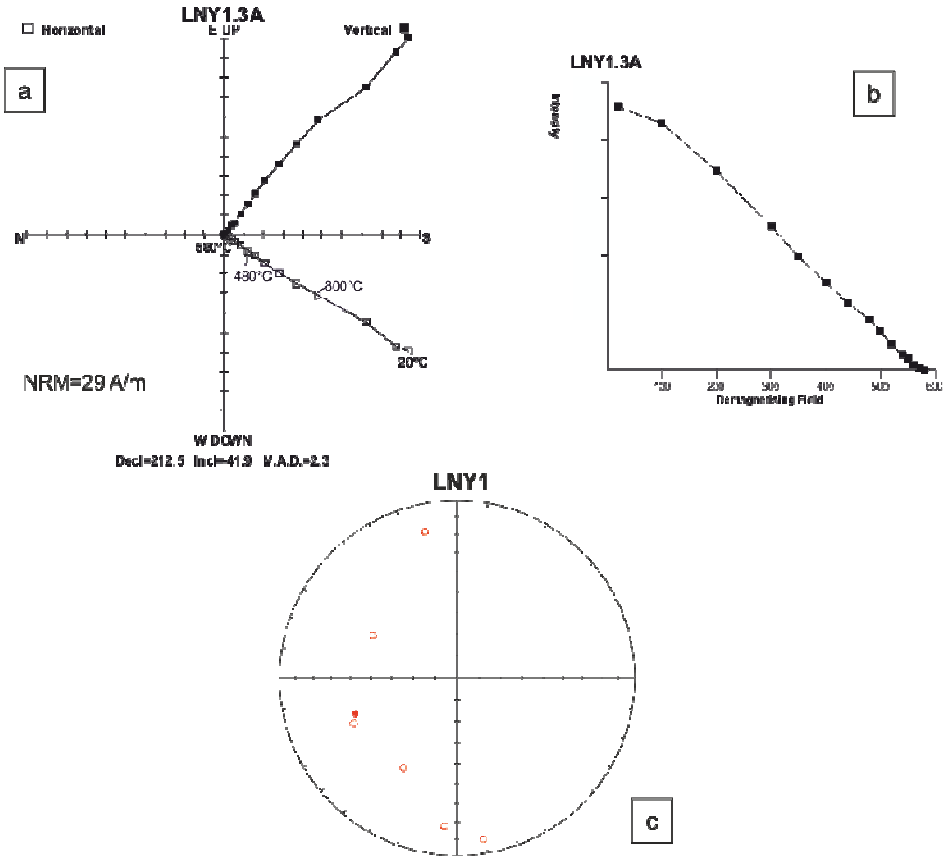

Figure 6.6. Orthogonal vector plots (a &b) and equal area projections (c), showing demagnetisation and clustering of directions for LNY1. Data presented in the equal area projections are in-situ. Filled points represent the lower hemisphere, open points represent the upper hemisphere.

6.4.1.2 LNY2

A total of 15 samples were collected from site LNY2. Of those, 13 core samples, further subdivided into specimens, were subjected to demagnetisation treatment. Three of the measured samples (LNY2.6, LNY2.7 and LNY2.8) are characterised by a low temperature overprint which is unblocked below 440°C. A high temperature direction is unblocked

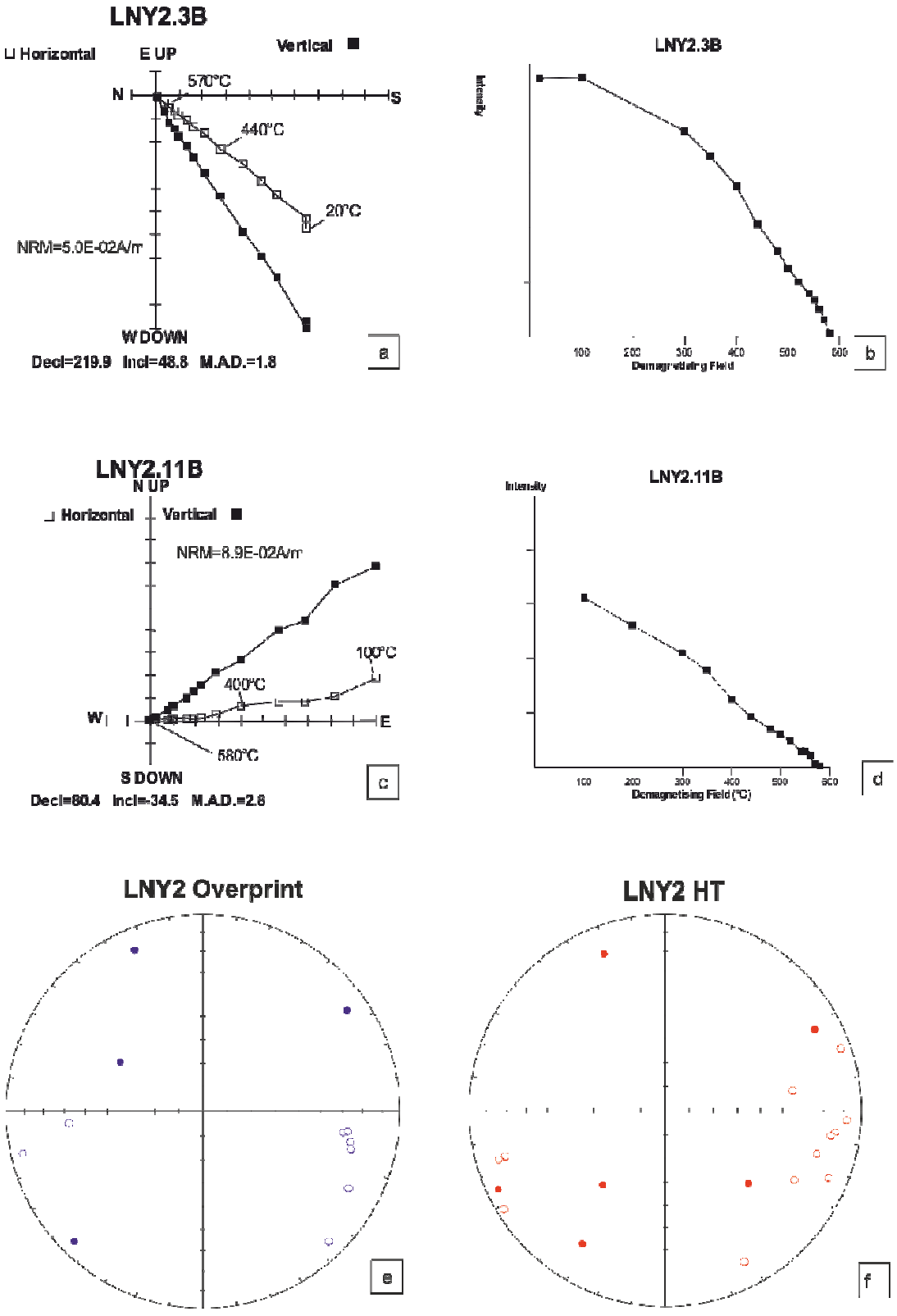

Figure 6.7. Orthogonal vector plots and equal area projections, showing demagnetisation and clustering of directions for LNY2. Data presented in the equal area projections are in-situ. Filled points represent the lower hemisphere, open points represent the upper hemisphere.

above the low temperature direction in the temperature range 20mT/520°C to 90mT/580° C. The overprint and high temperature directions are too scattered to obtain meaningful site means (see Figure 6.7).

The remaining samples are typically characterised by a single direction of magnetisation unblocked between 20°C-580°C/90mT. Samples LNY2.2 and LNY2.5 are seen to carry a low stability overprint which is removed by 300°C and is interpreted to be the result of sample handling. Overall, the single direction was seen to be scattered, with the exception of samples LNY2.11 to LNY2.15 were directions cluster as a shallow east component (see Figure 6.7). The measured NRM intensities range between 10^{-2} to 89 A/m. The unidirectional nature of the isolated directions combined with the elevated NRM intensities points towards the magnetisation carried by the samples site LNY2 having been overprinted as a result of lightning strikes.

As seen in Figure 6.8 the LNY2 samples were collected from a series of blocky outcrops. Samples LNY2.1 to LNY2.5 were collected close to one another. Samples LNY2.6 to LNY2.8 were collected from the lowest sampled block which was relatively sheltered compared to the other sampled blocks. Samples LNY2.9 to LNY2.15 were collected from a single south

Figure 6.8. Photographs showing sampling site LNY2. All samples shown with the exception of LNY2.8 which had yet to be drilled at the time the photograph was taken.

facing block, approximately 50cm away from samples LNY2.1 to LNY2.8. Due to being more sheltered, it is not unlikely that the multi direction behaviour seen in samples LNY2.6 to LNY2.8 results from them being affected by lightning strikes to a lesser extent.

The close location of samples LNY2.9 to LNY2.15 might explain the clustering in the directions seen in the East of the equal area projection shown in Figure 6.7. It is possible that the block was struck by a single lightning bolt and given the close proximity of the samples a single overprint direction was imparted.

6.4.1.3 LNY3

A total of nine samples were collected from site LNY3. Of those, 5 core samples, further subdivided into specimens, were subjected to demagnetisation treatment. The measured samples are characterised by multi component Zijderveld Plots. A low temperature overprint is removed below 440°C. A high temperature component is unblocked in the temperature range 3mT/440°C to 70mT/570°C. The overprint and high temperature directions are overall scattered but generally give an easterly to south direction. See Figure 6.9 for the directions plotted on a equal area projection. The measured NRM intensities range 10^{-3} to 10^{-2} A/m.

The demagnetisation behaviour observed in the Zijderveld Plots warrants interpretation of overprint and high temperature components, but, as is seen in the Equal Area Projections, the directions of both the components are strikingly similar. Given that sites LNY1 and LNY2 are largely affected by lightning strikes, this is one obvious interpretation for the observed results. However, the demagnetisation behaviour of the LNY3 samples is not what one might expect of lightning struck samples. Overall, the plots are noisy instead of a single clear convergent component as would be expected for lightning struck samples and seen in sites LNY1 and LNY2 (see Figures 6.6 and 6.8), for example.

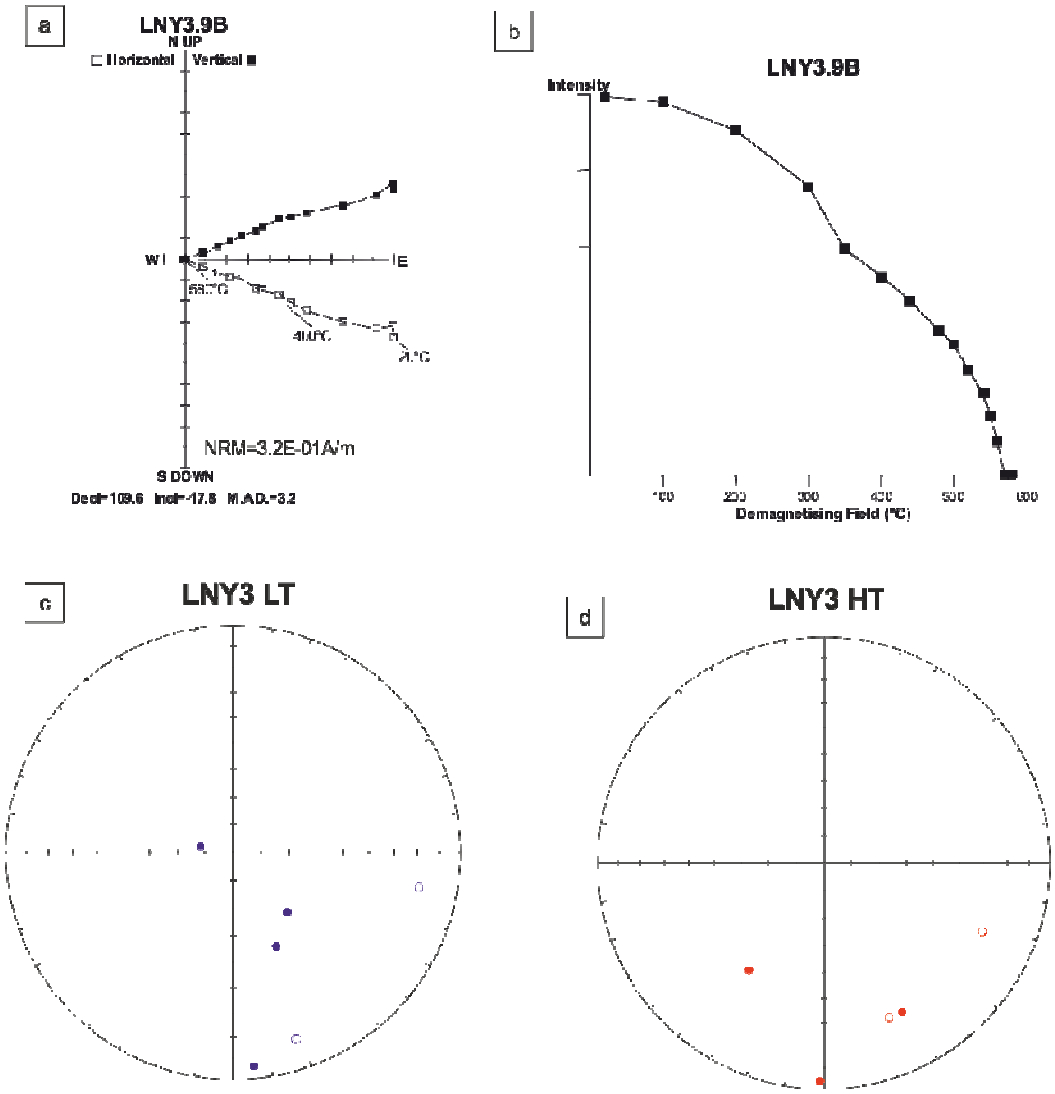

Figure 6.9. Orthogonal vector plots and equal area projections, showing demagnetisation and clustering of directions for LNY3. Data presented in the equal area projections are in-situ. Filled points represent the lower hemisphere, open points represent the upper hemisphere.

6.4.1.4 LNY4

A total of ten samples were collected from site LNY4. Of those, 6 core samples, further subdivided into specimens, were subjected to demagnetisation treatment. The measured samples are characterised by noisy, multi component Zijderveld Plots. A low temperature overprint is removed below 400°C. A high temperature component is unblocked in the temperature range 3mT/400°C to 70mT/580°C. The overprint and high temperature directions are overall scattered but generally give an easterly to south direction (see Fig. 6.10c & d). Samples LNY4.5a and LNY4.9b (shown in Fig 6.10a) are the exception to this, as they are characterised by a single component of magnetisation isolated in temperatures between 100°C and 540°C. The measured NRM intensities range between 10^{-3} to 89 A/m.

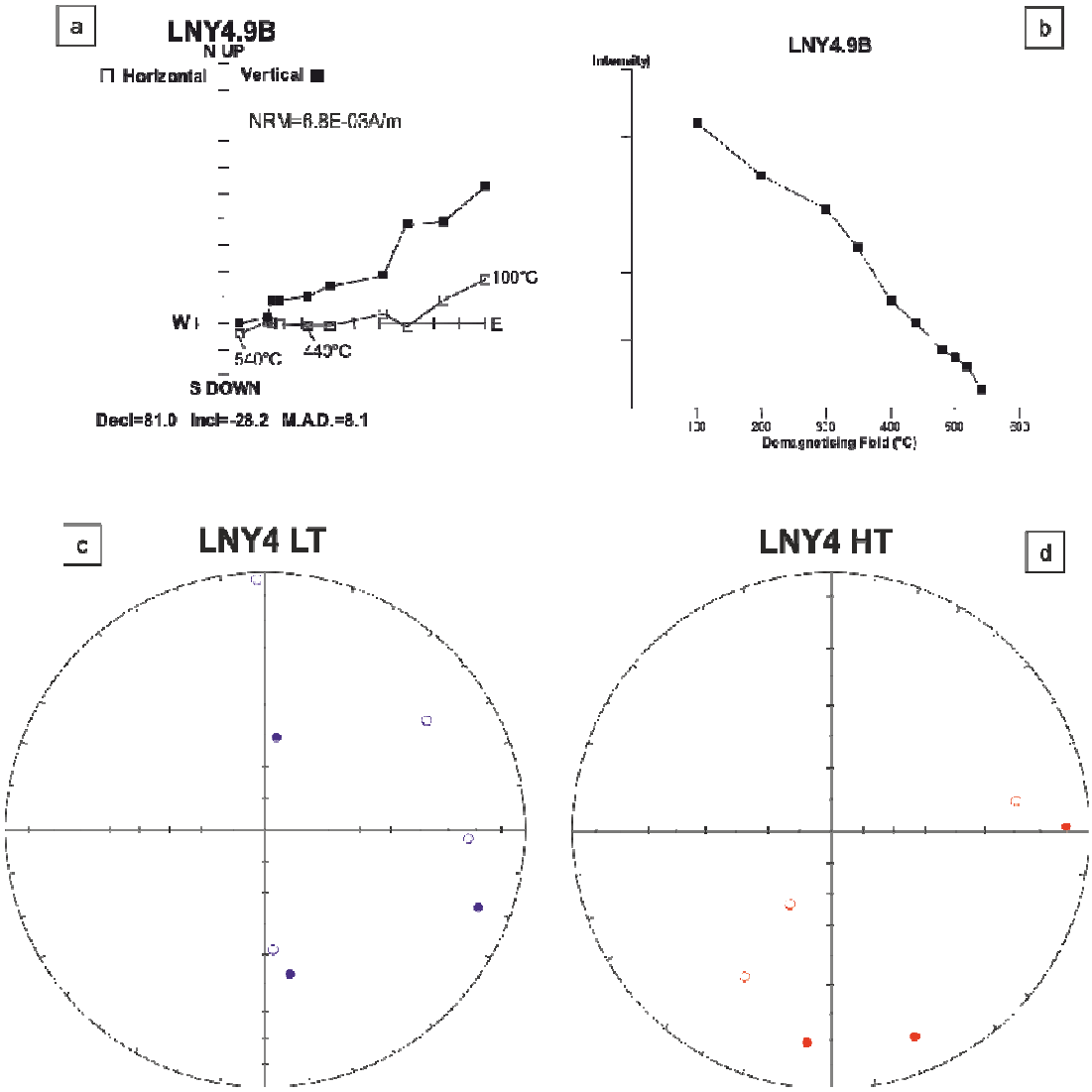

Figure 6.10. Orthogonal vector plots and equal area projections, showing demagnetisation and clustering of directions for LNY4. Data presented in the equal area projections are in-situ. Filled points represent the lower hemisphere, open points represent the upper hemisphere.

6.4.2. Rock Magnetic Characterisation

Site	Lithology	Sample	Ms (Am^2/kg)	Mrs (Am^2/kg)	Hc (mT)	Hcr (mT)	Mrs/Ms	Hcr/Hc	Tc (°C)
LNY1	Dyke/Sill	LNY1.9cc	5.063	0.38	5.5	28.8	0.075054	5.236364	595
LNY2		LNY2.7cc	-	-	-	-	-	-	323/553
LNY3		LNY3.2cc	-	-	-	-	-	-	-
		LNY3.5bb	0.015	0.0014	9	48.8	0.093333	5.422222	609
LNY4		LNY4.5cc	-	-	-	-	-	-	-
		LNY4.10bb	-	-	-	-	-	-	-

Table 6.1. Hysteresis parameters for the Noisy Complex, M_s, saturation magnetisation; M_r, saturation remanence; H_c, coercivity, H_{cr}, coercivity of remanence; T_c, Curie Temperature.

Of the eight samples for which rock magnetic experiments were performed, only samples from site LNY1 show strong ferromagnetic contribution, as is shown in Fig. 6.11a. The fer-

romagnetic signal is completely swamped by the paramagnetic fraction in samples from sites LNY2-4, as is shown in Figure 6.11c &d. As a result, it was not possible to obtain magnetic parameters (Saturation magnetisation: M_s M_r, M_s, Corecivity: H_c; H_{cr}).

Results from site LNY1 indicate that the magnetic carrier in this site is MD magnetite. Thermomagnetic curves measured in the VFTB for samples LNY1.9c (Figure 6.11e) gives a T_c of 599°C. In addition, IRM acquisition curves exhibit saturation below 200mT suggesting the presence of a low coercivity mineral, such as magnetite or maghemite, which is also consistent with the hysteresis curve analysis (Figure 6.11 a and b). Hysteresis parameters are plotted on a Day plot for magnetite showing (M_{rs}/ M_s) vs (H_{cr}/ H_c) and indicate samples from site LNY1 plot in the MD (multi domain) section of the plot (Figure 6.12).

Whilst samples from sites LNY2-4 are predominately paramagnetic, thermomagnetic curve results for sites LNY2 and LNY3 are not classically so. It was possible calculate T_c for sample LNY2.7cc (alteration temperature = 329°C and T_c = 549°C), as shown in Fig 6.11g. Whilst these temperatures may be affected by the paramagnetic contribution, they indicate that a new magnetic phase is being created upon heating of the sample at 329°C, potentially titanomaghaemite unmixing to magnetite. In addition the second T_c could be that of the newly created phase, rather than the original minerals carrying the magnetic signal recorded in the LNY2 samples. Cooling curves, after heating of all measured samples from LNY2 and LNY3 were found to be unreproducible indicating the samples alter upon heating. However, it was not possible to calculate T_c for samples from LNY3 due to the paramagnetic contribution dominating the signal in the heating curve (Fig. 6.11h). Hysteresis parameters from a single sample from site LNY3 are plotted on a Day plot (M_{rs}/ M_s) and (H_{cr}/ H_c) and their position suggests MD (multi domain) grain sizes (see Figure 6.12).Results from the measured samples from site LNY4 were too strongly dominated by the paramagnetic signal for any interpretations to be made (Fig. 6.11f)

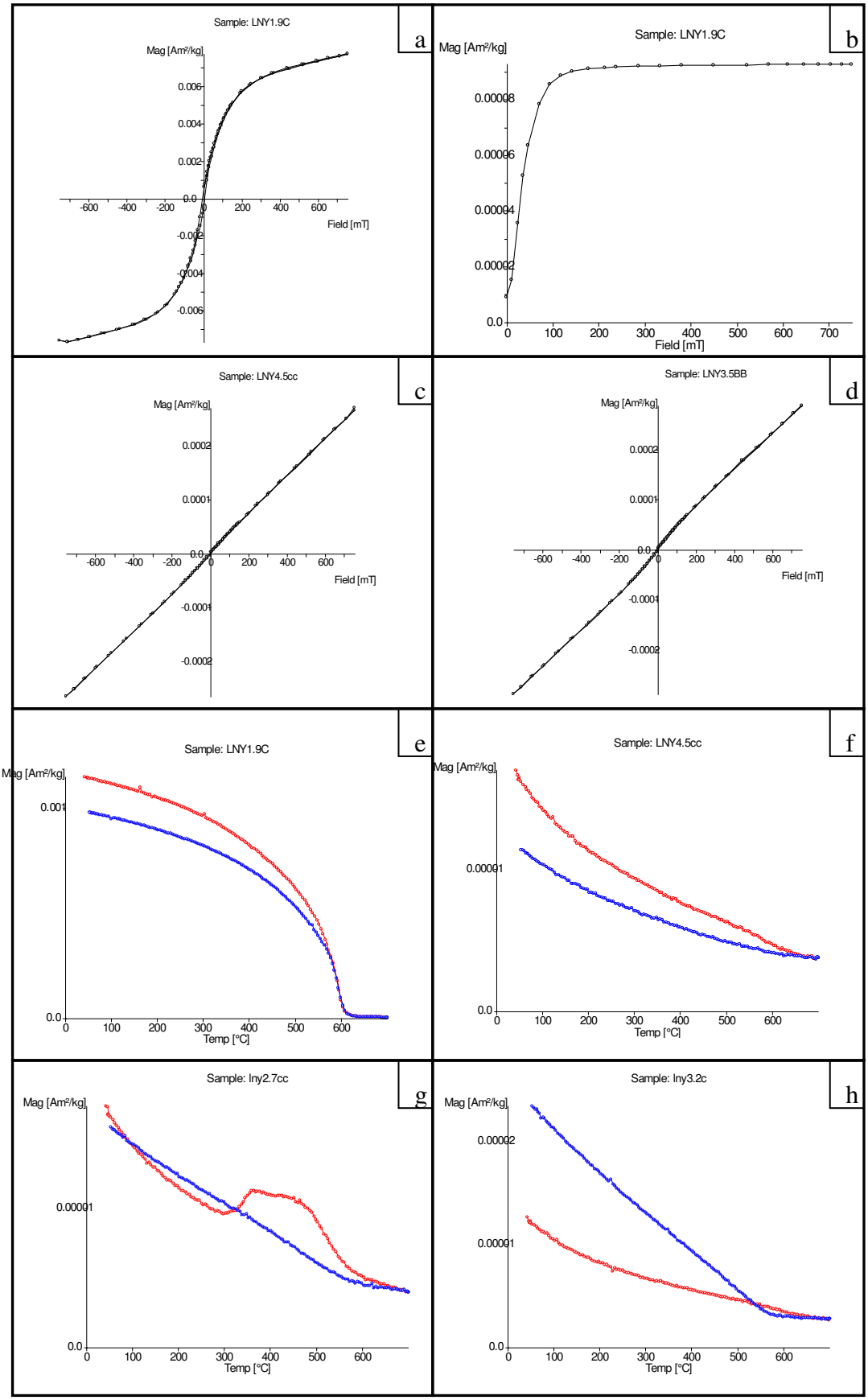
a
Sample: LNY1.9C
Mag [Am²/kg]
0.006
0.004
0.002
0.0
-0.002
-0.004
-0.006
-600 -400 -200 0 200 400 600
Field [mT]
b
Sample: LNY1.9C
Mag [Am²/kg]
0.00008
0.00006
0.00004
0.00002
0.0
0 100 200 300 400 500 600 700
Field [mT]
c
Sample: LNY4.5cc
Mag [Am²/kg]
0.0002
0.0001
0.0
-0.0001
-0.0002
-600 -400 -200 0 200 400 600
Field [mT]
d
Sample: LNY3.5BB
Mag [Am²/kg]
0.0002
0.0001
0.0
-0.0001
-0.0002
-600 -400 -200 0 200 400 600
Field [mT]
e
Sample: LNY1.9C
Mag [Am²/kg]
0.001
0.0
0 100 200 300 400 500 600
Temp [°C]
f
Sample: LNY4.5cc
Mag [Am²/kg]
0.00001
0.0
0 100 200 300 400 500 600
Temp [°C]
g
Sample: Iny2.7cc
Mag [Am²/kg]
0.00001
0.0
0 100 200 300 400 500 600
Temp [°C]
h
Sample: Iny3.2c
Mag [Am²/kg]
0.00002
0.00001
0.0
0 100 200 300 400 500 600
Temp [°C]

Figure 6.11. Representative hysteresis loops and thermomagnetic curves for the Noisy Complex. (a, b & e) Hysteresis loop, IRM acquisition curve and thermomagnetic curve (heating step in red, cooling in blue) indicating the magnetic carrier in site LNY1 is multidomain magnetite. (c & f) Hysteresis loop and thermomagnetic curve showing the paramagnetic fraction that dominates the signal in the samples of sites LNY2-4. (d) Hysteresis loop for sample LNY3.5bb shows some ferromagnetic contribution to the overall signal. (g & h) Thermomagnetic curves for samples LNY2.7cc and LNY 3.2c showing significant alteration on heating of the samples. Hysteresis loops for both samples are dominated by the paramagnetic fraction.

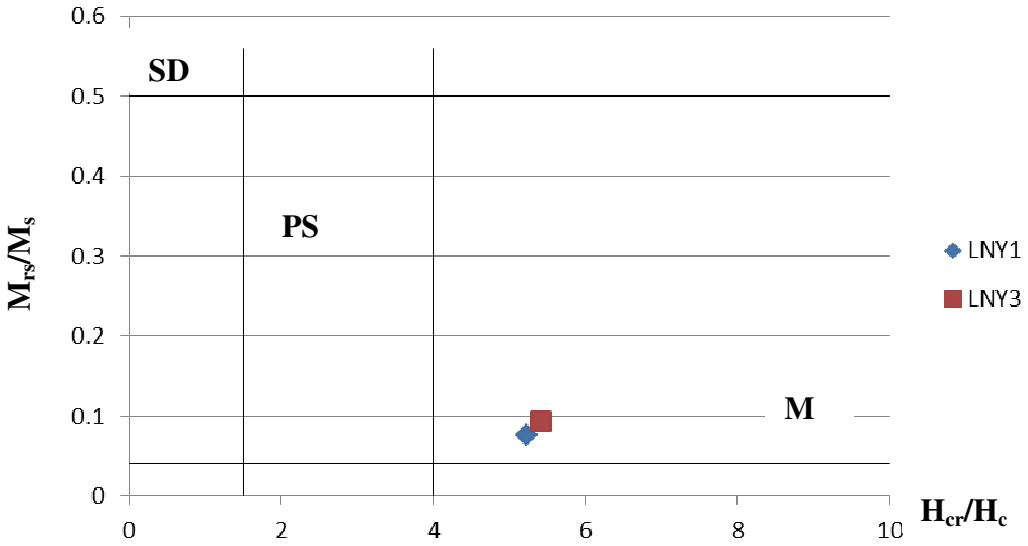

Figure 6.12. Day Plot, (Day et al., 1977) for samples of this study and also samples of the Komati Formation from Yoshihara & Hamano, 2004 (referredto as Y&H04, in plot). SD: Single Domain; PSD: Pseudosingle domain; MD: Multidomain.

6.4.3. Microscopy Observations

The rocks of the Noisy Complex were examined using an optical microscope and Philips XL30 tungsten filament SEM to better understand the mineralogy and thermal history of the unit, whilst the scanning electron microscope (SEM) was also used to analyse the composition of the minerals.

Only one sample from the Noisy Complex sites was available for thin section study: LNY2.10a. The sample is representative of the sites studied as part of the work presented in this chapter.

Previous microscopy work of the Noisy Complex has been focused on understanding Archean hydrothermal fluids or identifying single magnetite grains within single crystals (Tarduno et al., 2007) to measure past geomagnetic field intensity. There is little in the way of detailed microscopy studies of the complex as a whole in the published literature.

Biggin et al., (2011) studied three samples from the Etimambeni section using optical microscopy: a dacitic conglomerate clast, a sample from the conglomerate matrix and a tuff sample. The conglomerate samples were characterised by extensive sericitation (the process by which plagioclase alters to fine grained micas in the presence of hydrothermal fluids). Carbonate minerals and veinlets were also common in the samples and also thought to have been deposited as a result of hydrothermal alteration. Biggin et al., (2011) identified opaque minerals (submicron to tens of microns) were often associated with the feldspar dominated groundmass. In the tuff sample, which was also found to be extensively altered by hydrothermal fluids, opaque minerals were distributed along the carbonitised grain rims and micro-fractures. The authors argue the magnetisation in the sample was reset during the hydrothermal alteration. Usui et al., (2009), used electron microscopy to study dacite clasts and found the sample was dominated by a microcrystalline texture of plagioclase and quartz with some phenocrysts which had been hydrothermally altered to clay minerals (micas). Accessory minerals in the sample included magnetite and apatite.

Sample LNY2.10a is characterised by a fine grained, equigranual matrix of plagioclase and quartz. Large, euhedral opaques were also identified within the thin section. When studied in reflected light these were found not to be 'bright and shinny', as one might expect from iron oxides. The plagioclase phenocrysts were largely sericitised implying significant hydrothermal alteration.

6.5. Discussion and Conclusions

Despite the success and promising palaeomagnetic results obtained in the studies of Usui et al., (2009), Tarduno et al., (2010) and Biggin et al., (2011), it was not possible to obtain meaningful results from the Noisy Complex sampled as part of this study.

Samples from site LNY1 are dominated by a single direction of magnetisation with elevated NRM intensities, consistent with lightning strikes being the source of the magnetisation recorded in the site. The site was mistaken for the felsic volcanics, but on closer inspection of hand specimens it was identified as mafic in composition and likely one the ultramafic dyke or sills that occur in the western part of the OF limb, see Figure 6.2 for details.

Sites LNY2 to LNY4 sample the felsic volcanics that outcrop in the uppermost part of the northern limb of the OF fold. The directions from the sites are overall scattered and no

meaningful overprint or high temperature site mean directions were obtained from the samples. However there is a tendency for directions to cluster towards the east and south shallow, possibly suggesting a contaminated high stability component. A number of samples from each site are affected by lightning strikes, resulting in a single convergent component observed in the Zijderveld Plots. However, the directions do have a tendency to cluster towards the east and relatively south shallow potentially suggesting a contaminated high stability component.

Rock magnetic characterisation of the samples shows that samples from LNY1 are dominated by the ferromagnetic fraction and hysteresis parameters indicate the magnetisation in the LNY1 samples is carried by multidomain grains. The magnetisation in sites LNY2 to LNY4 is dominated by the paramagnetic contribution. Curie temperatures for samples of LNY1 are indicative of maghemite. Curie temperatures from site LNY2 indicate that the samples from this site alter readily upon heating. It was not possible to calculate a Curie temperature for sites LNY3 and LNY4 due to paramagnetism dominating the signal observed in the thermomagnetic curve.

The sampling rationale was driven by the need to increase the available data set and more importantly, in the hope of performing field stability tests that would build upon the findings of previous studies and more robustly determine the time of acquisition of the magnetisation recorded in the rocks of the Noisy Complex. In order to achieve this, it was important to sample localities not previously studied, to ascertain results were robust over a wide geographical area. In addition, the type locality in the southern OF has limited exposure and has been heavily sampled. In order to preserve the geological textures and field relationships for further study of the geology of the BGB, it was not advisable to sample this locality further. For these reasons the outcrops of the Noisy Complex in the northern limb of the OF were chosen for sampling as part of this study.

The locality is relatively inaccessible and there is no water supply readily available, meaning it is not the ideal candidate for palaeomagnetic study but precisely for these reasons offered an attractive alternative to localities of previous studies. However, the elevated position of the sampling sites on the uppermost section of a ridge meant that lightning strikes were likely (see Figure 6.13). In order to minimise the likelihood of sampling sites which had been lightning struck, we were careful not to sample outcrop tops and focused on the bases of outcrops which were less exposed. An alternative area for sampling was a

nearby valley, which would mean outcrops were more sheltered. However, outcrop of the Noisy Complex in the valley was very poor and further obscured by dense vegetation meaning sampling would have been extremely hard.

Figure 6.13. Panoramic picture showing the Noisy Complex Outcrop on the northern limb of the Onverwacht Fold. The image is taken facing South towards the Komati River and Tjakstad can be seen in the distance. The boxed area marks the area in which the LNY sites were sampled. The lowermost photograph shows Andy Biggin using a sun compass to orient the samples of LNY2. Note the blocky nature of the outcrop and how samples are taken of the least exposed lower sections of the outcrops.

Despite the effort to minimise the likelihood of sites being affected by lightning strikes, the results show that the magnetic signal recorded by the rocks in this locality is significantly affected by lightning strikes. The relatively scarce number of samples collected in the Noisy Complex mean that the effects of lightning strikes on the quality of the data is significant and obscures any primary signal that the rocks might have otherwise recorded. Wider spacing of sampling sites, as well as increasing the number of sites sampled might have gone some way to minimise the effects of potential lightning strikes. In addition, attempts to sample even more remote localities in the steep valleys (seen in Figure 6.9) might further reduce the risk of primary signals being overprinted by lightning strikes.

Given the poor quality of the data obtained from the sites LNY2 to LNY4 it is not possible to put our results in the wider context of the already published work for the paleomagnetism of the Noisy Complex. Site LNY1 is the most dominated by the effects of lightning

overprints, however, the data would not be comparable to previous studies of the Noisy Complex, due to its origin, composition and exact age being unclear.

Given the success and promising results of the work of Usui et al., (2009), Tarduno et al., (2010) and Biggin et al., (2011), further study of the rocks of the Noisy complex is advocated. Despite the results presented in this chapter not being hugely encouraging the primary reasons (outlined in the introduction to this chapter) for studying the paleomagnetism of the rocks of the Noisy Complex remain valid and true.

Further sampling of the northern limb of the OF would allow for a fold test when combined with the results from the southern limb by Usui et al., (2009) and Biggin et al., (2011). Tarduno et al., (2010) sampled the felsic intrusives in the northern OF. Sampling the intrusives further to the west or east would increase the geographical extent of the present data set, whilst still being relatively accessible via the valleys off the Komati River. The outcrop of the felsic volcanics is fairly blocky in the western OF northern limb where we attempted our sampling due to the normal listric faults offsetting the unit (see Figure 6.2). Sampling further localities in this area would still be of benefit; however, to avoid sites which have a high likelihood of being lightning struck it would be advisable to invest time in identifying outcrops in the valleys away from the ridge. The eastern section of the northern limb of the OF fold offers thick packages of felsic volcanics and would be viable for sampling. Outcrop exposure in this area is also good. However, the area is remote and accessibility might be an issue.

7 Paleomagnetism of the Nelshoogte Pluton

7.1. Introduction

The Nelshoogte Pluton (NSP) is one of a number of tonalitic-trondjhemitic-granodioritc bodies (collectively known as the TTG Series) which surround the Barberton Greenstone Belt (BGB). It is the youngest unit studied in this thesis; dated at 3236 ± 1Ma (De Ronde and Kamo, 2000a) and significantly different to the rocks of the Onverwacht Group in terms of its composition and emplacement history.

TTG Series are associated with all Archaean cratons but are absent from the post-Archaean rock record. As is true of the rocks of the Onverwacht Group also studied in this thesis, better understanding of the TTG genesis can shed light on how the early Earth continental crust developed and feed into larger scale geodynamic models of the Archaean.

Given that the TTGs have (mostly) experienced limited post-emplacement metamorphism and their tectonic history is relatively simple when compared to the BGB, requiring straightforward tilt corrections (if any at all); palaeomagnetically, they have long been of interest to researchers. One of the earliest and most influential Precambrian palaeomagnetic studies was that of the Modipe Gabbro (2784 ± 1Ma, Denyszyn, et. al., 2013) carried out by Evans and McElhinny in 1966. Further studies of the TTGs followed that of Evans & McElhinny (Denyszyn et al., 2013; Feinberg et al., 2010; Layer et al., 1996; Layer et al., 1989; Layer et al., 1998; Muxworthy and Evans, 2013; Muxworthy et al., 2013; Tarduno et al., 2007) with the aim of shedding light on the tectonic growth and setting of the Kaapval Craton. The key questions being addressed, given that some of the TTG genesis represent the last major intrusive event in the BGB's Archaean history, concerned the formation of the Kaapvaal Craton and the possibility that it may have behaved as a single cratonised block (Layer et al., 1989) : when was cratonisation complete and how long did the Kaapvaal Craton behave as a single block? In addition, VGPs calculated from directional results from the TTG genesis have been used to discuss the tectonic setting of the Kaapvaal Craton (Denyszyn et al., 2013), including its palaeolatitude during the Archean, which has implications for the existence of the Vaalbara Supercontinent as suggested by Cheney, (1996) and Zegers et al., (1998) and discussed further in chapters 2 and 8 of this thesis.

As the previous studies of the TTGs genesis have identified that they are able to hold stable, Archaean aged remanences, more recently research has focused on their ability to yield information regarding the planetary magnetic dipole moment at this early stage

in the Earth's history (Muxworthy et al., 2013; Tarduno et al., 2007; Tarduno et al., 2010). The research of Tarduno et al., (2007 & 2010) focused on the tonalitic Kaap Valley Pluton (3227±1Ma, Kamo and Davies, 1994), which neighbours on the NSP to the North) and the granodioritic 3216 ±2 Ma (Kamo and Davies, 1994) Dalmein Pluton, located along the southern margin of the BGB. Using the single crystal method, where the palaeointensity of single domain (SD) or pseudosingle domain (PSD) magnetic inclusions within a silica host, (typically feldspar, quartz or hornblend) is determined (Cottrell and Tarduno, 2000; Tarduno et al., 2006), Tarduno et al., (2007) were able to determine that field strength at ca.3.2Ga was 50% of the present day values, indicating a viable magnetosphere in the Archaean that was able to protect the atmosphere from solar wind erosion, which has implications for the early origins of life on Earth (Tarduno et al., 2007; Tarduno et al., 2010). Muxworthy et al., (2013) revisited the palaeomagnetism of the Modipe Gabbro and produced palaeointensity data using the Thellier-Thellier-Coe method (Coe, 1967). The results showed a Magnetic Dipole moment of 6 x 10^{22} Am^2 indicating a geomagnetic field strength in the late Archaean of 80% of the modern day values. When compared to the results of Tarduno et al., (2007), the results of Muxworthy et al., (2013), imply a 30% increase in field strength from ca. 3.22 Ga to ca. 2.78 Ga. The mechanism by which this increase in field strength, over a period of 440Ma, might have occurred has implications for inner core growth and convection of the inner core. Large differences in the average dipole moment over short-time scales (a few decades-100Ma) have been observed in other data sets (Prévot and Perrin, 1992; Shaar et al., 2011) and are suggestive of possible changes in the flow of heat between the core-mantle boundary, which in turn could be related to crustal or mantle driven changes such as crustal accretion (Prévot and Perrin, 1992).

The work of Layer et al., (1998) on the palaeomagnetism of the NSP is of direct relevance to the results presented in this chapter. Whilst verifying the reliability of the age of the magnetisation recorded in the rocks of this formation is still of key importance, but the well constrained ages published by Layer et al, (1998) mean this is not the primary focus of the work carried out in this study on the NSP. Crucially, Layer et al., (1998) argue that antipodal directions, (A+ and A-), isolated from the NSP represent a primary magnetisation and indicate a reversing magnetic field in the Archaean. The A- direction in particular is scattered, with elevated α95, despite which, Layer et al. (1998) argue for the A- and A+ directions being antipodal and combined to produce a single pole. A further direction with steep antipodal positive and negative inclinations was isolated by Layer et al. (1998), B+

and B-. However, this time the VGPs were not to be fully antipodal and therefore the directions were not combined to produce a single pole.

The results of Layer et al., (1998) are extremely encouraging. They have implications for our understanding of the core structure and are suggestive of a dipolar field, similar, to the present day field, being present in the Archaean. However, the scatter in both the B and A directions needs to be addressed in order to further constrain the reliability of the results presented by Layer et al., (1998). Collection of new samples will further add to the dataset available for the NSP, allowing for more robust interpretation of new results, particularly in light of the findings of Layer et al., (1998). Surface samples were collected from nine sites across the NSP. Sites not previously by Layer et al., (1998) were targeted to increase the geographical distribution of the dataset. Localities close to sites which yielded good directional data in the work of Layer et al., (1998) were also sought in order to validate previously published finding.

This chapter outlines the geological context of the samples collected for this study, as well as including a short summary of previous palaeomagnetic studies of the rocks of the NSP. The chapter focuses on the directional results obtained from the samples collected as part of this study, in addition to establishing the carriers of the magnetisation via rock magnetic characterisation and optical and scanning electron microscopy. The new results are put into the context of the already published work. The chapter concludes with some final observations.

7.1.1. Geological Background

The BGB is surrounded on all sides by plutons and gneisses of tonalitic to trondhjemitic composition, which were emplaced over a period of ca. 500Ma, from 3662 to 3105Ma (Kamo and Davis, 1994; Schoene et al., 2008). Collectively, the plutons and gneisses are known as the tonalite-trondhjemite-granodiorite series (TTG). The plutonic rocks surrounding the BGB are arranged in a series of groups depending on their age and relationship with the BGB; with the Kaap Valley Pluton and the Nelshoogte Pluton (NSP) comprising the Kaap Valley Domain (Kisters et al., 2010). The NSP is a coarse grained trondhjemite pluton dated at 3236 ± 1Ma (De Ronde and Kamo, 2000) which crops out over an area of approximately 450Km^2 ,as shown in Figure 7.1. The size of the NSP is not well constrained as its westernmost exposure is covered by the younger Traansval Supergroup (2670 – 2050 Ma). The contact of the NSP with the BGB to the east is along a sheared margin

(Layer et al., 1988). To the south the NSP is intruded into by the rocks of the Badplaas Trondhjemite Cell (Kisters et al., 2010). The contact is characterised by a 1000m wide intrusive breccia and fragments of the NSP are also found within the Badplaas pluton (Matsumura, 2014). To the north, the exposure is poor and the exact nature of the contact with the Kaap Valley Pluton is unclear; however, regional geological models and isotopic evidence presented by Robb et al., (1986), suggests that the NSP intrudes the Kaap Valley Pluton (Layer et al., 1988). The NSP is characterised by northwest- southeast trending joints (Layer et al., 1998 and this study, see section 7.2.1 of this chapter) of potassic composition. A series of dolerite dykes (DD, after Layer et al., 1998), thought to be of Proterozoic age (Robb et al., 1986) intrude the NSP along the joint pattern. In addition, Layer et al., (1998) identified a second set of coarser grained dykes: microgabbro dykes, (MGD)

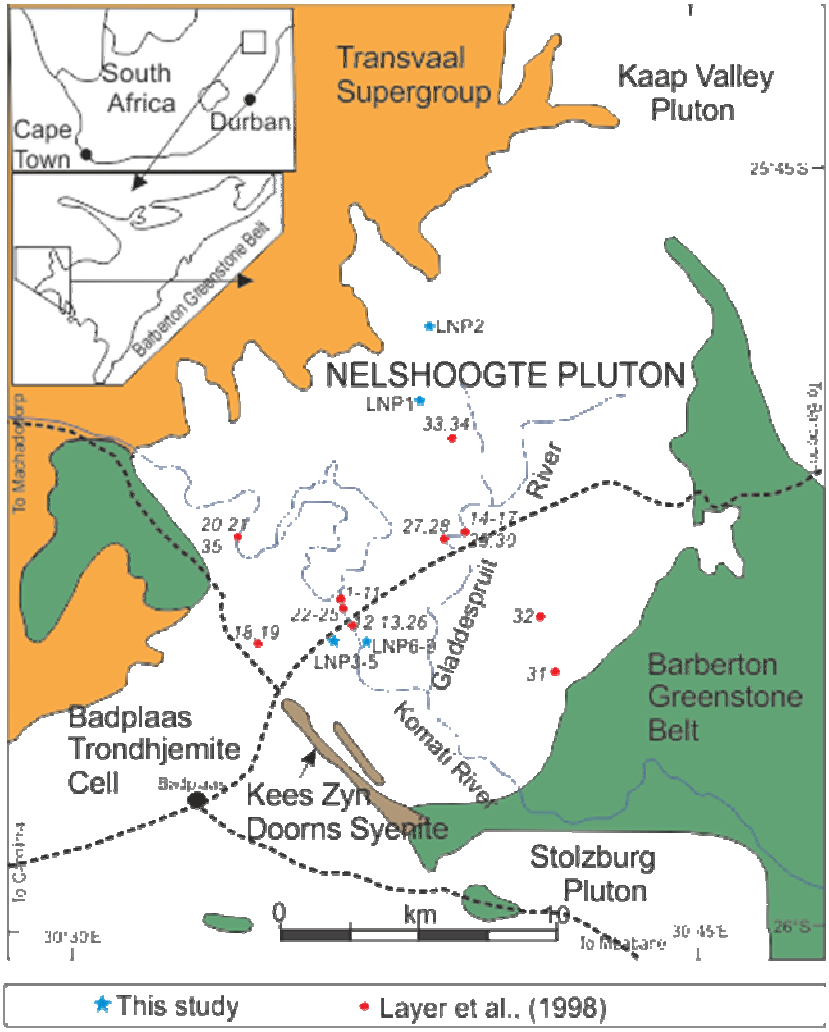

Figure 7.1 Geological map of the Nelshoogte Pluton. Sampling sites for this study are shown with blue stars, whilst the sampling sites of Layer et al., (1998) are reperesented by a red circle. The dotted line shows the main roads in the area.

with a similar trend to the DD dykes. The coarser grain size is indicative of a slower cooling time. The intrusives appear in greater abundances closer to the eastern margin of the NSP, in the vicinity of the contact with the BGB (Matsumura, 2014).

The BGB formed through two terrain accretionary events: D1 and D2 at ca. 3445 and 3225 Ma respectively (Armstrong et al., 1990; de Ronde and de Wit, 1994; de Wit et al., 1992; Kisters et al., 2003); see also Introductory chapter of this thesis for further details of tectonic history of the BGB. It is thought the plutons surrounding the BGB were emplaced simultaneously with the D1 and D2 events (de Ronde and de Wit, 1994; De Ronde and Kamo, 2000a; de Wit, 1987; Kamo and Davis, 1994; Kisters et al., 2003; Lowe and Byerly, 1999a). The TTG series is considered to have been emplaced during the D2 event, at a subducting plate margin, in an arc-arc style setting characterised by continuous magmatism and a prolonged period of convergence (Matsumura, 2014). This tectonic setting is supported by metamorphic evidence from garnet-albite mineral assemblages studied by Moyen et al., (2006) from the Inyoni shear zone (ISZ), exhumed simultaneously to the emplacement of the Kaap Valley Domain at ca. 3.2Ma (Nédélec et al., 2012) . These indicate that rocks of the ISZ record a geothermal gradient of 12-15°C/Km, which is similar to the conditions observed in present day subduction zones. Moyen et al., (2006) suggest that the ~3200 Ma plutons represent a mixture of low and high pressure styles of melting (therefore, shallow and deep magma sources); a consequence of slab break-off and asthenospheric upwelling, whereas the older trondhjemites (3500-3450Ma) represent slab melts within a steep subduction zone, of shallow and deep sources (Matsumura, 2014).

The source of the rocks for the NSP has been highly debated; it has been suggested the source rocks could be derived from the Ancient Gneiss Complex (AGC, Kroner and Tegtmeyer, 1994), the rocks of the Onverwacht Group (Kröner et al., 1996) or the rocks of the Fig Tree Group (Sanchez-Garrido et al., 2011). However, based on geochemical and experimental evidence, there is now a broad consensus that the TTGs resulted from partial melting of hydrous metabasalts, possibly amphibolites or eclogites (Moyen et al., 2006; Nédélec et al., 2012).

Layer et al., (1998) argue that the NSP has experienced very limited tilting since ca. 2500Ma as the sediments of the Traansval Supergroup (2670 – 2050 Ma) have a gentle dip of <5° (Layer et al., 1998). In addition, the lack of internal deformation and tilting

(Anhaeusser and Robb, 1983; Robb and Anhaeusser, 1983; Westraat et al., 2005) in the Mpuluzi Batholith (ca. 3.1Ma) to the south of the BGB, which intrudes the ca.3.2Ga Plutons, provides further evidence that the NSP was not tilted prior to this time, (Layer et al., 1998). However, Matsumura (2014), argues that the domal structure observed from geological mapping of the NSP reflects later stage folding and steepening of the initially flat fabrics, meaning structural deformation of the NSP cannot be ruled out.

The NSP is predominantly of trondhjemitic composition with well-developed gneissosity. The style of gneissosity is varied throughout the pluton (towards the north, the Pluton is not strongly foliated) and indicative of a protracted emplacement history (Matsumura, 2014). The ages obtained for the Pluton support this theory: De Ronde and Kamo (2000) published a 3236 ± 1 Ma age from the main trondhjemitic phase within the Pluton, whilst Bletcher et al., (2005), present an age of 3225 ± 2 Ma for the late tonalitic phase seen in the Pluton. These ages indicate that the NSP was emplaced over a period of ca. 10Myr (Matsumura, 2014).

7.1.2. Palaeomagnetic Background

An extensive and detailed study of the palaeomagnetism of the NSP was carried out by Layer et al., (1998). The work followed on from a number of studies published during the 1960s and 1980s that aimed to address whether apparent polar wander was active in South Africa in Archaean times (Evans and McElhinny, 1966; McElhinny and Gough, 1963).

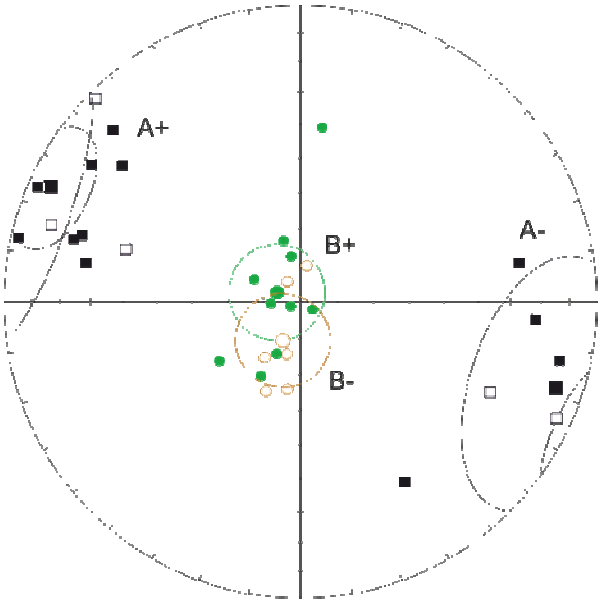

Figure 7.2. Equal Area projections showing the directions isolated by Layer et al., (1998). Modified from Layer et al., (1998).

Evans, (1967)was the first to suggest that there was evidence for significant polar wander based on his work on Proterozoic rocks, such as the Modipe Gabbro. However, Hale

	Poles	N	Dec (° C)	Inc (° C)	k	α95 (°)	λ (°C)	ϕ (°C)	K	A95
Layer et al., (1998)	A+	11	293.1	7.0	13	13	19	314.3	28	9
	A-	6	104	11.8	7	28	14.7	121.3	9	24
	A	17	285.1	0.6	9	13	17.6	309.8	16	9
	B+	6	224.7	80.0	28	13	37.6	15.0	9	23
	B-	5	212.9	-80.6	27	15	11.9	220.3	9	28

Table 7.1. Mean components identified by Layer et al., (1998) from the Nelshoogte Pluton. Where N represents the number of sites used in the calculation of the pole. The Fisherian precision parameter is represented by k and α95 is the radius of the circle of 95% confidence about the direction mean. K and A95 are the Fisherian precision parameter and the radius of the circle of 95% confidence about the mean pole.

(1987b), based on the findings from the Komati Formation pole (Hale and Dunlop, 1984), argued against apparent polar wander in the Archean. The aim of the work of Layer et al., (1998) was to clarify the debate.

Layer et al., (1998) sampled a total of 31 sites in the body of the NSP, (see Figure 7.1), and a further 5 sites were sampled in the cross cutting dykes: microgabbro dykes (MGD) and dolerite dykes (DD, 1902 ±6 Ma, Layer et al., (1998)). The majority of the NSP sites were located in the south and central areas of the pluton as access to the northern area, as well as exposure, was limited. The majority of samples were obtained from river-cut outcrops where exposure was freshest, although some rounded dome outcrops away from rivers were also sampled. Samples were Alternating Field (AF) demagnetised to 80mT and selected samples were also thermally demagnetised (TH) to 700°C. Layer et al., (1998) found samples were characterised by stable univectorial behaviour. Two dominant directions were obtained from the NSP samples, see Table 7.1. A direction with steep antipodal positive and negative inclinations was isolated from the NSP and DD samples, B+ and B -. The equal area projection in Figure 7.2 shows the directions isolated by Layer et al., (1998). The VGPs of the B+ and B– directions were found not to be fully antipodal and therefore the directions were not combined to produce a single pole. The B+ and B– directions are not distributed with a Fisher distribution, but rather appear smeared along a south-west to north-east path; the implication thus being that the directions could have been acquired at different times and reflect a polar wander path. Antipodal north-

westerly (A+) and scattered south-easterly (A-) directions were also isolated in the NSP samples. The components have a distributed unblocking temperature spectrum but are resolved by 560°-580° C and are always the highest coercivity or unblocking temperature component. The scatter in the A- direction gives rise to a large α95; consequently, despite the VGPs for both directions being 167° apart, Layer et al., (1998) argue the directions are antipodal and warrant being combined into a mean pole. Albeit rarely, the B- appears to overprint the A- component, suggesting the B direction is younger than the A direction. In addition, the B+ and B- directions are comparable to other early Proterozoic directions, e.g. Witwatersrand Supergroup overprint (Layer et al., 1988). Furthermore, the B+ and B- directions are isolated in the Proterozoic aged DD dykes. The age of the A direction is interpreted by the authors to be best represented by an age obtained from a single Hornblende grain from a MGD dyke at 3179 ±18 Ma (Layer et al., 1998). The direction is similar to the C1 direction seen in the neighbouring Kaap Valley Pluton (Layer et al., 1996).

Layer et al., (1998) argue that given that the B+ and B- directions are widespread across the Kaapval Craton, the NSP was not rotated relative to the craton after ca. 2000 Ma. In addition the similarity between components observed in the NSP and Kaap Valley Pluton is thought to indicate the plutons behaved as a single structural block since ca. 3180 Ma. The findings presented by Layer et al., (1998) contradict those of Hale, (1987) suggesting limited polar wander in the Archaean. Crucially, the antipodal directions, A+ and A-, indicate a reversing magnetic field in the Archaean.

7.2. Methodology

7.2.1. Sampling

In May 2011, 78 core samples were sampled at nine sites (LNP1-9) of the Nelshoogte Pluton, collected as part of a large sampling trip of the Onverwacht Group; see Figure 7.1 for sample locations. The Nelshoogte Pluton covers an area of 450km^2, much of which is now privately owned and used for agricultural, forestry and mining purposes, meaning access to outcrops can be restricted and difficult. Outcrop of the trondhjemitic/tonalitic rocks is predominantly along river beds and scarce in other areas.

Site LNP1 is located in the central part of the Pluton. It is an isolated dome-like outcrop surrounded by an area of grass land and chosen due to it being an area not sampled previously by palaeomagnetic studies, see Figure 7.3 a & b. The same is true for LNP2 sampled

in a river within forestry commission land. Sites LNP3-5 were sampled along a tributary of the Komati River. Access to the sites was via a bridge off the R38 road. Sites LNP3-5 are located 1Km away from sites 22-25 of Layer et al., (1998). Originally, the aim was to obtain samples in close proximity to the sites of Layer at al., (1998); however, it was not possible to access the outcrop due to it now being on private land. Sites LNP6-9 are located along the Komati River bed (Fig 7.3 c & d), in an area not previously sampled by palaeomagnetic studies, 0.5 km away from sites 22-25 of Layer et al., (1998). Access to the sites was granted by the land owner.

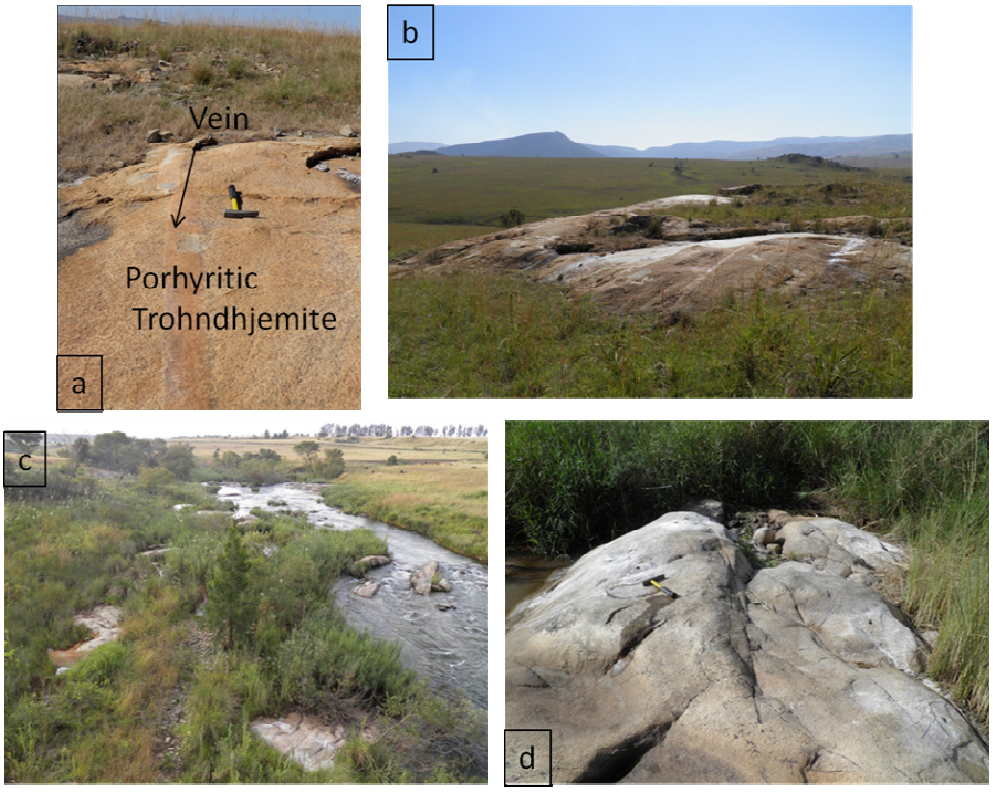

Figure 7.3 (a) Sampling site LNP1, showing a potassic vein. (b) Sampling site LNP1. Note the domal nature of the outcrop. (c) Komati River bed where sites LNP6-9 where drilled. (d) Close up of site LNP8.

Overall, the samples taken from the Nelshoogte Pluton are heterogeneous. In outcrop the rocks of the Pluton tend to weather a light brown/orange colour. The weathering effects do not seem to penetrate deep into the rock; fresh exposure can be obtained once the uppermost layer of rock is chipped away. In hand specimen the rock is coarse grained (phaneritic texture) and dominated by quartz and plagioclase. Dark accessory minerals, interpreted to be pyroxenes are also present. The mineralogy is consistent with what is expected of a rock of trondhjemitic/tonalitic composition. The outcrops at sites LNP1-5 are characterised by numerous quartz veins which can be up to 20cm wide. The veins are less profuse in sites LNP6-9 and typically only a few cm wide.

7.2.2. Experimental Methodology

A total of 73 discrete core samples from nine sites were subjected to demagnetisation treatment. The discrete core samples were further subdivided to create specimens, of which a total of 25 samples were demagnetised using the combined thermal and AF treatment, whilst 61 were treated using thermal techniques alone. Details of the demagnetisation techniques are given in Chapter 3, Section 3.3.1.

Temperature dependent susceptibility measurements on nine core samples from sites LNP1 to LNP9 have been carried out. A total of 59 measurements (which include measurement of sister samples) were made of bulk susceptibility from samples across LNP1 to LNP9.

In chapter four of the thesis, thermomagnetic curve results obtained from the VFTB were noted to overestimate Curie Temperatures when compared to results obtained from the Kappa Bridge. On further investigation it was established that the position of the thermocouple in the furnace of the VFTB was misaligned (see chapter four for further details). However, it is not know when the original misalignment occurred. The Nelshoogte Pluton samples were measured prior to this problem being identified and therefore thermomagnetic curves are unreliable and can only provide maximum estimates of Curie Temperature and be used to identify alteration.

7.3. Results

7.3.1. Directional Results

The analysis of the palaeomagnetic data was conducted using principal component analysis and standard statistical analysis (Fisher, 1953: Kirschvink, 1980). On the whole samples were characterised by a single component of magnetisation. Samples from sites LNP3 to LNP8 did produce some multi-component Zijderveld Plots with one stable overprint removed during step-wise demagnetisation prior to a characteristic remanent magnetisation (ChRM) component being isolated. In most cases, (discussed in more detail below), the isolated directions were too scattered to produce a reliable site mean. In some cases it was not possible to isolate a stable overprint and/or ChRM components. Recorded overprint and ChRM components generally had a maximum angular deviation (MAD) of less

than 15°. Low NRM intensities (up to 10^{-3} A/m) in many samples resulted in very scattered directions that did not produce a reliable site mean direction.

The samples of LNP1-2 and LNP9 are dominated by a single component of magnetisation. The samples from the LNP3-8 sites are often characterised by two components, i.e. a low temperature overprint component and a high temperature component. However, in all the sites, some samples with single components of magnetisation are observed. Data collected from sites LNP1-2 and LNP6-9, were scattered and it was not possible to isolate site means from the results. NRM intensities for the LNP sites ranged from 0.01 to 34 A/m. See Table 7.2 for details of sampling sites and directions. Zijderveld plots and equal area projections of isolated directions can be found in Figures 7.4 and 7.5, respectively

In some cases the samples are weakly magnetised which adds significant noise to the data. In addition, in hand specimen the samples were noted to be considerably altered due to weathering and the presence of veins..

7.3.1.1 LNP1

A total of seven samples were collected from site LNP1. Of those, seven core samples, further subdivided into specimens, were subjected to demagnetisation treatment. All the measured samples are characterised by a single component of magnetisation (an example is shown in Figure 7.4a&b) which is isolated in the temperature range 20-580°C/90mT. The directions obtained from the LNP1 samples are scattered and, therefore, it was not possible to calculate a meaningful site mean direction, as is shown clearly in Figure 7.5.

The measured intensities from the samples of the LNP1 site are in the range 7-40 A/m. The elevated intensities recorded by the samples, when compared to intensities of other TTG gneiss rocks [0.5-1.0A/m for the Kaap Valley samples in Layer et al., (1996)], in combination with the single component behaviour observed in the samples, suggests that the samples of this site have acquired an overprint associated with lightning strikes. The samples were collected from an isolated and exposed dome like outcrop. At the time of sampling the risk of the samples being lightning struck was acknowledged and so samples were collected over a wide area with each sample a minimum of 0.7m, but up to 3m, apart.

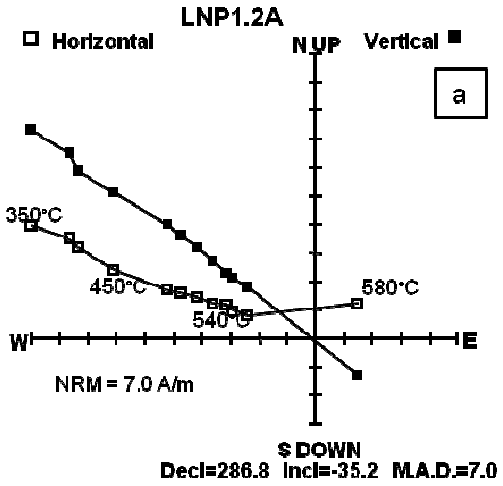
LNP1.2A
Horizontal
N UP
Vertical
a
350°C
450°C
540°C
580°C
W
E
NRM = 7.0 A/m
S DOWN
Decl=286.8 Incl=-35.2 M.A.D.=7.0

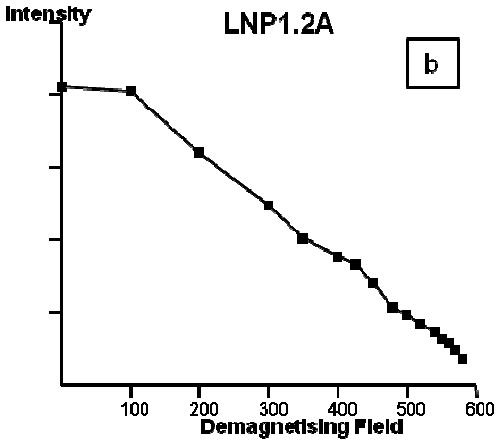
Intensity
LNP1.2A
b
100
200
300
400
500
600
Demagnetising Field

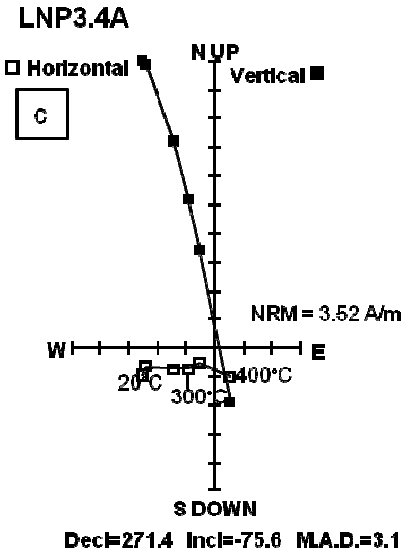
LNP3.4A
Horizontal
N UP
Vertical
c
NRM = 3.52 A/m
W
E
20°C
300°C
400°C
S DOWN
Decl=271.4 Incl=-75.6 M.A.D.=3.1

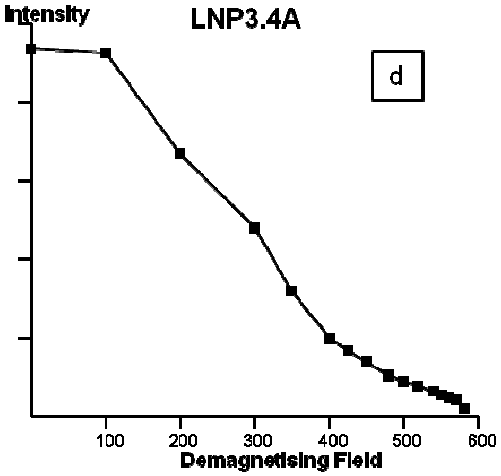
Intensity
LNP3.4A
d
100
200
300
400
500
600
Demagnetising Field

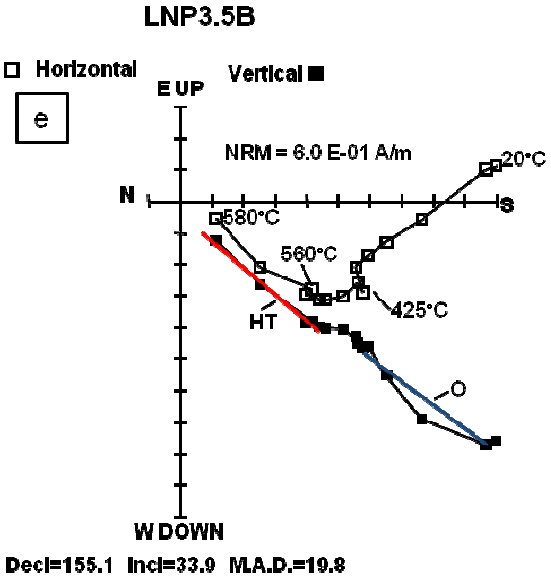
LNP3.5B
Horizontal
E UP
Vertical
e
NRM = 6.0 E-01 A/m
N
S
20°C
580°C
560°C
425°C
HT
O
W DOWN
Decl=155.1 Incl=33.9 M.A.D.=19.8

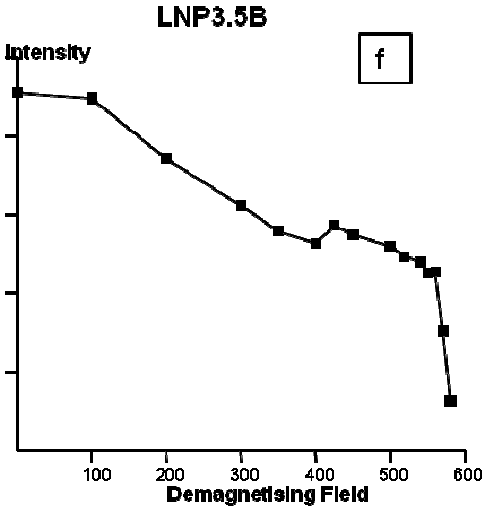
LNP3.5B
Intensity
f
100
200
300
400
500
600
Demagnetising Field

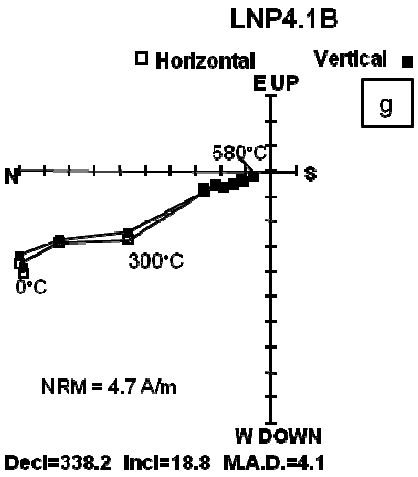
LNP4.1B
Horizontal
Vertical
E UP
g
580°C
N
S
300°C
0°C
NRM = 4.7 A/m
W DOWN
Decl=338.2 Incl=18.8 M.A.D.=4.1

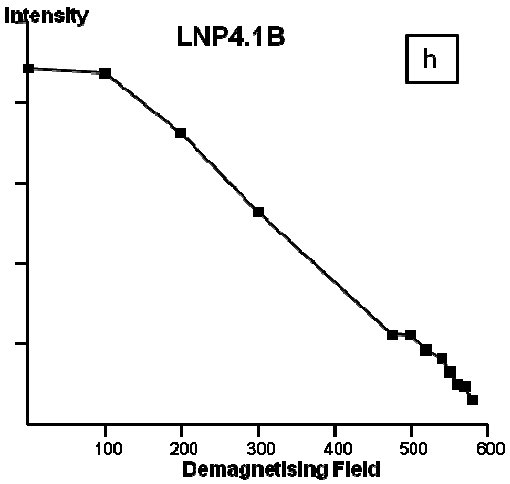
Intensity
LNP4.1B
h
100
200
300
400
500
600
Demagnetising Field

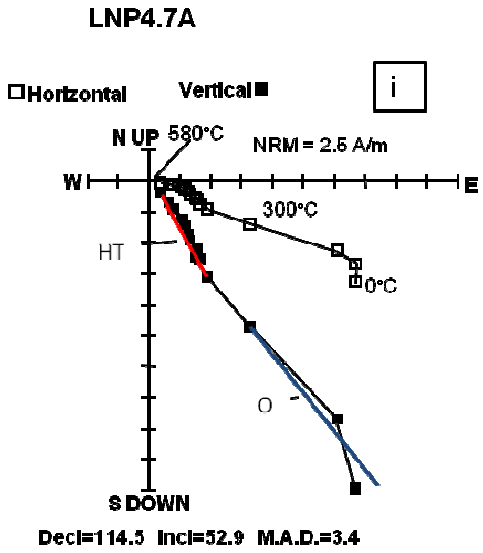
LNP4.7A
Horizontal
Vertical
i
N UP
580°C
NRM = 2.5 A/m
W
E
300°C
HT
0°C
O
S DOWN
Decl=114.5 Incl=52.9 M.A.D.=3.4

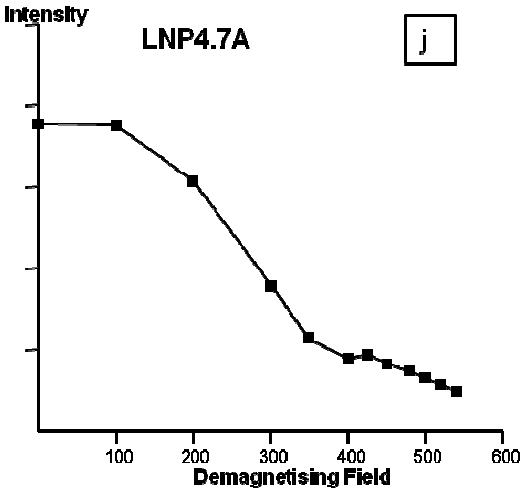
Intensity
LNP4.7A
j
100
200
300
400
500
600
Demagnetising Field

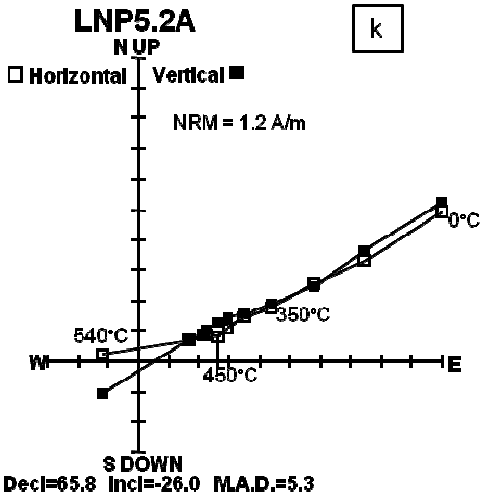
LNP5.2A
k
N UP
Horizontal
Vertical
NRM = 1.2 A/m
0°C
350°C
540°C
W
E
450°C
S DOWN
Decl=65.8 Incl=-26.0 M.A.D.=5.3

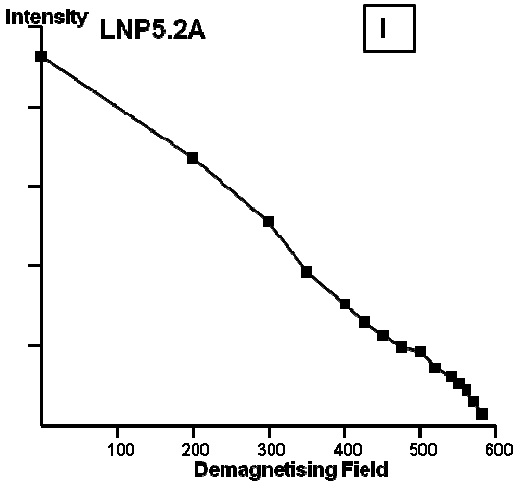
Intensity
LNP5.2A
l
100
200
300
400
500
600
Demagnetising Field

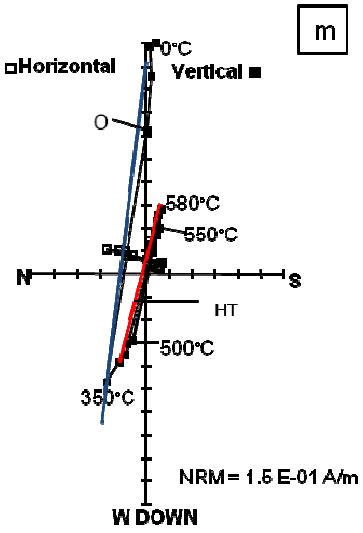
m
Horizontal
Vertical
0°C
O
580°C
550°C
N
S
HT
500°C
350°C
NRM= 1.5 E-01 A/m
W DOWN

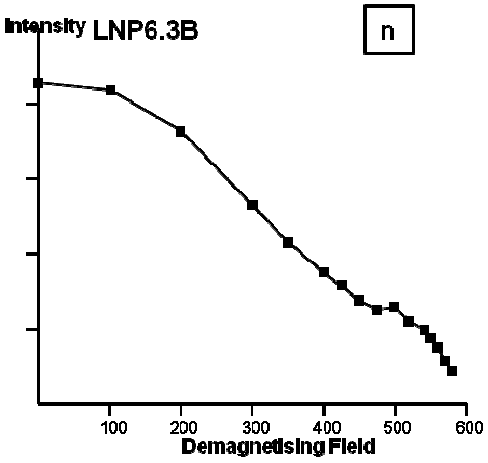
n
Intensity
LNP6.3B
100
200
300
400
500
600
Demagnetising Field

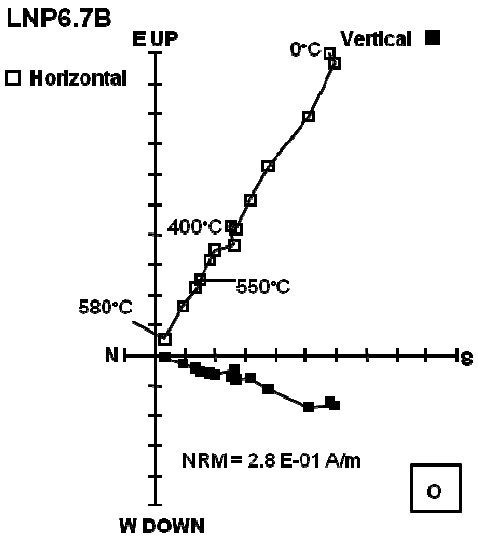
LNP6.7B
E UP
Horizontal
Vertical
0°C
400°C
550°C
580°C
N
S
NRM= 2.8 E-01 A/m
o
W DOWN

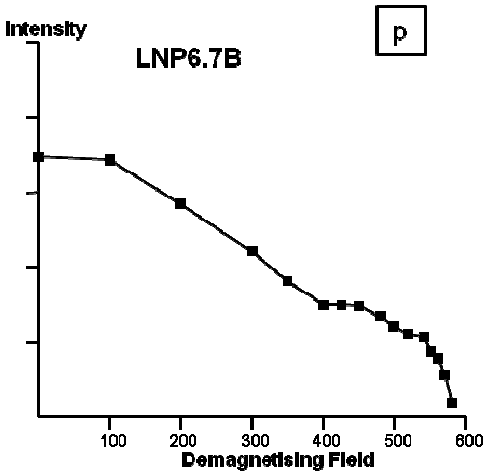
p
Intensity
LNP6.7B
100
200
300
400
500
600
Demagnetising Field

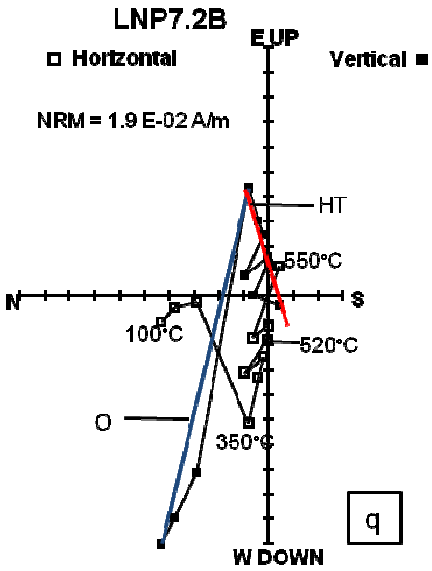
LNP7.2B
E UP
Horizontal
Vertical
NRM= 1.9 E-02 A/m
HT
550°C
N
S
100°C
520°C
O
350°C
q
W DOWN

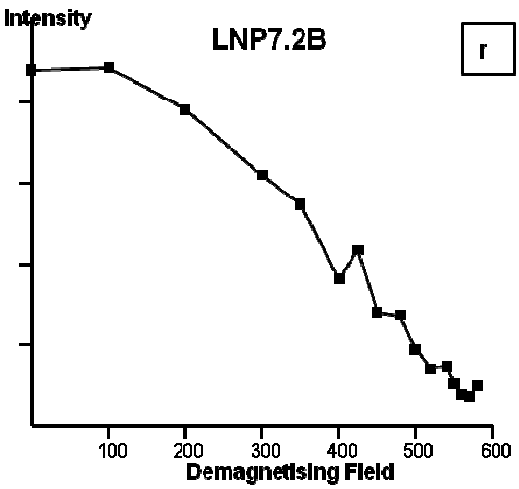
r
Intensity
LNP7.2B
100
200
300
400
500
600
Demagnetising Field

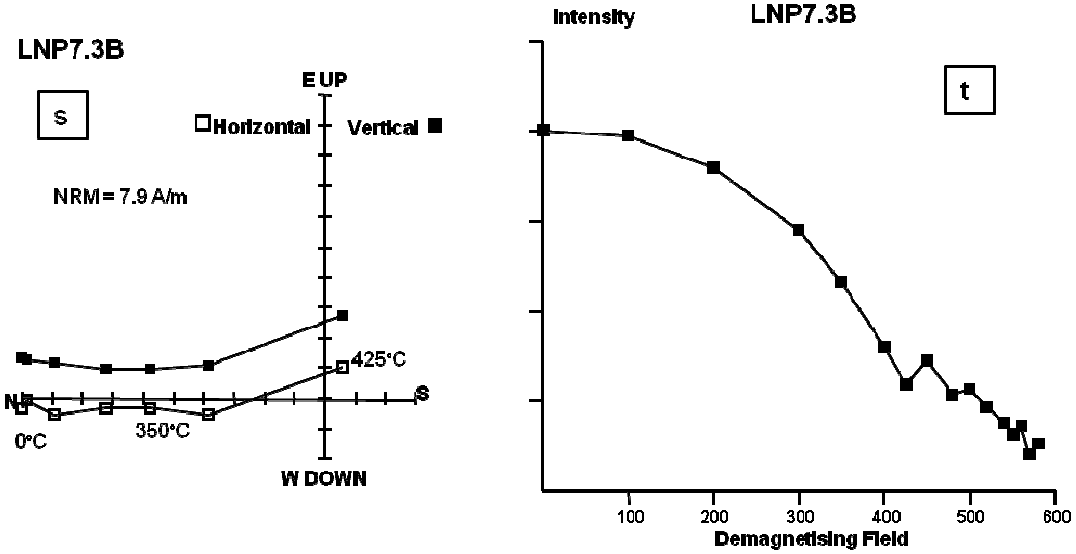
LNP7.3B
s
E UP
Horizontal
Vertical
NRM = 7.9 A/m
425°C
N
S
0°C
350°C
W DOWN
Intensity
LNP7.3B
t
100
200
300
400
500
600
Demagnetising Field

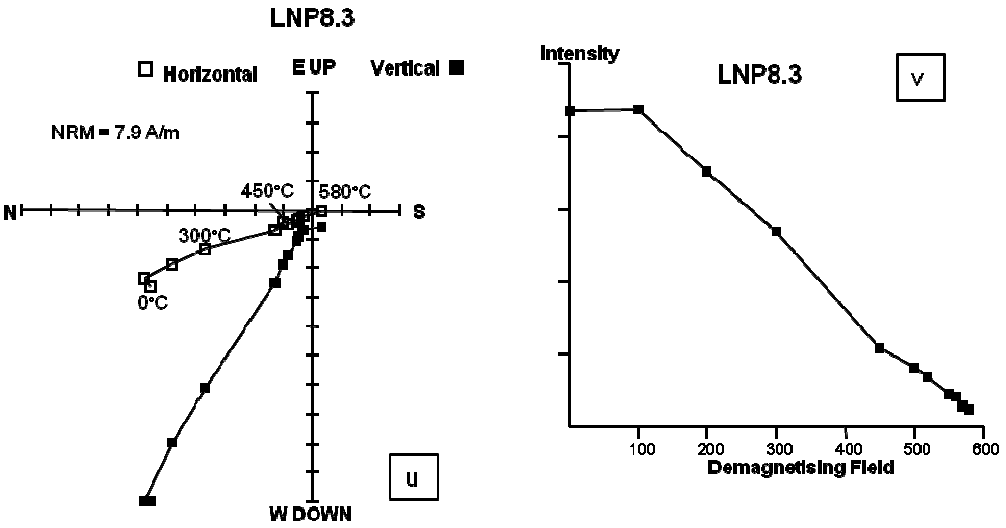
LNP8.3
Horizontal
E UP
Vertical
NRM = 7.9 A/m
450°C
580°C
N
S
300°C
0°C
u
W DOWN
Intensity
LNP8.3
v
100
200
300
400
500
600
Demagnetising Field

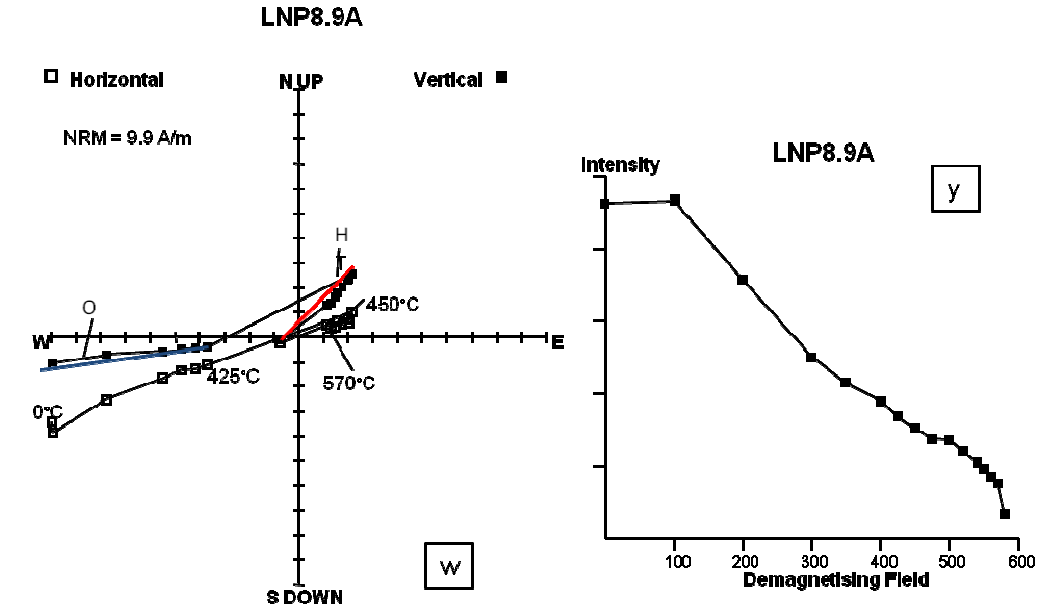
LNP8.9A
Horizontal
N UP
Vertical
NRM = 9.9 A/m
H
O
W
E
450°C
425°C
570°C
0°C
w
S DOWN
Intensity
LNP8.9A
y
100
200
300
400
500
600
Demagnetising Field

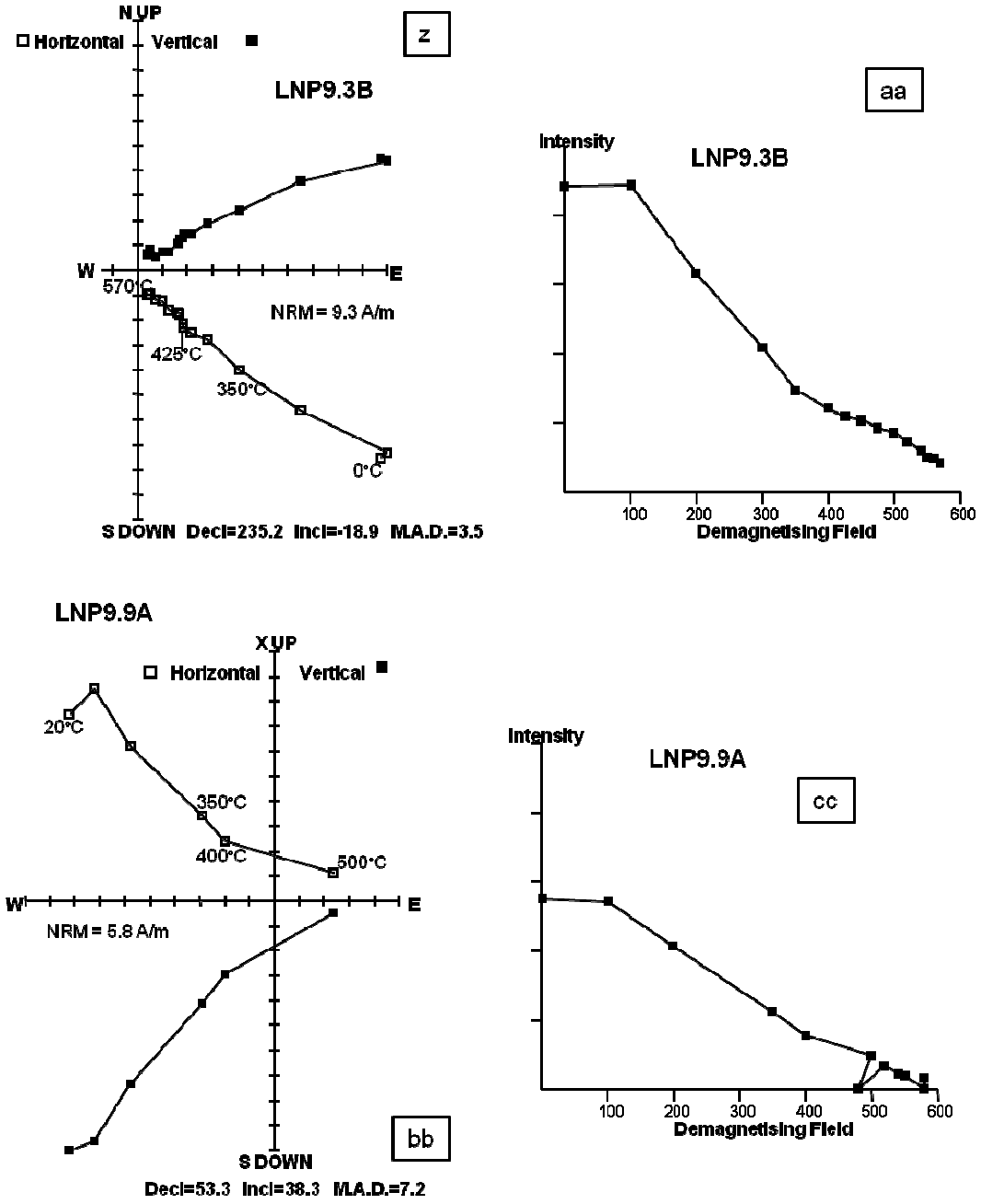

Figure 7.4. Orthogonal vector plots and equal area projections and demagnetisation diagrams to accompany each sample. (a & b) Site LNP1 shows a single component of magnetisation and significant loss of magnetisation prior to 500°C, characteristic of lightning struck samples. (c & d) Sample LNP3.4 is affected by a lightning strike as is evident from the single component of magnetisation and significant loss of NRM in the original parts of the experiment. (e & f) Sample LNP3.5a shows multi-component behaviour and a steep loss of magnetisation in the final heating step of the experiment. (g through to j) The demagnetisation behaviour observed in samples from site LNP4 is comparable to that of site LNP3. (k & l) Site LNP5 is affected by lightning strikes as is evident from the single component of magnetisation isolated from the samples. (m,n,o & p) LNP6 produces samples with single components of magnetisation as well as multi-component Zijderveld plots. (q through to y) The same is true for sites LNP7 and LNP8. (z to cc)The demagnetisation spectra of site LNP9 are dominated by single components; elevated NRM intensities along with significant loss of NRM intensity in the early part of the experiment indicates samples are significantly affected by lightning strikes.

7.3.1.2 LNP2

A total of ten samples were collected from site LNP2. Of those, six core samples, further subdivided into specimens, were subjected to demagnetisation treatment. Of the nine specimens measured, seven were characterised by a single component of magnetisation which was isolated in the temperature range 100-570°C/90mT.Specimens LNP2.9a and LNP2.9b were characterised by a single component of magnetisation removed below 400° C, above which the demagnetisation spectra observed in the Zijderveld Plots became too noisy for further interpretation. It was not possible to calculate a meaningful direction mean for the single component of magnetisation as the isolated directions are significantly scattered (see Figure 7.5).

The measured intensities from the samples of the LNP site are in the range 10^{-1} – 2.4A/m. The elevated intensities recorded by the samples, when compared to intensities of other TTG gneiss rocks (0.5-1.0A/m for the Kaap Valley samples in Layer et al., (1996)), in combination with the single component behaviour observed in the samples indicates that the samples of this site which display a single component have acquired an overprint associated with lightning strikes. In addition, the NRM of the samples is observed to decrease rapidly with increasing temperature, a characteristic signature of samples affected by lightning strikes e.g. (Strik et al., 2003). The samples were collected alongside a stream, where the outcrop was relatively exposed and could be prone to lightning strikes. However, there were some higher ridges in the vicinity of the sampling site and it was expected those would be more likely to be struck by lightning than the lower lying land closer to the stream.

7.3.1.3 LNP3

A total of nine samples were collected from site LNP3. Of those, nine core samples, further subdivided into specimens, were subjected to demagnetisation treatment. Of the eleven measured specimens, four were characterised by a single component of magnetisation (Fig. 7.4c & d) which was isolated in the temperature range 100-580°C/90mT.Seven measured specimens give multi-component Zijderveld Plots (shown in Figure 7.4e) with a low temperature overprint unblocked below 550°C and a high temperature component unblocked in temperature ranges between 540°C/40mT to 580°C/80mT.

The samples characterised by the single component of magnetisation have high NRM intensities ranging between 1.7A/m to 8.8A/m and are located in close proximity to one

	Lithology	Site	Bedding Strike/Dip (°)	Lat (°)	Long (°)	Demag	N	n	NRM (A/m)	Component	T Range (°C/mT)	Dm	Im	k	a95
Noisy Complex	Trondhjemitic/Tonalitic	LNP1	-	-25.8226	30.651	TH, TH+AF	7	7	7-40	SC	20-580°C/90mT		Scattered to the W		
								2		O	20°C-400°C		-		
		LNP2	-	-25.7900	30.6460	TH, TH+AF	7	0	10^{-1}- 2.4	HT	-		-		
								6		SC	100°C-570°C/90mT		Scattered to the N		
								6		O	20°C-550°C		Scattered to the N		
		LNP3	-	-25.8989	30.6153	TH, TH+AF	8	3	10^{-2}-8.8	HT	540°C/40mT - 580°C/80mT	231.9	48.7	32.4	22
								4		SC	100°C-580°C/90mT		Scattered		
								3		O	20°C-440°C	92.4	60.2	14.4	33.5
		LNP4	-	-25.8990	30.653	TH, TH+AF	9	3	10^{-1}- 11	HT	350°C/7mT-550°C/90mT		Scattered, overall steep		
								5		SC	20°C-580°C		Scattered		
								4		O	0°C-440°C/10		Scattered to the E		
		LNP5	-	-25.8993	30.6155	TH, TH+AF	7	4	10^{-1}- 3	HT	500°C/25mT - 580°C/90mT	238.4	67.2	11.7	28
								4		SC	20°C-580°C		Scattered to the E		
								2		O	0°C-440°C		Scattered to the S		
		LNP6	-	-25.8956	30.6259	TH, TH+AF	8	2	10^{-2} -10^{-1}	HT	520°C/25mT - 560°C/90mT		Scattered to the S/SW		
								6		SC	20°C-580°C		Scattered, overall shallow		
								5		O	20°C-440°C/35		Scattered		
		LNP7	-	-25.8956	30.6258	TH, TH+AF	9	3	10^{-3}- 1.2	HT	520°C/0mT-550°C/50mT		Scattered		
								3		SC	100°C-560°C/50mT		Scattered		
								3		O	20°C-425°C		Scattered		
		LNP8	-	-25.8954	30.6258	TH	9	3	10^{-2} -34	HT	400°C-580°C		Scattered		
								6		SC	20°C-580°C		Scattered		
		LNP9	-	-25.8953	30.6258	TH	9	9	4.8-9.2	SC	20°C-580°C		Scattered		

Table 7.2 Summary of directions obtained from the Nelshoogte Pluton. Also shown are sampling locations; treatment given to samples; samples measured (N); specimens used (n) and NRM intensities

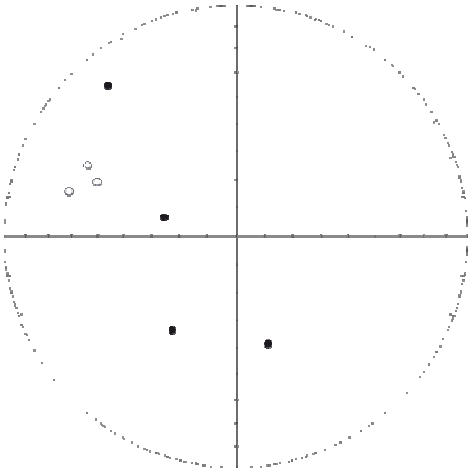

LNP1

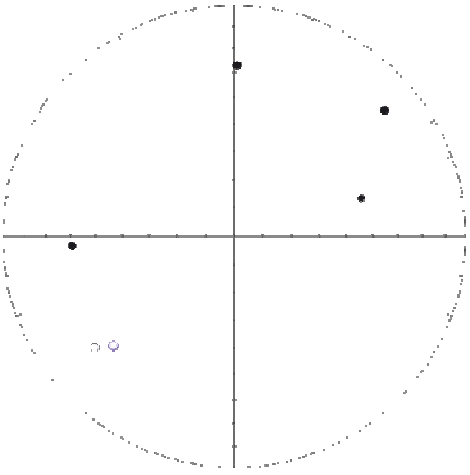

LNP2

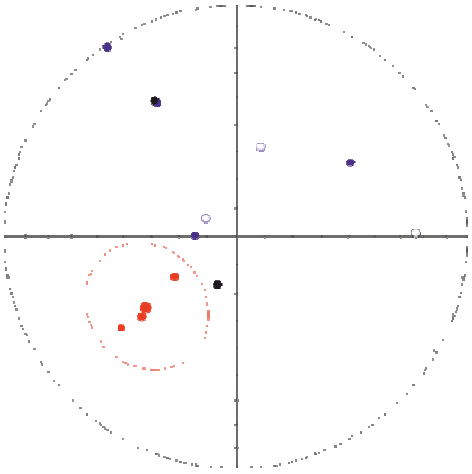

LNP3

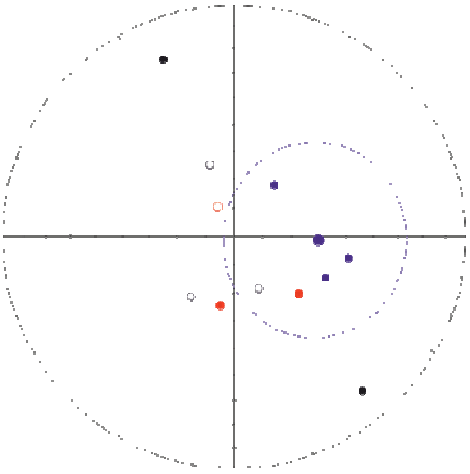

LNP4

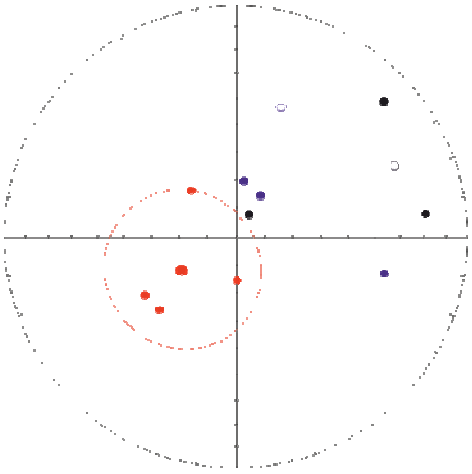

LNP5

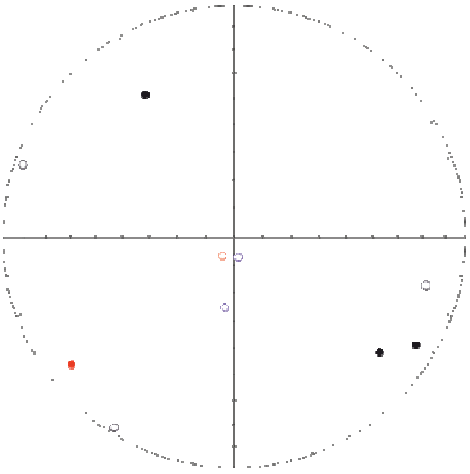

LNP6

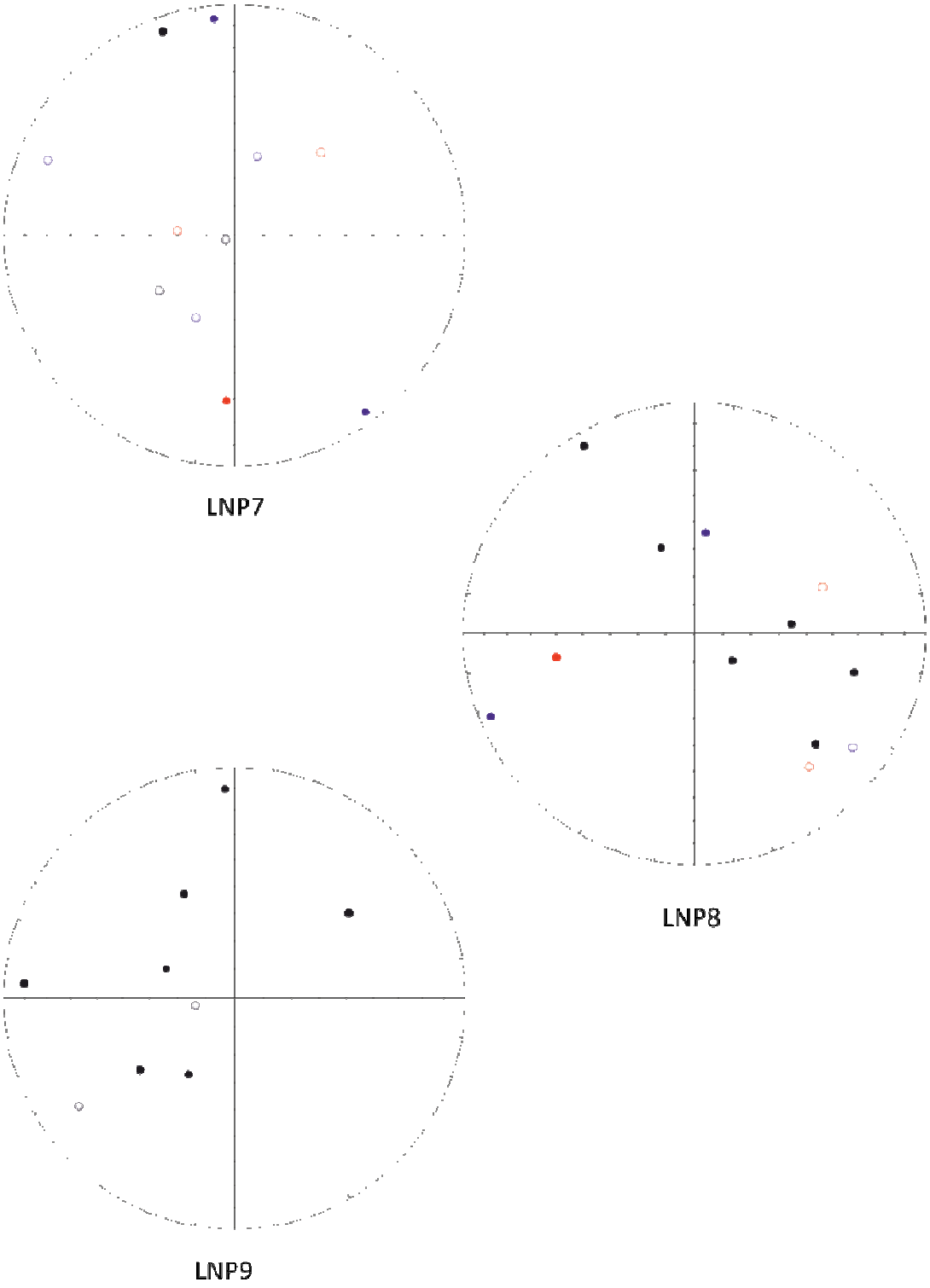

Figure 7.5. Equal area projections for all LNP sites, showing clustering and scatter of measured direction. Filled points represent the lower hemisphere, open points represent the upper hemisphere. Points in blue represent overprint components, whilst points in red are for high temperature components. Black points are indicative of single components of magnetisation. Directions in sites LNP1, LNP2 and LNP9 are dominated by single components of magnetisation. All directions in sites LNP6-8 are too scattered to obtain meaningful site mean directions. LNP3 and LNP5 give both scattered overprint and single component directions, but clustered directions (with mean direction and α95 error envelope) are shown. Site LNP4 gives a well clustered overprint direction (shown with mean direction and α95 error envelope), whilst high temperature and single component directions remain scattered.

another (LNP3.1b to LNP3.3b are no more than 30cm apart). The components isolated from these samples are scattered and it was therefore not possible to calculate a meaningful site mean. In conjunction with high initial NRMs, the single component nature of the Zijderveld Plots point towards the samples LNP3.1 to LNP3.3 and potentially LNP3.4 being lightning struck. Specimen LNP3.1a is characterised by a single component of magnetisation unblocked between 0-440°C, above which the sample is almost fully demagnetised (less than 10% the original NRM remains) and the demagnetisation spectra becomes too noisy to interpret. However, a single component of magnetisation is isolated in specimen LNP3.1b (0-550°C). Similar demagnetisation behaviour is to be expected from specimens from the same core; it is possible that specimen LNP3.1a acquired a laboratory induced IRM which explains the differences in the demagnetisation behaviour.

Overprint components were isolated from a total of six specimens (LNP3.5 to LNP3.9), with NRM intensities ranging between 0.05-0.06 A/m. However, the directions were too scattered to calculate a direction mean. The high temperature component was isolated from four samples; however, the direction isolated in samples LNP3.7b was of too poor a quality (maximum angular deviation, MAD=30.2) to be included in further interpretations. High temperature components cluster reasonably well, giving a mean direction of declination/inclination (D/I)=226.3°/44.9°, $\hat{k}$= 26.4, $\alpha 95$=18.2°, N=3), see Figure 7.5. Note that samples LNP3.5 to LNP3.9 were collected between 3m and 10m) away from samples LNP3.1 to LNP3.4. This can explain why the samples have not been severely affected by the effects of the lightning strike which has overprinted the original NRM in samples LNP3.1 to LNP3.4.

7.3.1.4 LNP4

A total of ten samples were collected from site LNP4. Of those, nine core samples, further subdivided into specimens, were subjected to demagnetisation treatment. Of the ten measured specimens, five are characterised by a single component of magnetisation which is isolated in the temperature range 20-580°C. The Zijderveld Plots, shown in Figure maining five specimens show a low temperature overprint unblocked below 440°C and a high temperature component unblocked in the temperature ranges between 350°C/7mT to 550°C/90mT.

Two specimens (LNP4.9a and LNP4.9b) from the same sample were measured and the directions i (which were consistent with one another) isolated, were averaged for the pur-

440°C and a high temperature component unblocked in the temperature ranges between 350°C/7mT to 550°C/90mT.

Two specimens (LNP4.9a and LNP4.9b) from the same sample were measured and the directions i (which were consistent with one another) solated, were averaged for the purpose of attempting to calculate a direction mean. Although a low temperature component was isolated in sample LNP4.10a, it was not used when attempting to calculate a direction mean due to it being of poor quality (it only took in three temperature steps), in addition to which the unblocking temperature range was elevated (300-400°C) when compared to the other samples. The overprint components gives a mean direction (which can be seen in Figure 7.5) of declination/inclination (D/I)=92.3°/60.2°, $\hat{k}$= 14.4, α95=33.7°, N=3).

The high temperature component is isolated infour samples but the direction identified in specimen LNP4.5a was of too poor a quality (MAD = 27.3) to be used in any further interpretations. High temperature components are also identified in specimens LNP4.9a and LNP4.9b; again, their results were combined when attempting to calculate a site mean. The three high temperature directions isolated from site LNP4 are scattered, (but overall are characterised by steep down inclinations); as a result it was not possible to calculate a direction mean.

The samples carrying a single component of magnetisation gave scattered directions from which it was not possible to calculate a site mean. Measured NRM intensities from the site range from 11-0.7A/m. Those elevated levelsin conjunction with the single component nature of some of the Zijderveld Plots studied are indicative of the site being affected, to some extent by lightning strikes.

7.3.1.5 LNP5

A total of eight samples were collected from site LNP5. Of those, seven core samples, further subdivided into specimens, were subjected to demagnetisation treatment. Of the eight measured specimens, four give multi-component Zijderveld Plots, showing a low temperature overprint unblocked below 440°C/10mT with a high temperature component unblocked above 500°C/25mT. The overprint components isolated from these samples are scattered (α95=94), but overall give a moderate to steep north easterly direction. The high temperature component is isolated from four samples and gives a mean direction of declination/inclination (D/I)=238.39°/67.27°, $\hat{k}$= 11.6, α95=28.0°, N=4). The direction isolated

from specimen LNP5.5a gave an elevated MAD of 19°, above the 15° cut-off used throughout this thesis. However, given that the unblocking temperature of the component is consistent with those of the other samples and the overall noisy nature of the Zijderveld Plot, the sample was used to calculate the direction mean. The remaining four specimens are characterised by a single component of magnetisation which is isolated in the temperature range 20-580°C. The single component directions are scattered and therefore, it was not possible to calculate a meaningful site mean direction (Figure 7.5).

The measured NRM intensities from the samples of the LNP5 site are similar to the NRM intensities reported by Layer et al., (1998), between 0.2-1.1 A/m with the exception of sample LNP5.1 which gives an elevated intensity of 3.04A/m. The demagnetisation behaviour observed in the Zijderveld Plots for samples LNP5.1 and LNP5.2 (see Figure 7.4), in addition to the high NRM intensity suggests these samples have been affected by a lightning strike. Samples LNP5.5 and LNP5.6 also display single component behaviour in their Zijderveld Plots alongside moderate intensities (1.1A/m). Compared to the 10^{-1} A/m intensities characteristic of the other samples in the site, this may also indicate the samples have been affected by a lightning strike. From the equal area projection shown in Figure 7.5, note that the single component direction is to the east, as are the overprint directions. Both are scattered so a direct comparison is problematic; nevertheless, one possible explanation is that the whatever caused the primary magnetic signal to be fully overprinted in the single component samples (likely a lightning strike), may not have fully overprinted the remaining samples and so multi-component behaviour is observed.

7.3.1.6 LNP6

A total of eight samples were collected from site LNP6. Of those, eight core samples, further subdivided into specimens, were subjected to demagnetisation treatment. Of the ten measured specimens, six are characterised by a single component of magnetisation which is isolated in the temperature range 20-580°C/90mT. The single component directions are scattered and, therefore, it was not possible to calculate a meaningful site mean direction. In addition, two samples, LNP6.1a and LNP6.3b, , produce multi-component Zijderveld Plots, showing a low temperature overprint unblocked below 440°C with a high temperature component unblocked above 520°C/25mT. However, both the overprint and high temperature components isolated from these samples are also scattered and no meaningful site mean direction was obtained.

The Zijderveld Plots of specimens LNP6.1a, LNP6.4a LNP6.5b and LNP6.5c (see Figure 7.4) were observed to be particularly noisy. In the case of samples demagnetised using thermal techniques, the poor quality of the demagnetisation curves can be explained by their readiness to alter during the experiment. During TH demagnetisations, samples were reversed (along the Y-Z axis), in the oven at each demagnetisation step. If samples are prone to alteration and/or if residual field is significant, this results in the demagnetisation curves being characterised by a zigzag.

The measured NRM intensities from the samples of the LNP6 site are in the range $3x10^{-2}$-2 $x10^{-1}$A/m, which are comparable to the intensities reported by Layer et al., (1996) of 0.5-1.0A/ for the Kaap Valley Pluton samples. The samples of site LNP6 were taken in close proximity to sites LNP7-9 (see Figure 7.3). Sites LNP8 and LNP9 have been largely affected by lightning strikes (see sections 3.1.8 and 3.1.9, below). Lightning strikes can affect the NRM of a surface outcrop by as much as 25 m² (Graham, 1961). As a result,, it is not unlikely that these samples would have felt the effects of nearby lightning strikes which have more severely affected their neighbours. Given the proximity of the sampling sites, it is not unreasonable to propose that the samples of LNP6 might have been overprinted by the lightning strikes affecting the neighbouring sites. However, the demagnetisation behaviour of the LNP6 samples is not what one might expect of lightning stuck samples. Whilst the majority of the directions isolated are from single components, these result from noisy and zigzag demagnetization curves, whereas lightning struck curves are characteristically very straight (see Figure 7.4 for sites LNP8 and LNP9). However, NRM decay curves show strong loss of NRM in the early parts of the demagnetisation experiments, behaviour typical of lightning strikes.

7.3.1.7 LNP7

In total, nine samples were collected from site LNP7. Of those, nine core samples, further subdivided into specimens, were subjected to demagnetisation treatment. Overall, the samples of site LNP7 produce multi-component Zijderveld Plots. However, the quality of the Zijderveld Plots is poor and often results in difficult interpretation of the components. This is particularly true for specimen LNP7.2b, where it was not possible to isolate any components. NRM intensities range from 0.1A/m to $5x10^{-2}$ A/m.

Seven of the measured specimens (three of those specimens are from a single core and so directions are averaged to produce a single sample direction) are characterised by a low temperature overprint which is unblocked below 440°C/35mT, shown in Figure 7.4. A high temperature component is unblocked above the low temperature component in three samples in the temperature range 0mT/520°C to 50mT/550°C. At high temperatures the Zijderveld Plots of specimens from sample LNP7.4 became too unstable to isolate components. The overprint and high temperature directions are too scattered to obtain meaningful site means (Figure 7.5). A further three samples yield single components of magnetisation which are unblocked in the temperature range 100°C to 50mT/560°C. The directions isolated from these samples are also scattered to the west and north and no meaningful site mean direction was obtained.

Samples from site LNP7 were also collected in very close proximity to sites LNP6 and LNP8-9. As is the case for site LNP6, it may be that, whilst samples from site LNP7 have not been directly struck by lightning, they have been overprinted by the lightning strikes affecting sites LNP8 and LNP9.

7.3.1.8 LNP8

Altogether nine samples were collected from site LNP8. Of those, nine core samples, further subdivided into specimens, were subjected to thermal demagnetisation treatment. Of the nine measured samples, six are characterised by a single component of magnetisation which is isolated in the temperature range 20-580°C. The single component directions are scattered and, therefore, it was not possible to calculate a meaningful site mean direction. In addition, three samples, LNP8.6b, LNP8.8 and LNP8.9a, produce multi-component Zijderveld Plots, showing a low temperature overprint unblocked between 20-425°C with a high temperature component unblocked between 400-580°C (seen in Figure 7.4). However, both the overprint and high temperature components isolated from these samples are also scattered and no significant site mean direction was obtained.

The measured intensities from the samples of the LNP site are in the range $4x10^{-2}$ 33A/m. The elevated intensities recorded by the samples, when compared to intensities of other TTG gneiss rocks [0.5-1.0A/ for the Kaap Valley samples in Layer et al., (1996)] in combination with the single component behaviour observed in the samples indicates that the sam-

ples of this site which display a single component have acquired an overprint associated with lightning strikes. In addition, the NRM of the samples is observed to decrease rapidly with increasing temperature, a characteristic signature of samples affected by lightning strikes (Strik et al., 2003).

The samples were collected along the Komati River bed, which is usually more protected from lightning strikes as throughout the Pluton it tends to carve out shallow valleys. However, at this locality the river is relatively broad (when compared to other LNP outcrops) and does not cut out a valley (as seen in Figure 7.3) and outcrops are relatively exposed. Therefore, it is not unexpected that the location of the sampling site might have been affected by a lightning induced IRM.

The multi component behaviour observed in samples LNP8.6b, LNP8.8 and LNP8.9a is likely to be explained by the least stable part of the blocking temperature spectra being contaminated during sample handling, given the low unblocking temperature of the overprint component. The samples across this site were taken in relatively close proximity to one another (between 0.5m to 2.4m apart, although the average distance was 1m). Lightning strikes can affect the NRM of a surface outcrop by as much as 25 m² (Graham, 1961). Consequently, it is not unlikely that these samples would have felt the effectsof nearby lightning strikes which have more severely affected their neighbours.

7.3.1.9 LNP9

In all, ten samples were collected from site LNP9. Of those, nine core samples, further subdivided into specimens, were subjected to thermal demagnetisation treatment. All the measured samples are characterised by a single component of magnetisation (see Figure 7.4) which is isolated in the temperature range 20-580°C. The directions obtained from the LNP9 samples are scattered and, therefore, it was not possible to calculate a meaningful site mean direction, as can be clearly seen in Figure 7.5.

The measured intensities from the samples of the LNP site are in the range 9-5A/m. The elevated intensities recorded by the samples, when compared to intensities of other TTG gneiss rocks [0.5-1.0A/ for the Kaap Valley samples in Layer et al., (1996)] in combination with the single component behaviour observed in the samples indicates that the samples of this site have acquired an overprint associated with lightning strikes. In addition, the

NRM of the samples is observed to decrease rapidly with increasing temperature, a characteristic signature of samples affected by lightning strikes (Strik et al., 2003).

The samples were collected along the Komati River bed, which is usually more protected from lightning strikes as throughout the Pluton it tends to carve out shallow valleys. However, at this locationthe river is relatively broad (when compared to other LNP outcrops) and does not cut out a valley (as seen in Figure 7.3) meaning outcrops are relatively exposed. Therefore, it is not unexpected that the location of the sampling site might have been affected by a lightning induced IRM.

7.3.2. Rock Magnetic Characterisation

The unblocking temperature spectra observed in the rocks of the Nelshoogte Pluton (NSP) are problematic for identifying magnetic carriers in the samples, given their often very noisy or single component behaviour, as discussed in section 7.3.3.

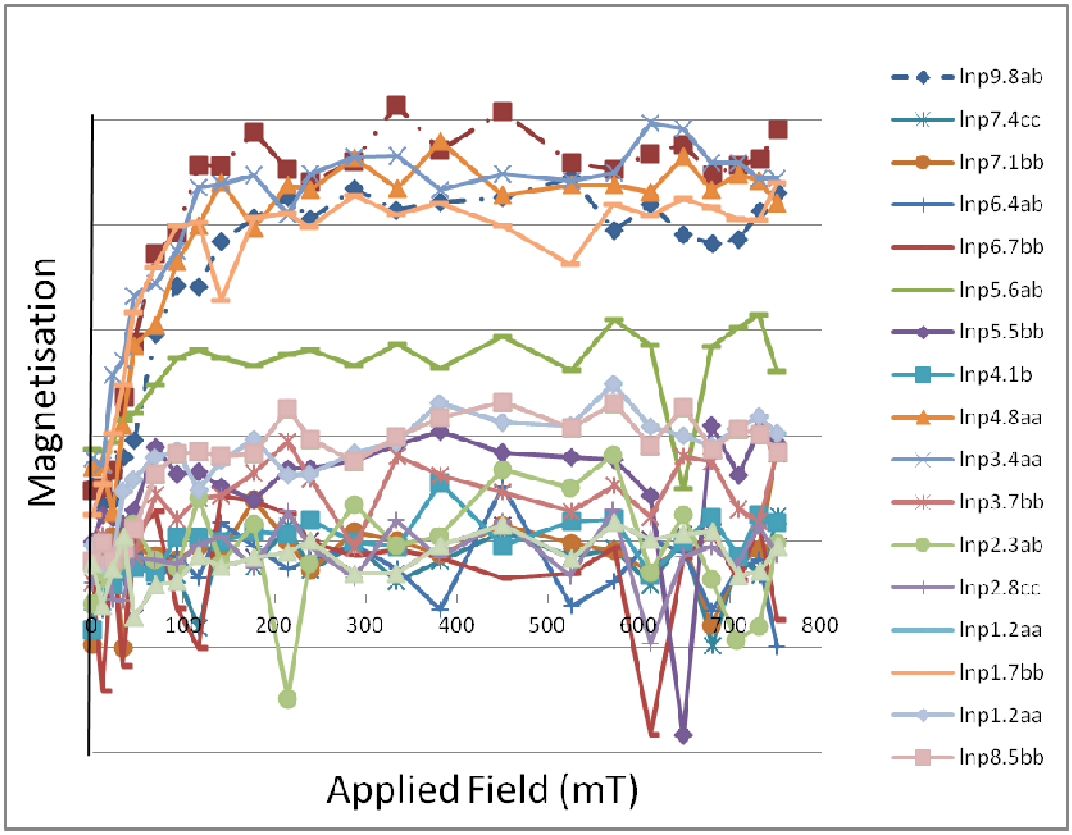

Figure 7.6. IRM acquisition curves for all samples of the LNP. Note that some curves are particularly noisy. Saturation is observed between 200-300mT.

Curie Temperatures (T_c) = 598°- 624°C established from thermomagnetic curves are indicative of the presence of maghemite in the samples, Figure 7.7 (b, d,e). VFTB thermomagnetic curves for sites LNP1-3, LNP 5, and LNP7-9 are highly reproducible (Fig. 7.7 b & d),

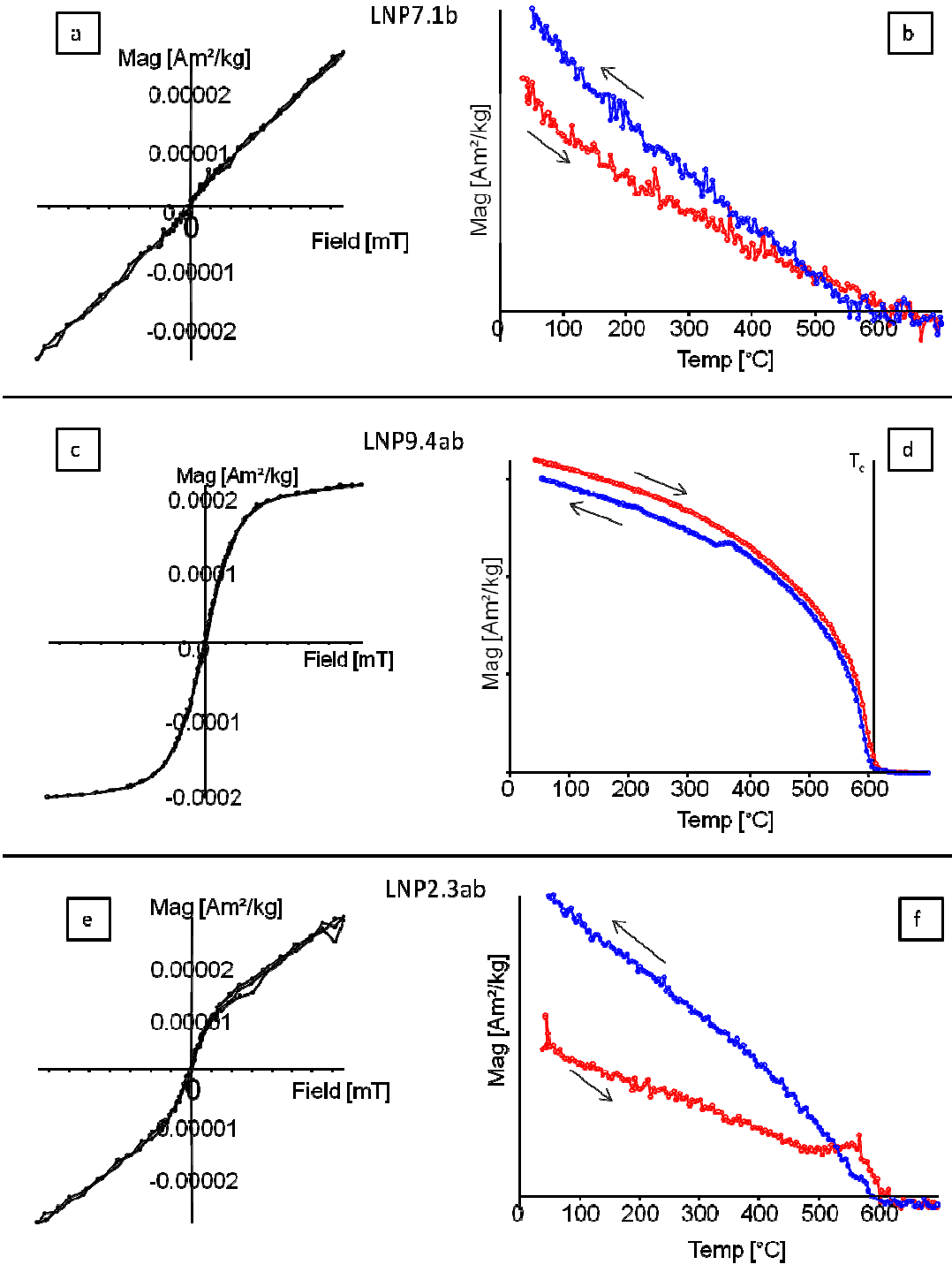

Figure 7.7. Representative rock magnetic parameters, acquired from the VFTB, for sites across the NSP. Hysterisis curves are displayed on the left, whilst thermomagnetic curves are shown on the right. The downwards arrow on the thermomagnetic curve represents a heating cycle, whilst the upward arrow indicates the cooling cycle. (a & b) Sample 7.1b displayed dominantly paramagnetic behaviour, both in both results. It was not possible to obtain rock magnetic data from this sample. (c & d) Sample LNP9.4ab is strongly dominated by the ferromagnetic fraction and thermomagnetic curves are fully reproducible. (e & f) Sample LNP2.3ab shows a strong paramagnetic contribution, where the hysteresis loop had to be significantly corrected to remove that contribution in order to obtain rock magnetic parameters. Thermomagnetic curve for the same sample shows strong alteration on heating with a new phase being created in the oxidation process.

whilst curves for sites LNP4, 6 and 8, as well as sample LNP2.3ab, as seen in Fig. 7.7f are not. This indicates that the samples from these sites alter significantly on heating. Reproducible curves are indicative of samples where alteration on heating is minimal or non-existent. IRM acquisition curves exhibit saturation between 200-300mT, as shown in Figure 7.6. In combination with hysteresis curve analysis, this suggests the presence of a low coercivity mineral, such as magnetite or maghemite. In order to acquire rock magnetic parameters, it was necessary to correct all hysteresis curves for a contribution from the paramagnetic fraction (as seen in sample LNP2.3ab, shown in Figure 7.7e & f). In most cases, the samples were dominated by the ferromagnetic fraction and only a small correction was applied, e.g. Site LNP1, (see Figure 7.7d). However, in some cases a significant paramagnetic contribution was removed before the curves could be analysed, e.g. LNP7.4cc. Only sample LNP7.1bb displayed dominantly paramagnetic behaviour as seen Figure 7.7b. Hysteresis parameters and thermomagnetic curves measured for samples from the same site are reproducible and suggest uniform distribution of magnetic carriers throughout the individual units sampled. Sites LNP4 and LNP8 are the exception. Sample LNP4.1bb is strongly paramagnetic and the thermomagnetic curve shows significant alteration. However, LNP4.8aa has a lesser paramagnetic contribution and does not alter on heating. This is in agreement with temperature dependant susceptibility measurements made on the Kappa Bridge from sample LNP4.8bb. Sample LNP8.5bb is dominated by the ferromagnetic fraction and only has a small paramagnetic contribution, a T_c 602°C and does not alter on heating. Sample LNP8.9ab has a significant contribution from the paramagnetic fraction and the thermomagnetic curve shows significant alteration. The alteration on heating is also seen clearly in the high temperature frequency dependency results performed on the Kappa Bridge from sample LNP8.9ab. Hysteresis parameters are plotted on a Day plot (M_{rs}/ M_s) and (H_{cr}/ H_c) for magnetite, (after Day et al., (1977a) and Dunlop (2002)) and show the majority of the samples from this study plot in the MD (multi domain) section of the plot (Figure 7.8).

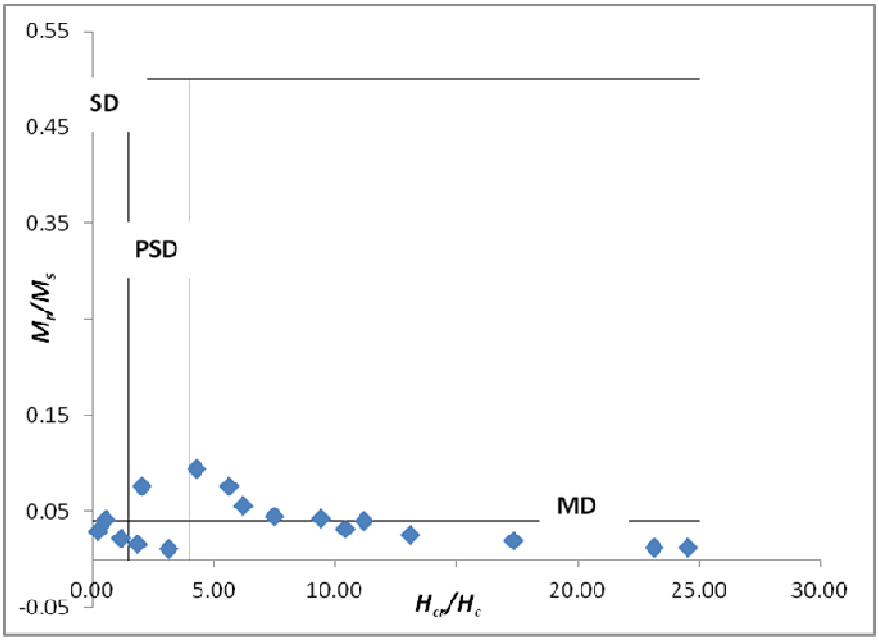

Figure 7.8. Day plot for LNP rock magnetic results. Theoretical Day plot after Day et al., (1977) and Dunlop (2002). SD: Single Domain; PSD: Pseudosingle domain; MD: Multidomain.

High and low temperature magnetic susceptibility experiments performed on a Kappa Bridge on nine LNP samples mostly support the findings of the experiments performed on the VFTB. In samples which are not dominated by the paramagentic fraction, a clear change in slope is measured at 568°C- 584°C, (see Fig.7.9a) indicating the presence of magnetite. Calculated Verwey transitions at 146K-148K also indicate the presence of magnetite. In cases where the signal is dominated by the paramagnetic contribution (LNP6.2ab and LNP7.1bb, see Figure 7.9b) results can be noisy and so establishing the magnetic carrier is difficult. Samples which show strong paramagnetic contribution are from the same sites that showed significant paramagnetic contribution during the VFTB experiments also. The majority of thermomagnetic curves show some degree of alteration, with the most extreme cases being observed in samples LNP6.2ab, LNP7.1aa and LNP8.9ab, (shown in Figure 7.9c). Thermomagnetic curves for samples LNP1.2b, LNP5.6ab and LNP9.4ab are fully reproducible and clearly indicate the presence of magnetite, as observed in Figure 7.9a.

Curie temperatures calculated from the VFTB and the approximated Curie Temperature calculated from the Hopkinson peak on the Kappa Bridge and differ by up to 40°C. The VFTB Curie Temperatures indicate the magnetic carrier in the samples is likely to be maghemite. However, both low temperature Verwey Transitions and high temperature dependence susceptibility results are consistent with magnetite. This T_c (VFTB) and ap-

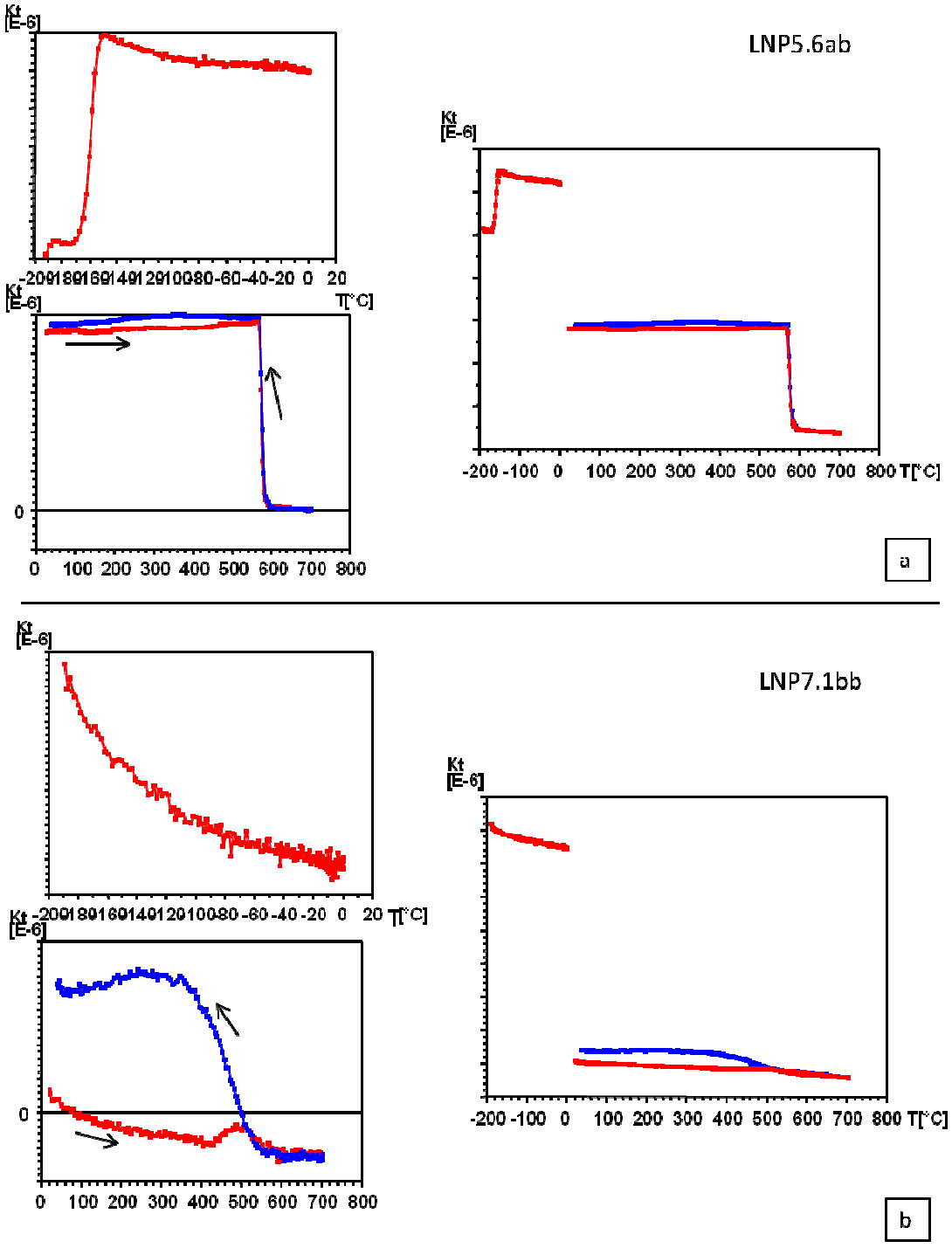

Figure 7.9. Representative temperature dependant susceptibility measurements for samples across the LNP sites. Low (-200°C to room temperature) temperature dependant susceptibly and high (0°C to 700° C) temperature dependant susceptibility (carried out in argon), corrected for the sample holder, are show on the left (above and below respectively). Downward arrows on the high temperature dependant susceptibility indicates the heating cycle, whilst upwards arrows indicate the cooling cycle. Combined results for low and high temperature experiments are displayed on the right, however, it should be noted these are not corrected for the contribution the sample holder may have to the susceptibility. (a) Sample LNP5.6ab displays a clear Hopkison's Peak at 148K and a T_c of 577°C, indicating magnetite is the magnetic carrier. The sample does not show significant alteration upon heating and curves in the high temperature experiment are highly reproducible. (b) Sample LNP7.1 is dominated by the paramagnetic contribution, meaning no Hopkison's Peak is observed and T_c approximation is difficult to establish. (Continued overleaf).

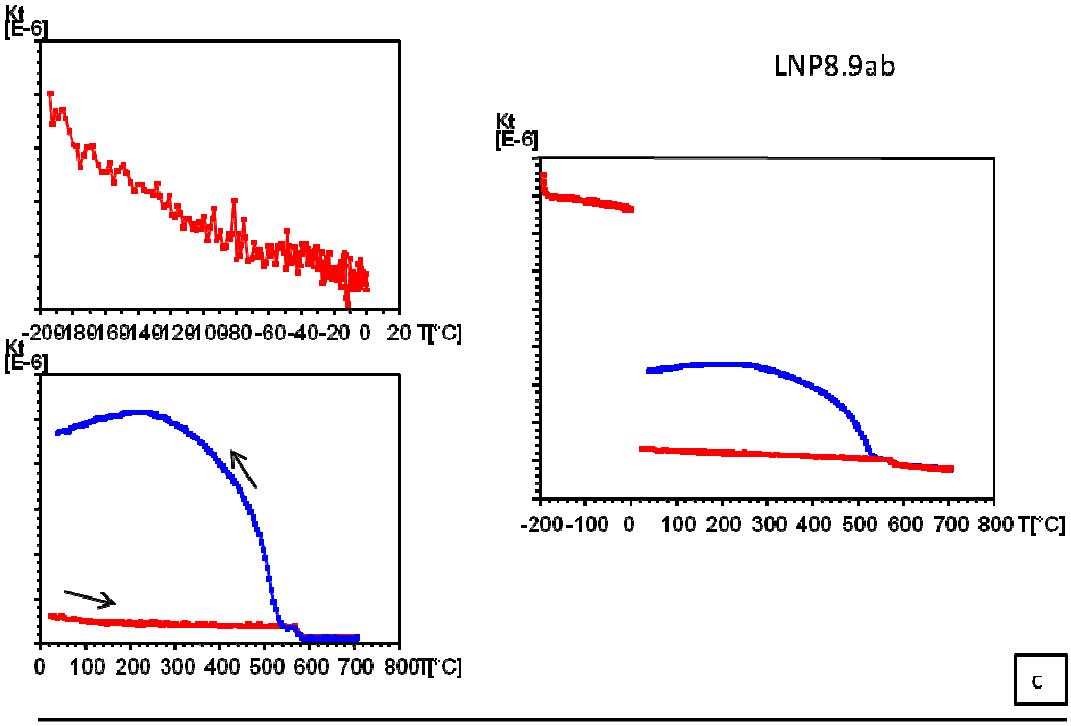

Figure 7.9. Representative temperature dependant susceptibility measurements for samples across the LNP sites. Low (-200°C to room temperature) temperature dependant susceptibly and high (0°C to 700°C) temperature dependant susceptibility (carried out in argon), corrected for the sample holder, are show on the left (above and below respectively). Downward arrows on the high temperature dependant susceptibility indicates the heating cycle, whilst upwards arrows indicate the cooling cycle. Combined results for low and high temperature experiments are displayed on the right, however, it should be noted these are not corrected for the contribution the sample holder may have to the susceptibility. (c) LNP8.9ab is dominated by the paramagnetic contribution, meaning no Hopkison's Peak is observed and T_c approximation is difficult to establish.

proximated T_c (High temperature susceptibility) discrepancy was also observed in results from the Komati Formation (See Chapter 4). For the Komati Formation samples further experiments, comparing results from the same core were carried out, and showed the discrepancy was consistent and observed in all samples. Investigation of the VFTB identified that the thermocouple was incorrectly positioned within the oven and not flush against the samples. Therefore the T_c are a measurement of temperature within the oven, rather than the sample itself. On average, sampled temperature is overestimated by 20°C -30°C in the VFTB. Therefore, despite the elevated T_c calculated from the VFTB results which indicate that maghemite is the magnetic carrier, the high and low temperature magnetic susceptibility results from the Kappa Bridge are considered to be the most reliable. Magnetite, which in many cases is susceptible to alteration on heating, is identified as the magnetic carrier in the LNP samples.

Rock magnetic characterisation results from the Nelshoogte Pluton indicate that the magnetic carrier in the Formation is MD magnetite. Thermomagnetic curves for samples LNY1.9c (Figure 7.7) and LNY1.0 give a T_c of 599°C and 588°C, respectively. However the shape and reproducibility of both the heating and cooling curves are consistent with magnetite. In addition, IRM acquisition curves exhibit saturation below 200mT suggesting the presence of a low coercivity mineral, such as magnetite, which is also consistent with the hysteresis curve analysis (Figure 7.7 a and b). Hysteresis parameters are plotted on a Day plot (M_{rs}/ M_s) and (H_{cr}/ H_c) and show samples from the majority of the sites site plot in the MD (multi domain) section of the plot (Figure 7.8), meaning they have have low Mrs/Ms but high Hcr/Hc. However some samples are plotting in the bottom left corner of the plot, indicating low Hcr/Hc, unlikely for magnetite, and their validity must be questioned.

7.3.3. Microscopy Observations

The rocks of the NSP range in composition from tonalites, granodirites, trondjhemites and granites (Matsumura, 2014). Samples from sites LNP3 and LNP7 were examined using an optical microscope and a Philips XL30 tungsten filament scanning electron microscope (SEM) to understand the mineralogy and thermal history of the sample in more depth. The samples were chosen at random, as at the time of selection, no palaeomagnetic interpretations had started. In particular, the SEM was used to analyse the mineral composition of these rocks using backscatter electron imaging (BEI) and energy dispersive spectroscopy (EDS). The microscopy investigations were carried out with the aim of supplementingthe findings of the rock magnetic work and further characterise the magnetic minerals in the

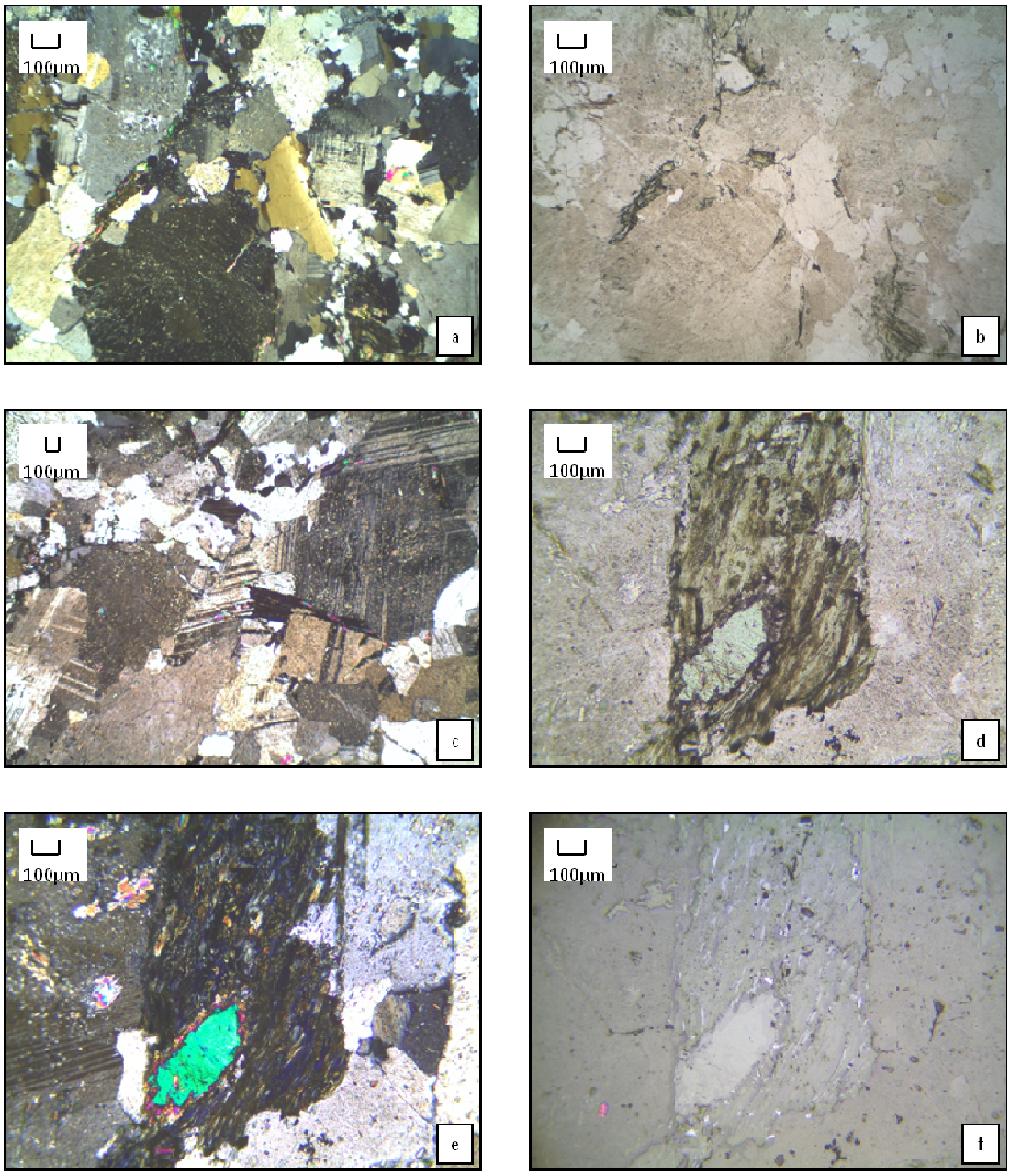

Figure 7.10. Optical Photomicrographs (a,b, c and e) show the primary mineralogy of the Nelshoogte Pluton. dominated by quartz although it has a granular texture formed by plagioclase and accompanied by biotite, often altered to chlorite. (a) Ribbon-like quartz is observed. (c) Faint sercitization of plagioclase is seen (d, e & f) Transmitted (Plain Polarised light /Cross Polarised Light) and reflected light microscopy showing Fe-oxides (as black and bright particles respectively) forming along chlorite mineral boundaries, as seen in LNP7.8bb. (e) A large hornblend grain is observed in the centre of the field of viw.

NSP samples. The secondary aim was to better understand the timing of the acquisition of the ChRM isolated in the samples, by establishing the petrological history of the rocks studied.

Previous results have shown the common microscopic assemblage for the NSP to comprise plagioclase, quartz, biotite as the major phases (Matsumura, 2014), whilst microcline, epidote, muscovite and minor opaques are present as accessory minerals (Layer et al., 1998). In addition, hornblendeis found in granodiorites and tonalites of the northern and eastern margins of the pluton (Matsumura, 2014). The biotites can often be altered to chlorite [up to 50% of grains, Layer et al., (1998)]. Chlorite is a common secondary mineral of biotite and can form under a number of conditions, including the presence of hydrothermal fluids or as a result of metamorphism. Layer et al., (1998) found that muscovite in the rocks of the NSP can occur closely associated with biotite, or alternatively as sericite (a common alteration product of plagioclase which has been subjected to hydrous conditions) prisms in saussuritised (fluids present at late stages of plagioclase crystalisation lead to the formation of saussurite) plagioclase. The presence of epidote as an accessory mineral further indicates it is likely the rocks of the NSP have experienced some degree of hydrothermal alteration. In the northern part of the pluton the textures observed are generally magmatic and include porphyritic and granitic textures (Matsumura, 2014). The southern and southeastern areas of the pluton are dominated by deformation textures such as foliations and xenomorphic textures (Matsumura, 2014). The reader is directed to the work of Matsumura, (2014) for a very detailed study of the mineralogy of the NSP.

Samples LNP3.8ab and LNP7.8bb were found to be very similar both in composition and texturally. Sample LNP3.8ab is dominated by quartz although it has a granular texture formed by plagioclase and accompanied by biotite, often altered to chlorite. In addition, small proportions of hornblende and biotite are also observed in the thin section. The plagioclaseis often sericitised, whilst the quartz can be seen to form elongate ribbons in some places (Figure 7.10 c and Fig7.10 a, respectively). Sample LNP7.8bb was found to be slightly coarser grained than LNP3.8ab and dominated by equigranular quartz and plagioclase. Biotite altered to chlorite was commonly observed, as seen in Figure 7.10d. The plagioclasess are often normally zoned and sericitised (Figure 7.10a). Rare muscovite was also observed, (Fig 7.10e) Opaques were usually observed along the rims and within the chlorite grains (Fig 7.10d). Reflected light microscopy indicated these were likely to be iron oxides, given their shinny lustre, as shown in Figure 7.10f.

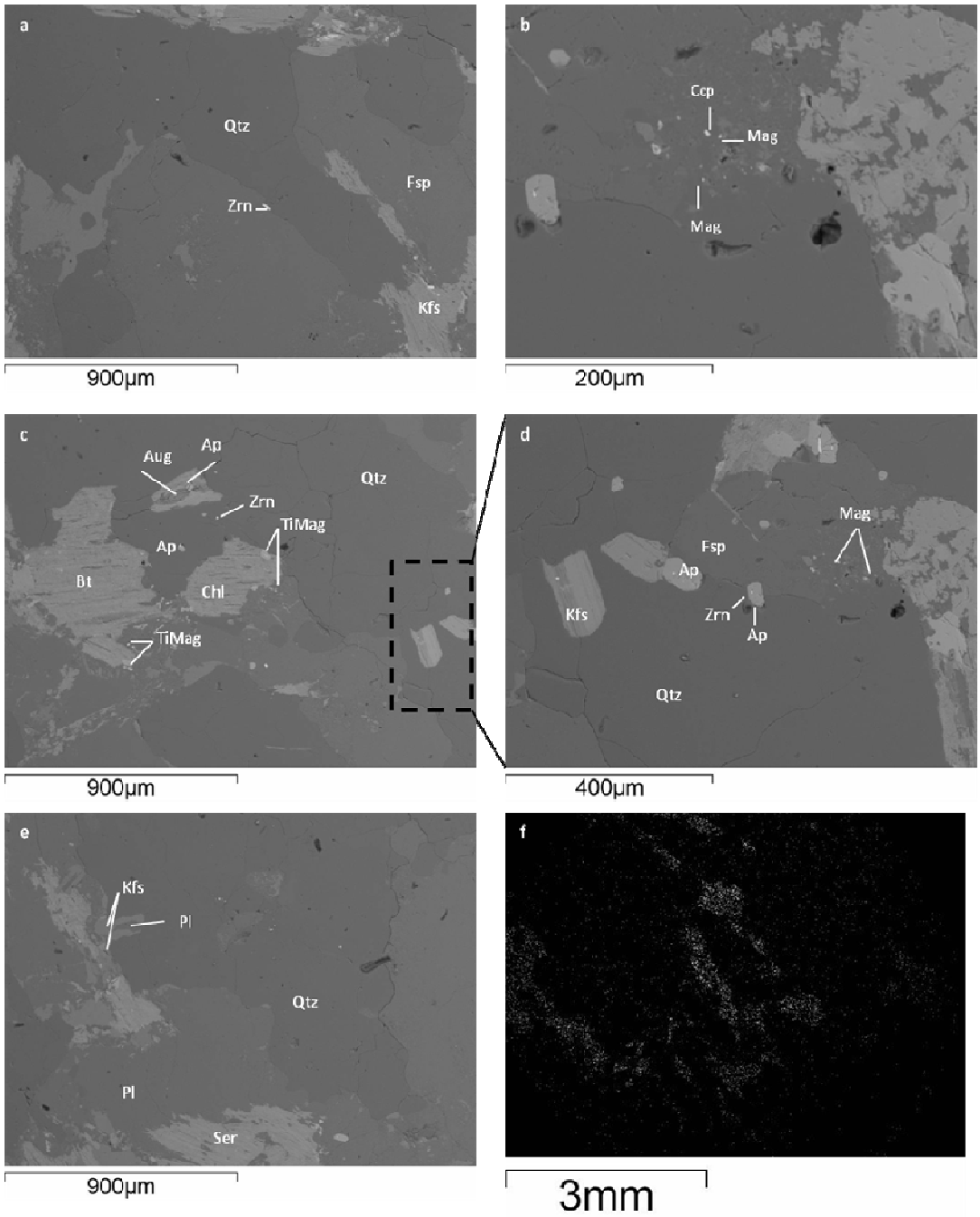

Figure 7.11. Scanning Electron Micrographs of LNP3.8ab. (a, c, d) Show mineralogy expected of a rock of tonalitic/trondhjemitic composition: quartz (Qtz), K-feldspar (Kfs), Feldspar (Fsp), Plagioclase (Pl), Sericite (Ser), Augite (Ag),Chlorite (Chl), Biotite (Bt), Apatite (Ap) and Zircon (Zn). Iron- oxides including magnetite (Mag), Chalcopyrite (Ccp) and titanomagnetite (TiMag) were identified in the sample, as seen in a, b and c. (e)Magnified area of edge of olivine mineral where magnetite is expected to be found. (f) Fe element X-ray map of area (e). Map indicates iron is well distributed across the imaged area, rather than concentrated, therefore indicating Fe-Oxides in the thin section are sparse and small in scale.

Further work was carried out on the SEM to try and identify the opaque minerals and their relationship to the primary mineralogy. Energy dispersive X-ray spectra (EDX) were also acquired to try and identify the main minerals in the sample. Opaques tend to be bright when observed under the SEM and so minerals with these properties were targeted for X-ray analysis in order to identify likely FeO. Magnetite, titanomagnetite and a single grain of chalcopyrite were identified in the studied samples (Figure 7.11c, d and e). Opaque minerals were observed on a micron scale (50µm-10µm) and in close proximity to chlorite and biotite grains, as was observed during the optical microscopy work. All the minerals expected to be identified in a rock of tonalitic to trondhjemitic composition were recognised-quartz, plagioclase and K-feldspar (intergrowths of which give rise to perthitic texture seen in Figure 7.11e and Fig Bc), sericite (Figure 7.11 e), biotite and chlorite. In addition, augite, apatite and numerous zircons (which also tend to be bright and euhedral, as expected of Fe-oxides) were identified, e.g.Figures7.11c and d. Element x-ray mapping was carried out on three distinct areas of the sample to try and identify clusters of iron that may indicate the presence of Fe bearing opaque minerals. However, in all three maps produced, iron was found to be well scattered throughout the sample with no obvious clusters, indicating Fe bearing ore minerals are sparse. Figure Cf shows an Fe element map, for the area shown in Fig. Ce. Well defined clusters of Fe are seen in Fig. Cf; however, they are associated with large phenocrysts which contain Fe within their chemical formula, e.g. chlorite, biotite and epidote .

The findings of the microscopy work carried out on site LNP 3 and 7, for the most part, support the results of the rock magnetic characterisation experiments performed on the sites. Whilst no opaques were identified in the optical microscopy examination of LNP3.8ab, iron oxides were clearly identified during the electron microscopy work and support the findings of the rock magnetic characterisation. Whilst the discrepancy of the T_c described in section 3.2 is resolved due to the experimental error during VFTB experiments, it might have been possible to use the electron microscopy to further clarify the problem. However, the EDX spectra acquired for the Fe Oxides cannot distinguish between minerals that have the same composition, i.e., magnetite and maghemite, but different lattice structures. If magnetite in the samples had been hydrothermally altered by low temperature oxidation to maghemite, one would expect to see cracking at the surface of the iron oxide grain ((Tauxe, 2010). Unfortunately, it was not possible to distinguish between the two potential carriers identified through rock magnetic characterisation using optical and electron backscatter imaging techniques.

The rock magnetic characterisation of the samples of site LNP7 were dominated strongly by the paramagnetic fraction. Although in reflected light optical microscopy some opaques were observed along chlorite grain rims (see Figure 7.10), as the sample was not studied using electron microscopy it was not possible to confirm these were iron oxides. Samples LNP7.1 and LNP 7.4 were studied for rock magnetic characterisation purposes. The presence of opaques in sample LNP7.8bb might indicate that the magnetic carriers were not distributed evenly within the area sampled and rock magnetic results for sample LNP7.8 might have been more strongly dominated by the ferromagnetic fraction. Alternatively, the opaques identified in sample LNP7.8bb might be largely paramagnetic, such as iron sulphides, e.g. pyrite and in that case, would support the findings of the rock magnetic characterisation. Finally, it is important to mention that the remanence carrying grains may well be too small to see even with an SEM and may have their signal drowned out by larger, lower coercivity grains in high field rock magnetic experiments (such as hysteresis), therefore thequestion arises whether minerals observed under the (optical or electron) microscope are representative of theremanence carrying grains (Davies, 2009)?

7.4. Discussion

Despite the success and promising palaeomagnetic results obtained by Layer et al., (1998) it was difficult to obtain consistent site mean directions from the Nelshoogte Pluton sampled as part of this study.

The LNP sites are evenly distributed across the NPS and compositionally very similar. The directions from the sites are overall scattered and only consistent overprint directions were obtained from site LNP4, whilst high temperature site mean directions were obtained from the samples of sites LNP3 and LNP5. A number of samples from each site are affected by lightning strikes, resulting in a single convergent component observed in the Zijderveld Plots.

Rock magnetic characterisation and microscopy work suggests the magnetic carrier in the NSP to be multidomain magnetite, although site LNP7 is dominated by the paramagnetic fraction, possibly due to the presence of iron sulphides, although it was not possible to confirm these findings.

7.4.1. Comparison with Previously Published Palaeomagnetic Data

Despite only one meaningful overprint site mean and two high temperature site means being obtained from the samples of the NSP presented in this work, it is still worthwhile comparing the results to previously published data. It is important to establish if the mean directions calculated are relevant in the context of the current state of knowledge. The results will not confirm, nor disprove, the findings of the earlier studies, but they have the potential to contribute to the available data set as sites LNP3-5 are of a geographical area not previously studied.

The works most relevant to the results presented in this chapter are those of Layer et al., (1998) of the Nelshoogte Pluton and Tarduno et al., (2007) of the Kaap Valley Pluton. Extensive reference to these and other palaeomagnetic works worthy of note is made in sections 7.1 and 7.3 of this chapter; the reader is directed there for more detail. Layer et al., (1998), identified two antipodal, ChRM directions:- shallow southeast (A-) and shallow northwest (A+), (A-= (D/I)=104.0°/11.8°, $\hat{k}$= 7, α95=28°, n=6); (A+=(D/I)=293.1°/7.0°, $\hat{k}$= 13, α95=13, n=11). In addition, this direction is also recorded in microgabbro dykes of similar age and the authors consider the directions wereacquired simultaneously. Tarduno et al., (2007) studied the tonalitic Kaap Valley Pluton (3227±1Ma, Kamo and Davies, 1994). Whilst the focus of this study was measuring palaeointensities, the authors also identified two antipodal east (KVP+ = (D/I)=101°/56.1°, $\hat{k}$= 26.2, α95=13°, n=8) and shallow west directions (KVP- = (D/I)=273°/-24.1°, $\hat{k}$= 46, α95=7°, n=7). In addition, Layer et al., (1998) also identified two antipodal overprint directions:- B+, (D/I)=224.7°/80.0°, $\hat{k}$= 28, α95=13°, n=6) and B-, (D/I)=212.9°/-80.6°, $\hat{k}$= 27, α95=25, n=5. The palaeomagnetic poles corresponding to the directions are similar to others dated at 2500Ma and are also isolated in a dolerite dykes, dated by Layer et al., (1998) at 1902±6 Ma, leading the authors to interpret the magnetisation to be post-Archaean in age, likely Proterozoic, which affected a large proportion of the Kaapval Craton.

7.4.1.1 LNP3-5

7.4.1.1.1 LNP4

The overprint direction isolated from LNP4 was plotted against the B+ and B- directions of Layer et al., (1998) –the reasoning for this approach being that as an overprint direction, it cannot be compared to the ca.3.2Ga A+ and A- direction which is always present as a primary direction in the Layer et al., (1998) study. The equal area projection in Figure 7.12

shows that directions means for B+ and B- and overprint direction do not overlap, but their α95 confidence limit envelopes do. Therefore it was necessary to perform a common true mean test for randomness to statistically compare the directions and establish if they are distinguishable from one another. The test gave a negative results, indicating the two directions do not share a common mean and are distinguishable from one another. It should be noted that the α95 confidence limit envelope for the mean calculated from samples in

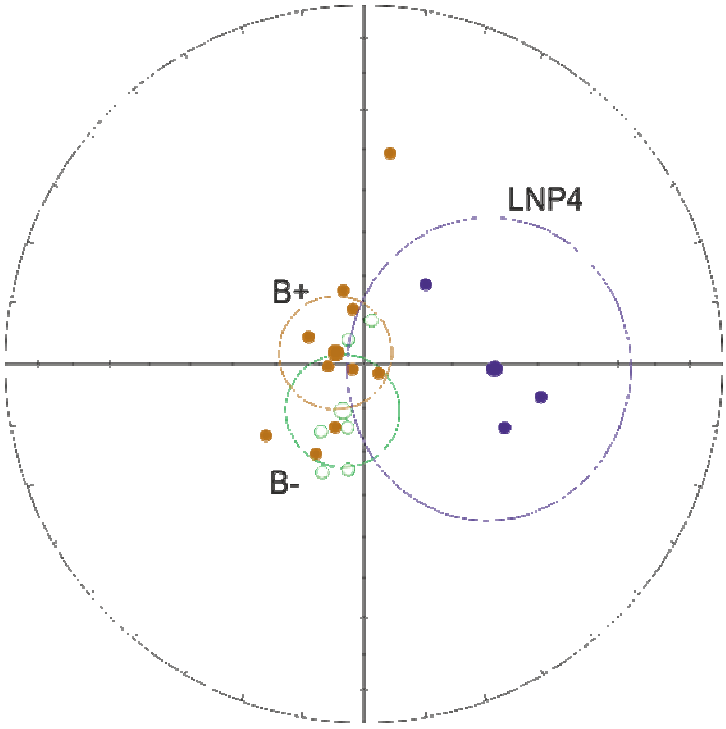

Figure 7.12. Equal area projections showing Layer et al., (1998) B+ and B- directions, as well as site LNP4 overprint direction. Directions means for B+ and B- and overprint direction do not overlap, but their α95 confidence limit envelopes do. Therefore it was necessary to perform a common true mean test for randomness to statistically compare the directions and establish if they are distinguishable from one another.

LNP4 is large, owing to the small number of samples used to calculate the mean. It is likely that with a larger sample set, the α95 confidence limit envelope would decrease, in which case the direction would be clearly distinguishable from the Layer et al., (1998) directions.

7.4.1.1.2 LNP3 and LNP5

As the mean directions for sites LNP3 and LNP5 are isolated from high temperature components, they were compared to Layer et al., (1998) A+ and A- direction, as well as the antipodal direction of Tarduno et al., (2007) KPV+ and KPV-. As is clearly shown in the equal area plot in Figure 7.13, the α95 confidence limit envelopes of the direction means do not overlap, clearly indicating that the directions are distinguishable from one another.

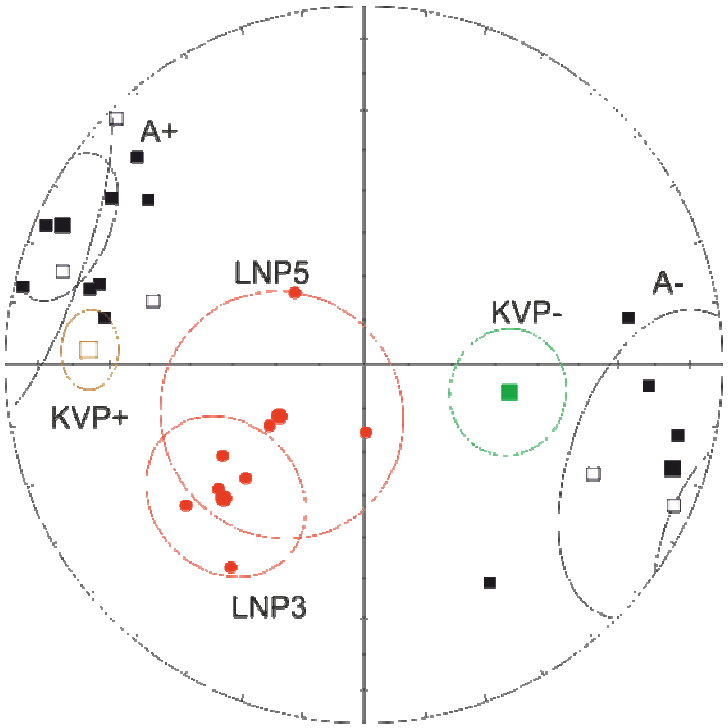

Figure 7.13. Equal area projections showing Layer et al., (1998) A+ and A- directions, as well as Tarduno et al., (2007) Kaap Valley KVP+ and KVP- directions. High temperature site means for LNP3 and LNP5 are shown for comparison. Neither the direction means, nor their α95 confidence limit envelopes overlap, clearly indicating that the directions are distinguishable from one another.

Layer et al., (1998)'s B- direction is south and steep, whilst the LNP3 and LNP5 means are south westerly and of moderate steepness. As the B+ and B- can appear as primary components, it was appropriate to compare the directions. The equal area projection in Figure 7.14, shows that direction mean and the α95 confidence limit envelopes of the overprint directions of site LNP3 do not overlap with the B+ and B- directions. Therefore, the direction isolated from site LNP3 is distinguishable from those of Layer at al., (1998). In the case of site LNP5 the α95 confidence limit envelope does overlap those of the B+ and B- direction and therefore it was necessary to perform a common true mean test for randomness to statistically compare the directions and establish if they are distinguishable from one another. The test gave a negative results, indicating the two directions do not share a common mean and are distinguishable from one another.

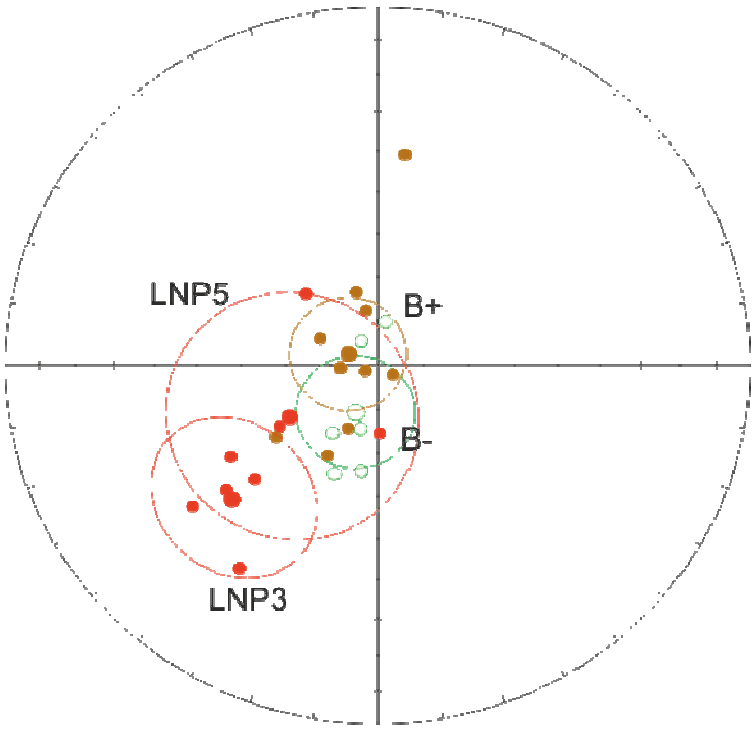

Figure 7.14. Equal area projections showing Layer et al., (1998) B+ and B- directions, as well as site LNP3 and LNP5 high temperature directions. Directions means for B+ and B- and overprint direction do not **overlap, but the α95 confidence limit envelopes of site LNP5 do. Therefore it was necessary to perform a common true mean test for randomness to statistically compare the directions and establish if they are distinguishable from one another. The α95 confidence limit envelope of site LNP3 does not overlap those of Layer et al., (1998) directions and therefore the directions are distinguishable form one another.**

The test for LNP5 gave a negative results, indicating the two directions do not share a common mean and are distinguishable from one another. As was the case for site LNP4, the α95 confidence limit envelopes for the mean calculated from sites LNP3 and LNP5 is large, owing to the small number of samples used to calculate the mean. It is likely that with a larger sample set, the α95 confidence limit envelope would decrease. However, even a significant reduction in the α95 confidence limit envelope for site LNP5 would probably still mean the envelope would overlap with those calculated by Layer et al., (1998) and it would be necessary to perform a common true mean test for randomness to continue to ascertain how statistically distinguishable the directions are.

7.4.1.2 Lightning Struck Sites

Whilst there is evidence that all sites sampled in the NSP as part of this work have suffered the effects of lightning strikes, sites LNP1, LNP2 and LNP6-9 are most clearly affected, given the elevated NRM intensities measured and predominantly single component behaviour observed in the Zijderveld Plots from samples in the sites. In the case of LNP6 and LNP7, whilst NRM intensities are moderate and crucially, comparable to those presented by Layer et al., (1996) for the Kaap Valley Pluton, their proximity to LNP8 and LNP9 and the scattered nature of the directions isolated from them warrants their inclusion in the group of sites affected by lightning.

An approach similar to that taken in the Komati Formation Chapter (Chapter 4), where direction means were calculated, as opposed to site means, might have been appropriate in the case of the NSP sites. Some of the overprint and high temperature directions isolated from the lightning affected sites (mainly LNP6, LNP7 and LNP8) might be comparable, in particular to the B+ and B- directions of Layer et al., (1998), but also to the A+ and A- (see LNP8). However, when comparable directions are seen in the LNP samples, they can appear both as overprint and/or high temperature components within a site, which is not the case in the data of Layer et al., (1998), where they are the high temperature component only [with one exception, where the B- component appeared as an overprint on the A+ component, Layer et al., (1998)]. Crucially, to what extent the samples have been affected by the lightning strikes cannot be accurately quantified and, therefore, it cannot be said with certainty that the few directions that might be similar to those of Layer et al., (1998) truthfully record a magnetisation that is ca. 2500Ma old, or whether the analogous directions are purely coincidental. A larger sample set might assist in clarifying the situation, as it could result in a smaller proportion of samples being affected by lighting and observation of more potentially primary directions.

7.5. Summary

It was not possible to obtain meaningful results from the Nelshoogte Pluton sampled as part of this study.

A single overprint site mean direction was calculated for site LNP4 and a high temperature site mean directions were obtained from sites LNP3 and 5. The LNP4 site mean is not comparable to previously published directions and given the data set is so small it was not viable to calculate a Virtual Geomagnetic Pole (VGP) for comparison with other Kaapval Cra-

ton poles. The direction mean calculated for site LNP3 is not comparable to directions presented in previously published studies by Layer et al., (1998) and Tarduno et al., (2007). Given the limited number of directions obtained when calculating the site mean, it was also not viable to calculate a VGP for comparison with other Kaapval Craton poles.

The remaining six sites were too largely affected by lightning strikes for any meaningful site means to be calculated.

The sampling rationale was driven by the need to increase the available data set and more importantly, the hope to confirm the findings of Layer et al., (1998) that the samples of the LNP record a reversing magnetic field at ca. 3.2Ga. In order to achieve this, it was important to sample localities not previously studied, to ascertain results were robust over a wide geographical area. For this reasons the outcrops of sites LNP1 and 2 were chosen. Layer et al., (1998) found access to the northern part of the NSP difficult and they carried out limited sampling in this area. In addition, it was important to select spots/locations/ sites in relatively close proximity to those sampled by Layer et al., (1998) to establish if their results were reproducible.

However, the exposed position of some the sampling sites: LNP1, LNP2 and LNP6-9 in particular, meant that lightning strikes could not be ruled out. In order to minimise the likelihood of sampling sites which had been lightning struck, we were careful not to sample outcrop tops and focused on the bases of outcrops which were less exposed (where these were present). In addition, collection of samples was distributed over larger areas than usual, with significant spacing between samples (between 1-4m), when possible.

Despite the effort to minimise the likelihood of sites being influencedby lightning strikes, the results show that the magnetic signal recorded by the rocks of the NSP is significantly affected. The number of samples collected in the NSP and the wide spacing between them mean that in some cases (e.g. LNP5) the effects of lightning strikes on the quality of the data has been mitigated to some extent. However, in other cases (LNP1 and LNP9, for example) it significantly obscures any primary signal that the rocks might have otherwise recorded. Wider spacing of sampling sites, particularly in the case of samples LNP6-9, as well as increasing the number of locationssampled might have gone some way to minimise the effects of potential lightning strikes. In addition, attempts to sample more localities might further reduce the risk of primary signals being overprinted by lightning strikes.

However, this would require a considerable amount of preparation work and would benefit from working with a local collaborator, in order to establish relationships with the landowners in the area of the NSP, who might allow access to otherwise inaccessible sampling sites.

A small proportion of the total sample set was measured using a combined thermal (TH) and alternating field (AF) demagnetisation technique. The advantage of this technique is that secondary magnetisation is fully removed by the thermal steps. However, it is in the samples where the combined methodology was used that more multi-component directions are isolated in the Zijderveld Plots. In some instances, distinguishing the overprint and high temperature components was not always straightforward due to the components overlapping, e.g. LNP6.3b. Overall, thermally demagnetised samples do not appear to resolve potentially overlapping components as well as the combined technique does. The combined technique has yielded positive results in other studies of Onverwacht Group samples (Biggin et al., 2011). Layer et al., (1998) also employ a largely AF demagnetisation technique and only a limited sample set is demagnetised using thermal techniques.In future, it would be advantageous to employ the combined methodology on a large proportion of obtained samples in order to increase the likelihood of producing clean Zijderveld Plots.

The success and promising results of the work of not only of Layer et al., (1998) in the Nelshoogte Pluton, but other palaeomagnetic work carried out in the TTG terrain of the BGB (discussed in detail in the introduction to this chapter), means further study of the rocks of the NSP is encouraged. Despite the results presented in this chapter not adding to the work of Layer et al., (1998), the opportunity to confirm a magnetic reversal in the Archaean means the reasons to study the palaeomagnetism of the rocks of the Nelshoogte Pluton, and indeed its neighbouring TTG terrain, remain valid and should be pursued.

Further sampling of the bed of the Gladdespruit River, past Layer's sampling sites 14-17 and the Gladdespruit River tributary to the North, past Layer's sites 33-34 would increase the geographical extent of the present data set, whilst still being relatively accessible via dirt tracks. However, it is likely the area covers sections of private land, necessitating permission to access the sites from the landowners. The Gladdespruit carves out a small valley and so sites along the river bed may be offered some protection from lightning strikes. During the field work, we attempted to sample the sites 1-11 of Layer et al., (1998), but

these now form part of land associated with the Vygeboom Dam and we were unable to secure access to the site. The same is true of sites 22-25, which now belong to a privately owned estate. Despite attempting to drill the site, the landowner was unwilling to cooperate. Re-sampling of these locations would allow for the findings of Layer et al., (1998) to be validated whilst at the same time adding to the existing dataset. Our experiences in the area of the Nelshoogte Pluton highlight the importance of establishing good working relationships with the local community prior to and during any future palaeomagnetic investigations in order to access the largest number of sites possible.

8 Conclusion

8.1. Overall Conclusions

The work presented in this thesis has highlighted the difficulties of trying to obtain a robust record of the direction of the geomagnetic field during the Archean Aeon. Four formations of the Onverwacht Group of the BGB were studied with mixed results. Despite the complications that result from the study of rocks of this age the new palaeomagnetic data presented here, following detailed rock magnetic, microscopy and directional investigations, indicate the existence of a stable geomagnetic field at ca. 3.4Ga.

Palaeomagnetic results presented from samples collected from the Noisy Complex and Nelshoogte Pluton were inconclusive given the primary magnetic signal was obscured by the effects of lightning induced IRMs. These results in particular continue to highlight the difficulties associated with working with rocks of Archaean age, especially when collected in thunderstorm prone areas. Despite these disappointing findings, previous studies of both Formations have yielded encouraging and also exciting palaeomagnetic results. Results which may have contributed to those previous studies might have also been obtained from the samples studied here had they not been lighting struck and therefore do not discourage further palaeomagnetic investigation into both the Noisy Complex and Nelshoogte Pluton.

The rocks of the Komati Formation provide further support for the validity of the world's oldest pole and have strengthened the findings of previous studies by decreasing the uncertainty associated with the already published pole, aged 3472-3482 Ma. The age of the magnetisation is further confirmed as it is only observed in the Komati Formation komatiites and not in the younger intrusive units also sampled as part of this work dated at 3.2Ga (Kamo and Davis, 1994) but which are potentially as old as 3.4Ga. In addition, new antipodal directions are obtained from the Komati Formation. The age is not well constrained as the performed baked contact tests were inconclusive and the age of the majority of the dykes used in the tests are unknown. However, given the age and geological correlations between the sampled dykes and the Stolzburg, Doorhoek and Theespruit plutons, one possibility is that the directions are ca. 3450Ma in age. However, this interpretation is difficult to reconcile with the proposed stable field and modest drift rates from the comparison of the KOM and HT poles. Without constraining the age of the directions via direct dating of the dykes and/or field stability tests, ages attributed to the direction

are somewhat speculative and should be considered with caution. The limited dataset and quality of the results preclude any further discussion regarding the implications of the antipodal directions with regards to geodynamo and inner core structure during the Archaean. Nevertheless, they highlight the possibility of successful results should further research be conducted and provide a framework in which these results can be interpreted.

The palaeomagnetic investigation of volcanic units of the Hooggenoeg Formation show that interpretation of the results obtained from Archaean aged rocks is far from straightforward. Previous studies of the formation have focused on the southern limb of the Onverwacht Fold; here we also sample the northern limb of the Onverwacht fold to take advantage of the opportunity that offers to carry out field stability tests which can contribute towards constraining the age of the isolated directions, both in this study and previously published works. The existence of a mid temperature component of ca 2.7Ga (Biggin et al., 2011) is confirmed by the work presented here. After acquiring data from both sides of the Onverwacht fold, this study confirms that the magnetisation was acquired after the formation of the OF at 3.2Ga. Whilst the presence of a previously published high temperature component HT1 is also confirmed by the findings of this work, the error envelope is increased meaning the results are less reliable than previously thought. A final high temperature component is identified in the rocks of the Hooggeneog Formation, HT2N, from the northern limb of the fold. It's similarity to the MT direction mentioned above cannot be ignored. The implication being that the MT direction could overprint the post 2.7Ga magnetic signal in the northern limb of the fold. If this is the case, then the source of the HT2S magnetisation identified in a previous study is unknown and casts some doubt over the interpretations. However, it is argued that the HT2N direction is in fact distinct from the MT direction. When compared to previously published results which identify the HT2S direction in the southern limb of the fold, clustering of the directions is seen to increase once a tectonic correction is applied. This results in a positive fold test for the HT2 direction. As the age of formation of the fold is thought to be ca 3.2Ga, the minimum age of component is at least synchronous with the formation of the fold. The new VGP calculated for the HT2 component places the BGB at equatorial latitudes at the time of the acquisition of the HT2 magnetisation.

Using the newly obtained poles for the Komati and Hoggeneog Formations it is possible to make some inferences on the palaeogeography during the Archaean Aeon. When com-

pared to poles of similar ages from rocks from the Pilbara Craton (Western Australia) the error bounds of the poles are seen to overlap and therefore tentatively support the hypothesis that the Pilbara Craton and the Kaapvaal Craton may have been conjoined at ca. 3.5-3.2Ga. This is in agreement with the results of a previous study which considered the poles in the same manner. Nevertheless, the results are far from conclusive given the loose fit of the poles and the issues associated with result quality address throughout this thesis.

8.2. Implication of Findings for the Early Earth

In this section, the findings of the palaeomagnetic investigations of the Komati and Hooggenoeg Formations will be placed into the wider context of Archaean Aeon.

As a result of the inconclusive nature of the findings of the reversal test of the Komati Formation and its very tentative suggestion of a reversing geomagnetic field, it would be unwise to advocate for the presence of a dipolar field in the Archean. Even if reversals were established, this would not necessarily imply that the field was dipolar. The only real way to get a handle on whether GAD holds is by comparing palaeomagnetic and palaeoenvironmental data sets (see e.g. Evans, 2006, Nature). The results are intriguing and encouraging and have the potential to contribute towards the understanding of the activity in the conducting liquid core at this early stage of the Earth's history. The same remains true for the Nelshoogte and Kaap Valley Plutons (Layer et al., 1996; Layer et al., 1998; Tarduno et al., 2007). Given the presence of antipodal directions in the published data sets, the results provide tentative evidence of a reversing field. One of the main reasons for sampling the Nelshoogte Pluton was to validate the findings of Layer et al., (1998) and potentially contribute towards the discussion on the operation of the geodynamo at this time. However, the results were too significantly affected by lighting induced IRMs to contribute meaningful data that might allow for further discussion on this subject. Therefore, as it the case with the Komati Formation, further study of the Nelshoogte Pluton is encouraged, but taking into consideration the sampling recommendations made in Chapter 7.

Given the unreliable directional results obtained from the Noisy Complex and Nelshoogte Pluton, these will not be considered further. However, the results presented in the Komati Formation and Hooggenoeg chapters can contribute towards developing the understanding of the palaeogeography of the Archaean. In order to discuss the implications of the directional results obtained, it is assumed that the geocentric axial dipole (GAD) model

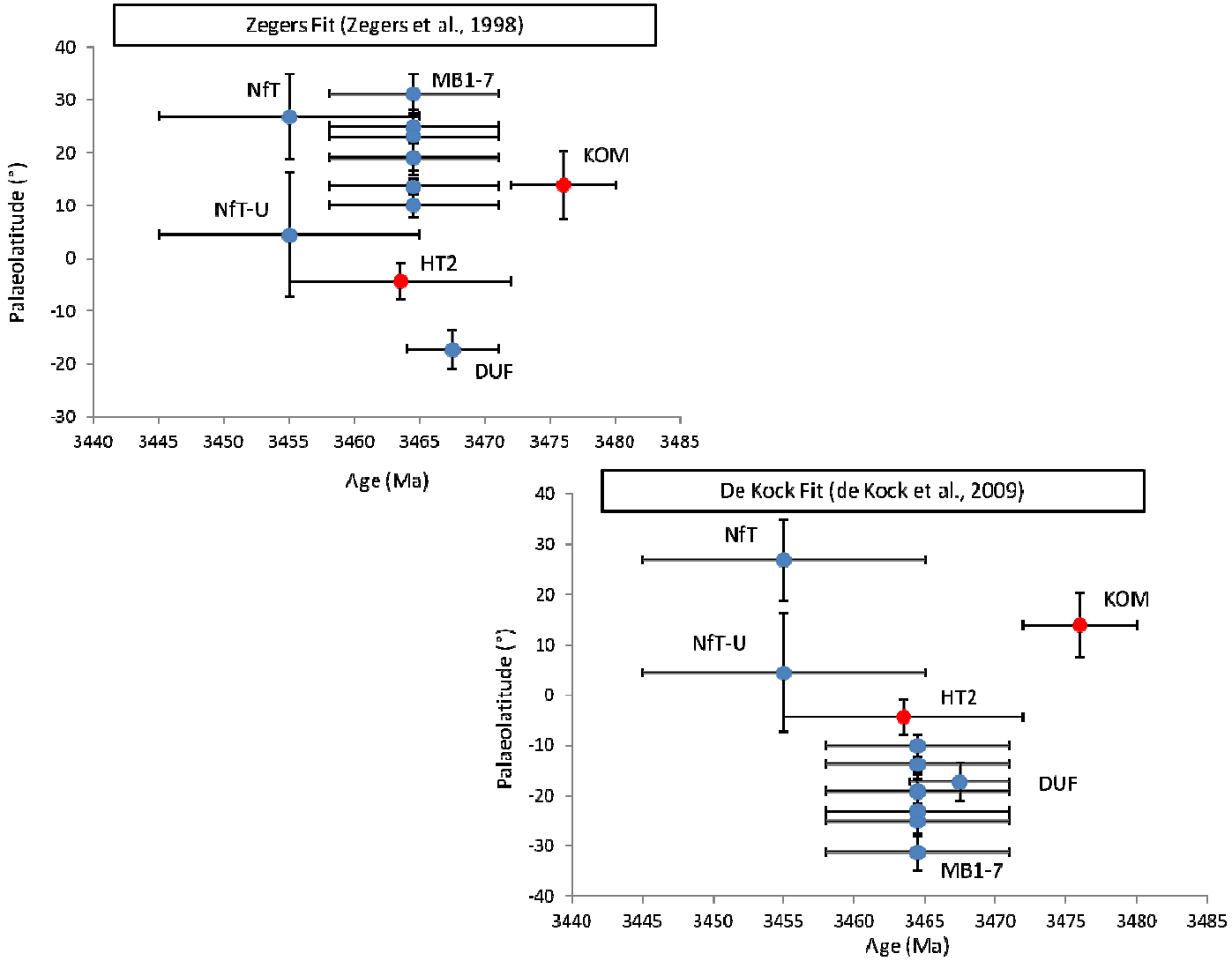

Figure 8.1. Tests of two previously proposed configurations of the Vaalbara supercontinent (de Kock et al., 2009; Zegers et al., 1998) comparing absolute palaeolatitudes from BGB (red) Pilbara (blue). Note that the darker red points are taken from Biggin et al., (2011) and the brighter red points correspond to the new palaeolatitudes from BGB calculated as part of this work. Note also that the polarities for the Pilbara Craton poles are reversed. Figure based on Biggin et al., (2011).

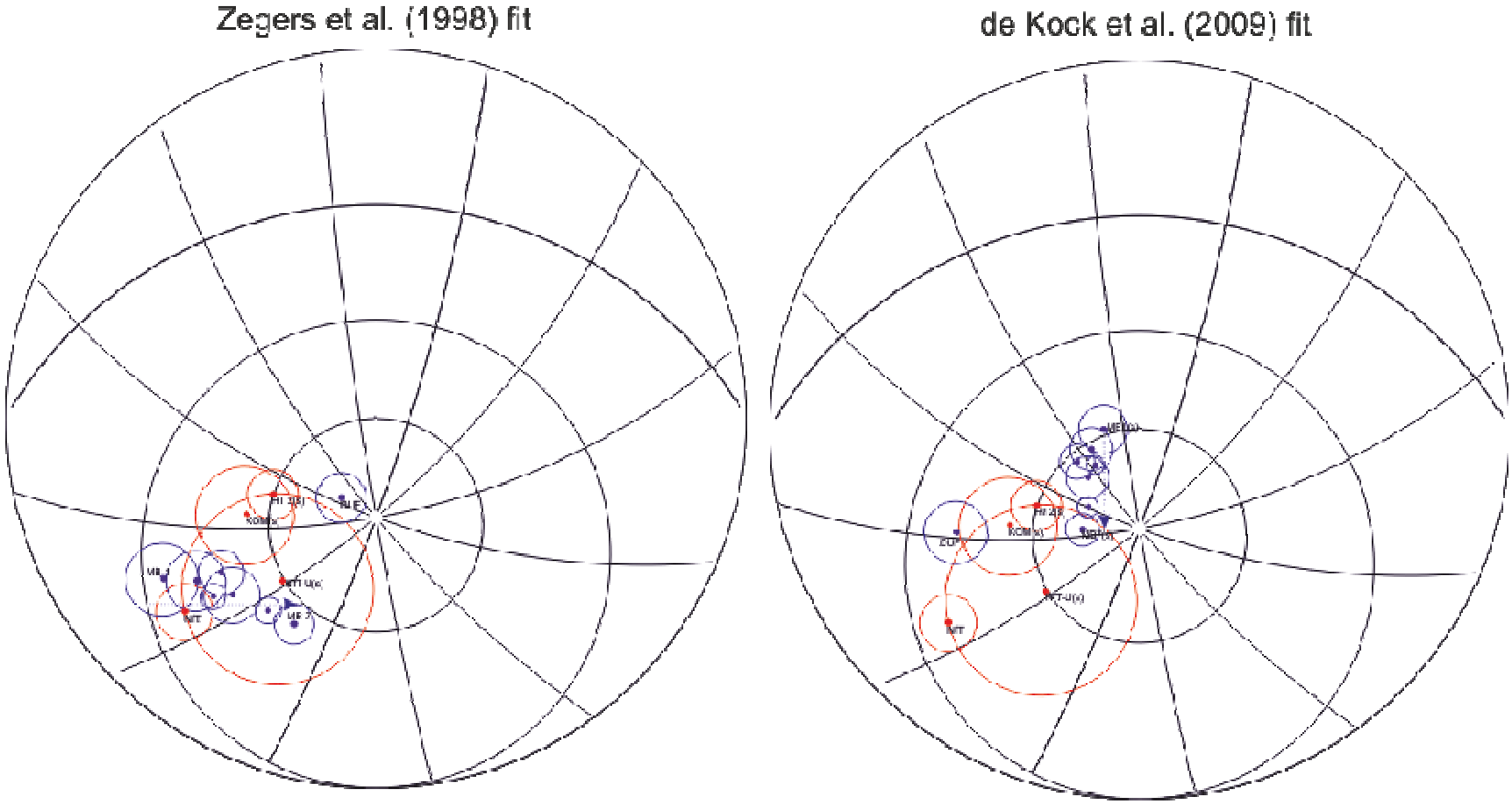

Figure 8.2. Comparisons of poles from the Kaapval Craton (red) and Pilbrara Craton (blue), (north unless marked with an S) after the Euler rotations were applied (Zegers et al., 1998; Euler pole =28.1°, N256.5°, angle= 177.1°; de Kock et al., 2009: Euler pole =52.0°, N71.4°, angle= -90.8°) to the Pilbara poles. The projections were produced using GMAP software (Torsvik and Smethurst, 1999).

holds true, even in the Archean. This is not an unreasonable assumption as GAD theory validity is supported for the past 2 Gyr by global palaeoclimatic–palaeomagnetic data (Evans, 2006). It is further supported by theoretical studies which provide no evidence to suggest it would not hold true in deep geological time(Roberts and Glatzmaier, 2001).

Of particular relevance to the results presented here is the Vaalbara theory (see Chapter 2 for further detail). The new palaeolatitudes calculated for the Komati Formation and Hooggenoeg Formation can contribute to the debate of a) whether Vaalbara existed at all and b) which of the two proposed fits (de Kock et al., 2009; Zegers et al., 1998) for the Kaapvaal and Pilbara Cratons is most likely. The new palaeolatitudes identified for the poles of the Hooggenoeg and Komati Formations are comparable to those presented by Biggin et al. (2011) and cluster well with the NfT and NfT-U poles of Biggin et al., (2011). For further discussion and details on these poles see Chapters 4, 5 and 6, as well as Biggin et al., (2011), see also the average poles presented in Chapter 7. Palaeolatitudes calculated by Biggin et al., (2011) range between -22° and 36°. The new poles for the Hooggenoeg Formation and Komati formation do not contribute to reduce this range, as the limits are defined by the NfT and NFT-U poles. Net latitudinal rates of drift calculated using the new poles presented here remain limited and constrains the Kaapval Craton to equatorial latitudes in the Archean, supporting the findings of Biggin et al., (2011). The new Hooggenoeg Formation pole for HT2, along with the results of Biggin et al., (2011) continue to represent the most rapid latitudinal rate of drift shown by the data set, but is decreased somewhat given the new HT2 pole moves northwards towards a more equatorial latitude (see Figure 8.1a), when compared to the results of Biggin et al., (2011). Given the average 9 Myr difference in age estimates between the HT2 and NfT units, the ~1100 km motion and latitudinal velocity of ca.12 cm/year proposed by Biggin et al., (2011) are supported. This is comparable to the lowest rates suggested by Suganuma et al., (2006) and Klootwijk et al., (1992).

In Figure 8.1, a and b, the palaeolatitudes calculated from the inclination of the directions means, used to also establish the VGP poles, are shown in relation to the similarly aged Duffer Formation (DUF; 3470±6 Ma; (McElhinny and Senanayake, 1980; McNaughton et al., 1993) and Marble Arch Chert (MB; 3456–3476 Ma (McNaughton et al., 1993; Suganuma et al., 2006), of the Pilbara Craton in western Australia, and are plotted against the BGB VGPs from this study (HT2 and KOM) as well as NfT and NfT-U, following the approach taken by Biggin et al., (2011); see Chapter 5, for further details. The aim is to compare the palaolati-

tudes from both Cratons and establish if there is sufficient overlap to consider the existence of the Vaalbara supercontinent. As seen in the Figure 8.2, the BGB palaeolatitudes are within error of the Pilbara Craton poles, displaying a similar fit as established previously by Biggin et al., (2011), with the overlap remaining stronger when the antipodes of the Australian poles are taken. This tentatively favours the fit proposed by Zegres et al. (1998), where the Pilbara is located towards the east of Kaapvaal Craton. These results support the findings of Biggin et al., (2011) and continue to cautiously suggest the existence of the Vaalbara supercontinent at ca. 3.5Ga, some 600-700Myr older than suggested by other palaeomagnentic data.

However, as was the case with the findings of Biggin et al., (2011) the uncertainty associated with the directions established means these results should not be considered conclusive and encourage further work in this area. The poles from the Pilbara Craton have come under scrutiny with regards to the origin of the magnetisation carried by the volcanic rocks, as suggested Usui et al.,(2009), please see Chapter 4 for further discussion on this. Of course, the same consideration needs to be given to the source of the magnetisation in this study. Furthermore, the newly calculated HT2 pole is used in the discussion above, but as highlighted in Chapter 7, may well not be a reliable ChRM direction, but rather an overprint of ca. 2.7Ga. If this is true, then the only contribution this project can make to Archean palaeogeography is the KOM pole, which on its own is insufficient to add considerably to the debate on either of the fundamental questions regarding the existence and configuration of the Vaalbara supercontinent.

8.3. Further Work

Whilst the work presented here indicates that the rocks of the Barberton Greenstone Belt have the potential to record a magnetic field of ca. 3.2Ga, given their complex thermochemical history and age means accurately constraining the age of the magnetisation and reaching robust interpretations remains problematic.

The palaeomagnetic study of the Komati Formation has been focused on the northern limb of the Onverwacht fold. This may be partly due to the fact that exposure on the southern limb is limited due to tight folding and thinning of the volcanic units. In this study only six surface sites were sampled, which represents a relatively limited data set given the potential for lighting strikes and weathering to have affected the signal held by the rocks. Additional sampling in the hinge and southern limb of the OF would not only allow for investi-

gation of whether the results presented here and those of Yoshihara and Hammano (2004) are reliable over a wide geographical extent, but would also allow for a full fold test to be carried out. A positive fold test would further constrain the age of the StW/Kom direction identified. This study benefited from access to the BARB/ICDP cores. When the samples were collected in July 2011 the understanding of the volcanic textures, geochemistry and overall geology of the cores was at very preliminary stages. Sampling was targeted at units which had the potential to give good results (based primarily on the findings of Yoshihara and Hamano, (2004) and comparison with drill core logs) or which provided candidates for field stability tests. The palaeomagnetic understating of the cores has developed as a result of the work presented here; combined with advances in the understanding of the geochemistry and its implications for komatiite emplacement, (as a result of the work of the collaborators of the BARB projects), further sampling of promising and targeted units, (particularly in BARB2 where samples were collected from four sites only), would no doubt contribute to the reliability of results for the Komati Formation. Work to determine the age of the ShW/ShE direction is critical. The results tentatively point towards a reversing magnetic field at this time, which if more reliably constrained would allow us to make inferences of the structure of the Earth's magnetic field and the geodynamo. Therefore, dating of the dykes in the BARB cores in particular would hugely benefit the results presented in this work. Furthermore, a better understanding of the geochemistry of the dykes and their relation to the surrounding TTG terrain would provide an indirect age relationship which would go some way towards establishing an age for the ShE/ShW direction. Finally, the reversed drilling overprint direction is intriguing and might indicate some of the samples studied have the potential to self-reverse. This was only briefly explored during this PhD on a very limited sample set (six samples). If further access to the BARB cores were granted, it is recommend to collect samples to further investigate this issue.

The rocks of the Hooggenoeg Formation also reveal interesting results but further paleomagnetic work would be beneficial in order to clarify the findings presented here. In particular, further sampling of the northern limb of the OF is recommended. Samples as part of this work were collected, in the northern OF, from two, relatively nearby areas and it would be of interest to see if the clear directional and rock magnetic differences between samples of the southern and northern limbs of the fold are wide spread or purely coincidental. To this effect, further microscopy work, including further detailed electron microscopy is recommended in order to better understand the opaque mineralogy across the Hooggenoeg. This should be complimented with further rock magnetic characterisation to

better define the rock magnetic carriers. The rock magnetic interpretations presented here were hampered by the predominance of the paramagnetic signal in the majority of the samples studied. Kappa Bridge results were somewhat more informative than the VFTB experiments, but only one sample from each site was studied. The work presented here would benefit from further Kappa Bridge experiments. Further studies may consider alternative rock characterisation methods such as the use of a MicroMag Measurements Vibrating Sample Magnetometer (VSM) with high and low temperature capabilities and characterisation of grain size of magnetic carriers via first order reversal curves (FORC). Although these alternatives would not guarantee better results given the strong paramagnetic contribution of the samples it would be worthwhile exploring on a small initial sample set at least.

The results from the Noisy Complex and Nelshoogte Pluton are significantly affected by lighting induced IRMs and reflect the difficulties that arise from working in a storm prone area such as the BGB. Nevertheless, there is potential for good directional results to be obtained from both of the units as demonstrated in the literature and this alone should encourage further palaeomagnetic research of both Formations. Chapters 6 and 7 offer detailed discussions on alternative sampling locations in both the Noisy Complex and the Nelshoogte Pluton which could potentially yield better quality results than those obtained here. In the case of the Pluton, and this too is discussed in detail in Chapter 7, it is important to establish a good working relationship with the local community in order to be granted access to otherwise inaccessible and unknown exposures (sites LNP6-9 were chosen only after a local land owner pointed out their existence).

During the sampling of the BARB cores in July 2011, not only were samples collected from the two Komati Formation cores, but also from cores BARB3 (which samples the Buck Reef Chert, at the contact between the Hooggenoeg Formation and the Kromberg Formation) and BARB4 (which samples the upper most units of the Onverwacht Group and a proportion of the sediments of the overlying Fig Tree Group). Five sites were drilled in the BARB3 and BARB4 cores. Selected samples were demagnetised but no interpretation of the results was made, nor was any rock magnetic characterisation carried out, as a result of time constraints of the PhD. However, completion of this work is recommended as results from BARB4 might add to the discussion of the results presented for the Hooggenoeg Formation. With palaeomagnetic research of the BGB so far focusing primarily on the volcanic rocks of the Onverwacht Group, there are no published palaeomagnetic studies from the

Fig Tree Group yet available. The samples taken from the uppermost part of the BARB4 core, if successful, would represent the first palaeomagnetic directions obtained from sedimentary rocks of the BGB. In addition, the new dataset, again assuming reliable directions were obtained from the samples, might further contribute to the discussion regarding the configuration of Vaalbara and its existence prior to 2.7Ga.

9 References

Abbott, D. H., W. D. Mooney, and J. A. VanTongeren, 2013, The character of the Moho and lower crust within Archean cratons and the tectonic implications: Tectonophysics, v. 609, p. 690-705.

Allaby, A., and M. Allaby, 2003, Oxford dictionary of Earth Sciences, Oxford University Press Oxford, pp. 654.

Anhaeusser, C. R., 2010, Magmatic and structural characteristics of the ca. 3440 Ma Theespruit pluton, Barberton Mountain Land, South Africa: American Journal of Science, v. 310, p. 1136-1167.

Anhaeusser, C. R., and L. J. Robb, eds., 1983, Geological and geochemical characteristics of the Heerenveen and Mpuluzi batholiths south of the Barberton greenstone belt and preliminary thoughts on their petrogenesis.: Contributions to the Geology of the Barberton Mountain Land., v. 9, Special Publication of the Geological Society of South Africa, Johannesburg, p.223.

Armstrong, R. A., W. Compston, M. J. Dewit, and I. S. Williams, 1990, The stratigraphy of the 3.5-3.2Ga Barberton Greenstone-Belt revisited—A single Zircon Ion Microprobe Study: Earth and Planetary Science Letters, v. 101, p. 90-106.

Arndt, N., 2003, Komatiites, kimberlites, and boninites: Journal of Geophysical Research: Solid Earth, v. 108, B6, p. 2293 (ECV 5-1 to ECV 5-11).

Arndt, N., C. Ginibre, C. Chauvel, F. Albarède, M. Cheadle, C. Herzberg, G. Jenner, and Y. Lahaye, 1998, Were komatiites wet?: Geology, v. 26, p. 739-742.

Arndt, N., M. C. Lesher, and S. J. Barnes, 2008, Komatiite, Cambridge University Press, Cambridge, pp.467.

Aubert, J., S. Labrosse, and C. Poitou, 2009, Modelling the palaeo-evolution of the geodynamo: Geophysical Journal International, v. 179, p. 1414-1428.

Bédard, J. H., 2006, A catalytic delamination-driven model for coupled genesis of Archaean crust and sub-continental lithospheric mantle: Geochimica et Cosmochimica Acta, v. 70, p. 1188-1214.

Belcher, R. W., A. F. M. Kisters, M. Poujol, and G. Stevens, 2005, Structural emplacement of the 3.2 Ga Nelshoogte Pluton: implications for the origin of dome-and-keel structures in the Barberton granite greenstone terrain, Geo 2005 conference abstracts, Durban, South Africa, p. 14. .

Berry, A. J., L. V. Danyushevsky, H. St C. O'Neill, M. Newville, and S. R. Sutton, 2008, Oxidation state of iron in komatiitic melt inclusions indicates hot Archaean mantle: Nature, v. 455, p. 960-963.

Beswick, A. E., 1982, Some geochemical aspects of alteration and genetic relations in komatiitic suites: Komatiites, p. 147-157.

Biggin, A. J., G. H. M. A. Strik, and C. G. Langereis, 2008, Evidence for a very-long-term trend in geomagnetic secular variation: Nature Geoscience, v. 1, p. 395-398.

Biggin, A. J., Strik, G.H.M.A and Langereis, C.G., 2009, The intensity of the geomagnetic fiels in the late-Archean: new measurements and an analysis of the updated IAGA palaeointensity database: Earth Planets Space, v. 61, p. 9-22.

Biggin, A. J., M. J. de Wit, C. G. Langereis, T. E. Zegers, S. Voûte, M. J. Dekkers, and K. Drost, 2011, Palaeomagnetism of Archaean rocks of the Onverwacht Group, Barberton Greenstone Belt (southern Africa): Evidence for a stable and potentially reversing geomagnetic field at ca. 3.5Ga: Earth and Planetary Science Letters, v. 302, p. 314-328.

Bontognali, T. R. R., W. W. Fischer, and K. B. Föllmi, 2013, Siliciclastic associated banded iron formation from the 3.2 Ga Moodies Group, Barberton Greenstone Belt, South Africa: Precambrian Research, v. 226, p. 116-124.

Brandl, G., and M. J. de Wit, 1997, The Kaapval Craton, South Africa. In: de Wit, M.J., Ashwal, L.D. (Eds.), Greenstone Belts. Clarendon Press, Oxford, pp. 581.

Butler.R.F, 1992, Paleomagnetism: Magnetic Domains to Geological Terranes., Blackwell Scientific publications, pp. 319

Byerly, G. R., D. R. Lowe, B. W. Nocita, and B. L. Ransom, 1983, Apparent volcaninc cycles in the Archean Swaziland Supergroup, Barberton Mountain Land, South Africa: a result of non-magmatic processes: Lunar and Planetary Science XIV, P. 84-85. Abstract.

Byerly, G. R., A. Kröner, D. R. Lowe, W. Todt, and M. M. Walsh, 1996, Prolonged magmatism and time constraints for sediment deposition in the early Archean Barberton greenstone belt: evidence from the Upper Onverwacht and Fig Tree groups: Precambrian Research, v. 78, p. 125-138.

Campbell, I. H., R. W. Griffiths, and R. I. Hill, 1989, Melting in an Archaean mantle plume: heads it's basalts, tails it's komatiites: Nature, v. 339, p. 697-699.

Cheney, E. S., 1996, Sequence stratigraphy and plate tectonic significance of the Transvaal succession of southern Africa and its equivalent in Western Australia: Precambrian Research, v. 79, p. 3-24.

Coe, R.S., 1967, Paleo-intensities of Earths magnetic field determined from Teriary and Quaternary rocks, Journal of Geophysical Research, 72, p. 3247—3262.

Cloete, M., 1991, An overview of metamorphism in the Barberton greenstone belt: Two Cratons and an Orogen—Excursion Guidebook and Review Articles for a Field Workshop through Selected Archean Terranes of Swaziland, South Africa and Zimbabwe, p. 84-98.

Cloete, M., 1999, Aspects of volcanism and metamorphism of the Onverwacht Group lavas in the southwestern portion of the Barberton Greenstone Belt, Council for Geoscience (Geological Survey of South Africa), Johannesburg, pp. 232.

Coetzee, G., 2014, Petrology and Geochemistry of the Tjakastad (Barberton) ICDP Cores, M.Sc. Thesis, University of Witwatersrand, Johannesburg, pp. 212.

Condie, K. C., 1981, Archean Greenstone Belts, Elsevier Scientific Publishing, Amsterdam, pp.434.

Cottrell, R. D., and J. A. Tarduno, 2000, In search of high-fidelity geomagnetic paleointensities: A comparison of single plagioclase crystal and whole rock Thellier-Thellier analyses: Journal of Geophysical Research: Solid Earth, v. 105, p. 23579-23594.

Dann, J. C., 2000, The 3.5 Ga Komati Formation, Barberton Greenstone Belt, South Africa, Part I: New maps and magmatic architecture: South African Journal of Geology, v. 103, p. 47-68.

Davies, C. J., 2009, Assessing the Effect of Mineral Alteration on Palaeointensities Derived from Volcanic Rocks of Cretaceous Age, Ph.D. Thesis, University of Liverpool, Liverpool, pp. 262.

Day, R., M. Fuller, and V. A. Schmidt, 1977b, Hysteresis properties of titanomagnetites: Grain-size and compositional dependence: Physics of the Earth and Planetary Interiors, v. 13, p. 260-267.

de Kock, M. O., D. A. D. Evans, and N. J. Beukes, 2009, Validating the existence of Vaalbara in the Neoarchean: Precambrian Research, v. 174, p. 145-154.

de Ronde, C. E. J., and M. J. de Wit, 1994, Tectonic History of the Barberton greenstone belt, South Africa: 490 million years of Archean crustal evolution: Tectonics, v. 13.

de Ronde, C. E. J., and S. L. Kamo, 2000, An Archaean arc-arc collisional event: A short-lived (ca 3 Myr) episode, Weltevreden area, Barberton greenstone belt, South Africa: Journal of African Earth Sciences, v. 30, p. 219-248.

de Ronde, C. E. J., S. Kamo, D. W. Davis, M. J. de Wit, and E. T. C. Spooner, 1991, Field, geochemical and U-Pb isotopic constraints from hypabyssal felsic intrusions within the Barberton greenstone belt, South Africa: Implications for tectonics and the timing of gold mineralization: Precambrian Research, v. 49, p. 261-280.

De Vries, S. T., 2004, Early Archaean sedimentary basins: depositional environment and hydrothermal systems; examples from the Barbeton and Coppin Gap Greenstone Belts, v. 244, Faculteit Aardwetenschappen Universiteit Utrecht.

de Vries, S. T., and J. L. R. Touret, 2007, Early Archaean hydrothermal fluids; a study of inclusions from the approximately 3.4 Ga Buck Ridge Chert, Barberton greenstone belt, South Africa: Chemical Geology, v. 237, p. 289-302.

de Vries, S. T., W. Nijman, and R. A. Armstrong, 2006, Growth-fault structure and stratigraphic architecture of the Buck Ridge volcano-sedimentary complex, upper Hooggenoeg Formation, Barberton Greenstone Belt, South Africa: Precambrian Research, v. 149, p. 77-98.

de Wit, M. J., 1991, Archaean greenstone belt tectonism and basin development: some insights from the Barberton and Pietersburg greenstone belts, Kaapvaal Craton, South Africa: Journal of African Earth Sciences (and the Middle East), v. 13, p. 45-63.

de Wit, M. J., 1998, On Archean granites, greenstones, cratons and tectonics: does the evidence demand a verdict?: Precambrian Research, v. 91, p. 181-226.

de Wit, M. J., 2004, Archean Greenstone Belts Do Contain Fragments of Ophiolites, v. 13, p. 599-614.

de Wit, M. J., and L. D. Ashwal, 1995, Greenstone belts; what are they?: South African Journal of Geology, v. 98, p. 505-520.

de Wit, M. J., R. Hart, A. Martin, and P. Abbott, 1982, Archean abiogenic and probable biogenic structures associated with mineralized hydrothermal vent systems and regional metasomatism, with implications for greenstone belt studies: Economic Geology, v. 77, p. 1783-1802.

De Wit, M. J., R. E. P. Fripp, and I. G. Stanistreet, 1983, Tectonic and stratigraphic implications of new field observations along the southern part of the Barberton greenstone belt: Spec. Publ. Geol. Soc. S. Afr, v. 9, p. 21-29.

de Wit, M. J., Hart, R.A. and Hart, R.J., 1987, The Jamestown Ophiolite Complex, Barberton mountain belt: a section through 3.5 Ga oceanic crust: Journal of African Earth Sciences, v. 6.

de Wit, M. J., C. E. J. de Ronde, M. Tredoux, C. Roering, R. J. Hart, R. A. Armstrong, R. W. E. Green, E. Peberdy, and R. A. Hart, 1992, Formation of an Archaean continent: Nature, v. 357, p. 553-562.

de Wit, M. J., H. Furnes, and B. Robins, 2011, Geology and tectonostratigraphy of the Onverwacht Suite, Barberton Greenstone Belt, South Africa: Precambrian Research, v. 186, p. 1-27.

Denyszyn, S. W., J. M. Feinberg, P. R. Renne, and G. R. Scott, 2013, Revisiting the age and paleomagnetism of the Modipe Gabbro of South Africa: Precambrian Research, v. 238, p. 176-185.

Diener, J. F. A., G. Stevens, A. F. M. Kisters, and M. Poujol, 2005, Metamorphism and exhumation of the basal parts of the Barberton greenstone belt, South Africa: Constraining the rates of Mesoarchaean tectonism: Precambrian Research, v. 143, p. 87-112.

Dilek, Y., and H. Furnes, 2014, Evolution of archean crust and early life [electronic book] / edited by Yildirim Dilek, Harald Furnes: Modern approaches in Solid Earth Sciences: Springer, Dordrecht, 2014, pp. 418.

Doubrovine, P. V., and J. A. Tarduno, 2004, Self-reversed magnetization carried by titanomaghemite in oceanic basalts: Earth and Planetary Science Letters, v. 222, p. 959-969.

Doubrovine, P. V., and J. A. Tarduno, 2006, Alteration and self-reversal in oceanic basalts: Journal of Geophysical Research: Solid Earth, v. 111, p. B12S30.

Dunlop, D. J., 2002, Theory and application of the Day plot (Mrs/Ms versus Hcr/Hc) Theoretical curves and tests using titanomagnetite data: Journal of Geophysical Research, v. 107, B3, p. 4-11 to 4-22.

Dunlop, D. J., and Ö. Özdemir, 1997, Rock magnetism: fundamentals and frontiers, v. 3, Cambridge University Press, Cambridge, pp. 575.

Dunlop, D. J., and Y. Yu, 2004, Intensity and Polarity of the Geomagnetic Field During Precambrian Time: Geophysical Monograph Series, v. 145, p. 85-100.

Dziggel, A., G. Stevens, M. Poujol, C. R. Anhaeusser, and R. A. Armstrong, 2002, Metamorphism of the granite-greenstone terrane south of the Barberton greenstone belt, South Africa: an insight into the tectono-thermal evolution of the [`]lower' portions of the Onverwacht Group: Precambrian Research, v. 114, p. 221-247.

Dziggel, A., R. A. Armstrong, G. Stevens, and L. Nasdala, 2005, Growth of zircon and titanite during metamorphism in the granitoid-gneiss terrane south of the Barberton greenstone belt, South Africa: Mineralogical Magazine, v. 69, p. 1019-1036.

Eriksson, K. A., 1977, Tidal deposits from the Archaean Moodies Group, Barberton Mountain Land, South Africa: Sedimentary Geology, v. 18, p. 257-281.

Eriksson, K. A., E. L. Simpson, and W. Mueller, 2006, An unusual fluvial to tidal transition in the mesoarchean Moodies Group, South Africa: A response to high tidal range and active tectonics: Sedimentary Geology, v. 190, p. 13-24.

Evans, D. A. D., 2006, Proterozoic low orbital obliquity and axial-dipolar geomagnetic field from evaporite palaeolatitudes: Nature, v. 444, p. 51-55.

Evans, M. E., 1967, A Palaeomagnetic Study of the Gaberones Granite of Botswana: Geophysical Journal International, v. 12, p. 491-498.

Evans, M. E., and M. W. McElhinny, 1966, The paleomagnetism of the Modipe Gabbro: Journal of Geophysical Research, v. 71, p. 6053-6063.

Feinberg, J. M., S. W. Denyszyns, P. R. Renne, and G. R. Scott, 2010, Goldschmidt Abstracts 2010 – F: Geochimica et Cosmochimica Acta, v. 74, p. A276-A312.

Fisher, R., 1953, Dispersion on a sphere: Proceedings of the Royal Society of London. Series A. Mathematical and Physical Sciences, v. 217, p. 295-305.

Fliegel, D., J. Kosler, N. McLoughlin, A. Simonetti, M. J. de Wit, R. Wirth, and H. Furnes, 2010, In-situ dating of the Earth's oldest trace fossil at 3.34Ga: Earth and Planetary Science Letters, v. 299, p. 290-298.

Furnes, H., N. R. Banerjee, K. Muehlenbachs, H. Staudigel, and M. de Wit, 2004, Early Life Recorded in Archean Pillow Lavas: Science, v. 304, p. 578-581.

Furnes, H., Staudigel, H., Thorseth, I.H., Torsvik, T., Muehlenbachs, K., Ole, T., 2001, Bioalteration of basaltic glass in the oceanic crust: Geochemistry Geophysics Geosystems, v. 2.

Furnes, H., M. J. de Wit, B. Robins, and N. R. Sandstå, 2011, Volcanic evolution of the upper Onverwacht Suite, Barberton Greenstone Belt, South Africa: Precambrian Research, v. 186, p. 28-50.

Furnes, H., M. de Wit, and B. Robins, 2013, A review of new interpretations of the tectonostratigraphy, geochemistry and evolution of the Onverwacht Suite, Barberton Greenstone Belt, South Africa: Gondwana Research, v. 23, p. 403-428.

Glikson, A. Y., ed., 2014, The Moon and the Late Heavy Bombardment (LHB): The Archaean: Geological and Geochemical Windows into the Early Earth, Springer International Publishing, pp. 283.

Graham, J. W., 1949, The stability and significance of magnetism in sedimentary rocks: Journal of Geophysical Research, v. 54, p. 131-167.

Graham, K. W. T., 1961, The re-magnetization of a surface outcrop by lightning currents.: Geophysics Journal of the Royal Astronomical Society, v. 6, p. 85-102.

Grosch, E. G., N. McLoughlin, M. de Wit, and H. Furnes, 2009a, Drilling for the Archean Roots of Life and Tetonic Earth in the Barberton Mountains: Scientific Drilling., no. 8, p. 24-28.

Grosch, E. G., N. McLoughlin, M. Wit, and H. Furnes, 2009b, Deciphering Earth's deep history: drilling in Africa's oldest greenstone belt: Eos, Transactions American Geophysical Union, v. 90, p. 350-351.

Grosch, E. G., J. Kosler, N. McLoughlin, K. Drost, J. Slama, and R. B. Pedersen, 2011, Paleoarchean detrital zircon ages from the earliest tectonic basin in the Barberton Greenstone Belt, Kaapvaal craton, South Africa: Precambrian Research, v. 191, p. 85-99.

Grosch, E. G., and N. McLoughlin, 2014, Reassessing the biogenicity of Earth's oldest trace fossil with implications for biosignatures in the search for early life: Proceedings of the National Academy of Sciences, v. 111, p. 8380-8385.

Grove, T. L., Gaetani, G.A., and de Wit, M.J., 1994, Spinifex textures in 3.49 Ga Barberton Montain Belt komatiites: Evidence for crystallization of water-bearing, cool magmas in the Archean.: Eos (Transactions, American Geophysical Union), v. 75 (spring), p. 354.

Grove, T. L., and S. W. Parman, 2004, Thermal evolution of the Earth as recorded by komatiites: Earth and Planetary Science Letters, v. 219, p. 173-187.

Gubbins, D., and E. Herrero-Bervera, 2007, Encyclopedia of geomagnetism and paleomagnetism, Springer, pp. 1054.

Hale, C. J., and D. J. Dunlop, 1984, Evidence for an Early Archean Geomagnetic Field: A paleomagnetic study of the Komati Formation, Barberton Greenstone Belt, South Africa: Geophysical Research Letters, v. 11, p. 97-100.

Hale, C. J., 1987a, The intensity of the geomagnetic field at 3.5 Ga: paleointensity results from the Komati Formation, Barberton Mountain Land, South Africa: Earth and Planetary Science Letters, v. 86, p. 354-364.

Hale, C. J., 1987b, Palaeomagnetic data suggest link between the Archaean-Proterozoic boundary and inner-core nucleation: Nature, v. 329, p. 233-237.

Hall, A. L., 1918, The Geology of the Barberton Gold mining district: Geological Survey of South Africa, Pretoria, Memoir, v. 9, pp. 347.

Hamilton, W. B., 1998, Archean magmatism and deformation were not products of plate tectonics: Precambrian Research, v. 91, p. 143-179.

Heinrichs, T., 1984, The Umsoli chert, turbidite testament for a major phreatoplinian event at the onverwacht/fig tree transition (Swaziland supergroup, Archaean, South Africa): Precambrian Research, v. 24, p. 237-283.

Heubeck, C., and D. R. Lowe, 1994, Depositional and tectonic setting of the Archean Moodies Group, Barberton Greenstone Belt, South Africa: Precambrian Research, v. 68, p. 257-290.

Heubeck, C., J. Engelhardt, G. R. Byerly, A. Zeh, B. Sell, T. Luber, and D. R. Lowe, 2013, Timing of deposition and deformation of the Moodies Group (Barberton Greenstone Belt, South Africa): Very-high-resolution of Archaean surface processes: Precambrian Research, v. 231, p. 236-262.

Hofmann, A., 2005, The geochemistry of sedimentary rocks from the Fig Tree Group, Barberton greenstone belt: implications for tectonic, hydrothermal and surface processes during mid-Archaean times: Precambrian Research, v. 143, p. 23-49.

Hofmann, A., R. Bolhar, B. Orberger, and F. Foucher, 2013, Cherts of the Barberton Greenstone Belt, South Africa: Petrology and trace-element geochemistry of 3.5 to 3.3Ga old silicified volcaniclastic sediments: South African Journal of Geology, v.116, p297-322.

Huppert, H. E., and R. S. J. Sparks, 1985, Komatiites I: Eruption and Flow: Journal of Petrology, v. 26, p. 694-725.

Johnson, B. C., and H. J. Melosh, 2012, Impact spherules as a record of an ancient heavy bombardment of Earth: Nature, v. 485, p. 75-77.

Kamo, S. L., and D. W. Davis, 1994, Reassessment of Archean crustal development in the Barberton Mountain Land, South Africa, based on U-Pb dating Tectonics, v. 13., p. 167-192.

Kamo, S. L., W. U. Reimold, T. E. Krogh, and W. P. Colliston, 1996, A 2.023 Ga age for the Vredefort impact event and a first report of shock metamorphosed zircons in pseudotachylitic breccias and granophyre: Earth and Planetary Science Letters, v. 144, p. 369-387.

Kerr, A. C., and N. T. Arndt, 2001, A Note on the IUGS Reclassification of the High-Mg and Picritic Volcanic Rocks: Journal of Petrology, v. 42, p. 2169-2171.

Kirschvink, J. L., 1980, The least-squares line and plane and the analysis of palaeomagnetic data: Geophysical Journal International, v. 62, p. 699-718.

Kisters, A. F. M., G. Stevens, A. Dziggel, and R. A. Armstrong, 2003, Extensional detachment faulting and core-complex formation in the southern Barberton granite–greenstone terrain, South Africa: evidence for a 3.2 Ga orogenic collapse: Precambrian Research, v. 127, p. 355-378.

Kisters, A. F. M., R. W. Belcher, M. Poujol, and A. Dziggel, 2010, Continental growth and convergence-related arc plutonism in the Mesoarchaean: Evidence from the Barberton granitoid-greenstone terrain, South Africa: Precambrian Research, v. 178, p. 15-26.

Klootwijk, C. T., J. S. Gee, J. W. Peirce, G. M. Smith, and P. L. McFadden, 1992, An early India-Asia contact: paleomagnetic constraints from Ninetyeast ridge, ODP Leg 121: Geology, v. 20, p. 395-398.

Knauth, L. P., and D. R. Lowe, 2003, High Archean climatic temperature inferred from oxygen isotope geochemistry of cherts in the 3.5 Ga Swaziland Supergroup, South Africa: Geological Society of America Bulletin, v. 115, p. 566-580.#

Kröner, A., and A. Tegtmeyer, 1994, Gneiss-greenstone relationships in the Ancient Gneiss Complex of southwestern Swaziland, southern Africa, and implications for early crustal evolution: Precambrian Research, v. 67, p. 109-139.

Kröner, A., G. R. Byerly, and D. R. Lowe, 1991, Chronology of early Archaean granite-greenstone evolution in the Barberton Mountain Land, South Africa, based on precise dating by single zircon evaporation: Earth and Planetary Science Letters, v. 103, p. 41-54.

Kröner, A., E. Hegner, J. I. Wendt, and G. R. Byerly, 1996, The oldest part of the Barberton granitoid-greenstone terrain, South Africa: evidence for crust formation between 3.5 and 3.7 Ga: Precambrian Research, v. 78, p. 105-124.

Labrosse, S., J. W. Hernlund, and N. Coltice, 2007, A crystallizing dense magma ocean at the base of the Earth's mantle: Nature, v. 450, p. 866-869.

Lana, C., A. Kisters, and G. Stevens, 2010a, Exhumation of Mesoarchean TTG gneisses from the middle crust: Insights from the Steynsdorp core complex, Barberton granitoid-greenstone terrain, South Africa: Geological Society of America Bulletin, v. 122, p. 183-197.

Lana, C., E. Tohver, and P. Cawood, 2010b, Quantifying rates of dome-and-keel formation in the Barberton granitoid-greenstone belt, South Africa: Precambrian Research, v. 177, p. 199-211.

Layer, P. W., A. Kröner, M. McWilliams, and N. Clauer, 1988, Regional magnetic overprinting of Witwatersrand Supergroup Sediments, South Africa: Journal of Geophysical Research: Solid Earth, v. 93, p. 2191-2200.

Layer, P. W., A. Kröner, M. McWilliams, and D. York, 1989, Elements of the Archean thermal history and apparent polar wander of the eastern Kaapvaal Craton, Swaziland, from single grain dating and paleomagnetism: Earth and Planetary Science Letters, v. 93, p. 23-34.

Layer, P. W., A. Kröner, and M. McWilliams, 1996, An Archean Geomagnetic Reversal in the Kaap Valley Pluton, South Africa: Science, v. 273, p. 943-946.

Layer, P. W., M. Lopez-Martinez, A. Kroner, D. York, and M. McWilliams, 1998, Thermochronometry and palaeomagnetism of the Archean Nelshoogte Pluton, South Africa: Geophysics Journal International, v. 135, p. 16.

Leonhardt, R., 2006, Analyzing rock magnetic measurements: The RockMagAnalyzer 1.0 software: Computers & Geosciences, v. 32, p. 1420-1431.

Letts, S., T. H. Torsvik, S. J. Webb, and L. D. Ashwal, 2009, Palaeomagnetism of the 2054 Ma Bushveld Complex (South Africa): implications for emplacement and cooling: Geophysical Journal International, v. 179, p. 850-872.

López-Martínez, M., D. York, and J. A. Hanes, 1992, A 40Ar39Ar geochronological study of komatiites and komatiitic basalts from the Lower Onverwacht Volcanics: Barberton Mountain Land, South Africa: Precambrian Research, v. 57, p. 91-119.

Lowe, D. R., 2013, Crustal fracturing and chert dike formation triggered by large meteorite impacts, ca. 3.260 Ga, Barberton greenstone belt, South Africa: Geological Society of America Bulletin, v. 125, p. 894-912.

Lowe, D. R., and G. R. Byerly, 1986, Archaean flow-top alteration zones formed initially in a low-temperature sulphate-rich environment: Nature, v. 324, p. 245-248.

Lowe, D. R., and G. R. Byerly, 1999a, Geologic evolution of the Barberton Greenstone Belt, In: Lowe, D.R., Byerly, G.R. (Eds.), Geological Evolution of the Barberton Greenstone Belt, South Africa.: Geological Society of America Special Paper, v. 329, Boulder, Colorado, pp.321.

Lowe, D. R., and G. R. Byerly, 1999b, Stratigraphy of the west-central part of the Barberton Greenstone Belt, South Africa. In: Lowe, D.R., Byerly, G.R. (Eds.), Geological Evolution of the Barberton Greenstone Belt, South Africa.: Geological Society of America Special Paper, v. 329, Boulder, Colorado, pp.321.

Lowe, D. R., and G. R. Byerly, 2007, Chapter 5.3, An Overview of the Geology of the Barberton Greenstone Belt and Vicinity: Implications for Early Crustal Development., In: Martin J. van Kranendonk, R. Hugh Smithies and Vickie C. Bennett, (Eds.), Developments in Precambrian Geology, Elsevier, Vol. 15, p. 481-526.

Lowe, D. R., and G. R. Byerly, 2010, Did LHB end not with a bang but a whimper? The geological evidence., Lunar and Planetary Science Conference, p. 2563.

Lowe, D. R., and L. P. Knauth, 1977, Sedimentology of the Onverwacht Group (3.4 billion years), Transvaal, South Africa, and its bearing on the characteristics and evolution of the early earth: The Journal of Geology, p. 699-723.

Lowe, D. R., and B. W. Nocita, 1999, Foreland basin sedimentation in the Mapepe Formation, southern-facies Fig Tree Group: Geological Society of America Special Papers, v. 329, p. 233-258.

Lowe, D. R., and G. F. Worrel, 1999, Sedimentology, mineralogy, and implications of silicified evaporites in the Kromberg Formation, Barberton Greenstone Belt, South Africa. In: Lowe, D.R., Byerly, G.R. (Eds.), Geological Evolution of the Barberton Greenstone Belt, South Africa.: Geological Society of America Special Paper, v. 329, Boulder, Colorado, pp.321.

Lowe, D. R., G. R. Byerly, B. L. Ransom, and B. W. Nocita, 1985, Stratigraphic and sedimentological evidence bearing on structural repetition in early Archean rocks of the Barberton greenstone belt, South Africa: Precambrian Research, v. 27, p. 165-186.

Lowe, D. R., G. R. Byerly, F. T. Kyte, A. Shukolyukov, F. Asaro, and A. Krull, 2003, Spherule beds 3.47-3.24 billion years old in the Barberton Greenstone Belt, South Africa: a record of large meteorite impacts and their influence on early crustal and biological evolution: Astrobiology, v. 3, p. 7-48.

Macouin, M., J.-P. Valet, and J. Besse, 2004, Long-term evolution of the geomagnetic dipole moment: Physics of the Earth and Planetary Interiors, v. 147, p. 239-246.

Matsumura, R., 2014, The petrogenesis of the Nelshoogte pluton: The youngest and most compositionally variable TTG pluton in the Barberton Granite-Greenstone Terrain, MS.c Thesis, Stellenbosch University, Stellenbosch, pp. 120 .

McElhinny, M. W., 1964, Statistical Significance of the Fold Test in Palaeomagnetism: Geophysical Journal of the Royal Astronomical Society, v. 8, p. 338-340.

McElhinny, M. W., and D. I. Gough, 1963, The Palaeomagnetism of the Great Dyke of Southern Rhodesia: Geophysical Journal International, v. 7, p. 287-303.

McElhinny, M. W., and W. E. Senanayake, 1980, Paleomagnetic evidence for the existence of the geomagnetic field 3.5 Ga ago: Journal of Geophysical Research: Solid Earth, v. 85, p. 3523-3528.

McFadden, P. L., and M. W. McElhinny, 1990, Classification of the reversal test in palaeomagnetism: Geophysical Journal International, v. 103, p. 725-729.

McNaughton, N. J., W. Compston, and M. E. Barley, 1993, Constraints on the age of the Warrawoona Group, eastern Pilbara Block, Western Australia: Precambrian Research, v. 60, p. 69-98.

Merrill, R. T., M. W. McElhinny, and P. L. McFadden, 1998, The magnetic field of the earth: paleomagnetism, the core, and the deep mantle, v. 63, Academic Press., pp.531.

Moskowitz, B. M., 1981, Methods for estimating Curie temperatures of titanomaghemites from experimental< i> Js-T</i> data: Earth and Planetary Science Letters, v. 53, p. 84-88.

Moyen, J.-F., G. Stevens, and A. Kisters, 2006, Record of mid-Archaean subduction from metamorphism in the Barberton terrain, South Africa: Nature, v. 442, p. 559-562.

Muxworthy, A. R., and M. E. Evans, 2013, Micromagnetics and magnetomineralogy of ultrafine magnetite inclusions in the Modipe Gabbro: Geochemistry, Geophysics, Geosystems, v. 14, p. 921-928.

Muxworthy, A. R., M. E. Evans, S. J. Scourfield, and J. G. King, 2013, Paleointensity results from the late-Archaean Modipe Gabbro of Botswana: Geochemistry, Geophysics, Geosystems, v. 14, p. 2198-2205.

Nédélec, A., M. O. Chevrel, J. F. Moyen, J. Ganne, and S. Fabre, 2012, TTGs in the making: Natural evidence from Inyoni shear zone (Barberton, South Africa): Lithos, v. 153, p. 25-38.

Nisbet, E. G., 1982, The tectonic setting and petrogenesis of komatiites: Komatiites. George Allen & Unwin, London, p. 501-520.

Nisbet, E. G., M. J. Cheadle, N. T. Arndt, and M. J. Bickle, 1993, Constraining the potential temperature of the Archaean mantle: A review of the evidence from komatiites: Lithos, v. 30, p. 291-307.

Parman, S. W., J. C. Dann, T. L. Grove, and M. J. de Wit, 1997, Emplacement conditions of komatiite magmas from the 3.49 Ga Komati Formation, Barberton Greenstone Belt, South Africa: Earth and Planetary Science Letters, v. 150, p. 303-323.

Parman, S. W., T. L. Grove, and J. C. Dann, 2001, The production of Barberton komatiites in an Archean Subduction Zone: Geophysical Research Letters, v. 28, p. 2513-2516.

Parman, S. W., T. L. Grove, J. C. Dann, and M. J. de Wit, 2004, A subduction origin for komatiites and cratonic lithospheric mantle: South African Journal of Geology, v. 107, p. 107-118.

Pidgeon, R. T., 1978, 3450-m.y.-old volcanics in the Archaean layered greenstone succession of the Pilbara Block, Western Australia: Earth and Planetary Science Letters, v. 37, p. 421-428.

Prévot, M., and M. Perrin, 1992, Intensity of the Earth's magnetic field since Precambrian from Thellier-type palaeointensity data and inferences on the thermal history of the core: Geophysical Journal International, v. 108, p. 613-620.

Prior, D. J., P. W. Trimby, U. D. Weber, and D. J. Dingley, 1996, Orientation contrast imaging of microstructures in rocks using forescatter detectors in the scanning electron microscope: Mineralogical Magazine, v. 60, p. 859-869.

Puchtel, I. S., J. Blichert-Toft, M. Touboul, R. J. Walker, G. R. Byerly, E. G. Nisbet, and C. R. Anhaeusser, 2013, Insights into early Earth from Barberton komatiites: Evidence from lithophile isotope and trace element systematics: Geochimica et Cosmochimica Acta, v. 108, p. 63-90.

Pyke, D. R., A. J. Naldrett, and O. R. Eckstrand, 1973, Archean Ultramafic Flows in Munro Township, Ontario: Geological Society of America Bulletin, v. 84, p. 955-978.

Robb, L. J., and C. R. Anhaeusser, eds., 1983, Chemical and petrogenetic characteristics of the Archaean tonalite–trondhjemite gneiss plutons in the Barberton Mountain Land: Contributions to the Geology of the Barberton Mountain Land., v. 9, Special Publication of the Geological Society of South Africa.

Robb, L. J., J. M. Barton Jr, E. J. D. Kable, and R. C. Wallace, 1986, Geology, geochemistry and isotopic characteristics of the Archaean Kaap Valley pluton, Barberton Mountain Land, South Africa: Precambrian Research, v. 31, p. 1-36.

Roberts, P. H., and G. A. Glatzmaier, 2001, The geodynamo, past, present and future: Geophysical & Astrophysical Fluid Dynamics, v. 94, p. 47-84.

Robin-Popieul, C. C. M., N. T. Arndt, C. Chauvel, G. R. Byerly, A. V. Sobolev, and A. Wilson, 2012, A New Model for Barberton Komatiites: Deep Critical Melting with High Melt Retention: Journal of Petrology, v. 53, p. 2191-2229.

Rouchon, V., and B. Orberger, 2008, K-Si-metasomatism of 3.4-3.3 Ga volcanoclastic sediments: Implications for Archean seawater evolution: Geochimica et Cosmochimica Acta Supplement, v. 72, p. 808.

Sanchez-Garrido, C. J. M. G., G. Stevens, R. A. Armstrong, J.-F. Moyen, H. Martin, and R. Doucelance, 2011, Diversity in Earth's early felsic crust: Paleoarchean

peraluminous granites of the Barberton Greenstone Belt: Geology, v. 39, p. 963-966.

Schmidt, P. W., and B. J. J. Embleton, 1985, Prefolding and overprint magnetic signatures in Precambrian (~ 2.9–2.7 Ga) igneous rocks from the Pilbara Craton and Hamersley Basin, NW Australia: Journal of Geophysical Research: Solid Earth (1978–2012), v. 90, p. 2967-2984.

Schoene, B., M. J. de Wit, and S. A. Bowring, 2008, Mesoarchean assembly and stabilization of the eastern Kaapvaal craton: A structural-thermochronological perspective: Tectonics, v. 27. TC5010, 27 pages.

Schult, A., 1968, Self-reversal of magnetization and chemical composition of titanomagnetites in basalts: Earth and Planetary Science Letters, v. 4, p. 57-63.

Self, S., and R. S. J. Sparks, 1978, Characteristics of widespread pyroclastic deposits formed by the interaction of silicic magma and water: Bulletin volcanologique, v. 41, p. 196-212.

Shaar, R., E. Ben-Yosef, H. Ron, L. Tauxe, A. Agnon, and R. Kessel, 2011, Geomagnetic field intensity: How high can it get? How fast can it change? Constraints from Iron Age copper slag: Earth and Planetary Science Letters, v. 301, p. 297-306.

Sleep, N. H., and D. R. Lowe, 2014, Physics of crustal fracturing and chert dike formation triggered by asteroid impact,~ 3.26 Ga, Barberton greenstone belt, South Africa: Geochemistry, Geophysics, Geosystems, v. 15, p. 1054-1070.

Smirnov, A. V., and J. A. Tarduno, 2004, Secular variation of the Late Archean–Early Proterozoic geodynamo: Geophysical Research Letters, v. 31, p. L16607.

Smirnov, A. V., D. A. D. Evans, R. E. Ernst, U. Söderlund, and Z.-X. Li, 2013, Trading partners: Tectonic ancestry of southern Africa and western Australia, in Archean supercratons Vaalbara and Zimgarn: Precambrian Research, v. 224, p. 11-22.

Smith, D. K., and J. R. Cann, 1993, Building the crust at the Mid-Atlantic Ridge: Nature, v. 365, p. 707-715.

Stanistreet, I. G., M. J. de Wit, and R. E. P. Fripp, 1981, Do graded units of accretionary spheroids in the Barberton Greenstone Belt indicate Archaean deep water environment?: Nature, v. 293, p. 280-284.

Stiegler, M. T., D. R. Lowe, and G. R. Byerly, 2008, Abundant pyroclastic komatiitic volcanism in the 3.5–3.2 Ga Barberton greenstone belt, South Africa: Geology, v. 36, p. 779-782.

Strik, G., 2004, Palaeomagnetism of late Archaean flood basalt terrains: implications for early Earth geodynamics and geomagnetism, University of Utrecht, Utrecht, 160 p.

Strik, G., T. S. Blake, T. E. Zegers, S. H. White, and C. G. Langereis, 2003, Palaeomagnetism of flood basalts in the Pilbara Craton, Western Australia: Late Archaean continental drift and the oldest known reversal of the geomagnetic field: Journal of Geophysical Research: Solid Earth, v. 108, p. n/a.

Strik, G., M. J. de Wit, and C. G. Langereis, 2007, Palaeomagnetism of the Neoarchaean Pongola and Ventersdorp Supergroups and an appraisal of the 3.0–1.9 Ga apparent polar wander path of the Kaapvaal Craton, Southern Africa: Precambrian Research, v. 153, p. 96-115.

Suganuma, Y., Y. Hamano, S. Niitsuma, M. Hoashi, T. Hisamitsu, N. Niitsuma, K. Kodama, and M. Nedachi, 2006, Paleomagnetism of the Marble Bar Chert Member, Western Australia: Implications for apparent polar wander path for Pilbara craton during Archean time: Earth and Planetary Science Letters, v. 252, p. 360-371.

Tarduno, J. A., R. D. Cottrell, and A. V. Smirnov, 2006, The paleomagnetism of single silicate crystals: Recording geomagnetic field strength during mixed polarity intervals, superchrons, and inner core growth: Reviews of Geophysics, v. 44, p. RG1002.

Tarduno, J. A., R. D. Cottrell, M. K. Watkeys, and D. Bauch, 2007, Geomagnetic field strength 3.2 billion years ago recorded by single silicate crystals: Nature, v. 446, p. 657-660.

Tarduno, J. A., R. D. Cottrell, M. K. Watkeys, A. Hofmann, P. V. Doubrovine, E. E. Mamajek, D. Liu, D. G. Sibeck, L. P. Neukirch, and Y. Usui, 2010, Geodynamo, Solar Wind, and Magnetopause 3.4 to 3.45 Billion Years Ago: Science, v. 327, p. 1238-1240.

Tauxe, L., 2010, Essentials of paleomagnetism, Univ. of California Press, Oakland, pp. 512.

Tauxe, L., and G. S. Watson, 1994, The fold test: an eigen analysis approach: Earth and Planetary Science Letters, v. 122, p. 331-341.

Tauxe, L., Mullender,T.A.T., Pick, T., 1996, Potbellies, wasp-waists, and superparamagnetism in magnetic hysteresis: Journal of Geophysical Research, v. 101.

Tice, M. M., B. C. Bostick, and D. R. Lowe, 2004, Thermal history of the 3.5–3.2 Ga Onverwacht and Fig Tree Groups, Barberton greenstone belt, South Africa, inferred by Raman microspectroscopy of carbonaceous material: Geology, v. 32, p. 37.

Thellier, E. and O. Thellier, 1959, Sur l'intensité du champ magnétique terrestre dans le passé historique et géologique, Ann. Géophys, 15, p. 285 – 376.

Tolstikhin, I. N., and J. D. Kramers, 2008, The evolution of matter from Big Bang to the present day, Cambridge University Press, Cambridge, pp. 532.

Toulkeridis, T., S. L. Goldstein, N. Clauer, A. Kröner, and D. R. Lowe, 1994, Sm-Nd dating of Fig Tree clay minerals of the Barberton greenstone belt, South Africa: Geology, v. 22, p. 199-202.

Usui, Y., J. A. Tarduno, M. Watkeys, A. Hofmann, and R. D. Cottrell, 2009, Evidence for a 3.45-billion-year-old magnetic remanence: Hints of an ancient geodynamo from conglomerates of South Africa: Geochemistry Geophysics Geosystems, v. 10, pp.16.

Van Kranendonk, M. J., A. Kröner, E. Hegner, and J. Connelly, 2009, Age, lithology and structural evolution of the c. 3.53 Ga Theespruit Formation in the Tjakastad area,

southwestern Barberton Greenstone Belt, South Africa, with implications for Archaean tectonics: Chemical Geology, v. 261, p. 115-139.

Verwey, E. J. W., 1939, Electronic conduction of magnetite (Fe3O4) and its transition point at low temperatures: Nature, v. 144, p. 327-328.

Viljoen, M. J., and R. P. Viljoen, 1969a, Evidence for the existance of a mobile extrusive peridotitic magma from the Komati Formation of the Onverwacht Group, in: Upper Mantle Project. Geological Society of South Africa Special Publication 2, p. 87 – 112.

Viljoen, M. J., and R. P. Viljoen, 1969b, The geological and geochemical significance of the Upper Formations of the Onverwacht Group in: Upper Mantle Project. Geological Society of South Africa Special Publication 2, p. 113 –151.

Viljoen, M. J., and R. P. Viljoen, 1969c, The geology and geochemistry of the lower ultramafic unit of the Onverwacht Group and a proposed new class of igneous rocks in: Upper Mantle Project. Geological Society of South Africa Special Publication 2, p.55 – 85.

Viljoen, M. J., and R. P. Viljoen, 1969d, An introduction to the geology of the Barberton Granite-Greenstone Terrain in: Upper Mantle Project. Geological Society of South Africa Special Publication 2, p.9 – 28.

Viljoen, R. P., and M. J. Viljoen, 1969e, The effect of metamorphism and serpentinization on the volcanic and associated rocks of the Barberton Region in: Upper Mantle Project. Geological Society of South Africa Special Publication 2, p.29—53.

Viljoen, M. J., R. P. Viljoen, H. S. Smith, and A. J. Erlank, 1983, Geological, textural, and geochemical features of komatiitic flows from the Komati Formation in:Geological Society of South Africa Special Publication 9, p. 1 – 20.

Vlaar, N. J., P. E. Van Keken, and A. P. Van den Berg, 1994, Cooling of the Earth in the Archaean: consequences of pressure-release melting in a hotter mantle: Earth and Planetary Science Letters, v. 121, p. 1-18.

Watson, G. S., 1956, A test for Randomness of Directions: Geophysical Journal International, v. 7, p. 160-161.

Weis, D., and G. J. Wasserburg, 1987, Rb □ Sr and Sm □ Nd isotope geochemistry and chronology of cherts from the Onverwacht Group (3.5 AE), South Africa: Geochimica et Cosmochimica Acta, v. 51, p. 973-984.

Westraat, J., A. M. Kisters, M. Poujol, and G. Stevens, 2005, Transcurrent shearing, granite sheeting and the incremental construction of the tabular 3.1 Ga Mpuluzi batholith, Barberton granite–greenstone terrane, South Africa: Journal of the Geological Society, v. 162, p. 373-388.

Yoshihara, A., and Y. Hamano, 2004, Paleomagnetic constraints on the Archean geomagnetic field intensity obtained from komatiites of the Barberton and Belingwe greenstone belts, South Africa and Zimbabwe: Precambrian Research, v. 131, p. 111-142.

Zegers, W. De, Dann, and White, 1998, Vaalbara, Earth's oldest assembled continent? A combined structural, geochronological, and palaeomagnetic test: Terra Nova, v. 10, p. 250-259.

Zijderveld, J. D. A., 1967, AC demagnetization of rocks: Analysis of results, Methods in Paleomagnetism DW Collinson, KM Creer, SK Runcorn, Elsevier, New York, p. 254–286.

Abbreviations

AF	Alternating Field
BGB	Barberton Greenstone Belt
BARB1	Barberton Greenstone Belt Drilling Programme Core 1
BARB2	Barberton Greenstone Belt Drilling Programme Core 2
BRC	Buck Reef Chert
BR-vsc	Buck Ridge volcano sedimentary complex
BSDP	Barberton Scientific Drilling Programme
CRM	Chemical Remanent Magnetisation
Dec/D	Declination
EDX	Energy Dispersive X-Ray
GAD	Geocentric Axial Dipole
GPS	Global Positioning System
Hc	Coercivity
Hcr	Remanent Coercivity
ICDP	International Continental Scientific Drilling Programme
Inc/I	Inclination
IRM	Isothermal Remanent Magnetisation
k	Precision parameter
LHG	Samples from the Hooggenoeg Formation
LKM	Samples from the Komati Formation
LNP	Samples from the Nelshoogte Pluton
LNY	Samples from the Noisy Complex
MAD	Maximum Angular Deviation
MD	Multidomain
MM	Middle Marker
Mrs	Saturation Remanence
Ms	Saturation Magnetisation
N/n	Number of samples/number of specimens
NRM	Natural Remanent Magnetisation
NS	Nelshoogte Pluton
OF	Onverwacht Fold
SD	Single Domain
SEM	Scanning Electron Microscope
SP	Super paramagnetic
SQUID	Supercondution Quantum Interference Device
Tc	Curie Temperature
TH	Thermal Demagnetisation
TRM	Thermal Remanent Magnetisation
VDM	Virtual Dipole Moment
VFTB	Variable Translational Balance
VRM	Viscous Remanent Magnetisation
VGP	Virtual Geomagnetic Pole
a95	Radius of 95% confidence cone

λ	Palaeolatitude
ϕ	Palaeolongitude
χ	Susceptibility
χfd	Frequency Dependant Susceptibility

Appendices

Appendix A – Komati Formation Directional Results

Komati Formation directions obtained are presented here. Surface sampling sites are presented first followed by the directional results from the drill core samples from cores BARB1 and BARB2.

As direction means were calculated using sample means rather than site means some details on interpretation of results are also included.

LKM1

LKM1 Directions

Sample Name	Dec (°)	Inc (°)	MAD	Temp. Range (°C)	Notes
ONVELKM1.10a	264.8195	15.86034	1.552468	300-570	
ONVELKM1.10b	332.7031	-34.633	6.491936	* 100-350	
ONVELKM1.10c	266.0042	15.27958	5.689466	400-580x500-520	
ONVELKM1.15	251.7401	59.94736	10.86065	555-580	KOM
ONVELKM1.15	291.4968	-12.5161	37.1567	* 440-555	
ONVELKM1.3A	351.1816	-28.9523	20.57564	* 100-300	
ONVELKM1.3A	292.1194	11.8048	15.32322	* 300-560	
ONVELKM1.3A	306.5152	58.70245	2.832952	560-575	
ONVELKM1.4A	339.5416	-32.6551	13.51979	* 100-300	
ONVELKM1.4A	272.7049	11.76961	9.842776	* 400-560	
ONVELKM1.4A	288.3386	62.49501	4.630744	565-575	
ONVELKM1.5A	344.5881	-20.1075	13.44616	* 100-350	
ONVELKM1.5A	270.1249	12.45341	15.44725	* 440-560	
ONVELKM1.5A	315.002	73.67989	2.321486	565-580	
ONVELKM1.6C	263.1128	20.97703	6.010778	300-580x350x550	Not Fully de-mag'd
ONVELKM1.9A	106.2113	19.72117	2.706337	* 20-200	
ONVELKM1.9A	120.6517	23.11629	14.95131	* 300-520	irm?
ONVELKM1.9A	262.9166	11.75839	8.225291	* 530-565	
ONVELKM1.9A	253.2651	49.72277	5.845798	565-575	v small

LKM1

LKM1 Direction Means

Sample Name	Dec (°)	Inc (°)	MAD	Temp. Range (°C)	Notes
LT1	Recent overprint				
ONVELKM1.10b	332.7031	-34.633	6.491936	* 100-350	
ONVELKM1.3A	351.1816	-28.9523	20.57564	* 100-300	
ONVELKM1.4A	339.5416	-32.6551	13.51979	* 100-300	
ONVELKM1.5A	344.5881	-20.1075	13.44616	* 100-350	
ONVELKM1.9A	106.2113	19.72117	2.706337	* 20-200	outlier - direction above was different - IRM?

Dm	Im	k	a95	N	PAL-LAT
342.2154	**-29.2603**	**7.58E+01**	**10.62354**	**4**	**-15.64909842**

West and Shallow	isolated between 300 and 560, up to 580 in some samples where it appeared as convergent component					
ONVELKM1.10a	264.8195	15.86034	1.552468	300-570		
ONVELKM1.10c	266.0042	15.27958	5.689466	400-580x500-520		
	265.4127	15.57075				
ONVELKM1.3A	292.1194	11.8048	15.32322	* 300-560	KOM ABOVE	
ONVELKM1.4A	272.7049	11.76961	9.842776	* 400-560	KOM ABOVE	
ONVELKM1.5A	270.1249	12.45341	15.44725	* 440-560	KOM ABOVE	
ONVELKM1.6C	263.1128	20.97703	6.010778	300-580x350x550	Not fully de-mag'd	
ONVELKM1.9A	262.9166	11.75839	8.225291	* 530-565		

Dm	Im	k	a95	N	PAL-LAT
271.0733	**14.26394**	**51.48809706**	**9.425034**	**6**	**7.244188341**

Nsamples = 6
Nspecimen=7

ONVELKM1.15	291.4968	-12.5161	37.1567	* 440-555	KOM ABOVE

West and steep	isolated above 560 appearing as the convergent component in the most stable samples				
ONVELKM1.15	251.7401	59.94736	10.86065	555-580	KOM
ONVELKM1.3A	306.5152	58.70245	2.832952	560-575	
ONVELKM1.4A	288.3386	62.49501	4.630744	565-575	
ONVELKM1.5A	315.002	73.67989	2.321486	565-580	
ONVELKM1.9A	253.2651	49.72277	5.845798	565-575	v small

Dm	Im	k	a95	N	PAL-LAT
278.209	**63.36427**	**25.58960945**	**15.41508**	**5**	**44.90921252**

	LKM2 (Dyke) Directions					
	Sample Name	**Dec (°)**	**Inc (°)**	**MAD**	**Temp. Range (°C)**	**Notes**
LKM2	ONVELKM2.12	32.33865	45.66676	8.32716	100-520	
	ONVELKM2.2B	211.0037	24.40083	21.74463	* 200-510	noisy
	ONVELKM2.2B	257.4109	1.591293	21.14324	480-540	
	ONVELKM2.5B	29.45292	-29.6738	15.27598	* 20-200	
	ONVELKM2.5B	233.3876	23.65429	3.776002	440-500	
	ONVELKM2.4B	**Too noisy**				
	ONVELKM2.11B	57.45572	53.53134	13.54589	* 100-10	LT
	ONVELKM2.11B	269.4966	26.0887	13.64862	45-90	HT WSW Shallow
	ONVELKM2.11B	318.6812	69.52074	5.486602	* 15-30	

NOISY SITE AND ONLY 3 SAMPLES

2 OF THESE GAVE NOISY WSW AND SHALLOW DIRECTION AS CONVERGENT COMPONENT BUT INSUFFICIENT FOR SITE MEAN

	LKM3 Directons					
	Sample Name	**Dec (°)**	**Inc (°)**	**MAD**	**Temp. Range (°C/mT)**	**Notes**
LKM3	ONVELKM3.10	335.0459	-25.0158	7.109442	* 200-440	
	ONVELKM3.10	261.2272	-10.9651	3.740311	480-555	
	ONVELKM3.12	353.9561	-37.0105	10.39158	* 20-300	
	ONVELKM3.12	191.0024	23.37255	5.021863	* 350-500x440	
	ONVELKM3.12	274.3655	-11.37	5.53423	* 500-550x530	
	ONVELKM3.4A	9.299737	-69.9561	25.02519	* 20-400	
	ONVELKM3.4B	1.723953	-7.98319	19.41533	* 20-0	
	ONVELKM3.4A	260.4423	-10.6458	2.242869	480-570	combined
	ONVELKM3.4B	256.1232	-5.47877	0.487882	25-100	HT W and Shallow
		258.2689	-8.06792			
	ONVELKM3.5B	349.2684	-51.4416	15.01968	* 20-400	
	ONVELKM3.5B	258	-3.97169	2.809007	480-570	
	ONVELKM3.6A	340.7791	-70.0826	9.074266	* 20-400	
	ONVELKM3.6A	256.3316	-11.5465	3.628583	440-575	
	ONVELKM3.8A	323.3922	-67.2774	4.457466	* 20-200	
	ONVELKM3.8A	254.8015	-1.87269	3.908572	300-560x400-440	
	ONVELKM3.9B	180.2036	19.39213	4.843873	* 20-500	
	ONVELKM3.9B	269.2024	-10.5312	2.894577	510-560	

LKM3

LKM3 Mean Directions

Sample Name	Dec (°)	Inc (°)	MAD	Temp. Range (°C/mT)	Notes
Shallow west component observed as convergent					
ONVELKM3.12	274.3655	-11.37	5.53423	* 500-550x530	
ONVELKM3.10	261.2272	-10.9651	3.740311	480-555	
ONVELKM3.4	258.2689	-8.06792			
ONVELKM3.5B	258	-3.97169	2.809007	480-570	
ONVELKM3.6A	256.3316	-11.5465	3.628583	440-575	
ONVELKM3.8A	254.8015	-1.87269	3.908572	300-560x400-440	
ONVELKM3.9B	269.2024	-10.5312	2.894577	510-560	
ONVELKM3.4B	256.1232	-5.47877	0.487882	25-100 HT W and Shallow	

Dm	Im	k	a95	N	PAL-LAT
260.9936	**-8.02855**	**105.4012**	**5.420177**	**8**	**-4.034071977**

Recent field overprint - to slightly higher temps than LKM1					
ONVELKM3.10	335.0459	-25.0158	7.109442	* 200-440	
ONVELKM3.12	353.9561	-37.0105	10.39158	* 20-300	
ONVELKM3.4A	9.299737	-69.9561	25.02519	* 20-400	
ONVELKM3.5B	349.2684	-51.4416	15.01968	* 20-400	
ONVELKM3.6A	340.7791	-70.0826	9.074266	* 20-400	
ONVELKM3.8A	323.3922	-67.2774	4.457466	* 20-200	

Dm	Im	k	a95	N	PAL-LAT
344.7888	**-54.2801**	**15.46541**	**17.58556**	**6**	**-34.81006489**

South and Shallow overprint					
ONVELKM3.9B	180.2036	19.39213	4.843873	* 20-500	
ONVELKM3.12	191.0024	23.37255	5.021863	* 350-500x440	

	LKM4 Directions					
	Sample Name	**Dec (°)**	**Inc (°)**	**MAD**	**Temp. Range (°C)**	**Notes**
LKM4	ONVELKM4.3B	238.2359	-7.49083	12.15466	* 200-480	
	ONVELKM4.3B	254.6565	62.39438	19.89095	480-540	
	ONVELKM4.4A	12.37731	-24.9677	4.29783	* 100-440	IRM?
	ONVELKM4.4A	27.17353	-9.75578	8.96083	440-550	IRM?
	ONVELKM4.8C	337.3481	-60.1011	10.08129	* 100-350	
	ONVELKM4.8C	242.1198	53.0448	7.254583	440-560	
	ONVELKM4.5B	234.4109	-71.191	19.45822	* 100-440 X400	
	ONVELKM4.5B	247.1812	17.69532	8.796911	3-100 X80 W and Shallow	W and Shallow
	ONVELKM4.3C				**Too noisy**	

	Sample Name	**Dec (°)**	**Inc (°)**	**MAD**	**Temp. Range (°C)**	**Notes**
LKM4	**WSW AND SHALLOW AS OVERPRINT**					
	ONVELKM4.3B	238.2359	-7.49083	12.15466	* 200-480	
	WSW AND SHALLOW AS CONVERGENT with W and Steep Below					
	ONVELKM4.5B	247.1812	17.69532	8.796911	3-100 X80	W and Shallow
	RECENT FIELD OVERPRINT					
	ONVELKM4.8C	337.3481	-60.1011	10.08129	* 100-350	
	WEST AND STEEP AS CONVERGENT COMPONENT BUT 2 SAMPLES INSUFFICIENT AND NOT AS STEEP AS LKM1 OR YH04					
	ONVELKM4.3B	254.6565	62.39438	19.89095	480-540	
	ONVELKM4.8C	242.1198	53.0448	7.254583	440-560	

	LKM5 Directions					
	Sample Name	**Dec (°)**	**Inc (°)**	**MAD**	**Temp. Range (°C/mT)**	**Notes**
LKM5	ONVELKM5.11	149.4393	72.43967	21.89586	* 200-440	noisy
	ONVELKM5.11	221.8112	61.72756	13.81586	500-540	noisy
	ONVELKM5.12	233.7376	78.10352	13.54869	20-520x440	noisy
	ONVELKM5.13	59.53862	40.94334	22.37193	* 300-500	noisy
	ONVELKM5.13a	273.0026	60.58958	35.63893	480-580x570	
	ONVELKM5.13b	326.9307	62.74611	19.2064	400-500	noisy
	ONVELKM5.14	137.7391	-35.5703	7.124461	* 200-400	
	ONVELKM5.14	10.60822	79.33652	7.129107	400-540	
	ONVELKM5.1B	10.29278	-37.0614	10.70061	* 20-300	
	ONVELKM5.1B	264.8164	57.2677	5.766375	* 480-540	
	ONVELKM5.1B	248.3615	23.15586	8.645905	540-580	curvy shallow W above KOM.
	ONVELKM5.2C	53.97733	75.72382	10.8159	* 350-500	
	ONVELKM5.2C	283.2469	24.06711	5.028873	* 510-550	no conv
	ONVELKM5.4A	10.04555	-39.8464	8.369745	* 20-400	
	ONVELKM5.4A	289.0499	63.71771	11.66649	440-530	
	ONVELKM5.5C	7.156835	-21.8985	19.9364	* 20-300	
	ONVELKM5.5C	234.3507	50.49588	22.13023	500-560	noisy
	ONVELKM5.6B	23.75221	-15.8359	20.5842	* 20-400	LT1 ish
	ONVELKM5.6B	283.1081	75.2821	7.103442	7-70	W and Steep
	ONVELKM5.13	47.06282	-15.978	11.72355	* 20-300	
	ONVELKM5.13	322.186	71.11349	10.30718	20-50	W and Steep
	ONVELKM5.5A				**Too noisy**	
	ONVELKM5.6A				**Too noisy**	
	LKM5.6B	22.8	-22.2	19		
	LKM5.6B	285.3	74.9	2.8		Steep W
	LKM5.13D	25.8	-5.2	3		
	LKM5.13D	323.5	76.8	19.7		

LKM5

Sample Name	Dec (°)	Inc (°)	MAD		Temp. Range (°C)	Notes
NOISY AND OR RANDOM MID-RANGE						
ONVELKM5.11	149.4393	72.43967	21.89586	*	200-440	noisy
ONVELKM5.13	59.53862	40.94334	22.37193	*	300-500	noisy
ONVELKM5.14	137.7391	-35.5703	7.124461	*	200-400	
ONVELKM5.2C	53.97733	75.72382	10.8159	*	350-500	
SHALLOW WEST HIGH TEMP IN 1 SAMPLE						
ONVELKM5.2C	283.2469	24.06711	5.028873	*	510-550	no conv
near recent field						
ONVELKM5.1B	10.29278	-37.0614	10.70061	*	20-300	
ONVELKM5.4A	10.04555	-39.8464	8.369745	*	20-400	
ONVELKM5.5C	7.156835	-21.8985	19.9364	*	20-300	

Dm	Im	k	a95	N	PAL-LAT
9.049884609	**-32.96**	**68.88712**	**14.96817**	**3**	**-17.96286254**

West and steep						
ONVELKM5.1B	264.8164	57.2677	5.766375	*	480-540	
ONVELKM5.4A	289.0499	63.71771	11.66649		440-530	
ONVELKM5.5C	234.3507	50.49588	22.13023		500-560	noisy
ONVELKM5.6B	283.1081	75.2821	7.103442		7-70	W and Steep
ONVELKM5.13	322.186	71.11349	10.30718		20-50	W and Steep

Dm	Im	k	a95	N	PAL-LAT
271.1415924	**66.53075**	**22.42567**	**16.51159**	**5**	**49.02759737**

	LKM6 Directions					
	Sample Name	**Dec (°)**	**Inc (°)**	**MAD**	**Temp. Range (°C)**	**Notes**
LKM6	ONVELKM6.10a	63.66776	-29.1231	4.739063	20-440	noise above
	ONVELKM6.10b	67.90596	-33.4558	8.944148	300-530	
	ONVELKM6.1A	40.28827	-38.2702	13.80488	* 20-350	
	ONVELKM6.3C	245.6084	26.57677	7.868542	20-350	
	ONVELKM6.4A	103.3865	78.2145	11.23995	300-440	
	ONVELKM6.5C	110.725	-1.16665	15.42376	* 20-480	
	ONVELKM6.6B	67.15323	26.63236	10.63076	200-530	
	ONVELKM6.8A	11.21336	-26.0759	8.563592	* 100-350	
	ONVELKM6.8A	28.55747	2.778845	7.456305	350-520x480	
	ONVELKM6.6C			**Too noisy**		
	VERY SCATTERED TO NORTH AND EAST MOSTLY SHALLOW					
	ONVELKM6.10a	63.66776	-29.1231	4.739063	20-440	noise above
	ONVELKM6.10b	67.90596	-33.4558	8.944148	300-530	
	ONVELKM6.1A	40.28827	-38.2702	13.80488	* 20-350	NOISY AND SUSPISCOUS
	ONVELKM6.4A	103.3865	78.2145	11.23995	300-440	
	ONVELKM6.5C	110.725	-1.16665	15.42376	* 20-480	
	ONVELKM6.6B	67.15323	26.63236	10.63076	200-530	
	ONVELKM6.8A	11.21336	-26.0759	8.563592	* 100-350	
	ONVELKM6.8A	28.55747	2.778845	7.456305	350-520x480	
	1 SAMPLE WEST SHALLOW - COULD BE CHANCE					
	ONVELKM6.3C	245.6084	26.57677	7.868542	20-350	

BARB1B Directions

	Sample	DemagType	field/temp	Dec (°)	Inc (°)	MAD (blank if avg)	ChRM	Comment
	BA1B1	AF	0-15	119	-34.7	2.6	N	REV DRILL
	BA1B1	AF	25-100	28	-35	23.5	Y	NE-UP
	BA1B3	AF	1-10	127	-53	6.1	N	REV DRILL
	BA1B3	AF	25-60	19	-17	9.6	Y	NE-UP
	BA1B6	AF	0-15	124	-49	1.1	N	REV DRILL
BA1B	BA1B6	AF	15-30	5	-61		Y	NE-UP
	BA1B7	TH	100-480	126	-49	5.7	N	REV DRILL
	BA1B7	TH	520-580	81	-65	6	Y	UNRESOLVED NE-UP?
	BA1B8	TH	**OVERLAPPING UNBLOCKING TEMP SPECTRA**					
	BA1B2	TH	**MOLSPIN - UNRELAIBLE - OVERLAPPING UNBLOCKING T SPECTRA**					
	BA1B	**CONSISTENT NE-UP ChRMs ABOVE REV DRILLING OVERP**						OLIVINE SPINIFEX 2m ABOVE DOLERITE

	Drill	305-310	47.5	

REV DRILL OVERP **appears as an overprint only**

119	-34.7
127	-53
124	-49
126	-49

D_m	I_m	k	a_{95}	N	PAL-LAT
123.638	-46.4865	92.52686222	9.602146	4	-27.7724

BA1B

NE-UP **isolated above 15mT appears as ChRM**

28	-35
19	-17
5	-61
81	-65

D_m	I_m	k	a_{95}	N	PAL-LAT
27.96486	-47.0459	7.821584556	35.0978	4	-28.237

BA1C

BARB1C Directions

Sample	DemagType	field/temp	Dec (°)	Inc (°)	MAD (blank if avg)	ChRM	Comment
BA1C2	AF	0-15	113	-45	7.5	N	REV DRILL
BA1C2	AF	40-60	247	-18	9.8	?	W-SHALLOW - STEEP ABOVE?
BA1C5	AF	0-15	117	-44	1.2	N	REV DRILL
BA1C5	AF	40-60X55	277	-7		Y	W-SHALLOW - SCATTERED
BA1C6	TH	100-440	110	-46	4.9	N	REV DRILL - CANNOT RESOLVE CHRM
BA1C7	TH	0-560	112	-61	8.3	Y	REV DRILL
BA1C3	TH			**MOLSPIN - UNRELAIBLE- W-SHALLOW CHRM???**			
BA1C	WEST SHALLOW ONLY RESOLVED IN AF - REV DRILLING OVP DOMINANT						OLIVINE SPINIFEX 1 - 0m ABOVE DOLERITE

BA1C

REV DRILL OVERP — appears as an overprint and ChRM

113	-45
117	-44
110	-46
112	-61

D_m	I_m	k	a_{95}	N	PAL-LAT
113.118	-49.01091461	95.89863	9.430084594	4	-29.915413

W-SHALLOW - STEEP ABOVE? — isolated above 40mT ChRM

247	-18
277	-7

BA1D

BARB1D Directions

Sample	DemagType	field/temp	Dec (°)	Inc (°)	MAD (blank if avg)	ChRM	Comment
BA1D3	AF	10-45X20	271	29		Y	W-SHALLOW BUT DOES NOT DEMAG
BA1D5	AF	0-70X60	93	16		Y	E-SHALLOW BUT DOES NOT DEMAG
BA1D6	TH	300-400	101	-27	21.6	Y	E-SHALLOW BUT NOISY AND DEMAGD BY 400
BA1D1	TH	200-500X400	228	18	16.8	Y	MOLSPIN - W-SHALLOW - SELF REVERSED ABOVE?
BA1D1	TH	500-550	79	-24	12	N	SELF-REVERSED ?- NOT DEMAGD BY 570
BA1D	**O DRILLING OVERP - E AND W SHALLOW ABOVE - SEE BOTH IN D1 - SELF-REVERSEI**						18M THICK DOLERITE

BA1E

BARB1E Directions

Sample	DemagType	field/temp	Dec (°)	Inc (°)	MAD (blank if avg)	ChRM	Comment
BA1E5	AF	0-3	119	-27	5.5	N	REV-DRILL OVERP
BA1E5	AF	25-60	251	34	13.9	Y	W-SHALLOW
BA1E8	AF	15-35	266	11	3.5	N	W-SHALLOW - POSS DRILL OVERPRINT BELOW
BA1E8	AF	40-70	251	42	24.9	Y	W-STEEP NOT FULLY RESOLVED?
BA1E9	AF	0-7	139	-57	5.7	N	REV-DRILL OVERP
BA1E9	AF	10-60	243	42	10.3	Y	W-SHALLOW AND STEEP?
BA1E6	TH	0-350	122	-54	9.2	N	REV-DRILL OVERP
BA1E6	TH	500-580	202	-61	18.4	Y	W-STEEP
BA1E2	TH	**MOLSPIN - UNRELIABLE W-SHALLOW 400-480?**					
BA1E	**WEST SHALLOW AND POSS STEEP ABOVE (OVERLAPPING IN SOME) - REV DRILL OVERPRINT**						KOMATIIC BASALT 2m ABOVE GABBRO

BA1E

REV-DRILL OVERP — appears as an overprint only

119	-27
139	-57
122	-54

D_m	I_m	k	a_{95}	N	PAL-LAT
125.2250598	-46.3974	20.47206393	27.97835	3	-27.69889

W-SHALLOW — isolated between 10-60 appears as overprint and ChRM

251	34
266	11
243	42

D_m	I_m	k	a_{95}	N	PAL-LAT
254.4302294	29.4089	18.19175581	29.78246	3	15.739684

W-STEEP — isolated between 40/500-70/580 appears as ChRM only

251	42
202	-61

BA1F

BARB1F Directions

Sample	DemagType	field/temp	Dec (°)	Inc (°)	MAD (blank if avg)	ChRM	Comment
BA1F3	AF	0-5	146	-46	11.8	N	REV-DRILL OVERP
BA1F3	AF	10-25	319	66	16.5	N	DRILL OVERP?
BA1F3	AF	25-40	65	-5		Y	E-SHALLOW
BA1F4	TH	0-350	134	-36	7.4	N	REV-DRILL OVERP
BA1F4	TH	420-580	326	34	11.8	Y	DRILL OVERP? - POSS UNRESOLVED SHALLOW COMPONENT ABOVE?
BA1F6	TH	0-300	112	-36	5.1	N	REV-DRILL OVERP
BA1F6	TH	490-580	328	24	12.8	Y	DRILL OVERP? - POSS UNRESOLVED SHALLOW COMPONENT ABOVE?
BA1F	**DRILLING OVERPRINT - BOTH POLARITIES RESOLVED BY THERMAL. E-SHALLOW CHRM RESOLVED IN AF SAMPLE ONLY**						GABBRO - ~10m APPARENT THICKNESS

BA1F

REV-DRILL OVERP isolated btwn 0-350

146	-46
134	-36
112	-36

D_m	I_m	k	a_{95}	N	PAL-LAT
129.9466	-40.17616454	31.8514	22.21483203	3	-22.88786

DRILL OVERP?

319	66
326	34
328	24

D_m	I_m	k	a_{95}	N	PAL-LAT
325.5277	41.21458918	13.56168	34.86592261	3	23.650115

BA1G

BARB1G Directions

Sample	DemagType	field/temp	Dec (°)	Inc (°)	MAD (blank if avg)	ChRM	Comment
BA1G4	TH-AF	100-5	17	-49	5.7	N	LT1??? - DIFFICULT TO INTERPRET
BA1G4	TH-AF	5-25	169	-61	18.9	Y	REV-DRILL OVERP?
BA1G5	AF	TOO NOISY					
BA1G7	AF	1-20	92	-59	5.1	N	E-UP
BA1G7	AF	20-70X30+40	256	-21		Y	W-SHALLOW - VERY NOISY
BA1G3	TH	0-300	121	-46	16	N	REV-DRILL OVERP
BA1G3	TH	300-420	217	-49	6	Y	W-DOWN COMBO OF SHALLOW AND STEEP??
BA1G7	TH	350-520	128	-37	7.7	N	REV-DRILL OVERP
BA1G8	TH	540-580	69	25	5.3	Y	E-SHALLOW - NOT FULLY DEMAG'D - BA1G8?
BA1G9	TH	0-380	194	-21	7.1	Y	SINGLE COMPONENT S-SHALLOW
BA1G2	TH				**MOLSPIN - TOO NOISY**		

BA1G REV DRILL OVERP ONLY - SCATTERED CHRM DIRECTIONS (MAINLY WEST AND EAST) GABBRO -6m LOWER THAN F

BA1G

REV-DRILL OVERP appears as OVERP and ChRM

169	-61
121	-46
128	-37

D_m	I_m	k	a_{95}	N	PAL-LAT
135.1754	-49.60166174	17.13351	30.74744286	3	-30.43463

BA1H

BARB1H Directions

Sample	DemagType	field/temp	Dec (°)	Inc (°)	MAD (blank if avg)	ChRM	Comment
BA1H3	AF	0-10	353	-55	14.4	N	LT1? ABOVE SW-SHALLOW?
BA1H5	AF	0-15	94	-4	16.1	N	E-SHALLOW? NOISY
BA1H6	AF	TOO NOISY					
BA1H9	AF	TOO NOISY					
BA1H10	AF	TOO NOISY					
BA1H2	TH	TOO NOISY					

BA1H VERY NOISY SITE - TENDING TO CLUSTER WEST KOMATIITIC BASALT

BARB1I Directions

	Sample	DemagType	field/temp	Dec (°)	Inc (°)	MAD (blank if avg)	ChRM	Comment
BA1I	BA1I2	AF	1-5	306	46	7.3	N	DRILL OVERP
	BA1I2	AF	5-25	257	77	13	Y	W-STEEP
	BA1I4	TH+AF	100-10	335	65	3.2	N	WNW-STEEP
	BA1I4	TH+AF	15-35	58	-9	14.9	Y	E-SHALLOW ABOVE STEEP
	BA1I17	AF	0-10	293	39	6.8	N	W-DOWN - DRILL OVERP??
	BA1I17	AF	20-70	81	-8	8.6	Y	E-SHALLOW CLEARLY ABOVE W
	BA1I15	TH	0-380	196	62	17.4	N	SWS-STEEP
	BA1I15	TH	500-540	65	-12	6.7	Y	E-SHALLOW CLEARLY ABOVE STEEP
	BA1I3	TH	SPIN - UNRELIABLE					
	BA1I	**WEST OVERPRINT (PRESUMED DRILLING RELATED) WITH E SHALLOW CHRM**						POSSIBLY BAKED KOMATIITE

BA1I

E-SHALLOW CLEARLY ABOVE STEEP

58	-9
81	-8
65	-12

Dm	Im	k	a95	N	PAL-LAT
68.00117	-9.802267962	47.11941	18.16371997	3	-4.93726

BA1J

BARB1J Directions

Sample	DemagType	field/temp	Dec (°)	Inc (°)	MAD (blank if avg)	ChRM	Comment
BA1J1	AF	TOO NOISY					
BA1J4	AF	TOO NOISY					
BA1J6	AF	1-5	270	80	3.9	N	W-STEEP BUT TENUOUS
BA1J9	AF	0-15	300	-40	25.7	Y	W-UP??? VERY NOISY ZIJD
BA1J3	TH	200-350	67	-6	7.3	N	E-SHALLOW OVERPRINT
BA1J3	TH	380-420	269	54	14.7	Y	W-STEEP IN INTRUSION??
BA1J12	TH			**MOLSPIN - UNRELIABLE**			
BA1J		**NOISY SITE WITH LOW UNBLOCKING TEMP/COER**					GABBRO

BA1K

BARB1K Directions

Sample	DemagType	field/temp	Dec (°)	Inc (°)	MAD (blank if avg)	ChRM	Comment
BA1K4	AF	20-50	319	32	24.1	N	DRILL OVERP - E SHALLOW ABOVE?
BA1K7	AF	1-25	345	27	19	Y	DRILL OVERP? NOISY
BA1K7	TH	200-480	321	36	16.8	N	DRILL OVERP? BA1K9??
BA1K7	TH	520-580	72	-42	20.3	Y	E-UP? NOISY
BA1K2	TH			**MOLSPIN - UNRELIABLE**			
BA1K		**DRILL OVERPRINT - UNSTABLE ABOVE?**					WELL-BAKED KOMATIITE

BA1K

DRILL OVERP appears as OVERP and ChRM

319	32
345	27
321	36

D_m	I_m	k	a_{95}	N	PAL-LAT
328.6722	32.23077	37.69528531	20.36622	3	17.496818

BA1L

BARB1L Directions

Sample	DemagType	field/temp	Dec (°)	Inc (°)	MAD (blank if avg)	ChRM	Comment
BA1L1	AF	15-50	220	-77	11	Y	SWS STEEP UP! UNRESOLVED OVERPRINT
BA1L5	AF	10-70	282	-77	1.3	Y	WEST STEEP UP! UNRESOLVED OVERPRINT
BA1L3	TH	540-580	190	-80	2.7	Y	SWS STEEP UP - UNRESOLVED OVERP
BA1L(UPPER)	**STRANGE STEEP UP DIRECTION**						KOMATIITE
BA1L6	TH	200-400	291	41	13.7	N	DRILL OVERP
BA1L6	TH	500-580	298	6	13.9	Y	WEST SHALLOW
BA1L7	TH+AF	5-15	305	44	9.9	N	DRILL OVERP? NOISY
BA1L7	TH+AF	20-40	301	4	13.8	Y	WEST SHALLOW -CLEAN
BA1L8	AF	15-35	302	34	3	N	DRILL OVERP
BA1L8	AF	35-60	288	12	23.3	Y	WEST SHALLOW -NOISY
BA1L(LOWER)	**DRILL OVERP ABOVE WEST AND SHALLOW**						OLIVINE CUMULATE

TRANSITING FROM TOP OF KOMATIITE TO BASE OF NEW UNIT (CUMULATE) - BIG CHANGE IN BEHAVIOUR

BA1L

DRILL OVERP appear as overp

291	41
305	44
302	34

D_m	I_m	k	a_{95}	N	PAL-LAT
299.3388	39.82016861	114.0481	11.59741257	3	22.629953

WEST SHALLOW isolated between 20mT/580

298	6
301	4
288	12

D_m	I_m	k	a_{95}	N	PAL-LAT
295.7194	7.366340544	104.9907	12.09217767	3	3.6984513

BA2A

BARB2A

Sample	DemagType	field/temp	Dec (°)	Inc (°)	MAD (blank if avg)	ChRM	Comment
BA2A1	AF	20-70	50	41		Y	V NOISY; DRILLING OVERP?
BA2A6	TH+AF	15-60	38	41	24.7	Y	V NOISY; DRILLING OVERP?
BA2A8	AF	1-100	48	34	14.4	Y	DRILLING OVERP?
BA2A3	TH	400-540	51	61	18.3	Y	V NOISY; DRILLING OVERP?; VISCOUS OVERP
BA2A5	TH	400-540	44	41	15.2	Y	DRILLING OVERP?; VISCOUS OVERP
BA2A9	TH	400-520	326	18	5	Y	????; NOISY OVERP
2A	**LOTS OF FULL DRILLING OVERPRINTS WITH ONE STRANGE OUTLIER**						Komatiitic Basalt

BA2A

DRILL ORIENTATION - 036 / 43

BA2A1	DRILLING OVERP?	
BA2A6	50	41
BA2A8	38	41
BA2A3	48	34
BA2A5	51	61
	44	41

D_m	I_m	k	a_{95}	N	PAL-LAT
45.87883	43.651711	55.92136	10.32042	5	25.50074

BA2B

BARB2B Directions

Sample	DemagType	field/temp	Dec (°)	Inc (°)	MAD (blank if avg)	ChRM	Comment
BA2B4	TH	200-500	215	-66	12.2	N	SW-UP
BA2B7	TH	0-480	204	-51	11.3	N	SW-UP
BA2B8	TH	100-480X300	69	60	24.7	N	DRILLING OVERP?
BA2B2	AF	0-10	217	-54	2.7	N	CLEAN REV DRILLING OVERP?
BA2B3	AF	0-10	212	-56	3.6	N	CLEAN REV DRILLING OVERP?
BA2B9	AF	0-5	45	-12	22.2	N	NE-UP
BA2B4	TH	530-600	30	-61	11.2	Y	NE-UP
BA2B7	TH	560-600	204	27	1.7	Y	SW-DOWN
BA2B8	TH	440-550X500	308	51	15.2	Y	NW-STEEP?DOWN
BA2B2	AF	15-50	93	-71	13.3	Y	EAST-UP???
BA2B3	AF	20-70	36	-18	8.1	Y	NE-UP
BA2B9	AF	10-50	212	41	3.1	Y	SW-DOWN

2B **both polarities of drilling ovprint but 3 samples show no sign** Komatiite

ChRMs clean but not consistent except for a few NE-Up

BA2C

BARB2C Directions

Sample	DemagType	field/temp	Dec (°)	Inc (°)	MAD (blank if avg)	ChRM	Comment
BA2C2	AF	3-40	26	11	37.9	Y	EAST-SHALLOW
BA2C4	AF	TOO NOISY					
BA2C8	AF	35-65	55	-41		Y	NE-UP BUT MEAN DIR AS VERY NOISY
BA2C9	AF	25-90	85	-4	26.2	Y	E-SHALLOW - NOT FULLY DEMAGD
BA2CC13	AF	5-25	216	5	19.2	N	SW-SHALLOW
BA2CC13	AF	30-90X60	91	-6	17	Y	EAST-SHALLOW
BA2C14	AF	20-70	80	-16		Y	EAST-SHALLOW
BA2C15	AF	3-50	52	-57		Y	NE-UP BUT MEAN DIR AS VERY NOISY
BA2C6	TH	440-520	64	0.3	21.3	Y	EAST-SHALLOW
BA2C11	TH	420-500	99	-24		Y	EAST-SHALLOW

2C **NOISY ZIJDS BUT CONSISTENT CHRMs - EAST SHALLOW WITH SOME NOISY NE-UP** Komatiitic Basalt

IF WOULD BE FROM OPPOSITE SIDE OF CORE, WOULD BE WEST AND SHALLOW

BA2C

	EAST-SHALLOW		Isolated between 3mT and 90
BA2C2	26	11	
BA2C9	85	-4	
BA2CC13	91	-6	
BA2C14	80	-16	
BA2C6	64	0.3	
BA2C11	99	-24	

D_m	I_m	k	a_{95}	N	PAL-LAT
74.69037129	-7.03105	8.289889	24.72922	6	-3.528808

BA2D

BARB2D Directions

Sample	DemagType	field/temp	Dec (°)	Inc (°)	MAD (blank if avg)	ChRM	Comment
BA2D2	TH	300-570	176	12	8.3	Y	S-SHALLOW
BA2D3	TH	100-560	168	8	13.3	N	S-SHALLOW OVERPRINT - SMALL UNBLOCKING RANGE
BA2D3	TH	560-620	154	20	0.4	Y	SE-DOWN - SHARP UNBLOCKING 560-580
BA2D5	TH	200-520X400	185	-6	16.5	Y	S-SHALLOW
BA2D4	AF	7-45	175	14	7.3	Y	S-SHALLOW
BA2D5	AF	20-70	17	-25	5.8	Y	N-UP???
BA2D6	TH+AF	200-30	187	-7	14.3	Y	S-SHALLOW
BA2D7	AF	0-35	180	5	7.4	Y	S-SHALLOW
BA2D8	AF	1-15	156	4	6.8	N	S-SHALLOW
BA2D8	AF	15-25	141	15	3.5	Y	SE-DOWN

2D **HIGHLY CONSISTENT DIRECTIONS, CLEAR ZIJDS** Komatiitic Basalt

WHERE 2 COMPONENTS ARE PRESENT, S-SHALLOW IS OVERPRINT OF SE-DOWN

WHERE 1 COMPONENT, S-SHALLOW IS CHRM

BA2D

S-SHALLOW isolated between 0mT and 570, seen as ChRM, with one exception

BA2D2	176	12
BA2D3	154	20
BA2D5	185	-6
BA2D4	175	14
BA2D6	187	-7
BA2D7	180	5
BA2D8	156	4
BA2D3	168	8

D_m	I_m	k	a_{95}	N	PAL-LAT
173.4758485	6.141054	24.25089	12.50584	7	3.0793695

Appendix B – Hooggenoeg Formation Directional Results

Hooggenoeg Formation directions obtained are presented here. Generally, sites contained a lower temperature direction (LT), a mid temperature direction (MT) and high temperature direction (HT). Results presented here are split into these categories.

	LHG1 - LT					
	Sample	Dec (°)	Inc (°)	MAD	Temp(°C)/Field (mT)	Comment
LHG1	LHG1.1B	99.4	51.3	14	20-300	
	LHG1.2B	322.8762	-79.1908	7.812949	* 20-300 LT	
	LHG1.2C	330.2112	-20.444	26.8525	* 100-400	
		328.9898	-49.8495			
	LHG1.3B	311.0751	-70.8859	9.628954	* 100-350 LT	
	LHG1.3C	349.1949	-46.8707	14.02233	* 100-400 LT	
		337.0746	-60.1068			
	LHG1.4B	too noisy				
	LHG1.5B	347.5729	-13.778	15.30477	* 0-400 LT	
	LHG1.6B	323.8806	-45.4941	10.52267	* 100-400	
	LHG1.6C	too noisy				
	LHG1.7B	335.1	-33.7	9.1	100-400	
	LHG1.8B	359.1516	-40.1765	14.41999	* 100-400 LT	
	LHG1.8C	348.675	-52.2473	1.474053	* 100-300 LT	
		354.4927	-46.3302			
	LHG1.9B	337.6213	-66.9974	4.900526	* 20-350 LT	
	LHG1.9C	7.977414	-59.9878	6.279097	* 0-300 LT	
		354.7074	-64.284			
	LHG1.10B	349.7541	-27.6925	9.035487	* 100-350 LT	
	LHG1.10C	307.9	-19.3	5.3	100-300	
	LHG1.10C	354.2707	-49.1085	12.25704	* 100-350	
			335.2873			

	LHG1 - MT				
	Sample	Dec (°)	Inc (°)	MAD	Temp(°C)/Field (mT) Comment
LHG1	LHG1.1B				
	LHG1.2B				
	LHG1.2C				
	LHG1.3B	76.32841	-57.8556	8.602575	* 440-500
	LHG1.3C				
	LHG1.4B				**too noisy**
	LHG1.5B	295.4999	4.265481	4.082475	* 10-25 MT
	LHG1.6B				
	LHG1.6C				
	LHG1.7B				
	LHG1.8B	354.3676	-4.13032	10.17084	* 0-15 MT
	LHG1.8C	7.911092	4.617142	23.31054	* 350-10 MT
		1.137135	0.245123		
	LHG1.9B				
	LHG1.9C	26.53503	18.61781	12.8077	* 0-15 MT
	LHG1.10B	333.213	25.50685	14.82906	* 0-30 MT
	LHG1.10C				
	LHG1.10C				

	LHG1 - MT					
	Sample	Dec (°)	Inc (°)	MAD	Temp(°C)/Field (mT)	Comment
LHG1	LHG1.1B			**doesnt go to origin**		
	LHG1.2B	355.5052	58.84216	13.13005	350-540 HT	
	LHG1.2C	119.4741	-62.7644	15.01914	25-80	
			50.92001			
	LHG1.3B	272.2514	53.15514	6.127955	* 500-530	(not to origin)
	LHG1.3C	271.1156	67.88926	10.70114	* 25-70 HT	(not to origin)
		271.8134	60.52334			
	LHG1.4B				**Too noisy**	
	LHG1.5B				**Too noisy**	
	LHG1.6B	262.5779	78.16832	26.99577	* 7-45 HT	(not to origin)
	LHG1.6C	263.9074	55.66605	7.892655	* 3-60 HT	(not to origin)
		263.553	66.91827			
	lhg1.7b	270.3	64	16	440-540	
	LHG1.8B	297.1117	66.62209	13.16627	20-70 HT	
	LHG1.8C	287.6718	67.76263	9.330983	* 30-70 HT	(not to origin)
		292.5037	67.26179			
	LHG1.9B	221.4892	6.070351	8.523185	530-550 HT	
	LHG1.9C	254.7835	54.42439	15.32947	* 25-70 HT	(not to origin)
		233.6606	31.24832			
	LHG1.10B	357.9272	46.11351	22.16162	* 35-70	
	LHG1.10C				**Noisy**	
	LHG1.10C	19.64661	39.95138	8.310345	440-70	
		9.339231	43.54788			

	LHG2 - LT					
	Sample	Dec (°)	Inc (°)	MAD	Temp(°C)/Field (mT)	Comment
LHG2	LHG2.1B	242.7442	3.879666	10.51272	* 0-350 LT	
	LHG2.2A	244.2081	-4.31882	5.086311	* 20-400 LT	
	LHG2.2B	248.5934	8.746084	6.234911	* 0-400 LT	
		246.391	2.215255			
	LHG2.3B	258.1359	-12.5926	15.55915	* 0-350 LT	
	LHG2.4A	316.8427	-42.2655	9.680123	* 20-400 LT	
	LHG2.4B	298.5703	-62.9553	6.779109	* 0-400 LT	
		309.9062	-52.9424			
	LHG2.5A	263.6055	-39.386	8.826478	* 0-400	
	LHG2.5B					
	LHG2.6B	300.0463	-44.5126	6.902703	* 0-350 LT	
	LHG2.6C	221.5	-63.3	10.8	20-350	
		271.2852	-60.1436			
	LHG2.8B	74.5	52.6	8.5	20-350	
	LHG2.10A	341.012	-7.71071	6.683539	* 300-440	
	LHG2.11B	66.65578	56.01634	4.905597	* 20-350	
	LHG2.13A	94.13015	-48.8122	6.730447	* 0-350 LT	
	LHG2.13C	79.70014	-63.0085	5.719695	* 200-400 LT	
		88.24947	-56.1142			

	LHG2 - MT					
	Sample	Dec (°)	Inc (°)	MAD	Temp(°C)/Field (mT)	Comment
LHG2	LHG2.1B	186.7892	-4.57115	11.30295	* 3-20 MT	
	LHG2.2A					
	LHG2.2B					
	LHG2.3B	188.9705	-1.75823	10.47449	* 3-15 MT	
	LHG2.4A					
	LHG2.4B	239.879	52.84935	32.19649	* 20-50 MT	
	LHG2.4B					
	LHG2.5A	91.72877	65.06364	21.10487	* 0-20 MT	
	LHG2.5B					
	LHG2.6B	289.032	46.86841	16.80472	* 400-25 MT	
	LHG2.6C					
	LHG2.8A					
	LHG2.8B	224	57.5	19.2	400-480	
	LHG2.10A					
	LHG2.11B					
	LHG2.13A					
	LHG2.13C					

	LHG2 - HT				
	Sample	Dec (°)	Inc (°)	MAD	Temp(°C)/Field (mT)	Comment
LHG2	LHG2.1B	130.6073	63.18157	10.80619	35-50 HT	
	LHG2.2a			**Too noisy**		
	LHG2.2B			**Too noisy**		
	LHG2.3B	100.7252	-6.3172	23.21393	* 30-50 HT	
	LHG2.8B	335.4	-25.5	25.7	480-550	
	LHG2.4A	233.8174	73.21568	10.12595	480-560 HT	
	LHG2.4B	223.7406	66.98176	26.54267	50-90 HT	
	LHG2.4B	218.6234	58.53655	10.8083	10-90 HT	
		223.9309	66.36153			
	LHG2.5A	264.9809	61.88142	11.11584	45-70 HT	
	LHG2.5B	211.6677	58.88828	10.52302	480-540	
		237.0026	63.06275			
	LHG2.6B	195.9437	54.36162	7.147431	30-70 HT (HT1)	
	LHG2.6C			**Noisy**		
	LHG2.8A			**Too noisy**		
	LHG2.10a			**Too noisy**		
	LHG2.11b			**Too noisy**		
	LHG2.13A			**Too noisy**		
	LHG2.13C			**Too noisy**		

	LHG3 - LT					
	Sample	Dec (°)	Inc (°)	MAD	Temp(°C)/Field (mT)	Comment
LHG3	LHG3.2A	**Exp. Not completed (AF part)**				
	LHG3.3A	270.1794	0.495069	10.51741	* 100-440	
	LHG3.3B	265.7632	-48.4752	16.43805	* 0-400	Z-plot noisy
	LHG3.3C	250.3	23.8	7.3	20-300	Z-plot noisy
		260.6854	12.32667			
	LHG3.4A	227.0248	-51.3985	7.214503	* 100-400	
	LHG3.4B	268.3404	-65.5696	19.28695	* 100-350 LT	
	LHG3.4C	304.3034	-61.6745	3.845065	* 100-350	
		262.3327	-63.6652			
	LHG3.5A	241.8439	-50.9604	13.26767	* 0-350 LT	
	LHG3.5B	134.7586	-47.5541	10.98133	* 100-400 LT	
	LHG3.6A	276.3944	-55.4861	15.9708	* 100-400	
	LHG3.6B	236.7698	-53.4545	7.751532	* 300-440	
		256.0696	-56.1054			
	LHG3.8A	258.7406	-62.47	13.47526	* 100-400	
	LHG3.9A	282.9071	-49.1204	13.31237	* 0-400	
	LHG3.9B	329.1	-70.2	16.3	100-350	
		298.2831	-61.4849			

	LHG3 - MT				
	Sample	Dec (°)	Inc (°)	MAD	Temp(°C)/Field (mT)	Comment
LHG3	LHG3.2A	**Exp. Not completed (AF part)**			
	LHG3.3A				
	LHG3.3B	323.279	2.033254	9.716213	* 0-10 MT
	LHG3.3C				
	LHG3.4A				
	LHG3.4B				
	LHG3.4C				
	LHG3.5A	232.8205	31.11566	7.287976	* 3-20
	LHG3.5B	171.5761	68.44287	10.10305	* 10-30 MT
		215.4998	53.2104		
	LHG3.6A				
	LHG3.6B				
	LHG3.8A	237.0898	52.8882	6.244823	* 0-35 MT
	LHG3.9A	229.8253	55.84557	5.354855	* 0-25 MT
	LHG3.9B	331.2	24.3	20.9	350-440
		296.6947	51.89787		

	LHG3 - HT					
	Sample	Dec (°)	Inc (°)	MAD	Temp(°C)/Field (mT)	Comment
LHG3	LHG3.2A	completed (AF part)				
	LHG3.3A	233.0592	53.69407	7.531083	480-550	
	LHG3.3B	166.9984	25.43473	17.38614	50-90	
	LHG3.3C	30.9	81.9	9.4	480-560	
		192.3276	44.3221			
	LHG3.4A	205.6969	64.96967	7.75071	480-550	
	LHG3.4B	195.1892	58.74516	3.989027	30-90 HT	
	LHG3.4C	205.4651	57.55137	4.41911	480-540	
		201.9292	60.5129			
	LHG3.5A	169.7721	57.38411	5.216659	45-90 HT	note that this dir is the same as 3.5B MT dir!
	LHG3.5B	67.88239	65.00523	6.264239	480-560	
		127.318	70.69472			note that this dir is the same as 3.5B MT dir!
	LHG3.6A	189.5984	61.32922	5.975701	40-90 HT	
	LHG3.6B	196.8424	60.78316	1.601171	25-80	
		193.2517	61.10468			
	LHG3.8A	174.661	61.08426	9.380362	35-90 HT	
	LHG3.9A	171.5155	55.03095	3.894886	480-560	
	LHG3.9B	175.8	38.8	6.5		
			173.9845			

	LHG4 - LT				
	Sample	Dec (°)	Inc (°)	MAD	Temp(°C)/Field (mT)	Comment
LHG4	LHG4.1	331.2	16.9	3.2	20-350	
	LHG4.1A	350.7019	-15.7065	2.561736	* 20-350	
	LHG4.1B	**Exp. Not finished (AF part)**				
	LHG4.2C	**Too noisy**				
	LHG4.3A	166.1081	-72.7055	12.27332	* 20-350 LT	
	LHG4.3D	116.5	-65.9	10.7	20-350	
		137.1442	-71.0237			
	LHG4.4C	267.863	3.201717	8.625935	* 100-350	
	LHG4.4D	268.3491	12.3084	8.897131	* 20-400 LT	
		268.1034	7.755127			
	LHG4.5B	263.9166	4.138708	12.70611	* 100-350	
	LHG4.5C	255.7651	-2.63844	10.96448	* 100-400 LT	
		259.8377	0.752038			
	LHG4.6B	40.3282	72.35085	3.132153	* 100-350	
	LHG4.7D	308.5014	36.28092	10.87516	* 00-400	
	LHG4.8B	312.7973	34.50642	6.350006	* 00-440	
	LHG4.8C	212.9882	23.59332	10.28883	* 20-350	
	LHG4.8D	311.265	28.52052	6.700775	* 200-400	
	LHG4.8E					
		281.8677	38.70115			
	LHG4.9A	177.7825	15.30896	2.942023	* 100-350	
	LHG4.9C	**Exp. Not finished (AF part)**				
	LHG4.9D	185.4291	12.16825	2.614612	* 20-350 LT	
		181.6315	13.76808			
	LHG4.10A	258.033	-17.8656	2.678169	* 20-300	
	LHG4.10B	353.2745	-25.6718	5.378903	* 100-350	
	LHG4.10D	340.4118	-28.043	5.816268	* 100-350	
		318.9322	-30.8205			

	LHG4 - MT				
	Sample	Dec (°)	Inc (°)	MAD	Temp(°C)/Field (mT)	Comment
LHG4	LHG4.1A					
	LHG4.1B			**Exp. Not finished (AF part)**		
	LHG4.1C					
	LHG4.2C			**Too noisy**		
	LHG4.3A	304.2822	8.478518	189.9804	* 0-35 MT	
	LHG4.3D					
	LHG4.4C					
	LHG4.4D					
	LHG4.5B					
	LHG4.5C	273.4325	40.28694	78.68664	* 0-15	
	LHG4.6B					
	LHG4.7D					
	LHG4.8B					
	LHG4.8C					
	LHG4.8D					
	LHG4.8E					
	LHG4.9A					
	LHG4.9C			**Exp. Not finished (AF part)**		
	LHG4.9D					
	LHG4.10A					
	LHG4.10B					
	LHG4.10D					

	LHG4 - HT					
	Sample	Dec (°)	Inc (°)	MAD	Temp(°C)/Field (mT)	Comment
LHG4	LHG4.1A	too noisy				
	LHG4.1B	t finished (AF part)				
	LHG4.1	Noisy				
	LHG4.2C	Too noisy				
	LHG4.3A	178.2014	65.21758	15.419	40-70 HT	
	LHG4.3D	noisy				
	LHG4.4C	307.7234	80.47401	25.04152	440-540	
	LHG4.4D	79.34552	67.22103	19.71513	* 0-15 HT	
		55.29838	80.95985			
	LHG4.5B	221.8483	65.69159	13.8252	440-530	
	LHG4.5C	151.7601	63.15385	6.453841	40-50	
		184.9452	68.59147			
	LHG4.6B	218.2278	86.60905	17.36321	480-530	
	LHG4.7D	159.82	68.79098	15.04909	500-530	
	LHG4.8B	too noisy				
	LHG4.8C	163.1419	74.85913	4.044374	0-30 HT	
	LHG4.8D	too noisy				
	LHG4.8E					
	LHG4.9A	254.9745	-6.56201	4.337436	400-500	
	LHG4.9C	t finished (AF part)				
	LHG4.9D	293.2555	-27.007	8.522303	7-35 HT	
		273.0335	-17.7039			
	LHG4.10A	57.37917	27.40076	14.67455	60-80 HT	
	LHG4.10B	89.84599	33.55711	11.37222	480-540	
			73.08461			
	LHG4.10D	97.21394	241.8668	20.27096	480-540	weak Z-plot

	LHG5 - LT				
	Sample	Dec (°)	Inc (°)	MAD	Temp(°C)/Field (mT)	Comment
LHG5	LHG5.2A			**Too noisy**	
	LHG5.2B	284.3439	-56.4229	15.54676	* 200-350 LT	
	LHG5.3B	262.7297	-65.4133	28.09454	* 0-400 LT	
		275.0824	-61.3428			
	LHG5.3C	269.471	21.37179	14.50397	* 20-300 LT	
	LHG5.4A			**Too noisy**	
	LHG5.4B	226.9676	-2.8602	6.473127	* 200-350 LT	
	LHG5.5A	237.0711	54.02789	7.55019	* 0-350 LT	
	LHG5.5B	235.5216	50.62475	21.08551	* 0-350 LT	
	LHG5.5C	268.1162	49.28629	1.938288	* 100-300	
		247.2365	52.29974			
	LHG5.6A	226.7238	32.12927	5.403727	* 100-400	
	LHG5.6B	240.5201	53.72822	6.53735	* 0-400 LT	
	LHG5.6C	206.0047	44.24951	9.92433	* 20-350	
		223.6492	44.1877			
	LHG5.7A	215.5979	43.93293	3.483968	* 0-350 LT	
	LHG5.7B	227.1411	47.17381	6.377729	* 0-400 LT	
	LHG5.7C	203.6276	56.23513	0.52752	* 100-300	
		216.2141	49.48534			
	LHG5.8A	242.0204	20.79412	7.359074	* 0-400 LT	
	LHG5.8B	241.3	20.3	2.2	20-350	
		241.6596	20.54743			
	LHG5.10A			**Exp not finished (AF part)**	
	LHG5.10B	197.7792	84.47682	5.422115	* 0-400 LT	
	LHG5.11A	242.1801	83.4052	3.328333	* 200-440	
	LHG5.11B	186.5263	82.95882	7.412848	* 0-400 LT	
	LHG5.11C					

	LHG5 - MT					
	Sample	Dec (°)	Inc (°)	MAD	Temp(°C)/Field (mT)	Comment
LHG5	LHG5.2A					
	LHG5.2B					
	LHG5.3B	170.4209	-40.6101	14.92966	* 10-30 MT	
	LHG5.3C	332.3526	-23.9824	16.86532	* 0-15 MT	
	LHG5.4A					
	LHG5.4B	229.5389	68.53257	30.01036	* 480-25 MT	(HT1)
	LHG5.5A	298.1967	32.23949	14.48625	* 0-20 MT	
	LHG5.5B	2.795173	36.67549	36.73985	* 7-45 MT?	
		329.5334	39.06573			
	LHG5.5C					
	LHG5.6A					
	LHG5.6B	271.1267	44.68188	20.60095	* 480-50 MT	
	LHG5.6C					
	LHG5.7A	Too noisy				
	LHG5.7B	72.47713	58.39842	16.19165	* 0-20 MT	
	LHG5.7C					
	LHG5.8A	Too noisy				
	LHG5.8B					
	LHG5.10A	Exp not finished (AF part)				
	LHG5.10B	Too noisy				
	LHG5.11B	19.40738	69.18715	13.96129	* 0-25 MT	
	LHG5.11C					

	LHG5 - HT					
	Sample	Dec (°)	Inc (°)	MAD	Temp(°C)/Field (mT)	Comment
LHG5	LHG5.2A	Too noisy				
	LHG5.2B	298.2124	43.5966	18.47301	0-50 HT	
	LHG5.3B	79.78223	88.21367	8.288938		
	LHG5.3C	134.4007	-10.0638	18.44207	* 30-45 HT	
	LHG5.4A	Too noisy				
	LHG5.4B	75.194	54.64694	16.66151		
	LHG5.5A	44.85619	45.83448	19.53654	45-70 HT	(HT2S)
	LHG5.5B	174.6724	56.53492	26.02565	50-90 HT	(HT1)
	LHG5.5C	166.0315	56.24779	15.44248	500-560	
	LHG5.6A	Too noisy				
	LHG5.6B	311.4438	47.6929	25.18986	60-80 HT	
	LHG5.6C					
	LHG5.7A	Too noisy				
	LHG5.7B	186.2444	25.10484	28.38012	45-70 HT	
	LHG5.7C	Too noisy				
	LHG5.8A	Too noisy				
	LHG5.8B	noisy				
	LHG5.10A	Exp not finished (AF part)				
	LHG5.10B	Too noisy				
	LHG5.11A	303.2832	58.39141	18.44015	520-550	
	LHG5.11B	195.3197	47.43505	5.237267	40-50 HT	
	LHG5.11C	192.8562	80.07899	0.94452	100-580	
		230.8853	71.83178			

	LHG6 - LT				
	Sample	Dec (°)	Inc (°)	MAD	Temp(°C)/Field (mT)	Comment
LHG6	LHG6.1A	337.6142	-76.7015	14.86274	* 100-350	
	LHG6.1B	28.02053	-63.0753	14.25448	* 20-350 LT	(strange dir)
	LHG6.1C	306.652	-56.855	14.65411	* 100-350 LT (LT)	
		341.5328	-69.8819			
	LHG6.2A	319.4932	-83.2055	13.01986	* 100-400 LT	
	LHG6.4A	257.649	-38.8194	9.491903	* 100-350 LT	
	LHG6.4B	282.9	-45.5	10.6	20-350	
		269.5963	-42.8563			
	LHG6.6B	267.5728	-30.7176	16.23039	* 20-350 LT	
	LHG6.7A	320.6384	-60.3304	5.429522	* 20-400 LT	
	LHG6.7B	51.31906	-76.497	12.79226	* 20-350 LT	Z-plot noisy
	LHG6.8A	**Exp. Not finished (AF part)**				
	LHG6.8B	314.449	-64.195	7.954825	* 20-400 LT	
	LHG6.8C					
	LHG6.9B	348.2902	-66.1392	3.499651	* 100-350 LT	
	LHG6.9C	348.6	-57.6	8.8	100-350	
		348.4667	-61.8697			
	LHG6.10B	24.17561	-9.87741	4.741537	* 20-350 LT	
	LHG6.10B	**Too noisy/ altering**				
	LHG6.11A	344.9689	-83.1157	10.09684	* 20-400 LT	
	LHG6.11B	273.5857	-78.954	12.11686	* 200-440 LT	
	LHG6.11C	4.299522	-74.8071	4.888748	* 100-400	
		332.4861	-81.5112			

	LHG6 - MT				
	Sample	Dec (°)	Inc (°)	MAD	Temp(°C)/Field (mT)	Comment
LHG6	LHG6.1A	260.6786	68.39347	25.362	* 0-30 MT	
	LHG6.1B					
	LHG6.1C	277.0593	47.86452	10.56894	* 0-20 MT (MT)	
		271.2695	58.36933			
	LHG6.2A	311.3344	33.01114	3.251582	* 0-25 MT	
	LHG6.4A	296.9209	70.18551	15.55011	* 0-30 MT (MT)	
	lhg6.4b	343.4	-60.7	9.3	350-440	
	LHG6.6B	322.6243	67.48029	5.380694	* 0-15 MT	
	LHG6.7A					
	LHG6.7B					
	LHG6.8A	**Exp. Not finished (AF part)**				
	LHG6.8B	258.1996	76.13432	8.995407	* 7-35 MT	
	LHG6.8C					
	LHG6.9B	255.0835	72.60298	8.061763	* 3-25 MT	
	LHG6.9C					
	LHG6.10B	**Too noisy/ altering**				
	LHG6.11A					
	LHG6.11B					
	LHG6.11C					

	LHG6 - HT				
	Sample	Dec (°)	Inc (°)	MAD	Temp(°C)/Field (mT)	Comment
LHG6	LHG6.1A	148.5757	73.61076	4.547068	40-70 HT (HT1)	
	LHG6.1B	163.5786	44.16618	20.31785	* 480-550 HT (HT1 not to origin)	
	LHG6.1C	275.731	65.56038	18.40907	45-90 HT (HT2 N)	
		183.9812	70.88131			
	LHG6.2A	164.4489	78.49954	7.102839	35-90 HT (HT1)	
	LHG6.4A	205.2318	77.15006	6.138355	40-70 HT (HT1)	
	LHG6.4B	176.5	56	15.5	480-580	
		184.5679	67.10775			
	LHG6.6B	86.2616	61.02868	18.87588	* 35-70 HT (HT2S not to origin)	
	LHG6.7A	190.7596	61.10503	10.44833	480-550 HT (HT1)	
	LHG6.7B	156.6702	72.2969	5.842509	0-90 HT (HT1)	
		177.705	67.57245			
	LHG6.8A	**Exp. Not finished (AF part)**				
	LHG6.8B	194.0172	79.78181	8.329009	* 40-90 HT (HT1 not to origin)	
	LHG6.8C	181.281	54.7565	5.602689	480-550	
		184.2657	67.35977			
	LHG6.9B	185.2617	67.2288	5.130595	30-60 HT (HT1)	
	LHG6.9C	**Noisy**				
	LHG6.10B	**Too noisy/ altering**				
	LHG6.10B	**Too noisy**				
	LHG6.11A	176.5097	63.10355	15.39246	40-90 HT (HT1)	
	LHG6.11B	177.9958	58.33004	21.07442	* 520-560 HT (HT1 not origin)	
	LHG6.11C					
		177.308	60.71884			

Appendix C – Noisy Complex Directional Results

Noisy Complex directions obtained are presented here. Generally, sites contained a lower temperature direction (LT), a mid temperature direction (MT) and high temperature direction (HT). Results presented here are split into these categories.

	LNY1 - LT					
	Sample	Dec (°)	Inc (°)	MAD	Temp(°C)/Field (mT)	Comment
LNY1	LNY1.3AA	191.8884	-46.02377	1.378033	* 20-200	OHG
	LNY1.3A	**Single Component - lightning?**				
	LNY1.5A	**Single Component - lightning?**				
	LNY1.5B	**Too Noisy**				
	LNY1.6A	**Single Component - lightning?**				
	LNY1.6C	**Single Component - lightning?**				
	LNY1.7B	**Single Component - lightning?**				
	LNY1.7C	**Single Component - lightning?**				
	LNY1.8A	33.44862	-50.55145	33.60932	* 100-530	
	LNY1.8B	**Noisy in LT - particularly Th portion**				
	LNY1.9B	**Single Component - lightning?**				
	LNY1.9C	**Experiment not complet**				

	LNY1 - HT					
	Sample	Dec (°)	Inc (°)	MAD	Temp(°C)/Field (mT)	Comment
LNY1	LNY1.3AA	208.9039	-39.4977	2.271781	520-580	
	LNY1.3A	212.5	-41.5	2.3	20-580	Lightning Struck
		210.6751	-40.5128			
	LNY1.5A	347.4702	-16.7333	4.161763	7-90	Lightning?
	LNY1.5B	296.641	-45.6753	4.362396	400-580	
	LNY1.6A	248.0064	-39.3181	2.558664	20-580	Lightning
	LNY1.6C	244.2196	-33.5835	2.279806	100-580	Lightning
		246.0429	-36.4657			
	LNY1.7B	170.4646	-7.88368	1.62621	10-90	Lightning
	LNY1.7C	170.7432	-9.25738	1.220049	10-100	
		170.6036	-8.57055			
	LNY1.8A	178.4595	-24.0187	3.710712	530-580	
	LNY1.8B	196.8777	-13.1573	1.065333	20-90	
	LNY1.8C	179.496	-14.0524	2.002762	15-90	
		185.0676	-17.2497			
	LNY1.9B	250.5492	38.96982	3.079004	0-90	

	LNY2 - LT				
	Sample	Dec (°)	Inc (°)	MAD	Temp(°C)/Field (mT)	Comment
LNY2	LNY2.1B	Single Component, Lighting?				
	LNY2.1C	Single Component, Lighting?				
	LNY2.1D	256.6825	-6.56561	15.58784	* 20-0	
	LNY2.2B	264.8543	-32.016	15.6553	* 100-300	Ligtning? Small viscous, sample handling?
	LNY2.3B				**Lightning**	
	LNY2.5B	230.6997	-8.58819	0.278492	* 100-300	Ligtning? Small viscous, sample handling?
	LNY2.5C	218.2689	23.54485	5.248755	* 20-350	
		224.7202	7.521982			
	LNY2.6A	135.9686	-8.67031	20.64301	* 200-7	
	LNY2.7A	44.9879	7.372675	9.764165	* 300-440	
	LNY2.7B	77.94421	23.28848	6.177216	* 200-440	
	LNY2.7C	44.13985	2.512563	12.36248	* 200-440	
		54.94734	11.4434			
	LNY2.8A	267.2493	45.94731	7.409408	* 440-10	DONT USE BECAUSE Th & AF dont match very well
	LNY2.8A	259.4953	49.00605	6.179172	* 100-300	
	LNY2.8B	300.7108	49.48433	12.86804	* 100-400	
		275.382	49.51948			
	LNY2.9A	96.60714	-38.832	3.830535	* 200-440	
	LNY2.9B	100.2939	-18.9023	6.437497	* 200-440	
	LNY2.9C	98.62913	-28.8795	1.2	100-300	
		98.62913	-28.8795			
	LNY2.10A	130.7919	-28.0184	4.359162	* 100-440	
	LNY2.10B	118.0624	-11.3359	8.35415	* 100-15	
	LNY2.10C	106.451	-12.4737	5.674113	* 20-350	
		118.0215	-17.5018			
	LNY2.11B				**Single Component**	
	LNY2.12A	104.48	-23.4287	9.032088	* 100-400	
	LNY2.13A	336.9626	11.96137	3.997578	* 100-350	
	LNY2.14A	119.0917	-22.5337	14.7771	* 100-350	
	LNY2.14B	75.99355	-27.6284	6.199001	* 100-350	
		98.01374	-26.7109			
	LNY2.15B	101.9342	-24.6609	10.95624	* 200-7	

	LNY2 - HT					
	Sample	Dec (°)	Inc (°)	MAD	Temp(°C)/Field (mT)	Comment
LNY2	LNY2.1C	253.5305	-12.4316	3.711365	350-90	Lightning
	LNY2.3B	219.9	48.8	1.8	20-580 ex 200	Lightning Struck
	LNY2.8A	93.23324	-8.16822	4.109583	25-90	
	LNY2.9A	111.1104	-27.9758	8.727611	10-20	
	LNY2.9B	124.6242	-4.48999	5.705951	3-30	
	LNY2.9C	101.8	0.1	5.3	400-580	
		112.5465	-10.8748			
	LNY2.12A	106.0373	-20.65	2.911227	400-35	
	LNY2.14A	120.5325	-29.2568	3.713507	400-35	
	LNY2.14B	116.5141	-23.1294	4.789723	400-35	
		118.4704	-26.207			
	LNY2.15A	95.55166	-25.0264	5.492367	200-580	
	LNY2.15B	101.8052	-5.76592	7.449358	15-60	
		98.82467	-15.418			
	Outliers					
	LNY2.1B	253.8411	-16.0558	4.608523	100-580	Lightning?
	LNY2.1D	238.4472	-3.83403	2.957544	20-100	
		245.8141	-11.0319			
	LNY2.2B	244.6342	6.35857	3.763087	350-90	Lightning?
	LNY2.5B	212.6571	13.90665	1.508675	350-90	Lightning?
	LNY2.5C	211.0867	27.98144	2.455138	20-100	
		211.909	20.94584			
	LNY2.6A	97.31718	-13.4914	3.214881	20-90	
	LNY2.7A	72.14015	-10.8304	3.740709	15-90	
	LNY2.7B	78.39581	6.667677	5.869258	520-580	
	LNY2.7C	60.999	-12.671	1.75855	25-100	
		70.5687	-5.67874			
	LNY2.8B	61.53682	14.25983	5.259527	25-70	
	LNY2.10A	152.3043	-13.8438	18.7702	550-570	
						didnt average bc too
	LNY2.10B	131.2813	42.78903	14.99711	25-45	different
	LNY2.11B	81.1	-34.5	2.8	100-580	Lightning Struck ?
	LNY2.13A	338.6631	15.35382	2.217215	0-100	

	LNY3 - LT					
	Sample	Dec (°)	Inc (°)	MAD	Temp(°C)/Field (mT)	Comment
LNY3	LNY3.1A	155.4752	52.39578	10.60447	* 300-440	
	LNY3.1B	280.1146	78.15342	12.72101	* 100-440	
	LNY3.2A	172.8456	8.315416	7.107272	* 100-480	noisy
	LNY3.2B	182.7178	1.85744	3.883152	* 100-350	
	LNY3.2C	167.9601	7.560546	15.74017	* 200-440	
		174.5269	5.945875			
	LNY3.3A	138.2161	60.85776	6.738769	* 100-400	noisy
	LNY3.3B				**Too noisy**	
	LNY3.5B	161.416	-14.2165	8.479619	* 200-400	
	LNY3.9A				**Single Component Lightning**	
	LNY3.9B	100.7	-17.9	6.3	100-350	

	LNY3 - MT					
	Sample	Dec (°)	Inc (°)	MAD	Temp(°C)/Field (mT)	Comment
LNY3	LNY3.2C	173.8407	-7.36898	1.845074	* 15-40	

	LNY3 - HT				
	Sample	Dec (°)	Inc (°)	MAD	Temp(°C)/Field (mT)	Comment
LNY3	LNY3.1A	214.3828	34.14216	4.203238	7-70	
	LNY3.1B	215.6071	49.03794	8.840724	440-50	
		214.9239	41.59165			
	LNY3.2A	177.6935	10.14064	7.194428	500-560	noisy
	LNY3.2B	182.4663	3.712412	11.32686	500-570	
	LNY3.2C	183.1294	-2.67948	8.636462	45-100	
		181.113	3.727801			
	LNY3.3A				**Too noisy**	
	LNY3.3B	152.3708	26.38047	8.408658	3-40	
	Outliers					
	LNY3.5B	157.0806	-26.4545	0.659238	3-60	
	LNY3.9A	116.5555	-31.1467	2.921379	200-90	lightning
	LNY3.9B	110.9	-17.9	3.1	200-580	Single component
		113.5778	-24.5496			

	LNY4 - LT					
	Sample	Dec (°)	Inc (°)	MAD	Temp(°C)/Field (mT)	Comment
LNY4	LNY4.3B	6.957864	60.3618	3.347203	* 100-3	Noisy, espcially in Th (altering), Th & AF dont match well, v weak
	LNY4.3D	**Noisy, espcially in Th (altering), Th & AF dont match well, v weak**				
	LNY4.4A	181.4744	48.14964	7.61662	* 100-400	
	LNY4.4C	161.2	35.7	6.1	20-300	
		170.3339	42.36896			
	LNY4.5A	**Single Component**				
	LNY4.5B	123.552	13.9793	10.55566	* 100-300	
	LNY4.5C	97.027	12.35322	6.147898	* 200-400	
		110.2447	13.51397			
	LNY4.6A	176.2828	-51.3529	10.03972	* 200-20	
	LNY4.9A	358.0169	-3.18773	2.782873	* 200-350	
	LNY4.9B	**Single Component**				
	LNY4.10A	92.64843	-22.5832	13.40884	* 200-15	
	LNY4.10B	55.71503	-25.8178	9.136889	* 20-350	not averaged these two bc they are so different.

	LNY4 - MT					
	Sample	Dec (°)	Inc (°)	MAD	Temp(°C)/Field (mT)	Comment
LNY4	LNY4.10A	89.79719	-16.7571	10.6761	* 7-25	
	LNY4.10B	88.0265	-19.2728	3.237399	* 7-20	

	LNY4 - HT					
	Sample	Dec (°)	Inc (°)	MAD	Temp(°C)/Field (mT)	Comment
LNY4	LNY4.3B	234.5241	-50.3899	10.24839	3-35	
	LNY4.3D	164.1188	-67.0522	2.680652	3-40	
		208.9727	-63.2733			
	LNY4.4B	188.9539	16.71814	5.195262	3-25	
	LNY4.4C	183.9	20.1	15.9	400-570	
		186.4518	18.42578			
	LNY4.5A	84.26159	4.08948	2.868385	* 300-480	Single Component
	LNY4.5B	93.88158	15.19495	4.321978	400-40	
		88.99195	9.67564			I've averaged these, but they need checking as the direction is v different btwn them
	LNY4.9A				**Th & AF do not match - don't use**	
	LNY4.9B	81	-28.2	8.1	100-540	Single component
	LNY4.10A	145.9397	43.93407	8.796818	560-580	
	LNY4.10C	162.7035	-3.55735	9.252617	35-60	
	LNY4.10B	161.5684	5.156096	3.282154	35-70	
			157.8588			
	Outliers					
	LNY4.6A	210.6316	-34.5903	12.77469	30-50	

Appendix D – Nelshoogte Pluton Directional Results

Nelshoogte Pluton directions obtained are presented here. Generally, sites contained a lower temperature direction (LT), a mid temperature direction (MT) and high temperature direction (HT). Results presented here are split into these categories.

	LNP1 - LT					
	Sample	Dec (°)	Inc (°)	MAD	Temp(°C)/Field (mT)	Comment
LNP1	LNP1.1A			**Single component**		
	LNP1.2A			**Single component**		
	LNP1.2B			**Single component**		
	LNP1.3A			**Single component**		
	LNP1.3B			**Single component**		
	LNP1.4A			**Single component**		
	LMP1.5A			**Single component**		
	LNP1.5B			**Single component**		
	LNP1.6A			**Single component**		
	LNP1.6B			**Single component**		
	LNP1.7A			**Single component**		

	LNP1 - HT					
	Sample	Dec (°)	Inc (°)	MAD	Temp(°C)/Field (mT)	Comment
LNP1	LNP1.1A	285	-26.1	2.7	100-90	Single Component
	LNP1.2A	292.9	-33.2	3.1	350-550	Single Component
	LNP1.2B	289.4	-38.3	1.9	300-580	Single Component
		291.2061	-35.7627			
	LNP1.3A	321.6	19.9	3.7	100-90	Single Component
	LNP1.3B	317.6497	11.66545	2.176128	0-580	Single Component
		319.5846	15.79164			
	LNP1.4A	295.4747	-29.6194	2.604173	20-580	Single Component
	LNP1.5A	202.4	75	2.4	100-60 ex440	
	LNP1.58B	217.4	23.3	3.3	100-580	Single Component
		214.1188	49.31658			
	LNP1.6A	271.7	63.4	7.5	300-90	Single Component
	LNP1.6B	297.8	62.8	6.1	350-90	Single Component
		284.8871	63.70014			
	LNP1.7A	163.6255	49.69308	2.478337	20-580	Single Component

	LNP2 - LT				
	Sample	Dec (°)	Inc (°)	MAD	Temp(°C)/Field (mT)	Comment
LNP2	LNP2.2A			**Single Component**		
	LNP2.4A			**Single Component**		
	LNP2.5aa			**Exp not complete**		
	LNP2.6A			**Single Component**		
	LNP2.7AA			**Single Component**		
	LNP2.8A			**Single Component**		
	LNP2.8B			**Single Component**		
	LNP2.9A	227.758	-30.0518	15.57804	* 100-400	
	LNP2.9B	227.8	-30.1	15.6	100-400	

	LNP2 - HT				
	Sample	Dec (°)	Inc (°)	MAD	Temp(°C)/Field (mT)	Comment
LNP2	LNP2.2A	231.2901	-23.8801	3.371233	200-560	Single Component
	LNP2.4A	266.6	30.6	4.5	100-90	Single Component
	LNP2.5aa			**Exp not complete**		
	LNP2.6A	0.9	27	3.4	200-90	Single Component
	LNP2.7AA	50	16.3	2.6	200-560	Single Component
	LNP2.8A	80.6	41.5	2.4		Single Component
	LNP2.8B	66.1	42.5	3.7	100-570	Single Component
		73.40727	42.22878			
	LNP2.9A			**Too noisy**		
	LNP2.9B			**Too noisy**		

	LNP3 - LT					
	Sample	Dec (°)	Inc (°)	MAD	Temp(°C)/Field (mT)	Comment
LNP3	LNP3.1A	329.413	33.35993	2.366977	100-3	fully dmaged - handling overprint?
	LNP3.1B				**Single Component**	
	LNP3.2A				**Single Component**	
	LNP3.3A				**Single Component**	
	LNP3.3B				**Single Component**	
	LNP3.4a	271.4	75.6	3.1	0-400	fully dmaged - handling overprint?
	LNP3.5b	144.4	32	7.3	0-400	
	LNP3.6	57.02151	40.96507	6.693609	* 20-500	
	LNP3.7B	15.3	-57	14.8	200-400	
	LNP3.8AA	325.7267	1.525883	12.99255	* 20-3	
	LNP3.9A	300.3465	-77.4775	3.201189	* 20-300	

	LNP3 - HT				
	Sample	Dec (°)	Inc (°)	MAD	Temp(°C)/Field (mT)	Comment
LNP3	LNP3.1A				**too noisy**	
	LNP3.1B	328.9	32.1	1.7	20-550	Single Component
	LNP3.2A	201.6662	71.57742	1.130549	100-580	Single Component
	LNP3.3A	86.7	-16.7	8.2	300-580	Single Component - not properly resolved - overlapping
	LNP3.3b	91.6	-30.2	6.1	200-90 ex.440-0	Single Component
		89.02414	-23.4691			
	LNP3.4a				**Sample handling overprint**	
	LMP3.5b	213.3	32.6	8	500-580	
	LNP3.6	237.0172	64.18536	16.87197	540-580	
	lnp3.7b	303.2	-19.3	30.2	425-580	EX. 540-570 - DONT USE High MAD!
	LMP3.8AA	231.4843	36.63446	7.808909	50-80	
	LNP3.9A	229.3824	45.41431	13.67929	40-60	non convergent

	LNP4 - LT					
	Sample	Dec (°)	Inc (°)	MAD	Temp(°C)/Field (mT)	Comment
LNP4	LNP4.1B			**Single Component**		
	LNP4.3AA			**Single Component**		
	LNP4.4A			**Single Component**		
	LNP4.5A	38	67.1	3.4	0-350 ex. 100	
	LNP4.6A			**Single Component**		
	LNP4.7A	114.5	54.5	8.2	0-300	
	LNP4.8A			**Single Component**		
	LNP4.9A	110.1913	52.16288	4.268641	* 100-440	
	LNP4.9B	92.8	44	1.3	20-300	
		100.7992	48.40842			
	LNP4.10A	308.4934	-66.3072	4.387031	* 300-400	

	LNP4 - MT					
	Sample	Dec (°)	Inc (°)	MAD	Temp(°C)/Field (mT)	Comment
LNP4	LNP4.3AA					
	LNP4.5A	45	-71.4		10	350-480
	LNP4.9A	101.3877	61.45587	8724.308	4.205483	* 0-15
	LNP4.10A					

	LNP4 - HT					
	Sample	Dec (°)	Inc (°)	MAD	Temp(°C)/Field (mT)	Comment
LNP4	LNP4.1B	338.2	18.8	4.1	0-580 ex. 350-450	Single Component
	LNP4.3AA	215.708	-63.6757	1.124491	20-580	Single Component
	LNP4.4A	154.8	-69.7	4.5	100-580 ex.300-350	Single Component
						DONT USED MAD
	LNP4.5A	176	26.4	27.3		TOO HIGH
	LNP4.6A	140.4	14.4	4.5	100-580 ex. 350-450	
	LNP4.7A	131.3	59.4	4.9	350-540	
	LNP4.8A	341	-63.3	2.1	0-550	Single Component
	LNP4.9A	223.6354	50.48369	5.920516	35-90	
	LNP4.9B	137.4	65.6	7.3	350-550	
		191.7809	65.09334			
	LNP4.10A	330.8015	-77.8946	16.03913	7-40	

	LNP5 - LT				
	Sample	Dec (°)	Inc (°)	MAD	Temp(°C)/Field (mT)	Comment
LNP5	LNP5.1			**Single Component**	
	LNP5.2A			**Single Component**	
	LNP5.4A	104.1269	34.50669	6.358649	* 100-10
	LNP5.5A	30.84127	73.19446	4.323173	* 20-440
	LNP5.6A	19.08791	-40.4483	6.33329	* 100-400
	LNP5.6B			**Single Component**	
	LNP5.7A			**Single Component**	
	LNP5.8A	8.3	70.3	4	20-400

	LNP5 - MT					
	Sample	Dec (°)	Inc (°)	MAD	Temp(°C)/Field (mT)	Comment
LNP5	LNP5.1					
	LNP5.4A	101.3877	61.45587	4.205483	* 0-15	
	LNP5.5A					
	LNP5.6A	14.34351	-31.1957	8.252048	* 3-25	
	LNP5.6B					

Total Cores 10

	LNP5 - HT					
	Sample	Dec (°)	Inc (°)	MAD	Temp(°C)/Field (mT)	Comment
LNP5	LNP5.1	83.09248	18.78182	3.344467	20-580	Single Component
	LNP5.2A	65.8	-26	5.3	0-540 ex 100	Single Component
	LNP5.4A	237.0941	51.10046	5.68714	25-90	
	LNP5.5A	178.5711	74.43548	19.43157	* 500-570	not convergent
	LNP5.6A	226.1214	52.0757	14.08338	40-90	
	LNP5.6B	29.87186	81.10678	4.894444	100-80	Single Component
	LNP5.7A	47.4	14.4	4.4	0-580 ex 300-350	Single Component
	LNP5.8B	316	67.3	10.5	500-570	

	LNP6 - LT					
	Sample	Dec (°)	Inc (°)	MAD	Temp(°C)/Field (mT)	Comment
LNP6	LNP6.1A	187.5952	-64.6425	3.435067	* 100-440	
	LNP6.2A	**Single Component**				
	LNP6.3B	169.4	-82.6	3	0-400	
	LNP6.4A	**Single Component**				
	LNP6.4C	**Single Component**				
	LNP6.5A	**Single Component**				
	LNP6.5B	**Single Component**				
	LNP6.6B	**Single Component**				
	LNP6.7B	**Single Component**				
	LNP6.8A	**Single Component**				

	LNP6 - MT				
	Sample	Dec (°)	Inc (°)	MAD	Temp(°C)/Field (mT)	Comment
LNP6	LNP6.1A	182.3806	-63.4059	6.699656	* 3-25	
	LNP6.4A					
	LNP6.4C					
	LNP6.5A					
	LNP6.5B					
	LNP6.8A					

	LNP6 - HT					
	Sample	Dec (°)	Inc (°)	MAD	Temp(°C)/Field (mT)	Comment
LNP6	LNP6.1A	229.7224	10.76552	10.8315	35-90	
	LNP6.4A	110.7314	-26.5831	1.789184	25-90	
	LNP6.1A	231.7	11.5	10.2	35-80	
	LNP6.2A	288.9	-4	6.1	0-550	
	LNP6.3B	211.4	-81.9	8.6	520-580	NOISY
	LNP6.4a	109.2	-26.7	2.8	300-90	
	LNP6.4C	100	-4.9	6.3	300-90	
		104.3488	-15.8484			
	LNP6.5A	211.8	-8.7	18.7	200-560	not convergent, noisy
	LNP6.5B	212.4	3.2	12.4	350-90mT	not convergent
		212.1	-2.8			
	LNP6.6B	128.6	339.2	6	100-500	
	LNP6.7B	120.9	9.3	6.7	0-580 ex. 425	
	LNP6.8A	328.1	28.5	2.4	100-580 ex. 570	

	LNP7 - LT					
	Sample	Dec (°)	Inc (°)	MAD	Temp(°C)/Field (mT)	Comment
LNP7	LNP7.1A	16.05271	-60.8928	4.750947	* 20-400	
	LNP7.2b				**Too noisy**	
	LNP7.3B	354.5	6.5	8.7	0-425	
	LNP7.4A	174.85	-65.0302	7.017422	* 100-350	
	LNP7.4B	205.6457	76.62829	6.486087	200-35	
	LNP7.4C	299.4	-77.9	16.5	20-440	
		204.9586	-57.5196			
	LNP7.5A	291.8168	-14.0179	8.858701	* 100-300	
	LNP7.6A				**Single Component**	
	LNP7.7B				**Single Component**	
	LNP7.8A	143.5241	5.337429	15.41813	* 200-440	
	LNP7.9B				**Single Component**	

	LNP7 - HT					
	Sample	Dec (°)	Inc (°)	MAD	Temp(°C)/Field (mT)	Comment
LNP7	LNP6.1A	229.7224	10.76552	10.8315	35-90	
	LNP6.4A	110.7314	-26.5831	1.789184	25-90	
	LNP7.1A	46.26942	-46.908	12.56753	3-20	
	LNP7.2B				**Too noisy**	
	LNP7.3B	9.4	13.2	24.9	500-570 ex.560	DON'T USE, MAD too high
	LNP7.4A				**Too noisy**	
	LNP7.4B				**Too noisy**	
	LNP7.4C				**Too noisy**	
	LNP7.5A	274.4612	-69.8223	8.658797	520-550	
	LNP7.6A	243.4214	-86.4012	4.159753	200-50	
	LNP7.7B	340.5	7.2	23.2	100-560	
	LNP7.8A	182.9172	28.85155	14.28917	0-25	
	LNP7.9B	233.6	-56.5	2.6	100-560	

	LNP8 - LT					
	Sample	Dec (°)	Inc (°)	MAD	Temp(°C)/Field (mT)	Comment
LNP8	LNP8.1			**Single Component**		
	LNP8.2B			**Single Component**		
	LNP8.3			**Single Component**		
	LNP8.4B			**Single Component**		
	LNP8.5A			**Single Component**		
	LNP8.6B	6.328104	53.79693	11.67671	* 20-400	
	LNP8.7B			**Single Component**		
	LNP8.8	125.8128	-16.5836	3.006835	* 20-300	
	LNP8.9A	247.7	5.2	3.1	0-425	

	LNP8 - MT				
	Sample	Dec (°)	Inc (°)	MAD	Temp(°C)/Field (mT)	Comment
LNP8	LNP8.1					
	LNP8.2B					
	LNP8.6B	26.72576	16.06605	24.87903	* 400-520	
	LNP8.7B					
	LNP8.8					

	LNP8 - HT					
	Sample	Dec (°)	Inc (°)	MAD	Temp(°C)/Field (mT)	Comment
LNP8	LNP6.1A	229.7224	10.76552	10.8315	35-90	
	LNP6.4A	110.7314	-26.5831	1.789184	25-90	
	LNP8.1	84.38158	55.28014	2.519085	20-560	Single Component
	LNP8.2B	329.4	6.4	2.7	100-580	Single Component
	LNP8.3	338.6	57.3	2.6	0-580 ex. 350 & 480	Single Component
	LNP8.4B	103.7	29.6	4.7	100-580	Single Component
	LNP8.5A	132.4	29.6	9.7		Single Component
	LNP8.6B	260.1721	38.99574	5.002031	530-560	
	LNP8.7B	125.466	73.5817	0.761957	100-580	Single Component
	LNP8.8	139.4289	-24.7739	2.495653	400-570	
	LNP8.9A	70.2	-40.7	7.1	450-580	

	LNP9 - LT					
	Sample	Dec (°)	Inc (°)	MAD	Temp(°C)/Field (mT)	Comment
LNP9	LNP9.1B			**Single component**		
	LNP9.2B			**Single component**		
	LNP9.3B			**Single component**		
	LNP9.4			**Single component**		
	LNP9.5A			**Single component**		
	LNP9.6			**Single component**		
	LNP9.7A			**Single component**		
	LNP9.9A			**Single component**		
	LNP9.10B			**Single component**		

	LNP9 - HT				
	Sample	Dec (°)	Inc (°)	MAD	Temp(°C)/Field (mT)	Comment
LNP9	LNP9.1B	232.7	47.3	2.9	20-580	
	LNP9.2B	258.8	-75.9	1.4	20-580	
	LNP9.3B	235.2	-18.9	3.5	100-570	
	LNP9.4	293.3	63.6	1.2	100-560	
	LNP9.5A	211	58.1	4.3	0-540 ex. 100 & 520	
	LNP9.6	357.3	10.3	6.5	0-550 ex. 425	
	LNP9.7A	334.1	48.5	5.4	0-580 ex. 425	
	LNP9.9A	53.3	38.3	7.2	0-500	
	LNP9.10B	274.0	9.6	8.1	550-580	